Dissertation zur Erlangung des Doktorgrades

der Fakultät für Chemie und Pharmazie

der Ludwig-Maximilians-Universität München

The Role of Open-shell Intermediates in Biological and Pharmaceutical Systems

von

Florian Achrainer

aus

München, Deutschland

2015

Erklärung

Diese Dissertation wurde im Sinne von §7 der Promotionsordnung vom 28. November 2011 von Herrn Prof. Dr. Hendrik Zipse betreut.

Eidesstattliche Versicherung

Diese Dissertation wurde eigenständig und ohne unerlaubte Hilfe bearbeitet.

München, den 10. April 2015

……

Florian Achrainer

Dissertation eingereicht am: 13. 04. 2015

1. Gutachter: Prof. Dr. Hendrik Zipse

2. Gutachter: Prof. Dr. Thomas Carell

Mündliche Prüfung am: 19. 05. 2015

Keep on dreaming boy,

cause when you stop dreamin' it's time to die.

Shannon Hoon

Danksagung

Zuallererst gilt mein Dank natürlich meinem Doktorvater Prof. Dr. Hendrik Zipse.

Ich danke ihm für sein stetes Vertrauen in mir und dass seine Tür stets bei Problemen und persönlichen Anliegen offenstand. Danke für ihre Inspiration und die mir überlassenen Freiräume. Des Weiteren danke ich Prof. Dr. Thomas Carell für die Übernahme des Zweitgutachtens und allen Mitgliedern meines Prüfungskomitees. Prof. Dr. Sergey Verevkin bin ich für die Hilfe und die Durchführung der kalorimetrischen Messungen überaus dankbar.

Ebenso danke ich meinen alten und neuen Laborkollegen Florian Barth, Carola Draxler, Harish, Julian Helberg, Dr. Johnny Hioe, Dr. Sandhiya Lakshmanan, Dr. Evgeny Larionov, Dr. Christoph Lindner, Dr. Boris Maryasin, Pascal Patschinski, Dr. Raman Tandon, Jutta Tumpach und Dr. Cong Zhang für eine unvergessliche Zeit inner- und noch mehr außerhalb des Labors. Ich danke meinen Praktikanten Renata Aguilar Torres, Leonhard Kade und Stefan Thumser für ihre tolle Arbeit. Ich hoffe, ihr konntet etwas mitnehmen…

Mein Aufenthalt in Kroatien wäre ohne Davor Šakić, Domagoj Bošnjak, Valerije Vrček, Karmen Condic-Jurkic und David Smith nicht möglich gewesen. Hvala vam za veliku vrijeme.

Ich danke allen ehemaligen und kommenden Mitgliedern der Fachschaft Chemie für die verrücktesten Augenblicke in meinem Leben. Lasst euch nicht unterkriegen. „Revolution ist nicht ein kurzer Akt, wo mal irgendwas geschieht und dann ist alles anders. Revolution ist ein langer komplizierter Prozess, wo der Mensch anders werden muss.“ (Rudi Dutschke).

Ganz besonders möchte ich meinen Freunden und Kommilitonen Tobias Blümke, Annette Frischmuth, Matthias „Knecht Ruprecht“ Ludwig und Familie, Ramona und Stefan Pichl, Martina Preiner und Veronika Werner danken. Ohne euch wäre dies alles nicht möglich gewesen. Ihr bedeutet mir sehr viel…

Abschließend möchte ich meiner Familie danken; zuerst meinen Eltern Dietmar und Evi Achrainer, dann meinen Großeltern Herbert und Theresia Gassel. Ohne eure stete Unterstützung und Zuneigung in jeder Lebenslage wäre ich heute nicht hier. Ebenso gilt mein Dank Lisa Türk und Günter Wildfeuer. Danke, dass eure Tür immer für mich offenstand. Gina, deine Hilfe und vor allem Geduld mit mir lassen sich nicht in Gold aufwiegen. Für alles, danke mein * ….

Allen, die ich hier vergessen habe, vielen Dank.

Publications

1.) **Free Radical *5-exo-dig* Cyclization as the Key Step in the Synthesis of *bis*-butyrolactone natural products: experimental and theoretical studies**
G. V. M. Sharma, D. H. Chary, N. Chandramouli, F. Achrainer, S. Patrudu, H. Zipse, *Org. Biomol. Chem.* **2011**, *9*, 4079.

2.) **The Catalytic Potential of Substituted Pyridines in Acylation Reactions: Theoretical Prediction and Experimental Validation**
E. Larionov, F. Achrainer, J. Humin, H. Zipse, *ChemCatChem* **2012**, *4*, 559.

3.) **The Chemical Fate of Paroxetine Metabolites. Dehydration of Radicals Derived from 4-(4-Fluorophenyl)-3-(hydroxymethyl)piperidine**
D. Sakič, F. Achrainer, V. Vrček, H. Zipse, *Org. Biomol. Chem.* **2013**, *11*, 4232.

4.) **New In Situ Trapping Metalations of Functionalized Arenes and Heteroarenes with TMPLi in the Presence of $ZnCl_2$ and Other Metal Salts**
A. Frischmuth, M. Fernandez, N. M. Barl, F. Achrainer, H. Zipse, G. Berionni, H. Mayr, K. Karaghiosoff, P. Knochel, *Angew. Chem. Int. Ed.* **2014**, *53*, 7928.

5.) **Transfer Hydrogenation as a Redox Process in Nucleotides**
F. Achrainer, V. N. Emel'yanenko, W. Tantawy, S. P. Verevkin, H. Zipse, *J. Phys. Chem. B* **2014**, *118*, 13863.

6.) **Transfer Hydrogenation in Open-Shell Nucleotides – A Theoretical Survey**
F. Achrainer, H. Zipse, *Molecules* **2014**, *19*, 21486.

7.) F. Achrainer, F. Barth, C. Draxler, C. Lindner, H. Zipse, „Versuche zur Experimentalvorlesung Organische Chemie", 2nd Ed., *Shaker Verlag*, **2014** [ISBN 978-3-8440-2850-8].

8.) **Preparation of Tri- and Tetrasubstituted Allenes via Regioselective Lateral Metalation of Benzylic Trimethylsilyl Alkynes Using TMPZnCl•LiCl**
P. Quinio, C. François, A. E. Cuesta, A. Steib, F. Achrainer,H. Zipse, K. Karaghiosoff, P. Knochel, *Org. Lett.* **2015**, *17*, 1010.

Poster Presentations

1.) **The Environmental Fate of Cationic Open Shell Paroxetine Metabolites**
F. Achrainer, V. Vrček, H. Zipse, March 2013, Winterschool „Computational Life Sciences on Open Shell Intermediates",Ludwig-Maximilians-Universität Munich.

2.) **Radicals in Enzymatic Catalysis**
J. Hioe, F. Achrainer, H. Zipse, March 2013, 5th SFB749 Workshop, Wildbad Kreuth, Germany.

Oral Presentations

1.) **Microwave-Assisted Syntheses in Organic Chemistry (MAOS) – An Introduction for Technicians, PhDs and Students**, September 2011, University of Zagreb, Croatia.

2.) **Hydrogen Transfer in Enzymatic Radical Reactions**, March 2013, 5th SFB749 Workshop, Wildbad Kreuth, Germany.

3.) ***Ab-initio* Calculations of pK_a values in Aqueous Solution**, August 2013, Summerschool „Computational Life Sciences on Open Shell Intermediates“, Primošten, Croatia.

Table of Contents

1 Summary

1.1 General

The application of theoretical concepts in chemistry has wittnessed a remarkable evolution due to the development of efficient and powerful computers and software. The support of experimental results by theoretical predictions is the current field of work of numerous chemists worldwide, especially if highly reactive intermediates, *e.g.* open-shell systems with one or more unpaired electrons, are involved. A central question hereby is their thermodynamic stability, particularly for biological systems, where accurate values and structural information are not easily accessible. The enthalpy change ΔH of a molecular transformation is an easily computable value and a universal descriptor for the outcome of a reaction. The stability of *C*-centered radicals can conveniently be defined using the isodesmic hydrogen atom transfer of **Scheme 1.1**. In literature the reaction enthalpy of this process is referred to radical stabilization energy (RSE) of radical $R_3C\bullet$ compared to its parent methyl radical $H_3C\bullet$. Simple reaction equation analysis reveals that the bond strength of R_3C-H (bond dissociation energy, BDE) is exactly the sum of the theoretically calclulated RSE and the CH-BDE of methane.

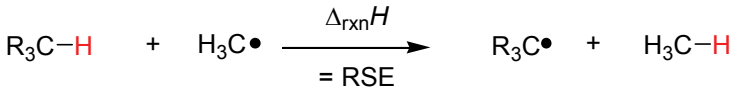

$$BDE\ (R_3C\text{-}H) = RSE + BDE\ (H_3C\text{-}H,\ exp.)$$

Scheme 1.1 General definition of radical stability and calculation of bond dissociation energies.

1.2 Transfer Hydrogenation as a Redox Process in Nucleotides

The fidelity of biological information storage is tightly linked to the chemical stability of DNA and RNA oligonucleotides. As a possible threat reduction of the pyrimidine and purine bases as a result of transfer hydrogenation from the sugar-phosphate-backbone (as a free hydroxyl group is present in C2' position of RNA) have been

studied herein. Using a combined theoretical and experimental strategy the heats of hydrogenation of the different bases have been determined.

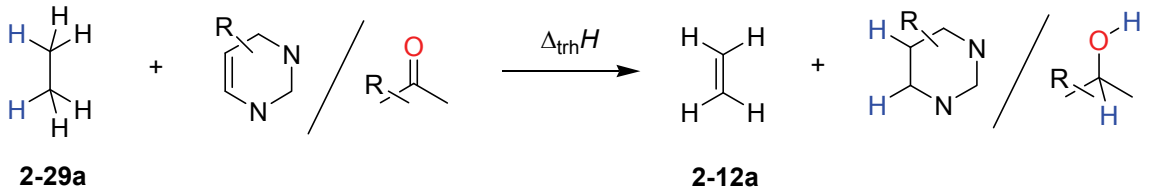

Scheme 1.2 Reaction scheme to calculate heats of hydrogenation $\Delta_{hyd}H$ of various substrates.

The best agreement of theory and experiment for $\Delta_{hyd}H$ has been obtained for the reaction involving transfer hydrogenation of ethane (**2-29a**) and ethylene (**2-12a**) at G3B3 level of theory in addition to the experimental heat of hydrogenation of ethylene ($\Delta_{hyd}H$(**2-12a**, exp.) = -136.3 kJ mol^{-1}).

The most easily hydrogenated base is uracil (**2-32a**), followed by thymine (**2-32b**) and cytosine (**2-76**). Comparison of these hydrogenation enthalpies with those of ketones and aldehydes derived from sugar models indicates the possibility of near thermoneutral hydrogen transfer between uracil (**2-32a**) and the sugar phosphate backbone (see **Figure 1.1**). Regardless of the position, the hydrogenation of purine-derived bases is always endothermic. Upon coupling base and sugar to complete nucleosides, the driving force for the intramolecular transfer hydrogenation of uridine (**2-99**) is decreased due to omission of stabilizing hydrogen bonds upon oxidation to yield **2-100a**.

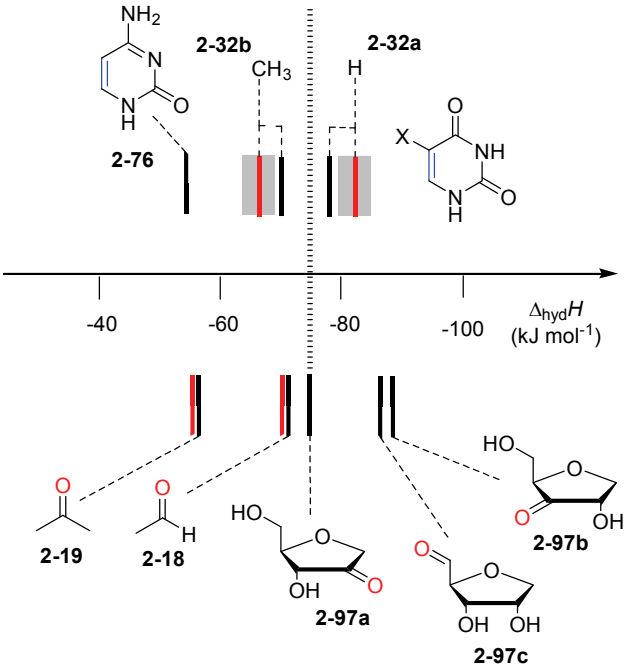

Figure 1.1 Heats of hydrogenation $\Delta_{hyd}H$ at 298.15 K of selected nucleobases and carbonyl compounds (G3B3 are shown as black, experimental hydrogenation enthalpies as red lines.

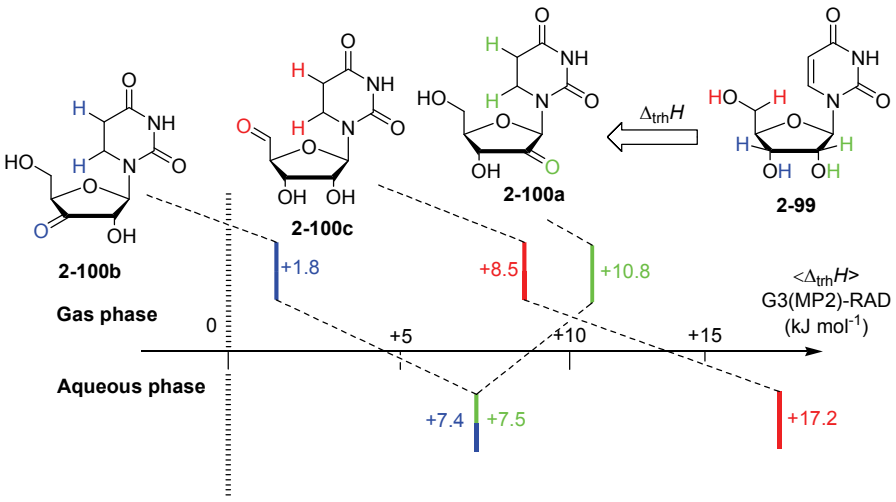

Figure 1.2 Intramolecular transfer hydrogenation of uridine (**2-99**) at G3(MP2)-RAD level in kJ mol^{-1}.

Undoubtedly, the kinetic barrier for direct hydrogen transfer is very high, but the residues present in enzyme active sites may be effective in catalyzing a stepwise mechanism. All analytical methods used for this purpose, mostly mass spectrometry, would not be able to predict the correct structure of this reaction.

1.3 Enhanced Redox Properties in Open-shell Nucleotides – A Theoretical Survey

The potential of biologically inspired open-shell intermediates to act as reductants in transfer hydrogenation reactions to alkenes has been investigated theoretically. The radical-induced changes in dihydrogen transfer energetics are likely to impact the chemistry of nucleotide and peptide-derived radicals. This may be particularly relevant for cases where oxidations of nucleotide radicals have been observed under reducing conditions. A prominent example is the outcome of the substrate reaction of the E441Q mutant of *E. coli* class I ribonucleotide reductase (RNR). The possibility that the base present in *e.g.* radical **3-11R** can act as internal redox partner to the adjacent C3'-ribosyl radical, thus generating product radical **3-14R** (and not **3-13R**) through a transfer hydrogenation process has been examined theoretically. Mass spectrometry as the major tool for the analysis of oligonucleotides gives for this type of reaction no meaningful conclusion and a dihydro cytosine motif has presumably no significant influence on the EPR parameters.

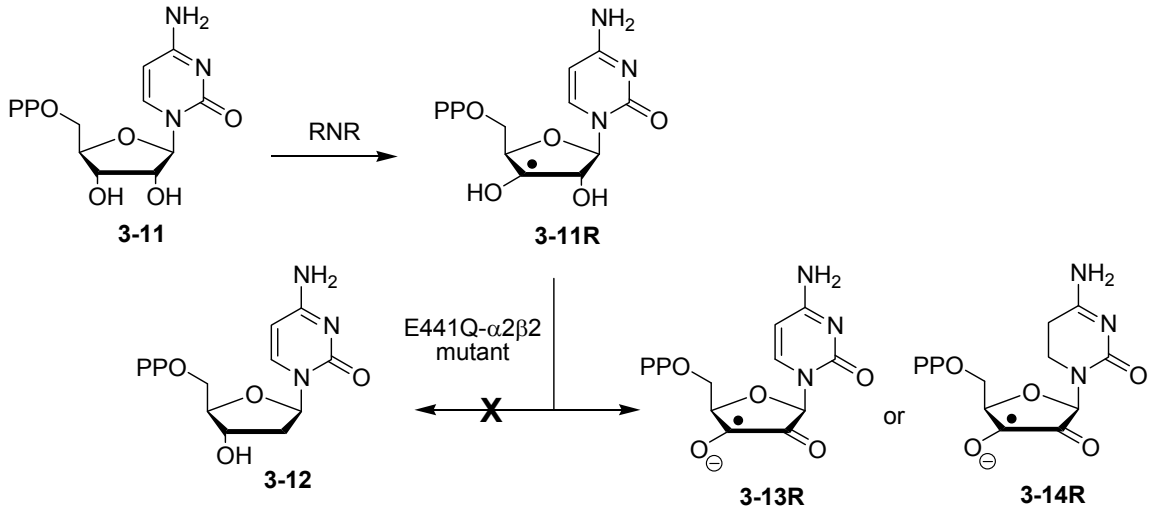

Scheme 1.3 Substrate reaction of class I RNR E441Q mutant.

The results fully support the strongly reductive nature of these species, if the oxidized product is a captodatively stabilized radical. As revealed through comparison to hydrogenation energies for individual nucleotide bases and also seen in the reaction energies for intramolecular transfer hydrogenation, the strongly reductive nature of ribosyl radicals implies that pyrimidine bases can be reduced in an exothermic fashion (see **Figure 1.3**).

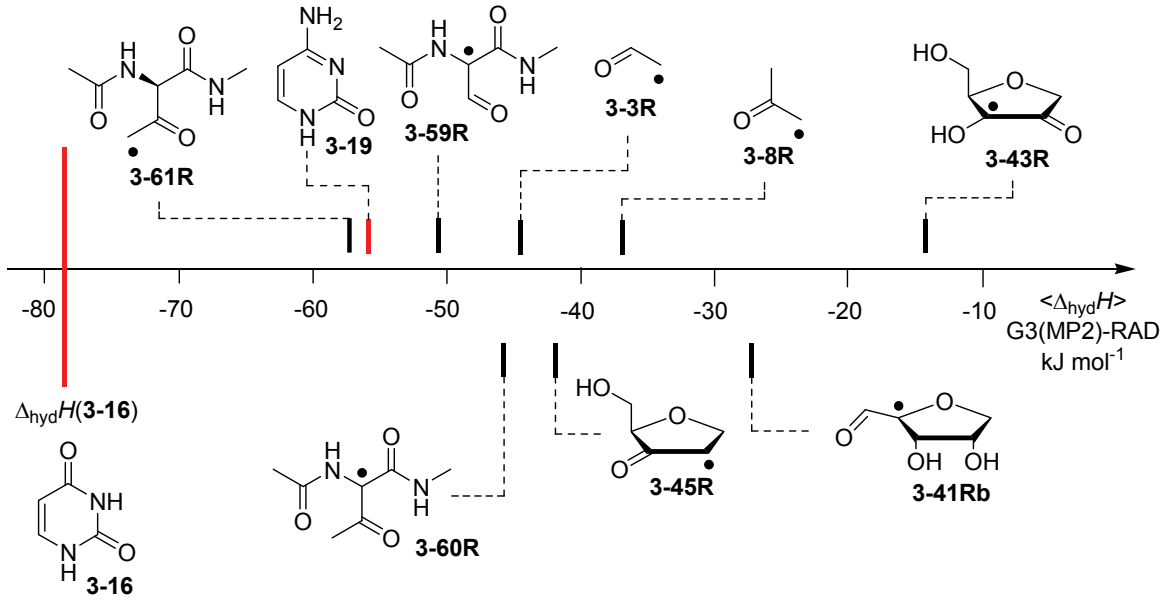

Figure 1.3 *Boltzmann*-averaged transfer hydrogenation enthalpy scale $\langle\Delta_{trh}H\rangle$ for *C*-centered peptide radicals (G3(MP2)-RAD, in kJ mol^{-1}) compared to selected carbonyl and sugar radicals.

The reaction energies for inter- and intramolecular transfer hydrogenation presented herein permit no statement on the pathways how such a process may occur. Nevertheless, some speculations on possible pathways can be made:

1.) Reactions involving open-shell intermediates at the nucleotide base. This may be accompanied with either initial single hydrogen atom or proton-coupled electron transfer to the uracil C6 position, followed by a second H• transfer to yield product radical **3-48Ra**. 2.) An ionic pathway, where the unpaired spin never leaves the ribose unit. This may involve, for example, initial protonation of the pyrimidine C4 carbonyl oxygen, followed by hydride transfer between the ribose C2' and the uracil C6 position. After deprotonation and tautomerization of radical cation **3-63Rb** the captodatively stabilized product **3-48Ra** is formed.

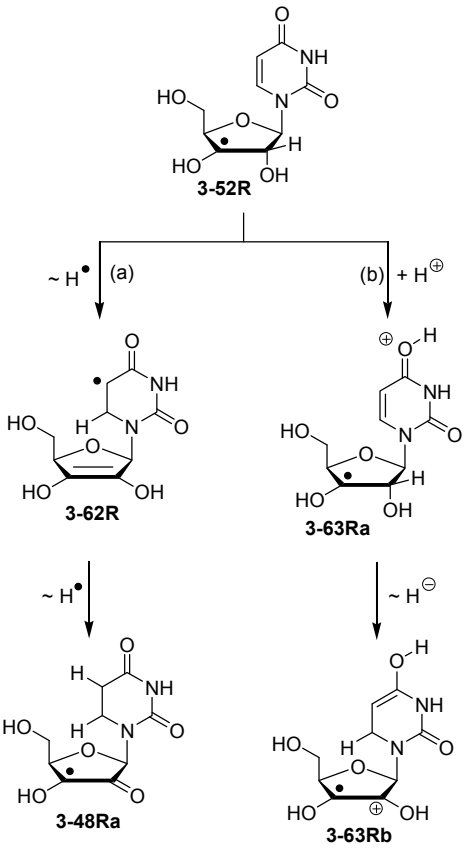

Scheme 1.4 Possible pathways for stepwise hydrogen transfer reactions using C3' radical **3-52R** as example.

1.4 Calculation of Chemical Properties of Allenic Zinc Compounds

In collaboration with the group of Prof. *Paul Knochel*, the formation of allenic zinc compounds has been studied spectroscopically and supported theoretically by NMR shift calculations and thermochemical analysis. The zinc base TMPZnCl•LiCl (**4-14**) has been used to synthesize neutral allenic zinc intermediates from benzylic propynes which can be quenched by the addition of various electrophiles. The analogous zincates have been prepared by transmetallation of the corresponding Li organyls with $ZnCl_2$ in THF.

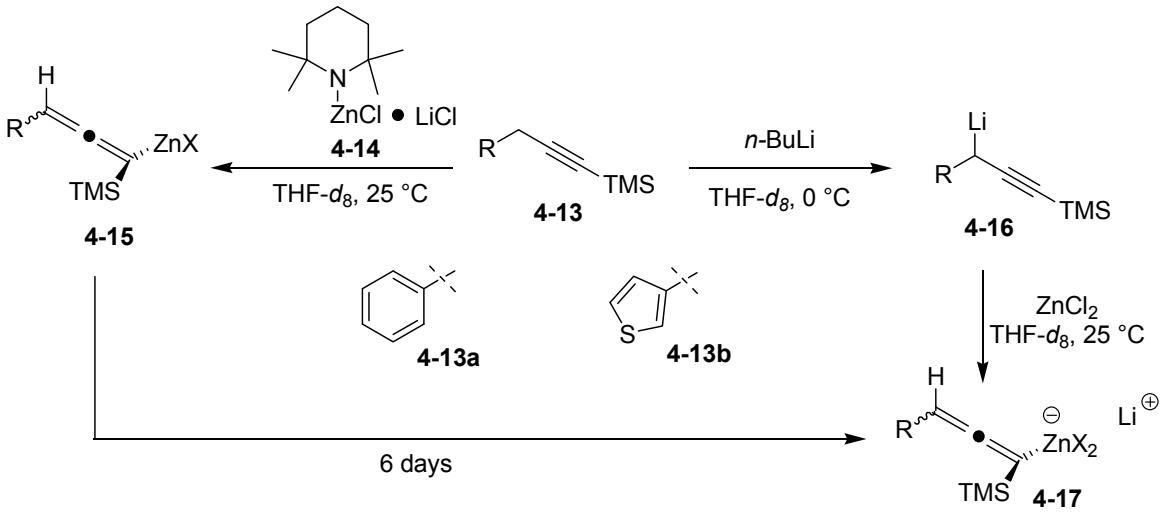

Scheme 1.5 Syntheses of allenic zinc compounds of proposed structure **4-15** and **4-17**.

Different basis sets, functionals and solvation states have been benchmarked with the well-known *Reformatsky* reagent **4-9**. B3LYP/631SVP geometries in combination with GIAO/mPW1K/IGLO-III calculations in the gas phase are sufficient enough to perform well in calculating ^{1}H and ^{13}C NMR shifts of organozinc reagents in THF solution.

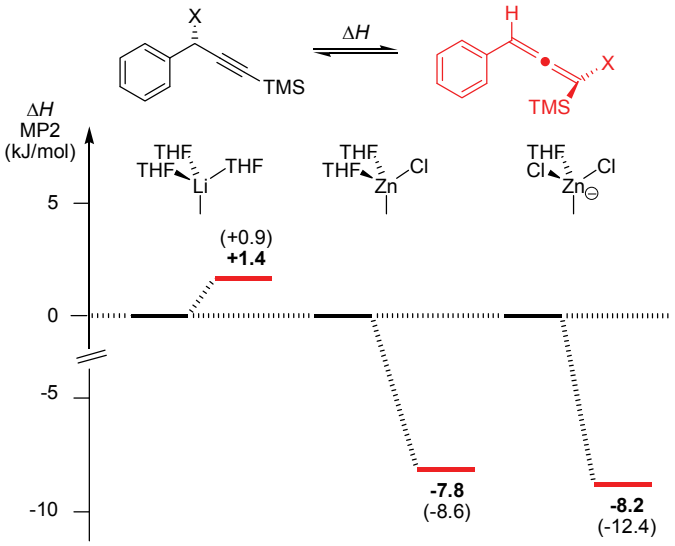

Figure 1.4 Propargyl to allenyl isomerization in THF solution (SMD/B3LYP/6-31G(d)) at MP2(FC)/6-31+G(d,p) level (gas phase values in parenthesis).

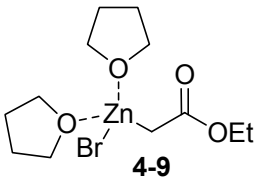

The reaction outcome of neutral and anionic zinc allenes as well as for the corresponding organolithium isomers were successfully predicted by thermochemical analysis of propargyl-allenyl isomerization at MP2 level of theory (**Figure 1.4**). Metalation of propynes with *n*-BuLi yielded only propargylic organometalics, whereas zincation or transmetalation with the aid of $ZnCl_2$ afforded only allenic products. The preferred location of metalation of various substrates has been examined in terms of their pK_a values. Since the experimental determination of

acidities or basicities of organic and inorganic compounds is rather challenging, a computational method that predicts protonation patterns in terms of pK_a values in a fast and reliable way would be of general use. The B3LYP/6-311++G(2df,2p) level of theory in combination with SMD/B3LYP/6-31G(d) free solvation energies and DMSO (**4-24H**, pK_a = +35.1) has been identified as a good compromise between accuracy and computational effort (see **Scheme 1.6**).

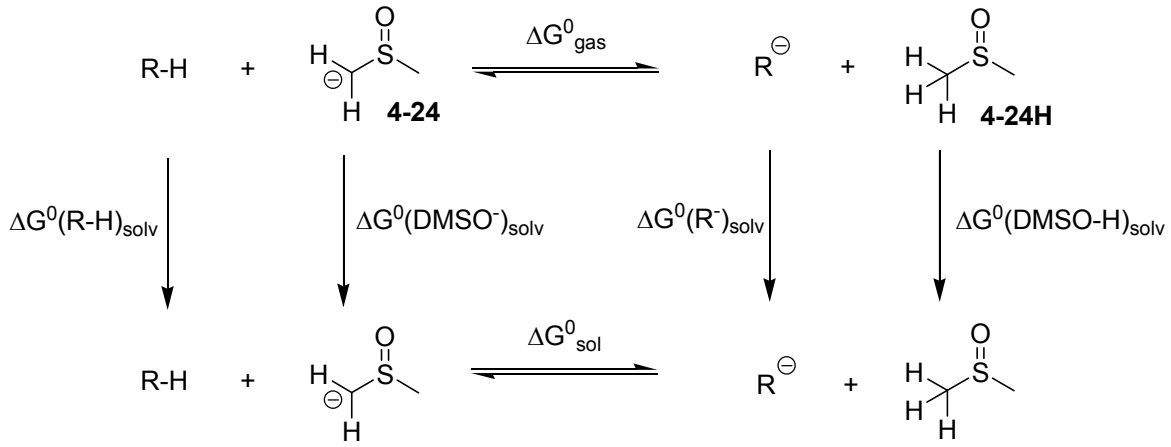

Scheme 1.6 Thermochemical cycle for the calculation of pK_a values in solution.

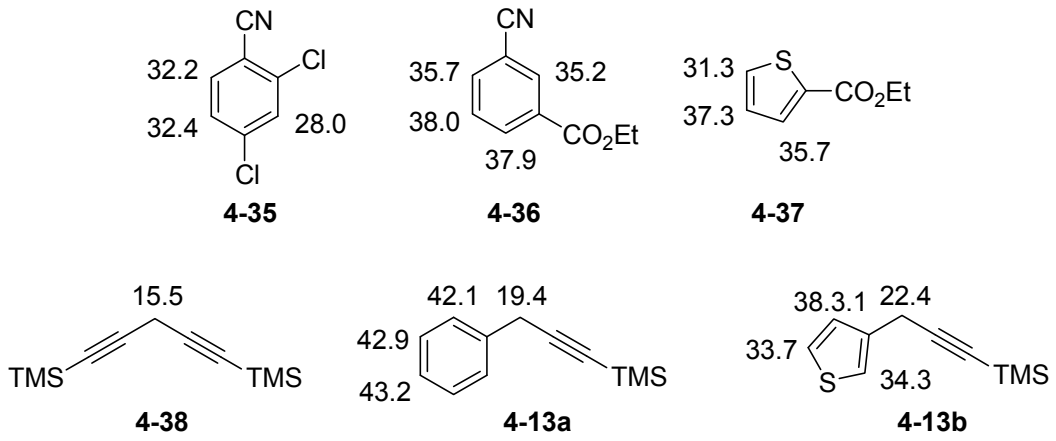

Figure 1.5 SMD/B3LYP/6-31G(d)//B3LYP/6-311++G(2df,2p) calculated pK_a values using DMSO as reference for various substrates (corrected to THF solution).

1.5 The Chemical Fate of Paroxetine Metabolites

The accumulation of pharmaceutically active compounds in waste or drinking water is of growing importance for world's population. With respect to environmental risk

assessment a prominent example for these pharmaceuticals is the selective serotonine reuptake inhibitor paroxetine (**5-7**).

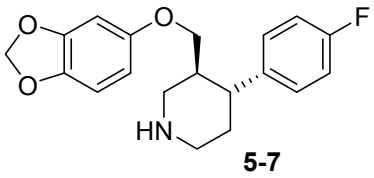

5-7

Quantum chemical calculations have been used to evaluate the chemical properties and possible reaction channels of open-shell piperidine **5-12R⁺,** which is considered to be the key intermediate in the environmental (photo)degradation of paroxetine (**5-7**). This includes, for example, bond dissociation processes, hydrogen atom transfer reactions and radical-induced dehydrations, which should not exceed an experimentally determined barrier of *ca.* +100 kJ mol^{-1}.

Considering the hydrogen atom transfer, the [1,4]-H shift is the most favorable pathway if a cluster continuum model with water as solvent and reagent is included. In the gas phase without explicit solvation the formation of α-hydroxy radical **5-18R** is preferred. The unpaired spin at the nitrogen atom has a significant impact on the bond strength of the α-CH bond, which is decreased dramatically and opens a dehydration pathway never considered before with iminium radical **5-22R** as intermediate.

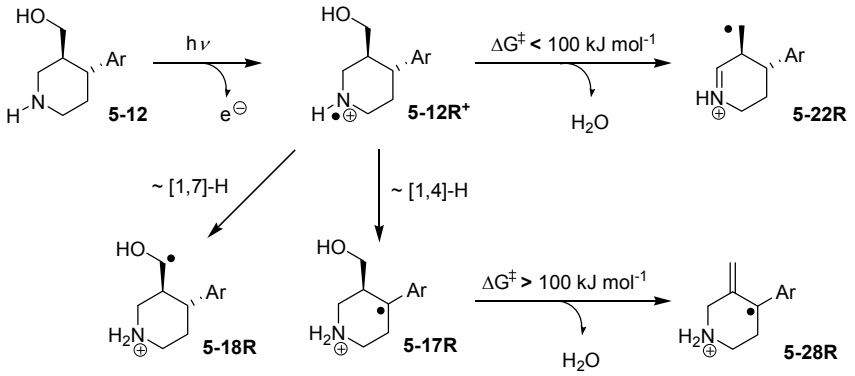

Scheme 1.7 Exemplary reaction pathways of the hydrolysis product **4-12** of paroxetine (**5-7**) upon photolysis (Ar = *p*-F-C_6H_5).

Table 1.1 Theoretically calculated bond dissociation energies (G3(MP2)-RAD level) in the gas phase for various piperidines.

	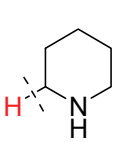 **5-14**	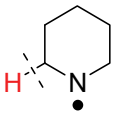 **5-14R**	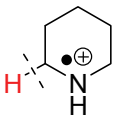 **5-14R⁺**	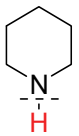 **5-14**	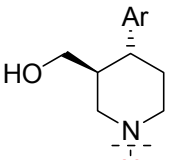 **5-12**	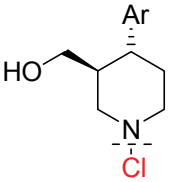 **5-12Cl**
BDE (kJ mol^{-1})	+390.5	+95.1	+75.2	+403.4	+401.7	+247.2

In addition, the stability of a range of proposed dehydrated product radicals has been evaluated to support the existence of proposed reaction products.

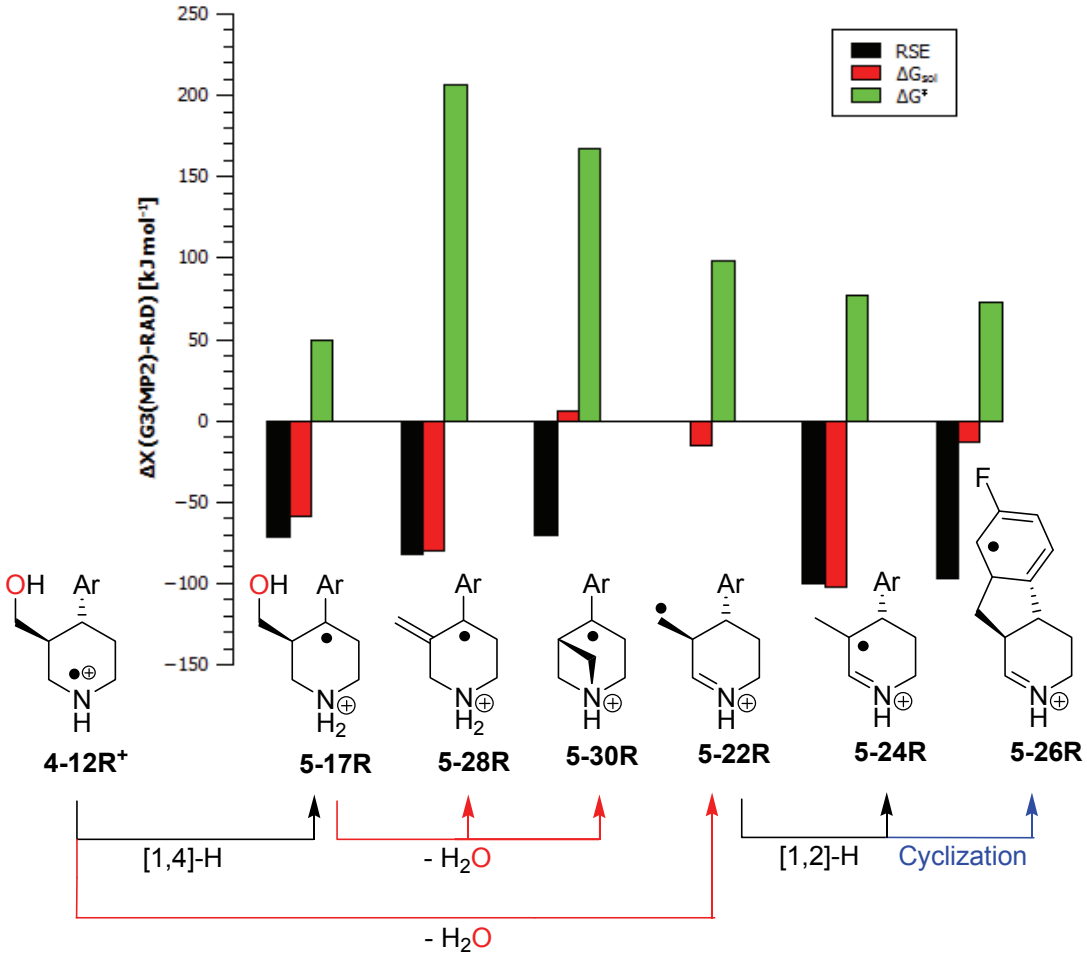

Figure 1.6 Comparison of barriers, reaction free energies for hydrogen atom transfer reactions (black), dehydrations (red) and cyclizations (blue) and radical stabilization energies obtained at G3(MP2)-RAD level of theory.

2 Transfer Hydrogenation as a Redox Process in Nucleotides

Parts of this chapter have been published in

Transfer Hydrogenation as a Redox Process in Nucleotides

F. Achrainer, V. N. Emel'yanenko, W. Tantawy, S. P. Verevkin, H. Zipse, *J. Phys. Chem. B* **2014**, *118*, 10426 – 10429.

2.1 Introduction

Desoxyribonucleic acid (DNA) is by far the most valuable molecule found in nature. It conserves the genetic code in form of chemical information, which finally is translated in a two-step process into proteins.[1] A complementary role is played by ribonucleic acid (RNA), which contains the information of genomic DNA after the transcription as messenger RNA (*m*RNA). This process is followed by the translation of the mRNA by the ribosome using its ribosomal RNA (*r*RNA) and with amino acid charged transfer RNA (*t*RNA) to form polypeptides. Genomic DNA is a polymer consisting of four different nucleobases connected to 2'-deoxribose-3',5'-phosphate backbone, the two purines adenine (dA, **2-1**) and guanine (dG, **2-2**) and the two pyrimidines thymine (dT, **2-3**) and cytosine (dC, **2-4**). The three-dimensional structure of DNA was revealed by *James Watson* and *Francis Crick* in the early 50ies of the last century and represents a double helix consisting of two complementary strands connected by hydrogen bonds and further stabilized by π-π base stacking.[2]

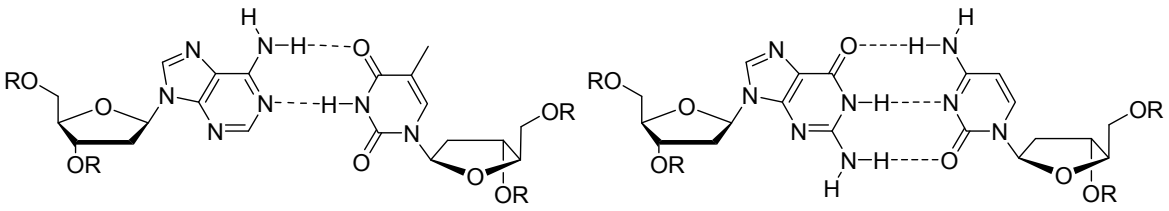

Figure 2.1 *Watson-Crick* base pairing of the complementary nucleotides in DNA.

On the other hand, RNA is only intended to be a short-lived intermediate, capable of hydrolytic strand cleavage due to the free C2' OH group (**Scheme 2.1**).

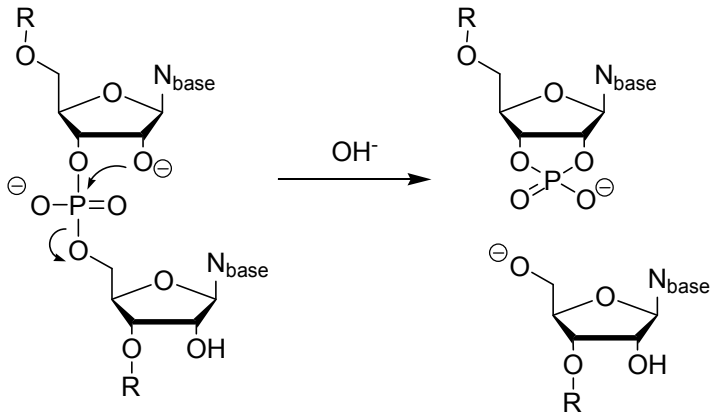

Scheme 2.1 RNA hydrolysis in aqueous solution.

In ribosomes RNA participates in the catalytic formation of peptide bonds.[3] More than 100 post-transcriptional RNA modifications have been discovered till today with the largest amount and diversity present in *t*RNA.

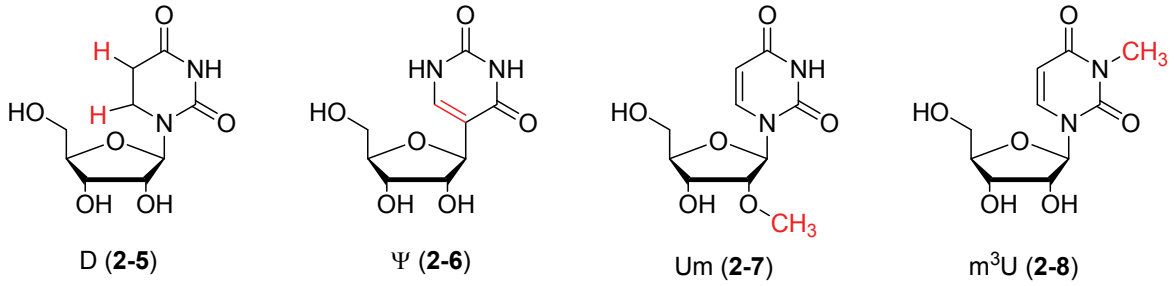

Figure 2.2 Selected uridine-derived RNA modifications marked in red color.

A very prominent example of RNA modification is dihydrouridine (D, **2-5**), which exhibits a strong conformational flexibility due to its missing base planarity.[4] It promotes C2'-*endo* conformation formation of the sugar moiety thus mainly found at positions where tertiary interactions and loop-formation are necessary.[5] As exemplified by dihydrouridine (**2-5**) the degree of saturation has a large impact on base-pairing and the conformational degree of freedom and can lead to point mutations at the wrong position. Mutagens can cause molecular changes to the DNA that can affect their transcription or replication which in severe case can also lead to cell death or serious diseases. In aqueous solution spontaneous deamination of cytitidine (**2-4**), the so called *Pucherer* reaction, results in the formation of ammonia and uridine (U, **2-9**) which represents a very potent transition mutation. In DNA, this unwanted nucleotide is corrected by the enzyme uracil-DNA glycolase generating an

abasic site (AP). These abasic sites are finally repaired by the DNA base excision repair (BER) pathway involving AP endonucleases.[6] A very mutagenic chemical is nitrous acid HNO_2, which can potentially be generated from a mixture of NaCl, $NaNO_2$ and $NaNO_3$ added as a preservative to numerous meat products.[7] Nitrous acid reacts with the free amino-group to form unstable diazonium ions, which hydrolyze to the deaminated products (see **Scheme 2.2**). This hydrolytic deamination is even faster for dihydrocytosines as examined theoretically by *Labet* and coworkers.[8]

Herein, we are studying the thermodynamics of CC-hydrogenation of biological-relevant nucleobases as potential threat for mutations in combination with oxidations of the sugar-backbone. This follows the large differences in hydrogenation enthalpies of molecular systems containing C-C and C-O double bonds.

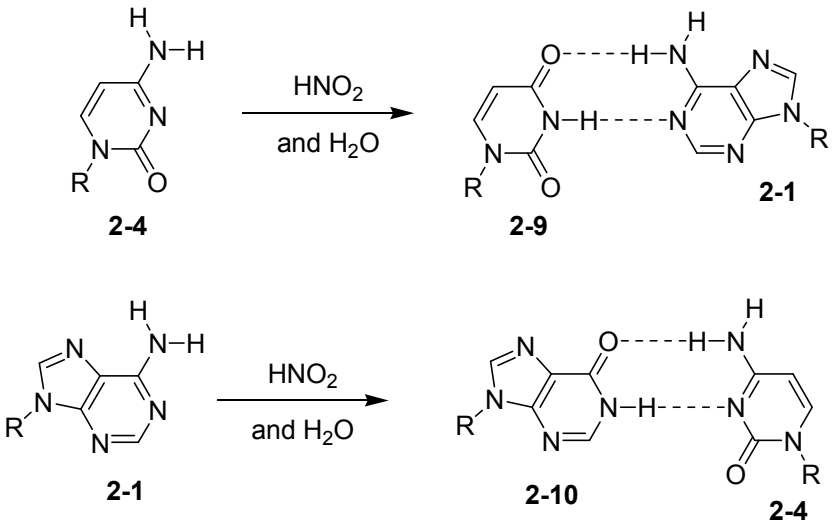

Scheme 2.2 Nitrous acid-induced hydrolytic deamination of cytidine (**2-4**) and adenosine (**2-1**) forming post-replicative transition mutations.

2.2 Evaluation of Methods for the Determination of Heats of Hydrogenation

Heats of hydrogenation of alkenes are historically important in defining essential chemical concepts like conjugation, aromaticity,[9] anti-aromaticity[10] and molecular strain.[11] However, the determination of enthalpy values for potentially interesting substrates sometimes cannot be carried out due to their instability or difficult syntheses. Therefore, the field of theoretical chemistry has provided a number of valuable methods to predict accurate thermochemical data with kcal mol^{-1} accuracy.

The "Gaussian-*n*" (G*n*) theories, and especially G3,[12] were the first methods to produce enthalpies of chemical accuracy, but relied on relatively small basis sets and empirical corrections. *Petersson* introduced his complete basis set (CBS) methods implementing similar concepts, but included pair correlation extrapolations to the corrections.[13] Today, the main focus of theoretical chemists is on merging relative computational effort with accuracy. The Weizmann-*n* (W*n*) theories, developed by *Martin*, represent probably the most valuable method for benchmarking thermochemical properties,[14] but are only applicable for very small or highly symmetric systems. Since the number of valence electrons of the examined nucleotides exceed the usage of Weizmann and CBS theory the performance of four different approaches, including DFT, MP2 and Gaussian theory, have been analyzed with a test set of 23 alkenes and arenes and 5 carbonyl compounds (see **Theoretical Appendix**). Results for the direct hydrogenation with molecular hydrogen (**2-11**) are summarized in **Table 2.1** and **Table 2.2**. The corresponding experimental values can either be obtained from actual measurements for the hydrogenation reaction ($\Delta_{hyd}H$) or from heats of formation of all participating reactants/products ($\Delta_{rxn}H$). The largest difference between these two data sets of 5 kJ mol^{-1} can be seen for cylohexanone (**2-16**). Calculations with the G3B3 compound method reproduce the experimental $\Delta_{hyd}H$ and $\Delta_{rxn}H$ values with RMSD values of 2.3 kJ mol^{-1} and 2.8 kJ mol^{-1}, respectively (**Figure 2.3**). Deviations are slightly larger for the G3(MP2)-RAD composite method and significantly larger for the much more economical MP2(FC)/6-311+G(3df,2p) method. Deviations are largest for the hydrogenation onf benzene (**2-14**) to cyclohexane, when only the G3B3 method yields satisfactory results.

Table 2.1 Calculated hydrogenation enthalpies $\Delta_{hyd}H$ of some selected alkenes in the gas phase (at 298.15 K and 1 atm) and experimental values in kJ mol^{-1}.

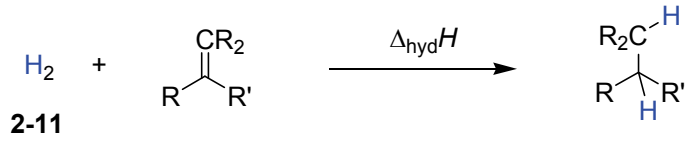

2-11

	$\Delta_{hyd}H$				$\Delta_{rxn}H$
	MP2(FC)/ 6-311+G(3df,2p)	G3(MP2)-RAD	G3B3	$\Delta_{hyd}H$(exp.)	$\Delta_{rxn}H$(exp.)[15]
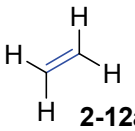 **2-12a**	-140.04	-127.31	-133.76	**-136.31 ± 0.21**[9]	**-136.4**
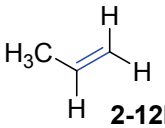 **2-12b**	-127.66	-116.54	-122.70	**-124.98 ± 0.21**[16]	**-123.8**
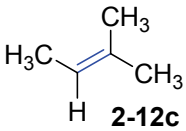 **2-12c**	-114.37	-105.43	-110.79	**-111.63 ± 0.25**[17]	**-111.9**
 **2-13a**	-120.75	-110.31	-116.52	**-118.83 ± 0.42**[18]	**-118.4**

Table 2.2 Calculated hydrogenation enthalpies $\Delta_{hyd}H$ of some selected alkenes and carbonyl compounds in the gas phase (at 298.15 K and 1 atm) and experimental values in kJ mol^{-1}.

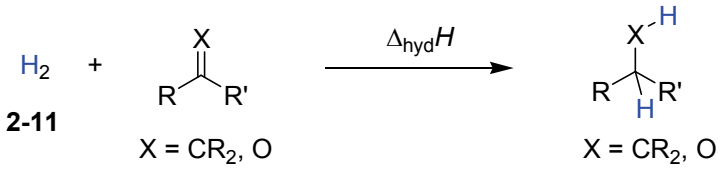

	$\Delta_{hyd}H$				$\Delta_{rxn}H$
	MP2(FC)/ 6-311+G(3df,2p)	G3(MP2)-RAD	G3B3	$\Delta_{hyd}H$(exp.)	$\Delta_{rxn}H$(exp.)[15]
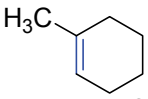 **2-13b**	-114.77	-105.53	-110.96	**-111.40 ± 0.37**[19]	**-111.4**
 **2-14**	-186.12	-183.67	-201.04	**-205.27 ± 0.63**[9]	**-206.3**
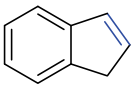 **2-15**	-98.59	-93.34	-99.51	**-98.9 ± 0.63**[20]	**-103.2**
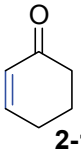 **2-16**	-108.09	-98.82	-104.51	**-109.20 ± 2.9**[21]	**-104.2**
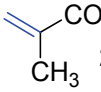 **2-17**	-120.47	-110.62	-116.26	**-118.0 ± 1.3**[22]	**-117.3**
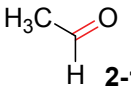 **2-18**	-65.23	-62.91	-66.47	**-69.08 ± 0.42**[23]	**-68.6**
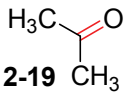 **2-19**	-52.40	-50.85	-54.04	**-55.60 ± 0.42**[24]	**-55.5**
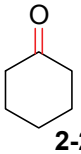 **2-20**	-58.74	-57.31	-60.14	**-63.51 ± 0.63**[23]	**-60.1**
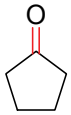 **2-21**	-47.45	-45.13	-47.92	**-51.25 ± 0.63**[23]	**-50.4**

From a chemical point of view it is important to note that hydrogenation of C-O double bond is significantly less exothermic than that of C-C double bonds.

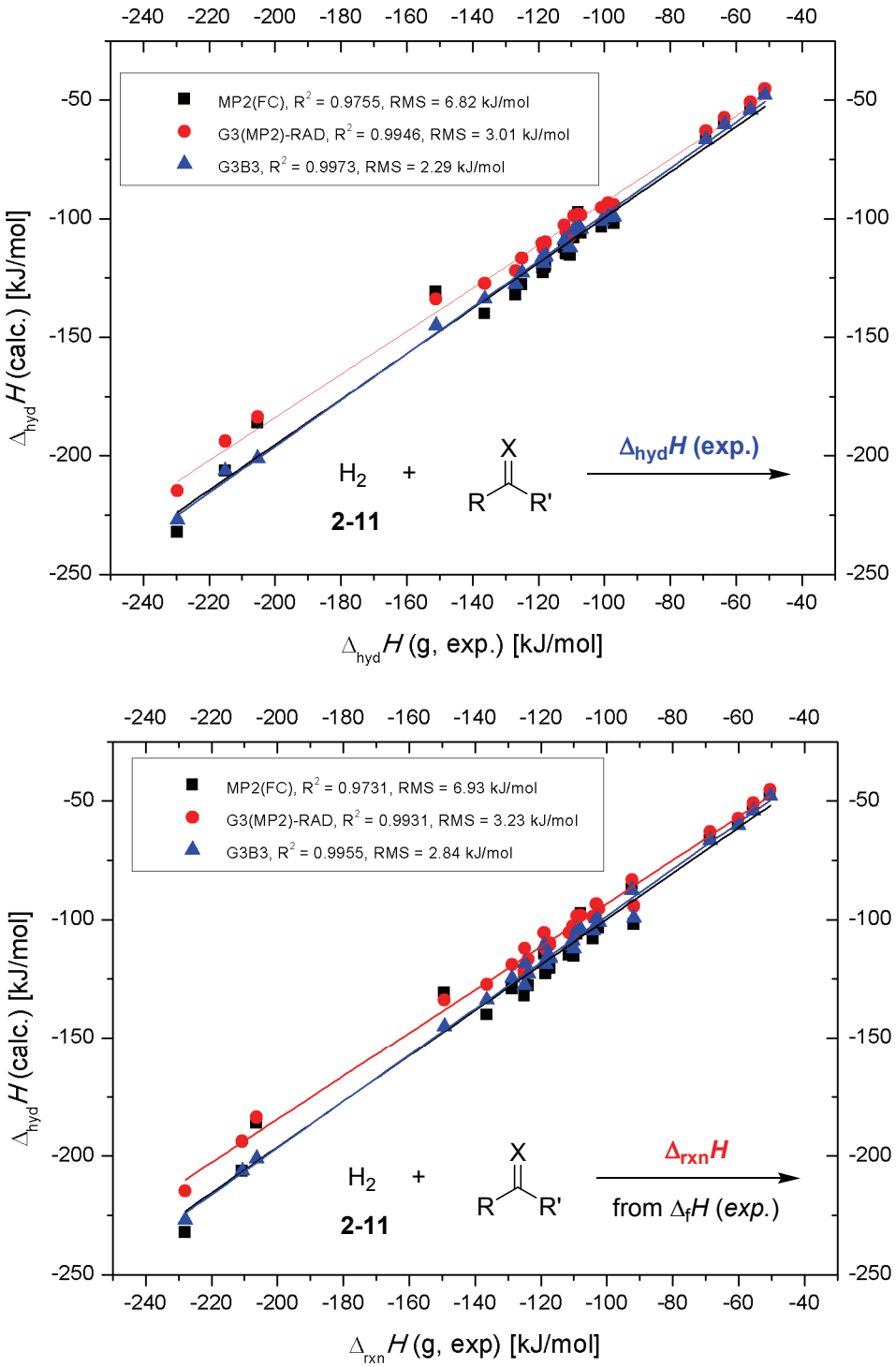

Figure 2.3 Evaluation of methods using experimentally available enthalpies in the gas phase (or gas phase corrected of the corresponding liquid or solid substrate).

Aside from using molecular hydrogen as the reducing agent, alternative reduction reactions employ hydrogen donors such as propan-2-ol (**2-22**), formic acid (**2-23**),[25] *Hantzsch*'s ester **2-24**[26], or thiazoline **2-25**[27] (**Figure 2.4**).

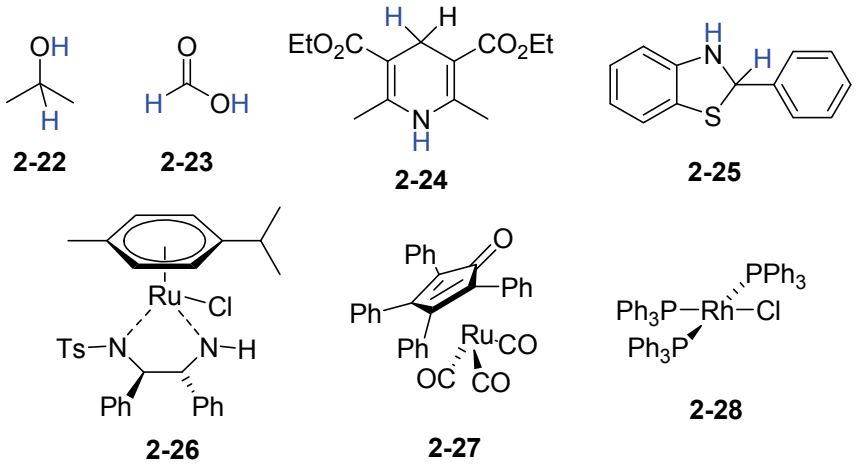

Figure 2.4 Selected organic hydrogen donors and transition metal catalysts.

Since transfer hydrogenations are equilibrium reactions, the formation of volatile or stabilized byproducts like acetone, carbon dioxide or pyridine represents, together with different bond energies for C-O and C-C bonds, the main driving force.[28]

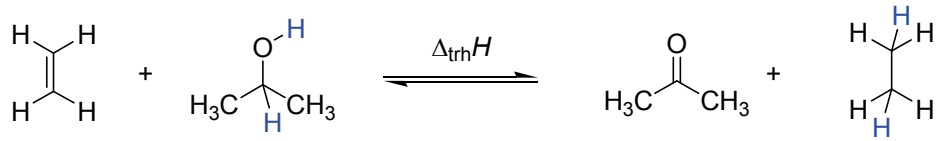

Scheme 2.3 Transfer hydrogenation of ethylene (**2-12a**) using propan-2-ol (**2-22**).

Fujita et al. recently reported an iridium-based catalyst system (**2-30**) for the mild reversible dehydrogenative oxidation of alcohols even in water.[29]

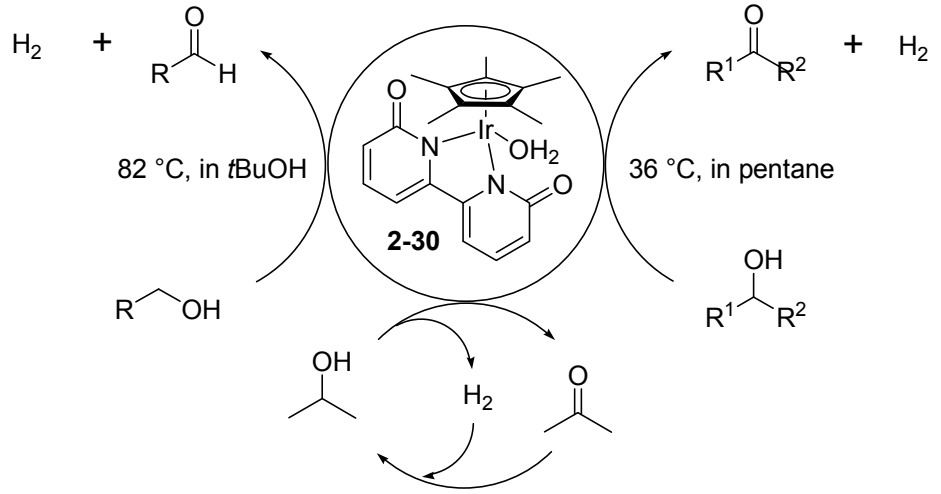

Scheme 2.4 Dehydrogenative oxidation of alcohols using the water-soluble Ir(III) catalyst **2-30** developed by *Fujita* and coworkers.[29]

The energetics of transfer hydrogenation reactions can be calculated with the same theoretical medthods used before. The accuracy in these calculations is expected to be higher as compared to that for direct hydrogenation reactions simply because the bonding situation in reactants and products is quite comparable. Using ethane (**2-29a**) as hydrogen donor a very good correlation of calculated vs. experimentally available values is found for alkenes (**Table 2.3**) and carbonyl compounds (**Table 2.4**).

Table 2.3 Calculated transfer hydrogenation enthalpies $\Delta_{trh}H$ of some selected alkenes (at 298.15 K and 1 atm) and experimental values in kJ mol^{-1}.

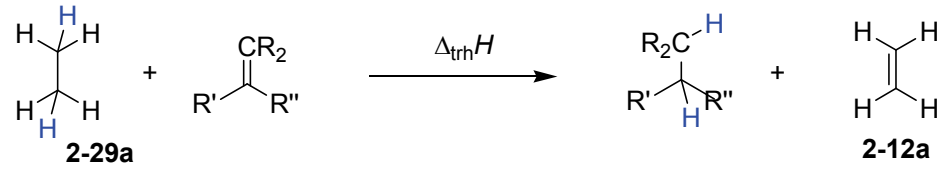

	$\Delta_{trh}H$			
	MP2(FC)/ 6-311+G(3df,2p)	G3(MP2)-RAD	G3B3	$\Delta_{trh}H$(g, exp.)[15]
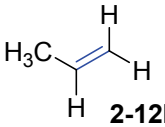 **2-12b**	+12.39	+10.77	+11.06	**+12.6**
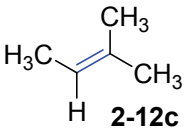 **2-12c**	+25.68	+23.29	+22.97	**+24.5**
 **2-13a**	+19.29	+16.99	+17.24	**+18.0**
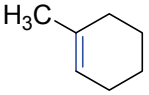 **2-13b**	+25.27	+21.77	+22.80	**+25.0**
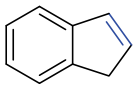 **2-15**	+41.45	+33.97	+34.25	**+33.2**
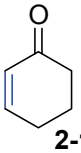 **2-16**	+31.96	+28.49	+29.25	**+32.2**
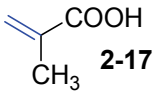 **2-17**	-19.58	+16.68	+17.50	**+19.1**

Table 2.4 Calculated transfer hydrogenation enthalpies $\Delta_{trh}H$ of some selected carbonyl compounds (at 298.15 K and 1 atm) and experimental values in kJ mol^{-1}.

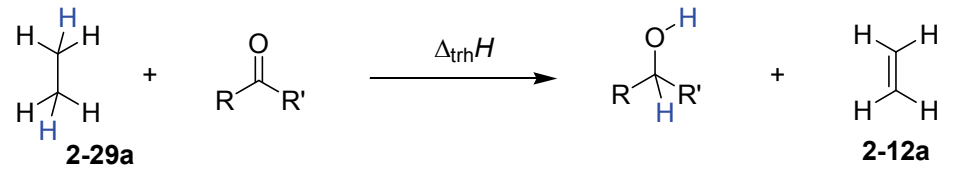

	$\Delta_{trh}H$			
	MP2(FC)/ 6-311+G(3df,2p)	G3(MP2)-RAD	G3B3	$\Delta_{trh}H$(g, exp.)[15]
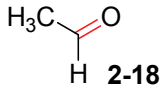 **2-18**	+75.65	+65.05	+67.88	**+67.8**
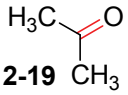 **2-19**	+87.64	+76.45	+79.73	**+80.9**
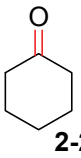 **2-20**	+81.31	+69.99	+73.62	**+76.3**
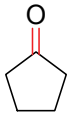 **2-21**	+92.59	+82.18	+85.85	**+86.0**

By addition of the experimental heats of hydrogenation for ethylene (**2-12a**, $\Delta_{hyd}H$ = -136.3 kJ mol^{-1})[9] to the heat of transfer hydrogenation $\Delta_{trh}H$ the newly corrected $\Delta_{hyd}H$* is obtained, representing the best correlation at G3B3 level of theory (see **Figure 2.5** and **Table 2.5**). The R^2 and RMSE values and the slope of the regression line are similar for direct and transfer hydrogenation, but the intercept as a mark for the accuracy is closer to the origin. Therefore, for all following thermodynamical considerations this approach in combination with the G3B3 values is used:

$$\Delta_{hyd}H^* \text{ (G3B3)} = \Delta_{trh}H \text{ (G3B3)} + \Delta_{hyd}H \text{ (}\mathbf{2\text{-}12a}\text{, exp.)} \qquad \textbf{(eq. 2.1)}$$

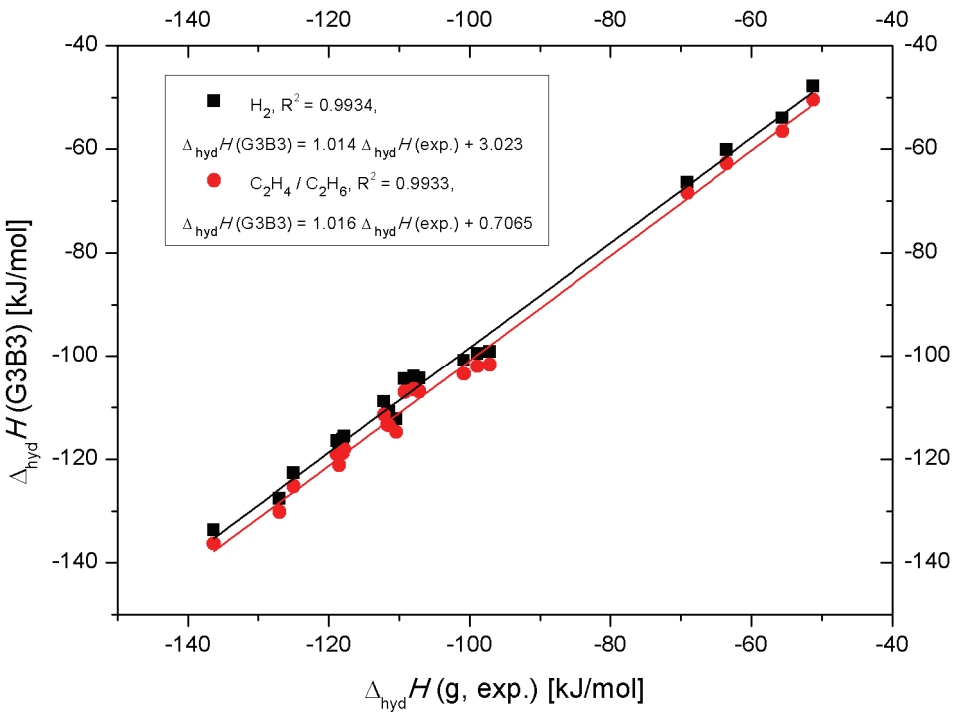

Figure 2.5 Correlation of direct vs. transfer hydrogenation at G3B3 level of theory in the gas phase.

Table 2.5 Calculated corrected hydrogenation enthalpies $\Delta_{hyd}H^*$ of some selected alkenes and carbonyls (at 298.15 K and 1 atm) and experimental values in kJ mol^{-1}.

	MP2(FC)/ 6-311+G(3df,2p	G3(MP2)-RAD	G3B3	$\Delta_{hyd}H$(g, exp.)
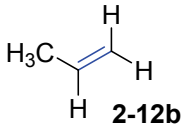 **2-12b**	-123.91	-125.53	-125.24	**-124.98 ± 0.21**[16]
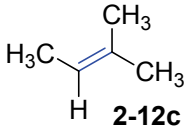 **2-12c**	-110.62	-113.01	-113.33	**-111.63 ± 0.25**[9]
 **2-13a**	-117.01	-119.31	-119.06	**-118.83 ± 0.42**[18]
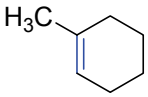 **2-13b**	-111.03	-114.53	-113.50	**-111.40 ± 0.37**[19]
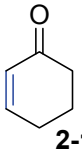 **2-16**	-104.34	-107.81	-107.05	**-109.20 ± 2.9**[21]
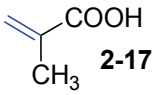 **2-17**	-116.72	-119.62	-118.80	**-118.00 ± 1.3**[22]
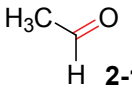 **2-18**	-60.65	-71.25	-68.42	**-69.08 ± 0.42**[23]
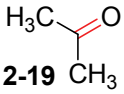 **2-19**	-48.66	-59.85	-56.57	**-55.60 ± 0.42**[24]
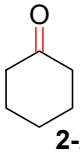 **2-20**	-54.99	-66.31	-62.68	**-63.51 ± 0.63**[23]
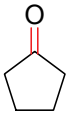 **2-21**	-43.71	-54.12	-50.45	**-51.25 ± 0.63**[23]

2.3 Synthesis of Substrates for Calorimetric Measurements

2.3.1 Determination of Thermochemical Values

In order to match the theoretically calculated values for the heats of formation ($\Delta_f H$) and heats of hydrogenation ($\Delta_{hyd} H$) of nucleobases and nucleotides with experimental values, a series of model compounds has been synthesized and their respective thermochemical values have been measured. In contrast to measure the heats of hydrogenation $\Delta_{hyd} H$ the indirect approach using $\Delta_f H$ does not require the use of any hydrogenation catalyst and, more importantly, allows an accurate characterization of the reaction products. The experimental determination of the molar enthalpy of formation $\Delta_f H$ in the gas phase is quite sensitive to experimental inaccuracies or substrate impurities. Therefore, great attention was paid to the synthesis and purification of the investigated compounds. The thermochemical target value is the standard enthalpy of formation in the gaseous state, which for liquid substrates is defined as:

$$\Delta_f H^0(g) = \Delta_f H^0(l) + \Delta_{vap} H^0 \qquad \textbf{(eq. 2.2)}$$

or for solids

$$\Delta_f H^0(g) = \Delta_f H^0(s) + \Delta_{sub} H^0 \qquad \textbf{(eq. 2.3)}$$

Three principle methods are used and combined to measure standard heats of formation $\Delta_f H^0$ in the liquid or solid state: 1.) determination of the heat of combustion in a bomb calorimeter; 2.) calorimetric measurement of reaction enthalpies; and 3.) identification of equilibrium constants, where the thermochemical properties of the involved species are well-known. Nevertheless, the interpretation of enthalpies in the condensed phase is connected to complications, caused by intermolecular interactions present in all matter. More reliable are values for the gas phase in which ideal behavior of molecules is expected. Enthalpies of vaporization $\Delta_{vap} H$ or sublimation $\Delta_{sub} H$ are defined as the amount of energy needed to convert condensed to gaseous phase. A well-established procedure to obtain $\Delta_{vap} H$ from the temperature dependence of the vapor pressure is the transpiration method.[30]

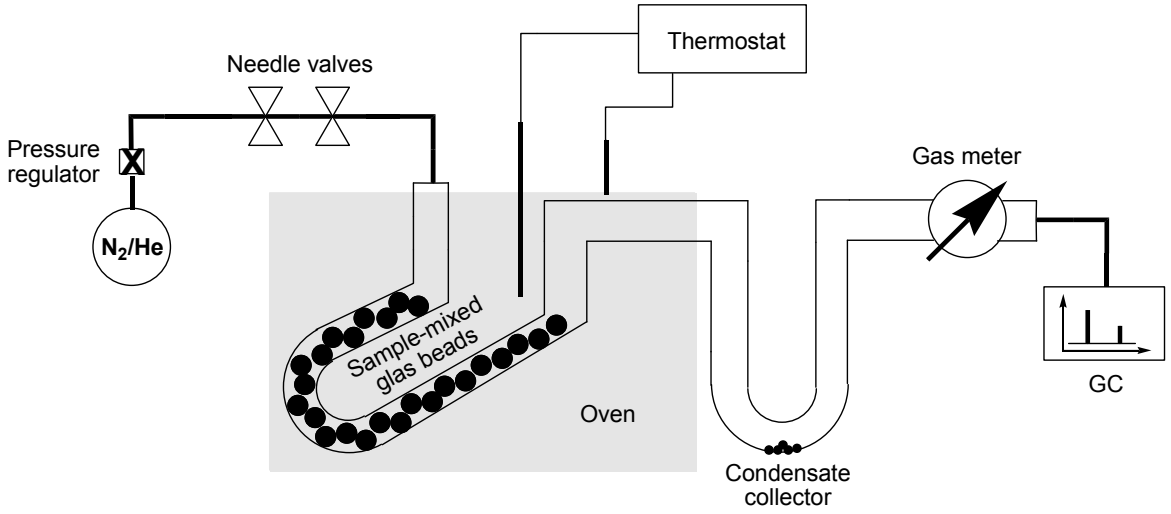

Figure 2.6 Schematical setup for the determination of $\Delta_{vap}H$ via transpiration method.[31]

A schematic overview of the apparatus is shown in **Figure 2.6**. The desired values are obtained by measuring the transference in a saturated inert gas stream applying the *Clausius-Clapeyron* equation. Therefore, the preheated carrier gas is passed through the U-tube with different flow rates to ensure that the gas is in equilibrium with the coexisting liquid phase at each temperature of the study. The saturated vapor pressure p_i^{sat} at each temperature T is calculated from the amount of product found in the condensate collector within a definite period of time. Assuming the validity of *Dalton*'s law of partial pressures and the ideal gas law, p_i^{sat} can be calculated through:

$$p_i^{sat} = m_i \, R \, T \, / \, V \, M_i \, ; \qquad V = V_{TG} + V_i \qquad \textbf{(eq. 2.4)}$$

where m_i is the mass of the transported compound, M_i is its molar mass and V_i its volume contribution to the gaseous phase. The volume of transporting gas V_{TG} is determined from the flow rate and time measurements. The following equation

$$R \ln p_i^{sat} = a + b/T + \Delta_s^g C_p \ln (T/T_0) \qquad \textbf{(eq. 2.5)}$$

is fitted to the experimental p and T data using a and b as adjustable parameters.

Herein, $\Delta_s{}^g C_p$ represents the difference of molar heat capacities of the gaseous and the solid phase and finally, the enthalpy of sublimation at a defined temperature T can be derived according the *Clausius-Clapeyron* equation:

$$\Delta_{sub}H(T) = \text{-b} + \Delta_s{}^g C_p\, T \qquad \textbf{(eq. 2.6)}$$

2.3.2 Modified Uracil and Thymine Models

For the correct numerical assignment of thermodynamic properties of chemical compounds a large quantity of substance is needed in high purity. Attempts to synthesize the required amounts of nucleosides of type **2-31a** or **2-31b** were not successful due to low-yielding reaction steps and purification problems. Therefore, methyl derivatives of pyrimidine bases were considered as promising synthetic targets, since the dihydro derivatives of uracil (**2-32a**) and thymine (**2-32b**) are commercially available.

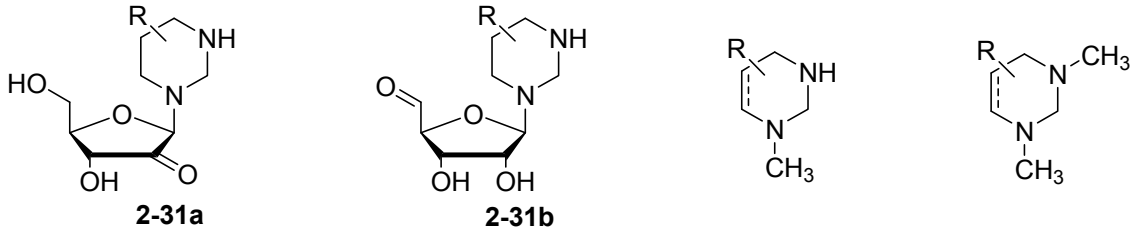

Figure 2.7 Proposed targets for the synthesis of pyrimidine models.

The synthesis of nucleosides involves the coupling of a nucleophilic heterocyclic base and an electrophilic sugar part. The simple alkylation of pyrimdinones is not specific in terms of regioselectivity and multiple substitution. A common and widely used method to introduce pyrimidine-derived bases, like uracil or thymine, is the *Hilbert-Johnson* reaction[32] and the improved silyl variant also known as *Vorbrüggen* procedure.[33] The advantage of the latter is, asides from higher yields and milder reaction conditions, the application of easily available acylated sugars, which are more stable than halo sugars and preserve the requested diastereoselectivity of the anomeric center (see **Scheme 2.5**).

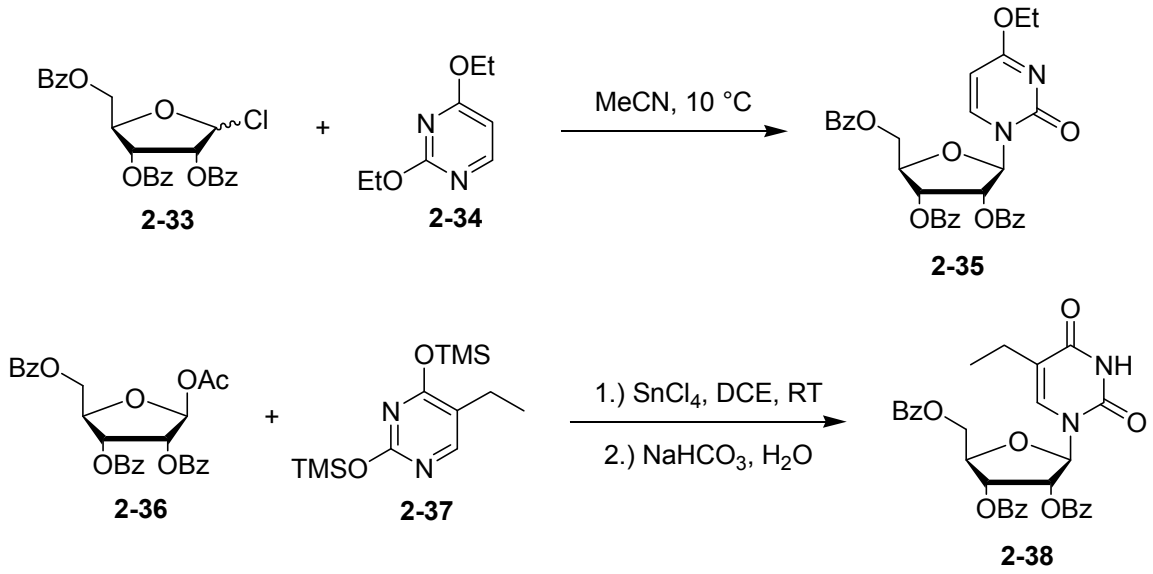

Scheme 2.5 Examples for the *Hilbert-Johnson* reaction (top) and its silyl variant (bottom).

The first *Vorbrüggen* synthesis of 1-methyl uracil (**2-39a**) was achieved by *Micklitz et al.* using a mixture of uracil (**2-32a**), TMSCl, hexamethyldisilazane $(TMS)_2NH$ and methyl iodide.[34] However, regarding the expenses of the used reagents and the moisture sensitivity of TMS-protected pyrimidinones it turned out, that this method is not beneficial for the large-scale synthesis of 1-methyl pyrimidines.

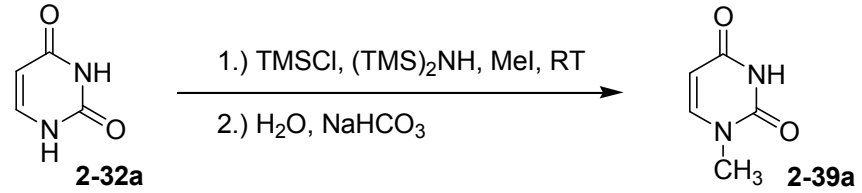

Scheme 2.6 Synthesis of 1-methyl uracil (**2-39a**) according to *Micklitz*.[34]

Another literature-known way to introduce a methyl group is the reductive cleavage of carbamate protecting groups by complex aluminium hydrides.[35] Regioselective *tert*-butoxycarbonyl (Boc) protected uracil (**2-40**) was prepared by DMAP-catalyzed carbamoylation with Boc_2O at room temperature in 42 % yield.[36] The correct regioselectivity was proven by crystal structure determination (see **Scheme 2.7**).

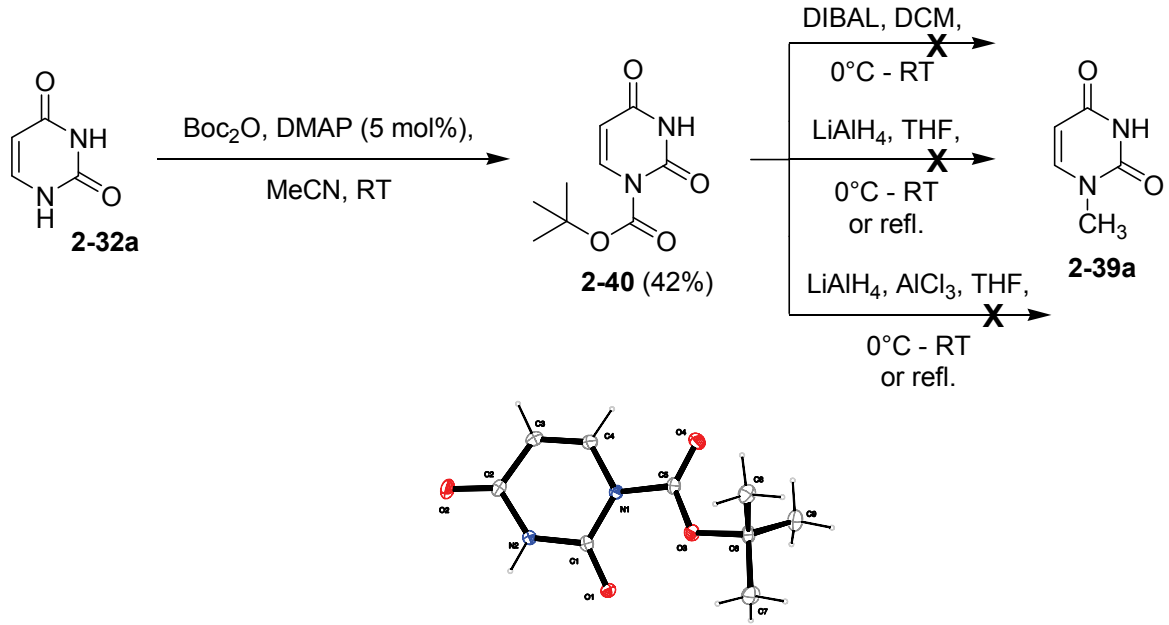

Scheme 2.7 Regioselective carbamoylation of uracil (**2-32a**) and failed reductive cleavage of the Boc group.

Unfortunately, all attempts to reduce the Boc group to a methyl moiety failed. The methyl group was finally introduced using the *Hilbert-Johnson* reaction of electron-rich pyrimidines (see **Scheme 2.8**).[37] The methoxy-substituted pyrimidines **2-42a** and **2-42b** were available from the natural bases uracil (**2-32a**) and thymine (**2-32b**) via chlorination[38] and subsequent nucleophilic aromatic substitution.

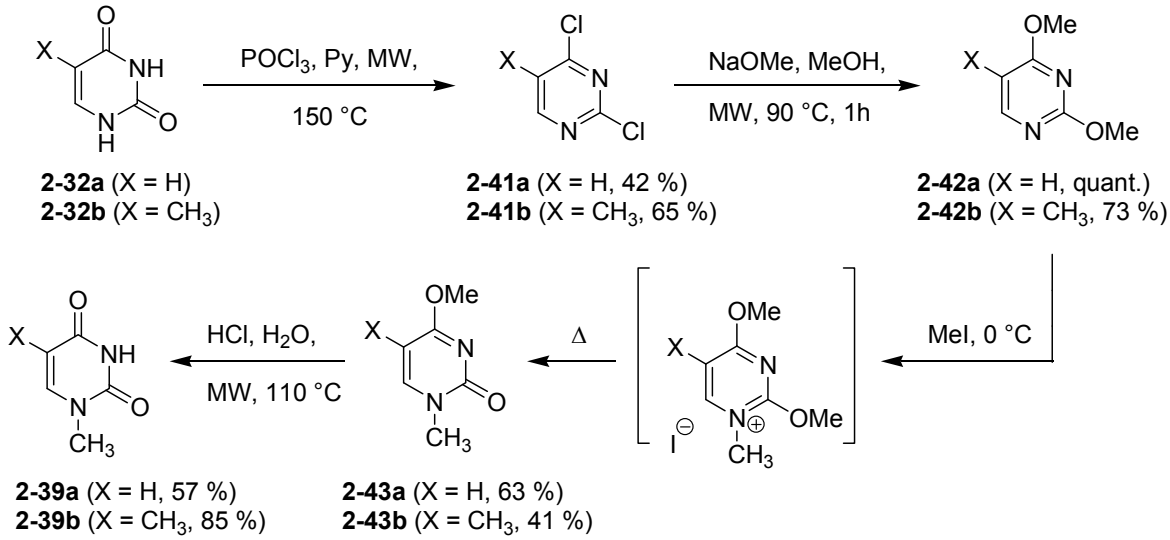

Scheme 2.8 *Hilbert-Johnson* reaction to give 1-methyl pyrimidines.

Microwave heating under closed-vessel conditions led to improved yields for the substititution reaction and at least a 2-fold reduction of reaction time compared to conventional heating. Transformation to the methyl pyrimidinium salt was smoothly accomplished over night characterized by the formation of yellowish crystals, which give the related 4-methoxy pyrimidones **2-43a** and **2-43b** in good yields on heating. The last step involved simple ether cleavage by acidic hydrolysis. The two nitrogen centers in pyrimidine **2-44b** possess different Lewis basicity and react preferably at N1-position, as indicated by the high methyl cation affinity (MCA)[39] of +552.4 kJ mol^{-1}, in contrast to +497.3 kJ mol^{-1} for N3 (**Scheme 2.9**). Suitable crystals for X-ray analysis were obtained by the reaction of methyliodide with diethoxy pyrimidine **2-44b** at 0 °C, thus confirming the theoretically MCA calculated values.[40]

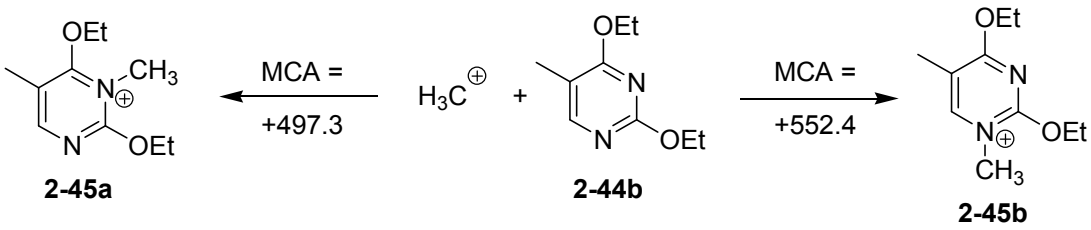

Scheme 2.9 Methyl cation affinities obtained at MP2(FC)/6-31+G(2d,p)//B98/6-31G(d) level (*Boltzmann*-averaged, in kJ mol^{-1}).

The dihydro compounds of 1-methyl uracil (**2-39a**) or thymine (**2-39b**) were synthesized in quantitative yield by simple low-pressure hydrogenation over heterogenous transition metals in absolute ethanol.

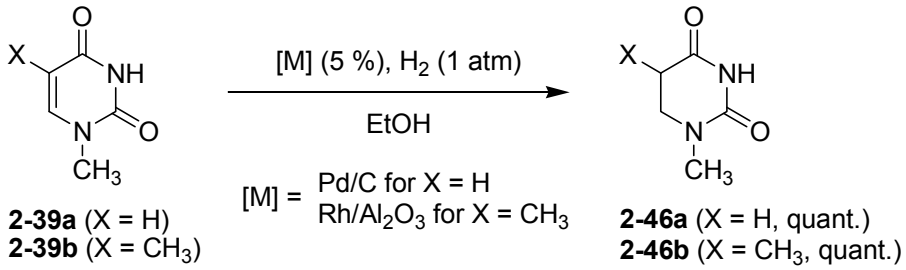

Scheme 2.10 Synthesis of 1-methyl dihydropyrimidines **2-46a** and **2-46b**.

Since the largest effort and also the largest errors are connected to the determination of the heats of sublimation $\Delta_{sub}H$, minimization of the latter is highly desirable. In order to break the strong three-dimensional framework in the solid, the *N*-methylated

derivatives of thymine und uracil together with their dihydro isomers have been synthesized. *N,N'*-dimethyl pyrimidines are simply prepared by nucleophilic substitution in basic media with excess dimethyl sulfate $(CH_3O)_2SO_2$ as methylating agent.

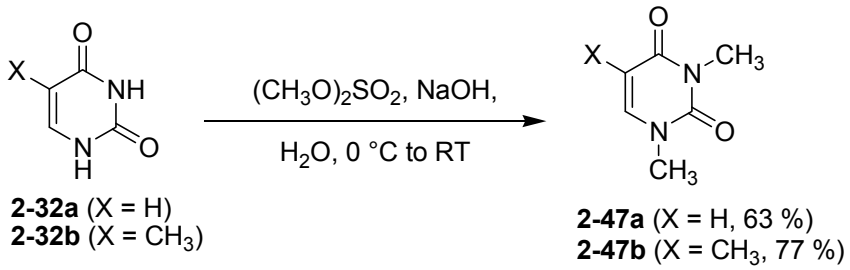

Scheme 2.11 Synthesis of *N,N'*-dimethyl pyrimidines **1-47a** and **1-47b**.

Besides the simple reduction of **2-47a** or **2-47b** with H_2, 5,6-dihydrouracils can be synthesized following a procedure published by *Lee* and *Shim* involving the fast tandem Michael addition/condensation of acrylic acids and substituted ureas.[41] By varying the substitution pattern of either urea or acrylic acid, a multitude of differently functionalized dihydropyrimidines is accessible.

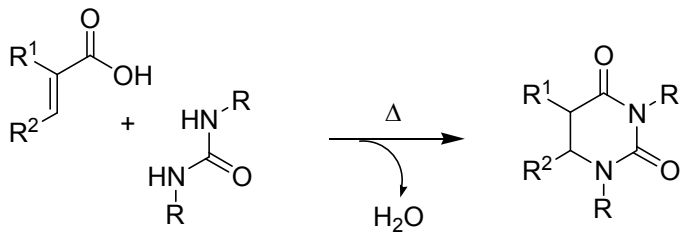

Scheme 2.12 Dihydro pyrimidine synthesis according to *Lee* and *Shim*.

No additional solvent is needed as most of the acrylic acids are liquids, but high-pressure conditions are needed to induce the reaction. The synthesis and purification was optimized using microwave heating under closed-tube conditions. Impurities of polymeric acrylates were removed by silica gel filtration followed by repeated distillation and precipitation steps. The low yields are mainly the result of the purification methods and incidental polymerization.

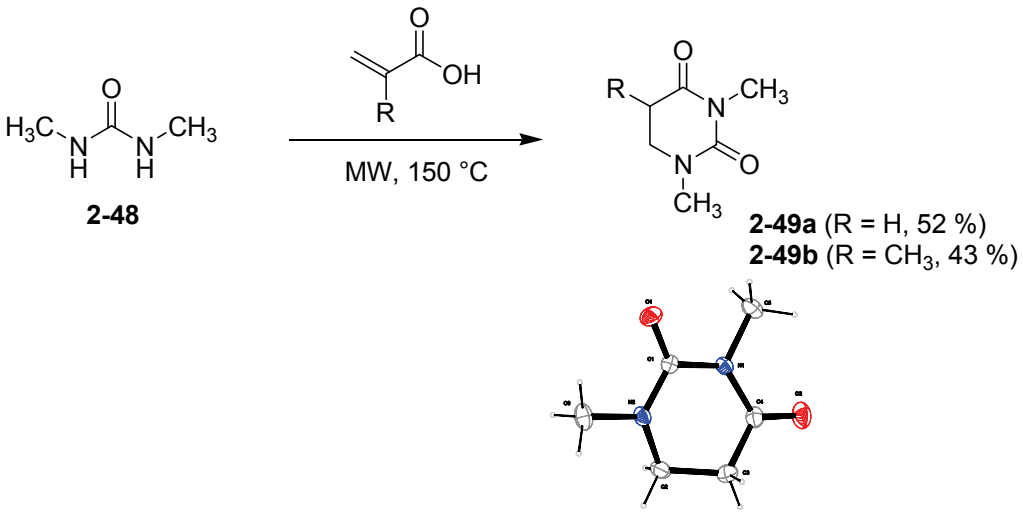

Scheme 2.13 Synthesis of dimethylated dihydropyrimidines **2-49a** and **2-49b**, together with the ORTEP plot of **2-49a**.

Indeed, the yield for **2-49b** was almost doubled by the usage of synthesis microwave machines from 25 % (conventional heating in a stainless steel tube, 190 °C, 2 h)[41] to 43 % (microwave glass vial, 150 °C, 1 h). Similarily, the yield for the dihydro derivative of dimethyl uracil **2-49a** was also increased from 27 % (Pyrex pressure tube, 190 °C, 2 h) to 52 % (microwave glass vial, 150 °C, 2 h).

2.3.3 Modified Cytosine Models

Inspired by the work by *Leonard* and *Hosmane*[42] the synthesis of 1-methyl cytosine (**2-50a**) was accomplished in a two-step procedure displayed in **Scheme 2.14**.

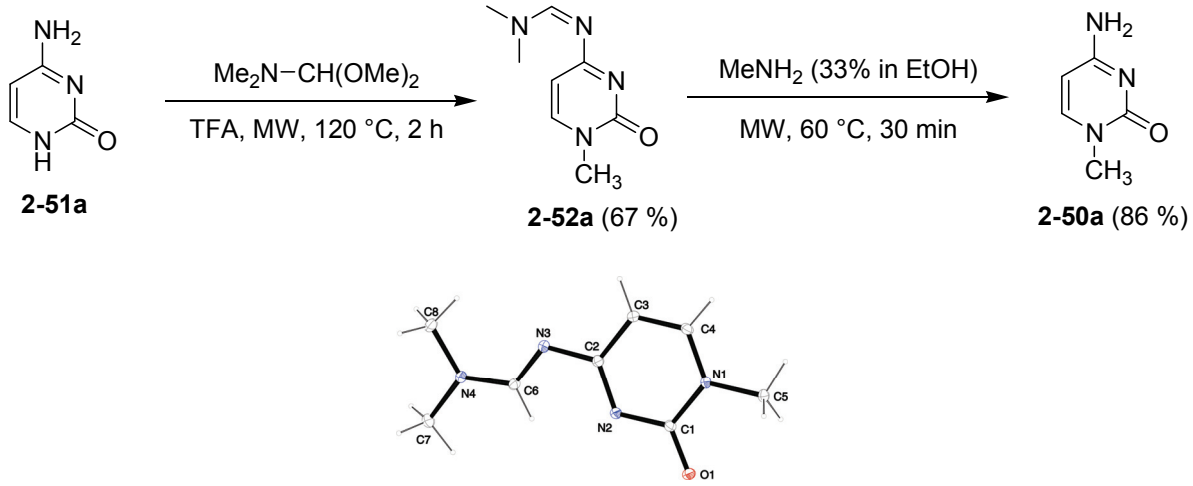

Scheme 2.14 Modified synthesis of 1-methylcytosine according to *Leonard* and *Hosmane*.[42]

The applied microwave heating reduced the reaction times for the synthesis of **2-52a** from published 15 to 2 hours.[42] Replacing ammonium hydroxide NH_4^+ OH^- with ethanolic methylamine in the deprotection step simplified the purification very effectively. No time-consuming removal of ammonia and water was needed and the product isolation is simply accomplished by filtration and repeated recrystallization. In 1995, the *Golankiewicz* group published a novel route for the synthesis of 1-substituted cytosines, including 1,5-dimethylcytosine (**2-50b**).[43] Unfortunately, their synthesis starts from 1-methylthymine (**2-39b**), whose extensive synthesis via *Hilbert-Johnson*-alkylation was already described in the previous chapter (**Scheme 2.15**).

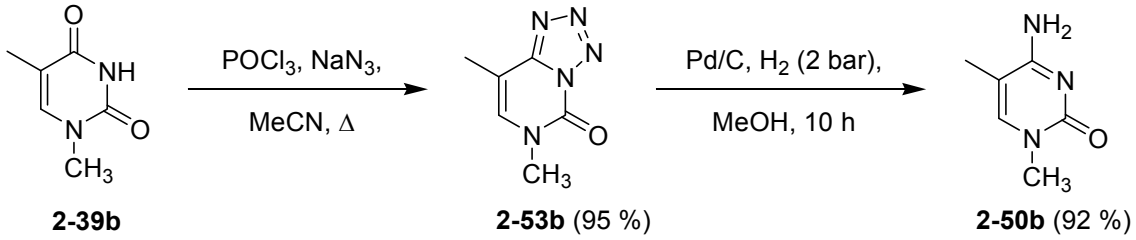

Scheme 2.15 1,5-Dimethylcytosine (**2-50b**) synthesis according to *Golankiewicz*.[43]

The isolation of pure nitrogen-rich compounds in substance can be quite dangerous and the formation of HN_3 under the reaction conditions represents another potential hazard. Therefore, the synthesis of **2-50b** was attempted by simple nucleophilic aromatic substitution of **2-54b** by methanolic ammonia solution under high-pressure microwave conditions to save three reaction steps.

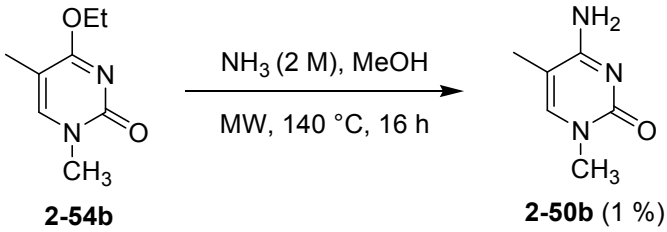

Scheme 2.16 Microwave-assisted synthesis of 1,5-dimethylcytosine (**2-50b**).

Mainly unreacted starting material **2-54b** and only traces of desired product could be isolated. The synthesis of gram-quantities of highly pure 5,6-dihydrocytosines was more difficult than expected due to their high acid sentivity. It is commonly known,

that in catalytical hydrogenations over Pd/C, cytosine is often partly hydrogenated to 5,6-dihydrocytosine (**2-55**) which is then readily hydrolyzed to the dihydrouracil derivative.[8, 44] The number of articles describing the chemospecific synthesis and isolation of dihydrocytosines is very limited and mainly consists of Brønstedt base-induced cyclizations of urea derivatives of type **2-56**[45] or the aminolysis of 4-thio-5,6-dihydrouracils (**2-57**) in liquid ammonia.[46]

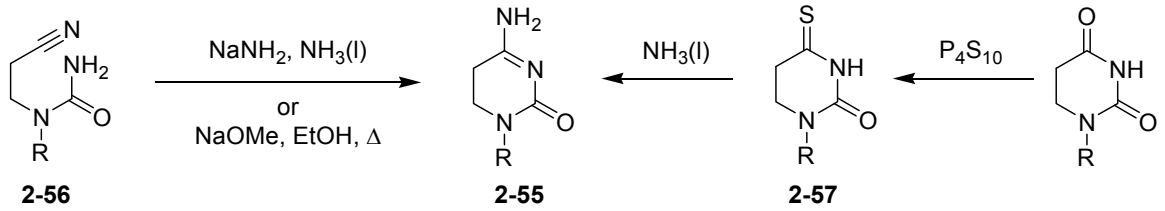

Scheme 2.17 Literature known syntheses for 5,6-dihydrocytosines.

In order to avoid handling and exposure to hazardous phosphorous pentasulfide and its byproducts, the cyclization route was envisaged as the only alternative. The appropriate urea compounds were synthesized from commercially available secondary amine **2-58a** and *in situ* generated aqueous isocyanic acid in 60 % yield. Slow evaporation of an ethanolic solution of urea **2-59b** gave crystals suitable for X-ray analysis with four crystallographically independent urea molecules in the triclinic cell. The cyclization was performed according to *Cheng et al.*[45b] using sodium methoxide in refluxing absolute ethanol. Conventional heating was crucial for successful synthesis of dihydrocytosine **2-55a**. All attempts to optimize the reaction by means of temperature variation, increased pressure or reaction time using microwave irradiation failed and only inseparable mixtures of byproducts were formed.

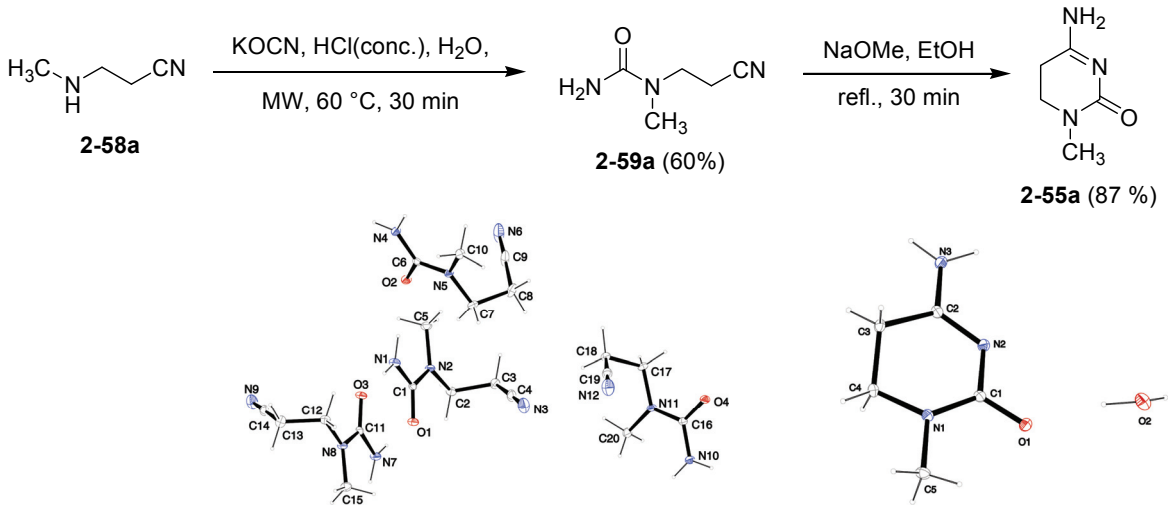

Scheme 2.18 Modified synthesis of 1-methyl-5,6-dihydrocytosine (**2-55a**) according to *Cheng et al.*[45b] and ORTEP plots of urea **2-59a** and 1-methyl-5,6-dihydrocytosine (**2-55a**)•hemihydrate.

Nevertheless, *N*-methylated dihydrocytosine (**2-55a**) was obtained in good yield (87 %) and structural properties were proven by X-ray structure determination from crystals grown from ethanol at -10 °C. Closer inspection of ^{1}H NMR spectra in DMSO-d_6 (**Figure 2.9**) revealed, that with increased water content the fast rotation of the amino group is retarded (**Figure 2.9**), resulting in the appearance of two broad singlets around 7.5 ppm.

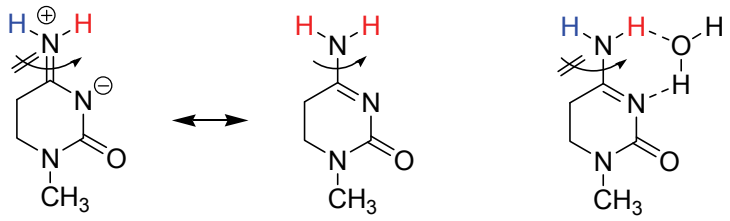

Figure 2.8 Decreased rate of rotation of the amino group in **2-55a** upon coordination with water resulting in two NMR-distinguishable amino protons.

In addition, the rotation barrier around the C-NH_2 bond has been determined spectroscopically by analyzing temperature-dependent ^{1}H NMR spectra (**Figure 2.10**). The relative population of the intramolecular motion as a result of the temperature-dependent equilibrium and the conclusive rate constant k is defined by the *Eyring* equation:

$$k = (R\,T/N_A\,h)\,\exp(-\Delta G^{\ddagger}/R\,T) \qquad \textbf{(eq. 2.7)}$$

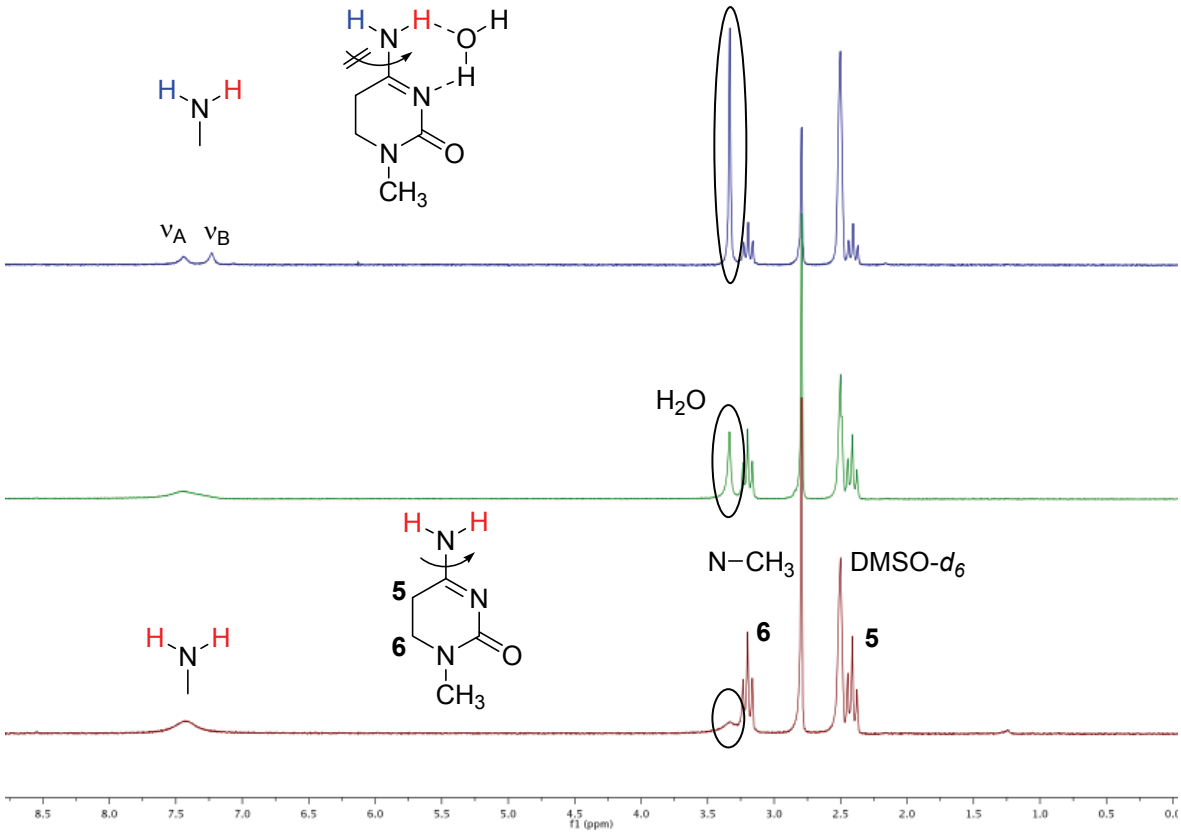

Figure 2.9 ^{1}H NMR (200 MHz) of 1-methyl-5,6-dihydrocytosine (**2-55a**) in DMSO-d_6 with different water content.

The coalescence temperature T_c, at which the rotation barrier is overcome and the two signals merge into one is connected to the rate constant k_c by the following relation:

$$\pi/\sqrt{2}\ |\nu_A - \nu_B| = (R\,T_c/N_A\,h)\exp(-\Delta G^{\ddagger}/R\,T_C) \qquad \textbf{(eq. 2.8)}$$

where ν_A and ν_B are the chemical shifts of the respective amino protons. If T_c is measured in K and the shifts ν in Hz, the free energy of activation $\Delta G^{\ddagger}$ is given in kJ mol^{-1} by

$$\Delta G^{\ddagger} = 19.1\ 10^{-3}\ T_c\ (9.97 + \log T_c - \log |\nu_A - \nu_B|) \qquad \textbf{(eq. 2.9)}$$

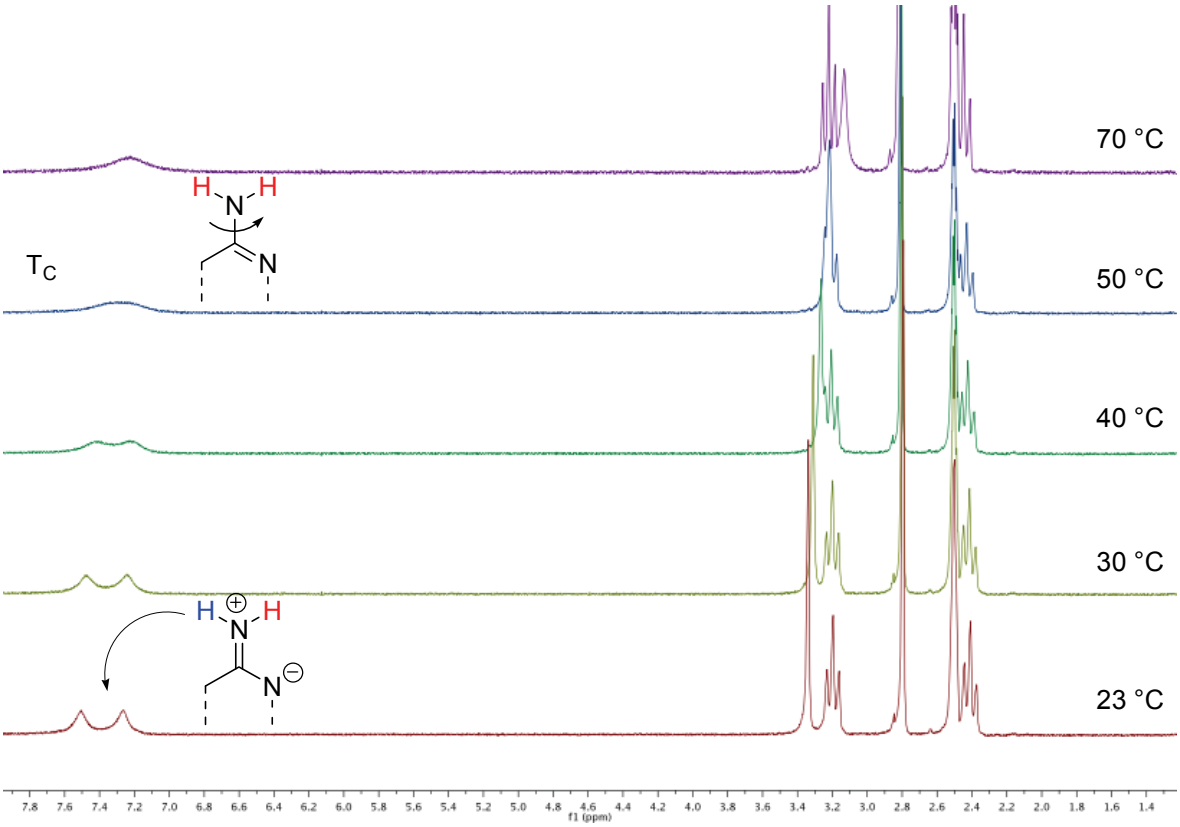

Figure 2.10 Temperature-dependent ^{1}H NMR (200 MHz, DMSO-d_6) of dihydrocytosine **2-55a** to determine its coalescence temperature T_c.

Table 2.6 Activation free energy ΔG‡ for the intramolecular rotation of the amino group in **2-55a** in DMSO together with literature data for related systems.

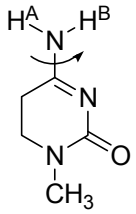

δ(NH^A) [ppm]	δ(NH^B) [ppm]	Δν [Hz][a]	k_c [s^{-1}]	T_c [K]	ΔG‡[kJ mol^{-1}]
7.51	7.26	50	111	323.15 ± 3 K	**+66.54 ± 0.64**
	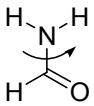 **2-60a**	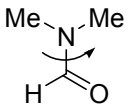 **2-60b**	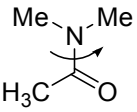 **2-60c**	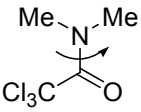 **2-61**	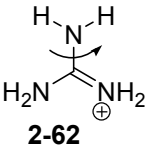 **2-62**
ΔG‡[kJ mol^{-1}]	+76.1[47] in H_2O	+92.0[47] in H_2O	+79.1[47] in H_2O	+62.8[48] neat	+54.4[49] nematic solution

[a] ^{1}H NMR (200 MHz, DMSO-d_6).

The coalescence is reached at approximately 50 °C (**Figure 2.10**) leading to a barrier of +66.5 kJ mol^{-1}. Assuming a spectra- and temperature sensor-specific deviation of 3 °C during this kinetic study, an error of ±0.6 kJ mol^{-1} should be included to the free activation energy. Comparison with literature-known rotation barriers (see **Table 2.6**) for model systems like DMF (**2-60b**) or *N*,*N*-dimethyl acetamide (**2-60c**) indicates that the rotation barrier for **2-55a** is in between that for trichloro acetamide (**2-61**) and the guanidinium cation (**2-62**). The ring structure of dihydro compound **2-55a** can therefore be classified as weak acceptor. Unfortunatelly, from this study no statement on the influence of the water content on the internal rotation can be made.

The reported synthesis of dihydrocytosine can also be extended to the formation of 5-methyl-5,6-dihydrocytosine **2-55b**.[40] The respective racemic urea **2-59b** was simply synthesized by *Michael* addition of methylamine to acrylonitrile (**2-63**) at ambient temperature, followed by addition to isocyanic acid. In contrast to the parent dihydrocytosine **2-55a**, the 5-methyl derivative **2-55b** can be synthesized in the microwave in modest yield (see **Scheme 2.19**).

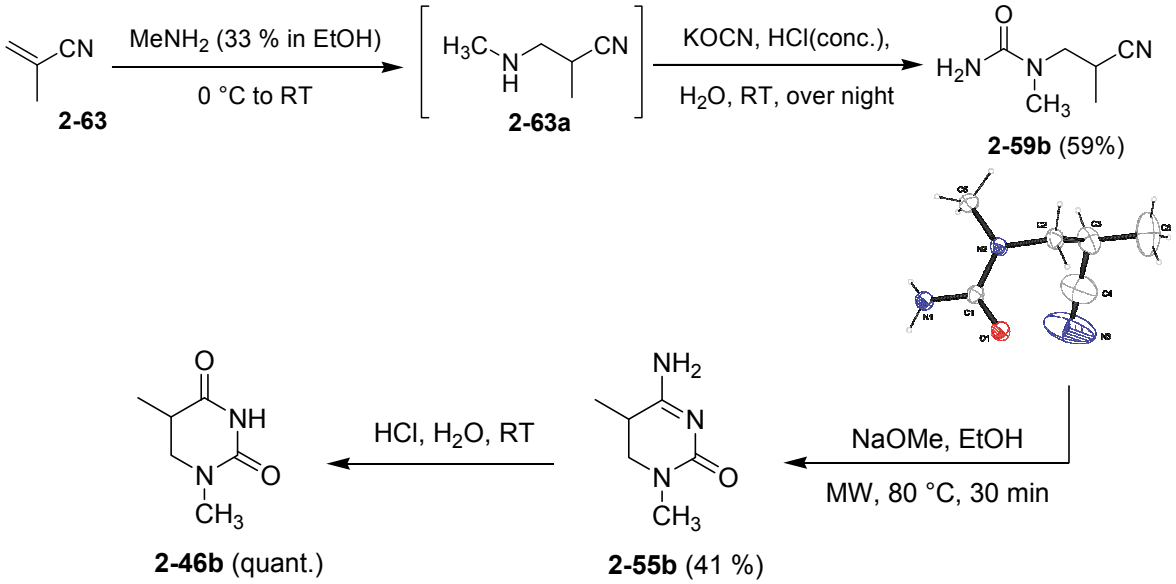

Scheme 2.19 Synthesis of 5-methyl dihydrocytosine **2-55b**.

Increased stability of **2-55b** against hydrolysis in acidic media by attaching a methyl group was not observed. Overall the synthesized dihydrocytosine derivates represent relatively instable, hydrolysable compounds, which should be stored under dry and oxygen-free conditions.

In conclusion, three *N*-methylated pyrimidine pairs of each pyrimidine nucleobase, respectively, were synthesized in high amount and purity and their heats of formation in the gas phase $\Delta_f H^0$(g) were experimentally determined via bomb calorimetry together with the commercially available nucleobases uracil (**2-32a**) and thymine (**2-32b**) and their dihydro derivatives. These measurements were performed in collaboration with the group of *Prof. Dr. Sergey Verevkin* at the university of Rostock. The results are displayed in **Table 2.7**. For unknown reasons, the heat of formation $\Delta_f H^0$(g) of dihydrocytosine **2-55a** could not be determined accurately due to incomplete combustion to H_2O, CO_2 and NH_3. An unknown residue remained in the combustion chamber that was not detected by elemental analysis. Purification by reversed-phase silica (RP-18) using a mixture of acetone and methanol (15:1) led to hydrolysis of **2-55a** to 1-methylated dihydrouracil (**2-46a**) in a ratio of 1:3 (**2-55a**:**2-46a**) determined by ^{1}H NMR spectroscopy. A short-term amino-protection strategy using the benzyloxycarbamate (CBz) group to mask the reactivity against hydrolysis to facilitate purification failed. After silica gel chromatography an inseparable mixture of CBz-protected **2-64a** and **2-46a** in the ratio 1:1 was obtained.

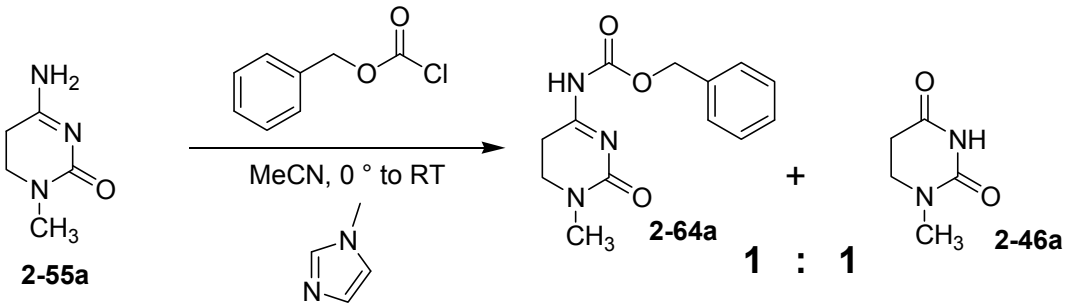

Scheme 2.20 Failed synthesis of CBz-protected **2-64a**.

Table 2.7 Thermochemical data obtained in this work at 298.15 K and 1 atm.

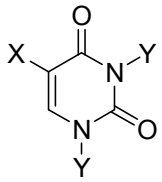	$\Delta_c H^0$ (s)	$\Delta_f H^0$ (s)	$\Delta_{sup} H^0$	$\Delta_f H^0$ (g)
X = H, Y = H (**2-32a**)	-1715.2±1.0	-430.5±1.1	+131.9±0.7	**-298.6±1.3** -292.5±2.6[50]
X = CH_3, Y = H (**2-32b**)	-2359.3±1.0	-465.7±1.2	126.3±1.2	**-339.4±1.7** -327.5±1.6[51]
X = H, Y = CH_3 (**2-47a**)	-3088.5±1.8	-415.9±2.0	95.6±0.6	**-320.3±2.1** -314.9±1.5[52]
X = CH_3, Y = CH_3 (**2-47b**)	-3735.9±1.5	-447.9±1.8	95.1±0.6	**-352.8±1.9**
X = H, Y = CH_3, O→NH_2 (**2-50a**)	-2749.1±2.9	-218.8±3.0	142.8±1.3	**-76.0±3.3**
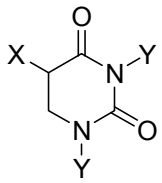	$\Delta_c H^0$ (s)	$\Delta_f H^0$ (s)	$\Delta_{sup} H^0$	$\Delta_f H^0$ (g)
X = H, Y = H (**2-65a**)	-1936.7±1.4	-494.9±1.5	114.8±1.7	**-380.1±2.3** -378.2±2.1[53]
X = CH_3, Y = H (**2-65b**)	-2585.3±1.4	-525.6±1.5	118.6±0.6	**-407.0±1.6**
X = H, Y = CH_3 (**2-49a**)	-3314.9±1.2	-475.3±1.4	87.4±0.7	**-387.9±1.6**
X = CH_3, Y = CH_3 (**2-49b**)	-3966.9±2.5	-502.6±2.7	83.4±1.0	**-419.2±2.9**
X = H, Y = CH_3, O→NH_2 (**2-55a**)	n/a	n/a	n/a	n/a

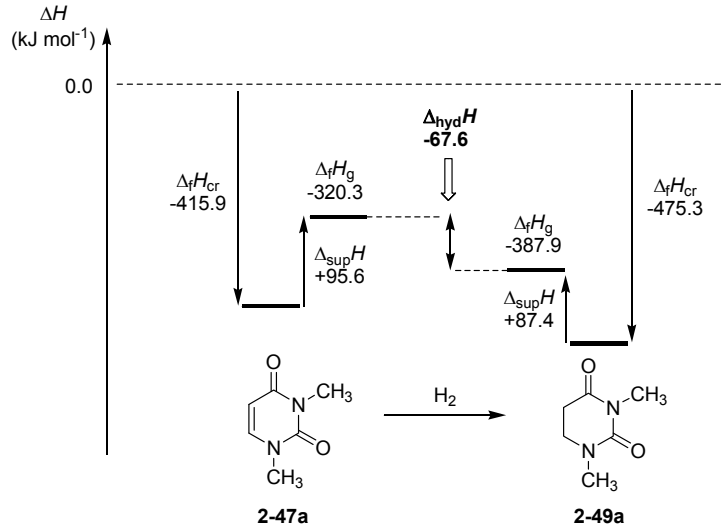

Figure 2.11 Schematic representation of energies required for the determination of $\Delta_{hyd}H$ of dimethyl uracil (**2-47a**).

2.3.4 Modified Sugar Models

The number of heats of hydrogenation $\Delta_{hyd}H$ for carbonyl compounds is, compared to those for alkenes or alkynes, comparatively small and even the specific standard heats of formation $\Delta_f H^0(g)$ are very limited. For instance, available thermochemical data of polyols is mainly restricted to simple systems like glycol, glycerine or 1,2-diols in their standard state, usually liquids at room temperature. No gas phase values for α-hydroxy ketones are available.

The most simple RNA-related substrate acting as H_2 donor is the commercially available 1,4-anhydroerithritol (**2-66**) and its oxidized α-hydroxy keto derivative **2-67a**.

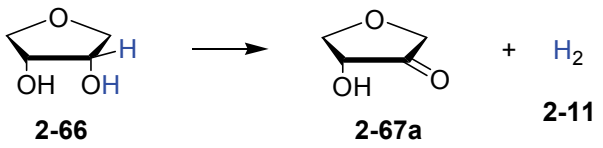

Scheme 2.21 1,4-Anhydroerithritol (**2-66**) and its dehydrogenated keto form **2-67a**.

Attempts to synthesize **2-67a** in one step via standard oxidation using chromium in high oxidation states failed and only decomposition was observed.

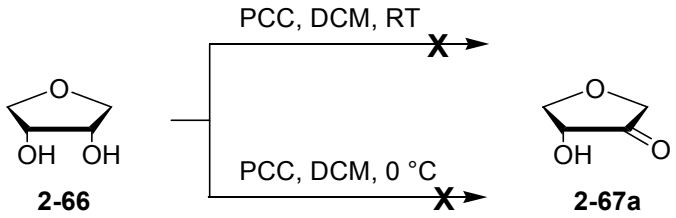

Scheme 2.22 Attempted synthesis of **2-67a** via Cr(VI)-oxidation.

Using a two-step synthesis including selective mono-protection of the hydroxyl functionality by an acetyl group, followed by Cr(VI)-oxidation yielded tetrahydrofuranone **2-69a** in modest yield.[54] Mono-acetylation was achieved using the triethyl ortho acetate and catalytic amounts of trifluoro acetic acid in refluxing THF. With the aid of microwave heating the yield could be increased to 89 % and accelerated to be finished after 15 minutes compared to 48 h with conventional oil bath heating.[54] The hydroxyl group was oxidized using pyridinium chlorochromate

(PCC) in DCM using celite as absorbant for the precipitating polymeric chromium oxides.

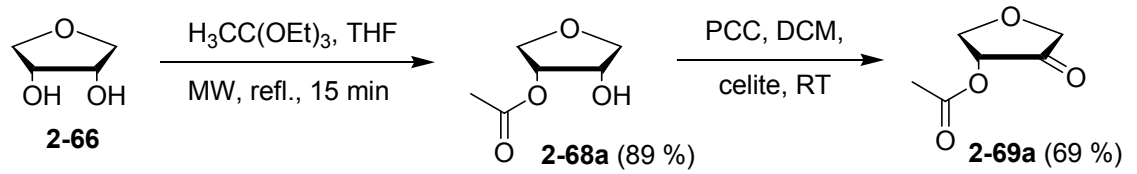

Scheme 2.23 Synthesis of acetoxy-protected tetrahydrofuranone **2-69** according to *Buechi* and coworkers.[54]

Nevertheless, several attempts to achieve deprotection of **2-69a** under basic conditions resulted either in decomposition or unsuccessful isolation after work-up due to the good solubility of acyloin **2-67a** in water.

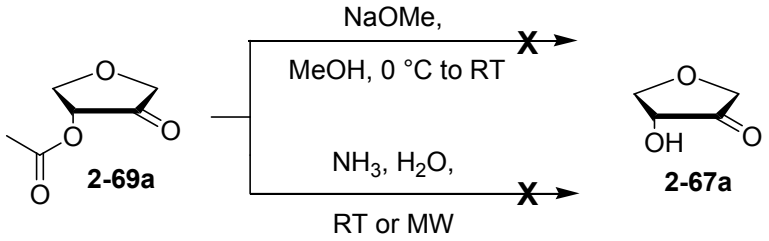

Scheme 2.24 Failed synthesis of α-hydroxy ketone **2-67a**.

Replacement of the acetyl by a benzyl group led to no improvement. The mono-benzylation was accomplished using 1.1 equivalents of benzyl bromide and NaH in refluxing THF under microwave irradiation. The *Buechi* conditions (PCC, DCM, celite, RT) gave rise to ether cleavage and benzaldehyde was isolated as main product.

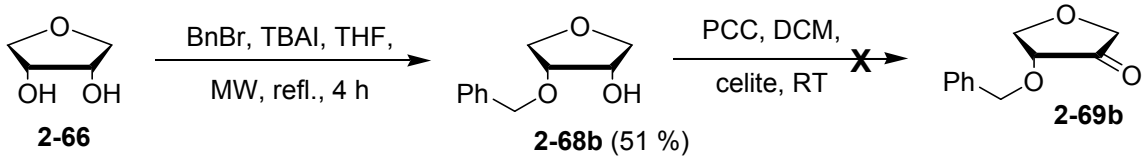

Scheme 2.25 Benzylation of **2-66** and subsequent PCC-oxidation.

A one-step synthesis of **2-67a** inspired by the well-known acyloin condensation using sodium metal, the ethyl ester of diglycolic acid **2-70** and TMSCl as anion scavenger brought no success. This may indicate that stepwise one-electron reduction of the

carbonyl group in **2-70** gives rise to ketyl radical **2-71** which can easily be cleaved in α-position to give ethyl acetate and ethyl glycolate (**2-72**).

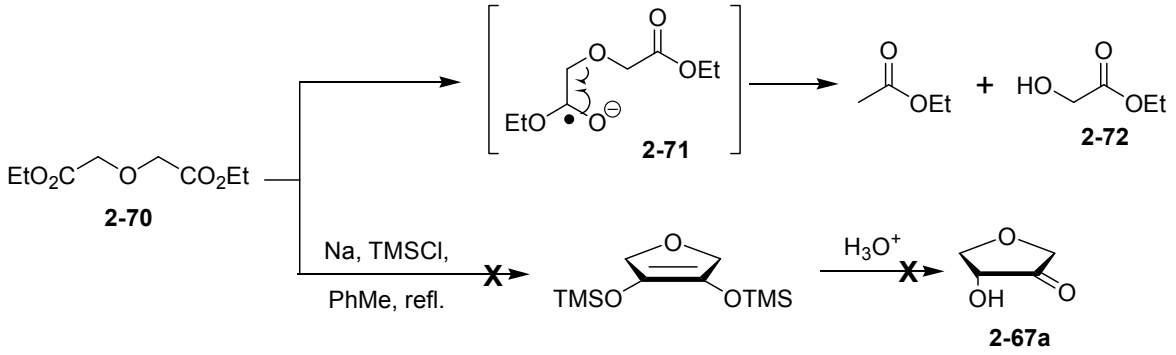

Scheme 2.26 Failed acyloin condensation of ethyl ester **2-70**.

Synthesis of the desired sugar compound **2-67a** could thus not be achieved in the required purity and amount. This can have the effect that syntheses of the even more complex models like **2-73** or **2-74a** is not likely to be completed successfully since they are not commercially available and require long expensive reaction steps (**Scheme 2.27**).

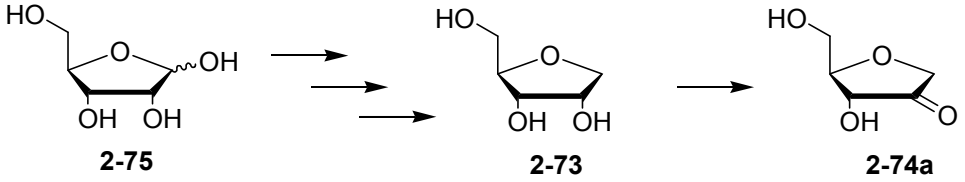

Scheme 2.27 Proposed synthesis of **2-73** and **2-74a** based on D-ribose (**2-75**).

2.4 Experimental vs. Theoretical Heats of Hydrogenation

2.4.1 Thermochemistry of Nucleobases

The heats of hydrogenation $\Delta_{hyd}H^*$ at G3B3 level together with the experimentally obtained values from **Chapter 2.3.3** are summarized in **Table 2.8**.

Table 2.8 Heats of hydrogenation $\Delta_{hyd}H$ of pyridine nucleobases and alkene models at G3B3 level of theory in kJ mol^{-1} (at 298.15 K and 1 atm, only the starting materials are shown).

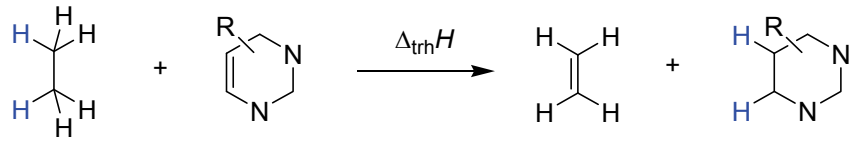

2-29a **2-12a**

	$\Delta_{trh}H$(calc.)[a]	$\Delta_{hyd}H$*(calc.)[b]	$\Delta_{hyd}H$(exp.)
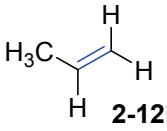 **2-12b**	+11.06	-125.24	**-125.0±0.2**[16] -123.8[c]
 **2-13a**	+17.24	-119.06	**-118.8±0.4**[18] -118.4[c]
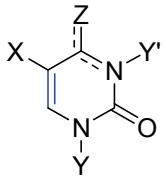	$\Delta_{trh}H$(calc.)[a]	$\Delta_{hyd}H$*(calc.)[b]	$\Delta_{hyd}H$(exp.)
X = H, Y, Y' = H, Z = O (**2-32a**)	+58.19	-78.11	**-81.5±2.6**[c] -75.7±3.0[53]
X = H, Y = CH_3, Z = O (**2-39a**)	+58.47	-77.83	n/a
X = H, Y, Y' = CH_3, Z = O (**2-47a**)	+63.96	-72.34	**-67.6±2.6**[c]
X = CH_3, Y = H, Z = O (**2-32b**)	+66.09	-70.51	**-67.6±2.3**[c]
X = CH_3, Y = CH_3, Z = O (**2-39b**)	+66.66	-69.64	n/a
X = CH_3, Y, Y' = CH_3, Z = O (**2-47b**)	+70.65	-65.65	**-66.4±3.5**[c]
X = F, Y = CH_3, Z = O (**2-39c**)	+48.01	-88.29	n/a
X = H, Y = H, Z = NH_2 (**2-76**)	+81.62	-54.68	n/a
X = H, Y = CH_3, Z = NH_2 (**2-50a**)	+86.99	-49.31	n/a
X = CH_3, Y = CH_3, Z = NH_2 (**2-50b**)	+91.28	-45.02	n/a
X = F, Y = CH_3, Z = NH_2 (**2-50c**)	+67.74	-68.58	n/a

[a] Defined as $\Delta_{trh}H = \Delta_fH(C_2H_4) + \Delta_fH(RCH_2\text{-}CH_2R) - \Delta_fH(RHC{=}CHR) - \Delta_fH(C_2H_6)$. [b] Addition of the reaction enthalpies $\Delta_{trh}H$ to the experimentally determined hydrogenation enthalpy of ethylene $\Delta_{hyd}H$ (C_2H_4, **2-12a**) = -136.3±0.2 kJ mol^{-1} yields the hydrogenation enthalpy $\Delta_{hyd}H$* of the respective double bond. [c] Calculated using heats of formation Δ_fH.[15]

As is readily seen in **Table 2.8** the most easily reduced naturally occuring base is uracil (**2-32a**) with an experimental heat of hydrogenation $\Delta_{hyd}H$(exp.) of -81.5 kJ mol^{-1} and a G3B3 value of -78.1 kJ mol^{-1}. This value is hardly affected by

alkylation at the N1 position as illustrated by the value for 1-methyluracil (**2-39a**) of $\Delta_{hyd}H$(**2-39a**) = -77.8 kJ mol^{-1}. Introduction of a second methyl group at N3 position in **2-47a** leads to $\Delta_{hyd}H$(**2-47a**) = -72.3 kJ mol^{-1} and thus to a more significant change.

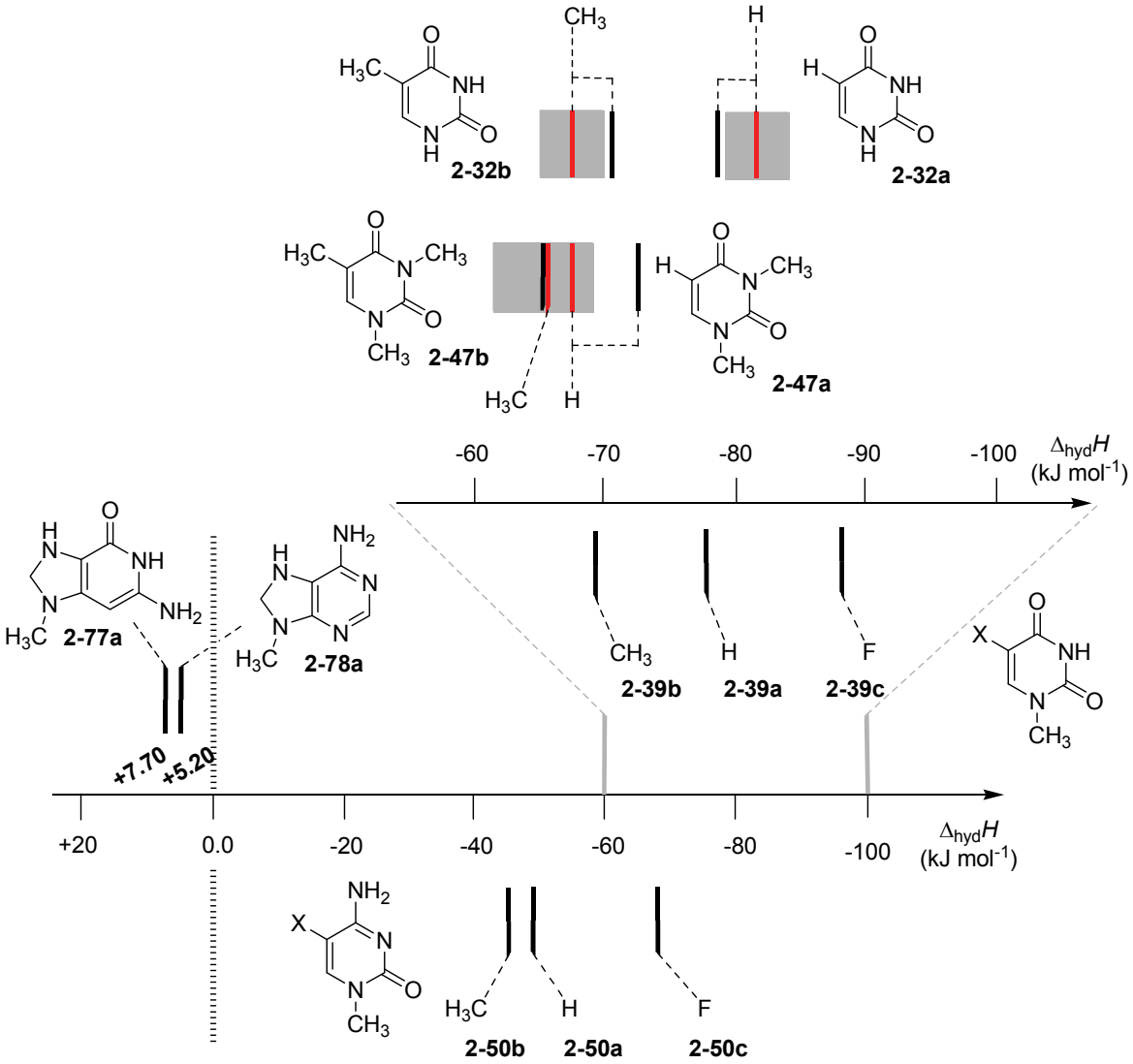

Figure 2.12 Heats of hydrogenation $\Delta_{hyd}H$ of nucleobases at G3B3 level of theory at 298.15 K. Experimental hydrogenation enthalpies (red lines) are shown together with their standard deviations as gray bars.

This effect is almost identical to the introduction of a methyl group in C5 position of thymine (**2-32b**) which reduces the hydrogenation enthalpy by 7 kJ mol^{-1} ($\Delta_{hyd}H$(**2-32b**) = -70.5 kJ mol^{-1}). Alkylation of the N1 and N3 position in thymine again reduces the enthalpy by a small margin to $\Delta_{hyd}H$ = -65.7 kJ mol^{-1} in **2-47b**. A similar reduction of hydrogenation enthalpies occurs on moving to more highly substituted

systems like ethylene (**2-12a**)/propene (**2-12b**) or cyclohexene (**2-13a**)/1-methylcylohexene (**2-13b**) and can thus be considered to be a general phenomenon (see **Chapter 2.2**). Exchange of the methyl group in 1-methyl thymine (**2-39b**) by a fluoro substituent increases the driving force for the reduction of the C-C double bond by *ca.* 19 kJ mol^{-1} ($\Delta_{hyd}H$(**2-39c**) = -88.3 kJ mol^{-1}). The enhanced driving force is more a result of large electronegativity differences than steric hindrance. Compared to the parent uracil derivate **2-39a** the reaction enthalpy of **2-39c** is around 10 kJ mol^{-1} more exothermic. 5-Fluoro-5,6-dihydrouracil (**2-65c**) is a metabolite of the widely prescribed cytostatic drug 5-fluorouracil (**2-32c**) most commonly used in the treatment of breast and colorectal cancer.[55] **2-65c** is produced by the enzyme dihydropyrimidine dehydrogenase (**Scheme 2.28**), followed by two subsequent enzymatic degradation steps to low toxic fluoro-β-alanine (**2-79**).[56] The large difference in heats of hydrogenation can be the reason for the lack in specifity of the dehydrogenase enzyme.

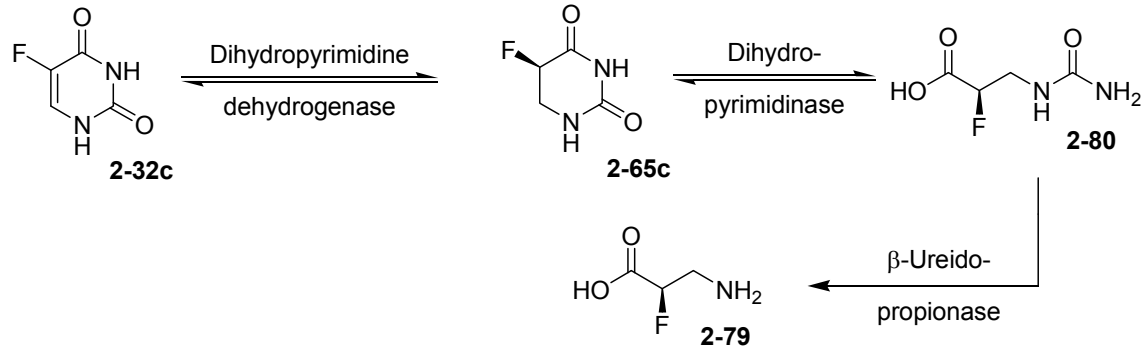

Scheme 2.28 Metabolic pathway of the degradation of 5-fluorouracil (**2-32c**).

The hydrogenation of pyrimidine bases is much more exothermic than the purine bases adenine (**2-81**) or guanine (**2-82**). The most stable reaction products are in both cases those involving reduction of the C8-N7 double bond with positive heats of hydrogenation of $\Delta_{hyd}H$(**2-77a**) = +7.70 kJ mol^{-1} and $\Delta_{hyd}H$(**2-78b**) = +5.20 kJ mol^{-1} (**Figure 2.12**). Regardless at which position the reduction occurs, all enthalpic values are positive and hydrogenation is therefore unlikely to happen as graphically displayed in **Figure 2.13**. The large differences between pyrimidine- and purine-based nucleobases reflect the intrinsically large discrepancy in hydrogenations of C-C and C-N double bonds. This can readily be seen in hydrogenation enthalpies of small

model systems like propene ($\Delta_{hyd}H$(**2-12b**) = -125.0 kJ mol^{-1}) and *N*-methylimine ($\Delta_{hyd}H$(**2-83**) = -62.8 kJ mol^{-1}).[15, 57]

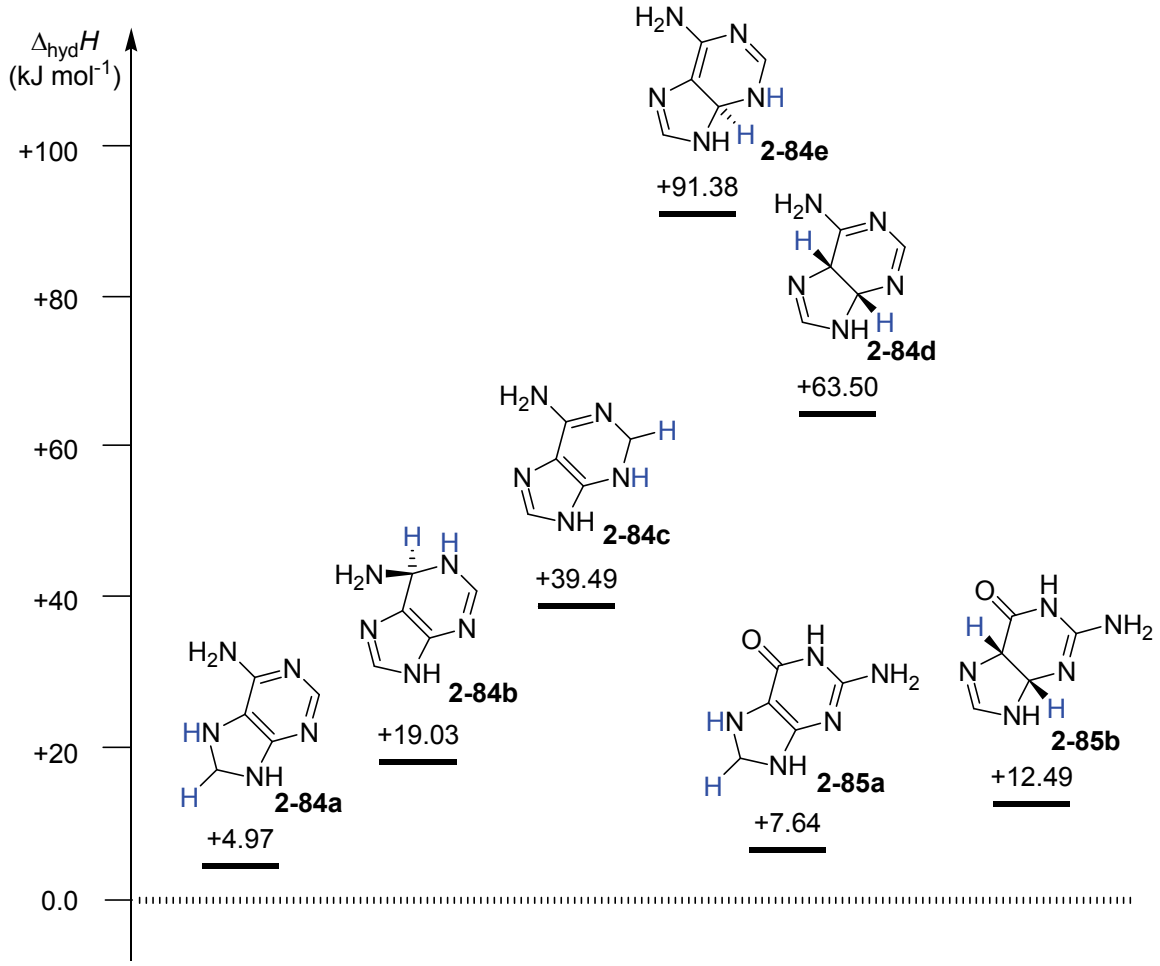

Figure 2.13 Regioselective hydrogenation of adenine (**2-81**) and guanine (**2-82**) at G3B3 level of theory obtained at 298.15 K and 1 atm (in kJ mol^{-1}).

The most difficult pyrimidine base to reduce is cytosine (**2-76**) with a hydrogenation value of $\Delta_{hyd}H$(**2-76**) = -54.7 kJ mol^{-1}, which is probably a result of the different substitution pattern at C4 position (amino vs. carbonyl group). The order of hydrogenation energies found here in the gas phase parallels that of the experimentally measured one-electron reduction potentials in the gas phase and in polar organic solvents.[58] A different energetic outcome is observed, if the tautomeric forms of uracil or cytosine are considered to be relevant. The isomerization enthalpies $\Delta_{iso}H$ in gas phase at G3B3 level are displayed in **Figure 2.14**. For uracil (**2-32a**) the canonical structure of its reduced form **2-65a** is the most stable among the

tautomeric amides. The high endothermicity of *bis*-enol **2-88a** ($\Delta_{iso}H$(**2-88a**)= +134.7 kJ mol^{-1}) is without doubt the consequence of abolition of the aromatic stabilization. Recently, *Ribeiro da Silva* and coworkers used this approach in combination with its hydrogenation energy to verify the question wether uracil (**2-32a**) is aromatic.[53] For cytosine (**2-76**) the canonical dihydro structure **2-89** is not the global minimum, but imine tautomer **2-90** either in its *E* or *Z* form with $\Delta_{iso}H$(*E*-**2-90**) = -20.3 kJ mol^{-1} and $\Delta_{iso}H$(*Z*-**2-90**) = -16.9 kJ mol^{-1}, respectively.

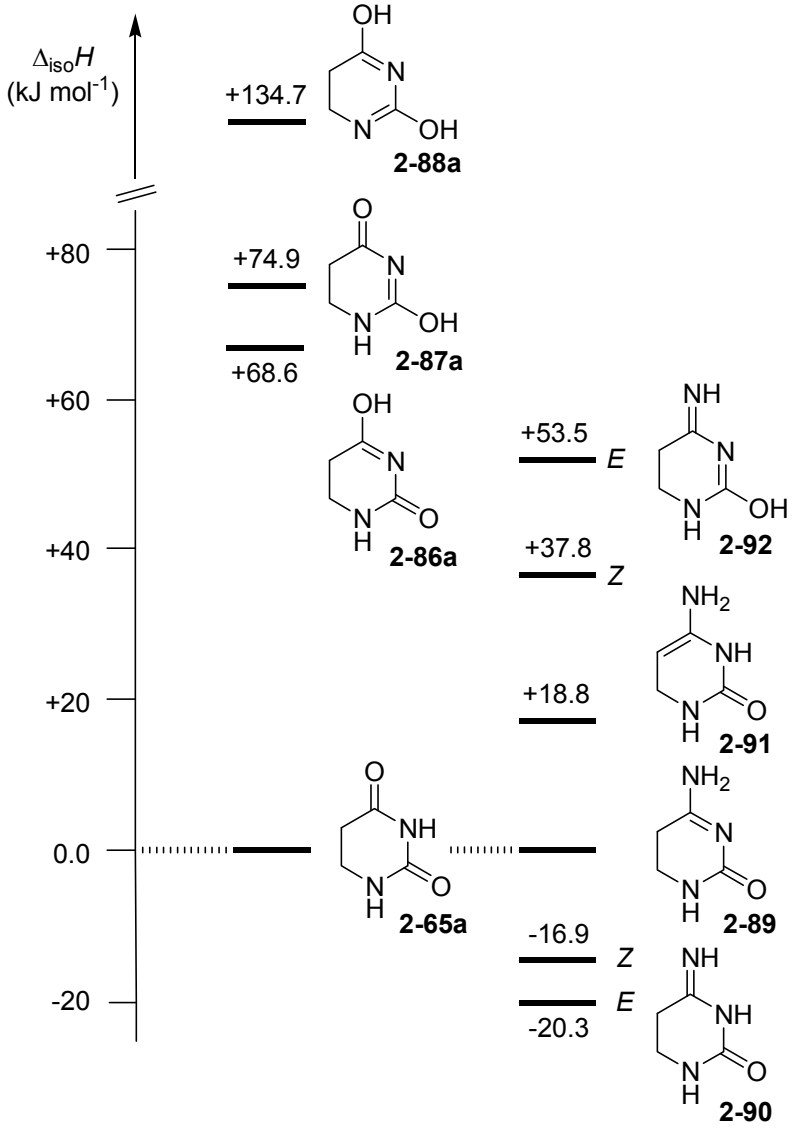

Figure 2.14 Isomerization enthalpies $\Delta_{iso}H$ of the hydrogenated pyrimidines **2-65a** and **2-89** at G3B3 level of theory in kJ mol^{-1}.

Besides of increased rates of hydrolysis as cause for the mutagenetic properties of dihydrocytosines, these results also indicate an impact of the tautomeric equilibrium on base-pairing. The experimentally measured heats of hydrogenation are closely similar to the theoretically obtained G3B3 values and therefore provide a quantitative guideline for the redox properties of nucleobases with respect to reductive hydrogenation.

2.4.2 Thermochemistry of Sugar Models

The theoretically obtained numbers for the sugar models together with available experimental values of selected carbonyl compounds are found in **Table 2.9** and **Table 2.10**.

Table 2.9 *Boltzmann*-averaged heats of hydrogenation $\langle\Delta_{hyd}H\rangle$ of some selected carbonyl compounds at G3B3 level of theory in kJ mol^{-1} (at 298.15 K and 1 atm, only the starting materials are shown).

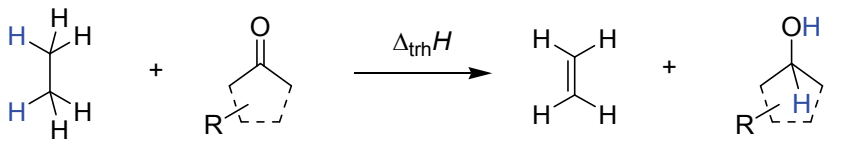

2-29a **2-12a**

	$\langle\Delta_{trh}H\rangle$(calc.)[a]	$\langle\Delta_{hyd}H^*\rangle$(calc.)[b]	$\Delta_{hyd}H$(exp.)
CH_3-CHO (**2-18**)	+67.88	-68.42	**-69.1 ± 0.4**[23] -68.6[c]
$(CH_3)_2CO$ (**2-19**)	+79.73	-56.57	**-55.6 ± 0.4**[24] -55.5[c]
$(CH_3)_2CH$-CHO (**2-93**)	+66.65	-69.65	-68.1[c]
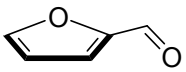 **2-94**	+72.36	-63.94	-60.8[c]
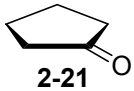 **2-21**	+85.85	-50.45	**-51.3 ± 0.6**[23] -50.4[c]

[a] Defined as $\Delta_{trh}H = \Delta_fH(C_2H_4) + \Delta_fH(R_2CH\text{-}OH) - \Delta_fH(R_2C{=}O) - \Delta_fH(C_2H_6)$. [b] Addition of the reaction enthalpies $\Delta_{trh}H$ to the experimentally determined hydrogenation enthalpy of ethylene $\Delta_{hyd}H$ (C_2H_4, **2-12a**) = -136.3±0.2 kJ mol^{-1} yields the hydrogenation enthalpy $\Delta_{hyd}H^*$ of the respective double bond. [c] Calculated using heats of formation Δ_fH.[15]

Table 2.10 *Boltzmann*-averaged heats of hydrogenation <$\Delta_{hyd}H$> of ribose and desoxyribose models at G3B3 level of theory in kJ mol^{-1} (at 298.15 K and 1 atm, only the starting materials are shown).

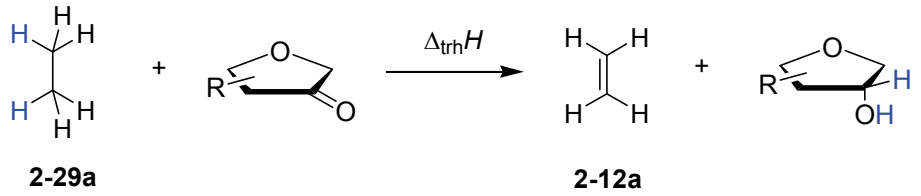

2-29a **2-12a**

	<$\Delta_{trh}H$>(calc.)[a]	<$\Delta_{hyd}H^*$>(calc.)[b]
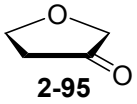 **2-95**	+74.18	-62.12
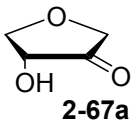 **2-67a**	+65.87	-70.43
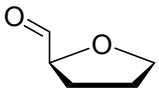 **2-96**	+50.41	-85.89
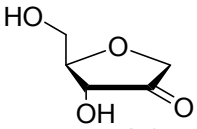 **2-97a**	+61.71	-74.59
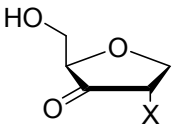		
X = OH (**2-97b**)	+48.21	-88.09
X =H (**2-98b**)	+73.60	-62.70
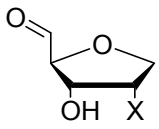		
X = OH (**2-97c**)	+52.84	-83.46
X =H (**2-98c**)	+55.31	-80.99

[a] Defined as $\Delta_{trh}H$ = $\Delta_fH(C_2H_4)$ + $\Delta_fH(R_2CH\text{-}OH)$ – $\Delta_fH(R_2C{=}O)$ – $\Delta_fH(C_2H_6)$. [b] Addition of the reaction enthalpies $\Delta_{trh}H$ to the experimentally determined hydrogenation enthalpy of ethylene $\Delta_{hyd}H$ (C_2H_4, **2-12a**) = -136.3±0.2 kJ mol^{-1} yields the hydrogenation enthalpy $\Delta_{hyd}H^*$ of the respective double bond.

Systematic differences in hydrogenation enthalpies between compounds containing a formyl or ketone functionality are not observed, since multiple secondary factors like ring strain, electrostatic interactions and stabilizing hydrogen bonds have to be

considered. For example, the heat of hydrogenation is lowered by *ca.* 4 kJ mol^{-1} if the ketone moiety is incorporated into the cyclopentane ring of **2-21** ($\Delta_{hyd}H$(**2-21**, exp.) = -51.3±0.6 kJ mol^{-1}, $\Delta_{hyd}H$ (**2-21**, G3B3) = -50.5 kJ mol^{-1}) compared to acyclic acetone (**2-19**). Installing an electronegative oxygen atom, present in all furanose sugars, reduces the driving force of hydrogenation by approximately 12 kJ mol^{-1} ($\Delta_{hyd}H$(**2-95**) = -62.1 kJ mol^{-1}), which is even further reduced by attaching a hydroxyl group in α position resulting in **2-67a** ($\Delta_{hyd}H$(**2-67a**) = -70.4 kJ mol^{-1}).

The hydrogenation enthalpies for the sugar-derived reaction partners collected in **Table 2.9** and **Table 2.10** are shown graphically in **Figure 2.15** in a comparable way (that is, as the hydrogenation enthalpies of the respective oxidized forms) in order to allow side-by-side comparison. That means all sugar building blocks with a less favorable (less negative) hydrogenation enthalpy are in principle able to reduce the respective nucleobase. The important sugar models are all located in the range of -70.4 to -88.1 kJ mol^{-1} and thus bracket the hydrogenation enthalpies of uracil (**2-32a**), its *N*-methylated derivatives and thymine (**2-32b**). The most effective reducing agent found in the RNA sugar models is the C2' hydroxyl group, whose transfer hydrogenation with uracil (**2-32a**) to yield dihydrouracil **2-65a** and **2-97a** is predicted to be exothermic by -78.1 - (-74.6) = -3.5 kJ mol^{-1}. Removal of the C2' hydroxyl group as is the case in DNA leaves only over the C3' and C5' hydroxyl groups as reducing agents. The former of these is reactive enough ($\Delta_{hyd}H$(**2-98b**) = -62.7 kJ mol^{-1}) to reduce uracil and thymine in an exothermic fashion. Overall it can be concluded that transfer hydrogenation from sugar components to uracil (**2-32a**) may be thermochemically favorable.

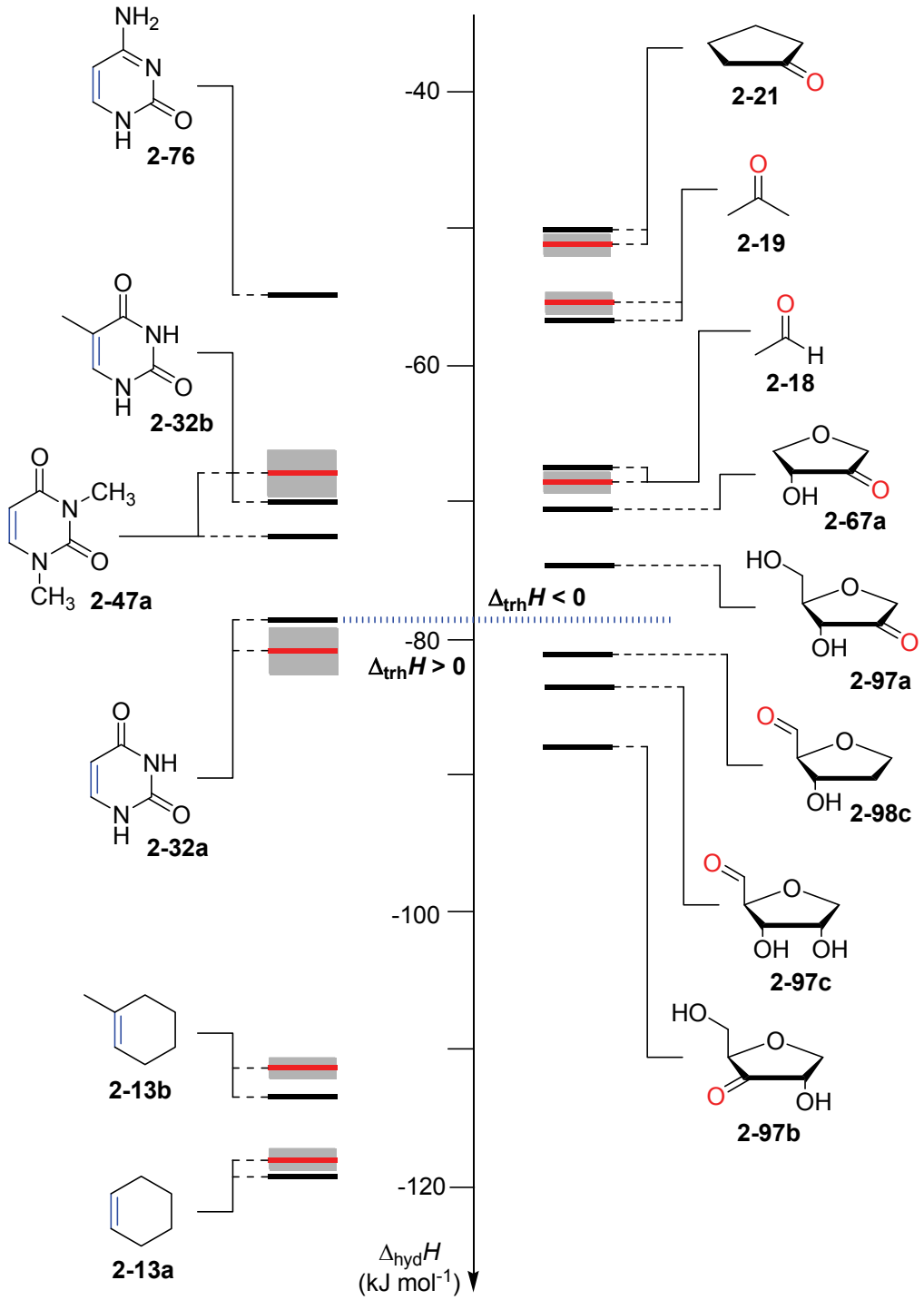

Figure 2.15 Heats of hydrogenation $\Delta_{hyd}H$ at 298.15 K of selected nucleobases and carbonyl compounds. Experimental hydrogenation enthalpies (red lines) are shown together with their standard deviations as gray bars.

2.4.3 Complete Nucleosides

Comparison of the computed data for the individual components of **Figure 2.15** with those for the nucleosides in **Figure 2.16** shows that sugar-to-base transfer hydrogenation energetically becomes more positive on covalent coupling of both redox partners. However, even for the least favorable process, the formation of C2' oxidized nucleoside **2-100a** from uridine (**2-99**), the endothermicity amounts to only +10.8 kJ mol^{-1} in the gas phase, which is a result of the loss of the hydrogen bond upon oxidation.[59] Using either the C3' (as in **2-100b**) or the C5' (as in **2-100c**) hydroxyl groups as redox partners leads to even less positive reaction energies. This difference, which is obtained from *Boltzmann*-averaged enthalpies, can potentially be modified through intermolecular interactions as present in base-paired systems or in polar solvents.

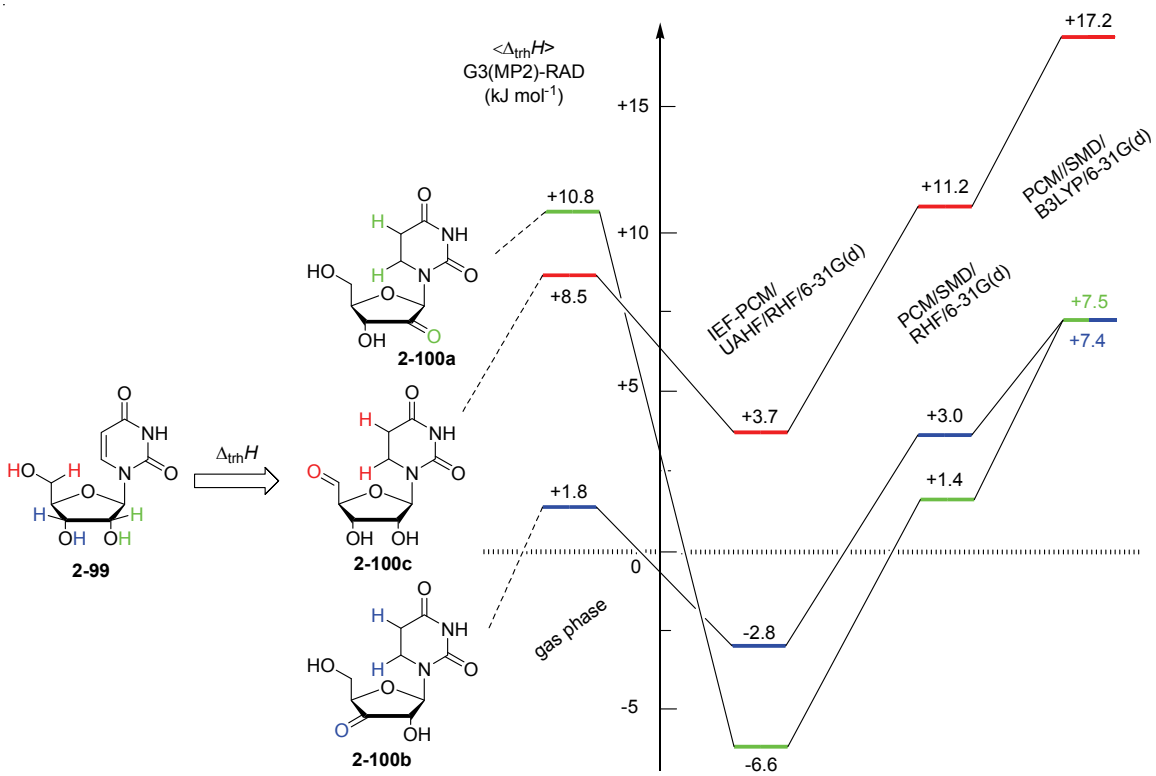

Figure 2.16 Heats of transfer hydrogenation <$\Delta_{trh}H$> of uridine (**2-99**) to the three possible reaction products as obtained at G3(MP2)-RAD level at 298.15 K in the gas phase (left) and in aqueous solution (right).

Implicit water solvation using an IEF-PCM model in combination with UAHF radii led to exothermic values for the keto models with the largest change for **2-100a**

($\Delta_{trh}H$(sol) = -6.6 kJ mol^{-1}). The oxidation of the C3' position present in **2-100b** gives only moderate changes in structural parameters concerning the base and the C2' hydroxy substituent, which is important for hydrogen-bonding. Application of the more recent SMD solvation model by *Truhlar* and *Cramer*[60] leads to uniformly more endothermic values. Irrespective of the used theory the relative order remains unchanged. The large endothermicity for the transfer of dihydrogen upon implicit solvation from the C5' hydroxyl group to form **2-100c** is a combination of the weak redox power of the formyl residue and the poor solvation of relevant hydrogen bonds between the base and the C2'-OH group. The strong impact of solvation after omission of the C2' hydroxyl group is depicted in **Figure 2.17**, where the black bars represent the most favorable and the red bars the least favorable conformers in the gas phase.

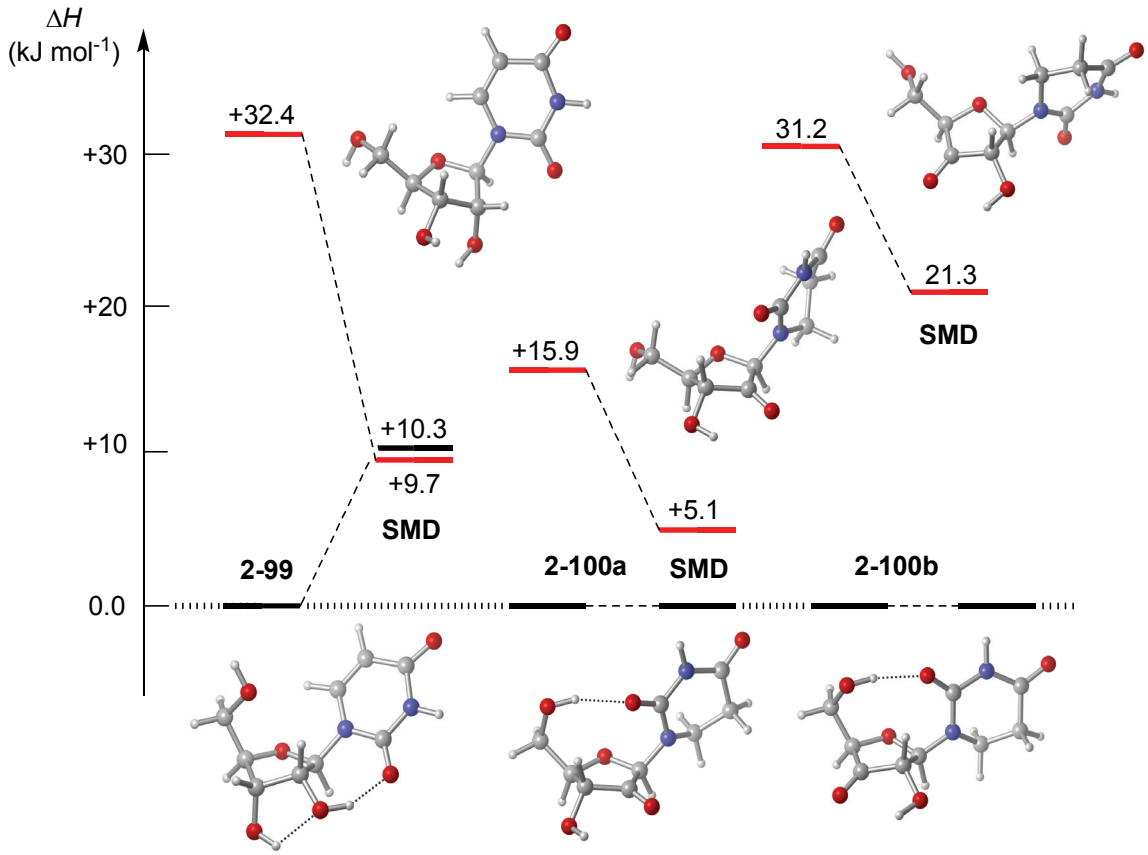

Figure 2.17 Relative stabilities of uridine (**2-99**) and its redox products **2-100a** and **2-100b** at G3(MP2)-RAD level of theory in the gas phase and with implicit solvation (water, SMD/B3LYP/ 6-31G(d)).

The small energy gap of herein considered conformers of **2-100a** shows a distinct stabilization in the gas phase. Most of the conformers of C2' oxidized **2-100a** possess

a *syn* base orientation, pointing its C2 carbonyl residue directly to the C3' hydrogen atom. For the least stable conformer of **2-100a** in the gas phase this hydrogen atom exhibits the highest *Mulliken* charge of all ring protons. The distance of the proton at C3' position to the carbonyl oxygen in the base (r(C3'H-C2O) = 259 pm) is only slightly longer than the related C3'OH and C2'CO distance (r(C3'OH-C2'CO) = 231 pm). The similar stabilization in the SMD model of *ca.* 10 kJ mol^{-1} of **2-100a** and **2-100b** is the result of weak interactions of the OH proton and the neighboring carbonyl oxygen atom.

The close proximity of nucleobases in RNA opens the possibility of inter-nucleotide transfer hydrogenation. Therefore, the energetics for an intermolecular transfer hydrogenation including two uridine molecules, where one is acting as hydrogen donor to give **2-101a** and the other as acceptor yielding 5,6-dihydrouridine (**2-5**), have also been investigated theoretically using G3(MP2)-RAD and SMD calculations (see **Scheme 2.29**). Compared to the intramolecular transfer hydrogenation, the intermolecular process is slightly less favorable by 2.9 kJ mol^{-1} ($<\Delta_{trh}H>_{inter}$ = +13.7 kJ mol^{-1}). Secondary effects are again almost compensated by implicit water solvation yielding an endothermic reaction enthalpy of +10.1 kJ mol^{-1}.

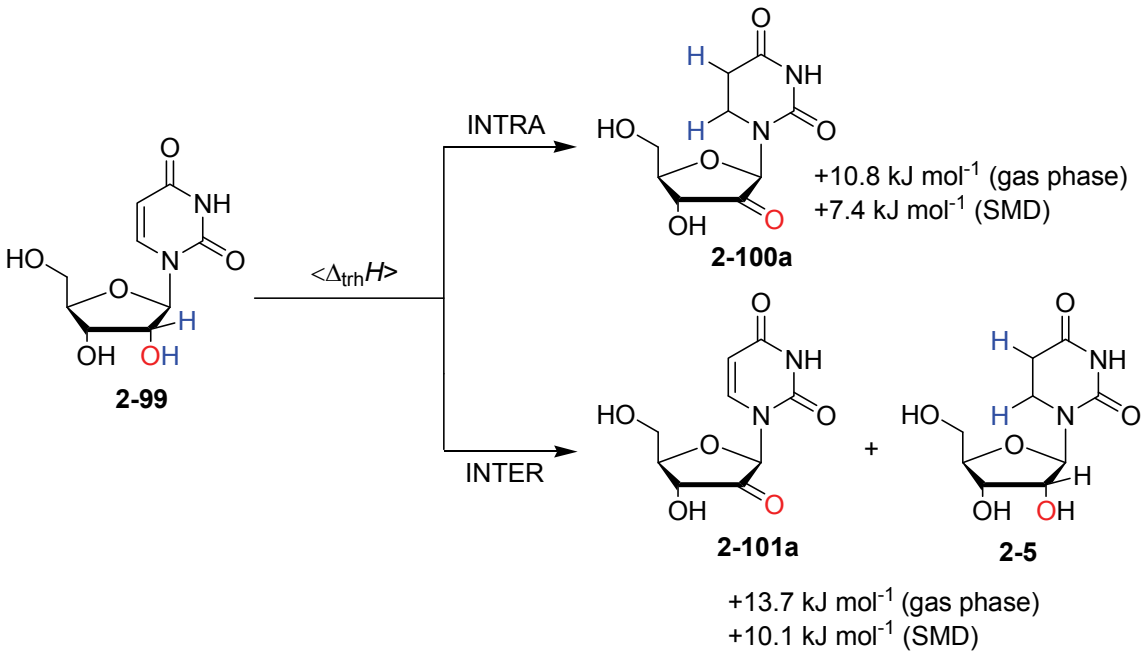

Scheme 2.29 Intra- vs. intermolecular transfer hydrogenation of uridine (**2-99**) at G3(MP2)-RAD level and 298.15 K.

DNA systems, in contrast, are much less prone to this type of redox process due to the removal of the C2' hydroxyl group und exchange of the uracil base by thymine. This limits the risk of transfer hydrogenation to the terminal C3' and C5' positions carrying thymine (**2-32b**) as redox partner. The results of a hypothetical 2'-desoxyuridine nucleoside **2-102** are depicted in **Figure 2.18**. A redox reaction involving the C5' hydroxyl group leading to the formylated redox product **2-103c** features an even larger endothermic enthalpy of +21.5 kJ mol^{-1} compared to **2-100c** (<$\Delta_{trh}H$>(**2-100c**) = +8.5 kJ mol^{-1}) in the gas phase. On the other hand, the hydrogen transfer from the C3' OH group is slightly exothermic (<$\Delta_{trh}H$>(**2-103b**) = -0.74 kJ mol^{-1}). As expected, **2-103b** profits mostly from the displacement of the hydroxyl group with a simple hydrogen atom upon solvation and is the only example where the driving force for transfer hydrogenation is increased.

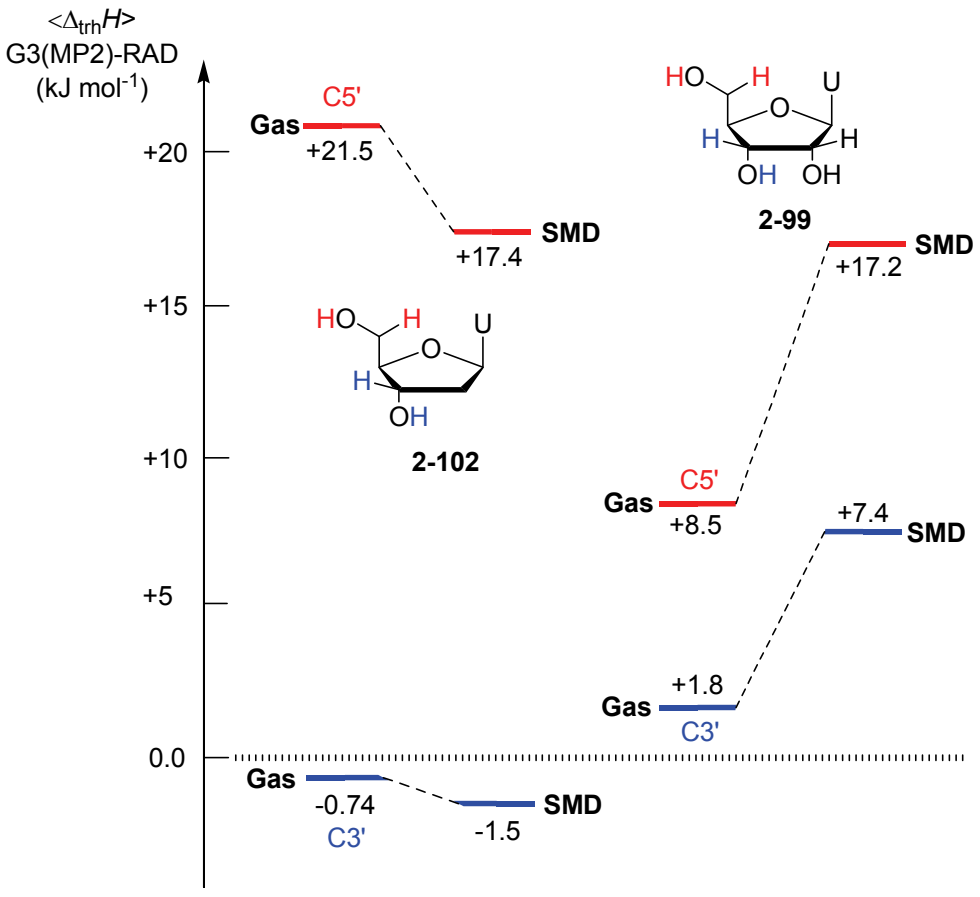

Figure 2.18 Comparison of *Boltzmann*-averaged heats of transfer hydrogenation <$\Delta_{trh}H$> of ribose and 2'-desoxyribose derived nucleosides at 298.15 K (G3(MP2)-RAD level, SMD/B3LYP/6-31G(d) implicit water solvation).

2.5 C5-modified Dihydrocytosines as Intermediates in their Demethylation Process

Epigenetic modifications play a crucial role in the development and differentiation of cells. Unlike simple genetics based on the change of the genotype, the changes in gene expression have other causes or mechanisms such as non-coding RNAs, histone modifications[61] or DNA methylation.[62] The latter is usually observed at the C5 position of cytosine in CpG (cytosine-phosphatidyl-guanine) rich areas in the genome promoter region.[63] The so-called 5th base 5-methyl desoxycytosine (m^5dC, **2-4a**) is an epigenetic mark which correlates with gene silencing due to prohibition of the transcription by m^5dC-affine proteins.[64] Recently, conversion of m^5dC in neurons or embryonic stem cells by TET (ten-eleven translocation) enzymes, which utilize α-keto glutarate and an iron(II)-oxo species, was found to lead to 5-hydroxymethylcytosine (hm^5dC, **2-4b**)[65] and further to 5-formylcytosine (f^5dC, **2-4c**)[66] and 5-carboxycytosine (ca^5dC, **2-4d**).[67]

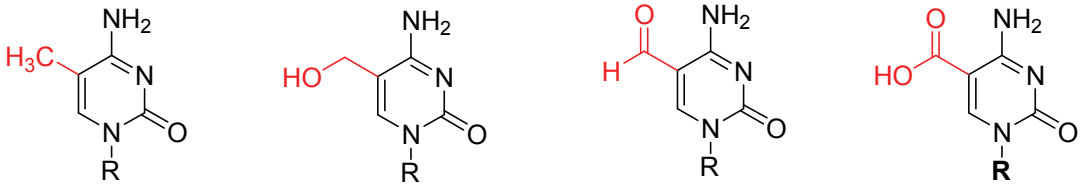

2-4a, m^5dC **2-4b**, hm^5dC **2-4c**, f^5dC **2-4d**, ca^5dC

Figure 2.19 Selection of modified DNA bases, R = 2'-desoxyribose.

The biological effects of active cytosine demethylation is believed to revert the native state of stem cells.[68] Two mechanisms are currently discussed extensively in the literature (see **Scheme 2.30**), one involving special glycosylases,[69] followed by base excision repair (BER) and second the active decarboxylation of ca^5dC (**2-4d**).

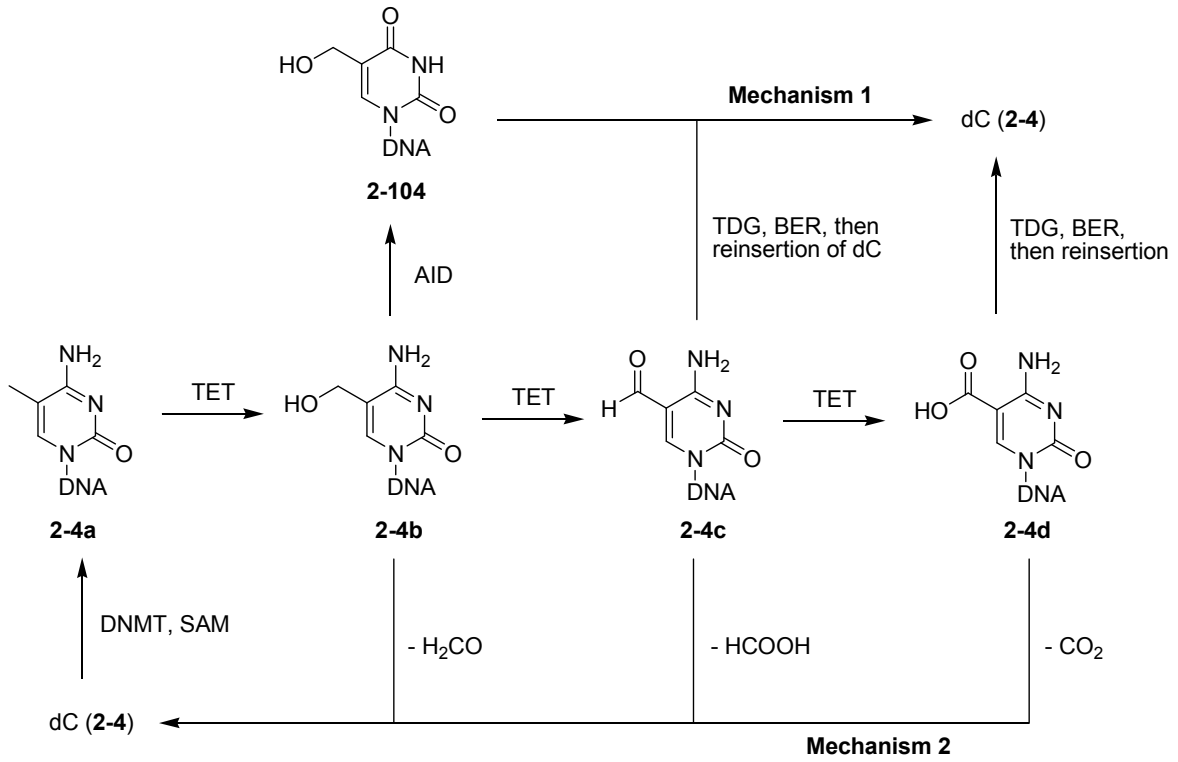

Scheme 2.30 Proposed mechanisms for the oxidative demethylation of m^{5}dC (**2-4a**).

Chemical model studies have shown, that decarboxylation of ca^{5}dC (**2-4d**) is accelerated by saturation of the C5-C6 double bond either by nucleophilic attack of a thiol residue[70] or complete reduction (see **Scheme 2.31**).[68]

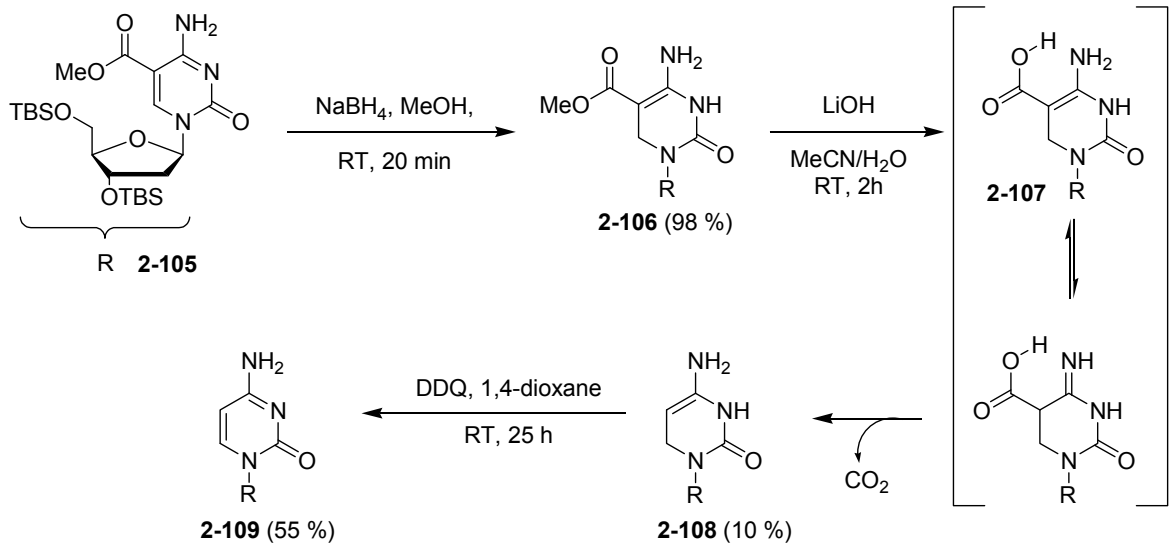

Scheme 2.31 *In-vitro* decarboxylation of silylated 2'-desoxycytidine **2-105**.

The influence of the side chain on the reduction potential in terms of C5-C6-transfer hydrogenation has been examined at the G3B3 level of theory and the isodesmic reaction as discussed in the previous chapters. The results are summarized in **Table 2.11**. The ease of hydrogenation of cytosine derivatives apparently depends on three main criteria: 1.) π- and σ-accepting properties of the group at C5 position; 2.) intramolecular interactions and steric effects; and 3.) solvent interactions. The first criterion is mainly relevant for the dihydro compounds, whereas the second has to be included for the unsaturated parent system. The largest hydrogenation enthalpy in the gas phase, apart from the non-natural 5-fluoro derivative **2-50c**, is observed for the 1-methylcytosine derivate with R = H (**2-50a**). The stereo-electronic influences of a methyl (**2-50b**) or a hydroxymethyl group (**2-50d**) is comparable low, giving almost the same hydrogenation enthalpies (<$\Delta_{hyd}H$>(**2-50b**) = -45.0 kJ mol^{-1}, <$\Delta_{hyd}H$>(**2-50d**) = -42.5 kJ mol^{-1}). The very low driving force of C-C double bond reduction in 5-formyl cytosine **2-50e** of only -3.8 kJ mol^{-1} is a consequence of the loss of the vinylogous amide resonance mainly responsible for the strong hydrogen bond (**Scheme 2.32**).

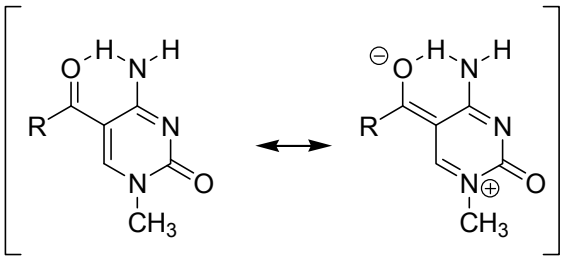

Scheme 2.32 Vinylogous amide resonace in cytosines **2-50e** (R = H) and **2-50f** (R = OH).

In addition, the electron-withdrawing ability as π acceptor to increase the electrophilicity of the C-C double bond is disabled. The final oxidization product **2-50f** exhibits the second lowest hydrogenation enthalpy (<$\Delta_{hyd}H$>(**2-50f**) = -11.7 kJ mol^{-1}). Abstraction of a proton to give carboxylate **2-50g** enhances the driving force by *ca.* 31 kJ mol^{-1}, implying that electronic effects are negligible. Implicit water solvation (SMD/B3LYP/6-31G(d)) of the hydroxyl group in **2-50d** is compensated by the enlarged size of the group.

Table 2.11 *Boltzmann*-averaged heats of hydrogenation <$\Delta_{hyd}H^*$> of cytosine derivatives at G3B3 level of theory in kJ mol^{-1} (at 298.15 K and 1 atm).

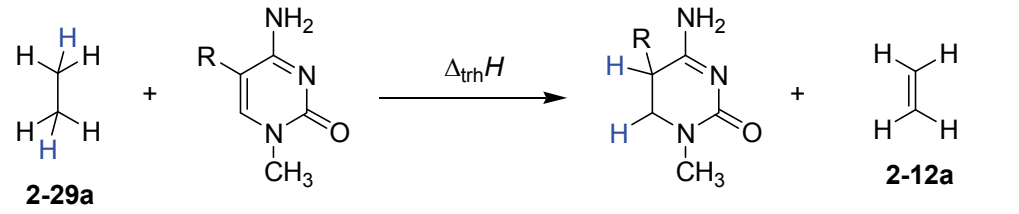

R	<$\Delta_{trh}H$>	<$\Delta_{trh}H$>(sol)[a]	<$\Delta_{hyd}H^*$>[a]	<$\Delta_{hyd}H^*$>(sol)[b]
-H (**2-50a**)	+86.99	+79.50	**-49.31**	**-56.80**
-CH_3 (**2-50b**)	+91.28	+86.02	**-45.02**	**-50.28**
-CH_2OH (**2-50d**)	+93.78	+85.66	**-42.45**	**-50.64**
-CHO (**2-50e**)	+132.52	+117.11	**-3.78**	**-19.19**
-COOH (**2-50f**)	+124.57	+106.83	**-11.73**	**-19.47**
-COO^- (**2-50g**)	+93.43	+100.38	**-42.87**	**-35.92**

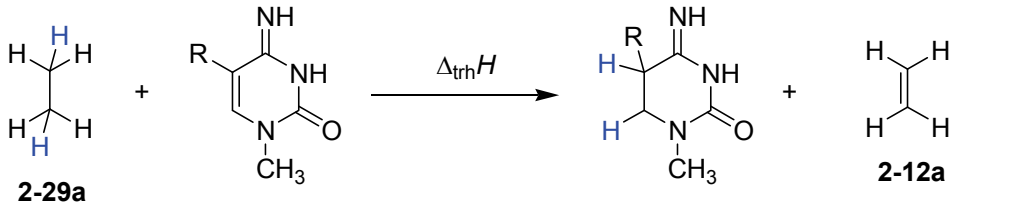

R[c]	<$\Delta_{trh}H$>	<$\Delta_{trh}H$>(sol)[a]	<$\Delta_{hyd}H^*$>[a]	<$\Delta_{hyd}H^*$>(sol)[b]
-H (**2-110a**)	+57.18	+49.37	**-79.12**	**-86.93**
-CH_3 (**2-110b**)	+64.23	+57.12	**-72.07**	**-79.18**
-CH_2OH (**2-110d**)	+58.58	+58.12	**-77.72**	**-78.18**
-CHO (**2-110e**)	+85.74	+85.73	**-50.56**	**-50.57**
-COOH (**2-110f**)	+77.30	+76.41	**-59.00**	**-59.89**
-COO^- (**2-110g**)	+89.47	+67.14	**-46.83**	**-69.16**

[a] Addition of the reaction enthalpies $\Delta_{trh}H$ to the experimentally determined hydrogenation enthalpy of ethylene $\Delta_{hyd}H$(C_2H_4, **2-12a**) = -136.3±0.2 kJ mol^{-1} yields the hydrogenation enthalpy $\Delta_{hyd}H^*$ of the respective double bond. [b] Addition of ΔG_{solv} (SMD/B3LYP/6-31G(d)) to the enthalpies H_{298} yields ΔH(sol). [c] Mixture of (*E*)- and (*Z*)-imines.

As already discussed in **Chapter 2.4.1**, the imine tautomer of cytosine has a significant effect on the C-C bond hydrogenation. The same trend is observed for C5-modified cytosines (see **Table 2.11**), with the overall order remaining constant. Implicit solvation has only an impact on carboxylate **2-110f**, which indicates that the tautomeric imine form, claimed to be involved in the decarboxylation of silylated ca^{5}dC (**2-105**, **Scheme 2.30**), is a populated structural motif in aqueous solution.

Since the driving force for C5-C6 hydrogenation shows a minimal value for formylated cytosine **2-50d**, the energetics for a combined inter- and intramolecular redox reaction of hydroxymethyl-substituted **2-50c** have been examined and depicted in **Table 2.12**.

Table 2.12 *Boltzmann*-averaged heats of transfer hydrogenation $<\Delta_{trh}H>$ of hydroxymethyl cytosine **1-50c** at G3B3 level of theory in kJ mol^{-1} (at 298.15 K and 1 atm).

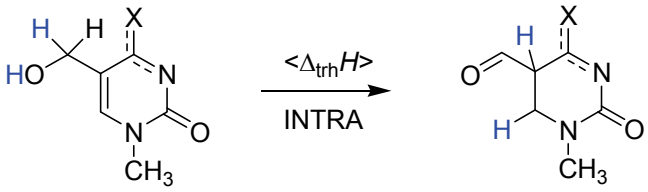

X	$<\Delta_{trh}H>$	
	G3B3	G3B3 + ΔG_{solv} (SMD/B3LYP/6-31G(d))
-NH_2	+40.21	+39.91
=NH[a]	+10.59	+14.35

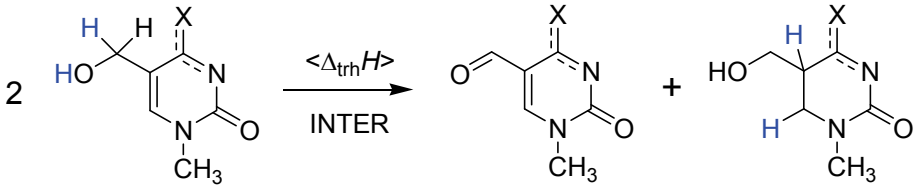

X	$<\Delta_{trh}H>$	
	G3B3	G3B3 + ΔG_{solv} (SMD/B3LYP/6-31G(d))
-NH_2	+1.47	+8.46
=NH[a]	-17.11	-13.26

[a] Mixture of (*E*)- and (*Z*)-imines.

As expected, an intramolecular hydrogenation reaction transferring H_2 from the side chain to the pyrimidine scaffold is not very likely from a thermochemical point of view. Again tautomerization increases the driving force by approximately 30 kJ mol^{-1}. On the other hand an intermolecular reaction has an almost thermoneutral reaction enthalpy value of +1.5 kJ mol^{-1}, which is shifted to exothermic -17.1 kJ mol^{-1} for the imine tautomer in the gas phase. In conclusion, no clear evidence for a preferred decarboxylation mechanism of m^{5}dC (**2-4a**) has been found on the basis of the

thermochemical results. Especially, it remains currently open at which oxidation step a C-C bond cleavage occurs to regain 2'-desoxycytosine in the DNA strand, and no supporting argument can be derived from the calculations. Due to the formation of toxic byproducts (CH_2O for **2-4b** and HCOOH for **2-4c**) hints for deprotonated carboxylate **2-4d** as plausible intermediate can be assumed.

2.6 Conclusion

The fidelity of biological information storage is tightly linked to the chemical stability of DNA and RNA oligonucleotides. As a possible threat reduction of the pyrimidine and purine bases as a result of transfer hydrogenation from the sugar-phosphate-backbone (as a free hydroxyl group is present in C2' position of RNA) have been studied herein. Using a combined theoretical and experimental strategy the heats of hydrogenation of the different bases have been determined. The best agreement of theory and experiment for $\Delta_{hyd}H$ has been obtained for the isodesmic reaction involving transfer hydrogenation of ethane (**2-29a**) and ethylene (**2-12a**) at G3B3 level of theory (**Scheme 2.33**) in combination with the experimental heat of hydrogenation of ethylene ($\Delta_{hyd}H$(**2-12a**, exp.) = -136.3 kJ mol^{-1}).

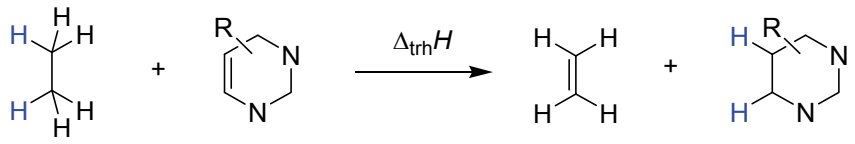

2-29a **2-12a**

Scheme 2.33 Isodesmic reaction to calculate various heats of hydrogenation $\Delta_{hyd}H$.

The most easily hydrogenated base is uracil (**2-32a**), followed by thymine (**2-32b**) and cytosine (**2-76**). Comparison of these hydrogenation enthalpies with those of ketones and aldehydes derived from sugar models indicates the possibility of near thermoneutral hydrogen transfer between uracil (**2-32a**) and the sugar phosphate backbone (see **Figure 2.20**). Regardless of the position, the hydrogenation of purine-derived bases is always endothermic.

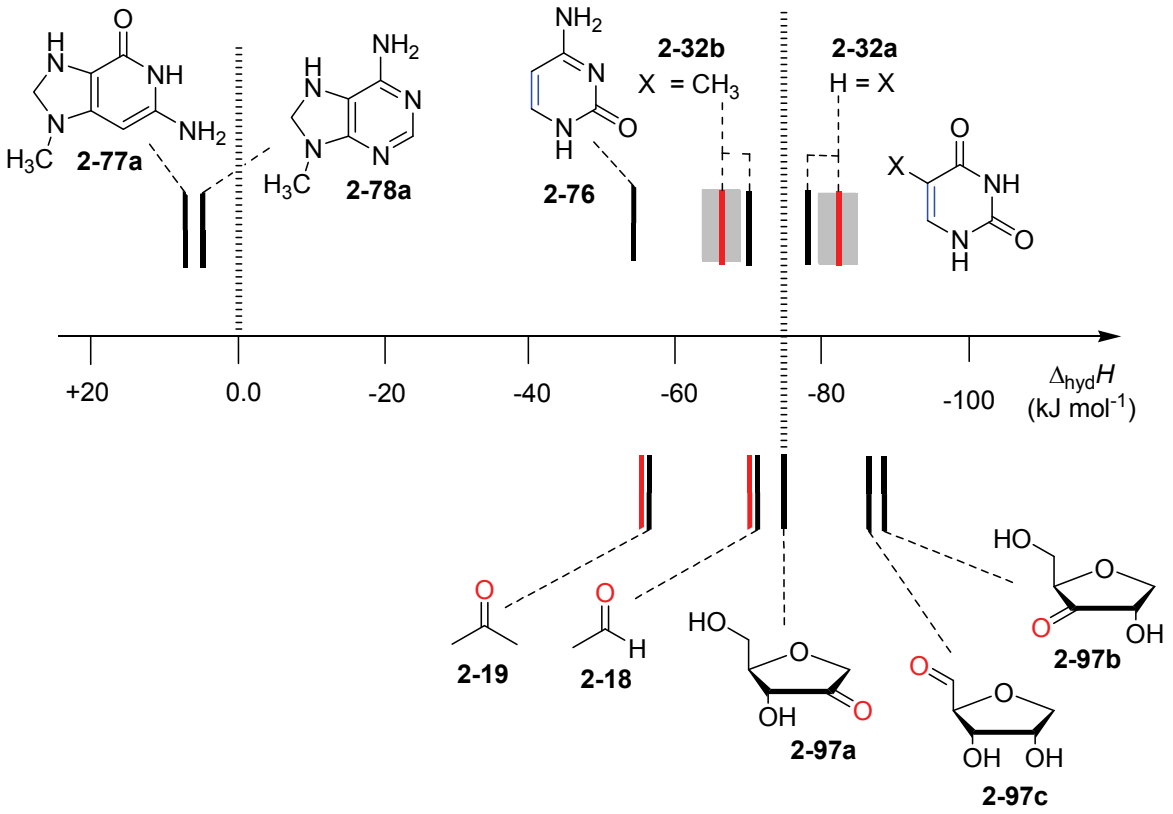

Figure 2.20 Heats of hydrogenation $\Delta_{hyd}H$ at 298.15 K of selected nucleobases and carbonyl compounds. Experimental hydrogenation enthalpies (red lines) are shown together with their standard deviations as gray bars.

Upon coupling base and sugar to complete nucleosides, the driving force for the intramolecular transfer hydrogenation of uridine (**2-99**) is decreased due to changes in the hydrogen bonding pattern upon oxidation to yield **2-100a**. All analytical methods used for this purpose, mostly mass spectrometry, would not be able to predict the correct structure of the reaction products. The rather similar hydrogenation enthalpies found here for some of the sugar and base components of nucleosides raise the question how the information stored in oligonucleotides can be preserved under the potential threat of internal hydrogen transfer reactions, undoubtedly with a very high kinetic barrier. End-capping and post-transcriptional methylation including the formation of cyclic DNA will of course eliminate the risk of transfer hydrogenation as an unwanted redox process.

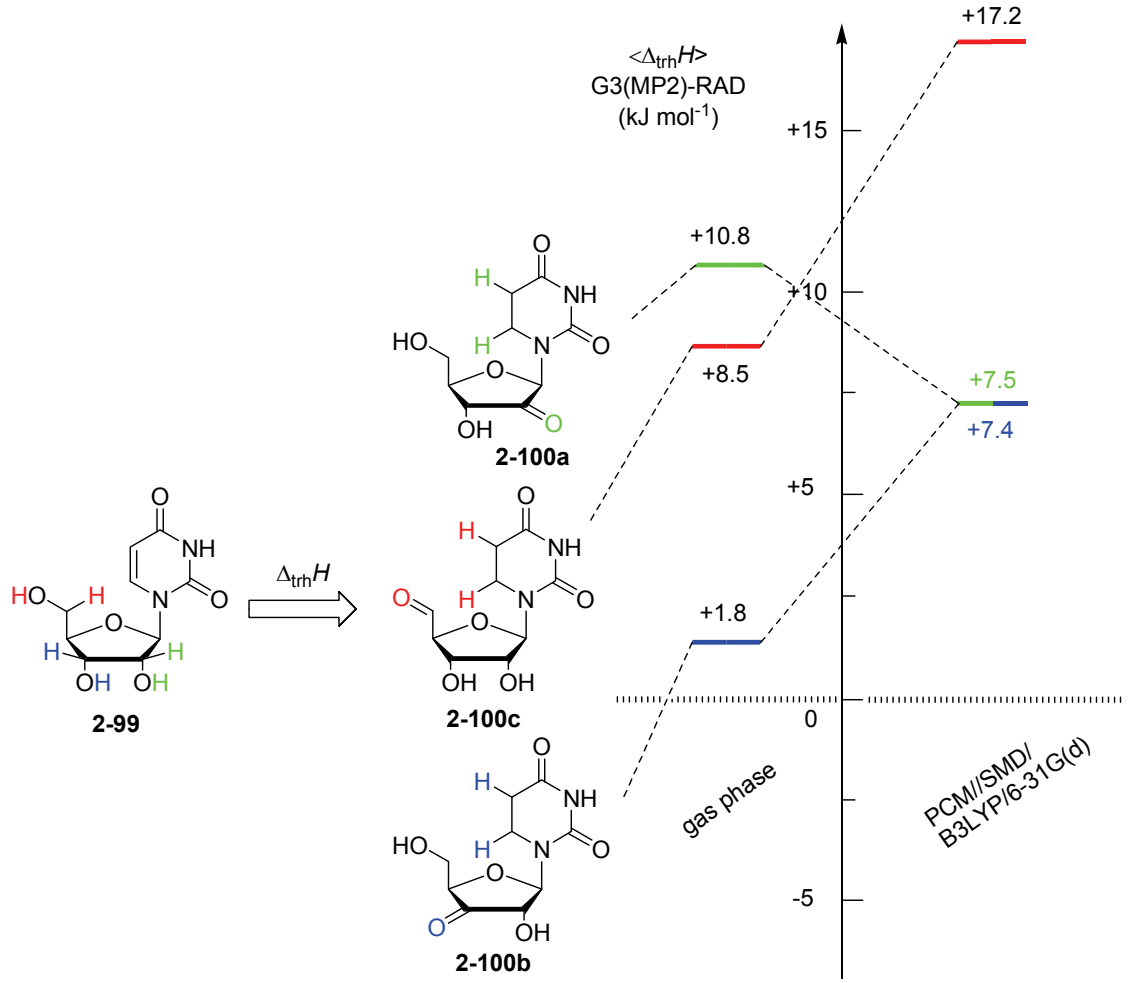

Figure 2.21 Intramolecular transfer hydrogenation of uridine (**2-99**) at G3(MP2)-RAD level and 298.15 K.

2.7 Experimental

2.7.1 General Considerations

All reactions were carried out under magnetic stirring and, if air or moisture sensitive, in flame-dried glass flasks using standard *Schlenk* techniques and P_4O_{10}-predried N_2 as inert gas. Syringes were used to transfer reagents and solvents and were purged with N_2 prior to use. Microwave syntheses were performed in a CEM Discover Synthesis System.

Solvents (p.a. quality) were dried according to standard methods[71] by distillation from drying agents and were stored under N_2 over 4 Å molecular sieves. Reagents were purchased from Across, Aldrich, Alfa Aesar and Fluka and used without further purification if not otherwise noted.

Thin layer chromatography (TLC) was performed using aluminium plates coated with SiO_2 (Merck 60, F_{254}). The spots were visualized by either UV light or staining the TLC plates with the reagents listed below, followed by heating with a heat gun:

- Neat iodine
- Ninhydrine (0.3 g) in 100 mL *n*-butanol and 3 mL glacial acetic acid
- $Ce(SO_4)_2$ (5.0 g), $(NH_4)_6Mo_7O_{24}$•4 H_2O (25.0 g), conc. H_2SO_4 (50 mL) in 450 mL water

Flash column chromatography was performed according to recommendations by *Still* using SiO_2 60 (0.04-0.063 mm, 230-300 mesh) from *Across*.[72] The solvents for the chromatography were of technical grade and distilled prior to use.

2.7.2 Analytical Methods

Nuclear magnetic resonance spectra were recorded on either *Varian Mercury 200*, *Varian Inova 400* or *Varian 600 instruments*. The chemical shifts δ were specified in ppm relative to the deuterated solvent:[73]

- $CDCl_3$ (^{1}H: 7.26, ^{13}C: 77.0)
- DMSO-d_6 (^{1}H: 2.50, ^{13}C: 39.5)
- CD_3OD (^{1}H: 3.31, ^{13}C: 40.0)

The signals were assigned to the corresponding nuclei by $^{1}H^{1}H$-COSY, $^{1}H^{13}C$-HSQC or $^{1}H^{13}C$-HMBC experiments. For the characterization of the observed signal multiplicities, the following abbreviations were used: s (singlet), d (doublet), t (triplet), q (quartet), dd (doublet of doublets), br (broad) and m (multiplet). The coupling constants ^{n}J with n = 2,3,4 (distance between the protons) are given in Hz.

Melting points are uncorrected and were measured on a *Büchi B-540* apparatus.

Infrared spectra were recorded from 4000-500 cm^{-1} on a *Perkin-Elmer FT-IR Spectrum BX*-spectrometer using the ATR-technique. For the band characterization, the following abbreviations were used: vs (very strong), s (strong), m (medium) and w (weak).

Mass spectra were recorded on a *Finnigan MAT 95q* or *MAT90* instrument for electron impact ionisation (EI, 70 eV). Electron spray ionisation (ESI) measurements were performed on a *Thermo Finnigan LTQ FT* apparatus. High resolution mass spectra (HRMS) were recorded on the same instruments.

Elemental analyses (CHNS) were performed by the microanalytical laboratory of the central analytics divison of the faculty for chemistry and pharmacy using either an *Elementar vario EL* or *Elementar vario micro cube* device.

2.7.3 Calorimetry

Combustion calorimetry and **enthalpy measurements** were performed by the group of *Prof. Dr. Sergey Verevkin* at the university of Rostock. The details can be found herein.[74]

2.7.4 Typical Procedures

2.7.4.1 Typical procedure for the methylation of pyrimidines (TP1)

To a suspension of the corresponding pyrimidine derivative in 20% aqueous NaOH was added dimethyl sulfate dropwise at 0 °C. After one hour the ice bath was removed and stirring at room temperature was continued for an additional hour. The colorless solution was transferred to a separating funnel and extracted with $CHCl_3$. The organic

phase was dried over $MgSO_4$ and concentrated under reduced pressure to yield the crude methylated pyrimidines as colorless solids.

2.7.4.2 Typical procedure for the synthesis of *N,N'*-dimethyl dihydropyrimidines (TP2)

A dry and nitrogen-flushed 10-mL microwave vessel was charged with *N,N'*-dimethyl urea, the corresponding acrylic acid and a magnetic stir bar. It was sealed and irradiated (200 W, closed vessel, PowerMAX) to 150 °C. After cooling to room temperature the crude mixtures were purified either by fractional distillation or column chromatography.

2.7.4.3 Typical procedure for the chlorination of pyrimidine bases (TP3)

A pressure tube was charged with the corresponding pyrimidine base and mixed with phosphoryl chloride $POCl_3$ followed by pyridine as HCl scavenger. The tube was quickly sealed and heated either in the oil bath or in the microwave to 150 °C until all starting material was consumed (TLC control). The dark solution was poured onto ice water/sat. $NaHCO_3$ solution and extracted with CH_2Cl_2. The combined organic extracts were dried over $MgSO_4$ filtered and evaporated to dryness.

2.7.4.4 Typical procedure for the nucleophilic aromatic substitution of chloro pyrimidines (TP4)

Sodium methoxide was slowly added under stirring to its parent alcohol in a microwave vial. The resulting suspension was cooled by an ice bath and the chloro pyrimidine was added in small portions or dropwise via syringe. The vial was sealed and heated under microwave irradiation to 90 °C (200 W, closed vessel, PowerMAX) until TLC control showed complete consumption of the starting material. The suspension was diluted with water and extracted with CH_2Cl_2. The combined organic phase was dried over $MgSO_4$, filtered and evaporated under reduced pressure.

2.7.4.5 Typical procedure for the methylation/rearrangement of electron rich pyrimidines (TP5)

In a round-bottom flask alkoxy-substituted pyrimidines were dissolved in methyl iodide, sealed by a stopper and placed in the refrigerator overnight. Excess of methyl iodide was removed under reduced pressure and the remaining solid was melted and cooled down again. The melting steps were monitored by TLC. If further purification was needed column chromatography was applied.

2.7.4.6 Typical procedure for the acidic demethylation of pyrimidones (TP6)

A 10 mL microwave vial was charged with the pyrimidone and dissolved in aqueous HCl. The reaction mixture was heated in the microwave under closed-shell conditions for 30 minutes. The crude product was either collected by filtration after cooling to 0 °C or by column chromatography.

2.7.5 Target Compounds

2.7.5.1 1,3-Dimethylpyrimidine-2,4(1*H*,3*H*)-dione (2-47a)

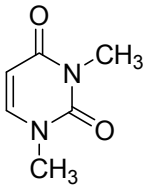

According to **TP1** the title compound was prepared by reacting uracil (4.48 g, 40.0 mmol) with dimethyl sulfate (8.5 mL, 11.3 g, 89.6 mmol) in 20 mL aqueous NaOH solution. After extraction with $CHCl_3$ (3x 100 mL) the crude uracil was purified by column chromatography on silica using $CHCl_3$/MeOH (20:1) as eluent to yield **2-47a** as colorless solid (3.54 g, 25.3 mmol, 63.2 %). Alternatively, **2-47a** can be purified by recrystallization from EtOH.

M.p. 122.1 - 123.0 °C. $\mathbf{R_f}$ ($CHCl_3$/MeOH, 20:1) = 0.55.

^{1}H NMR (600 MHz, $CDCl_3$) δ 7.10 (d, ^3J 7.9 Hz, 1H, C(6)H), 5.66 (d, ^3J 7.9 Hz, 1H, C(5)H), 3.34 (s, 3H, N(3)CH_3), 3.27 (s, 3H, N(1)CH_3) ppm.

^{13}C NMR (150 MHz, $CDCl_3$) δ 163.2 (C(4)), 151.8 (C(2)), 142.7 (C(6)), 101.1 (C(5)), 36.9 (NCH_3), 27.6 (NCH_3) ppm.

IR (ATR) ν (cm^{-1}) = 3079 (w), 1714 (m), 1700 (m), 1653 (vs), 1483 (m), 1438 (s), 1399 (m), 1372 (s), 1343 (s), 1264 (w), 1234 (m), 1178 (m), 1147 (m), 1002 (w), 985 (w), 932 (w), 812 (vs), 759 (vs), 726 (m), 684 (m), 625 (w).

HRMS (EI, 70 eV, m/z): $[M]^+$ calcd for $C_6H_8N_2O_2$, 140.0586; found, 140.0588.

EA (% calcd, % found for $C_6H_8N_2O_2$): C (51.42, 51.49), H (5.75, 5.91), N (19.99, 20.05).

NMR spectra are in agreement with already published data.[75]

2.7.5.2 1,3,5-Trimethylpyrimidine-2,4(1*H*,3*H*)-dione (2-47b)

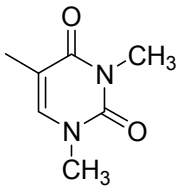

According to **TP1** the methylated thymine derivative **2-47b** was prepared by the reaction of thymine (2.52 g, 19.98 mmol) with dimethyl sulfate (4.0 mL, 3.01 g, 23.9 mmol) in 10 mL aqueous NaOH solution. After extraction with $CHCl_3$ (3x 100 mL) the crude product was purified by column chromatography on silica using $CHCl_3$/MeOH (20:1) as eluent to yield **2-47b** as colorless solid (2.38 g, 15.4 mmol, 77 %).

M.p. 148.3 - 150.0 °C. $\mathbf{R}_f$ ($CHCl_3$/MeOH, 20:1) = 0.57.

^{1}H NMR (300 MHz, $CDCl_3$) δ 6.97 (q, ^4J 1.2 Hz, 1H, C(6)H), 3.34 (s, 3H, N(3)CH_3), 3.33 (s, 3H, N(1)CH_3), 1.90 (d, ^4J 1.2 Hz, 3H, CHCH_3) ppm.

^{13}C NMR (75 MHz, $CDCl_3$) δ 164.0 (C(4)), 151.8 (C(2)), 138.9 (C(6)), 109.5 (C(5)), 36.6 (NCH_3), 27.9 (NCH_3), 12.9 (C(5)CH_3) ppm.

IR (ATR) ν (cm^{-1}) 3066 (w), 2992 (w), 2954 (w), 2929 (w), 2850 (w), 1700 (m), 1661 (s), 1633 (vs), 1508 (w), 1450 (s), 1421 (m), 1382 (m), 1366 (m), 1339 (s), 1230 (s),

1193 (s), 1069 (m), 1048 (m), 1001 (s), 960 (m), 926 (m), 840 (w), 808 (w), 776 (s), 763 (vs), 753 (vs), 667 (m).

HRMS (EI, 70 eV, m/z): $[M]^+$ calcd for $C_7H_{10}N_2O_2$, 154.0742; found, 154.0741.

EA (% calcd, % found for $C_7H_{10}N_2O_2$): C (54.54, 54.23), H (6.54, 6.53), N (18.17, 18.15).

NMR spectra are in agreement with already published data.[75]

2.7.5.3 1,3-Dimethyl-5,6-dihydropyrimidine-2,4-dione (2-49a)

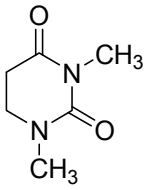

2-49a was prepared according to **TP2** by heating *N,N'*-dimethyl urea (2.20 g, 25.0 mmol) and acrylic acid (1.7 mL, 1.81 g, 25.1 mmol) at 150 °C for two hours. After cooling to room temperature the yellowish oil was distilled fractionally under reduced pressure (p = 0.29 mbar, b.p. = 114 - 116 °C) to yield dihydrouracil **2-49a** as colorless oil which solidified upon standing (1.85 g, 13.0 mmol, 52.1 %).

M.p. 40.7 - 42.2 °C. $\mathbf{R_f}$ ($CHCl_3$/MeOH, 20:1) = 0.53.

^{1}H NMR (600 MHz, $CDCl_3$) δ 3.26 (dt, ^3J 6.9 Hz, ^3J 4.4 Hz, 2H, C(6)H_2), 3.03 (d, ^3J 6.8 Hz, 3H, N(3)CH_3), 2.92 (d, ^3J 5.9 Hz, 3H, N(1)CH_3), 2.61 (dt, ^3J 6.8 Hz, ^3J 5.2 Hz, 2H, C(5)H_2) ppm.

^{13}C NMR (150 MHz, $CDCl_3$) δ 169.1 (C(4)), 153.7 (C(2)), 42.6 (C6), 35.5 (N(3)CH_3), 31.1 (C5), 27.2 (N(1)CH_3) ppm.

HRMS (EI, 70 eV, m/z): $[M]^+$ calcd for $C_6H_{10}N_2O_2$, 142.0742; found, 142.0731.

EA (% calcd, % found for $C_6H_{10}N_2O_2$): C (50.69, 50.54), H (7.09, 6.87), N (19.71, 19.79).

NMR spectra were in agreement with already published data.[41]

2.7.5.4 *rac*-1,3,5-Trimethyl-5,6-dihydropyrimidine-2,4-dione (2-49b)

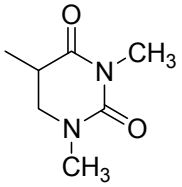

According to **TP2** the racemic dihydropyrimidine **2-49b** was prepared by heating *N,N'*-dimethyl urea (2.20 g, 25.0 mmol) with methacrylic acid (2.15 g, 2.13 mL, 25.0 mmol) at 150 °C for one hour. After cooling to room temperature the highly viscous mixture was directly transferred to a silica gel filled column to be purified by chromatography. The product was obtained as colorless oil which solidified upon cooling (1.66 g, 10.6 mmol, 43 %).

M.p. 39.4 - 40.9 °C. **R_f** ($CHCl_3$/MeOH, 20:1) = 0.55.

^{1}H NMR (300 MHz, $CDCl_3$) δ 3.24 (dd, ^2J 12.3 Hz, ^3J 6.1 Hz, 1 H, C(6)H_a), 3.06 (s, 3H, N(3)CH_3), 3.05 (dd, ^2J 12.3 Hz, ^3J 10.5 Hz, 1H, C(6)H_b), 2.96 (s, 3H, N(1)CH_3), 2.72 - 2.58 (m, 1H, C(4)H), 1.15 (dd, ^3J 7.0 Hz, ^4J 0.85 Hz, 3H, C(4)CH_3) ppm.

^{13}C NMR (75 MHz, $CDCl_3$) δ 172.2 (C(4)), 153.8(C(2)), 49.5 (C(6)), 35.4 (C(5)), 35.4 (N(3)CH_3), 27.6 (N(1)CH_3), 13.1 (C(5)CH_3) ppm.

IR (ATR) ν (cm^{-1}) 3353 (w), 2997 (w), 2968 (w), 2935 (w), 2898 (w), 2797 (w), 1706 (s), 1659 (vs), 1525 (w), 1494 (s), 1450 (s), 1418 (vs), 1402 (s), 1377 (s), 1343 (m), 1284 (s), 1270 (s), 1209 (s), 1160 (m), 1134 (s), 1092 (s), 1030 (s), 985 (w), 949 (w), 911 (m), 889 (w), 761 (s), 731 (m).

HRMS (EI, 70 eV, m/z): $[M]^+$ calcd for $C_7H_{12}N_2O_2$, 156.0899; found, 156.0875.

EA (% calcd, % found for $C_7H_{12}N_2O_2$): C (53.83, 53.81), H (7.74, 7.63), N (17.94, 18.03).

NMR spectra are in agreement with already published data.[41]

2.7.5.5 2,4-Dichloropyrimidine (2-41a)

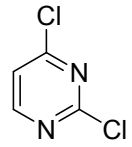

According to **TP3** uracil (**2-32a**, 1.76 g, 15.70 mmol) was reacted with $POCl_3$ (2.8 mL, 1.67 g, 10.9 mmol) and pyridine (1.2 mL, 1.22 g, 15.4 mmol) for two hours at 150 °C (oil bath). After work-up and purification by column chromatography (SiO_2, PE/EtOAc, 10:1) the title compound **2-41a** was isolated as colorless, sublimable solid (0.97 g, 6.51 mmol, 42 %).

M. p. 59.4 – 61.1 °C (no decomp.). $\mathbf{R}_f$ (SiO_2, PE/EtOAc, 10:1) 0.26.

^{1}H NMR (400 MHz, $CDCl_3$) δ 8.53 (d, ^3J 5.3 Hz, 1H, C(6)H), 7.34 (d, ^3J 5.2 Hz, 1H, C(5)H) ppm.

^{13}C NMR (100 MHz, $CDCl_3$) δ 162.8 (C(4)), 161. 2 (C(2)), 160.2 (C(6)), 120.5 (C(5)) ppm.

HR-MS (EI, 70 eV) m/z calc. for $C_4H_2{}^{35}Cl_2N_2$ 147.9595 (M^+), found 147.9601.

NMR spectra are in agreement with already published data.[76]

2.7.5.6 2,4-Dichloro-5-methylpyrimidine (2-41b)

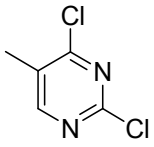

According to **TP3** the mixture of thymine (**1-32b**, 1.89 g, 15.00 mmol), $POCl_3$ (2.8 mL, 1.67 g, 10.9 mmol) and pyridine (1.2 mL, 1.22 g, 15.4 mmol) was heated for one hour to 150 °C in the microwave (100 W, closed vessel, PowerMAX on). After work-up and purification by column chromatography (SiO_2, PE/EtOAc, 5:1) the chlorinated methylpyrimidine **2-41b** was obtained as colorless oil (1.59 g, 9.76 mmol, 65 %)

$\mathbf{R}_f$ (SiO_2, PE/EtOAc, 5:1) 0.48.

^{1}H NMR (300 MHz, $CDCl_3$) δ8.41 (s, 1H, C(6)H), 2.35 (s, 3H, C(5)CH_3) ppm.

^{13}C NMR (300 MHz, $CDCl_3$) δ 162.61 (C(2)), 160.08 (C(4)), 158.29 (C(6)), 129.11 (C(5)), 15.89 (C(5)*C*H_3) ppm.

HR-MS (EI, 70 eV) m/z calc. for $C_5H_4{}^{35}Cl_2N_2$ 161.9746 (M^+), found 161.9749.

NMR spectra are in agreement with already published data.[77]

2.7.5.7 2,4-Dimethoxypyrimidine (2-42a)

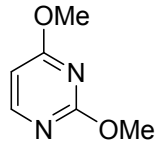

An excess of NaOMe (2.50 g, 46.3 mmol) was heated with chloro pyrimidine **2-41a** (1.50 g, 10.1 mmol) in methanol (20 mL) under microwave conditions (closed vessel, 100 W, POWERMax on) for one hour to 90 °C. Following the work-up procedure in **TP4**, 2,4 dimethoxypyrimidine (**2-42a**) was obtained after purification by column chromatography (SiO_2, PE/EtOAc, 5:1) as colorless liquid (1.40 g, 10.0 mmol) in 99 % yield.

R_f (SiO_2, PE/EtOAc, 5:1) 0.45.

^{1}H NMR (300 MHz, $CDCl_3$) δ 8.15 (d, ^3J 5.7 Hz, 1 H, C(6)H), 6.34 (d, ^3J 5.7 Hz, 1 H, C(5)H), 3.96 (s, 3 H, OMe), 3.93 (s, 3 H, OMe) ppm.

^{13}C NMR (75 MHz, $CDCl_3$) δ 171.4 (C(4)), 165.4 (C(2)), 158.2 (C(6)), 102.0 (C(5)), 54.6 (OMe), 53.6 (OMe) ppm.

HR-MS (EI, 70 eV) m/z calc. for $C_6H_8N_2O_2$ 140.0586 (M^+), found 140.0581.

NMR spectra are in agreement with already published data.[77]

2.7.5.8 2,4-Dimethoxy-5-methylpyrimidine (2-42b)

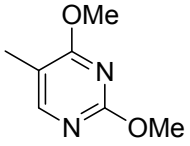

Following **TP4 2-42b** was synthesized by the reaction of sodium methoxide (1.50 g, 27.8 mmol) with chloropyrimidine **2-41b** (1.04 g, 6.38 mmol) in MeOH (5 mL) in the microwave (90 °C, closed vessel, 100 W, POWERMax on) for 90 min. After work-up

and purification by column chromatography (SiO_2, PE/EtOAc, 5:1) **2-42b** was isolated as colorless sublimable solid (0.72 g, 4.67 mmol, 73 %).

M. p. 57.0 – 58.2 °C (no decomp.). $\mathbf{R_f}$ (SiO_2, PE/EtOAc, 5:1) 0.31.

^{1}H NMR (300 MHz, $CDCl_3$) δ 7.85 (q, ^4J 0.8 Hz, 1 H, C(6)H), 3.96 (s, 3 H, OMe), 3.93 (s, 3 H OMe), 2.02 (q, ^4J 0.8 Hz, 3 H, C(5)CH_3) ppm.

^{13}C NMR (75 MHz, CDCl3) δ 169.5 (C(4)), 164.0 (C(2)), 156.8 (C(6)), 111.0 (C(5)), 54.5 (OMe), 53.7 (OMe), 11.8 (C(5)*C*H_3) ppm.

HR-MS (EI, 70 eV) m/z calc. for $C_7H_{10}N_2O_2$ 154.0742 (M^+), found 154.0729.

2.7.5.9 2,4-Diethoxy-5-methylpyrimidinium iodide (2-45b)

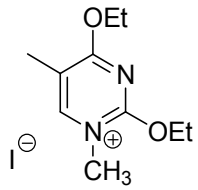

According to **TP5** pyrimidine **2-44b** (0.63 g, 3.46 mmol) was dissolved in methyl iodide (0.28 mL, 0.63 g, 4.46 mmol) and stored over night at around 0 °C in the refrigerator. Excess MeI was removed from the crystalline precipitate under high vacuum.[40]

2.7.5.10 4-Ethoxy-1,5-dimethylpyrimidine-2(1*H*)-one (2-111a)

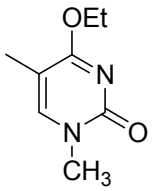

The pyrimidinium salt **2-45b** was melted with the aid of a heat gun and subsequently cooled to room temperature again. The precipitated solid was purified by column chromatography (SiO_2, EtOAc/MeOH, 10:1) to yield pyrimidone **2-111** as colorless solid (0.35 g, 2.07 mmol, 60 %).[40]

M. p. 109.5 – 110.5 °C (no decomp.). $\mathbf{R_f}$ (SiO_2, EtOAc/MeOH, 10:1) 0.28.

^{1}H NMR (300 MHz, $CDCl_3$) δ 7.17 (s, 1H, C(6)H), 4.43 (q, ^3J 7.1 Hz, 2H, OCH_2CH_3), 3.44 (s, 3H, C(5)CH_3), 1.92 (s, 3H, N(1)CH_3), 1.35 (t, ^3J 7.1 Hz, 3H, OCH_2CH_3) ppm.

^{13}C NMR (75 MHz, $CDCl_3$) δ 170.6 (C(4)), 157.4 (C(2)), 144.7 (C(6)), 104.6 (C(5)), 63.3 (OCH_2CH_3), 37.7 (N(1)CH_3), 14.4 (OCH_2CH_3), 12.1 (C(5)CH_3) ppm.

IR (ATR) ν (cm^{-1}) 3041(w), 2992 (w), 1656 (vs), 1632 (vs), 1566 (m), 1535 (s), 1462 (s), 1422 (vs), 1390 (s), 1365 (s), 1343 (vs), 1324 (vs), 1252 (s), 1179 (m), 1159 (vs), 1109 (s), 1060 (s), 1032 (vs), 934 (s), 917 (s), 902 (m), 815 (m), 780 (vs), 745 (s), 693 (m).

HR-MS (EI, 70 eV) m/z calc. for $C_8H_{12}N_2O_2$ 168.0893 (M^+), found 168.0890.

2.7.5.11 4-Ethoxy-1-ethyl-5-methylpyrimidine-2(1*H*)-one (2-111b)

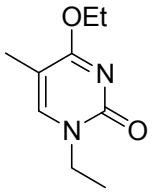

2-111b was isolated as side product after melting the pyrimidinium salt **2-45b** (0.83 g, 2.56 mmol) for two times (99.0 mg, 0.54 mmol, 21 %).[40]

M. p. 75.1 – 77.5 °C (no decomp.). **R_f** (SiO_2, EtOAc/MeOH, 10:1) 0.46.

^{1}H NMR (300 MHz, $CDCl_3$) δ 7.16 (s, 1H, C(6)H), 4.42 (q, ^3J 7.1 Hz, 2H, OCH_2CH_3), 3.84 (q, ^3J 7.2 Hz, 2H, NCH_2CH_3), 1.91 (s, 3H, C(5)CH_3), 1.34 (t, ^3J 7.1 Hz, 2H, OCH_2CH_3), 1.30 (t, ^3J 7.1 Hz, 2H, OCH_2CH_3) ppm.

^{13}C NMR (75 MHz, $CDCl_3$) δ 170.3 (C(4)), 156.7 (C(2)), 143.5 (C(6)), 104.7 (C(5)), 63.2 (OCH_2CH_3), 45.2 (NCH_2CH_3), 14.6 (OCH_2CH_3), 14.4 (NCH_2CH_3), 12.2 (C(5)CH_3) ppm.

IR (ATR) ν (cm^{-1}) 3048 (w), 2975 (m), 2951 (w), 1665 (vs), 1636 (vs), 1571 (w), 1527 (s), 1483 (m), 1461 (s), 1443 (s), 1426 (vs), 1393 (m), 1376 (vs), 1361 (s), 1328 (vs), 1279 (m), 1234 (vs), 1172 (m), 1154 (vs), 1106 (s), 1098 (m), 1074 (m), 1031 (s), 1012 (m), 972 (m), 938 8m), 902 (m), 885 (w), 806 (m), 784 (vs), 761 (m), 744 (s), 690 (w), 620 (w), 582 (m), 566 (w).

HR-MS (EI, 70 eV) m/z calc. for $C_9H_{14}N_2O_2$ 182.1050 (M^+), found 182.1052.

2.7.5.12 4-Methoxy-1-methylpyrimidine-2(1*H*)-one (2-43a)

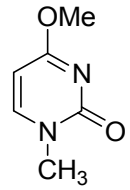

According to **TP5 2-43a** was isolated from a mixture of 2,4-dimethoxypyrimidine (**2-42a**, 1.26 g, 8.99 mmol) and methyl iodide (0.60 mL, 1.36 g, 9.58 mmol) by column chromatography using silica as stationary phase (EtOAc/MeOH, 15:1). The colorless solid (**2-43a**) was obtained in a yield of 63 % (0.79 g, 5.64 mmol), together with 37 % starting material (**2-42a**, 0.47 g, 3.35 mmol).

M. p. 146.5 – 147.3 °C (no decomp.). **R_f** (SiO_2, EtOAc/MeOH, 15:1) 0.30.
^{1}H NMR (400 MHz, $CDCl_3$) δ 7.40 (d, ^3J 7.1 Hz, 1H, C(6)-H), 5.84 (d, ^3J 7.1 Hz, 1H, C(5)-H), 3.92 (s, 3H, OMe), 3.46 (s, 3H, NMe).
^{13}C NMR (75 MHz, $CDCl_3$) δ 171.8 (C(4)), 157.0 (C(2)), 147.4 (C(6)), 95.3 (C(5)), 54.3 (OCH_3), 37.9 (NCH_3) ppm.
IR (ATR) ν (cm^{-1}) 3009 (w), 2990 (w), 2950 (w), 1656 (s), 1632 (vs), 1574 (m), 1535 (s), 1488 (vs), 1471 (m), 1453 (s), 1430 (w), 1409 (s), 1351 (s), 1301 (vs), 1229 (s), 1200 (s), 1176 (m), 1123 (s), 1045 (m), 1023 (s), 989 (m), 898 (w), 785 (vs), 779 (vs), 720 (m), 618 (m), 564 (s).
HR-MS (EI, 70 eV) m/z calc. for $C_6H_8O_2N_2$ 140.0586 (M^+), found 140.0581.

2.7.5.13 4-Methoxy-1,5-dimethylpyrimidine-2(1*H*)-one (2-43b)

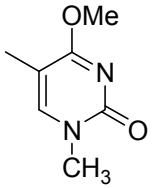

2-43b was isolated in 41 % yield (0.27 g, 1.75 mmol, **TP5**) after purification by column chromatography (SiO_2, EtOAc/MeOH, 10:1) of a mixture of **2-42b** (0.65 g, 4.22 mmol) and MeI (0.9 mL), together with 0.33 g of unreacted starting material (**2-42b**, 2.14 mmol, 51 %).

M. p. 141.1 – 142.1 °C (no decomp.). $\mathbf{R_f}$ (SiO_2, EtOAc/MeOH, 10:1) 0.32.

^{1}H NMR (300 MHz, $CDCl_3$) δ 7.18 (q, ^4J 1.1 Hz, 1 H, C(6)H), 3.96 (s, 3 H, OCH_3), 3.44 (s, 3 H, NCH_3), 1.92 (d, ^4J 1.1 Hz, 3 H, C(5)CH_3) ppm.

^{13}C NMR (75 MHz, $CDCl_3$) δ 170.8 (C(4)), 157.1 (C(2)), 144.6 (C(6)), 104.3 (C(5)CH_3), 54.5 (OMe), 37.6 (NCH_3), 11.9 (C(5)*C*H_3) ppm.

IR (ATR) ν (cm^{-1}) 3027 (w), 2959 (w), 1659 (vs), 1629 (vs), 1563 (w), 1538 (s), 1472 (s), 1434 (s), 1390 (m), 1377 (m), 1359 (s), 1329 (s), 1257 (s), 1191 (m), 1171 (s), 1135 (s), 1007 (m), 993 (vs), 932 (m), 887 (w), 779 (vs), 743 (s), 693 (w), 628 (s).

HR-MS (EI, 70 eV) m/z calc. for $C_7H_{10}N_2O_2$ 154.0742 (M^+), found 154.0724.

2.7.5.14 1-Methyluracil (2-39a)

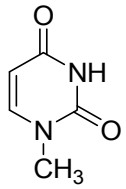

Following the general procedure **TP6**, pyrimidone **2-43a** (0.33 g, 2.35 mmol) was heated with HCl (3.8 % in H_2O) for 30 min to 110 °C in the microwave (100 W, closed vesell, PowerMAX on). The flask was placed in the fridge over night; the precipitated solid was filtered off and washed with pentane. After drying under high vacuum, uracil derivate **2-39a** was obtained as colorless needles (0.17 g, 1.35 mmol, 57 %).

M. p. 232.7 – 234.2 °C (no decomp.). $\mathbf{R_f}$ (SiO_2, EtOAc/MeOH, 10:1) 0.38.

^{1}H NMR (400 MHz, DMSO-d_6) δ 11.20 (s br, 1 H, NH), 7.60 (d, ^3J 7.8 Hz, 1 H, C(6)H), 5.51 (dd, ^3J 7.8 Hz, ^4J 2.3 Hz, 1 H, C(5)H), 3.22 (s, 3 H, NCH_3) ppm.

^{13}C NMR (100 MHz, DMSO-d_6) δ 163.9 (C(4)), 151.2 (C(2)), 146.4 (C(6)), 100.5 (C(5)), 35.2 (NCH_3) ppm.

IR (ATR) ν (cm^{-1}) 3000 (w), 2977 (w), 2874 (w), 2827 (w), 1759 (w), 1652 (s), 1619 (s), 1525 (m), 1482 (m), 1459 (m), 1420 (s), 1376 (s), 1329 (s), 1222(m), 1198 (m),

1159 (m), 1143 (m), 1046 (m), 990 (m), 855 (s), 802 (vs), 754 (vs), 722 (s), 627 (w), 558 (s).

HRMS (EI, 70 eV, m/z): calcd for $C_5H_6N_2O_2$, 126.0429 (M^+); found, 126.0420.

EA (% calcd, % found for $C_5H_6N_2O_2$): C (47.62, 47.50), H (4.80, 4.90), N (22.21, 22.07).

NMR spectra are in agreement with already published data.[78]

2.7.5.15 1-Methylthymine (2-39b)

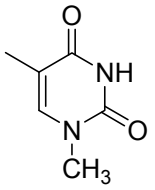

According to **TP6** 4-methoxypyrimidone **2-43b** (0.18 g, 1.17 mmol) was dissolved in 2 mL aqueous HCl (3.8 %) and heated in the microwave cavity for 30 min (110 °C, closed vessel, 100 W, PowerMAX on). Thymine **2-39b** (0.14 g, 0.99 mmol, 85 %) was obtained after purification by column chromatography (SiO_2, EtOAc/MeOH, 10:1).

M. p. 289.7 – 291.3 °C (decomp.). **R_f** (SiO_2, EtOAc/MeOH, 10:1) 0.51.

^{1}H NMR (400 MHz, DMSO-d_6) δ 11.19 (s broad, 1H, NH), 7.49 (d, ^4J 1.2 Hz, 1H, C(6)H), 3.19 (s, 3H, NMe), 1.74 (d, ^4J 1.2 Hz, 3H, C(5)CH_3) ppm.

^{13}C NMR (100 MHz, DMSO-d_6) δ 164.4 (C(4)), 151.2 (C(2)), 142.3 (C(6)), 108.1 (C(5)), 34.9 (NCH_3), 11.8 (C(5)CH_3) ppm.

IR (ATR) ν (cm^{-1}) 3148 (w), 3062 (m), 3001 (m), 2957 (m), 2927 (m), 2828 (m), 1762 (w), 1713 (s), 1696 (s), 1650 (vs), 1639 (vs), 1515 (m), 1484 (s), 1464 (s), 1422 (vs), 1378 (s), 1368 (s), 1328 (vs), 1208 (s), 1150 (s), 1066 (vs), 1050 (s), 1010 (m), 949 (s), 889 (s), 787 (s), 756 (vs), 693 (vs), 654 (m).

HRMS (EI, 70 eV, m/z): calcd for $C_6H_8N_2O_2$, 140.0586 (M^+); found, 140.0572.

EA (% calcd, % found for $C_6H_8N_2O_2$): C (51.42, 51.33), H (5.75, 5.86), N (19.99, 19.89).

2.7.5.16 1-*tert*-Butoxycarbonyluracil (2-40)

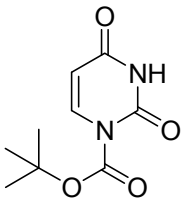

A suspension of uracil (**2-32a**, 1.12 g, 10.0 mmol), excess Boc_2O (2.23 g, 78.9 mmol) and catalytical amounts of DMAP (0.06 g, 0.049 mmol) in acetonitrile (20 mL) were stirred for two hours at room temperature until everything was dissolved. All volatile compounds were removed and the solid residue was purified by recrystallisation from EtOAc or column chromatography on silica using a mixture of petrol ether/ethyl acetate (1:1) as eluent. Boc-protected uracil **2-40** was isolated by recrystallisation as colorless solid (0.89 g, 4.19 mmol) in 41.9 % yield.

M. p. > 300 °C. $\mathbf{R_f}$ (SiO_2, PE/EtOAc, 1:1) 0.42.

^{1}H NMR (300 MHz, $CDCl_3$) δ 8.88 (s, 1H, NH), 7.87 (d, ^3J 8.4 Hz, 1H, C(6)H), 5.79 (d, ^3J 8.4 Hz, 1H, C(5)H), 1.60 (s, 9H, $C(CH_3)_3$) ppm.

^{13}C NMR (75 MHz, $CDCl_3$) δ 162.6 (C(4)), 148.2 ($NHCO_2$), 147.1 (C(2)), 139.7 (C(6)), 103.7 (C(5)), 87.3 ($C(CH_3)_3$), 27.8 ($C(CH_3)_3$) ppm.

IR ν (cm^{-1}) 3126 (w), 3105 (w), 3042 (w), 2982 (w), 2935 (w), 2842 (w), 1791 (w), 1753 (s), 1733 (s), 1703 (vs), 1634 (m), 1477 (w), 1459 (w), 1450 (w), 1403 (m), 1362 (s), 1265 (vs), 1234 (s), 1147 (vs), 1126 (vs), 1099 (vs), 1034 (w), 992 (w), 856 (s), 862 (m), 835 (vs), 777 (s), 765 (s), 754 (s), 733 (m), 659 (vs).

HRMS (EI, 70 eV, m/z): calcd for $C_9H_{13}N_2O_4$, 213.0875 $(M+H)^+$; found, 213.0848.

NMR spectra are in agreement with already published data.[36]

2.7.5.17 1-Methyl-5,6-dihydrouracil (2-46a)

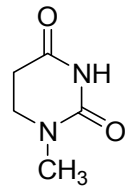

A 50 mL Schlenk flask equipped with stirring bar and additional stop-cock was charged with 1-methyluracil (**2-39a**, 0.19 g, 1.51 mmol), palladium on carbon (5%, 0.02 g, 0.94 μmol) and ethanol (10 mL). After flushing the flask for 30 seconds with hydrogen gas, the substrate was hydrogenated under atmospheric pressure until complete reduction was confirmed by ^{1}H NMR spectroscopy or TLC (SiO_2, $CHCl_3$/EtOH, 9:1). The hydrogen was replaced by nitrogen and the dark suspension was filtered over a plug of celite. After removal of the solvent the dihydro compound **2-46a** was obtained as colorless solid (0.19 g, 1.48 mmol) in almost quantitative yield.

An alternative way to synthesize **2-46a** is the following:
Dihydrocytosine **2-55a** (0.10 g, 0.79 mmol) was dissolved in aqueous HCl (1.9 %, 1.0 mL) and stirred at room temperature for five minutes. All volatile compounds were removed under reduced pressure and the remaining colorless solid was purified by column chromatography (SiO_2, $CHCl_3$/EtOH, 9:1) to obtain the hydrolysis product **2-46a** (0.06 g, 0.47 mmol) in 60 % yield.

M. p. 169.6 – 170.8 °C (no decomp.). **R_f** (SiO_2, $CHCl_3$/EtOH, 9:1) 0.49.
^{1}H NMR (400 MHz, DMSO-d_6) δ 10.04 (s broad, 1H, NH), 3.33 (t, ^{3}J 6.9 Hz, 2H, C(6)H_2), 2.85 (s, 3H, NCH_3), 2.54 (t, ^{3}J 6.9 Hz, 2H, C(5)H_2) ppm.
^{13}C NMR (100 MHz, DMSO-d_6) δ 170.5 (C(4)), 153.1 (C(2)), 43.1 (C(6)), 34.0 (NCH_3), 30.6 (C(5)) ppm.
IR (ATR) ν (cm^{-1}) 3386 (w), 3818 (m), 3069 (m), 2975 (w), 2946 (w), 2924 (w), 1692 (vs), 1505 (vs), 1458 (s), 1408 (vs), 1371 (s), 1335 (s), 1292 (s), 1267 (s), 1241 (vs), 1202 (vs), 1123 (m), 1070 (s), 1046 (m), 986 (m), 957 (m), 844 (s), 831 (vs), 767 (s), 736 (vs), 712 (s).
HRMS (EI, 70 eV, m/z): calcd for $C_5H_8N_2O_2$, 128.0586 (M^+); found, 128.0579.

EA (% calcd, % found for $C_5H_8N_2O_2$): C (46.87, 45.03), H (6.29, 6.13), N (21.86, 20.98).

2.7.5.18 *rac*-1-Methyl-5,6-dihydrothymine (2-46b)

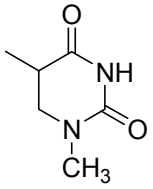

A 50 mL Schlenk flask equipped with stirring bar and additional stop-cock was charged with thymine derivative **2-39b** (0.14 g, 1.00 mmol), Rhodium on activated Al_2O_3 (5%, 0.03 g, 1.46 μmol) and ethanol (10 mL). After flushing the flask for 30 seconds with hydrogen gas, the stopper was closed and the substrate was hydrogenated under atmospheric pressure until complete reduction was confirmed by ^{1}H NMR spectroscopy or TLC (SiO_2, MeOH). The hydrogen was replaced by nitrogen and the dark suspension was filtered over a plug of celite and washed with EtOH. After removal of the solvent the dihydro compound **2-46b** was obtained as colorless solid (0.13 g, 0.91 mmol) in a yield of 91 %.

M. p. 150.4 – 151.8 °C (no decomp.). $\mathbf{R_f}$ (SiO_2, $CHCl_3$/EtOH, 9:1) 0.59.

^{1}H NMR (400 MHz, DMSO-d_6) δ 10.03 (s br, 1 H, NH), 3.35 (dd, ^2J 12.2 Hz, ^3J 6.3 Hz, 1 H, C(6)H^a), 3.17 – 3.06 (m, 1 H, C(6)H^b), 2.86 (s, 3 H, NCH_3), 2.72 – 2.60 (m, 1 H, C(5)H), 1.06 (d, ^3J 7.0 Hz, 3 H, C(5)CH_3) ppm.

^{13}C NMR (100 MHz, DMSO-d_6) δ 173.2 (C(4)), 153.2 (C(2)), 49.7 (C(6)), 34.5 (NCH_3), 34.0 (C(5)), 12.4 (C(5)CH_3) ppm.

IR (ATR) ν (cm^{-1}) 3199 (w), 3076 (w), 2980 (w), 2942 (w), 2883 (w), 1686 (vs), 1494 (s), 1449 (m), 1408 (m), 1392 (s), 1338 (m), 1240 (vs), 1151 (w), 1105 (w), 1069 (w), 1043 (w), 954 (w), 913 (w), 837 (s), 752 (vs), 728 (s), 678 (m).

HR-MS (ESI, m/z): calcd for $C_6H_9N_2O_2$, 141.0670 $(M-H)^-$; found, 141.0670.

EA (% calcd, % found for $C_6H_{10}N_2O_2$): C (50.69, 50.74), H (7.09, 7.08), N (19.71, 19.70).

2.7.5.19 1-(2-Cyanoethyl)-1-methylurea (2-59a)

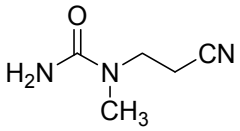

3-(Methylamino)propionitrile (4.26 g, 50.6 mmol), dissolved in 10 mL water and 5 mL conc. HCl was dropped slowly to a solution of potassium cyanate (5.70 g, 70.3 mmol) in 15 ml water. The reaction was completed by heating the reaction flask to 60 °C for 30 min (100 W, open vessel, PowerMAX on) in the microwave. After cooling to room temperature the solvent was removed under reduced pressure and the residue was purified by column chromatography on SiO_2 (crude mixture charged on SiO_2, EtOAc/MeOH, 10:1). Urea **2-59a** was obtained as colorless solid (3.86 g, 30.4 mmol, 60.0 %).

M.p. 116.7 - 117.7 °C (no decomp.). **R_f** (EtOAc/MeOH, 10:1) 0.25.

^{1}H NMR (400 MHz, DMSO-d_6) δ 5.94 (s broad, 2 H, NH_2), 3.43 (t, ^3J 6.7 Hz, 2 H, NCH_2CH$_2$CN), 2.83 (s, 3 H, NCH_3), 2.64 (t, ^3J 6.7 Hz, 2 H, NCH_2CH_2CN) ppm.

^{13}C NMR (100 MHz, DMSO-d_6) δ 158.3 (CO), 119.3 (CN), 44.0 (NCH_2CH_2CN), 34.5 (NCH_3), 16.0 (NCH_2CH_2CN) ppm.

IR (ATR) ν (cm^{-1}) 3396 (m), 3286 (w), 3182 (m), 2941 (w), 2775 (w), 2247 (w), 1656 (s), 1600 (vs), 1505 (vs), 1443 (m), 1411 (vs), 1361 (m), 1330 (m), 1288 (s), 1222 (m), 1159 (m), 1105 (s), 1066 (s), 1013 (vs), 990 (m), 820 (w), 775 (s), 728 (m).

HRMS (ESI, m/z): calcd for $C_5H_{10}N_3O$, 128.0824 $(M+H)^+$; found, 128.0819.

2.7.5.20 1-Methyl-5,6-dihydrocytosine (2-55a)

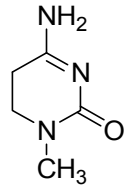

In a 10 mL round-bottom flask equipped with reflux condenser and magnetic stir bar a mixture of urea **2-59a** (1.05 g, 8.26 mmol) and sodium methoxide (0.17 g, 3.15 mmol) in absolute ethanol (10 mL) was refluxed for 30 minutes. The formed colorless

precipitate was filtered off upon cooling and washed with a small amount of cold ethanol. Recrystallization from ethanol yielded **2-55a** as colorless, acid sensitive solid (0.91 g, 7.16 mmol, 86.7 %).

M.p. 224.1 - 225.0 °C (decomp.).

^{1}H NMR (400 MHz, DMSO–d_6) δ 7.49 ppm (s broad, 1 H, NH_aH), 7.26 (s broad, 1 H, NH_bH), 3.19 (t, ^3J 7.0 Hz, 2 H, C(6)H_2), 2.79 (s, 3 H, NCH_3), 2.41 (t, ^3J 7.0 Hz, 2 H, C(5)H_2).

^{13}C NMR (100 MHz, DMSO–d_6) δ 168.3 ppm (C(4)), 159.5 (C(2)), 44.0 (C(6)), 35.0 (NCH_3), 25.8 (C(5)).

IR (ATR) ν (cm^{-1}) 3311 (m), 3016 (w), 2918 (w), 1654 (w), 1616 (s), 1538 (s), 1482 (m), 1464 (m), 1426 (vs), 1394 (s), 1315 (vs), 1273 (vs), 1256 (vs), 1180 (m), 1130 (s), 1071 (w), 1000 (w) 952 (w), 881 (m), 839 (w), 789 (vs), 753 (s), 710 (vs), 608 (s), 572 (vs).

HRMS (ESI, m/z): calcd for $C_5H_{10}N_3O$, 128.0824 $(M+H)^+$; found, 128.0819.

EA (% calcd, % found for $C_5H_9N_3O$): C (47.99, 47.95), H (5.64, 5.50), N (33.58, 33.48).

2.7.5.21 *rac*-2-Methyl-3-(methylamino)-propionitrile (2-63a)

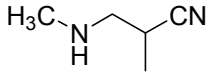

Methacrylonitrile (12.6 mL, 10.1 g, 147 mmol) was added via syringe under ice cooling to ethanolic $MeNH_2$ solution (33%, 6.74 mL, 54.1 mmol) and stirred over night at room temperature. The solvent was removed under reduced pressure and the crude propionitrile **2-63a** was obtained as yellowish oil (1.83 g, 18.6 mmol, 34 %), which was used without further purification.[40]

^{1}H NMR (200 MHz, $CDCl_3$) δ 2.89 – 2.61 ppm (m, 3 H, CH_2CHCN), 2.45 (s, 3 H, NCH_3), 1.30 (d, ^3J 5.9 Hz, 3 H, (CH)CNCH_3).

2.7.5.22 *rac*-1-(2-Cyanopropyl)-1-methylurea (2-59b)

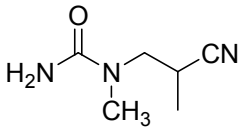

Propionitrile **2-63a** (0.40 g, 4.11 mmol) in water (1.25 mL) was carefully acidified with conc. HCl (0.41 mL, 4.91 mmol) and then added dropwise to a stirred solution of potassium cyanate (0.47 g, 5.75 mmol) in a 25 mL round bottom flask. After stirring over night at room temperature all volatile components were removed at the rotary evaporator and the remaining solid was purified by column chromatography (crude mixture charged on SiO_2, EtOAc/MeOH, 10:1). Title compound **2-59b** was isolated as colorless solid in 59 % yield (0.34 g, 2.41 mmol).[40]

M.p. 127.4 - 128.4 °C (no decomp.). $\mathbf{R_f}$ (EtOAc/MeOH, 10:1) 0.30.
^{1}H NMR (400 MHz, CD_3OD) δ 3.47 (qd, ^2J 14.1 Hz, ^3J 7.6 Hz, 2 H, NCH_2), 3.11 (m, 1 H, CH_2CHCN), 3.02 (s, 3 H, NCH_3), 1.27 (d, ^3J 7.1 Hz, 3 H, (CH)CNCH_3) ppm.
^{13}C NMR (100 MHz, CD_3OD) δ 161.8 (C=O), 123.1 (CN), 52.7 (CH_2), 36.3 (NCH_3), 26.2 (CH), 15.4 (CH_3) ppm.
IR (ATR) ν (cm^{-1}) 3400 (w), 3191 (m), 2943 (w), 2241 (w), 1656 (vs), 1601 (vs), 1504 (vs), 1453 (m), 1437 (m), 1414 (vs), 1381 (m), 1353 (m), 1333 (m), 1293 (s), 1176 (w), 1105 (s), 1075 (s), 1035 (s), 935 (w), 914 (w), 814 (w), 776 (s).
HRMS (ESI, m/z): calcd for $C_6H_{12}N_3O$, 142.0975 $(M+H)^+$; found, 142.0977.

2.7.5.23 4-Amino-1,5-dimethyldihydropyrimidin-2(1*H*)-one (2-55b)

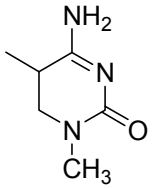

A 10 mL microwave vial was charged with urea **2-59b** (0.32g, 2.27 mmol), sodium methoxide (0.50 g, 0.93 mmol) and EtOH (3 mL). The suspension was heated in the microwave cavity for 30 min under closed vessel conditions (80 °C, 100 W, PowerMAX on). The suspension was filtered after cooling to room temperature and washed with

cold ethanol. After recrystallization from EtOH, **2-55b** was obtained as colorless, acid-sensitive solid (0.27 g, 1.91 mmol, 84 %).[40]

M.p. 183.7 - 185.0 °C (decomp.).

^{1}H NMR (400 MHz, CD_3OD) δ 3.48 (d, ^2J 12.5 Hz, 1 H, C(6)H^b), 3.29 (m, 1 H, C(5)H), 3.05 (d, ^2J 12.5 Hz, 1 H, C(6)H^a), 2.96 (s, 3 H, NCH_3), 1.24 (d, ^3J 6.5 Hz, 3 H, CH_3) ppm.

^{13}C NMR (100 MHz, CD_3OD) δ 174.7 (C(2)), 161.4 (C(4)), 52.0 (C(6)), 36.0 (NCH_3), 32.2 (C(5)), 16.1 (C(5)*C*H_3) ppm.

IR (ATR) ν (cm^{-1}) 2930 (w), 1685 (vs), 1626 (s), 1576 (m), 1493 (s), 1442 (vs), 1393 (vs), 1330 (m), 1292 (s) 1137 (m), 862 (m), 753 (s), 731 (s), 703 (s), 677 (s), 677 (s), 632 (s), 617 (s), 589 (vs), 565 (vs).

HRMS (ESI, m/z): calcd for $C_6H_{11}N_3O$, 141.0897 (M^+); found, 141.0896.

2.7.5.24 *N*,*N*-Dimethyl-*N'*-(1-methyl-2-oxo-1,2-dihydropyrimidin-4-yl)formimidamide (2-52a)

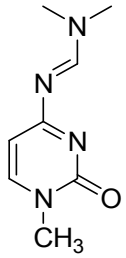

Cytosine (**2-51a**, 0.75 g, 6.75 mmol) was suspended in *N*,*N*-dimethylformamide dimethyl acetal (6 mL) in a dry and clean 10 mL microwave vial and sealed by a septum. Subsequently trifluoroacetic acid (0.1 mL, 0.15 g, 1.32 mmol) was added carefully via syringe and heated in the microwave cavity for two hours (200 W, closed vessel, PowerMAX on) to 120 °C. After cooling to room temperature the dark colored suspension was filtered off, washed with toluene and dried under high vacuum. Analytically pure samples were obtained after recrystallization from toluene as yellowish solid (0.81 g, 4.50 mmol, 67%).

M.p. 193.1 - 196.5 °C (decomp.).

^{1}H NMR (300 MHz, $CDCl_3$) δ 8.80 (s, 1H, NC*H*N$(CH_3)_2$), 7.33 (d, ^3J 6.9 Hz, 1H, C(6)H), 5.99 (d, ^3J 6.9 Hz, 1H, C(5)H), 3.45 (s, 3H, NCH_3), 3.12 (s, 3H, NCHN(C$H_3)_2$), 3.10 (s, 3H, NCHN(C$H_3)_2$) ppm.

^{13}C NMR (75 MHz, $CDCl_3$) δ 172.1 (C(4)), 158.3 (N*C*HN$(CH_3)_2$), 157.5 (C(2)), 146.5 (C(6)), 102.4 (C(5)), 41.3 (NCH_3), 38.0 (NCHN(*C*$H_3)_2$), 35.0 (NCHN(*C*$H_3)_2$) ppm.

IR (ATR) ν (cm^{-1}) 3008 (w), 2951 (w), 2918 (w), 2805 (w), 1654 (m), 1589 (vs), 1576 (s), 1510 (s), 1458 (m), 1440 (m), 1415 (s), 1393 (s), 1347 (s), 1325 (vs), 1269 (s), 1248 (s), 1200 (m), 1172 (m), 1152 (m), 1132 (w), 1098 (vs), 1058 (,), 1040 (m), 1007 (m), 980 (s), 950 (m), 884 (m), 820 (w), 814 (m), 799 (vs), 785 (s), 729 (m), 718 (m).

HRMS (ESI, m/z): calcd for $C_8H_{13}N_4O$, 181.1089 $(M+H)^+$; found, 181.1083.

NMR spectra are in agreement with already published data.[42]

2.7.5.25 1-Methylcytosine (2-50a)

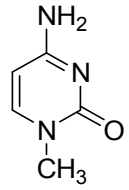

A 10 mL microwave vial equipped with septum and stirring bar was charged with formimidamide **2-52a** (0.50 g, 2.77 mmol) and ethanolic $MeNH_2$ solution (33 wt.%, 5.0 mL). The resulting suspension was heated for 30 minutes to 60 °C under closed-shell conditions (100 W, PowerMAX on). The precipitated colorless solid was filtered off and washed with toluene. After recrystallization from EtOH and drying under high vacuum, 1-methylcytosine (**2-50a**, 0.30 g, 2.40 mmol, 86 %) was obtained as colorless solid.

M.p. 295.5 - 296.2 °C (decomp.).

^{1}H NMR (400 MHz, DMSO-d_6) δ 7.53 (d, ^3J 7.1 Hz, 1H, C(6)H), 6.96 (s broad, 1H, NH^aH), 6.89 (s broad, 1H, NH^bH), 5.59 (d, ^3J 7.1 Hz, 1H, C(5)H), 3.17 (s, 3H, NCH_3) ppm.

^{13}C NMR (100 MHz, DMSO-d_6) δ 166.1 (C(4)), 156.4 (C(2)), 146.6 (C(6)), 92.9 (C(5)), 36.7 (NCH_3) ppm.

IR (ATR) ν (cm^{-1}) 3337 (m), 3129 (m), 2919 (w), 2786 (w), 1968 (w), 1899 (w), 1749 (w), 1619 (vs), 1525 (s), 1485 (s), 1436 (m), 1419 (s), 1370 (s), 1325 (s), 1260 (s), 1209 (s), 1156 (s), 1127 (s), 1050 (m), 987 (m), 949 (m), 807 (m), 799 (s), 781 (vs), 770 (s), 665 (vs).

HRMS (ESI, m/z): calcd for $C_5H_8N_3O$, 126.0667 $(M+H)^+$; found, 126.0662.

EA (% calcd, % found for $C_5H_7N_3O$): C (47.99, 47.95), H (5.64, 5.50), N (33.58, 33.48).

NMR spectra are in agreement with already published data.[42]

2.7.5.26 4-Amino-1,5-dimethylpyrimidin-2(1*H*)-one (2-50b)

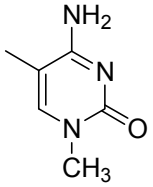

In a pressure tube equipped with stirring bar and screw cap 4-ethoxypyrimidinone **2-54b** (0.48 g, 2.85 mmol) was mixed with excess methanolic ammonia (2 M, 15 mL, 30.0 mmol), closed and heated in the microwave for 16 h and 140 °C (300 W, PowerMAX on). All volatile components were removed under reduced pressure und the residue was purified by column chromatography (SiO_2, DCM/MeOH, 10:1) to give **2-50b** as colorless solid (38 mg, 0.27 mmol, 1 %).[40]

M.p. 280 - 290 °C (under slow decomp.). **R_f** (DCM/MeOH, 10:1) 0.20.

^{1}H NMR (300 MHz, CD_3OD) δ 7.42 (q, ^4J 1.0 Hz, 1 H, C(6)H), 3.35 (s, 3 H, NCH_3), 1.93 (d, ^4J 1.1 Hz, 3 H, C(5)CH_3) ppm.

^{13}C NMR (100 MHz, CD_3OD) δ 167.5 (C(4)), 159.6 (C(2)), 145.7 (C(6)), 103.9 (C(5)), 37.5 (NCH_3), 13.0 (C(5)CH_3) ppm.

IR (ATR) ν (cm^{-1}) 3381 (m), 3095 (m), 2928 (w), 1810 (w), 1668 (s), 1612 (vs), 1517 (s), 1480 (s), 1426 (s), 1394 (s), 1363 (vs), 1326 (s), 1278 (m), 1223 (m), 1161 (s), 1104 (s), 1065 (m), 1044 (m), 909 (m), 879 (w), 781 (vs), 756 (m), 704 (m).

HRMS (ESI, m/z): calcd for $C_6H_{10}N_3O$, 140.0818 $(M+H)^+$; found, 140.0821.

2.7.5.27 *rac-cis*-4-Hydroxytetrahydrofuran-3-yl acetate (2-68a)

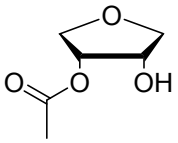

A dry N_2-flushed 100 mL round bottom Schlenk flask, equipped with stirring bar and reflux condenser, was charged with 1,4-anhydroerithritol (**2-66**, 5.20 g, 50.0 mmol), triethyl orthoacetate (13.8 mL, 12.21 g, 75.3 mmol) and 25 mL dry THF. Via syringe, TFA (0.1 mL, 0.15 g, 1.32 mmol) was slowly added to the colorless solution and the mixture was refluxed for 15 min in the microwave (80 °C, 200 W, open vessel, PowerMAX on). After cooling to room temperature the solution was concentrated to a colorless oil, which was redissolved in 20 mL of a mixture of 5 % aqueous oxalic acid and acetone (1:10) and stirred for 30 minutes at ambient temperature. Solid Na_2SO_4 and $NaHCO_3$ was added to remove traces of water and acid. The resulting slurry was filtered over a pad of silica and washed with acetone. The filtrate was concentrated and finally purified by column chromatography (SiO_2, EtOAc) to give acetate **2-68a** as colorless liquid (6.22 g, 42.6 mmol, 89 %)

R_f (EtOAc) 0.56.

^{1}H NMR (300 MHz, $CDCl_3$) δ 5.11 (td, ^3J 4.2 Hz, ^3J 5.62 Hz, 1 H, C(3)H), 4.43 (q, ^3J 5.5 Hz, 1 H, C(4)H), 4.05 (dd, ^2J 10.2 Hz, ^3J 5.8 Hz, 1H, C(2)H^a), 3.96 (dd, ^2J 9.5 Hz, ^3J 5.8 Hz, 1 H, C(5)H^a), 3.81 (dd, ^2J 10.2 Hz, ^3J 4.2 Hz, 1 H C(2)H^b), 3.70 (dd, ^2J 9.4 Hz, ^3J 5.3 Hz, 1 H, C(5)H^b), 2.33 (s br, 1 H, OH), 2.13 (s, 3 H, CH_3) ppm.

^{13}C NMR (75 MHz, $CDCl_3$) δ 170.7 (CO), 73.7 (C(3)HOAc), 72.3 (C(5)H_2), 70.8 (C(4)H), 70.5 (C(2)H_2), 20.8 (CO*C*H_3) ppm.

NMR spectra are in agreement with already published data.[54]

2.7.5.28 *rac*-(*R*)-Tetrahydro-4-oxofuran-3-yl acetate (2-69a)

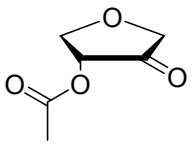

To a solution of acetate **2-68a** (7.17 g, 49.1 mmol) and DCM (150 mL) in a 250 mL round bottom flask was added celite (5.5 g), followed by PCC (20.84 g, 96.7 mmol) at room temperature The dark colored suspension was stirred two days at room temperature and then filtered over a plug of silica and washed with EtOAc. The filtrate was concentrated under reduced pressure and the dark residual oil was purified by column chromatography (SiO_2) using EtOAc as eluent. Ketone **2-69a** was obtained as yellowish liquid in 69 % yield (4.92 g, 34.1 mmol).

R_f (EtOAc) 0.81.

^{1}H NMR (300 MHz, $CDCl_3$) δ 5.18 (t, ^3J 8.0 Hz, 1 H, C(4)H), 4.53 (dd, ^2J 9.8 Hz, ^3J 8.1 Hz, 1 H, C(5)H^a), 4.11 (d, ^2J 17.5 Hz, 1 H, C(2)H^a), 4.07 (d, ^2J 17.5 Hz, 1 H, C(2)H^b), 3.87 (t, ^3J 9.2 Hz, 1 H, C(5)H^b), 2.13 (s, 3 H, CH_3) ppm.

^{13}C NMR (75 MHz, $CDCl_3$) δ 209.0 (C(3)O), 169.8 (CH_3CO), 71.5 (C(4)H), 69.7 ($C(2)H_2$), 69.2 ($C(5)H_2$), 20.4 (CH_3) ppm.

NMR spectra are in agreement with already published data.[54]

2.7.5.29 *rac-cis*-4-(Benzyloxy)tetrahydrofuran-3-ol (2-68b)

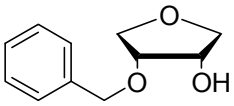

In a 100 mL Schlenk flask equipped with stirring bar and reflux condenser 1,4-anhydroerithritol (**2-66**, 0.52 g, 5.00 mmol) was dissolved in dry THF (50 mL). Under ice cooling NaH (60 % in oil, 0.15 g, 6.25 mmol) was added in small portions, followed by tetrabutylammonium iodide (0.20 g, 0.054 mmol) and benzyl bromide (0.6 mL, 0.86 g, 5.03 mmol). The reaction mixture was refluxed for 4 h under microwave irradiation (100 W, open vessel PowerMAX on). Saturated aqueous NH_4Cl-solution was added to quench the reaction and the mixture was extracted with CH_2Cl_2 (3x 20 mL). The organic phase was dried over $MgSO_4$, filtered and evaporated to

dryness. The residue was purified by column chromatography (SiO_2, PE/EtOAc, 1:1) and benzyl ether **2-68b** was obtained as yellowish oil (0.50 g, 2.57 mmol, 51 %).

R_f (PE/EtOAc, 1:1) 0.43.
^{1}H NMR (400 MHz, $CDCl_3$) δ 7.53 – 7.29 (m, 5 H, Ph), 4.62 (s, 2 H, $PhCH_2$), 4.26 (qd, ^3J 5.4 Hz, ^3J 4.0 Hz, 1 H, C(4)H), 4.07 (q, ^3J 5.5 Hz, 1 H, C(3)H), 3.90 (ddd, ^2J 9.7 Hz, ^3J 5.5 Hz ^4J 2.4 Hz, 2 H, $C(5)H_2$), 3.83 – 3.71 (m, 2 H, $C(2)H_2$), 2.77 (d, ^3J 5.6 Hz, 1 H, OH).
^{13}C NMR (100 MHz, $CDCl_3$) δ 137.1 (Ph, C^q), 128.6 (Ph, C^o), 128.2 (Ph, C^p), 127.9 (Ph, C^m), 78.3 (C(3)H), 73.4 ($C(5)H_2$), 72.6 ($PhCH_2$), 70.3 (C(4)H), 70.0 ($C(2)H_2$) ppm.
IR (ATR) ν (cm^{-1}) 3427 (w), 3064 (w), 3031 (w), 2942 (w), 2870 (w), 1733 (w), 1606 (w), 1586 (w), 1497 (w), 1454 (m), 1403 (w), 1371 (w), 1331 (w), 1247 (w), 1209 (m), 1125 (s), 1066 (vs), 1027 (s), 1005 (s), 904 (s), 736 (vs), 697 (vs).
HRMS (EI, 70 eV, m/z): calcd for $C_{11}H_{14}O_3$, 194.2271 (M^+); found, 194.0945.

2.8 Theoretical Appendix

Geometry optimizations of all systems have been performed at the B3LYP/6-31G(d) level of theory. Thermochemical corrections to 298.15 K have been calculated at the same level of theory using the rigid rotor/harmonic oscillator model. A scaling factor of 0.9806 has been used for this latter part. Single point energies have then been calculated at the MP2(FC)/6-311+G(3df,2p) level. Combination of the MP2 total energies with thermochemical corrections obtained at B3LYP level yield the enthalpies termed as "MP2" in the text.

$$H(HL) = E_{tot}(HL) + H(B3LYP, scal.) - E_{tot}(B3LYP) \qquad (\textbf{eq. 2.10})$$

In the conformationally flexible sugar systems enthalpies and free energies have been calculated as *Boltzmann*-averaged values ($w \geq 1\%$) over all available conformers obtained by a preliminary conformational search using the MM3* force field[79] implemented in *MacroModel 9.7*.[80]
The *Boltzmann*-averaged enthalpies of n conformers are obtained by **eq. 2.11**:

$$w_i = \exp\left(\frac{-\Delta H_{298}}{R\,T}\right) \Big/ \sum_{i=1}^{n} \frac{-\Delta H_{298}}{R\,T}$$

$$<\mathrm{H}_{298}> = \sum_{i=1}^{n} w_\mathrm{i} H_\mathrm{i} \qquad \textbf{(eq. 2.11)}$$

Improved relative energies are obtained using the G3(MP2)-RAD scheme proposed by *Radom et al.*[81] These are based on the same geometries and thermal corrections as the MP2 level:

$$\mathrm{E_{tot}(G3(MP2)\text{-}RAD) = E_{tot}(CCSD(T)/6\text{-}31G(d)//B3LYP/6\text{-}31G(d) + } \\ + \mathit{DE}(\mathrm{G3MP2large}) + \mathit{DE}(\mathrm{HLC}) \qquad \textbf{(eq. 2.12)}$$

$$\mathit{DE}(\mathrm{G3MP2large}) = \mathrm{MP2(FC)/G3MP2large - MP2(FC)/6\text{-}31G(d)} \qquad \textbf{(eq. 2.13)}$$

$$\mathit{DE}(\mathrm{HLC}) = \mathrm{-A\ n(\beta)} \qquad \textbf{(eq. 2.14)}$$

with A = 9.413x10^{-3} au and n(β) representing the β valence electrons, respectively.
G3B3 theory as the most expensive method is used in addition for the prediction of accurate thermochemical data. This composite method is a variant of G3 theory in which structures and zero point vibrational energies are again obtained at the B3LYP/6-31G(d) level of theory, but scaled by a factor of 0.9600:

$$\mathrm{E_{tot}(G3B3) = E_{tot}(QCISD(T)/6\text{-}31G(d)//B3LYP/6\text{-}31G) + } \\ + \mathit{DE}(+) + \mathit{DE}(\mathrm{2df,p}) + \mathit{DE}(\mathrm{G3large}) + \mathit{DE}(\mathrm{HLC}) \qquad \textbf{(eq. 2.15)}$$

$$\mathit{DE}(+) = \mathrm{MP4(FC)/6\text{-}31{+}G(d) - MP4(FC)/6\text{-}31G(d)} \qquad \textbf{(eq. 2.16)}$$

$$\mathit{DE}(\mathrm{2df,p}) = \mathrm{MP4(FC)/6\text{-}31G(2df,p) - MP4(FC)/6\text{-}31G(d)} \qquad \textbf{(eq. 2.17)}$$

$$\mathit{DE}(\mathrm{G3large}) = \mathrm{MP2(Full)/G3large - MP2(FC)/6\text{-}31G(2df,p) - } \\ - \mathrm{MP2(FC)/6\text{-}31{+}G(d) + MP2(FC)/6\text{-}31G(d)} \qquad \textbf{(eq. 2.18)}$$

$$\mathit{DE}(\mathrm{HLC}) = \mathrm{-A\ n(\beta)} \qquad \textbf{(eq. 2.19)}$$

with A = 6.760x10^{-3} au and the number of β valence electrons (n(β)), respectively.

Additional consideration of solvation was included by calculating free energies using the polarizable continuum solvation model in its IEF-PCM,[82] or SMD[60] variant and adding them to the gas phase enthalpies. In case for the IEF-PCM calculations the United Atom Hartree Fock (UAHF) radii in combination with HF/6-31G(d) theory have been used.[83]

Methyl cation affinities are defined as the negative of the reaction enthalpy for attaching the methyl cation CH_3^+ to a Lewis base. These values are obtained from MP2(FC)/6-31+G(d,p)//B98/6-31G(d) single-point calculations on B98/6-31G(d) optimized geometries.[39b]

CCSD(T) calculations have been performed with *MOLPRO*,[84] the geometry optimizations, frequencies and PCM calculations with *Gaussian03 Rev. D.01*.[85] The SMD model is implemented in *Gaussian09 Rev. C.01*.[86]

Table 2.13 Total energies and enthalpies at different levels of theory for the evaluation of the thermodynamics of hydrogenations in Hartree (Enthalpies are scaled by a factor of 0.9806, bold style scaling factor 0.960).

	E_{tot}(B3LYP)	H_{298}(B3LYP)	E_{tot}(MP2)	E_{tot}(G3(MP2)-RAD)	E_{tot}(G3B3)
H_2 (**2-11**)	-1.1754824	-1.162230 **-1.162439**	-1.1627376	-1.1797548	-1.1772139
C_2H_4 (**2-12a**)	-78.5874583	-78.533222 **-78.534261**	-78.3932565	-78.4841764	-78.5584753
C_2H_6 (**2-29a**)	-79.8304175	-79.752210 **-79.753731**	-79.6200539	-79.7231382	-79.7970825
 (**2-12b**)	-117.9075622	-117.823957 **-117.825562**	-117.8188568	-117.7498898	-117.8617142
 (**2-12b_H**)	-119.1442484	-119.036632 **-119.038730**	-118.8387761	-118.9847913	-119.0961374
 (**2-12d**)	-157.2272881	-157.114574 **-157.116735**	-156.8420116	-157.0170527	-157.1664745
 (**2-12d_H**)	-158.4588061	-158.322279 **-158.324922**	-158.0609392	-158.2492313	-158.3980083
 (**2-12e**)	-157.2247688	-157.111721 **-157.113891**	-156.8374652	-157.0132640	-157.1625634
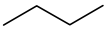 (**2-12e_H**)	-158.4580417	-158.320984 -**158.323644**	-158.0577369	-158.2466245	-158.3954185
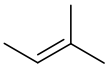 (**2-12c**)	-196.5435871	-196.401462 **-196.404186**	-196.0622753	-196.2797744	-196.4667624
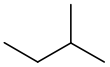 (**2-12c_H**)	-197.7711161	-197.605112 **-197.608325**	-197.2791990	-197.5103125	-197.6965220
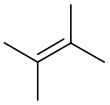 (**2-12f**)	-235.8566952	-235.685358 **-235.688638**	-235.2823275	-235.5982599	-235.8068708
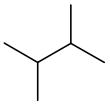 (**2-12f_H**)	-237.0824808	-236.887348 **-236.891117**	-236.4996100	-236.8293853	-237.0370979

Table 2.14 Total energies and enthalpies at different levels of theory for the evaluation of the thermodynamics of hydrogenations in Hartree (Enthalpies are scaled by a factor of 0.9806, bold style scaling factor 0.960).

	E_{tot}(B3LYP)	H_{298}(B3LYP)	E_{tot}(MP2)	E_{tot}(G3(MP2)-RAD)	E_{tot}(G3B3)
 (**2-13a**)	-234.6482949	-234.497636 **-234.500560**	-234.0907903	-234.3346521	-234.5599626
 (**2-13a_H**)	-235.8804308	-235.705840 **-235.709253**	-235.3102004	-235.5671030	-235.7919572
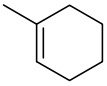 (**2-13b**)	-273.9679943	-273.788360 **-273.791835**	-273.3164436	-273.6020693	-273.8651663
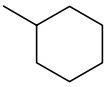 (**2-13b_H**)	-275.1956310	-274.992155 **-274.996117**	-274.5334849	-274.8326090	-275.0949548
 (**2-111a**)	-195.3271387	-195.206463 **-195.208803**	-194.8640872	-195.1120818	-195.2866149
 (**2-111c**)	-194.1010581	-194.004811 **-194.006652**	-193.6543158	-193.8393857	-194.0276521
 (**2-111a_H**)	-196.5570824	-196.421194 **-196.415027**	-196.0714928	-196.3328989	-196.5159818
 (**2-111b**)	-234.6481260	-234.498408 **-234.501299**	-234.0902607	-234.3894031	-234.5990778
 (**2-111b_H**)	-235.8725613	-235.698748 **-235.702131**	-235.3032829	-235.6163327	-235.8252866

Table 2.15 Total energies and enthalpies at different levels of theory for the evaluation of the thermodynamics of hydrogenations in Hartree (Enthalpies are scaled by a factor of 0.9806, bold style scaling factor 0.960).

	E_{tot}(B3LYP)	H_{298}(B3LYP)	E_{tot}(MP2)	E_{tot}(G3(MP2)-RAD)	E_{tot}(G3B3)
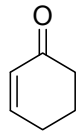 (**2-112**)	-308.6661323	-308.533542 **-308.536069**	-308.0237581	-308.2794877	-308.5495467
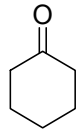 (**2-20**)	-309.8912545	-309.734975 **-309.737983**	-309.2381019	-309.5073166	-309.7767310
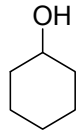 (**2-20_H**)	-311.0903700	-310.910427 **-310.913908**	-310.4336237	-310.7193125	-310.9869990
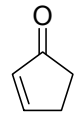 (**2-113**)	-269.3493447	-269.246710 **-269.248654**	-268.8008516	-269.0135973	-269.2465050
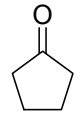 (**2-21**)	-270.7528268	-270.446741 **-270.449158**	-270.1926349	-270.4194450	-270.6514230
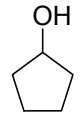 (**2-21H**)	-271.7666701	-271.616566 **-271.619466**	-271.2042119	-471.4471532	-271.6773793
 (**2-14**)	-232.2486519	-232.144431 **-232.146423**	-231.7204866	-231.9272682	-232.1539252
 (**2-113**)	-233.4189363	-233.292286 **-233.294720**	-232.8748896	-233.1044328	-233.3302537

Table 2.16 Total energies and enthalpies at different levels of theory for the evaluation of the thermodynamics of hydrogenations in Hartree (Enthalpies are scaled by a factor of 0.9806, bold style scaling factor 0.960).

	E_{tot}(B3LYP)	H_{298}(B3LYP)	E_{tot}(MP2)	E_{tot}(G3(MP2)-RAD)	E_{tot}(G3B3)
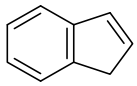 (**2-15**)	-347.7628540	-347.617217 **-347.619981**	-346.9846288	-347.2846510	-347.6260014
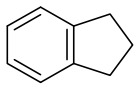 (**2-15_H**)	-348.9881530	-348.818330 **-348.821587**	-348.4301190	-348.5108895	-348.8517656
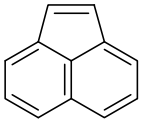 (**2-114**)	-462.0881956	-461.922716 **-461.925828**	-461.0759667	-461.4478683	-461.9049122
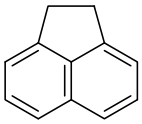 (**2-114_H**)	-463.3149440	-463.125949 **-463.129536**	-462.2860819	-462.6752734	-463.1317287
 (**2-115**)	-230.0205817	-229.947034 **-229.948421**	-229.5720577	-229.7850438	-229.9663352
 (**2-116**)	-231.2217833	-231.124790 **-231.126648**	-230.7544168	-230.9884512	-231.1689219
 (**1-115_H**)	-232.4492889	-232.328040 **-232.330394**	-231.9685290	-232.2167178	-232.3966020
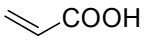 (**2-17a**)	-267.1607213	-267.088420 **-267.089746**	-266.6965087	-266.8689034	-267.0682344
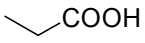 (**2-17a_H**)	-268.3966254	-268.300724 **-268.302524**	-267.9199367	-268.1054945	-268.3041419
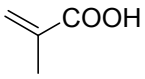 (**2-17**)	-306.4800904	-306.378691 **-306.380572**	-305.9218865	-306.1363530	-306.3732717
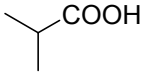 (**2-17_H**)	-307.7102187	-307.585051 **-307.587411**	-307.1410246	-307.3687575	-307.6050132

Table 2.17 Total energies and enthalpies at different levels of theory for the evaluation of the thermodynamics of hydrogenations in Hartree (Enthalpies are scaled by a factor of 0.9806, bold style scaling factor 0.960).

	E_{tot}(B3LYP)	H_{298}(B3LYP)	E_{tot}(MP2)	E_{tot}(G3(MP2)-RAD)	E_{tot}(G3B3)
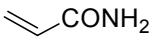 (**2-117a**)	-247.2915608	-247.207201 **-247.208758**	-246.8293544	-247.0088563	-247.2053282
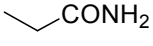 (**2-117a_H**)	-248.5268483	-248.418748 **-248.420784**	-248.0517816	-248.2444024	-248.4402537
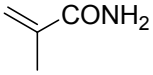 (**2-117**)	-286.6097901	-286.496121 **-286.498241**	-286.0539105	-286.2754358	-286.5095110
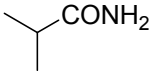 (**2-117_H**)	-287.8410266	-287.703689 **-287.706283**	-287.2737922	-287.5083306	-287.7418860
H_2CO (**2-118**)	-114.5004726	-114.470349 **-114.470898**	-114.3062517	-114.3794877	-114.4595066
CH_3OH (**2-118_H**)	-115.7144073	-115.659682 **-115.660724**	-115.5135682	-115.6022827	-115.6811433
CH_3CHO (**2-18**)	-153.8301215	-153.770515 **-153.771634**	-153.5380635	-153.6538781	-153.7717845
CH_3CH_2OH (**2-18_H**)	-155.0342871	-154.950239 **-154.951848**	-154.7365194	-154.8685341	-154.9850011
$(CH_3)_2CO$ (**2-19**)	-193.1556945	-193.066834 **-193.068510**	-192.7680241	-192.9263032	-193.0819798
$(CH_3)_2HCOH$ (**2-19_H**)	-194.3534513	-194.240614 **-194.242772**	-193.9614458	-194.1361519	-194.4166760

Table 2.18 Experimental reaction enthalpies $\Delta_{hyd}H$ at 298.15 K and 1 atm. Only the starting material is shown, if not otherwise noted leads the reaction to fully saturated products.

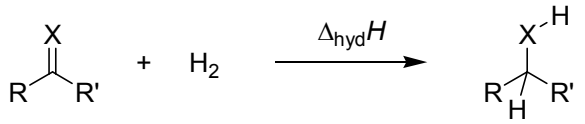

	$\Delta_{hyd}H$(g, exp.)	$\Delta_{rxn}H$(g, exp.)		$\Delta_{hyd}H$(g, exp.)	$\Delta_{rxn}H$(g, exp.)
C_2H_4 (**2-12a**)	-136.31 ± 0.21	-84.0[13]–(+52.4[13])= = **-136.4**	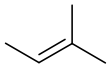 (**2-12c**)	-111.63 ± 0.25	-153.6[13]–(-41.7[13])= = **-111.9**
 (**2-12b**)	-124.98 ± 0.21	-103.8[13]–(+20.0[13])= = **-123.8**	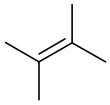 (**2-12f**)	-110.40 ± 0.42	-178.1[13]–(-68.1[13])= = **-110.0**
 (**2-12d**)	-117.78 ± 0.42	-134.2[13]–(-16.9[1][3])= = **-117.3**	 (**2-13a**)	-118.83 ± 0.42	-123.4[13]–(-5.0[13])= = **-118.4**
 (**2-12e**)	-118.53 ± 0.42	-125.7[13]–(-7.1[13])= = **-118.6**	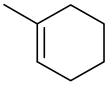 (**2-13b**)	-111.40 ± 0.37	-154.7[13]–(-43.3[18])= = **-111.4**
 (**2-111a**)	-112.13 ± 0.84	-76.4[13]– (+34.0[13])= = **-110.4**	 (**2-116**)	-107.11 ± 2.5	-184.1[13]– (-75.0[17])= = **-109.1**
 (**2-111c**)	-215.10 ± 0.42	-76.4[13]– (+134.3[13])= =**-210.7**	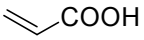 (**2-17a**)	-127.00 ± 0.8	-455.7[13]– (-330.7[25])= = **-125.0**
 (**2-111b**)	-100.80 ± 0.63	-106.2[13]– (-3.8[13])= = **-102.4**	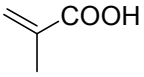 (**2-17**)	-118.00 ± 1.3	-532.1[26]– (-414.8[25])= = **-117.3**
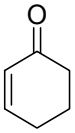 (**2-16**)	-109.20 ± 2.9	-226.1[13]– (-121.9[5])= = **-104.2**	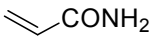 (**2-117a**)	n/a	-259.0[13]– (-130.2[13])= = **-128.8**
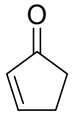 (**2-113**)	-97.10 ± 2.7	-192.1[13]– (-100.3[5])= = **-91.8**	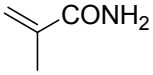 (**2-117**)	n/a	-282.6[14]– (-157.7[15])= = **-124.9**

Table 2.19 Experimental reaction enthalpies $\Delta_{hyd}H$ at 298.15 K and 1 atm. Only the starting material is shown, if not otherwise noted leads the reaction to fully saturated products.

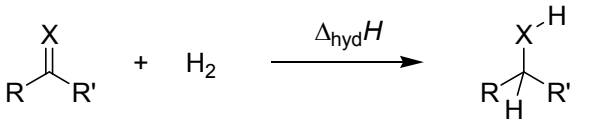

	$\Delta_{hyd}H$(g, exp.)	$\Delta_{rxn}H$(g, exp.)		$\Delta_{hyd}H$(g, exp.)	$\Delta_{rxn}H$(g, exp.)
 (**2-14**)	-205.27 ± 0.63	-123.4[13]– (+82.9[13])= = **-206.3**	H_2CO (**2-118**)	n/a	-201.0[13]– (-108.6[13])= = **-92.4**
 (**2-113**)	-229.62 ± 0.42	-123.4[13]– (+104.6[23])= = **-228.0**	CH_3CHO (**2-18**)	-69.08 ± 0.42	-234.8[13]– (-166.2[13])= = **-68.6**
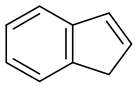 (**2-15**)	-98.90 ± 0.63	-163.51[28]– (-60.33[28])= =**-103.18**	$(CH_3)_2CO$ (**2-19**)	-55.60 ± 0.42	-272.6[13]– (-217.1[13])= = **-55.5**
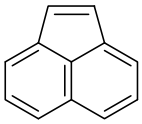 (**2-114**)	-107.90 ± 4.2	155.9[21]– (+263.8[21])= = **-107.9**	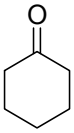 (**2-20**)	-63.51 ± 0.63	-286.2[13]– (-226.1[13])= = **-60.1**
 (**2-115**)	-151.13 ± 0.50	-184.1[13]– (-34.8[13]) = = **-149.3**	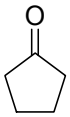 (**2-21**)	-51.25 ±0.63	-242.5[13]– (-192.1[13])= = **-50.4**

Table 2.20 Total energies and enthalpies at different levels of theory for the calculation of methyl cation affinities in Hartree (298.15 K, 1 atm).

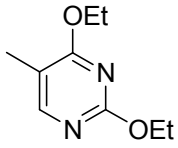 (**2-44b**)	E_{tot}(B98) **H_{298}(B98)**	E_{tot}(MP2)	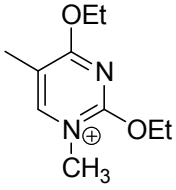 (**2-45b**)	E_{tot}(B98) **H_{298}(B98)**	E_{tot}(MP2)
1	-611.1161887 **-610.873842**	-609.7211139	1	-650.8067520 **-650.520970**	-649.2934405
3	-611.1178437 **-610.875378**	-609.7229677	3	-650.8060519 **-650.520195**	-649.2929392
5	-611.1145925 **-610.872055**	-609.7200057	5	-650.8051392 **-650.519158**	-649.2922938
7	-611.1168212 **-610.874107**	-609.7222598	9	-650.8051247 **-650.519171**	-649.2923529
9	-611.1168454 **-610.874105**	-609.7222944	29	-650.8058740 **-650.519946**	-649.292805
10	-611.1172867 **-610.874756**	-609.7224794			
13	-611.1154176 **-610.872972**	-609.7206011			
21	-611.1147290 **-610.872161**	-609.7202038			
25	-611.1147292 **-610.872163**	-609.7201984			
29	-611.1155970 **-610.873053**	-609.7207422			
31	-611.1174031 **-610.874775**	-609.7227726			
43	-611.1147276 **-610.872174**	-609.7201900	$\oplus CH_3$	-39.4629218 **-39.427474**	-39.3523741

Table 2.21 Total energies and enthalpies of **2-46b** at different levels of theory for the calculation of methyl cation affinities in Hartree (298.15 K, 1 atm).

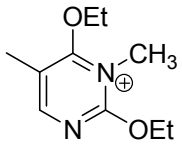 (**2-46b**)	E_{tot}(B98) **H_{298}(B98)**	E_{tot}(MP2)
1	-650.7859814 **-650.500113**	-649.2722425
2	-650.7854689 **-650.500427**	-649.2718718
3	-650.7856311 **-650.499767**	-649.2722384
5	-650.7851171 **-650.499292**	-649.2718906
9	-650.7806036 **-650.495061**	-649.2688269
10	-650.7851724 **-650.499366**	-649.2718622
16	-650.7843227 **-650.498329**	-649.2712649
21	-650.7842847- **-650.498194**	-649.271112
23	-650.7835741 **-650.598033**	-649.270848
25	-650.7854689 **-650.499485**	-649.2718645
27	-650.7805203 **-650.495062**	-649.2690546
31	-650.7810252 **-650.495705**	-649.2694903
33	-650.7853882 **-650.499452**	-649.2718343

Table 2.22 Total energies and enthalpies of pyrimdines in Hartree (enthalpies (in bold) are scaled by a factor of 0.960).

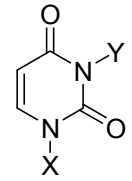	E_{tot}(B3LYP) **H_{298}(B3LYP)**	E_{tot}(G3B3)	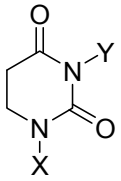	E_{tot}(B3LYP) **H_{298}(B3LYP)**	E_{tot}(G3B3)
X, Y =H (**2-32a**)	-414.8159434 **-414.724772**	-414.6572476	X, Y =H (**2-65a**)	-416.0289298 **-415.914487**	-415.8734750
X = CH_3, Y =H (**2-39a**)	-454.1274497 **-454.007679**	-453.9580397	X = CH_3, Y =H (**2-46a**)	-455.3400379 **-455.197082**	-455.1740712
X, Y =CH_3 (**2-47a**)	-493.4392316 **-493.290815**	-493.2538114	X, Y =CH_3 (**2-49b**)	-494.6502952 **-494.478691**	-494.4677559
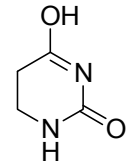 (**2-86a**)	-415.9980937 **-415.884173**	-415.8468161	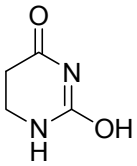 (**2-87a**)	-415.9954471 **-415.881679**	-415.8442822
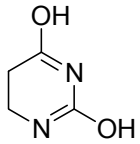 (**2-88a**)	-415.9640223 **-415.850845**	-415.8208951			
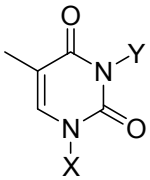	E_{tot}(B3LYP) **H_{298}(B3LYP)**	E_{tot}(G3B3)	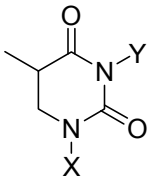	E_{tot}(B3LYP) **H_{298}(B3LYP)**	E_{tot}(G3B3)
X, Y =H (**2-32b**)	-454.1363070 **-454.016574**	-453.9697571	X, Y =H (**2-65b**) 1	-455.3449323 **-455.201904**	-455.1832440
			2	-455.3431628 **-455.200035**	-455.1824297
X = CH_3, Y =H (**2-39b**)	-493.4477629 **-493.299382**	-493.2643087	X = CH_3, Y =H (**2-46b**)	-494.6560380 **-494.484519**	-494.4771760
X, Y =CH_3 (**2-47b**)	-532.7590321 **-532.582022**	-532.5594004	X, Y =CH_3 (**2-49b**)	-533.9660220 **-533.765876**	-533.5706006

Table 2.23 Total energies and enthalpies of 5-fluorouracils in Hartree (enthalpies (in bold) are scaled by a factor of 0.960).

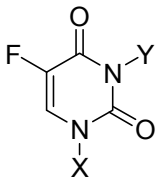	E_{tot}(B3LYP) **H_{298}(B3LYP)**	E_{tot}(G3B3)	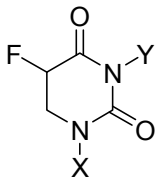	E_{tot}(B3LYP) **H_{298}(B3LYP)**	E_{tot}(G3B3)
X = CH_3, Y =H (**2-39c**)	-533.3476842 **-533.234925**	-553.1453376	X = CH_3, Y =H (**2-39c_H**) 1	-554.5618042 **-554.425684**	-554.3653367
			2	-554.5413167 **-554.425136**	-554.3657365

Table 2.24 Total energies and enthalpies of cytosines in Hartree (enthalpies (in bold) are scaled by a factor of 0.960).

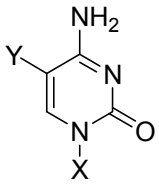	E_{tot}(B3LYP) **H_{298}(B3LYP)**	E_{tot}(G3B3)	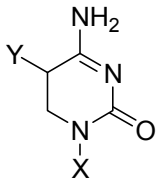	E_{tot}(B3LYP) **H_{298}(B3LYP)**	E_{tot}(G3B3)
X, Y = H (**2-51a**)	-394.9280116 **-394.825402**	-394.7861943	X, Y = H (**2-89**)	-396.1318383 **-396.005912**	-395.9935408
Y = H, X = CH_3 (**2-50a**)	-434.2405254 **-434.109345**	-434.1019629	Y = H, X = CH_3 (**2-55a**)	-435.4426401 **-435.288341**	-435.3070659
Y = F, X = CH_3 (**2-50c**)	-533.4646979 **-533.340568**	-533.2718708	Y = F, X = CH_3 (**2-50c_H**) 1	-534.6720074 **-534.524314**	-534,4848121
			2	-534.6662343 **-534.518614**	-534.4806182
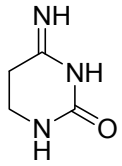 (**2-90**)			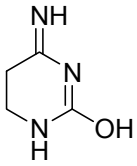 (**2-92**)		
(*Z*)	-396.1382092 **-396.011889**	-396.0003783	(*Z*)	-396.1129394 **-395.987035**	-395.9791404
(*E*)	-396.1396599 **-396.013164**	-396.0018491	(*E*)	-396.1061293 **-395.980325**	-395.9730619
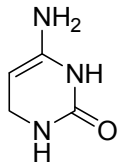 (**2-91**)	-396.1202114 **-395.994175**	-395.9865041			

Table 2.25 Total energies and enthalpies of purines in Hartree (enthalpies (in bold) are scaled by a factor of 0.960).

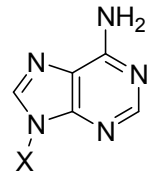	E_{tot}(B3LYP) **H_{298}(B3LYP)**	E_{tot}(G3B3)	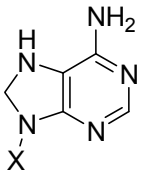	E_{tot}(B3LYP) **H_{298}(B3LYP)**	E_{tot}(G3B3)
X = H (**2-81**)	-467.3181723 **-467.20185**	-467.1472225	X = H (**2-84a**)	-468.4966380 **-468.357056**	-468.3318829
X = CH_3 (**2-78**)	-506.6323182 **-506.487227**	-506.4435314	X = CH_3 (**2-78a**)	-507.8101382 **-507.642105**	-507.6276997
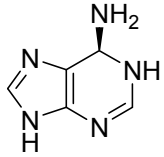 (**2-84b**)	-468.4878746 **-468.348256**	-468.3264731	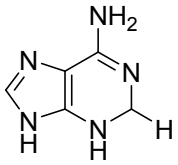 (**2-84c**)	-468.4799493 **-468.341103**	-468.3180097
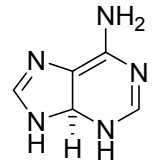 (**2-84e**)	-468.4587445 **-468.320171**	-468.2978730	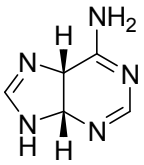 (**2-84d**)	-468.4729584 **-468.334040**	-468.3088378
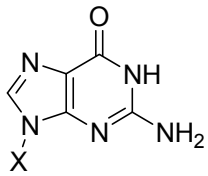	E(B3LYP) **H(B3LYP)**	E(G3B3)	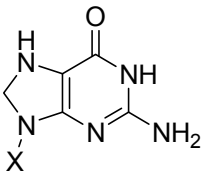	E(B3LYP) **H(B3LYP)**	E(G3B3)
X = H (**2-82**)	-542.5500873 **-542.428237**	-542.3566067	X = H (**2-85a**)	-543.7270992 **-543.582282**	-543.5398687
X = CH_3 (**2-77**)	-581.8638077 **-581.713213**	-581.6526319	X = CH_3 (**2-77a**)	-583.0404668 **-582.867234**	-582.8355398
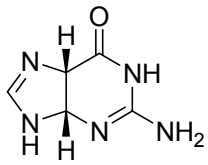 (**2-85b**)	-543.7224349 **-543.577733**	-543.5379056			

Table 2.26 Total energies and enthalpies of selected sugar models in Hartree (enthalpies (in bold) are scaled by a factor of 0.960).

	E_{tot}(B3LYP) **H_{298}(B3LYP)**	E_{tot}(G3B3)		E_{tot}(B3LYP) **H_{298}(B3LYP)**	E_{tot}(G3B3)
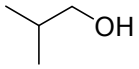 (**2-93_H**) 1	-233.6618379 **-233.522060**	-233.5858929	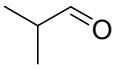 (**2-93**) 1	-232.4580811 **-232.341867**	-232.3718377
2	-233.6625681 **-233.522728**	-233.587655	2	-232.4593316 **-232.343227**	-232.3726607
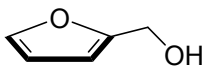 (**2-94_H**) 1	-344.5448134 **-344.438299**		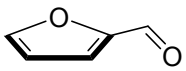 (**2-94**) 1	-343.3463411 **-343.263072**	-343.2136285
2	-344.5454703 **-344.438896**		2	-343.3480306 **-343.264785**	-343.2147455
3	-344.5424526 **-344.436072**				
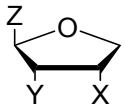	E_{tot}(B3LYP) **H_{298}(B3LYP)**	E_{tot}(G3B3)	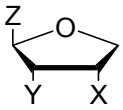	E_{tot}(B3LYP) **H_{298}(B3LYP)**	E_{tot}(G3B3)
X = OH; Y, Z = H (**2-95_H**) 1	-307.6577335 **-307.533899**	-307.5564863	X = O; Y, Z = H (**2-95**)	-306.4597096 **-306.359471**	-306.3464079
2	-307.6575200 **-307.533735**	-307.5563964			
3	-307.6593194 **-307.535268**	-307.5575085			
4	-307.6558074 **-307.532020**	-307.5540924			
X, Y = H;Z = CH_2OH (**2-96_H**) 1	-346.9766601 **-346.823487**	-346.8603195	X, Y = H;Z = CHO (**2-96**) 1	-345.7669591 **-345.637832**	-345.6411485
2	-346.9778207 **-346.824637**	-346.8609139	2	-345.7662732 **-345.637020**	-345.6402498
10	-346.9732134 **-346.820299**	-346.8574578	4	-345.7638860 **-345.634574**	-345.6383975
			6	-345.7642283 **-345.635036**	-345.6392464
X, Y = OH; Z = H (**2-67a_H**)	-382.8706514 **-382.741106**	-382.7510111	X = O; Y = OH; Z = H (**2-67**)	-381.6667793 **-381.561212**	-381.5370053

Table 2.27 Total energies and enthalpies of selected sugar models in Hartree (enthalpies (in bold) are scaled by a factor of 0.960).

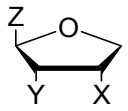	E_{tot}(B3LYP) **H_{298}(B3LYP)**	E_{tot}(G3B3)	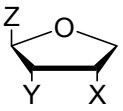	E_{tot}(B3LYP) **H_{298}(B3LYP)**	E_{tot}(G3B3)
X, Y = OH; Z = CH_2OH (**2-97_H**) 1	-497.3972201 **-497.233613**	-497.249057	X = O; Y = OH; Z = CH_2OH (**2-97a**) 1	-496.1930950 **-496.053292**	-496.0336568
2	-497.3966623 **-497.233200**	-497.2486509	2	-496.1914556 **-496.051718**	-496.031876
3	-497.396408 **-497.232676**	-497.2474595	3	-496.1867202 **-496.046887**	-496.0291221
X = OH; Y = O; Z = CH_2OH (**2-97b**) 1	-496.1883279 **-496.048049**	-496.0291077	X, Y = OH; Z = CHO (**2-97c**) 1	-496.1889342 **-496.049109**	-496.030260
2	-496.1867424 **-496.046697**	-496.028740	2	-496.1852568 **-496.045196**	-496.0263953
3	-496.1879531 **-496.047759**	-496.0283554	3	-496.1849254 **-496.045335**	-496.0267649
4	-496.1864131 **-496.046279**	-496.0279963	4	-496.1840697 **-496.044422**	-496.0260538
5	-496.1885387 **-496.048272**	-496.0277656			

Table 2.28 Total energies and enthalpies of selected sugar models in Hartree (enthalpies (in bold) are scaled by a factor of 0.960).

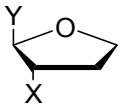	E_{tot}(B3LYP) **H_{298}(B3LYP)**	E_{tot}(G3B3)	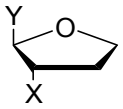	E_{tot}(B3LYP) **H_{298}(B3LYP)**	E_{tot}(G3B3)
X = OH; Y = CH_2OH (**2-98_H**) 1	-422.1838555 **-422.025546**	-422.052147	X = O; Y = CH_2OH (**2-98b**) 1	-420.9859207 **-420.850984**	-420.8410426
2	-422.1831374 **-422.024915**	-422.007705	2	-420.9846209 **-420.849734**	-420.8411106
3	-422.1830676 **-422.024661**	-422.0497733	3	-420.9838296 **-420.848370**	-420.8409192
4	-422.1825881 **-422.024374**	-422.0507128	4	-420.9848834 **-420.850029**	-420.8412873
			5	-420.9827371 **-420.848125**	-420.8409637
X = OH; Y = CHO (**2-98c**) 1	-420.9763079 **-420.841856**	-420.8338108			
2	-420.6743994 **-420.840167**	-420.8336657			
3	-420.9734584 **-420.839131**	-420.8325499			

Table 2.29 Total energies and enthalpies of **2-99** in Hartree (IEF-PCM = IEF-PCM/UAHF/RHF/6-31G(d), SMD/RHF = SMD/RHF/6-31G(d), SMD/B3LYP = SMD/B3LYP/6-31G(d)). Enthalpies (in bold) are scaled by a factor of 0.9806.

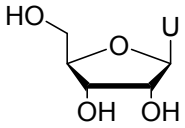 (**2-99**)	E_{tot}(B3LYP) **H_{298}(B3LYP)**	E_{tot}(G3(MP2)-RAD)	ΔG_{solv} (IEF-PCM)	ΔG_{solv} (SMD/RHF)	ΔG_{solv} (SMD/B3LYP)
3	-911.0212169 **-910.781544**	-910.0447029	-0.0373859	-0.1892244	-0.1436952
4	-911.0204214 **-910.780870**	-910.0424546	-0.0371309	-0.1860212	-0.1406832
5	-911.0228334 **-910.783386**	-910.0434866	-0.0318721	-0.1741648	-0.1300220
7	-911.0237487 **-910.784341**	-910.0454086	-0.0338641	-0.1630256	-0.1231536
8	-911.0211417 **-910.781848**	-910.0412588	-0.0344537	-0.1782923	-0.1316156
12	-911.0150796 **-910.775838**	-910.0389124	-0.0431070	-0.2010330	-0.1574957
14	-911.0193592 **-910.779999**	-910.0425980	-0.0370991	-0.1776230	-0.1378944
15	-911.0206915 **-910.781176**	-910.0434705	-0.0382624	-0.1910251	-0.1448904
20	-911.0208040 **-910.781488**	-910.0411089	-0.0367644	-0.1776230	-0.1331455
26	-911.0217813 **-910.782356**	-910.0423789	-0.0362226	-0.0182627	-0.1334802
30	-911.0177153 **-910.778192**	-910.0396637	-0.0398879	-0.1987701	-0.1499580
32	-911.0140701 **-910.774939**	-910.0380209	-0.0418639	-0.2042999	-0.1589619
38	-911.0196752 **-910.780438**	-910.0408434	-0.0365413	-0.1746907	-0.1308188
46	-911.0089992 **-910.769985**	-910.0326888	-0.0472344	-0.2263713	-0.0179918
52	-911.0149713 **-910.775724**	-910.0389055	-0.0414655	-0.2020369	-0.1566830

Table 2.30 Total energies and enthalpies of **2-100a** in Hartree (IEF-PCM = IEF-PCM/UAHF/RHF/6-31G(d), SMD/RHF = SMD/RHF/6-31G(d), SMD/B3LYP = SMD/B3LYP/6-31G(d)). Enthalpies (in bold) are scaled by a factor of 0.9806.

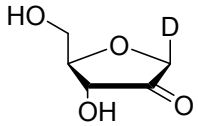 (**2-100a**)	E_{tot}(B3LYP) **H_{298}(B3LYP)**	E_{tot}(G3(MP2)-RAD)	ΔG_{solv} (IEF-PCM)	ΔG_{solv} (SMD/RHF)	ΔG_{solv} (SMD/B3LYP)
3	-911.0263257 **-910.787378**	-910.0404475	-0.0407803	-0.0450671	-0.0330513
4	-911.0273771 **-910.788420**	-910.0418003	-0.0425811	-0.0453539	-0.0333541
12	-911.0235957 **-910.784703**	-910.0388268	-0.0427404	-0.0467085	-0.0343899
14	-911.0251896 **-910.786278**	-910.0405951	-0.0425811	-0.0464854	-0.0343262
20	-911.0210149 **-910.782422**	-910.0377503	-0.0450990	-0.0493061	-0.0367963
22	-911.0193315 **-910.780773**	-910.0358254	-0.0456089	-0.0494973	-0.0368122
26	-911.0238742 **-910.784929**	-910.0377293	-0.0394417	-0.0475212	-0.0344378
28	-911.0239698 **-910.785123**	-910.0390913	-0.0408122	-0.0456408	-0.0334816
29	-911.0198328 **-910.780921**	-910.0360959	-0.0454495	-0.0492423	-0.0369078
32	-911.0215563 **-910.782713**	-910.0367788	-0.0441747	-0.0486049	-0.0362545
35	-911.0214100 **-910.782748**	-910.0373742	-0.0457523	-0.0502144	-0.0374497
36	-911.0197080 **-910.781074**	-910.0354080	-0.0463738	-0.0504535	-0.0374975

Table 2.31 Total energies and enthalpies of **2-100b** in Hartree (IEF-PCM = IEF-PCM/UAHF/RHF/6-31G(d), SMD/RHF = SMD/RHF/6-31G(d), SMD/B3LYP = SMD/B3LYP/6-31G(d)). Enthalpies (in bold) are scaled by a factor of 0.9806.

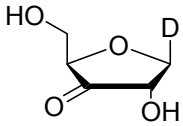 (**2-100b**)	E_{tot}(B3LYP) **H_{298}(B3LYP)**	E_{tot}(G3(MP2)-RAD)	ΔG_{solv} (IEF-PCM)	ΔG_{solv} (SMD/RHF)	ΔG_{solv} (SMD/B3LYP)
5	-911.0304761 **-910.791385**	-910.0440071	-0.0390433	-0.0436010	-0.0317605
1	-911.0298031 **-910.790674**	-910.0429591	-0.0390911	-0.0434575	-0.0314896
31	-911.0225138 **-910.783658**	-910.0365456	-0.0455611	-0.0492742	-0.0359198
43	-911.0242865 **-910.785195**	-910.0374874	-0.0439675	-0.0473778	-0.0346290
11	-911.0252970 **-910.785893**	-910.0396597	-0.0430910	-0.0449874	-0.0335931
41	-911.0247679 **-910.785427**	-910.0396816	-0.0432026	-0.0466607	-0.0350593
12	-911.0223091 **-910.783331**	-910.0340028	-0.0452105	-0.0475212	-0.0348362
29	-911.0223898 **-910.783494**	-910.0363806	-0.0446687	-0.0491786	-0.0358083
23	-911.0179882 **-910.779506**	-910.0315295	-0.0483499	-0.0473459	-0.0355214
22	-911.0212167 **-910.782287**	-910.0337362	-0.0454177	-0.0481587	-0.0351549
16	-911.0232252 **-910.783904**	-910.0370678	-0.0437125	-0.0454495	-0.0338162
24	-911.0226481 **-910.783776**	-910.0358720	-0.0437444	-0.0483180	-0.0352346
15	-911.0235880 **-910.784849**	-910.0386462	-0.0426289	-0.0472981	-0.0351071
45	-911.0218448 **-910.782803**	-910.0353906	-0.0446687	-0.0481587	-0.0353461
18	-911.0231484 **-910.784448**	-910.0384192	-0.0429317	-0.0471706	-0.0350433
26	-911.0227501 **-910.783841**	-910.0360538	-0.0434257	-0.0482384	-0.0352346
14	-911.0228695 **-910.784094**	-910.0373376	-0.0431388	-0.0489395	-0.0363341

Table 2.32 Total energies and enthalpies of **2-100c** in Hartree (IEF-PCM = IEF-PCM/UAHF/RHF/6-31G(d), SMD/RHF = SMD/RHF/6-31G(d), SMD/B3LYP = SMD/B3LYP/6-31G(d)). Enthalpies (in bold) are scaled by a factor of 0.9806.

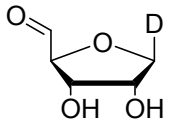 (**2-100c**)	E_{tot}(B3LYP) **H_{298}(B3LYP)**	E_{tot}(G3(MP2)-RAD)	ΔG_{solv} (IEF-PCM)	ΔG_{solv} (SMD/RHF)	ΔG_{solv} (SMD/B3LYP)
3	-911.0272732 **-910.788350**	-910.0413697	-0.0343581	-0.0393620	-0.0273940
4	-911.0266050 **-910.787656**	-910.0402824	-0.0351867	-0.0405094	-0.0282386
1	-911.0242927 **-910.785713**	-910.0379924	-0.0364616	-0.0401747	-0.0280474
2	-911.0239887 **-910.785282**	-910.0369889	-0.0366688	-0.0411468	-0.0285733
5	-911.0218560 **-910.783048**	-910.0381677	-0.0355533	-0.0408600	-0.0292745
9	-911.0182163 **-910.779527**	-910.0360793	-0.0441587	-0.0476647	-0.0356011
22	-911.0172687 **-910.778431**	-910.0339739	-0.0450511	-0.0484933	-0.0355692
29	-911.0185799 **-910.779921**	-910.0358754	-0.0430910	-0.0465332	-0.0347087
10	-911.0169287 **-910.778293**	-910.0343487	-0.0442384	-0.0476168	-0.0353939
12	-911.0175012 **-910.778900**	-910.0345217	-0.0434257	-0.0464216	-0.0344856
23	-911.0171919 **-910.778382**	-910.0345503	-0.0438559	-0.0482702	-0.0356330
24	-911.0152672 **-910.776495**	-910.0321516	-0.0450033	-0.0515212	-0.0380712
17	-911.0142450 **-910.775577**	-910.0305657	-0.0455133	-0.0525092	-0.0388042
18	-911.0166327 **-910.777872**	-910.0337989	-0.0431070	-0.0490352	-0.0359676

Table 2.33 Total energies and enthalpies of 2'-desoxyuridine derivatives in Hartree (IEF-PCM = IEF-PCM/UAHF/RHF/6-31G(d), SMD/RHF = SMD/RHF/6-31G(d), SMD/B3LYP = SMD/B3LYP/6-31G(d)). Enthalpies (in bold) are scaled by a factor of 0.9806.

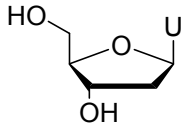 (**2-102**)	E_{tot}(B3LYP) **H_{298}(B3LYP)**	E_{tot}(G3(MP2)-RAD)	ΔG_{solv} (IEF-PCM)	ΔG_{solv} (SMD/RHF)	ΔG_{solv} (SMD/B3LYP)
16	-835.8095887 **-835.575484**	-834.8921372	-0.0357286	-0.041114948	-0.0306290
4	-835.8094814 **-835.575384**	-834.8921402	-0.0356967	-0.041130884	-0.0307087
17	-835.8064828 **-835.572462**	-834.8885524	-0.0372744	-0.043887817	-0.0328123
11	-835.8057103 **-835.571914**	-834.8891138	-0.0368760	-0.041290244	-0.0317446
19	-835.7999511 **-835.566409**	-834.8839495	-0.0416568	-0.046660685	-0.0360314
25	-835.8045845 **-835.570772**	-834.8873804	-0.0372903	-0.042134854	-0.0322386
20	-835.8019848 **-835.568330**	-834.8846159	-0.0397285	-0.044652746	-0.0344696
8	-835.8035680 **-835.569370**	-834.8873750	-0.0382305	-0.044079049	-0.0330035
21	-835.8014477 **-835.567699**	-834.8841822	-0.0400472	-0.045194571	-0.0349477
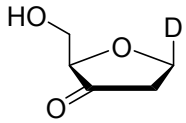 (**2-102a**)	E_{tot}(B3LYP) **H_{298}(B3LYP)**	E_{tot}(G3(MP2)-RAD)	ΔG_{solv} (IEF-PCM)	ΔG_{solv} (SMD/RHF)	ΔG_{solv} (SMD/B3LYP)
4	-835.8203423 **-835.586613**	-834.8924698	-0.0392982	-0.0426607	-0.0305653
5	-835.8179974 **-835.584470**	-834.8907488	-0.0350274	-0.0423102	-0.0308521
10	-835.8179955 **-835.584187**	-834.8903383	-0.0385811	-0.0420870	-0.0305175
6	-835.8173347 **-835.583937**	-834.8913796	-0.0369556	-0.0422783	-0.0308840
3	-835.8164597 **-835.582940**	-834.8880846	-0.0352027	-0.0388998	-0.0278243
15	-835.8155124 **-835.581893**	-834.8891498	-0.0410990	-0.0441906	-0.0323183

Table 2.34 Total energies and enthalpies of **2-102b** in Hartree (IEF-PCM = IEF-PCM/UAHF/RHF/6-31G(d), SMD/RHF = SMD/RHF/6-31G(d), SMD/B3LYP = SMD/B3LYP/6-31G(d)). Enthalpies (in bold) are scaled by a factor of 0.9806.

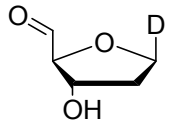 (**2-102b**)	E_{tot}(B3LYP) **H_{298}(B3LYP)**	E_{tot}(G3(MP2)-RAD)	ΔG_{solv} (IEF-PCM)	ΔG_{solv} (SMD/RHF)	ΔG_{solv} (SMD/B3LYP)
3	-835.8074053 **-835.574272**	-834.8833873	-0.0378321	-0.0445731	-0.032127029
11	-835.8073201 **-835.574091**	-834.8827890	-0.0369716	-0.0444456	-0.031903925
10	-835.8074380 **-835.574075**	-834.8834016	-0.0380234	-0.0399835	-0.028812336
7	-835.8064560 **-835.573308**	-834.8831734	-0.0408281	-0.0421508	-0.030772467
12	-835.8059451 **-835.572852**	-834.8808612	-0.0349636	-0.0396488	-0.027935854
9	-835.8059253 **-835.572737**	-834.8818252	-0.0361110	-0.0400154	-0.028844208
8	-835.8058083 **-835.572678**	-834.8824767	-0.0372266	-0.0419277	-0.030135026
2	-835.8054852 **-835.572416**	-834.8823594	-0.0418480	-0.0429476	-0.031330228
5	-835.8053664 **-835.571870**	-834.8831479	-0.0342465	-0.0394576	-0.028541423

Table 2.35 Total energies and enthalpies of **2-101a** in Hartree (SMD/B3LYP = SMD/B3LYP/6-31G(d)). Enthalpies (in bold) are scaled by a factor of 0.9806.

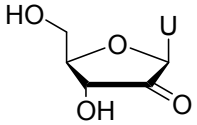 (**2-101a**)	E_{tot}(B3LYP) **H_{298}(B3LYP)**	E_{tot}(G3(MP2)-RAD)	ΔG_{solv} (SMD/B3LYP)
1	-909.8061657 **-909.591280**	-908.8155227	-0.0323183
2	-909.8123978 **-909.597240**	-908.8223991	-0.0319836
3	-909.8081638 **-909.593056**	-908.8173047	-0.0331788
5	-909.8096299 **-909.594523**	-908.8208075	-0.0328123
19	-909.8081346 **-909.593092**	-908.8190508	-0.0322386
20	-909.8065770 **-909.591410**	-908.8178018	-0.0344378

Table 2.36 Total energies and enthalpies of **2-5** in Hartree (SMD/B3LYP = SMD/B3LYP/6-31G(d)). Enthalpies (in bold) are scaled by a factor of 0.9806.

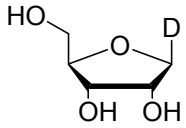 (**2-5**)	E_{tot}(B3LYP) **H_{298}(B3LYP)**	E_{tot}(G3(MP2)-RAD)	ΔG_{solv} (SMD/B3LYP)
1	-912.2346594 **-911.971495**	-911.2609410	-0.0309000
2	-912.2352624 **-911.972025**	-911.2616209	-0.0314099
4	-912.2358271 **-911.972564**	-911.2613678	-0.0303900
5	-912.2348283 **-911.971566**	-911.2600266	-0.0328282
6	-912.2337086 **-911.970528**	-911.2593800	-0.0315533
7	-912.2337596 **-911.970552**	-911.2587305	-0.0327007
17	-912.2327437 **-911.969646**	-911.2580174	-0.0328760
21	-912.2326890 **-911.969415**	-911.2589268	-0.0350274
22	-912.2327064 **-911.969505**	-911.2575578	-0.0331469
24	-912.2340577 **-911.970624**	-911.2614736	-0.0358401
25	-912.2348474 **911,971416**	-911.2627737	-0.0358401
26	-912.2332681 **-911.970125**	-911.2589568	-0.0330354
30	-912.2336469 **-911.970339**	-911.2604294	-0.0348521
31	-912.2326054 **-911.969529**	-911.2578578	-0.0337525
34	-912.2337008 **-911.970465**	-911.2605727	-0.0359039
45	-912.2341964 **-911.970938**	-911.2615065	-0.0358242

Table 2.37 Total energies and enthalpies of cytosine derivatives in Hartree (SMD/B3LYP = SMD/B3LYP/6-31G(d)). Enthalpies (in bold) are scaled by a factor of 0.960.

	E_{tot}(B3LYP) **H_{298}(B3LYP)**	E_{tot}(G3B3)	ΔG_{solv} (SMD/B3LYP)
C_2H_6 (**2-29a**)	-79.8304175 **-79.753731**	-79.7203960	+0.0029004
C_2H_4 (**2-12a**)	-78.5874583 **-78.534261**	-78.5052780	+0.0022789
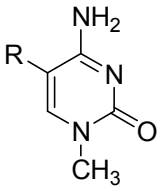	E_{tot}(B3LYP) **H_{298}(B3LYP)**	E_{tot}(G3B3)	ΔG_{solv} (SMD/B3LYP)
R = H (**2-50a**)	-434.2405254 **-434.109345**	-434.2331433	-0.0257367
R = CH_3 (**2-50b**)	-473.5584583 **-473.398611**	-473.3854549	-0.0251470
R = CH_2OH (**2-50d**) 1	-548.7651036 **-548.599088**	-548.5753134	-0.0303581
2	-548.7677647 **-548.601634**	-548.5769431	-0.0295773
3	-548.7608470 **-548.594935**	-548.5722890	-0.0312984
4	-548.7593125 **-548.593748**	-548.5709093	-0.0322545
R = CHO (**2-50e**) 1	-547.5770463 **-547.434425**	-547.3731338	-0.0243981
2	-547.5667770 **-547.424454**	-547.3636529	-0.0272506
R = COOH (**2-50f**) 1_cis	-622.8237269 **-622.675041**	-622.6018475	-0.0263582
2_cis	-622.8198331 **-622.671191**	-622.5977883	-0.0274100
1_trans	-622.8085409 **-622.660175**	-622.5884452	-0.0341509
2_trans	-622.8076541 **-622.658666**	-622.5868574	-0.0308043
R = COO^- (**2-50g**)	-622.2773582 **-622.142163**	-622.0695262	-0.1050025

Table 2.38 Total energies and enthalpies of cytosine derivatives in Hartree (SMD/B3LYP = SMD/B3LYP/6-31G(d)). Enthalpies (in bold) are scaled by a factor of 0.960.

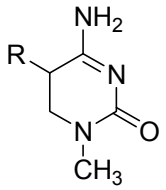	E_{tot}(B3LYP) **H_{298}(B3LYP)**	E_{tot}(G3B3)	ΔG_{solv} (SMD/B3LYP)
R = H (**2-50a_H**)	-435.4426401 **-435.288341**	-435.4613650	-0.0279677
R = CH_3 (**2-50b_H**) 1	-474.7566525 **-474.573777**	-474.5891094	-0.0263104
2	-474.7560883 **-474.573253**	-474.5879469	-0.0273303
R = CH_2OH (**2-50d_H**) 1	-549.9633330 **-549.774349**	-549.7793027	-0.0304537
2	-549.9611157 **-549.772345**	-549.7783167	-0.0324617
3	-549.9646092 **-549.775688**	-549.7792427	-0.0323979
4	-549.9581624 **-549.769483**	-549.7746694	-0.0346768
5	-549.9612629 **-549.772146**	-549.7766523	-0.0323342
6	-549.9633517 **-549.774208**	-549.7785414	-0.0314577
7	-549.9612243 **-549.772188**	-549.7765387	-0.0318402
9	-549.9590339 **-549.770231**	-549.7757985	-0.0339278
10	-549.9615959 **-549.772784**	-549.7779405	-0.0321111
11	-549.9544567 **-549.766001**	-549.7716961	-0.0372584
R = CHO (**2-50e_H**) 1	-548.7510620 **-548.586124**	-548.5563421	-0.0308362
2	-548.7553955 **-548.590231**	-548.5606182	-0.0276331
3	-548.7531804 **-548.588270**	-548.5594703	-0.0307087
4	-548.7565413 **-548.591506**	-548.5602137	-0.0285574

Table 2.39 Total energies and enthalpies of cytosine derivatives in Hartree (SMD/B3LYP = SMD/B3LYP/6-31G(d)). Enthalpies (in bold) are scaled by a factor of 0.960.

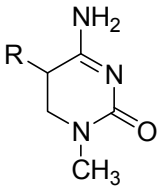	E_{tot}(B3LYP) **H_{298}(B3LYP)**	E_{tot}(G3B3)	ΔG_{solv} (SMD/B3LYP)
R = COOH (**2-50f_H**) 1_cis	-624.0062617 **-623.834764**	-623.7919499	-0.0330354
2_cis	-624.0053481 **-623.833541**	-623.7914946	-0.0316011
3_cis	-624.0052870 **-623.833673**	-623.7922157	-0.0329079
4_cis	-624.0026586 **-623.831009**	-623.7887904	-0.0328442
1_trans	-623.9957156 **-623.824275**	-623.7825411	-0.0361429
2_trans	-624.0052232 **-623.833458**	-623.7929951	-0.0309000
3_trans	-624.0000148 **-623.828296**	-623.7871639	-0.0349636
4_trans	-623.9958690 **-623.824099**	-623.7822311	-0.0347405
R = COO^- (**2-50g_H**) 1	-623.4759175 **-623.317740**	-623.2720404	-0.1017356
2	-623.4723049 **-623.313705**	-623.2670067	-0.1006041
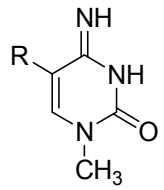	E_{tot}(B3LYP) **H_{298}(B3LYP)**	E_{tot}(G3B3)	ΔG_{solv} (SMD/B3LYP)
R = H (**2-110a**) 1_z	-434.2342507 **-434.102731**	-434.0760307	-0.0183902
1_e	-434.2371023 **-434.105420**	-434.0786424	-0.0168125
R =CH_3 (**2-110b**) 1_z	-473.5546156 **-473.394427**	-473.3819639	-0.0163026
1_e	-473.5562119 **-473.395874**	-473.3838536	-0.0159998

Table 2.40 Total energies and enthalpies of cytosine derivatives in Hartree (SMD/B3LYP = SMD/B3LYP/6-31G(d)). Enthalpies (in bold) are scaled by a factor of 0.960..

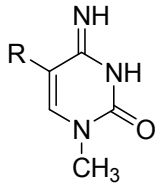	E_{tot}(B3LYP) **H_{298}(B3LYP)**	E_{tot}(G3B3)	ΔG_{solv} (SMD/B3LYP)
R = CH_2OH (**2-110d**) 1_z	-548.7631447 **-548.596750**	-548.5740513	-0.0230594
3_z	-548.7536463 **-548.587654**	-548.5661059	-0.0287645
5_z	-548.7581435 **-548.592271**	-548.5699223	-0.0221829
1_e	-548.7573473 **-548.591157**	-548.5695303	-0.0257207
3_e	-548.7601500 **-548.593795**	-548.5712023	-0.0244937
4_e	-548.7573997 **-548.591190**	-548.5702179	-0.0254339
5_e	-548.7576094 **-548.591633**	-548.5701593	-0.0239200
R = CHO (**2-110e**) 1_z	-547.5519348 **-547.409436**	-547.3509995	-0.0297685
2_z	-547.5614317 **-547.418610**	-547.3595335	-0.0213543
1_e	-547.566174 **-547.422983**	-547.3641067	-0.0218642
2_e	-547.5624143 **-547.419536**	-547.3601792	-0.0206531

Table 2.41 Total energies and enthalpies of cytosine derivatives in Hartree (SMD/B3LYP = SMD/B3LYP/6-31G(d)). Enthalpies (in bold) are scaled by a factor of 0.960.

	E_{tot}(B3LYP) **H_{298}(B3LYP)**	E_{tot}(G3B3)	ΔG_{solv} (SMD/B3LYP)
R = COOH (**2-110f**) 1_cis_z	-622.7989419 **-622.650227**	-622.5795887	-0.0308362
3_cis_z	-622.8017297 **-622.652806**	-622.5817134	-0.0282068
1_trans_z	-622.7861378 **-622.637654**	-622.5693547	-0.0366529
3_trans_z	-622.8159662 **-622.667168**	-622.5955925	-0.0259757
1_trans_e	-622.7978767 **-622.648931**	-622.5793543	-0.0310912
3_trans_e	-622.8003044 **-622.651184**	-622.5810062	-0.0267407
1_cis_e	-622.8133855 **-622.664080**	-622.5929472	-0.0231232
3_cis_e	-622.8121212 **-622.662792**	-622.5912299	-0.0226292
R = COO^- (**2-110g**) 1_z	-622.2335030 **-622.098321**	-622.0282506	-0.1209066
1_e	-622.2630732 **-622.126877**	-622.0560384	-0.1033133
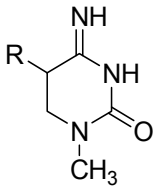	E_{tot}(B3LYP) **H_{298}(B3LYP)**	E_{tot}(G3B3)	ΔG_{solv} (SMD/B3LYP)
R = H (**2-110a_H**) 1_z	-435.4492329 **-435.294442**	-435.2940215	-0.0193304
1_e	-435.4505804 **-435.295615**	-435.2953803	-0.0190595

Table 2.42 Total energies and enthalpies of cytosine derivatives in Hartree (SMD/B3LYP = SMD/B3LYP/6-31G(d)). Enthalpies (in bold) are scaled by a factor of 0.960.

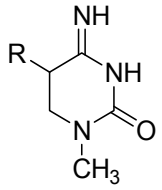	E_{tot}(B3LYP) **H_{298}(B3LYP)**	E_{tot}(G3B3)	ΔG_{solv} (SMD/B3LYP)
R = CH_3 (**2-110b_H**) 1_z	-474.7632422 **-474.579845**	-474.5965349	-0.0174659
2_z	-474.7645077 **-474.581175**	-474.5968633	-0.0174659
1_e	-474.7644661 **-474.580939**	-474.5976662	-0.0173065
2_e	-474.7651597 **-474.581630**	-474.5977392	-0.0183264
R = CHO (**2-110e_H**) 1_z	-548.7622965 **-548.596836**	-548.5682272	-0.0208921
2_z	-548.7622494 **-548.596775**	-548.5691788	-0.0206531
1_e	-548.7594360 **-548.593968**	-548.5656983	-0.0229957
2_e	-548.7596258 **-548.594083**	-548.5664423	-0.0216889
3_e	-548.7615166 **-548.596013**	-548.5686101	-0.0220555
4_e	-548.7600351 **-548.594527**	-548.5650274	-0.0225654
R = COO^- (**2-110g_H**) 1_z	-623.4490713 **-623.290738**	-623.2501482	-0.1166517
2_z	-623.4565970 **-623.298097**	-623.2593895	-0.1112335
1_e	-623.4725575 **-623.290738**	-623.2708916	-0.1015444
2_e	-623.4673347 **-623.298097**	-623.2652818	-0.1008910

Table 2.43 Total energies and enthalpies of 5-hydroxymethylcytosine in Hartree (SMD/B3LYP = SMD/B3LYP/6-31G(d)). Enthalpies (in bold) are scaled by a factor of 0.960.

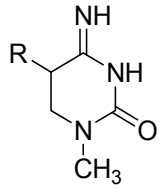	E_{tot}(B3LYP)	**H_{298}(B3LYP)**	E_{tot}(G3B3)	ΔG_{solv} (SMD/B3LYP)
R = CH_2OH (**2-110d_H**) 1_z	-549.9618560	**-549.772965**	-549.7802626	-0.0288761
2_z	-549.9677169	**-549.778465**	-549.7857887	-0.0245893
3_z	-549.9756513	**-549.786123**	-549.7900967	-0.0229638
4_z	-549.9690127	**-549.779891**	-549.7840751	-0.0239678
5_z	-549.9743994	**-549.784849**	-549.7897560	-0.0221033
6_z	-549.9718822	**-549.782434**	-549.7870924	-0.0233144
9_z	-549.9652735	**-549.776068**	-549.7825313	-0.0254180
10_z	-549.9672040	**-549.777891**	-549.7847642	-0.0244618
11_z	-549.9639815	**-549.774885**	-549.7822338	-0.0256092
1_e	-549.9671276	**-549.777880**	-549.7847945	-0.0252267
2_e	-549.9689878	**-549.779618**	-549.7869038	-0.0243502
3_e	-549.9687916	**-549.779342**	-549.7845836	-0.0258642
4_e	-549.9677159	**-549.778436**	-549.7848790	-0.0256411
5_e	-549.9698354	**-549.780339**	-549.7861214	-0.0251152
6_e	-549.9706906	**-549.781107**	-549.7870163	-0.0239359
7_e	-549.9665252	**-549.777331**	-549.7837855	-0.0269159
9_e	-549.9661910	**-549.776832**	-549.7831341	-0.0252745
10_e	-549.9681360	**-549.778728**	-549.7854841	-0.0244777
11_e	-549.9637211	**-549.774597**	-549.7817262	-0.0270594

Table 2.44 Total energies and enthalpies of 5-carboxylcytosine in Hartree (SMD/B3LYP = SMD/B3LYP/6-31G(d)). Enthalpies (in bold) are scaled by a factor of 0.960.

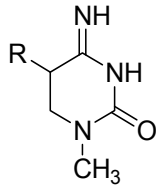	E_{tot}(B3LYP)	**H_{298}(B3LYP)**	E_{tot}(G3B3)	ΔG_{solv} (SMD/B3LYP)
R = COOH (**2-110f_H**) 1_cis_z	-624.0102209	**-623.838337**	-623.7979038	-0.0279996
2_cis_z	-624.0100184	**-623.838150**	-623.7989956	-0.0268044
1_trans_z	-624.0188390	**-623.847137**	-623.8042210	-0.0258323
2_trans_z	-624.0023838	**-623.830493**	-623.7918446	-0.0304378
3_trans_z	-624.0154545	**-623.843355**	-623.8017670	-0.0246212
1_trans_e	-624.0025596	**-623.830705**	-623.7905745	-0.0311709
2_trans_e	-624.0072582	**-623.835083**	-623.7964036	-0.0270594
3_trans_e	-624.0070404	**-623.835020**	-623.7958151	-0.0274896
4_trans_e	-624.0032904	**-623.831208**	-623.7912226	-0.0284617
1_cis_e	-624.0125869	**-623.840480**	-623.7993073	-0.0258642
2_cis_e	-624.0090833	**-623.836963**	-623.7966272	-0.0260554
3_cis_e	-624.0110725	**-623.839071**	-623.7992894	-0.0263423
4_cis_e	-624.0121306	**-623.839984**	-623.7983733	-0.0256729

2.9 Crystallographic Appendix

2.9.1 1,3-Dimethyl-5,6-dihydrouracil (2-49a)

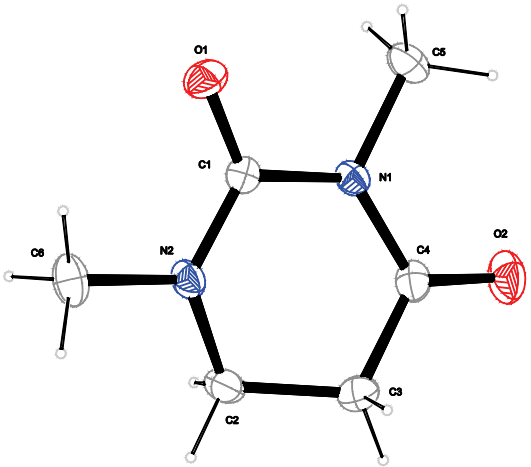

2-49a			
Formula	$C_6H_{10}N_2O_2$	T (K)	173(2)
M_r (g mol^{-1})	142.156	Diffractometer	Oxford Xcalibur (MoK_α)
Crystal sytem	Monoclinic	Angle	$4.25<\theta<26.32$
Space group	$P2_1/c$	Refls. measured	4972
a (Å)	8.5501(6)	Refls. in refinement	1425
b (Å)	12.0430(6)	Observed refls.	992
c (Å)	7.3700(6)	R_{int}	0.0250
α (°)	90	Mean σ(I)/I	0.0341
β (°)	111.828(8)	$R(F_{obs})$	0.0364
γ (°)	90	$R_w(F^2)$	0.0923
V (Å^3)	704.47(8)	*S*	0.954
Z	4	Hydrogen refinement	Constr.
ρ (g cm^{-1})	1.34035(15)	Shift/errormax	0.001
Crystal size (mm)	0.38 x 0.34 x 0.21	Max e$^-$ density (e Å^{-3})	0.129
μ (mm^{-1})	0.102	Min e$^-$ density (e Å^{-3})	-0.149

Hydrogen atoms of methyl group disordered, split model applied.

2.9.2 2,4-Diethoxy-5-methylpyrimidinium iodide (2-45b)

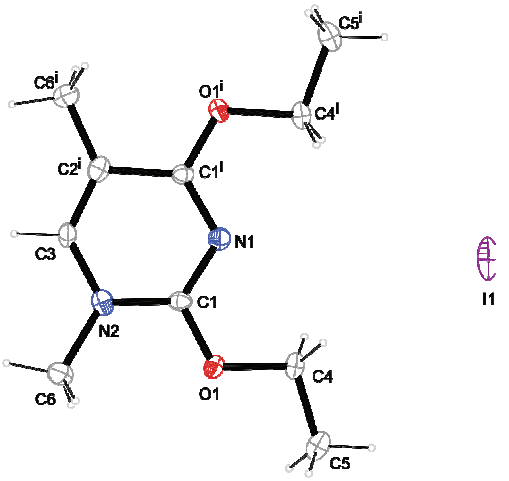

2-45b			
Formula	$C_{10}H_{17}IN_2O_2$	T (K)	100(2)
M_r (g mol^{-1})	324.159	Diffractometer	Bruker D8Venture (MoK_α)
Crystal sytem	Monoclinic	Angle	2.90<θ<27.58
Space group	*C2/c*	Refls. measured	17213
a (Å)	8.9980(7)	Refls. in refinement	1495
b (Å)	11.3959(9)	Observed refls.	1270
c (Å)	12.7487(11)	R_{int}	0.0578
α (°)	90	Mean σ(I)/I	0.0312
β (°)	97.786(3)	$R(F_{obs})$	0.0354
γ (°)	90	$R_w(F^2)$	0.0864
V (Å^3)	1295.20(18)	*S*	1.214
Z	4	Hydrogen refinement	Constr.
ρ (g cm^{-1})	1.6624(2)	Shift/errormax	0.001
Crystal size (mm)	0.166 x 0.087 x 0.075	Max e$^-$ density (e Å^{-3})	0.538
μ (mm^{-1})	2.458	Min e$^-$ density (e Å^{-3})	-0.523

2.9.3 1-*tert*-Butoxycarbonyluracil (2-40)

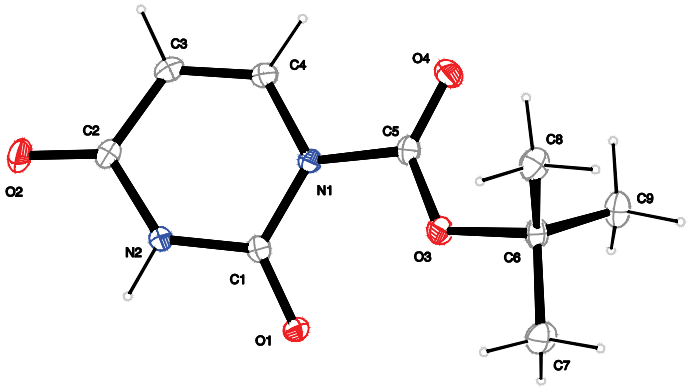

2-40			
Formula	$C_9H_{12}N_2O_4$	T (K)	173(2)
M_r (g mol^{-1})	212.203	Diffractometer	Oxford Xcalibur (MoK_α)
Crystal sytem	Monoclinic	Angle	4.19<θ<26.34
Space group	*P2$_1$*	Refls. measured	3484
a (Å)	9.1475(11)	Refls. in refinement	1112
b (Å)	6.2855(5)	Observed refls.	866
c (Å)	9.7621(13)	R_{int}	0.0323
α (°)	90	Mean σ(I)/I	0.0493
β (°)	116.975(16)	R(F_{obs})	0.00334
γ (°)	90	$R_w(F^2)$	0.0678
V (Å^3)	500.22(12)	*S*	0.931
Z	2	Hydrogen refinement	C bound constr. N bound refall.
ρ (g cm^{-1})	1.4089(3)	Shift/errormax	0.001
Crystal size (mm)	0.32 x 0.12 x 0.09	Max e$^-$ density (e Å^{-3})	0.139
μ (mm^{-1})	0.112	Min e$^-$ density (e Å^{-3})	-0.165

2.9.4 1-(2-Cyanoethyl)-1-methylurea (2-59a)

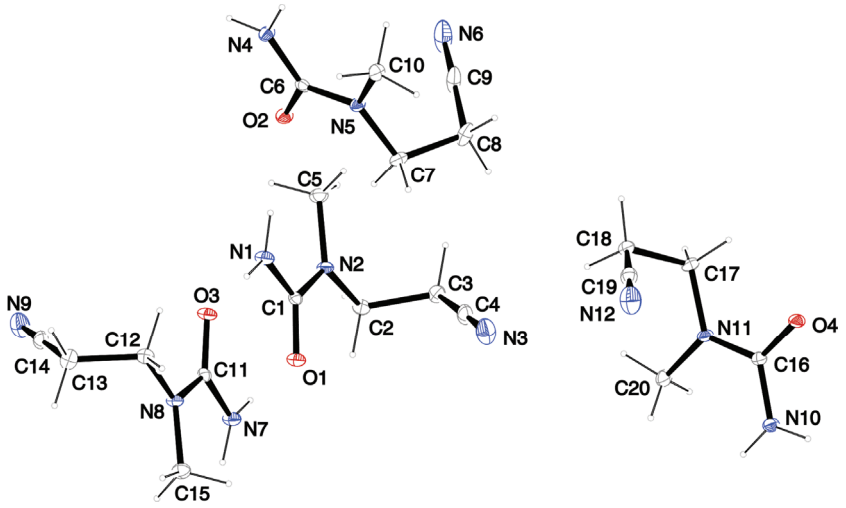

2-59a			
Formula	$C_5H_9N_3O$	T (K)	100(2)
M_r (g mol^{-1})	127.145	Diffractometer	Bruker D8Venture (MoK_α)
Crystal sytem	Triclinic	Angle	3.16<θ<25.09
Space group	*P1bar*	Refls. measured	8883
a (Å)	5.7659 (5)	Refls. in refinement	4541
b (Å)	13.0836(11)	Observed refls.	3101
c (Å)	18.1683(17)	R_{int}	0.0398
α (°)	77.013(3)	Mean σ(I)/I	0.0706
β (°)	82.897(3)	R(F_{obs})	0.0463
γ (°)	85.689(3)	$R_w(F^2)$	0.1136
V (Å^3)	1323.7(2)	*S*	1.016
Z	8	Hydrogen refinement	C bound constr. N bound refall.
ρ (g cm^{-1})	1.27601(19)	Shift/errormax	0.001
Crystal size (mm)	0.132 x 0.048 x 0.041	Max e$^-$ density (e Å^{-3})	0.226
μ (mm^{-1})	0.093	Min e$^-$ density (e Å^{-3})	-0.210

2.9.5 1-Methyl-5,6-dihydrocytosine • ½ H_2O (2-55a)

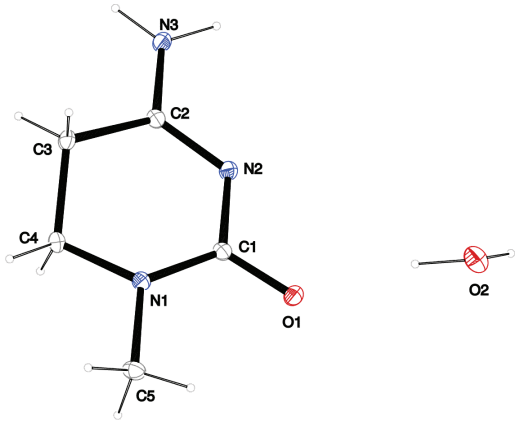

2-55a • ½ H_2O			
Formula	$C_5H_{10}N_3O_{1.5}$	T (K)	100(2)
M_r (g mol^{-1})	136.152	Diffractometer	Bruker D8Venture (MoK_α)
Crystal sytem	Orthorombic	Angle	3.28<θ<27.53
Space group	P*bcn*	Refls. measured	12062
a (Å)	12.4314(4)	Refls. in refinement	1496
b (Å)	8.6973(2)	Observed refls.	1357
c (Å)	12.0417(4)	R_{int}	0.0303
α (°)	90	Mean σ(I)/I	0.0188
β (°)	90	$R(F_{obs})$	0.0336
γ (°)	90	$R_w(F^2)$	0.0917
V (Å^3)	1301.94(7)	*S*	1.051
Z	8	Hydrogen refinement	Refall.
ρ (g cm^{-1})	1.38925(7)	Shift/errormax	0.001
Crystal size (mm)	0.157 x 0.127 x 0.120	Max e$^-$ density (e Å^{-3})	0.389
μ (mm^{-1})	0.105	Min e$^-$ density (e Å^{-3})	-0.168

2.9.6 *rac*-1-(2-Cyanopropyl)-1-methylurea (2-59b)

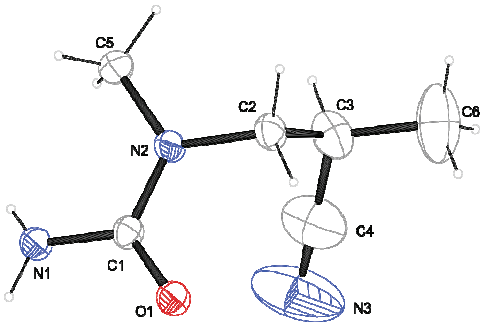

2-59b			
Formula	$C_6H_{11}N_3O$	T (K)	100(2)
M_r (g mol^{-1})	141.171	Diffractometer	Bruker D8Venture (MoK_α)
Crystal sytem	Monoclinic	range	3.16<θ<25.36
Space group	C2/c	Refls. measured	10282
a (Å)	25.977(5)	Refls. in refinement	1415
b (Å)	5.9042(8)	Observed refls.	1143
c (Å)	10.2324(156)	R_{int}	0.0461
α (°)	90	Mean σ(I)/I	0.0263
β (°)	97.469(4)	R(F_{obs})	0.0716
γ (°)	90	$R_w(F^2)$	0.2141
V (Å^3)	1556.1(4)	*S*	1.156
Z	8	Hydrogen refinement	Mixed
ρ (g cm^{-1})	1.2052(3)	Shift/errormax	0.001
Crystal size (mm)	0.253 x 0.093 x 0.018	Max e$^-$ density (e Å^{-3})	0.705
μ (mm^{-1})	0.086	Min e$^-$ density (e Å^{-3})	-0.306

2.9.7 *N,N*-Dimethyl-*N'*-(1-methyl-2-oxo-1,2-dihydropyrimidin-4-yl)formimidamide (2-52a)

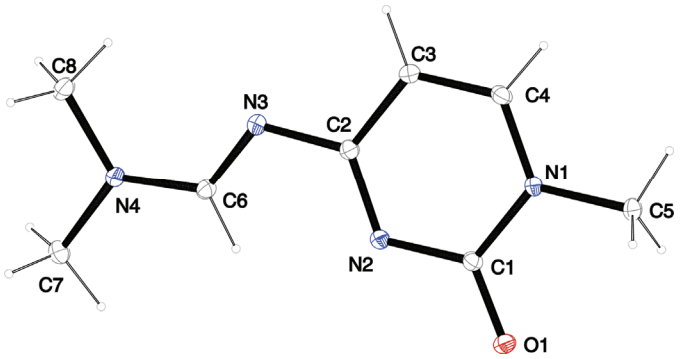

2-52a			
Formula	$C_8H_{12}N_4O$	T (K)	100(2)
M_r (g mol^{-1})	180.207	Diffractometer	Bruker D8Venture (MoK_α)
Crystal sytem	Monoclinic	range	$3.74<\theta<27.55$
Space group	$P2_1/n$	Refls. measured	11720
a (Å)	10.4269(5)	Refls. in refinement	
b (Å)	5.9290(3)	Observed refls.	1691
c (Å)	13.7501(6)	R_{int}	0.0288
α (°)	90	Mean σ(I)/I	0.0193
β (°)	90.7826(16)	$R(F_{obs})$	0.0371
γ (°)	90	$R_w(F^2)$	0.1025
V (Å^3)	849.97	*S*	1.063
Z	4	Hydrogen refinement	Constr.
ρ (g cm^{-1})	1.40826(12)	Shift/errormax	0.001
Crystal size (mm)	0.259 x 0.137 x 0.046	Max e$^-$ density (e Å^{-3})	0.355
μ (mm^{-1})	0.099	Min e$^-$ density (e Å^{-3})	-0.181

3 Enhanced Redox Properties in Open-shell Nucleotides – A Theoretical Survey

Parts of this chapter have been published in

Transfer Hydrogenation in Open-shell Nucleotides – A Theoretical Survey

F. Achrainer, H. Zipse, *Molecules* **2014**, *19*, 21489 – 21505.

3.1 Introduction

As already described in **Chapter 2** transfer hydrogenation between alcohols and alkenes represents a synthetically and technically relevant process to hydrogenate unsaturated compounds.[87] Over the past years numerous variants ranging from transition metal catalysis[88] over metal-free routes or organocatalytic approaches[89] have been developed to be compatible with sensitive starting materials or to induce high enantioselectivities. The driving force for this type of process derives from systematically higher heats of hydrogenation $\Delta_{hyd}H$ for alkenes as compared to aldehydes and ketones. For example taking the reaction of ethanol (**3-1**) with propene (**3-2**) of **Scheme 3.1** to yield acetaldehyde (**3-3**) and propane (**3-4**) the reaction enthalpy $\Delta_{trh}H$ amounts to -55.2 kJ mol^{-1} when experimentally measured heats of formation are used.[15]

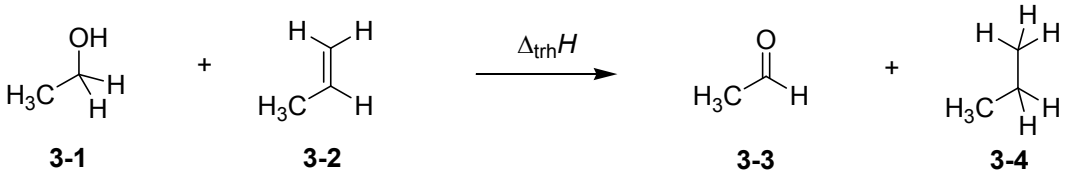

Scheme 3.1 Transfer hydrogenation of ethanol (**3-1**) to propene (**3-2**).

A multitude of actual pathways exist for utilizing this driving force, the most relevant of which will most likely involve open-shell intermediates under biological conditions. The combined theoretical and experimental study (see **Chapter 2.4**) to determine the heats of hydrogenation of pyrimidine und purine bases indicates that the hydrogenation enthalpies of oxidized sugar models are, in part, closely similar to those of the pyrimidine bases.[74]

How will these energetics change on introducing a radical center in direct neighbourhood of the reacting π system in the hydrogen-donor or -acceptor? This can in principle be discussed with reference to the reaction in **Scheme 3.2** with either ethanol (**3-1**) or ethanol-2-yl radical (**3-1R**). While the reaction of closed-shell reactants is exothermic ($\Delta_{trh}H$ = -55.2 kJ mol^{-1}) the latter is significantly more exothermic with a value of -84.6 kJ mol^{-1}. This increase in driving force of 29.4 kJ mol^{-1} implies that ethanol-2-yl radical (**3-1R**) is a better dihydrogen donor than its closed-shell parent ethanol. In contrast, installation of a radical center in the alkene partner leads to a close to thermoneutral reaction enthalpy of -4.4 kJ mol^{-1}.

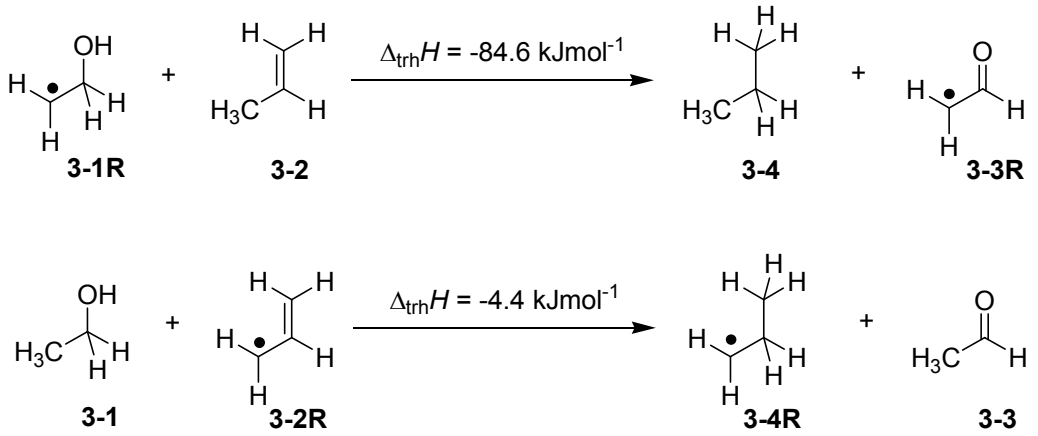

Scheme 3.2 Experimentally determined transfer hydrogenation enthalpy $\Delta_{trh}H$ for selected open-shell systems at 298.15 K in the gas phase.

On closer inspection of the reactant and product radicals involved, it also becomes evident that the driving force is identical to the differences in radical stabilization energies (RSE) of the reactant and product radicals.

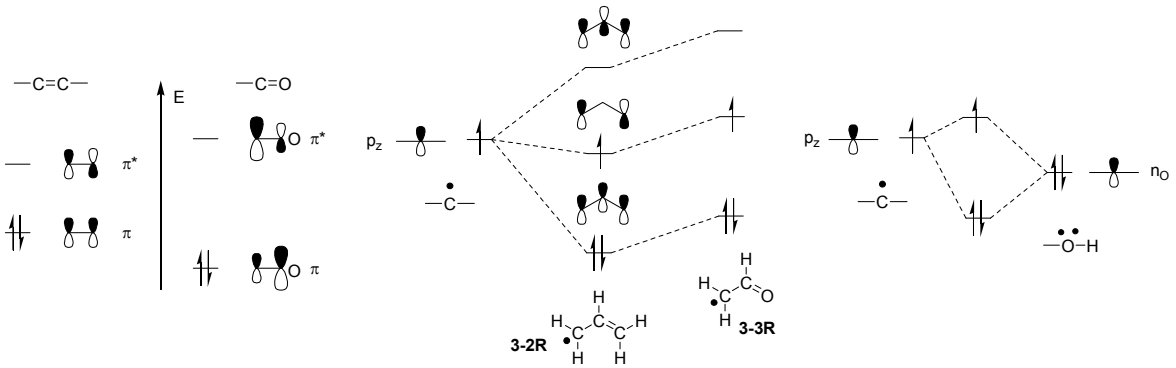

Figure 3.1 Qualitatitive frontier orbital interaction scheme for the formation of the allyl (**3-2R**) and the formyl methyl radical (**3-3R**).

Open-shell species like ribosyl radical **3-5R** possess enhanced stability because of their special substitution pattern of an electron-withdrawing and an electron-donating group in direct connection to the radical center (**Figure 3.1**). This synergistic effect is commonly referred in the literature as "captodative" or "push-pull" effect[90] with the open-shell glycyl model (**3-6R**)[91] and the semidehydroascorbate acid radical (**3-7R**)[92] as the most prominent examples (see **Scheme 3.3**).

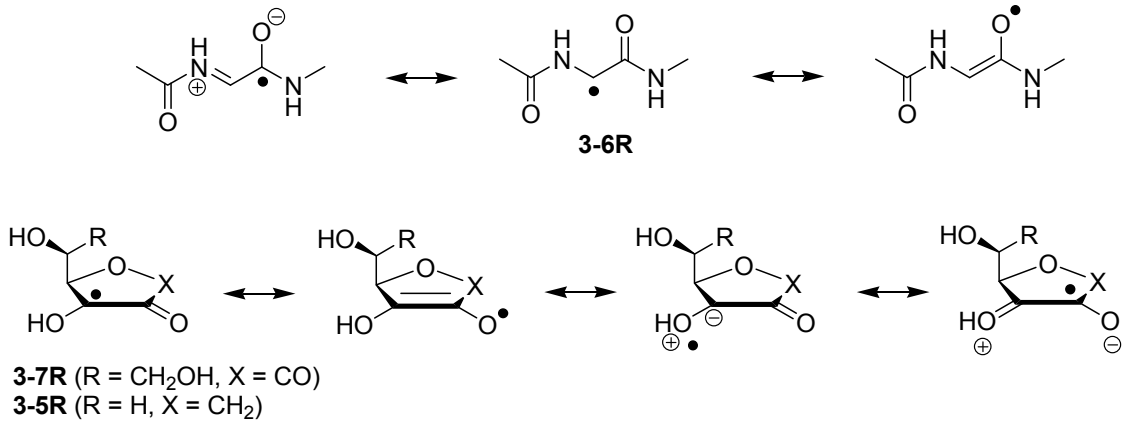

Scheme 3.3 Resonance contributions in the *C*-centered semiquinone radicals **3-5R** and **3-7R** and in glycyl peptide radical **3-6R**.

Another useful approach to define the captodative effect is the comparison of the radical stabilization energy (RSE) of the individual components. The sum of the calculated RSE of the hydroxyethyl radical (**3-1Rb**) and the acetonyl radical **3-8R** is -70.7 kJ mol^{-1}, whereas the RSE of **3-9R** in the *trans* form is -92.4 kJ mol^{-1} (see **Table 3.1**). The energetic difference of 21.7 kJ mol^{-1} indicates a substantial captodative stabilization.

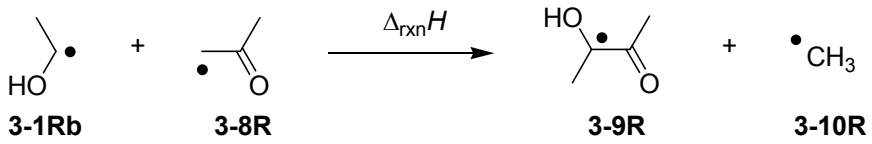

Scheme 3.4 EGroup exchange reaction to define the stabilizing captodative effect. The reaction enthalpy amounts to -40.7 kJ mol^{-1} at G3(MP2)-RAD level.

Table 3.1 Radical stabilization energies calculated at G3(MP2)-RAD level at 298.15 K, in kJ mol^{-1}.

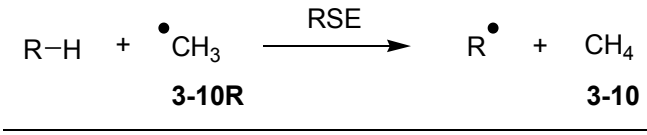

3-10R **3-10**

R-H	RSE(calc.)	RSE (exp.)[93]
 **3-1Rb**	-38.3	-42.7
 **3-8R**	-32.4	-38.1
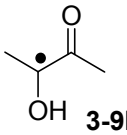 **3-9R**	-92.4	n/a

3.2 Ribonucleotide Reductase

The radical-induced changes in dihydrogen transfer energetics are likely to impact the chemistry of nucleotide radicals. This may be particularly relevant for cases where oxidations of nucleotide radicals have been observed under reducing conditions. A prominent example is the outcome of the substrate reaction of the E441Q mutant of *E. coli* class I ribonucleotide reductase (RNR).[94] This family of ubiquitous radical enzymes catalyzes the conversion of nucleotides to desoxynucleotides to provide the monomeric building blocks for cell growth and DNA synthesis.[95] The enzyme is classified in three different classes by the cofactor responsible for the radical generation: μ-oxo-di-iron-tyrosyl cofactor (class I, aerobic), coenzyme B_{12} (class II, facultative aerobic) and *S*-adenosyl methionine which forms a glycyl radical (class III, anaerobic).

Scheme 3.5 RNR-catalyzed reduction of ribonucleotides to 2'-desoxynucleotides.

Class I RNR, found in mammals and *E. coli*, is one of the best examined enzyme and is composed of two heterodimeric subunits, the large R1 (α2)[96] and the small R2 (β2).[97] The catalytic machinery and the binding site for the nucleotide reduction are located in the R1 section. The required radical for the reaction is formed and stored in the R2 unit by a di-iron-oxo tyrosyl (Y_{122}•) radical cofactor. Two remarkable facts have been the subject of scientific controversy in the last decades: 1.) The long half-life time of around four days of the radical, which results in a low affinity of the two subunits to form the active RNR; and 2.) the transport of the radical from the tyrosyl Y_{122}• of R2 to the cysteine moiety C_{439} in the active site of R1. A long-range proton-coupled electron transfer (PCET) has been proposed to initiate catalysis upon estimation of a distance of at least 25 Å on the basis of an MD docking model.[98]

As already mentioned, during the reaction progress the radical is transferred from the Y_{122} residue on β2 to cysteine C_{439} in the active site of α2. Essential residues for the catalytic activity are two additional cysteines (C_{225} and C_{462}),[99] a glutamate (E_{441}), acting as general acid-base catalyst[100] and an asparagine (N_{437}) which helps to stabilize the conformation of C_{225} and C_{462}.[101] These two cysteine residues provide the reducing equivalents to convert ribonucleotides into the desired 2'-desoxy derivatives (see **Figure 3.2**). The regeneration of the free thiol groups is achieved by subsequent thioredoxin/NADPH reduction.[102]

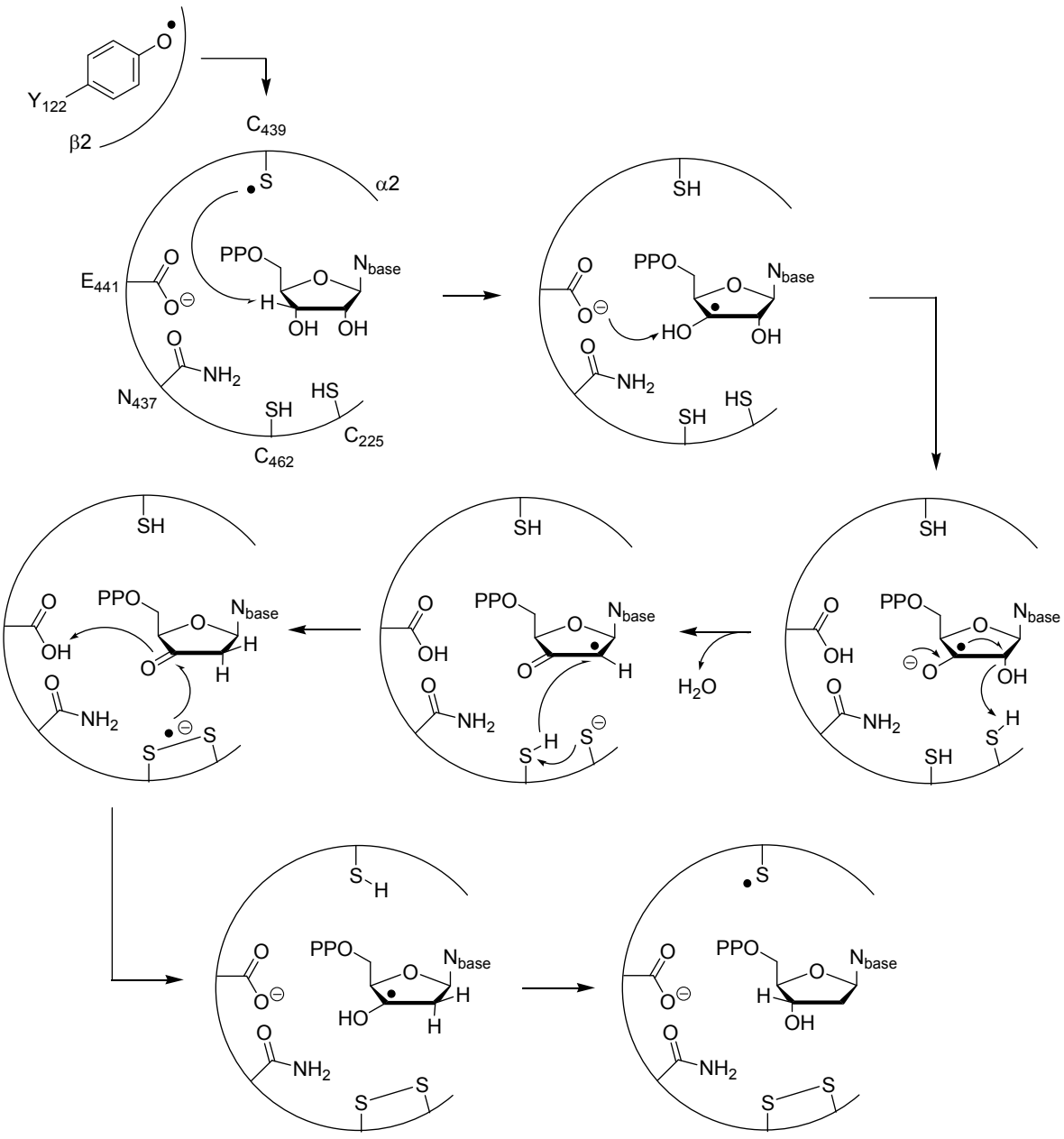

Figure 3.2 Proposed mechanisms for the RNR-catalyzed reduction of nucleoside diphosphates.

By replacing glutamate E_{441} with a glutamine and incubating with cytidine diphosphate the catalytical activity is suppressed completely and no 2'-reduction is detected. Instead, in a characteristic time-dependent manner signals of two open-shell intermediates are observed. Using a combination of high-field EPR and ENDOR measurements and computational predictions of EPR parameters, one of these intermediates has been identified as semidione radical anion **3-13R**.

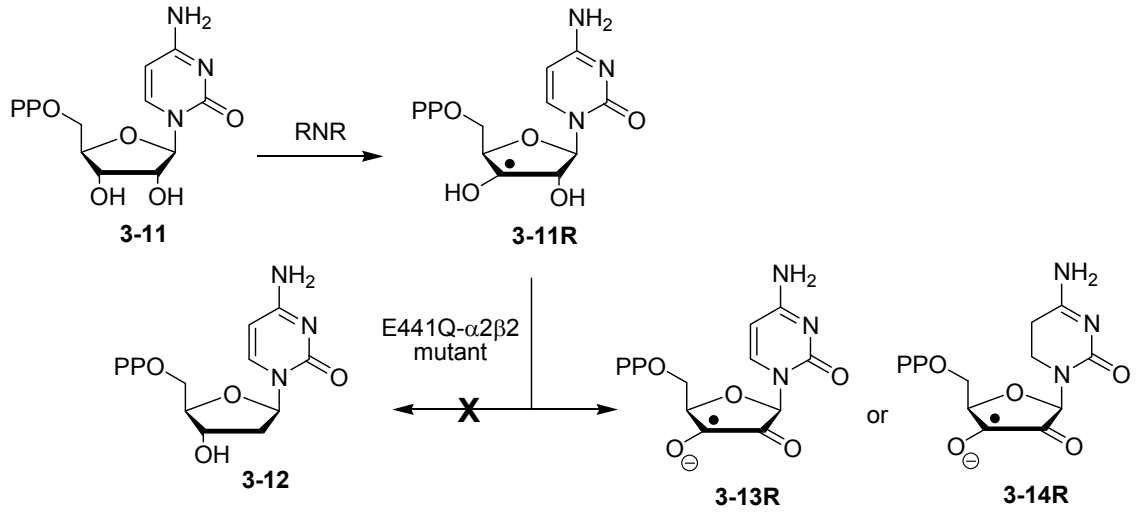

Scheme 3.6 Substrate reaction of class I RNR E441Q mutant.

How oxidized intermediate **3-13R** can be formed under the reductive conditions present in the experiment has still not been rationalized in a satisfactory way, but most likely a stepwise H atom transfer occurs.[103] The possibility that the cytosine base present in radical **3-11R** can act as internal redox partner to the adjacent C3'-ribosyl radical, thus generating product radical **3-14R** (and not **3-13R**) through a transfer hydrogenation process is feasible from a thermochemical point of view. Mass spectrometry as the major tool for the analysis of oligonucleotides gives for this type of reaction no meaningful conclusion and a dihydro cytosine motif has presumably no significant influence on the EPR parameters.

3.3 Validation of Theoretical Methods

3.3.1 Closed-shell Systems

The validation for the reaction energies of the transfer hydrogenation of closed-shell reactants has already been carried out in **Chapter 2.2** and the G3B3 method[104] has been identified as the method of choice in combination with the experimentally determined hydrogenation enthalpy of ethylene (**3-15**, $\Delta_{hyd}H$ = -136.3±0.2 kJ mol^{-1}).[105] Nevertheless, applying this method to open-shell molecules of the size of sugar models and complete nucleosides is difficult due to hardware limitations. Therefore, the also examined ROMP2(FC)/6-311+G(3df,2p) single point

approach[106] in combination with UB3LYP/6-31G(d) optimized structures and thermochemical corrections to 298.15 K using the rigid rotor/harmonic oscillator model were evaluated to estimate the driving force of the radical-induced hydrogenation of ethylene (**3-15**). Improved energies were obtained using the G3(MP2)-RAD composite method introduced by *Radom et al.*[81]

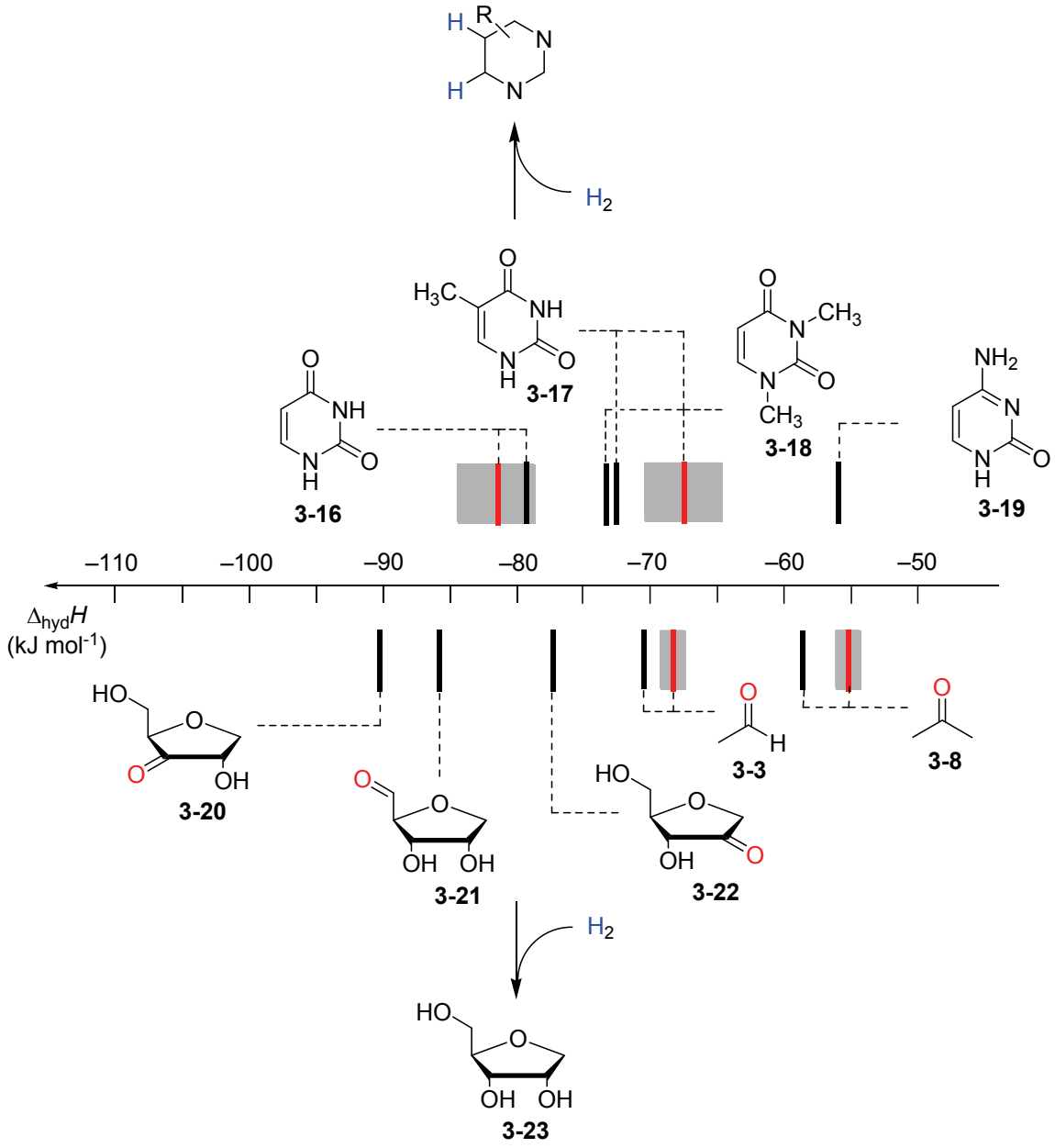

Figure 3.3 Heats of hydrogenation $\Delta_{hyd}H$ at 298.15 K (G3(MP2)-RAD, in kJ mol^{-1}) in the gas phase of selected pyrimidine bases and carbonyl compounds. Experimental hydrogenation enthalpies are shown as red lines together with their standard deviation as grey bars.

Table 3.2 Calculated and experimentally determined heats of hydrogenation $\Delta_{hyd}H$ at 298.15 K in the gas phase, in kJ mol^{-1}.

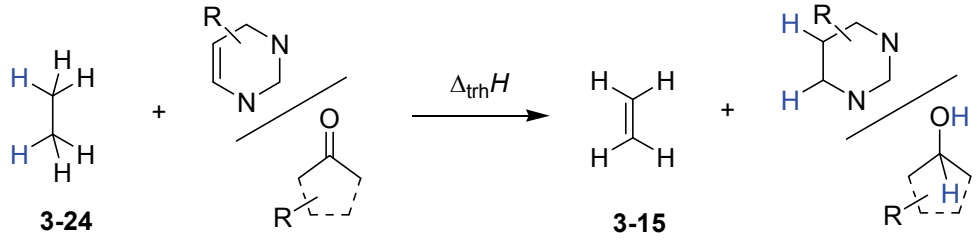

Reactants	MP2(FC)/ 6-311+G(3df,2p)		G3(MP2)-RAD		Exp.[15]	
	$\Delta_{trh}H^a$	$\Delta_{hyd}H^b$	$\Delta_{trh}H^a$	$\Delta_{hyd}H^b$	$\Delta_{trh}H^a$	$\Delta_{hyd}H^b$
Ethylene (**3-15**)	0.0	-136.3	0.0	-136.3	0.0	-136.3±0.2[105]
Propene (**3-2**)	+12.4	-123.9	+10.8	-125.5	+12.6	-125.0±0.2[16]
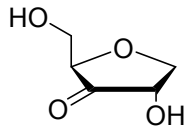 **3-20**	+44.5	-91.8	+44.9	-91.4	n/a	n/a
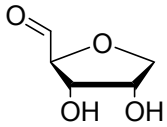 **3-21**	+50.3	-86.0	+50.2	-86.1	n/a	n/a
Uracil (**3-16**)	+56.1	-80.2	+57.0	-79.3	+53.6 ± 2.1[74]	-81.5±2.1
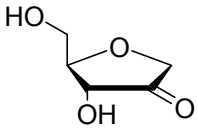 **3-22**	+58.3	-78.0	+58.8	-77.5	n/a	n/a
1,3-Dimethyl uracil (**3-18**)	+62.4	-73.9	+62.7	-73.6	+68.5± 2.1[74]	-67.6±2.6
Thymine (**3-17**)	+64.2	-72.1	+63.8	-72.5	+68.8 ± 4.2[74]	-67.6±2.3
Acetaldehyde (**3-3**)	+65.8	-70.5	+65.1	-71.2	+67.8	-69.1±0.4[23]
Acetone (**3-8**)	+77.8	-58.5	+76.5	-59.8	+80.9	-55.6±0.4[24]
Cytosine (**3-19**)	+82.4	-53.9	+80.2	-56.1	n/a	n/a
Adenine (**3-25**)	+152.6	+13.6	+139.0	+2.7	n/a	n/a
Guanine (**3-26**)	+155.2	+18.9	+141.2	+4.9	n/a	n/a

[a] Defined as $\Delta_{trh}H = \Delta_fH(C_2H_4) + \Delta_fH(R_2CH\text{-}OH) - \Delta_fH(R_2C{=}O) - \Delta_fH(C_2H_6)$ and $\Delta_{trh}H = \Delta_fH(C_2H_4) + \Delta_fH(RCH_2\text{-}CH_2R) - \Delta_fH(RHC{=}CHR) - \Delta_fH(C_2H_6)$, respectively. [b] Addition of the reaction enthalpies $\Delta_{trh}H$ to the experimentally determined hydrogenation enthalpy of ethylene $\Delta_{hyd}H$ (C_2H_4, **3-15**) = -136.3±0.2 kJ mol^{-1} yields the hydrogenation enthalpy $\Delta_{hyd}H$ of the respective double bond.

The hydrogenation enthalpies are summarized in **Table 3.2** and shown in **Figure 3.3** such that a side-by-side comparison of all possible hydrogen transfer reactions is possible in a graphical way. In accordance with **Chapter 2.4** and from this representation it is apparent that uracil (**3-16**) as the most easily reduced base can react exothermally with sugar models like 1'-anhydroribose **3-23** in a formal transfer hydrogen reaction to form ketone **3-22**.

The calculated reaction enthalpies obtained at G3(MP2)-RAD and MP2 level are in good agreement with experimental values and are found to fit the chemical accuracy of one kcal mol^{-1}. Introduction of two methyl groups present in dimethyl uracil **3-18** leads to $\Delta_{hyd}H$ = -73.6 kJ mol^{-1} vs. -79.3 kJ mol^{-1} for uracil (**3-16**) at G3(MP2)-RAD level, which is almost the same result as obtained for thymine (**3-17**, $\Delta_{hyd}H$ = -72.5 kJ mol^{-1}). The reduced hydrogenation enthalpy of around +7 kJ mol^{-1} ($\Delta\Delta_{hyd}H$ (**3-16**/**3-17**)) is also observed in related systems like ethylene/propene ($\Delta\Delta_{hyd}H$ (exp., **3-15**/**3-2**) = +11.3 kJ mol^{-1}), cyclohexene[18]/1-methylcyclohexene[19] ($\Delta\Delta_{hyd}$H(exp., **3-27**/**3-28**) = +7.4 kJ mol^{-1}) and cyclopentene[18]/1-methylcylopentene[19] ($\Delta\Delta_{hyd}H$(exp., **3-29**/**3-30**) =+11.3 kJ mol^{-1}) and can therefore be considered as general phenomenon. The most difficult pyrimidine base to reduce is cytosine (**3-19**, $\Delta_{hyd}H$ = -56.1 kJ mol^{-1}) due to the different substitution pattern. Hydrogenation of the purine bases adenine (**3-25**) and guanine (**3-26**) is significantly more difficult, a result of the intrinsically large differences in reductions of C-C and C-N double bonds.[15, 57]

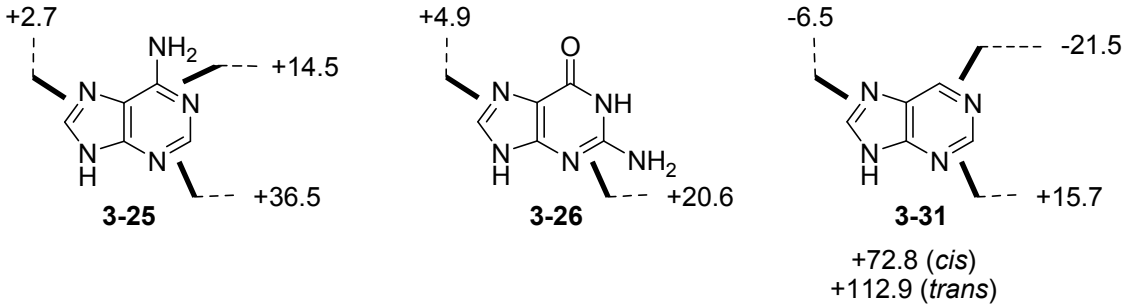

Figure 3.4 Hydrogenation enthalpies $\Delta_{hyd}H$ of adenine (**3-25**), guanine (**3-26**) and their parent lead structure purine (**3-31**) at G3(MP2)-RAD level of theory (gas phase, 298.15 K, in kJ mol^{-1}).

For instance the hydrogenation enthalpies for the canonical structures of adenine and guanine are all endothermic with energetically best values of $\Delta_{hyd}H$(**3-25**) = +2.7 and $\Delta_{hyd}H$(**3-26**) = +4.9 kJ mol^{-1}, respectively. The reduction of the oxidized sugar models

3-20, **3-21** and **3-22** (see **Table 3.2**) to give 1'-anhydroribose (**3-23**) are all located in a range from -77.5 to -91.4 kJ mol^{-1} in the gas phase at G3(MP2)-RAD level. As a result, transfer hydrogenation to yield 5,6-dihydro uracil and 2'-keto sugar **3-22** is predicted to be slightly exothermic by -79.3 – (-77.5) = -1.8 kJ mol^{-1}. The other two sugar derivatives **3-20** and **3-21** are, in contrast, not effective as dihydrogen donors to reduce uracil in an exothermic fashion.

3.3.2 Open-shell Systems

Substantial changes in reaction enthalpies are observed for open-shell systems as redox partners. Applying the same strategy of transfer hydrogenation with ethylene (**3-15**)/ethane (**3-24**) to radicals with reactive α- and β-hydrogen atoms gives overall more positive heats of hydrogenation due to the loss of radical stabilization. The redox data for a variety of small *C*-centered radicals obtained at various levels is collected in **Table 3.3** and validated with experimentally available values.

ROMP2 and G3(MP2)-RAD give almost the same results, but underestimate the experimental enthalpy constantly except for the cyclopentyl radical (**3-32R**) which is the result of the distinct ring strain. Inspection of the obtained correlation reveals a large discrepancy for the open-shell pair acetone (**3-8R**) and *iso*-propanol (**3-33R**), which is most likely caused by the experimentally determined heat of formation of propan-2-ol-1-yl radical **3-33R** ($\Delta_f H$(exp.) = -96.2±4.2 kJ mol^{-1}) supported by additional calculations (see **Appendix Table 3.35**).[107] Recent high-level calculations at CBS-QB3 level[108] gave a revised value of $\Delta_f H$ = -64.0 kJ mol^{-1} for **3-33R**[109] which gave an overall better correlation. The G3(MP2)-RAD correlation is mainly the result of the reaction enthalpies involving *C*-based reactants (see **Figure 3.5**). By abstracting a hydrogen atom from the parent closed-shell molecule the heats of hydrogenation $\Delta_{hyd}H$ are shifted significantly to less exothermic values, which is nothing else than a reflection of the radical stabilization energies of the respective open-shell intermediate.

Table 3.3 Validation of theoretical methods with experimentally available data for the open-shell induced transfer hydrogenation $\Delta_{trh}H$ at 298.15 K in the gas phase, in kJmol^{-1}.

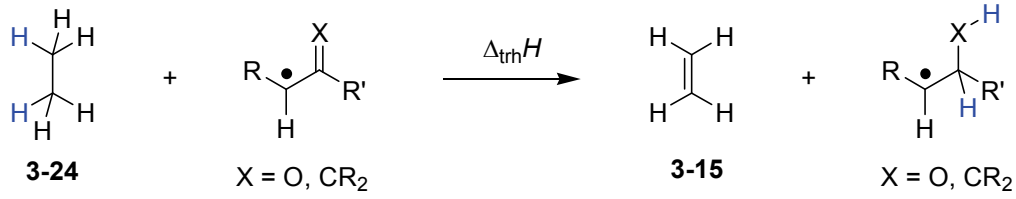

Initial radical	UB3LYP/6-31G(d)		ROMP2(FC)/ 6-311+G(3df,2p)		G3(MP2)-RAD		Exp.
	$\Delta_{trh}H$	$\Delta_{hyd}H$[a]	$\Delta_{trh}H$	$\Delta_{hyd}H$[a]	$\Delta_{trh}H$	$\Delta_{hyd}H$[a]	$\Delta_{trh}H$
3-2R	+82.8	-53.5	+71.5	-64.8	+72.7	-63.7	+65.4±5.9
3-34R	+88.4	-47.9	+72.9	-63.4	+72.8	-63.5	+64.6±2.2
3-35R	+79.5	-56.8	+62.5	-73.8	+64.9	-71.4	+55.4±17.3
3-27R	+96.3	-40.0	+85.8	-50.5	+81.6	-54.7	+74.9±4.9
3-29R	+88.3	-48.0	+79.9	-56.5	+75.9	-60.4	+82.7±7.6
3-3R	+137.3	+1.0	+90.1	-46.2	+91.4	-44.9	+94.9±17.1
3-8R	+149.0	+12.7	+98.3	-38.0	+99.3	-37.0	+74.1±8.1 +106.3±3.9[b]
3-36R	+161.6	+25.3	+105.7	-30.6	+106.6	-29.7	+106.6±13.5[c]
3-37R	+154.6	+18.3	+104.8	-31.5	+104.6	-31.7	+91.9±9.3

[a] Addition of the reaction enthalpies $\Delta_{trh}H$ to the experimentally determined hydrogenation enthalpy of ethylene $\Delta_{hyd}H$(C_2H_4, **2-15**) = -136.3±0.2 kJ/mol yields the hydrogenation enthalpy $\Delta_{hyd}H$ of the respective double bond. [b] With [a] Δ_fH^0(**2-33R**) = -64.02 kJ mol^{-1} at CBS-QB3 level of theory.[109] [c] Applying radical Δ_fH calculated by Benson group additivity values.

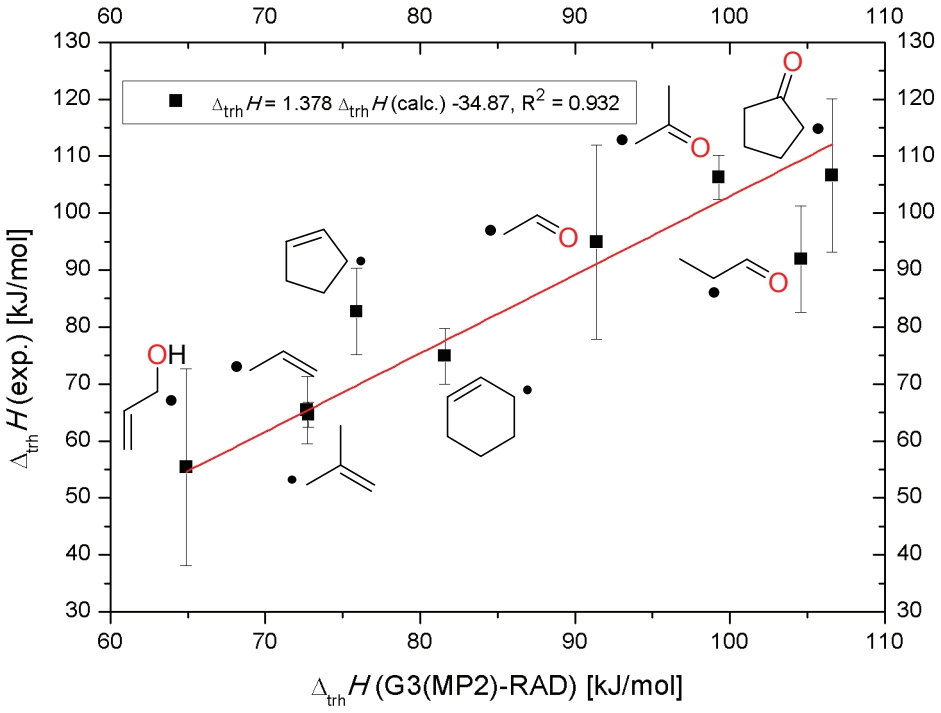

Figure 3.5 Correlation of experimentally available $\Delta_{trh}H$(exp.) vs. $\Delta_{trh}H$(calc.) at G3(MP2)-RAD level of theory in the gas phase at 298.15K.

According to these results all oxygen-containing open-shell intermediates are in principle able to hydrogenate the double bonds of the pyrimidine bases. For example, reaction of the ethanol derived radical **3-1R** with uracil (**3-16**) gives an increased driving force of -79.3 – (-44.9) = -34.4 kJ mol^{-1} at G3(MP2)-RAD level, compared to -8.1 kJ mol^{-1} for the closed-shell reaction (see **Figure 3.6**).[74] The enhanced redox power of ketones compared to aldehydes persists constantly despite the origin of the reactants indicated by almost the same difference in hydrogenation energies. Overall it can be concluded that the obtained G3(MP2)-RAD values reflect the real facts of radical-induced transfer hydrogenation.

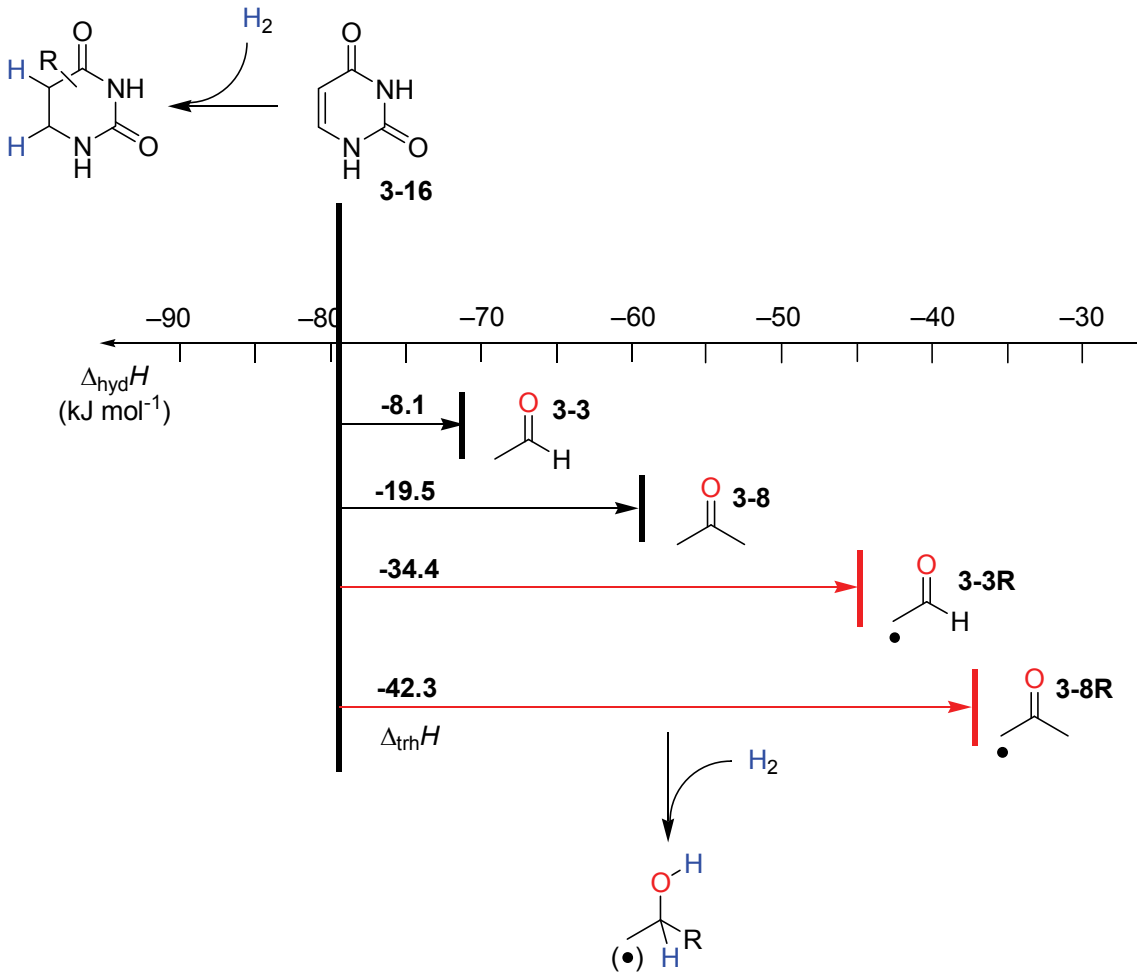

Figure 3.6 Comparison of open- and closed-shell-induced transfer hydrogenation of uracil (**3-16**).

3.4 Open-shell Sugar Models

The heats of hydrogenation of ribose-derived radicals are also shifted compared to their closed-shell counterparts and cover now a range from -14.4 to -94.5 kJ mol^{-1} depending on the position of the unpaired electron. The energies for pentose-derived aldehydes, ketones and alkenes are collected in **Table 3.4** and **Table 3.5**. The smallest hydrogenation enthalpies are found for donor/acceptor substituted radicals combining a hydroxyl group donor with a carbonyl acceptor-substituent as is the case in **3-43R**. Introduction of a hydroxymethyl substituent present in **3-43R** ($\Delta_{hyd}H$ = -14.4 kJ mol^{-1}), but not in radical **3-39Ra** ($\Delta_{hyd}H$ = -11.6 kJ mol^{-1}) has only a minor influence on the hydrogenation enthalpies. This conclusion is also supported by the almost negligible difference in energies of radical **3-42Ra** and **3-43R**, where the substituent and the radical center are interchanged.

Table 3.4 *Boltzmann*-averaged hydrogenation enthalpies $<\Delta_{hyd}H>$ at 298.15 K in the gas phase for diol-derived radicals. Only the initial radicals are shown.

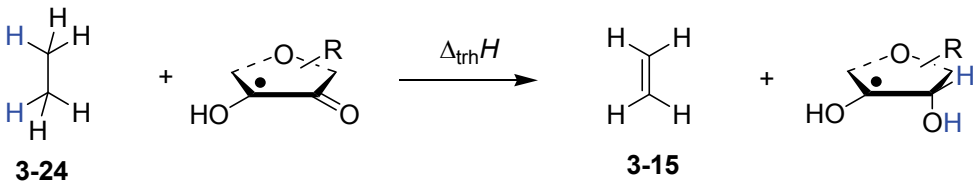

3-24 **3-15**

	ROMP2(FC)/ 6-311+G(3df,2p)		G3(MP2)-RAD	
	$<\Delta_{trh}H>$[a]	$<\Delta_{hyd}H>$[b]	$<\Delta_{trh}H>$[a]	$<\Delta_{hyd}H>$[b]
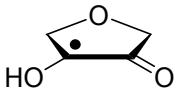 **3-39Ra**	+129.0	-7.28	+124.7	-11.6
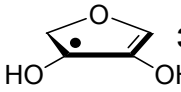 **3-39Rb**	+76.5	-59.8	+73.8	-62.5
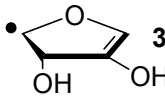 **3-40Ra**	+13.8	-122.5	+18.1	-118.2
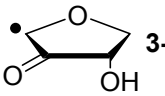 **3-40Rb**	+104.6	-31.7	+101.4	-34.9
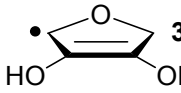 **3-40Rc**	+65.9	-70.4	+65.2	-71.1

[a] Defined as $\Delta_{trh}H = \Delta_fH(C_2H_4) + \Delta_fH(\bullet R_2CH\text{-}OH) - \Delta_fH(\bullet R_2C{=}O) - \Delta_fH(C_2H_6)$. [b] Addition of the reaction enthalpies $\Delta_{trh}H$ to the experimentally determined hydrogenation enthalpy of ethylene $\Delta_{hyd}H(C_2H_4$, **3-15**) = -136.3±0.2 kJ mol^{-1}[105] yields the hydrogenation enthalpy $\Delta_{hyd}H$ of the respective double bond.

Systematically larger enthalpies are calculated for ribose radicals carrying a carbonyl acceptor and the ring oxygen as alkoxy donor. A typical example is **3-44Ra** with Δ_{hyd}H = -33.1 kJ mol^{-1} at G3(MP2)-RAD level (see **Table 3.5**). This group also includes radicals **3-41Ra** and **3-41Rb**, in which the oxidized C5' position acts as acceptor substituent to the radical center. The influence of the C2' hydroxyl group present in **3-41Rb**, but not in **3-46Rb**, appears to be negligible according to the almost identical hydrogenation energies (Δ_{hyd}H (**3-46Rb**) = -26.7 vs. Δ_{hyd}H (**3-41Rb**) = -27.5 kJ mol^{-1}). The small hydrogenation enthalpies obtained herein for all push/pull-substituted radicals reflect the efficient interaction of the alkoxy/hydroxyl-donor and carbonyl-acceptor substituents.[90a, 93] As shown in **Scheme 3.7** for the example of radical

3-39Ra, these can be rationalized with the admixture of charge-transfer configurations such as **D** and **E** to the canonical Lewis structures **A** and **B**.

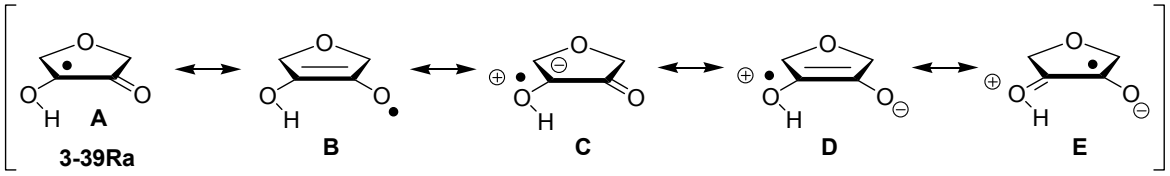

Scheme 3.7 Resonance stabilization of donor/acceptor substituted radical **3-39Ra**.

The relevance of the charge-transfer configurations **D** and **E** also implies that the carbonyl oxygen atom may be a better hydrogen-bond acceptor at the radical stage as compared to its closed-shell parent. Similarly, the hydroxyl group in **3-39Ra** may be a better hydrogen-bond donor as compared to closed-shell analogs (and also significantly more acidic).[100, 110] And indeed, optimized structures of the dimers of **3-39Ra** compared to **3-39a** at (U)B3LYP level show significantly shorter hydrogen bond distances for the open-shell species (**Figure 3.7**).

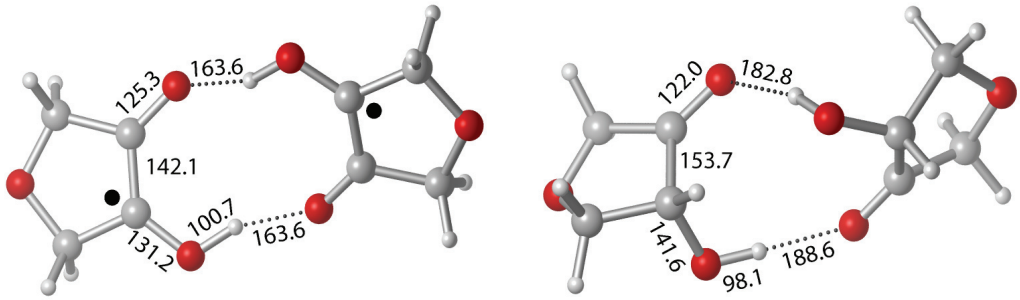

Figure 3.7 Dimers of radical **3-39Ra** (left) and its closed-shell parent **3-39a** (right) at (U)B3LYP/6-31G(d) level of theory. Distances are given in pm.

Table 3.5 *Boltzmann*-averaged hydrogenation enthalpies $\langle\Delta_{hyd}H\rangle$ at 298.15 K in the gas phase for ribose and 1'-desoxyribose-derived radicals. Only the initial radicals are shown.

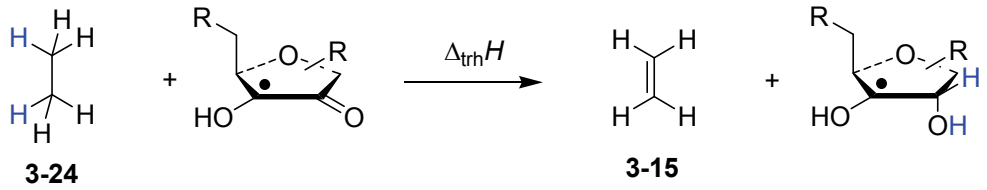

	ROMP2(FC)/ 6-311+G(3df,2p)		G3(MP2)-RAD	
	$\langle\Delta_{trh}H\rangle$[a]	$\langle\Delta_{hyd}H\rangle$[b]	$\langle\Delta_{trh}H\rangle$[a]	$\langle\Delta_{hyd}H\rangle$[b]
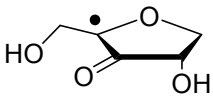 **3-41Ra**	+104.0	-32.3	+100.1	-36.2
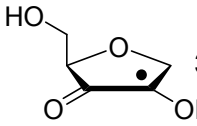 **3-42Ra**	+125.4	-11.0	+121.3	-15.0
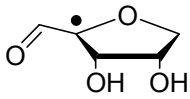 **3-41Rb**	+115.5	-20.8	+108.8	-27.5
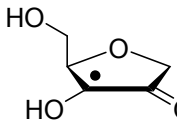 **3-43R**	+128.2	-8.09	+121.9	-14.4
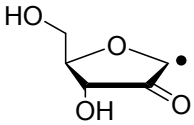 **3-44Ra**	+105.3	-31.0	+103.2	-33.1
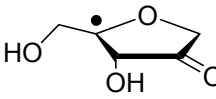 **3-41Rc**	+39.5	-96.8	+41.8	-94.5
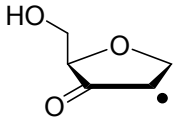 **3-45R**	+93.3	-43.0	+94.1	-42.3
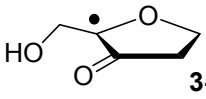 **3-46Ra**	+118.8	-17.5	+114.8	-21.5
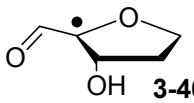 **3-46Rb**	+115.7	-20.7	+109.6	-26.7

[a] Defined as $\Delta_{trh}H = \Delta_fH(C_2H_4) + \Delta_fH(\bullet R_2CH\text{-}OH) - \Delta_fH(\bullet R_2C{=}O) - \Delta_fH(C_2H_6)$. [b] Addition of the reaction enthalpies $\Delta_{trh}H$ to the experimentally determined hydrogenation enthalpy of ethylene $\Delta_{hyd}H(C_2H_4$, **3-15**) = -136.3±0.2 kJ mol^{-1}[105] yields the hydrogenation enthalpy $\Delta_{hyd}H$ of the respective double bond.

The captodative effect of an alkoxy group is not that distinct than for an alcohol as electron-donating group ($\Delta\Delta_{hyd}$H(**3-42Ra/3-41Ra**) = -21.2 kJ mol^{-1}).

Again, hydrogenation enthalpies for sugar models containing an allyl radical such as **3-39Rb** and **3-40Rc**, are systematically larger compared to those of the respective tautomeric forms. This may be exemplified with radical **3-39Rb** whose hydrogenation energy of $\Delta_{hyd}H$(**3-39Rb**) = -62.5 kJ mol^{-1} is 50.9 kJ mol^{-1} larger than that of α-keto radical **3-39Ra**. The obtained hydrogenation product is identical for both species and the energy difference of 50.9 kJ mol^{-1} thus corresponds to the difference in stability of the enol and keto form. Radical **3-40Ra** or **3-41Rc** with isolated unpaired electrons react as typical alkene ($\Delta_{hyd}H$(*exp.*, propene) = -125.0±0.2 kJ mol^{-1} vs. $\Delta_{hyd}H$(**3-40Ra**) = -118.2 kJ mol^{-1}) or ketone ($\Delta_{hyd}H$(**3-22**) = -77.5 kJ mol^{-1} vs. $\Delta_{hyd}H$(**3-41Rc**) = -94.5 kJ mol^{-1}), respectively.

Reaction energies for the dihydrogen transfer between the open-shell sugar models and the nucleotide bases can be calculated from the hydrogenation energies in **Table 3.3** and **Table 3.5** in a straightforward manner. For the reduction of uracil (**3-16**) with C3' ribosyl radical **3-47R** as an example (see **Scheme 3.8**), the reaction enthalpy Δ_{trh}H is identical to the difference in hydrogenation enthalpy of uracil and oxidized ribose radical **3-43R**, which is $\Delta_{trh}H$ = -64.9 kJ mol^{-1}.

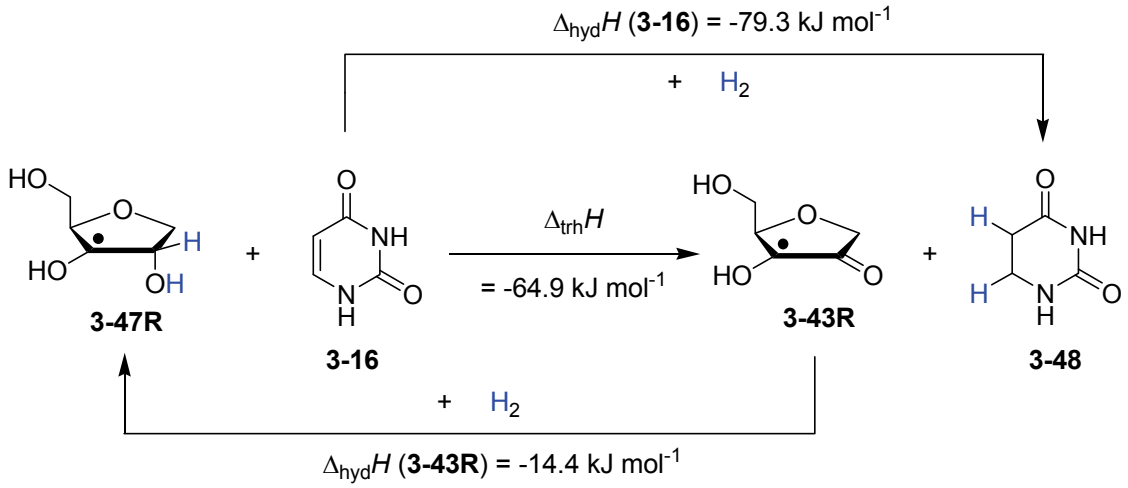

Scheme 3.8 Transfer hydrogenation between ribose model **3-47R** and uracil (**3-16**) using hydrogenation energies calculated at G3(MP2)-RAD level.

In pictoral terms, this difference equates to the horizontal distance on the hydrogenation enthalpy scale shown in **Figure 3.8**. Closer inspection of this scale also

shows that under these circumstances all resonance-stabilized radicals can act as hydrogen donor for the three pyrimidine bases (as well as their *N*-methylated derivatives) if the product represents an acetonyl or formyl radical.

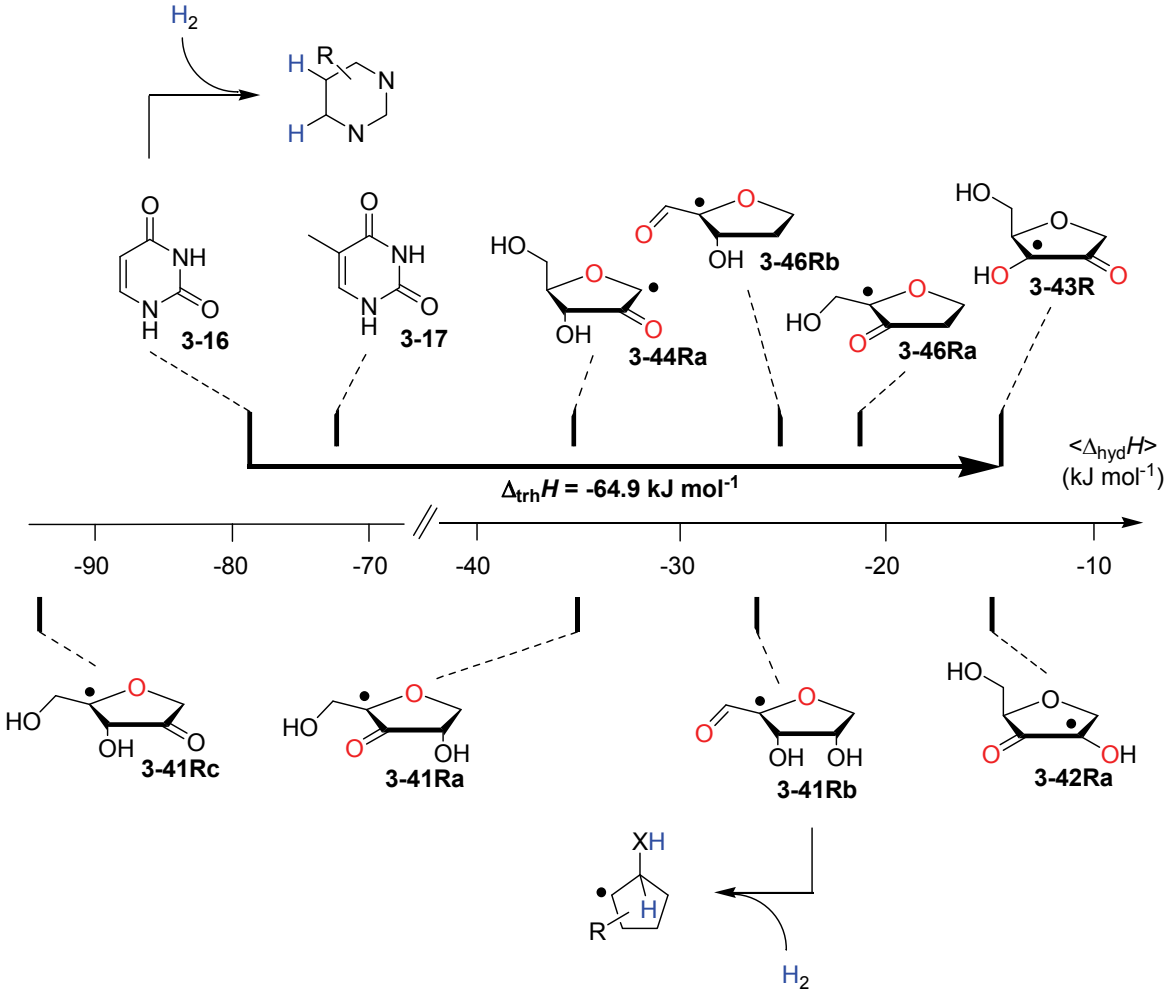

Figure 3.8 Graphical representation of hydrogenation enthalpies $<\Delta_{hyd}H>$ at 298.15 K (G3(MP2)-RAD, in kJ mol^{-1}) of selected open-shell systems in comparison to pyrimidine bases uracil (**3-16**) and thymine (**3-17**).

3.5 Open-shell Nucleotides

In order to assess the thermodynamics of such a process in complete nucleosides, intramolecular transfer hydrogenation reactions have been studied for different types of uridinyl radicals, where the unpaired spin is located on either C2', C3' or C4' position. The energies for intramolecular dihydrogen transfer between sugar and base fragments are depicted in **Figure 3.9**.

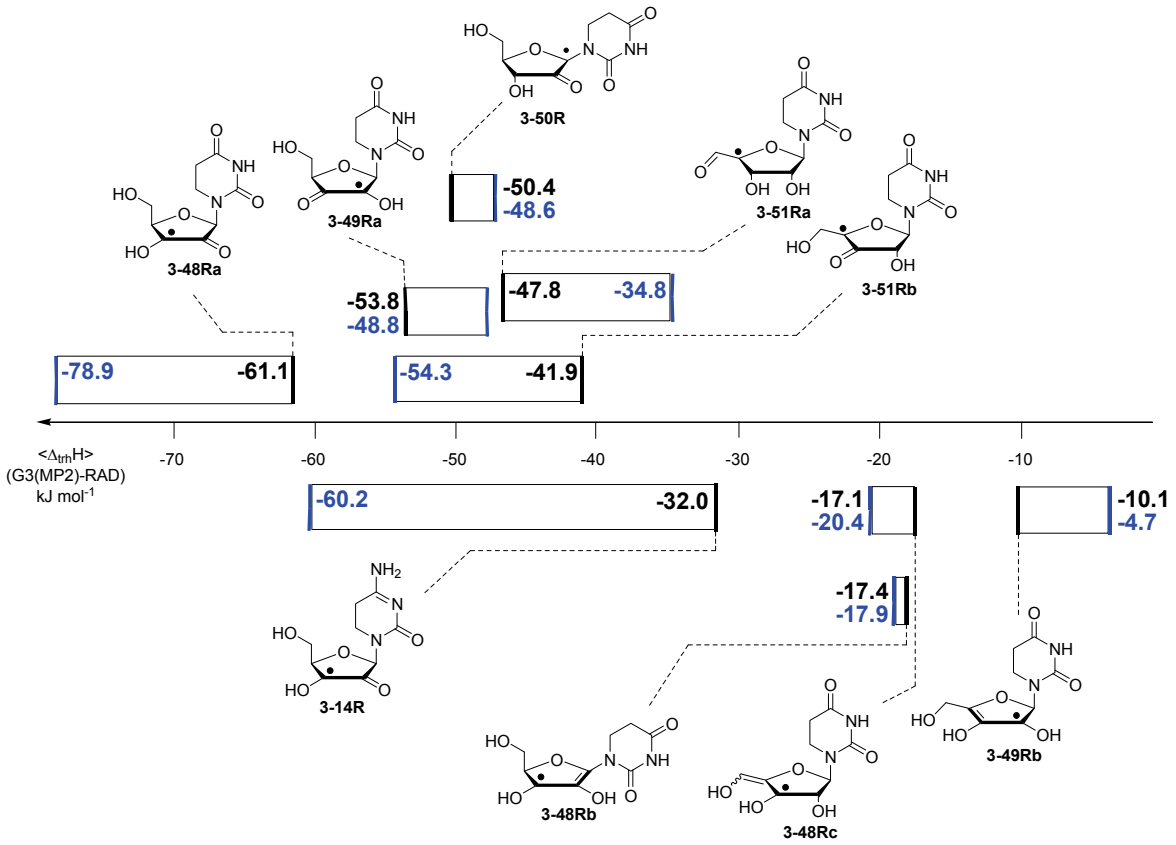

Figure 3.9 *Boltzmann*-averaged transfer hydrogenation enthalpy scale $<\Delta_{trh}H>$ for *C*-centered uridinyl and cytidinyl radicals (G3(MP2)-RAD, in kJ mol^{-1}), black bars gas phase, blue bars addition of ΔG_{solv} (IEF-PCM/UAHF/UHF/6-31G(d) in water). Only the product radicals are shown.

The reaction products are shown with the C-C or C-O double bond in the ribose fragment indicating the origin of the H_2 equivalent. The ROMP2 values can be found in the **Theoretical Appendix**. Energies have been calculated in the gas phase (black bars) as well as in aqueous phase (blue bars) in order to identify the influence of a polar (hydrogen-bonding) medium on the reaction outcome. Comparison of the data of individual components with those of the nucleosides in **Figure 3.9** shows that sugar-to-base transfer hydrogenation becomes slightly less effective on covalent coupling both redox partners. The only exception is uridin-1-yl radical **3-50R** with $\Delta_{trh}H$(**3-50R**) = -50.4 kJ mol^{-1}, compared to the hydrogenation energies of the separated fragments (see **Figure 3.10**).

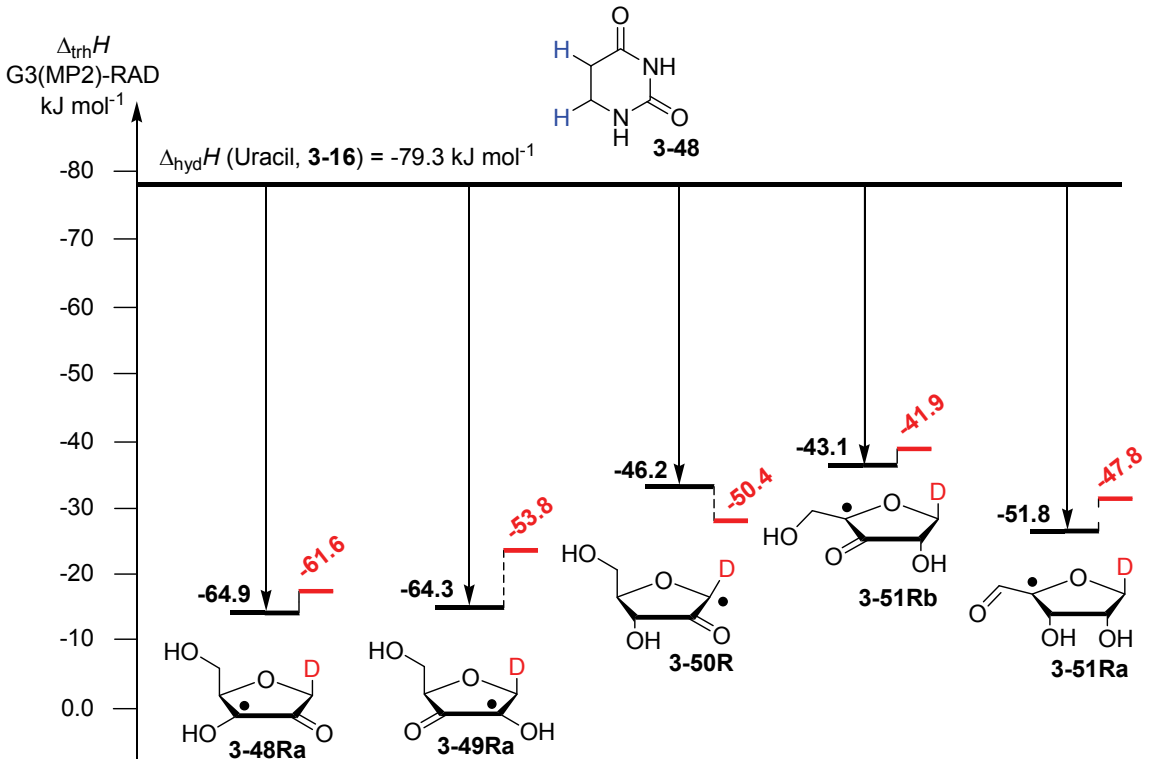

Figure 3.10 Comparison of the redox data for individual components (black bars) and nucleosides (red bars) in the gas phase at G3(MP2)-RAD level of theory.

This difference can be traced back to the presence of a second electron-donating substituent in radical **3-50R**, which is not present in ribose model **3-44Ra**. More generally, the most exothermic intramolecular transfer hydrogenation process is that of C3' uridinyl radical **3-52R** yielding the C2' oxidized open-shell product **3-48Ra** with a reaction energy of $\Delta_{trh}H$(**3-48Ra**) = -61.6 kJ mol^{-1} at G3(MP2)-RAD level in the gas phase. Transfer hydrogenation starting from the C2' radical to yield **3-49Ra** is somewhat less exothermic at $\Delta_{trh}H$(**3-49Ra**) = -53.8 kJ mol^{-1}, closely followed by the reaction of the C1' radical to give product radical **3-50R** with Δ_{trh}H (**3-50R**) = -50.4 kJ mol^{-1}. Hydrogenation energies under the circumstances of generating C-C (instead of C-O) double bonds in the ribose fragment are, in comparison, compararively less exothermic. Switching from uridine to cytosine leads to significantly smaller reaction energies, in line with the smaller hydrogenation energies of cytosine (**3-19**) as compared to uracil (**3-16**) summarized in **Table 3.2**. The above results have again been obtained from *Boltzmann*-averaged enthalpies for fully flexible nucleoside radicals and can potentially be modified through intermolecular interactions present in base-paired systems or polar solvents. In order

to obtain an estimate for the magnitude of these kind of effects, solvation free energies ΔG_{solv} in water were calculated using the continuum solvation model[82] (IEF-PCM/UAHF/UHF//UB3LYP/6-31G(d))[111] and combined with the gas phase results. The resulting hydrogenation energies (see **Figure 3.11**) in polar solution show that the C2'-oxidized uridinyl radical **3-48R** and the respective cytodinyl radical **3-14R** benefit most from the solvation resulting in a more exothermic reaction outcome. The usage of different PCM models, radii or theory leads to rather similar thermodynamics (see **Theoretical Appendix**) The higher exothermicity is the consequence of the better solvation of the product radical due to the omission of the hydrogen bond upon oxidation of the C2' hydroxyl group.

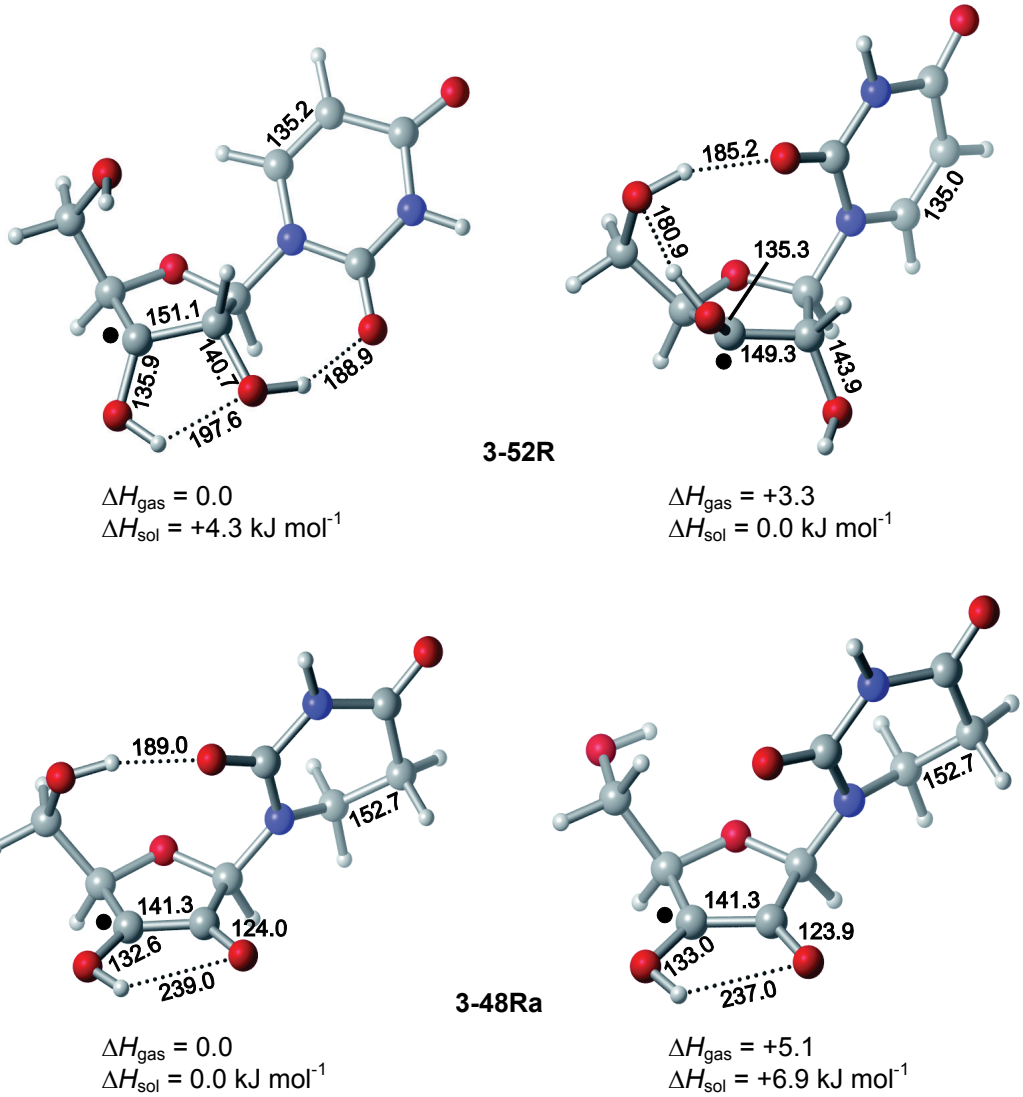

Figure 3.11 Graphical representation of the two most stable conformers of uridinyl radical **3-52R** and **3-48Ra** obtained at G3(MP2)-RAD level in gas phase and with implicit solvation of water.

3.6 Open-shell Peptides

An obvious, but never considered, alternative dihydrogen donor could be the RNR mutant with its redox active amino acid residues serine (Ser, **3-53**) and threonine (Thr, **3-54**) itself. The oxidized form of serine, α-formyl glycine (**3-55**) is a post-translational modification found in the active center of sulfatases and sulfotransferases. **3-55** is generated by the formyl generating enzyme (FGE) from a cysteine (Cys, **3-56**) under aerobic conditions (see **Scheme 3.9**).[112] Residue **3-55** forms a metastable hydrate **3-55-H_2O**, which attacks the sulfate ester in a nucleophilic manner to give the hydrolyzed product followed by fragmentation and the release of hydrogensulfate HSO_4^- and regenerated **3-55**.

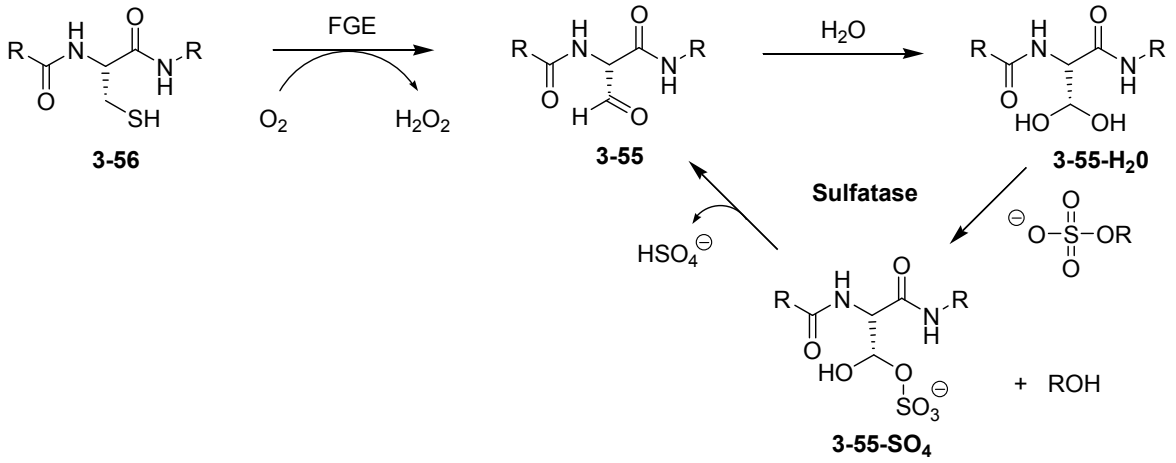

Scheme 3.9 FGE-catalyzed post-translational modification of cysteine to α-formyl glycine (**3-55**) and the following hydrolysis of sulfate esters.

Inspection of the linear sequence of the α subunit of class I RNR[96] shows that a serine moiety (S_{436}) is in close proximity to the spin-carrying cysteine C_{439}. Thermodynamic data for hydrogen atom transfer from all possible open-shell RNR cofactors to generate the redox precursor **3-53R** or **3-54R** are summarized in **Table 3.6**. All reactions involving peptide-derived radicals, like glycyl (**3-6R**), cysteinyl (**3-56R**) and the O-centered tyrosyl radical **3-57R**, are unfavored from a thermochemical point of view. The *C*-centered radical **3-53R** of serine is destabilized compared to the glycyl radical **3-6R** by a value of ΔRSE = +16.7 kJ mol^{-1}. The decrease of stability in C_α-substituted peptide radicals has already been investigated by *Hioe*.[113]

Table 3.6 Bond dissociation and radical stabilization energies of enzymatically relevant radicals at G3(MP2)-RAD level in the gas phase (at 298.15 K, in kJ mol^{-1}).

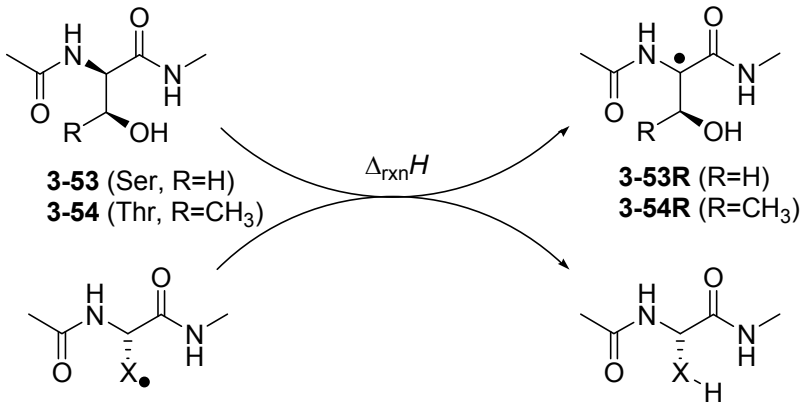

R•	RSE	BDE[a]	<$\Delta_{rxn}H$>		<$\Delta_{sol}H$>	
			Ser (**2-53**)	Thr (**2-54**)	Ser (**2-53**)	Thr (**2-54**)
3-53 (R=H)	-58.1	+381.2				
3-54 (R=Me)	-50.4	+388.9				
X•						
Cys-S• (**3-56R**)	-13.4	+368.2	**+13.0**	**+20.7**	+15.3[b] +11.7[c]	+23.0[b] +18.6[c]
Gly• (**3-6R**)	-74.8	+364.5	**+16.7**	**+24.4**	+9.15[b] +15.0[c]	+16.8[b] +21.8[c]
Tyr-O• (**3-57R**)	-151.0[113]	+346.1	**+35.1**	**+42.8**		
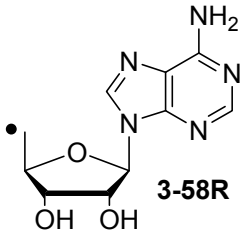 **3-58R**	-6.8[114]	+432.5	**-51.3**	**-43.6**		

[a] BDE(R-H)= RSE (R•) + BDE(Ref-H) with BDE(H_3C-H) = +439.3, BDE(HO-H) = +497.1 and BDE(HS-H) = +381.6 kJ mol^{-1}.[115]

[b]Addition of ΔG_{solv} in water at IEF-PCM/UAHF/UHF/6-31G(d)//UB3LYP/6-31G(d) level. [c] Addition of ΔG_{solv} in heptane at IEF-PCM/UAHF/UHF/6-31G(d)//UB3LYP/6-31G(d) level.

Due to repulsive interactions between the C_α substituent and the peptide backbone the radical stabilization is strongly conformation-dependent, which is shown in **Figure 3.12**. Hydrogen-bonding of the hydroxyl group has no supporting effect to the push-pull stabilization. The methyl group in the C_α radical of threonine (**2-54R**) leads to a reduction of +7.7 kJ mol^{-1} of the reduction of the RSE compared to serine.

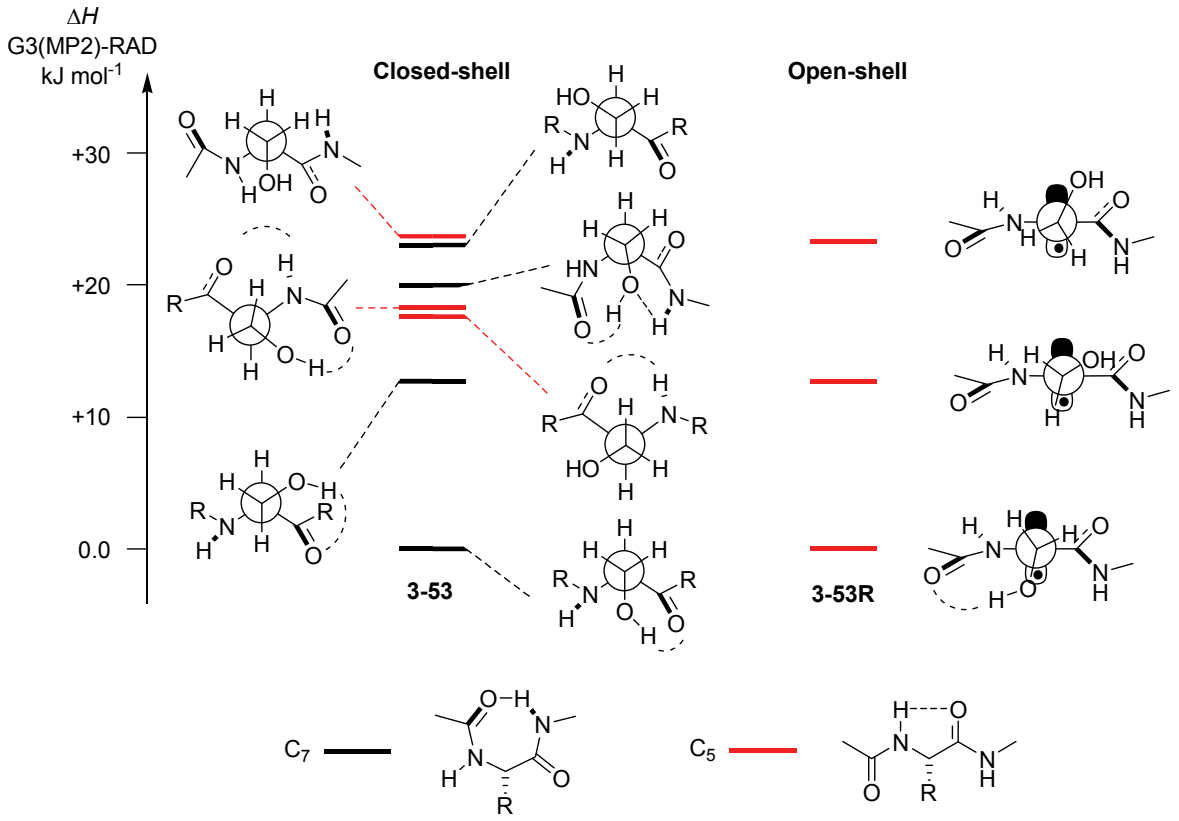

Figure 3.12 Relative conformational energies in the gas phase at 298.15 K for serine peptide **3-53** and its open-shell form **3-53R** obtained at G3(MP2)-RAD level (black bars C_7, red bars C_5 conformation).

In the case of serine, the radical formation in the gas phase is endothermic for either the cysteinyl ($\Delta_{rxn}H$(**3-56R**) = +13.0 kJ mol^{-1}) or the glycyl radical ($\Delta_{rxn}H$(**3-6R**) = +16.7 kJ mol^{-1}). Mimicking the environment in the active site of RNR and the role of hydrogen bonds by inclusion of implicit solvation lowers the enthalpy slightly, but negative values are not reached. Hydrogen transfer by glycine benefits from hydrophilic solvation in water ($\Delta_{sol}H$(**3-6R**) = +9.2 kJ mol^{-1}), whereas the reaction involving the cysteinyl radical profits from the hydrophobicity of heptanes to model the unpolar environment in the enzyme ($\Delta_{sol}H$(**2-65R**) = +11.7 kJ mol^{-1}). *Coote* and coworkers recently reported that the stability of carboxy-aminoxyl and peroxyl radicals is strongly affected by anionic point charges and an associated SOMO-HOMO conversion even on a long-range scale.[116] The glutamate residue (E_{441}), responsible for embedding the nucleotide in the active site, is located in near proximity to the serine residue and could have a positive effect on the hydrogen transfer on closer inspection. Unfortunately, this residue has been replaced in the E441Q mutant by a glutamine.

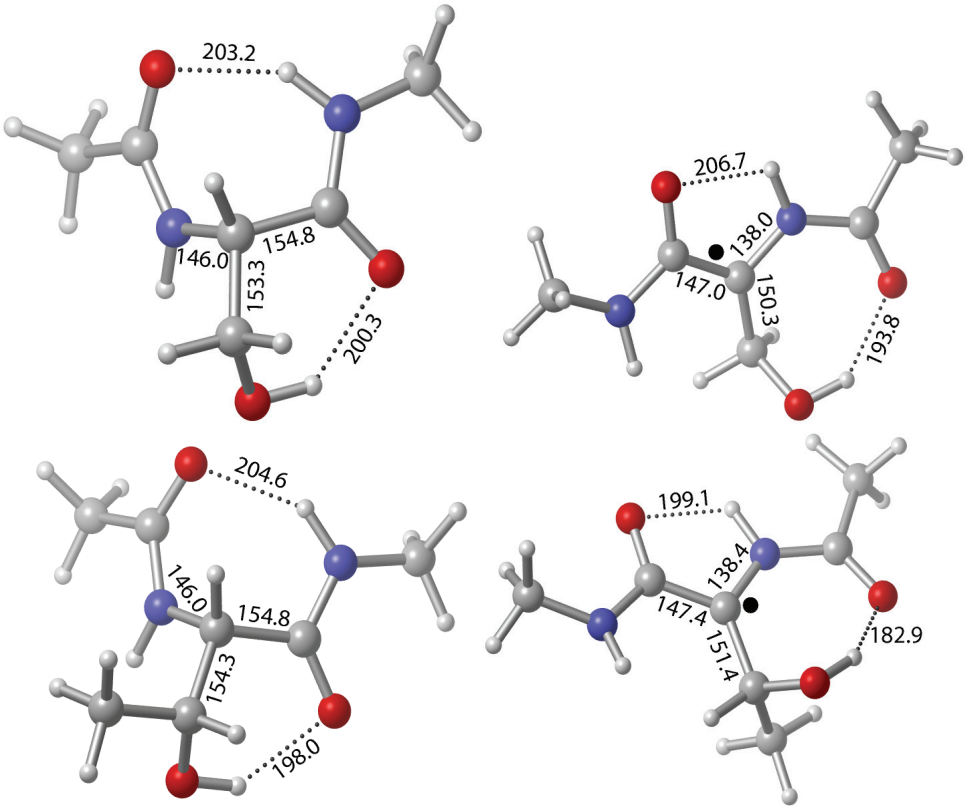

Figure 3.13 Graphical representation of the energetically most favorable conformations of closed-shell peptides serine (**3-53**) and threonine (**3-54**, left) and their radicals (right) at G3(MP2)-RAD level of theory.

As expected, only for the non-stabilized primary 5'-adenosyl radical **3-58R** the hydrogen exchange is strongly exothermic. Therefore, it is unlikely that the peptide backbone of RNR can act as dihydrogen donor. The reaction enthalpies for the subsequent transfer hydrogenation are nevertheless depicted in **Table 3.7** and graphically displayed in **Figure 3.14**.

Table 3.7 *Boltzmann*-averaged hydrogenation enthalpies $<\Delta_{hyd}H>$ at 298.15 K in the gas phase for serine- and threonine-derived radicals. Only the initial radicals are shown.

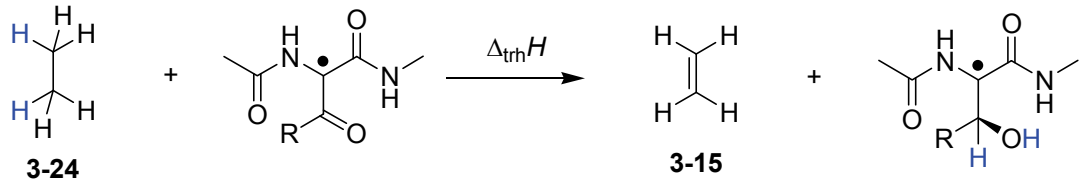

R	ROMP2(FC)/ 6-311+G(3df,2p)		G3(MP2)-RAD	
	$<\Delta_{trh}H>$[a]	$<\Delta_{hyd}H>$[b]	$<\Delta_{trh}H>$[a]	$<\Delta_{hyd}H>$[b]
H (**3-59R**)	+89.60	-46.7	+84.8	-51.7
CH_3 (**3-60R**)	+92.8	-43.5	+90.1	-46.2
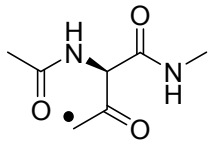 **3-61Ra**	+78.7	-57.6	+79.2	-57.1
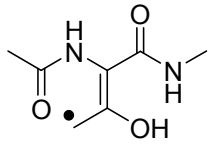 **3-61Rb**	+88.0	-48.3	+92.5	-43.8

[a] Defined as $\Delta_{trh}H = \Delta_fH(C_2H_4) + \Delta_fH(\bullet R_2CH\text{-}OH) - \Delta_fH(\bullet R_2C{=}O) - \Delta_fH(C_2H_6)$. [b] Addition of the reaction enthalpies $\Delta_{trh}H$ to the experimentally determined hydrogenation enthalpy of ethylene $\Delta_{hyd}H(C_2H_4$, **3-15**) = -136.3±0.2 kJ mol^{-1}[105] yields the hydrogenation enthalpy $\Delta_{hyd}H$ of the respective double bond.

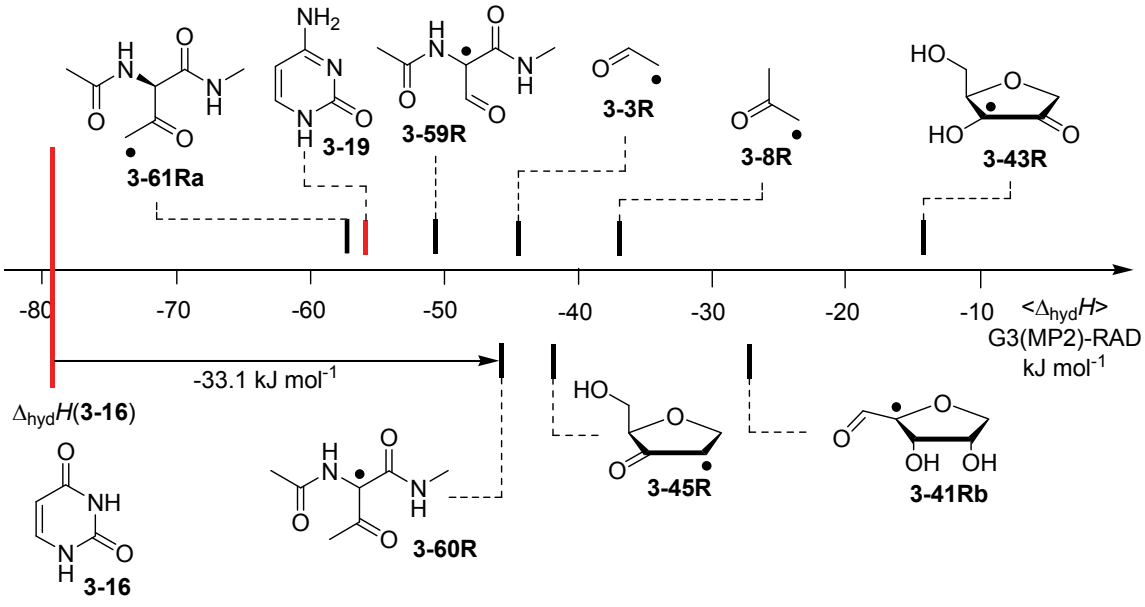

Figure 3.14 *Boltzmann*-averaged transfer hydrogenation enthalpy scale $<\Delta_{trh}H>$ for *C*-centered peptide radicals (G3(MP2)-RAD, in kJ mol^{-1}) compared to selected carbonyl radicals.

Again, all peptide-derived radicals are in principle capable to reduce the pyrimidine bases in an exothermic manner, except for radical **3-61Ra** in combination with cytosine ($\Delta_{trh}H$(**3-19**) = -56.1 – (-57.1) = +1.0 kJ mol^{-1}). The radical stabilization as a result of the push-pull effect of the electron-donating amino and the electron-accepting carbonyl group is not as as significant in glycyl radical **3-6R** due to the steric repulsion of the C_α substituent. The driving force at G3(MP2)-RAD level in the gas phase for the formation of 5,6-dihydrouracil is for serine C_α radical **3-53R** $\Delta_{trh}H$(**3-53R**) = -27.6 kJ mol^{-1} and for threonine radical **3-54R** $\Delta_{trh}H$(**3-54R**) = -33.1 kJ mol^{-1}, respectively. Upon oxidation, the resulting hydrogen bond accepting formyl group in **3-59R** cannot compensate the repulsive interactions on the RSE (see **Figure 3.15**). Therefore, **3-59R** and **3-60R** are acting in a comparable way just like simple delocalized π radicals. Oxidation of the threonine-derived radical to form **3-61Ra** with the unpaired spin in the side chain is unlikely due to simple thermochemical considerations.

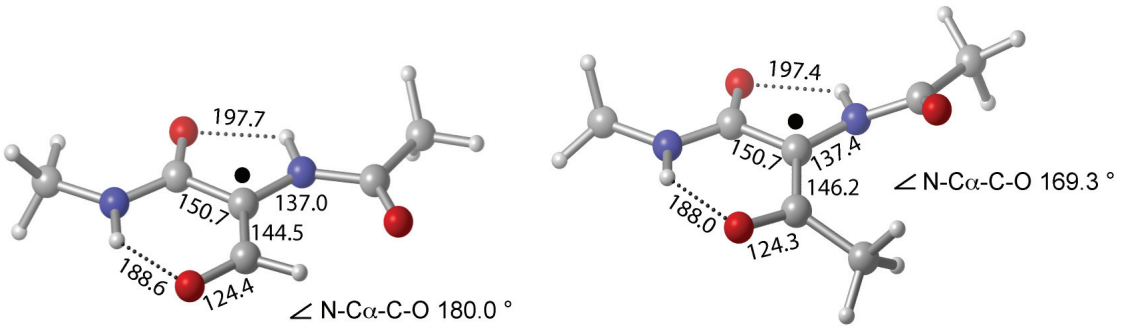

Figure 3.15 Graphical representation of the energetically most favorable conformations of oxidized peptide radicals **3-59R** (left) and **3-60R** (right) at G3(MP2)-RAD level of theory.

3.7 Conclusion

The potential of biologically inspired open-shell intermediates to act as reductants in transfer hydrogenation reactions to alkenes has been investigated theoretically. The results fully support the strongly reductive nature of these species, if the oxidized product is a captodatively stabilized radical. As revealed through comparison to hydrogenation energies for individual nucleotide bases and also seen in the reaction energies for intramolecular transfer hydrogenation in, for example, the C3' uridinyl

radical **3-52R**, the strongly reductive nature of ribosyl radicals implies that pyrimidine bases can be reduced in an exothermic fashion.

The reaction energies for inter- and intramolecular transfer hydrogenation presented herein permit no statement on the pathways how such a process may occur. Nevertheless, some speculations on possible pathways can be made. While a concerted dihydrogen shift can most likely be ruled out in view of the relative orientation of the donor and acceptor fragments in **3-52R**, two different reaction types for stepwise H_2 transfer are feasible (see **Scheme 3.10**): 1.) Reactions involving open-shell intermediates at the nucleotide base. This may either involve initial single hydrogen atom or proton-coupled electron transfer to the uracil C6 position, followed by a second H• transfer to yield product radical **3-48R**. *Giese et al.* recently reported that hydrogen atom transfer reactions in C4' desoxythymidine radicals can occur quite rapidly to give C5 dihydro thymyl radical, detected as the main open-shell species by EPR spectroscopy.[117] 2.) An ionic pathway, where the unpaired spin never leaves the ribose unit. This may involve, for example, initial protonation of the pyrimidine C4 carbonyl oxygen, followed by hydride transfer between the ribose C2' and the uracil C6 position. After deprotonation and tautomerization of radical cation **3-63Rb** the captodatively stabilized product **3-48Ra** is formed. What both pathways have in common is the direct inclusion of the uracil C6 position as shown in **Figure 3.11** due to the spatial proximity of this center to the reacting C2' ribose center.

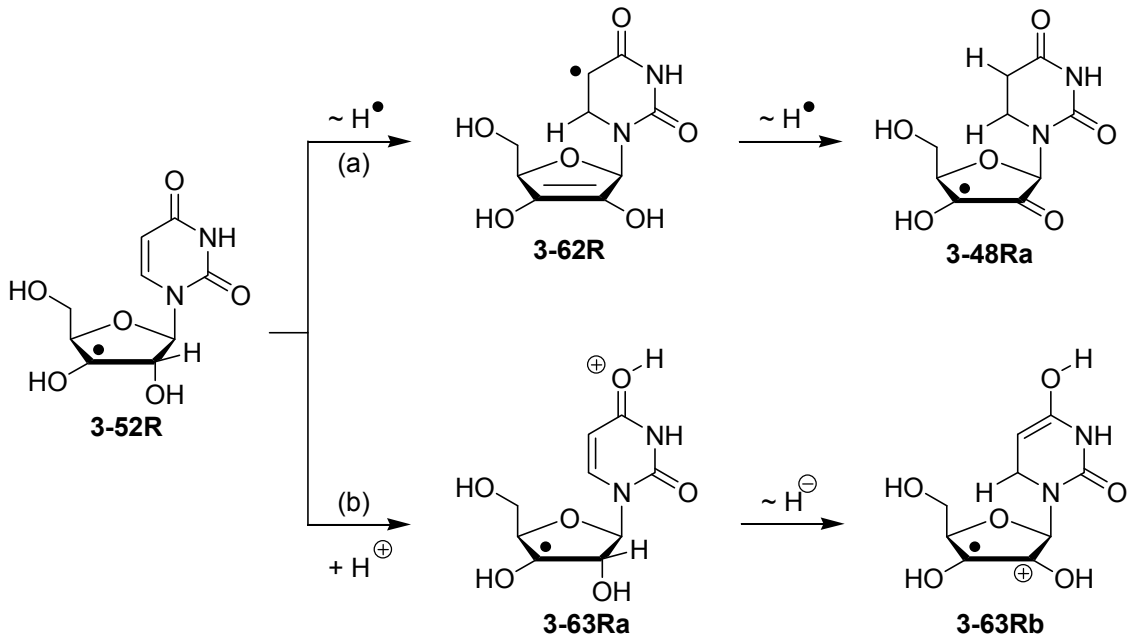

Scheme 3.10 Possible pathways for stepwise hydrogen transfer reactions using C3' radical **3-52R** as example.

Also, recent theoretical studies by *Gutowski* and coworkers on the strand cleavage of 2'-desoxycytosine-3'-phosphate revealed that the barriers for the hydrogen atom transfer from the C2' position of the sugar unit are lowered significantly upon addition of "H•" (either concerted or stepwise) to the N3 position of the cytosine base.[118]

3.8 Theoretical Appendix

Geometry optimizations of all systems have been performed at the (U)B3LYP/ 6-31G(d) level of theory. Thermochemical corrections to 298.15 K have been calculated at the same level of theory using the rigid rotor/harmonic oscillator model. A scaling factor of 0.9806 has been used for this latter part. Single point energies have then been calculated at the (RO)MP2(FC)/6-311+G(3df,2p) level. Combination of the MP2 total energies with thermochemical corrections obtained at B3LYP level yield the enthalpies termed as "ROMP2" in the text.

$$H(MP2) = E_{tot}(MP2) + H(B3LYP, 0.9806) - E_{tot}(B3LYP) \qquad \textbf{(eq. 3.1)}$$

In the conformationally flexible systems enthalpies and free energies have been calculated as *Boltzmann*-averaged values (w ≥ 1%) over all available conformers obtained by a preliminary conformational search using the MM3* force field[79] implemented in *MacroModel 9.7*.[80]

The *Boltzmann*-averaged enthalpies of n conformers are obtained by **eq. 3.2**:

$$w_i = \left. \exp\left(\frac{-\Delta H_{298}}{R\,T}\right) \middle/ \sum_{i=1}^{n} \frac{-\Delta H_{298}}{R\,T} \right.$$

$$<H_{298}> = \sum_{i=1}^{n} w_i H_i \qquad \textbf{(eq. 3.2)}$$

Improved relative energies are obtained using the G3(MP2)-RAD scheme proposed by *Radom et al.*[81] These are based on the same geometries and thermal corrections as the MP2 level:

$$E_{tot}(G3(MP2)\text{-}RAD) = E_{tot}((U)CCSD(T)/6\text{-}31G(d)//UB3LYP/6\text{-}31G(d) + \\ + DE(G3MP2large) + DE(HLC) \qquad \textbf{(eq. 3.3)}$$

$$DE(G3MP2large) = (RO)MP2(FC)/G3MP2large - (RO)MP2(FC)/6\text{-}31G(d) \qquad \textbf{(eq. 3.4)}$$

$$DE(HLC) = -A\,n(\beta) - B\,(n(\alpha) - n(\beta)) \qquad \textbf{(eq. 3.5)}$$

with A = 9.413×10^{-3} au, B = 3.969×10^{-3} au and n(α) and n(β) represent the valence electrons, respectively.

Additional consideration of solvation was included by calculating solvation free energies using the polarizable continuum solvation model in its IEF-PCM,[82] C-PCM[119] or SMD[60] variant and adding them to the gas phase enthalpies. In case for the IEF- and C-PCM calculations the United Atom Hartree Fock (UAHF) radii in combination with UHF/6-31G(d) theory have been used.[83] (U)CCSD(T) calculations have been performed with *MOLPRO*,[84] the geometry optimizations, frequencies and PCM calculations with *Gaussian03 Rev. D.01*.[85] The SMD model is implemented in *Gaussian09 Rev. C.01*.[86]

Table 3.8 Energies and enthalpies for closed- and open-shell compounds at various levels of theory in the gas phase in Hartree (298.15 K, 1 atm).

	C_2H_6 (**3-24**)	C_2H_4 (**3-15**)	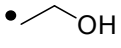 (**3-1R**)	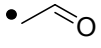 (**3-3R**)	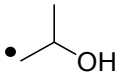 (**3-33R**)
	E_{tot} **H_{298}**	E_{tot} **H_{298}**	E_{tot} **H_{298}**	E_{tot} **H_{298}**	E_{tot} **H_{298}**
UB3LYP	-79.834175 **-79.752210**	-78.5874583 **-78.533222**	-154.3613832 **-154.291870**	-153.1715366 **-153.125159**	-193.6803856 **-193.581855**
ROMP2	-79.6200629 **-79.5380979**	-78.3932565 **-78.3390202**	-154.066633 **-153.9971198**	-152.8787261 **-152.8323485**	-193.2916261 **-193.1930955**
G3(MP2)-RAD	-79.7268957 **-79.6449307**	-78.4841764 **-78.4299401**	-154.1927918 **-154.1232786**	-152.989464 **-152.9430864**	-193.4603518 **-193.3618212**
	 (**3-8R**)	 (**3-4R**)	 (**3-2R**)	 (**3-34R_H**)	 (**3-34R**)
	E_{tot} **H_{298}**	E_{tot} **H_{298}**	E_{tot} **H_{298}**	E_{tot} **H_{298}**	E_{tot} **H_{298}**
UB3LYP	-192.4950213 **-192.419618**	-118.4711107 **-118.377919**	-117.2603540 **-117.190479**	-157.7856471 **-157.663659**	-156.5772554 **-156.478343**
ROMP2	-192.1068777 **-192.0314744**	-118.1690627 **-118.0758710**	-116.9739045 **-116.9040295**	-157.3910101 **-157.2690220**	-156.1966271 **-156.0977147**
G3(MP2)-RAD	-192.2600568 **-192.1846535**	-118.3090897 **-118.2158980**	-117.0984521 **-117.0285771**	-157.5736006 **-157.4516125**	-156.3632755 **-156.2643631**
	 (**3-27R_H**)	 (**3-27R**)	 (**3-29R_H**)	 (**3-29R**)	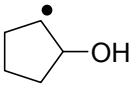 (**3-36R_H**)
	E_{tot} **H_{298}**	E_{tot} **H_{298}**	E_{tot} **H_{298}**	E_{tot} **H_{298}**	E_{tot} **H_{298}**
UB3LYP	-235.2139163 **-235.053530**	-234.0081729 **-233.871204**	-195.8948865 **-195.764645**	-194.6860804 **-194.579304**	-271.1017498 **-270.966094**
ROMP2	-234.6443077 **-234.4839214**	-233.4544966 **-233.3175277**	-195.4190525 **-195.2888110**	-194.2269215 **-194.1201451**	-270.5398569 **-270.4042011**
G3(MP2)-RAD	-234.8956477 **-234.7352614**	-233.6883126 **-233.5513437**	-195.6277641 **-195.4975226**	-194.4182277 **-194.3114513**	-270-7772463 **-270.6415905**

Table 3.9 Energies and enthalpies for closed- and open-shell compounds at various levels of theory in the gas phase in Hartree (298.15 K, 1 atm).

	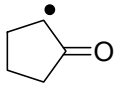 (**3-36R**)	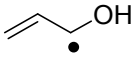 (**3-35R**)	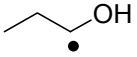 (**3-35R_H**)	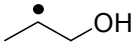 (**3-37R_H**)	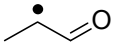 (**3-37R**)
	E_{tot} **H_{298}**	E_{tot} **H_{298}**	E_{tot} **H_{298}**	E_{tot} **H_{298}**	E_{tot} **H_{298}**
UB3LYP	-269.9214771 **-269.808652**	-192.4759940 **-192.400134**	-193.6887929 **-193.588901** -193.6887181 **-193.588740**	-193.6793493 **-193.580597** -193.6795750 **-193.580636**	-192.4957378 **-192.419812** -192.4968916 **-192.420785**
ROMP2	-269.3582119 **-269.2453868**	-192.0973633 **-192.0215033**	-193.2966386 **-193.1967467** -193.2968177 **-193.1968396**	-193.2877564 **-193.1890041** -193.2880859 **-193.1891469**	-192.1049337 **-192.0290079** -192.1062969 **-192.0301903**
G3(MP2)-RAD	-269.5800170 **-269.4671919**	-192.2511757 **-192.1753157**	-193.4654625 **-193.3655706** -193.4655549 **-193.3655768**	-193.4569905 **-193.3582382** -193.4572485 **-193.3583095**	-192.2582774 **-192.1823516** -192.2594781 **-192.1833715**
	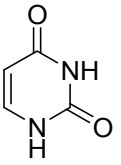 (**3-16**)	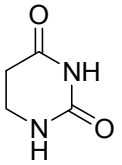 (**3-16_H**)	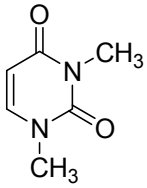 (**3-18**)	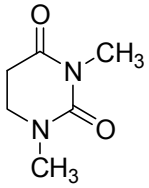 (**3-18_H**)	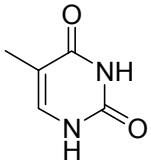 (**3-17**)
	E_{tot} **H_{298}**	E_{tot} **H_{298}**	E_{tot} **H_{298}**	E_{tot} **H_{298}**	E_{tot} **H_{298}**
B3LYP	-414.8159434 **-414.723082**	-416.0289298 **-415.912314**	-493.4392316 **-493.288006**	-494.6502952 **-494.475402**	-454.1363070 **-454.014332**
MP2	-414.0942780 **-414.0014156**	-415.2957353 **-415.1791195**	-492.5231659 **-492.3719403**	-493.7221289 **-493.5472357**	-453.3203336 **-453.1983586**
G3(MP2)-RAD	-414.3433253 **-414.2504637**	-415.5603634 **-415.4437476**	-492.8575198 **-492.7062942**	-494.0722892 **-493.8973960**	-453.6113003 **-453.4893302**

Table 3.10 Energies and enthalpies for nucleobases at various levels of theory in the gas phase in Hartree (298.15 K, 1 atm).

	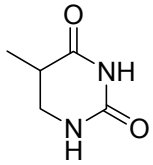 (**3-17_H**)	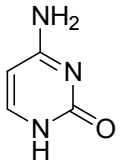 (**3-19**)	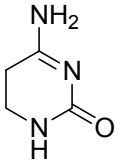 (**3-19_H**)	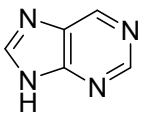 (**3-31**)	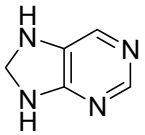 (**3-31_H**)
	E_{tot} **H_{298}**	E_{tot} **H_{298}**	E_{tot} **H_{298}**	E_{tot} **H_{298}**	E_{tot} **H_{298}**
B3LYP	-455.3449323 **-455.199176**	-394.9280116 **-394.823487**	-396.1318383 **-396.003514**	-411.9463521 **-411.846036**	-412.1301989 **-412.006589**
MP2	-454.5187530 **-454.3729967**	-394.2120332 **-394.1075086**	-395.4035169 **-395.2751926**	-411.1656980 **-411.0653819**	-412.3345434 **-412.2109335**
G3(MP2)-RAD	-454.8257664 **-454.6800101**	-394.1075086 **-394.3643732**	-395.6771488 **-395.5488245**	-411.4345202 **-411.3342041**	-412.6233834 **-412.4997735**
	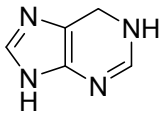 (**3-31a_H**)	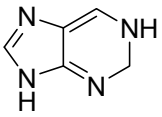 (**3-31b_H**)	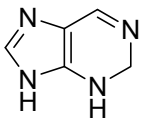 (**3-31c_H**)	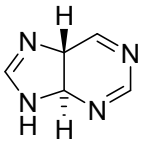 (**3-31d_H**)	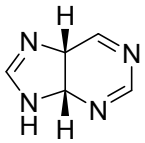 (**3-31e_H**)
	E_{tot} **H_{298}**	E_{tot} **H_{298}**	E_{tot} **H_{298}**	E_{tot} **H_{298}**	E_{tot} **H_{298}**
B3LYP	-413.1324971 **-413.008528**	-413.1109252 **-412.987804**	-413.1136403 **-412.990115**	-413.0741241 **-412.951611**	-4120932267 **-412.970365**
MP2	-412.3432303 **-412.2192612**	-412.3176429 **-412.1945217**	-412.3252181 **-412.2016928**	-412.2813681 **-412.1588550**	-412.2962836 **-412.1734219**
G3(MP2)-RAD	-412.6294486 **-412.5054795**	-412.6078629 **-412.4847417**	-412.6125301 **-412.4890048**	-412.5767815 **-412.4542684**	-412.5923974 **-412.4695357**
	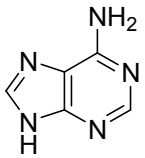 (**3-25**)	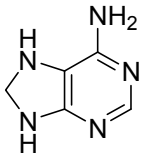 (**3-25_H**)	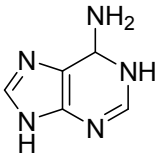 (**3-25a_H**)	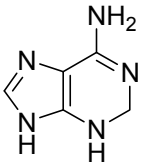 (**3-25b_H**)	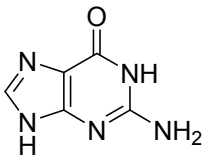 (**3-26**)
	E_{tot} **H_{298}**	E_{tot} **H_{298}**	E_{tot} **H_{298}**	E_{tot} **H_{298}**	E_{tot} **H_{298}**
B3LYP	-467.3181723 **-467.199675**	-468.4966380 **-468.354402**	-468.4878746 **-468.345603**	-468.4799493 **-468.338478**	-542.5500873 **-542.425985**
MP2	-466.4494932 **-466.3309998**	-467.6141961 **-467.4719598**	-467.6134757 **-467.4712041**	-467.6037901 **-467.4623188**	-541.5875930 **-541.4634907**
G3(MP2)-RAD	-466.75333230 **-466.6348350**	-467.9391229 **-467.7968866**	-467.9346456 **-467.7923740**	-467.9254881 **-467.7840168**	-541.9189154 **-541.7948131**

Table 3.11 Energies and enthalpies for nucleobases at various levels of theory in the gas phase in Hartree (298.15 K, 1 atm).

	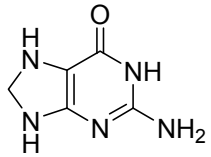 (**3-26_H**)	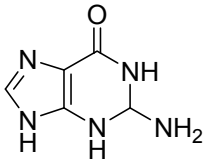 (**3-26a_H**)
	E_{tot} **H_{298}**	E_{tot} **H_{298}**
B3LYP	-543.7270992	-543.7145259
	-543.579564	**-543.566937**
MP2	-542.7510040	-542.7486877
	-542.6034689	**-542.6010988**
G3(MP2)-RAD	-543.1036030	-543.0976341
	-542.9560079	**-542.9500452**

Table 3.12 Energies and enthalpies for ribose models at various levels of theory in the gas phase in Hartree (298.15 K, 1 atm).

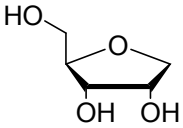

(**3-22_H**)

	B3LYP		MP2		G3(MP2)-RAD	
	E_{tot}	**H_{298}**	E_{tot}	**H_{298}**	E_{tot}	**H_{298}**
2	-497.397220	**-497.230477**	-496.5596005	**-496.3928574**	-496.8895632	**-496.7228201**
11	-497.396662	**-497.230071**	-496.5592698	**-496.3926785**	-496.8891756	**-496.7225843**
16	-497.39640	**-497.229533**	-496.5582756	**-496.3914006**	-496.8881060	**-496.7212310**

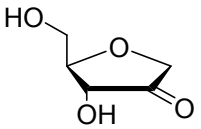

(**3-22**)

	B3LYP		MP2		G3(MP2)-RAD	
	E_{tot}	**H_{298}**	E_{tot}	**H_{298}**	E_{tot}	**H_{298}**
3	-496.1930950	**-496.050648**	-495.3584727	**-495.2160257**	-495.672666	**-495.5302185**
27	-496.1914556	**-496.049076**	-495.3567252	**-495.2143456**	-495.670863	**-495.5284832**
5	-496.1867202	**-496.044244**	-495.3538885	**-495.2114123**	-495.668127	**-495.5256512**

Table 3.13 Energies and enthalpies for ribose models at various levels of theory in the gas phase in Hartree (298.15 K, 1 atm).

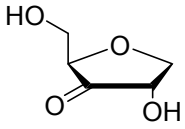

(**3-20**)

	B3LYP		MP2		G3(MP2)-RAD	
	E_{tot}	**H_{298}**	E_{tot}	**H_{298}**	E_{tot}	**H_{298}**
5	-496.1883279	**-496.045392**	-495.3537861	**-495.2108502**	-495.6679202	**-495.5249843**
2	-496.1867424	**-496.044049**	-495.353377	**-495.2106836**	-495.6676771	**-495.5249837**
8	-496.1879531	**-496.045105**	-495.3530798	**-495.2102317**	-495.667255	**-495.5244069**
6	-496.1864131	**-496.043627**	-495.3527991	**-495.210013**	-495.6668444	**-495.5240583**
4	-496.1885387	**-496.045615**	-495.352261	**-495.2093373**	-495.6666437	**-495.5237200**

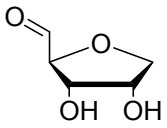

(**3-21**)

	B3LYP		MP2		G3(MP2)-RAD	
	E_{tot}	**H_{298}**	E_{tot}	**H_{298}**	E_{tot}	**H_{298}**
1	-496.1889342	**-496.046459**	-495.3553908	**-495.2129156**	-495.6693859	**-495.5269107**
7	-496.1852568	**-496.042536**	-495.3520419	**-495.2093211**	-495.6655164	**-495.5227956**
9	-496.1849254	**-496.042696**	-495.3518052	**-495.2095758**	-495.6659202	**-495.5236908**
13	-496.1840697	**-496.041779**	-495.3510202	**-495.2087295**	-495.6652322	**-495.5229415**

Table 3.14 Energies and enthalpies for 2'-desoxyribose model **3-45_H** at various levels of theory in the gas phase in Hartree (298.15 K, 1 atm).

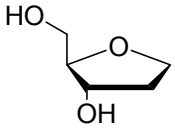

(**3-45_H**)

	B3LYP		MP2		G3(MP2)-RAD	
	E_{tot}	**H_{298}**	E_{tot}	**H_{298}**	E_{tot}	**H_{298}**
9	-422.1838555	**-422.022484**	-421.4342941	**-421.2729226**	-421.7357118	**-421.5743403**
6	-422.1831374	**-422.021856**	-421.4328604	**-421.271579**	-421.7343532	**-421.5730718**
3	-422.1830676	**-422.021595**	-421.4318483	**-421.2703757**	-421.7333124	**-421.5718398**
15	-422.1825881	**-422.021314**	-421.4325334	**-421.2712593**	-421.7342896	**-421.5730155**

Table 3.15 Energies and enthalpies for 2'-desoxyribose models at various levels of theory in the gas phase in Hartree (298.15 K, 1 atm).

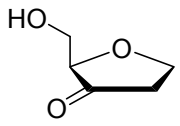

(**3-45**)

	B3LYP		MP2		G3(MP2)-RAD	
	E_{tot}	**H_{298}**	E_{tot}	**H_{298}**	E_{tot}	**H_{298}**
4	-420.9859207	**-420.848397**	-420.2375691	**-420.1000454**	-420.5228435	**-420.3853198**
6	-420.9846209	**-420.847150**	-420.2377431	**-420.1002722**	-420.5228589	**-420.385388**
5	-420.9838296	**-420.846388**	-420.2377331	**-420.1002915**	-420.5226863	**-420.3852447**
7	-420.9848834	**-420.847446**	-420.237967	**-420.1005296**	-420.5230925	**-420.3856551**
2	-420.9827371	**-420.845551**	-420.2377247	**-420.1005386**	-420.5227934	**-420.3856073**

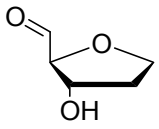

(**3-46**)

	B3LYP		MP2		G3(MP2)-RAD	
	E_{tot}	**H_{298}**	E_{tot}	**H_{298}**	E_{tot}	**H_{298}**
1	-420.9763079	**-420.839282**	-420.2305171	**-420.0934915**	-420.5159564	**-420.3789305**
3	-720.6743994	**-420.837599**	-420.2305048	**-420.0937044**	-420.5158041	**-420.3790037**
6	-720.9734584	**-420.836562**	-420.2295738	**-420.0926774**	-420.5146234	**-420.377727**

Table 3.16 Energies and enthalpies for open-shell sugar models at various levels of theory in the gas phase in Hartree (298.15 K, 1 atm).

	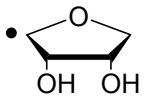 (**3-40R_H**)	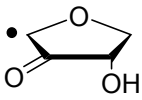 (**3-40Rb**)	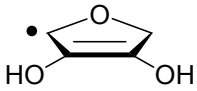 (**3-40Rc**)	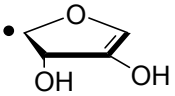 (**3-40Ra**)	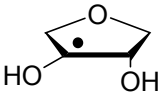 (**3-39R_H**)
	E_{tot} **H_{298}**	E_{tot} **H_{298}**	E_{tot} **H_{298}**	E_{tot} **H_{298}**	E_{tot} **H_{298}**
UB3LYP	-382.2095753 **-382.091592**	-381.0266100 **-380.931548**	-381.0020204 **-380.908302**	-380.9821186 -380.888269	-382.2110494 **-382.092602**
ROMP2	-381.5534556 **-381.4354723**	-380.3713030 **-380.2762410**	-380.3552209 **-380.2615025**	-380.3354956 **-380.2416460**	-381.5518970 **-381.4334496**
G3(MP2)-RAD	-381.8064076 **-381.6884243**	-380.6071139 **-380.5120519**	-380.591977 -380.4982586	-380.5741869 **-380.4803373**	-381.8047854 **-381.6863380**

	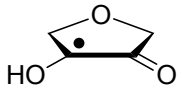 (**3-39Ra**)	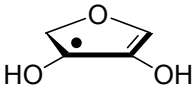 (**3-39Rb**)
	E_{tot} **H_{298}**	E_{tot} **H_{298}**
UB3LYP	-381.0374618 **-380.942058**	-381.0026090 **-380.908927**
ROMP2	-380.3789169 **-380.2835131**	-380.3571748 **-380.2634928**
G3(MP2)-RAD	-380.6142424 **-380.5188386**	-380.5931358 **-380.4994538**

Table 3.17 Energies and enthalpies for open-shell ribose models at various levels of theory in the gas phase in Hartree (298.15 K, 1 atm).

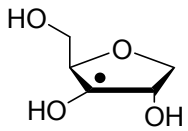

(**3-47R**)

	UB3LYP		ROMP2		G3(MP2)-RAD	
	E_{tot}	**H_{298}**	E_{tot}	**H_{298}**	E_{tot}	**H_{298}**
1	-496.7389357	**-496.585185**	-495.8984312	**-495.7446805**	-496.2230396	**-496.0692889**
22	-496.7389600	**-496.585192**	-495.8977324	**-495.7439644**	-496.2221522	**-496.0683842**
10	-496.7380026	**-496.584462**	-495.8968379	**-495.7432973**	-496.2214063	**-496.0678657**
4	-496.7378733	**-496.584388**	-495.8966704	**-495.7431851**	-496.2211722	**-496.0676869**
9	-496.7378587	**-496.584401**	-495.8960390	**-495.7425813**	-496.2205709	**-496.0671132**
26	-496.7364926	**-496.582910**	-495.8954764	**-495.7418938**	-496.2200524	**-496.0664698**
7	-496.7359818	**-496.582573**	-495.8948468	**-495.7414380**	-496.2195662	**-496.0661574**
28	-496.7353216	**-496.581984**	-495.8946429	**-495.7413053**	-496.2191180	**-496.0657804**

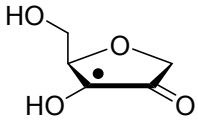

(**3-43R**)

	UB3LYP		ROMP2		G3(MP2)-RAD	
	E_{tot}	**H_{298}**	E_{tot}	**H_{298}**	E_{tot}	**H_{298}**
1	-495.5645486	**-495.433943**	-494.7248278	**-494.5942222**	-495.0311105	**-494.9005049**
3	-495.5643379	**-495.433710**	-494.7235412	**-494.5929133**	-495.0300378	**-494.8994099**
2	-495.5603865	**-495.430066**	-494.7221730	**-494.5918525**	-495.0287338	**-494.8984133**
8	-495.5625623	**-495.432013**	-494.7216880	**-494.5911387**	-495.0284445	**-494.8978952**
6	-495.5587599	**-495.428425**	-494.7191816	**-494.5888467**	-495.0257035	**-494.8953686**
7	-495.5595650	**-495.429135**	-494.7190198	**-494.5885898**	-495.0255795	**-494.8951495**
10	-495.5585514	**-495.428313**	-494.7183161	**-494.5880777**	-495.0250338	**-494.8947954**
11	-495.5592788	**-495.428702**	-494.7186330	**-494.5880562**	-495.0252295	**-494.8946527**

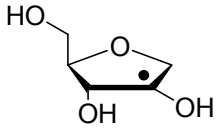

(**3-42R_H**)

	UB3LYP		ROMP2		G3(MP2)-RAD	
	E_{tot}	**H_{298}**	E_{tot}	**H_{298}**	E_{tot}	**H_{298}**
2	-496.7402859	**-496.586700**	-495.8989489	**-495.7453630**	-496.2231852	**-496.0695993**
1	-496.7382715	**-496.584579**	-495.8981496	**-495.7444571**	-496.2222990	**-496.0686065**
37	-496.7396709	**-496.586103**	-495.8976813	**-495.7441134**	-496.2220197	**-496.0684518**
3	-496.7375551	**-496.584125**	-495.8964631	**-495.7430330**	-496.2209669	**-496.0675368**
30	-496.7372751	**-496.583656**	-495.8962149	**-495.7425958**	-496.2204282	**-496.0668091**
4	-496.7346958	**-496.581372**	-495.8953572	**-495.7420334**	-496.2198706	**-496.0665468**

Table 3.18 Energies and enthalpies for open-shell ribose models at various levels of theory in the gas phase in Hartree (298.15 K, 1 atm).

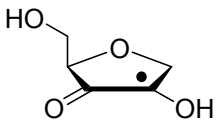

(3-42Ra)

	UB3LYP		ROMP2		G3(MP2)-RAD	
	E_{tot}	**H_{298}**	E_{tot}	**H_{298}**	E_{tot}	**H_{298}**
5	-495.5609850	**-495.430639**	-494.7230698	**-494.5927238**	-494.9005816	**-495.0309276**
7	-495.5643016	**-495.433721**	-494.7245314	**-494.5939508**	-494.9003491	**-495.0309297**
8	-495.5656280	**-495.434880**	-494.7240830	**-494.5933350**	-494.9000286	**-495.0307766**
9	-495.5639624	**-495.433378**	-494.7235357	**-494.5929513**	-494.8993588	**-495.0299432**
4	-495.5622536	**-495.431704**	-494.7231050	**-494.5925554**	-494.8988698	**-495.0294194**

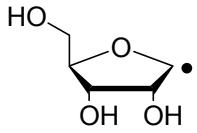

(3-44R_H)

	UB3LYP		ROMP2		G3(MP2)-RAD	
	E_{tot}	**H_{298}**	E_{tot}	**H_{298}**	E_{tot}	**H_{298}**
26	-496.7429036	**-496.589652**	-495.9034825	**-495.7502309**	-496.2276791	**-496.0744275**
6	-496.7419682	**-496.588778**	-495.9024489	**-495.7492587**	-496.2268552	**-496.0736650**
7	-496.7417069	**-496.588329**	-495.9018220	**-495.7484441**	-496.2261835	**-496.0728056**
9	-496.7400111	**-496.586627**	-495.9009916	**-495.7476075**	-496.2254693	**-496.0720852**
48	-496.7391764	**-496.586082**	-495.8998893	**-495.7467949**	-496.2245148	**-496.0714204**
10	-496.7391360	**-496.585818**	-495.8990543	**-495.7457363**	-496.2234430	**-496.0701250**

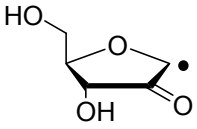

(3-44Ra)

	UB3LYP		ROMP2		G3(MP2)-RAD	
	E_{tot}	**H_{298}**	E_{tot}	**H_{298}**	E_{tot}	**H_{298}**
1	-495.5593527	**-495.429210**	-494.7214832	**-494.5913405**	-495.0289152	**-494.8987725**
3	-495.5585438	**-495.428430**	-494.7203944	**-494.5902806**	-495.0277781	**-494.8976643**
2	-495.5563707	**-495.426357**	-494.7194472	**-494.5894335**	-495.0268017	**-494.8967880**
8	-495.5565169	**-495.426425**	-494.7182927	**-494.5882008**	-495.0257388	**-494.8956469**
5	-495.5550092	**-495.425151**	-494.7181693	**-494.5883111**	-495.0253449	**-494.8954867**
7	-495.5556553	**-495.425510**	-494.7177302	**-494.5875849**	-495.0252485	**-494.8951032**
10	-495.5553354	**-495.425353**	-494.7177918	**-494.5878094**	-495.0250310	**-494.8950486**

Table 3.19 Energies and enthalpies for open-shell ribose models at various levels of theory in the gas phase in Hartree (298.15 K, 1 atm).

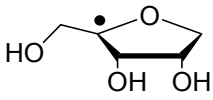

(**3-41R_H**)

	UB3LYP		ROMP2		G3(MP2)-RAD	
	E_{tot}	**H_{298}**	E_{tot}	**H_{298}**	E_{tot}	**H_{298}**
11	-496.7484927	**-496.594142**	-495.9057420	**-495.7513913**	-496.2303854	**-496.0760347**
3	-496.7495057	**-496.594905**	-495.9063667	**-495.7517660**	-496.2306135	**-496.0760128**
41	-496.7461084	**-496.592150**	-495.9039720	**-495.7500136**	-496.2286865	**-496.0747281**
34	-496.7440079	**-496.590081**	-495.9031911	**-495.7492642**	-496.2273662	**-496.0734393**
1	-496.7457353	**-496.591780**	-495.9026737	**-495.7487184**	-496.2269933	**-496.0730380**
40	-496.7457153	**-496.591134**	-495.9024036	**-495.7478223**	-496.2265507	**-496.0719694**

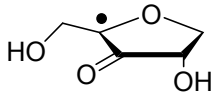

(**3-41Ra**)

	UB3LYP		ROMP2		G3(MP2)-RAD	
	E_{tot}	**H_{298}**	E_{tot}	**H_{298}**	E_{tot}	**H_{298}**
4	-495.5640058	**-495.433366**	-494.7228944	**-494.5922546**	-495.0299643	**-494.8993245**
1	-495.5635219	**-495.432894**	-494.7225180	**-494.5918901**	-495.0294867	**-494.8988588**
2	-495.5607439	**-495.430163**	-494.7208498	**-494.5902689**	-495.0282087	**-494.8976278**
7	-495.5606439	**-495.430036**	-494.7207735	**-494.5901656**	-495.0281588	**-494.8975509**
6	-495.5579128	**-495.427469**	-494.7187897	**-494.5883459**	-495.0261139	**-494.8956701**

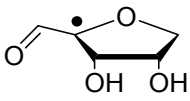

(**3-41Rb**)

	UB3LYP		ROMP2		G3(MP2)-RAD	
	E_{tot}	**H_{298}**	E_{tot}	**H_{298}**	E_{tot}	**H_{298}**
1	-495.5667105	**-495.436100**	-494.7268751	**-494.5962646**	-495.0328193	**-494.9022088**
7	-495.5608047	**-495.430291**	-494.7217550	**-494.5912413**	-495.0286335	**-494.8981198**

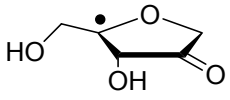

(**3-41Rc**)

	UB3LYP		ROMP2		G3(MP2)-RAD	
	E_{tot}	**H_{298}**	E_{tot}	**H_{298}**	E_{tot}	**H_{298}**
8	-495.5363043	**-495.406726**	-494.6972479	**-494.5676696**	-495.0067052	**-494.8771269**
1	-495.5344524	**-495.405050**	-494.6968455	**-494.5674431**	-495.0061551	**-494.8767527**
11	-495.5344614	**-495.404805**	-494.6962923	**-494.5666359**	-495.0054501	**-494.8757937**
13	-495.5354128	**-495.406026**	-494.6949241	**-494.5655373**	-495.0044191	**-494.8750323**
3	-495.5316145	**-495.402565**	-494.6940222	**-494.5649727**	-495.0033158	**-494.8742663**

Table 3.20 Energies and enthalpies for open-shell 2'-desoxyribose models at various levels of theory in the gas phase in Hartree (298.15 K, 1 atm).

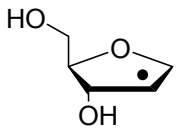

(**3-45R_H**)

	UB3LYP		ROMP2		G3(MP2)-RAD	
	E_{tot}	**H_{298}**	E_{tot}	**H_{298}**	E_{tot}	**H_{298}**
9	-421.5200951	**-421.373157**	-420.7696730	**-420.6227349**	-421.0654868	**-420.9185487**
3	-421.5184042	**-421.371589**	-420.7690937	**-420.6222785**	-421.0649586	**-420.9181434**
10	-421.5184392	**-421.371678**	-420.7688639	**-420.6221027**	-421.0646903	**-420.9179291**
11	-421.5183745	**-421.371513**	-420.7683399	**-420.6214784**	-421.0643432	**-420.9174817**
7	-421.5164382	**-421.369783**	-420.7676499	**-420.6209947**	-421.0635209	**-420.9168657**
8	-421.5174683	**-421.370555**	-420.7668700	**-420.6199567**	-421.0627337	**-420.9158204**
13	-421.5114896	**-421.365100**	-420.7637524	**-420.6173628**	-421.0597762	**-420.9133866**

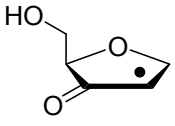

(**3-45R**)

	UB3LYP		ROMP2		G3(MP2)-RAD	
	E_{tot}	**H_{298}**	E_{tot}	**H_{298}**	E_{tot}	**H_{298}**
8	-420.3327589	**-420.209065**	-419.5829335	**-419.4592396**	-419.8630729	**-419.7393790**
9	-420.3343007	**-420.210456**	-419.5823908	**-419.4585461**	-419.8628199	**-419.7389752**
2	-420.3322767	**-420.208577**	-419.5816695	**-419.4579698**	-419.8619609	**-419.7382612**
5	-420.3295910	**-420.206103**	-419.5815823	**-419.4580943**	-419.8616669	**-419.7381789**
4	-420.3306986	**-420.207077**	-419.5812724	**-419.4576508**	-419.8614524	**-419.7378308**

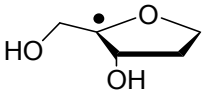

(**3-46R_H**)

	UB3LYP		ROMP2		G3(MP2)-RAD	
	E_{tot}	**H_{298}**	E_{tot}	**H_{298}**	E_{tot}	**H_{298}**
3	-421.5346756	**-421.385781**	-420.7808311	**-420.6319365**	-421.0767406	**-420.9278460**
1	-421.5322712	**-421.383791**	-420.7785680	**-420.6300878**	-421.0745078	**-420.9260276**
12	-421.5303108	**-421.381938**	-420.7775152	**-420.6291424**	-421.0737101	**-420.9253373**
13	-421.5298020	**-421.381327**	-420.7770852	**-420.6286102**	-421.0732112	**-420.9247362**
6	-421.5300162	**-421.381665**	-420.7751596	**-420.6268084**	-421.0713262	**-420.9229750**

Table 3.21 Energies and enthalpies for open-shell 2'-desoxyribose models at various levels of theory in the gas phase in Hartree (298.15 K, 1 atm).

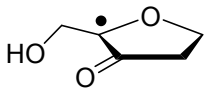

(**3-46Ra**)

	UB3LYP		ROMP2		G3(MP2)-RAD	
	E_{tot}	**H_{298}**	E_{tot}	**H_{298}**	E_{tot}	**H_{298}**
1	-420.3567811	**-420.231507**	-419.6032351	**-419.4779610**	-419.8816649	**-419.7563908**
2	-420.3530989	**-420.227885**	-419.6011761	**-419.4759622**	-419.8798062	**-419.7545923**
5	-420.3502802	**-420.225249**	-419.5991268	**-419.4740956**	-419.8776532	**-419.7526220**

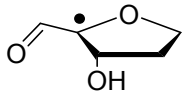

(**3-46Rb**)

	UB3LYP		ROMP2		G3(MP2)-RAD	
	E_{tot}	**H_{298}**	E_{tot}	**H_{298}**	E_{tot}	**H_{298}**
4	-420.3532614	**-420.228076**	-419.6018749	**-419.4766895**	-419.8794258	**-419.7542404**
5	-420.3512756	**-420.226069**	-419.6013255	**-419.4761189**	-419.8792097	**-419.7540031**

Table 3.22 Energies and enthalpies for **3-52R** at various levels of theory in the gas phase and in water solution in Hartree (IEF-PCM = IEF-PCM/UAHF/UHF/6-31G(d)//B3LYP/ 6-31G(d)).

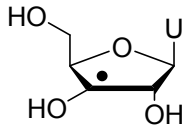

(**3-52R**)

	UB3LYP		ROMP2	G3(MP2)-RAD	IEF-PCM
	E_{tot}	**H_{289}**	E_{tot}	E_{tot}	ΔG_{solv}
7	-910.3664589	**-910.140049**	-908.8218201	-909.3774355	-0.0317446
22	-910.3653081	**-910.139071**	-908.8202557	-909.3760215	-0.0346130
29	-910.3645489	**-910.138495**	-908.8197226	-909.3756425	-0.0334816
1	-910.3647645	**-910.138453**	-908.8215667	-909.3772423	-0.0326848
16	-910.3646612	**-910.138337**	-908.8191918	-909.3750343	-0.0338003
6	-910.3640039	**-910.137808**	-908.8195240	-909.3753207	-0.0316489
11	-910.3637063	**-910.137285**	-908.8192463	-909.3749907	-0.0349158
2	-910.3624828	**-910.136200**	-908.8191042	-909.3747354	-0.0351549

Table 3.23 Energies and enthalpies for open-shell uridine derivatives at various levels of theory in the gas phase and in water solution in Hartree (IEF-PCM = IEF-PCM/UAHF/UHF/6-31G(d)//B3LYP/6-31G(d)).

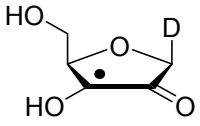

(**3-48Ra**)

	UB3LYP		ROMP2	G3(MP2)-RAD	IEF-PCM
	E_{tot}	**H_{289}**	E_{tot}	E_{tot}	ΔG_{solv}
18	-910.4000892	**-910.173117**	-908.8484744	-909.4013094	-0.0396488
6	-910.3980589	**-910.170862**	-908.8461554	-909.3986315	-0.0354736
34	-910.397375	**-910.170378**	-908.8460842	-909.399403	-0.0389636
40	-910.3967976	**-910.169766**	-908.8447738	-909.3976715	-0.0372106
31	-910.3964794	**-910.169468**	-908.8448253	-909.3983395	-0.0378321
25	-910.3961569	**-910.169164**	-908.8441937	-909.397007	-0.0373700
22	-910.3957370	**-910.168869**	-908.8451302	-909.3979019	-0.0385971

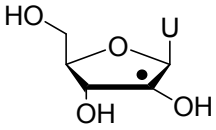

(**3-49R_H**)

	UB3LYP		ROMP2	G3(MP2)-RAD	IEF-PCM
	E_{tot}	**H_{289}**	E_{tot}	E_{tot}	ΔG_{solv}
25	-910.3674962	**-910.141315**	-908.8238780	-909.3796653	-0.0365254
6	-910.3663915	**-910.140426**	-908.8234801	-909.3794525	-0.0351708
17	-910.3661894	**-910.140144**	-908.8237596	-909.3793673	-0.0372425
14	-910.3660818	**-910.140032**	-908.8218777	-909.3778423	-0.0377524
10	-910.3661606	**-910.139888**	-908.8220833	-909.3779337	-0.0336728
5	-910.3655244	**-910.139435**	-908.8218906	-909.3778962	-0.0317446
20	-910.3644661	**-910.139360**	-908.8216169	-909.3775941	-0.0365413
18	-910.3644661	**-910.138423**	-908.8216348	-909.3775161	-0.0364776
4	-910.3641611	**-910.138064**	-908.8197640	-909.3758322	-0.0361907

Table 3.24 Energies and enthalpies for open-shell uridine derivatives at various levels of theory in the gas phase and in water solution in Hartree (IEF-PCM = IEF-PCM/UAHF/UHF/6-31G(d)//B3LYP/6-31G(d)).

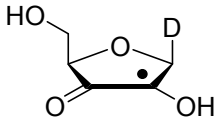

(**3-49Ra**)

	UB3LYP		ROMP2	G3(MP2)-RAD	IEF-PCM
	E_{tot}	**H_{289}**	E_{tot}	E_{tot}	ΔG_{solv}
4	-910.4012167	**-910.174298**	-908.8480150	-909.4009499	-0.0335294
8	-910.4009077	**-910.173946**	-908.8474979	-909.4003928	-0.0336888
7	-910.4006944	**-910.173603**	-908.8445872	-909.3978214	-0.0345334
3	-910.4003671	**-910.173463**	-908.8443338	-909.3975667	-0.0347405
14	-910.1721520	**-910.172152**	-908.8469492	-909.3998964	-0.0345493
19	-910.3982215	**-910.171548**	-908.8457340	-909.3989084	-0.0362704
17	-910.3982919	**-910.171204**	-908.8460953	-909.3990516	-0.0359198
34	-910.3980878	**-910.171018**	-908.8454791	-909.3992915	-0.0369716

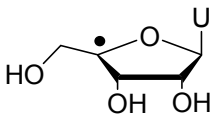

(**3-51R_H**)

	UB3LYP		ROMP2	G3(MP2)-RAD	IEF-PCM
	E_{tot}	**H_{289}**	E_{tot}	E_{tot}	ΔG_{solv}
25	-910.3684648	**-910.141883**	-908.8236613	-909.3799215	-0.0331788
8	-910.3661481	**-910.139772**	-908.8207562	-909.3769973	-0.0319358
36	-910.3657102	**-910.138977**	-908.8220360	-909.3780845	-0.0373222
48	-910.3655868	**-910.138791**	-908.8218973	-909.3780882	-0.0362067
15	-910.3644762	**-910.137891**	-908.8222872	-909.3788239	-0.0378321

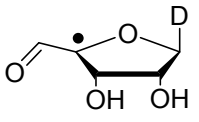

(**3-51Ra**)

	UB3LYP		ROMP2	G3(MP2)-RAD	IEF-PCM
	E_{tot}	**H_{289}**	E_{tot}	E_{tot}	ΔG_{solv}
23	-910.3965350	**-910.169704**	-908.8443837	-909.3981146	-0.0319039
25	-910.3947267	**-910.167927**	-908.8421603	-909.3959421	-0.0334178
8	-910.3940192	**-910.167364**	-908.8415184	-909.3946787	-0.0349796
7	-910.3930112	**-910.166435**	-908.8406424	-909.3937429	-0.0348999

Table 3.25 Energies and enthalpies for **3-51Rb** at various levels of theory in the gas phase and in water solution in Hartree (IEF-PCM = IEF-PCM/UAHF/UHF/6-31G(d)//B3LYP/ 6-31G(d)).

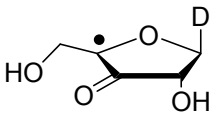

(**3-51Rb**)

	UB3LYP		ROMP2	G3(MP2)-RAD	IEF-PCM
	E_{tot}	**H_{289}**	E_{tot}	E_{tot}	ΔG_{solv}
17	-910.3939700	**-910.167430**	-908.8404581	-909.3942829	-0.0381349
11	-910.3939989	**-910.167312**	-908.8417578	-909.3963689	-0.0379756
14	-910.3933674	**-910.166754**	-908.8398747	-909.3937218	-0.0389636
26	-910.3930580	**-910.166500**	-908.8395743	-909.3933345	-0.0391708
24	-910.3924285	**-910.165864**	-908.8388548	-909.3926964	-0.0390592
16	-910.3920458	**-910.165378**	-908.8392185	-909.3938731	-0.0385652
47	-910.3916412	**-910.165033**	-908.8386118	-909.3932097	-0.0386130
31	-910.3907606	**-910.164173**	-908.8384723	-909.3925804	-0.0414496
4	-910.3907381	**-910.164108**	-908.8360205	-909.3909259	-0.0376728
9	-910.3905193	**-910.163887**	-908.8393586	-909.3942491	-0.0408600
3	-910.3903952	**-910.163778**	-908.8356604	-909.3906115	-0.0379118
29	-910.3900716	**-910.163519**	-908.8379142	-909.3920216	-0.0412424
61	-910.3899909	**-910.163352**	-908.8355369	-909.3902496	-0.0374975
57	-910.3895568	**-910.162941**	-908.8382875	-909.3931822	-0.0413699
5	-910.3895803	**-910.162906**	-908.8379664	-909.3932337	-0.0382783
7	-910.3894949	**-910.162903**	-908.8348492	-909.3895906	-0.0381030
18	-910.3888004	**-910.162372**	-908.8375249	-909.3916349	-0.0416568
10	-910.3888184	**-910.162210**	-908.8370766	-909.3919609	-0.0408918

Table 3.26 Energies and enthalpies for open-shell uridine derivatives at various levels of theory in the gas phase and in water solution in Hartree (IEF-PCM = IEF-PCM/UAHF/UHF/6-31G(d)//B3LYP/6-31G(d)).

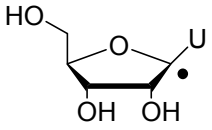

(**3-50R_H**)

	UB3LYP		ROMP2	G3(MP2)-RAD	IEF-PCM
	E_{tot}	**H_{289}**	E_{tot}	E_{tot}	ΔG_{solv}
22	-910.3709609	**-910.144709**	-908.8244957	-909.3812269	-0.0312984
9	-910.3707755	**-910.144399**	-908.8237197	-909.3805048	-0.0296569
73	-910.3705720	**-910.144115**	-908.8231906	-909.3801665	-0.0291948
10	-910.3700834	**-910.143879**	-908.8237039	-909.3805722	-0.0328920
14	-910.3693185	**-910.143173**	-908.8241676	-909.3808797	-0.0318880
3	-910.3695661	**-910.143131**	-908.8259405	-909.3821488	-0.0345971
5	-910.3691660	**-910.142914**	-908.8231324	-909.3798925	-0.0304219
15	-910.3689906	**-910.142449**	-908.8246616	-909.3808999	-0.0352346
23	-910.3682453	**-910.142178**	-908.8222318	-909.3790728	-0.0345812
17	-910.3677804	**-910.141771**	-908.8223483	-909.3791571	-0.0343740
26	-910.3679035	**-910.141711**	-908.8214930	-909.3780489	-0.0340872

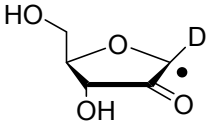

(**3-50R**)

	UB3LYP		ROMP2	G3(MP2)-RAD	IEF-PCM
	E_{tot}	**H_{289}**	E_{tot}	E_{tot}	ΔG_{solv}
3	-910.3998174	**-910.172796**	-908.8481619	-909.4014105	-0.0342306
4	-910.3986426	**-910.171605**	-908.8463553	-909.3997694	-0.0329398
12	-910.3966897	**-910.169768**	-908.8459416	-909.3978891	-0.0356011
6	-910.3959926	**-910.168975**	-908.8442775	-909.3964746	-0.0348362

Table 3.27 Energies and enthalpies for open-shell uridine derivatives at various levels of theory in the gas phase and in water solution in Hartree (IEF-PCM = IEF-PCM/UAHF/UHF/6-31G(d)//B3LYP/6-31G(d)).

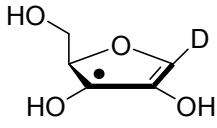

(**3-48Rb**)

	UB3LYP		ROMP2	G3(MP2)-RAD	IEF-PCM
	E_{tot}	**H_{289}**	E_{tot}	E_{tot}	ΔG_{solv}
13	-910.3767445	**-910.150730**	-908.8307220	-909.3831237	-0.0311071
15	-910.3763869	**-910.150556**	-908.8313908	-909.3835725	-0.0331788
50	-910.3760145	**-910.150190**	-908.8306331	-909.3832335	-0.0316171
9	-910.3757337	**-910.149737**	-908.8293879	-909.3816343	-0.0338322
77	-910.3756005	**-910.149604**	-908.8293250	-909.3815428	-0.0315533
10	-910.3753370	**-910.149541**	-908.8300332	-909.3820802	-0.0338322
29	-910.3749247	**-910.149144**	-908.8292525	-909.3817863	-0.0340234
52	-910.3746681	**-910.148951**	-908.8296750	-909.3826392	-0.0337206
64	-910.3733917	**-910.147801**	-908.8291477	-909.3810726	-0.0356170
32	-910.3734192	**-910.147785**	-908.8280928	-909.3809674	-0.0346927

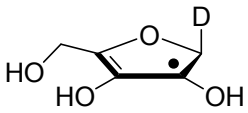

(**3-49Rb**)

	UB3LYP		ROMP2	G3(MP2)-RAD	IEF-PCM
	E_{tot}	**H_{289}**	E_{tot}	E_{tot}	ΔG_{solv}
4	-910.3748849	**-910.148801**	-908.8304122	-909.3832439	-0.0333063
2	-910.3747171	**-910.148707**	-908.8297656	-909.3832922	-0.0331469
3	-910.3730306	**-910.147143**	-908.8291285	-909.3824266	-0.0355533
1	-910.3728604	**-910.147141**	-908.8291756	-909.3817016	-0.0360473
9	-910.3730747	**-910.147067**	-908.8298582	-909.3832426	-0.0335613
14	-910.3728936	**-910.147045**	-908.8295389	-909.3834026	-0.0335135
13	-910.3725547	**-910.146817**	-908.8286920	-909.3822069	-0.0334497
26	-910.3728370	**-910.146695**	-908.8284112	-909.3817346	-0.0367007
11	-910.3726297	**-910.146691**	-908.8284132	-909.3823165	-0.0348202
5	-910.3724864	**-910.146595**	-908.8286255	-909.3816298	-0.0339437
32	-910.3729310	**-910.146524**	-908.8266122	-909.3798103	-0.0366210
8	-910.3721682	**-910.146428**	-908.8277617	-909.3810829	-0.0357604
34	-910.3723201	**-910.146184**	-908.8280655	-909.3813644	-0.0370991
20	-910.3722397	**-910.146048**	-908.8264528	-909.3777566	-0.0373062

Table 3.28 Energies and enthalpies for open-shell nucleosides at various levels of theory in the gas phase and in water solution in Hartree (IEF-PCM = IEF-PCM/UAHF/UHF/6-31G(d)//B3LYP/6-31G(d)).

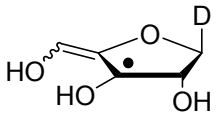

(**3-48Rc**)

	UB3LYP		ROMP2	G3(MP2)-RAD	IEF-PCM
	E_{tot}	**H_{289}**	E_{tot}	E_{tot}	ΔG_{solv}
16	-910.3738691	**-910.147993**	-908.8298603	-909.3831515	-0.0326370
7	-910.3732249	**-910.147421**	-908.8287356	-909.3820922	-0.0331788
12	-910.3722436	**-910.146427**	-908.8285703	-909.3827738	-0.0348840
11	-910.3717313	**-910.145989**	-908.8280772	-909.3821750	-0.0351071

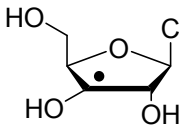

(**3-14R_H**)

	UB3LYP		ROMP2	G3(MP2)-RAD	IEF-PCM
	E_{tot}	**H_{289}**	E_{tot}	E_{tot}	ΔG_{solv}
7	-890.4849277	**-890.246767**	-888.9455584	-889.5085576	-0.03920262
16	-890.4832920	**-890.245216**	-888.9432443	-889.5063917	-0.04036595
29	-890.4831391	**-890.245185**	-888.9434718	-889.5066110	-0.03984007
6	-890.4821766	**-890.244315**	-888.9430036	-889.5060853	-0.03901139
22	-890.4821561	**-890.244292**	-888.9425999	-889.5056856	-0.04124244
1	-890.4821270	**-890.244060**	-888.9442329	-889.5073369	-0.03953728
11	-890.4819000	**-890.243714**	-888.9427660	-889.5059140	-0.04100340

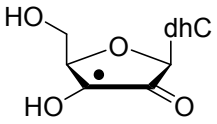

(**3-14R**)

	UB3LYP		ROMP2	G3(MP2)-RAD	IEF-PCM
	E_{tot}	**H_{289}**	E_{tot}	E_{tot}	ΔG_{solv}
18	-890.5064534	**-890.267775**	-888.9590225	-889.5207963	-0.04995944
34	-890.5032064	**-890.264483**	-888.9565121	-889.5188906	-0.04868456
6	-890.5031211	**-890.264261**	-888.9555468	-889.5169264	-0.04554516

Table 3.29 RSE-relevant energies and enthalpies for open- and closed-shell compounds at various levels of theory in the gas phase (298.15 K, 1 atm, in Hartree).

	 (**3-10R**)	 (**3-10**)	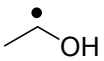 (**3-1Rb**)	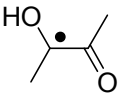 (**3-9R**)	 (**3-2**)
	E_{tot} **H_{298}**	E_{tot} **H_{298}**	E_{tot} **H_{298}**	E_{tot} **H_{298}**	E_{tot} **H_{298}**
(U)B3LYP	-39.8382922 **-39.804975**	-40.5183890 **-40.470240**	-154.3753608 **-154.304996**	-307.0460367 **-306.934651**	-117.9075622 **-117.823957**
(RO)MP2	-39.7316815 **-39.6983643**	-40.4055437 **-40.3573947**	-154.0785764 **-154.0082116**	-306.4710091 **-306.3596234**	-117.6166619 **-117.5330709**
G3(MP2)-RAD	-39.7851922 **-39.7518750**	-40.4651605 **-40.4170115**	-154.2043033 **-154.1339385**	-306.6936033 **-306.5822176**	-117.7498900 **-117.6662848**
	 (**3-4**)	 (**3-34**)	 (**3-34_H**)	 (**3-27**)	 (**3-27_H**)
	E_{tot} **H_{298}**	E_{tot} **H_{298}**	E_{tot} **H_{298}**	E_{tot} **H_{298}**	E_{tot} **H_{298}**
B3LYP	119.1442483 **-119.036640**	-157.2272881 **-157.114574**	-158.4588061 **-158.322279**	-234.6482883 **-234.497595**	-235.8804309 **-235.705840**
MP2	-118.8387689 **-118.7311606**	-156.8420116 **-156.7292975**	-158.0609392 **-157.9244121**	-234.0908015 **-233.9401082**	-235.3102004 **-235.1356095**
G3(MP2)-RAD	-118.9847884 **-118.8771801**	-157.0170527 **-156.9043386**	-158.2492314 **-158.1127043**	-234.3346577 **-234.1839644**	-235.5671031 **-235.3925122**
	 (**3-29**)	 (**3-29_H**)	 (**3-3**)	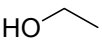 (**3-1**)	 (**3-8**)
	E_{tot} **H_{298}**	E_{tot} **H_{298}**	E_{tot} **H_{298}**	E_{tot} **H_{298}**	E_{tot} **H_{298}**
B3LYP	-195.3271387 **-195.206463**	-196.5570819 **-196.412193**	-153.8301215 **-153.770515**	-155.0342871 **-154.950239**	-193.1556942 **-193.066834**
MP2	-194.8640871 **-194.7434114**	-196.0804928 **-195.9356039**	-153.5380653 **-153.4784588**	-154.7365194 **-154.6524713**	-192.7680234 **-192.6791632**
G3(MP2)-RAD	-195.0650164 **-194.9443407**	-196.2948337 **-196.1499448**	-153.6538781 **-153.5942716**	-154.8685341 **-154.7844860**	-192.9263022 **-192.8374420**

Table 3.30 RSE-relevant energies and enthalpies for closed-shell compounds at various levels of theory in the gas phase (298.15 K, 1 atm, in Hartree).

	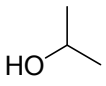 (**3-33**)	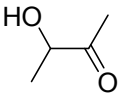 (**3-9**)
	E_{tot} **H_{298}**	E_{tot} **H_{298}**
B3LYP	-194.3534513 **-194.240614**	-307.6756355 **-307.551738**
MP2	-193.9614458 **-193.848685**	-307.1063382 **-306.9824407**
G3(MP2)-RAD	-194.1361518 **-194.0233145**	-307.3360457 **-307.2121482**

Table 3.31 Gas phase radical stabilization energies at various levels in kJ mol^{-1}.

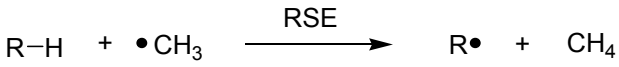

R•	RSE			RSE(exp.)[115]
	UB3LYP	ROMP2	G3(MP2)-RAD	
 (**3-2R**)	-83.44	-78.74	-71.97	-70.3 -70.7[93]
 (**3-4R**)	-17.18	-9.82	-10.12	-17.5 -17.1[93]
 (**3-34R**)	-76.23	-72.06	-66.06	-66.5
 (**3-34R_H**)	-17.45	-9.56	-10.62	-21.0 -20.1[93]
 (**3-27R**)	-102.06	-95.70	-85.37	-96.6
 (**3-27R_H**)	-34.01	-19.28	-20.70	-39.7 -23.0[93]
 (**3-29R**)	-100.05	-93.90	-84.66	-94.6
 (**3-29R_H**)	-46.52	-32.13	-33.38	-37.6 -39.3[93]
 (**3-3R**)	-52.27	-33.92	-36.63	-44.6
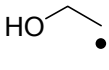 (**3-1R**)	-18.11	-9.66	-10.32	-17.5 -15.5[93]
 (**3-8R**)	-47.39	29.78	-32.42	-38.1
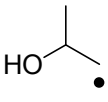 (**3-33R**)	-17.08	-9.03	-9.57	-44.9

Table 3.32 Benson increment system (BGVA) for the assignement of heats of formation (in kJ mol^{-1}). $\Delta_f H^0$(exp.) in bold style are estimated by the correlation in **Figure 3.16**.

	Benson notation	BGVA[115]	$\Delta_f H^0$(BGVA)	$\Delta_f H^0$(exp.)[115]
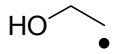 (**3-1R**)	C• – (C)(H$_2$) C – (C•)(O)(H$_2$) O – (C)(H)	+160.7 -39.6[120] -158.6[120]	-37.5	-31.0 ± 7.0
 (**3-3R**)	C• - (CO)(H$_2$) CO – (C•)(H)	+155.4[120] -145.0[120]	+10.4	+10.5 ± 9.20[121]
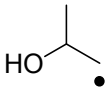 (**3-33R**)	C• - (C)(H$_2$) C-(C•)(C)(O)(H) C – (C)(H$_3$) O – (C)(H)	+160.7 -51.5[120] -41.8[122] -158.6[120]	-91.2	-96.2 ± 4.2
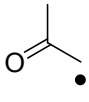 (**3-8R**)	C• -(CO)(H$_2$) CO – (C•)(C) C – (CO)(H$_3$)	+155.4[120] -146.9[120] -41.8[122]	-33.3	-33.9 ± 3.0
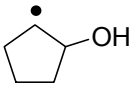 (**3-36R_H**)	C• – (C$_2$)(H) C – (C•)(C)(H2) 2x C – (C2)(H2) C – (C•)(C)(O)(H) O – (C)(H) Cyclopentane	+171.5[120] -20.9[120] 2x (-20.9)[121] -51.5[122] -158.6[121] +29.7[121]	-71.6	**-71.6 (corr.)**
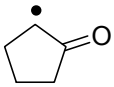 (**3-36R**)	C• - (CO)(C)(H) C – (C•)(C)(H$_2$) C – (C$_2$)(H$_2$) C – (CO)(C)(H$_2$) CO – (C•)(C) Cyclopentanone	+138.9[120] -20.9 -20.9[122] -21.8[122] -132.6[120] +25.9[122]	-31.4	-41.8 ± 12.6
 (**3-4R**)	C• - (C)(H$_2$) C – (C•)(C)(H$_2$) C – (C)(H$_3$)	+160.7 -20.9 -41.8[122]	+98.0	+100.0 ± 2.0
 (**3-2R**)	C• – (C$_D$)(H$_2$) C – (C•)(C)(H$_2$) C – (C)(H$_3$)	+108.4 +36.0 +26.4[122]	+170.8	+171.0 ± 3.0[123]
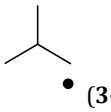 (**3-34R_H**)	C• – (C)(H$_2$) C – (C•)(C$_2$)(H) 2 x C – (C)(H$_3$)	+160.7 -10.0 2x (-41.8)	+67.1	+66.1 ± 1.3[124]
 (**3-34R**)	C• – (C$_D$)(H$_2$) C$_D$ – (C•)(C) C – (C$_D$)(H$_3$) C$_D$ – (H$_2$)	+108.4 +42.7 -41.8[122] +26.4[122]	+135.7	+137.9

Table 3.33 Benson increment system (BGVA) for the assignement of heats of formation (in kJ mol^{-1}). $\Delta_f H^0$(exp.) in bold style are estimated by the correlation in **Figure 3.16**.

	Benson notation	BGVA[115]	$\Delta_f H^0$(BGVA)	$\Delta_f H^0$(exp.)[115]
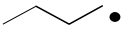 (**3-64R_H**)	C• – (C)(H$_2$) C – (C•)(C)(H$_2$) C – (C$_2$)(H$_2$) C – (C)(H$_3$)	+160.7 -20.9 -20.9[122] -41.8[122]	+77.1	+77.8 ± 2.1
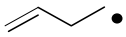 (**3-64R**)	C• – (C)(H$_2$) C – (C•)(C)(H$_2$) C$_D$ – (C)(C$_D$) C$_D$ – (H$_2$)	+160.7 -20.9 +36.8[122] +26.4[122]	+203.0	+192.5
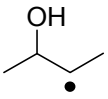 (**3-65R_H**)	C – (C•)(H$_3$) C• – (C$_2$)(H) C – (C•)(C)(O)(H) O – (C)(H) C – (C)(H$_3$)	-41.8[120] +171.5[120] -51.5[122] -158.6[121] -41.9[121]	-122.3	**-121.5 (corr.)**
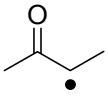 (**3-65R**)	C – (CO)(H$_3$) CO – (C)(C•) C• - (CO)(C)(H) C – (C•)(H$_3$)	-41.8[122] -132.6[120] +138.9[120] -41.8	-77.3	-70.3 ± 7.1
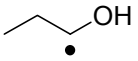 (**3-35R_H**)	C – (C)(H$_3$) C – (C)(C•)(H$_2$) C• - (C)(O)(H) O – (C•)(H)	-41.8[122] -17.4 +117.4[120] -146.3[120]	-88.1	-81.0 ± 8.0
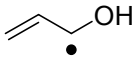 (**3-35R**)	C$_D$ – (C$_D$)(H$_2$) C$_D$ – (C$_D$)(H)(C•) C• - (C$_D$)(O)(H) O – (C•)(H)	+26.4[122] +36.0 +84.08[120] -146.25[120]	+0.23	0.0 ± 8.4
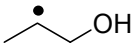 (**3-37R_H**)	C – (C•)(H$_3$) C• – (C$_2$)(H) C – (C•)(O)(H$_2$) O – (C)(H)	-41.8 +171.5 -39.6[120] -158.6[122]	-68.5	-78.7 ± 8.4
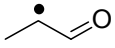 (**3-37R**)	C – (C•)(H$_3$) C• – (CO)(C)(H) CO – (C•)(H)	-41.8[120] +153.2[122] -145.0[122]	-33.6	**-34.2 (corr.)**
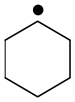 (**3-27R_H**)	C• – (C$_2$)(H) 2x C – (C•)(C)(H$_2$) 3x C – (C$_2$)(H$_2$) Cyclohexane	+171.5 2x (-20.9) 3x (-20.9)[122] +2.9[122]	64.1	+58.2 ± 4.0[120]

Table 3.34 Benson increment system (BGVA) for the assignement of heats of formation (in kJ mol^{-1}).

	Benson notation	BGVA[115]	$\Delta_f H^0$(BGVA)	$\Delta_f H^0$(exp.)[115]
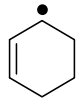 **(3-27R)**	C• – (C_D)(C)(H)	+109.6	+121.8	+119.7
	C – (C)(C•)(H_2)	-20.9		
	C – (C_2)(H_2)	-20.9[122]		
	C – (C)(C_D)(H_2)	-20.1[122]		
	C_D – (C)(H)	+36.0[122]		
	C_D – (C•)(H)	+36.0		
	Cyclohexene	+2.1[122]		
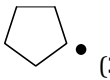 **(3-29R_H)**	C• – (C_2)(H)	+171.5	+117.6	+107.0 ± 2.5[120]
	2x C – (C•)(C)(H_2)	2x (-20.9)		
	2x C – (C_2)(H_2)	2x (-20.9)[122]		
	Cyclopentane	+29.7[122]		
 **(3-29R)**	C• – (C_D)(C)(H)	+109.6	+165.3	+160.7 ± 4.2
	C – (C•)(C)(H_2)	-20.9		
	C – (C)(C_D)(H_2)	-20.1[122]		
	C_D – (C)(H)	+36.0[122]		
	C_D – (C•)(H)	+36.0		
	Cyclopentene	+24.7[122]		

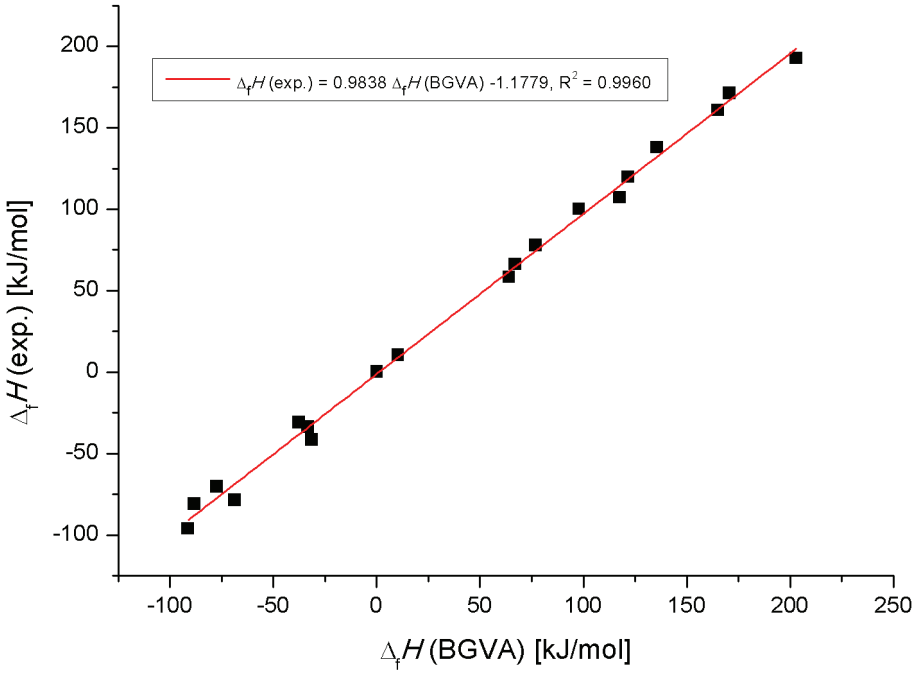

Figure 3.16 Correlation of experimental available heats of formation $\Delta_f H^0$(exp.) vs. calculated $\Delta_f H^0$(BGVA) using Benson's group additivity values.

Table 3.35 Calculated reaction enthalpies $\Delta_{trh}H$ for transfer hydrogenation of **3-8R** to **3-33R** at various levels of theory in the gas phase at 298.15 K (in kJ mol^{-1})

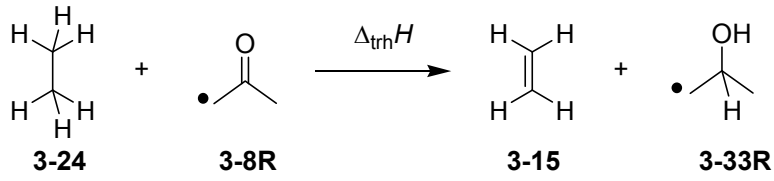

	$\Delta_{trh}H$ (calc.)	$\Delta_{trh}H$ (HL)[a]	$\Delta_{trh}H$ (exp.)	$\Delta_{trh}H$ (BGAV)[b]
G3(MP2)-RAD	+99.3			
G3B3	+104.5	+106.3	+74.1±8.1	+78.5
CBS-QB3	+105.3			

[a] $\Delta_f H^0(\bullet CH_2CH(OH)CH_3)$ = -64.02 kJ mol^{-1} at CBS-QB3 level of theory.[109] [b] $\Delta_f H^0$ estimated by Benson group additivity values.

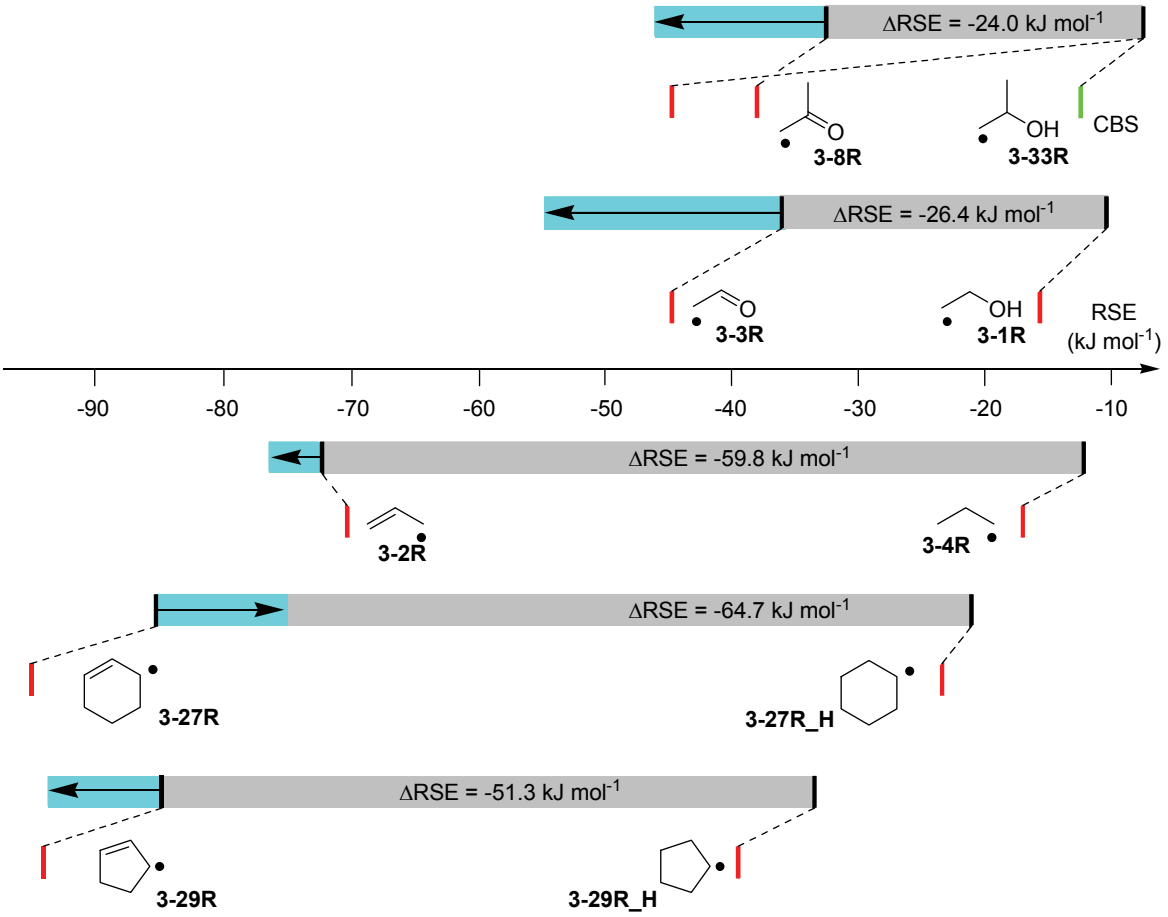

Figure 3.17 Relation of ΔRSE (red bars: experimental; black bars: G3(MP2)-RAD values) and $\Delta_{hyd}H$ (grey + light blue bar at G3(MP2)-RAD level in the gas phase).

Table 3.36 Calculated free solvation energies ΔG_{solv} in water (at 298.15 K and 1 atm, in Hartree). IEF-PCM = IEF-PCM/UAHF/UHF/6-31G(d), C-PCM = C-PCM/UAHF/UHF/6-31G(d), SMD/UHF = SMD/UHF/6-31G(d), SMD/B3LYP = SMD/UB3LYP/6-31G(d).

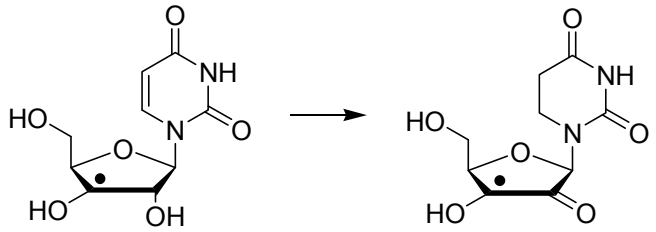

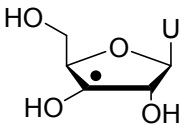 (**3-52R**)	G3(MP2)-RAD	IEF-PCM	C-PCM	SMD/UHF	SMD/UB3LYP
	H_{298}	ΔG_{solv}	ΔG_{solv}	ΔG_{solv}	ΔG_{solv}
7 (**A**)	**-909.1510256**	-0.0317446	-0.0321111	-0.0375293	-0.0269478
22 (**B**)	**-909.1497844**	-0.0346130	-0.0349796	-0.0407962	-0.0293860
29(**C**)	**-909.1495886**	-0.0334816	-0.0338481	-0.0379756	-0.0274259
1 (**D**)	**-909.1509308**	-0.0326848	-0.0330194	-0.0362704	-0.0268203
16(**E**)	**-909.1487101**	-0.0338003	-0.0341987	-0.0378321	-0.0269159
6(**F**)	**-909.1491248**	-0.0316489	-0.0319995	-0.0392345	-0.0287008
11 (**G**)	**-909.1485694**	-0.0349158	-0.0353302	-0.0392345	-0.0287486
2 (**H**)	**-909.1484526**	-0.0351549	-0.0355692	-0.0397285	-0.0290514
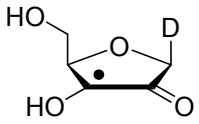 (**3-48Ra**)	G3(MP2)-RAD	IEF-PCM	C-PCM	SMD/UHF	SMD/UB3LYP
	H_{298}	ΔG_{solv}	ΔG_{solv}	ΔG_{solv}	ΔG_{solv}
18 (**A**)	**-909.1743372**	-0.0396488	-0.0400154	-0.0443181	-0.0342465
6 (**B**)	**-909.1714346**	-0.0354736	-0.0358242	-0.0439994	-0.0343103
34 (**C**)	**-909.1724060**	-0.0389636	-0.0392982	-0.0434894	-0.0340075
40 (**D**)	**-909.1706399**	-0.0372106	-0.0375453	-0.0437125	-0.0349477
31 (**E**)	**-909.1713281**	-0.0378321	-0.0381508	-0.0429954	-0.0340234
25 (**F**)	**-909.1700141**	-0.0373700	-0.0377046	-0.0442384	-0.0341987
22 (**G**)	**-909.1709090**	-0.0385971	-0.0388998	-0.0436806	-0.0347883

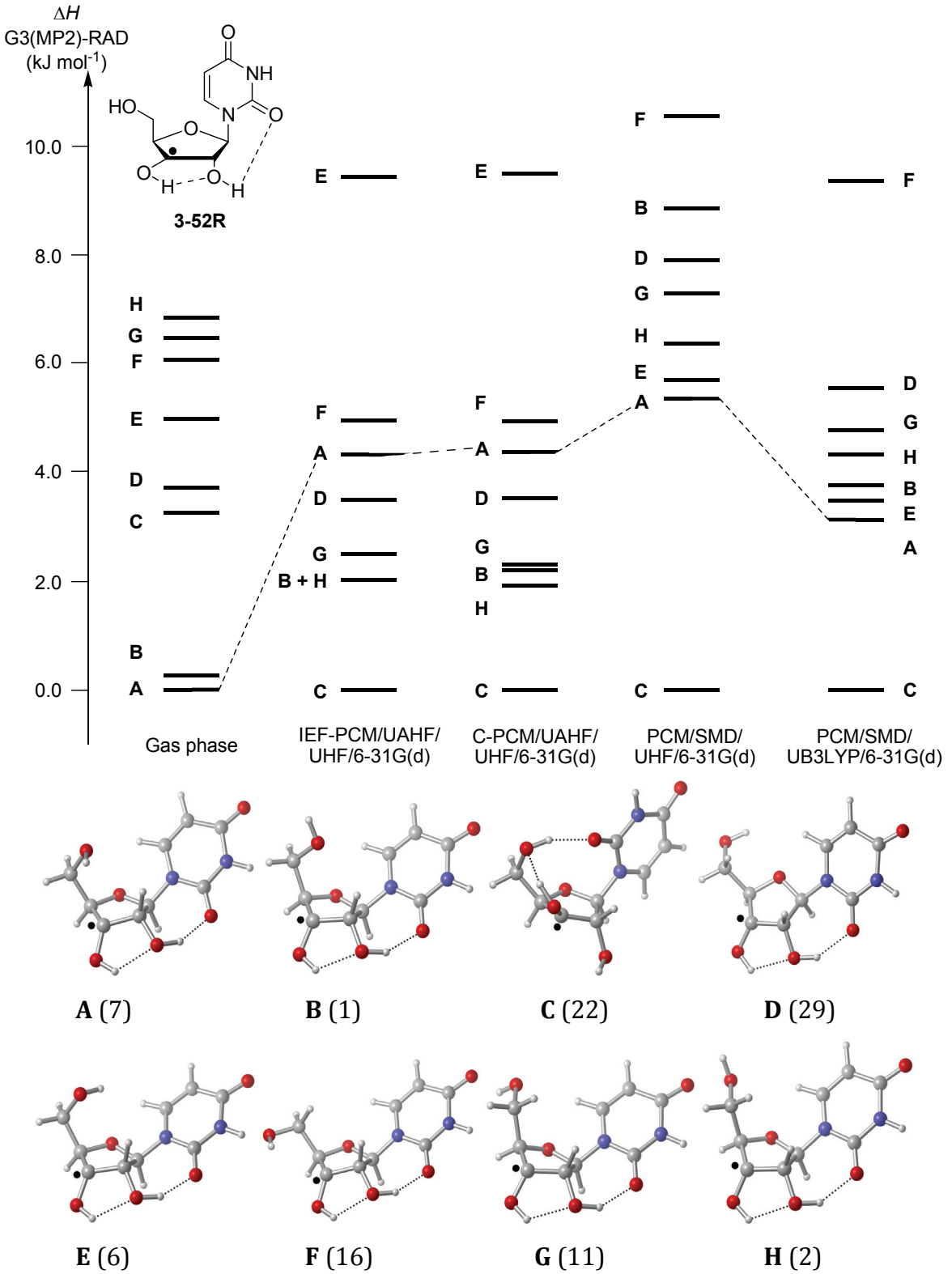

Figure 3.18 Relative stability of conformers of the C3' uridinyl radical **3-52R** in water (H_{298} + ΔG_{solv}) and in gas phase (G3(MP2)-RAD, at 298.15 K and 1 atm) and their graphical representations (conformer denotation in parenthesis).

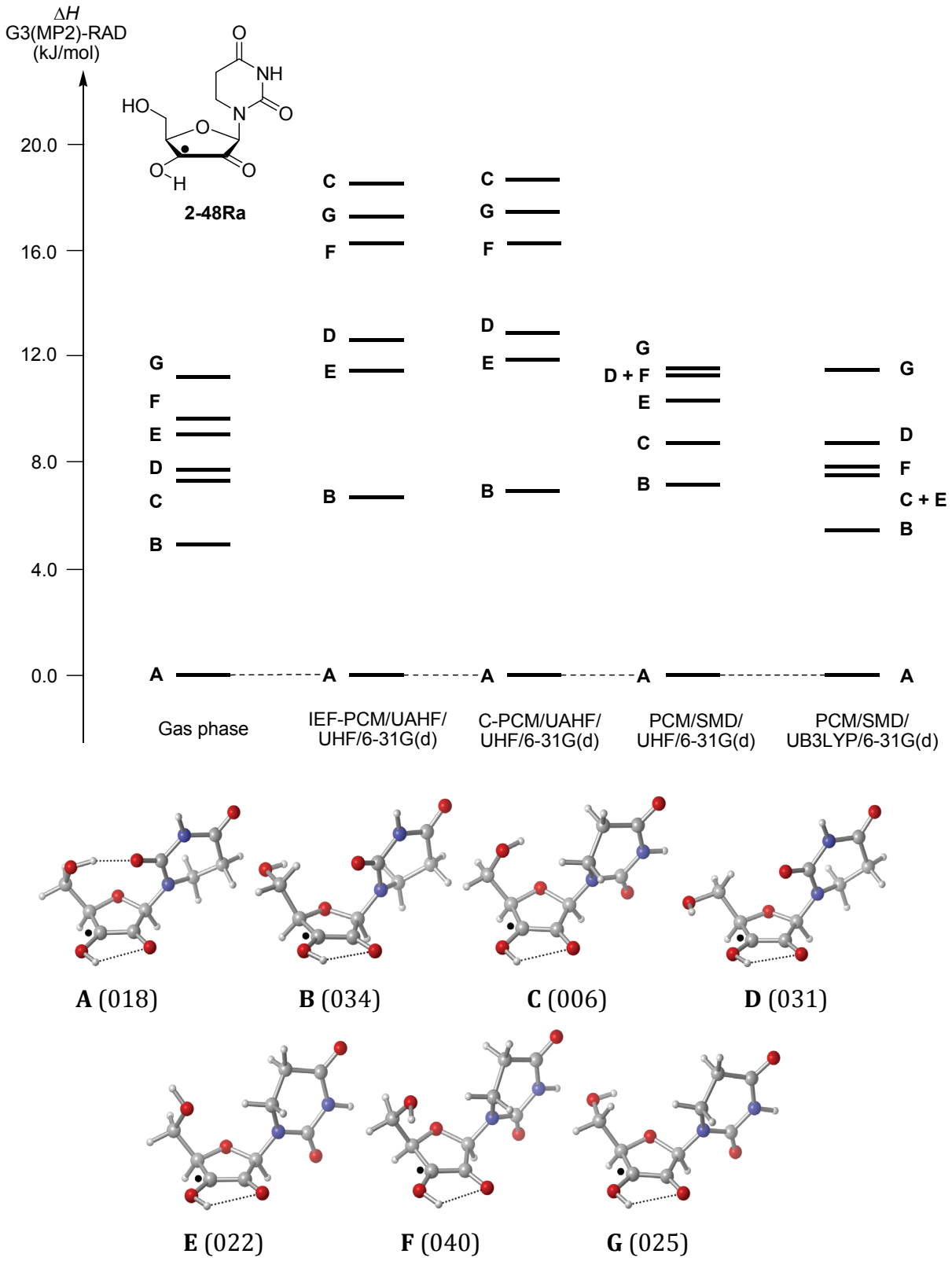

Figure 3.19 Relative stability of conformers of **3-48Ra** in water (H_{298} + ΔG_{solv}) and in gas phase (G3(MP2)-RAD, at 298.15 K and 1 atm) and their graphical representations (conformer denotation in parenthesis).

Table 3.37 *Boltzmann*-averaged <$\Delta_{trh}H$> at G3(MP2)-RAD level with and without implicit solvation.

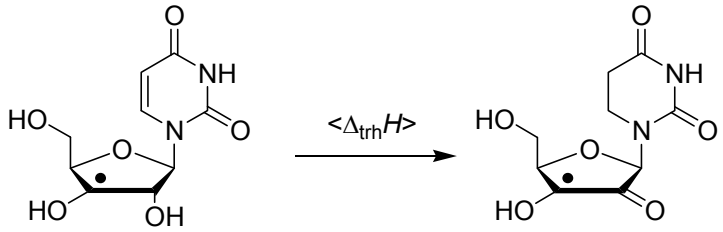

3-52R **2-48Ra**

Method	<$\Delta_{trh}H$>
Gas phase	**-61.14**
IEF-PCM/UAHF/UHF/6-31G(d)	**-78.87**
C-PCM/UAHF/UHF/6-31G(d)	**-78.99**
SMD/UHF/6-31G(d)	**-74.73**
SMD/UB3LYP/6-31G(d)	**-77.85**

Table 3.38 Energies and enthalpies for peptide models at various levels of theory in the gas phase, in polar and apolar media in Hartree (IEF-PCM = IEF-PCM/UAHF/UHF/ 6-31G(d)//B3LYP/6-31G(d)).

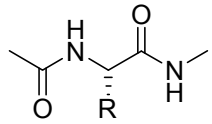	B3LYP		MP2	G3(MP2)-RAD	IEF-PCM
	E_{tot}	**H_{298}**	E_{tot}	E_{tot}	ΔG_{solv} (water) **ΔG_{solv} (heptane)**
R = CH_2OH (**3-53**) 1	-571.0620340	**-570.859332**	-570.0348734	-570.4316029	-0.0226451 **-0.0071075**
2	-571.0709906	**-570.867570**	-570.0425815	-570.4391284	-0.0185495 **-0.0058326**
3	-571.0655820	**-570.861955**	-570.0350951	-570.4316030	-0.0206372 **-0.0062947**
6	-571.0642011	**-570.861305**	-570.0352212	-570.4316541	-0.0237287 **-0.0073146**
7	-571.0649389	**-570.861801**	-570.0370142	-570.4339784	-0.0229638 **-0.0071075**
8	-571.0593294	**-570.856504**	-570.0326945	-570.4297998	-0.0230276 **-0.0068525**
14	-571.0584591	**-570.855887**	-570.032761	-570.4292377	-0.0270275 **-0.0070278**
R = $CH(CH_3)OH$ (**3-54**) 1	-610.3811404	**-610.149515**	-609.2618449	-609.7008546	-0.0201750 **-0.0060716**
2	-610.3894761	**-610.157305**	-609.2685995	-609.7075749	-0.0169081 **-0.0050039**
3	-610.3830920	**-610.150572**	-609.2607597	-609.6996555	-0.0192348 **-0.0057051**
4	-610.3799844	**-610.148278**	-609.259719	-609.6985144	-0.0223104 **-0.0067091**
5	-610.3788809	**-610.147158**	-609.2589904	-609.6985079	-0.0200953 **-0.0060398**
8	-610.3813687	**-610.149316**	-609.2602881	-609.6998488	-0.0183902 **-0.0060398**
10	-610.3797812	**-610.148074**	-609.2590826	-609.6984778	-0.0209877 **-0.0059760**
11	-610.3785290	**-610.146754**	-609.2575604	-609.6966008	-0.0242068 **-0.0065019**
12	-610.3773179	**-610.145193**	-609.2580187	-609.6972749	-0.0232188 **-0.0064860**

Table 3.39 Energies and enthalpies for open- and closed-shell peptide models at various levels of theory in the gas phase, in polar and apolar media in Hartree (IEF-PCM = IEF-PCM/UAHF/UHF/6-31G(d)//B3LYP/6-31G(d)).

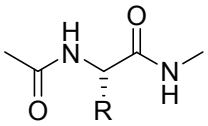	B3LYP		MP2	G3(MP2)-RAD	IEF-PCM
	E_{tot}	**H_{298}**	E_{tot}	E_{tot}	ΔG_{solv} (water) **ΔG_{solv} (heptane)**
R = CH_2SH (**3-56**) 1	-894.0363528	**-893.838306**	-892.6248366	-893.0401897	-0.0188683 **-0.0071075**
2	-894.0420128	**-893.843753**	-892.6297102	-893.0450819	-0.0133385 **-0.0058326**
3	-894.0345536	**-893.836784**	-892.6236602	-893.0387487	-0.0217049 **-0.0062947**
6	-894.0382031	**-893.840085**	-892.6263236	-893.0416149	-0.0151233 **-0.0073146**
7	-894.0381989	**-893.840031**	-892.6264810	-893.0418597	-0.0189479 **-0.0071075**
8	-894.0363536	**-893.838192**	-892.6238242	-893.0394555	-0.0184220 **-0.0068525**
14	-894.0345535	**-893.836785**	-892.6236587	-893.0387490	-0.0216889 **-0.0070278**
R = H (**3-6**) 1	-456.5361652	**-456.368827**	-455.6900430	-456.0154026	-0.0246052 **-0.0076652**
2	-456.5375162	**-456.369616**	-455.6921794	-456.0175637	-0.0214021 **-0.0069800**
3	-456.5333571	**-456.365764**	-455.6876553	-456.0128928	-0.0258960 **-0.0077449**
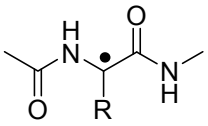	UB3LYP		ROMP2	G3(MP2)-RAD	IEF-PCM
	E_{tot}	**H_{298}**	E_{tot}	E_{tot}	ΔG_{solv} (water) **ΔG_{solv} (heptane)**
R = CH_2OH (**3-53R**) 1	-570.4201342	**-570.230115**	-569.3866481	-569.7778763	-0.0188842 **-0.0071553**
3	-570.4248155	**-570.234356**	-569.3921047	-569.7831742	-0.0187248 **-0.0065975**
5	-570.4142197	**-570.224153**	-569.3829485	-569.7740108	-0.0215296 **-0.0068684**

Table 3.40 Energies and enthalpies for open-shell peptide models at various levels of theory in the gas phase, in polar and apolar media in Hartree (IEF-PCM = IEF-PCM/UAHF/UHF/ 6-31G(d)//B3LYP/6-31G(d)).

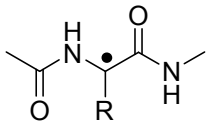	UB3LYP		ROMP2	G3(MP2)-RAD	IEF-PCM
	E_{tot}	**H_{298}**	E_{tot}	E_{tot}	ΔG_{solv} (water) **ΔG_{solv} (heptane)**
R = $CH(CH_3)OH$ (**3-54R**) 1	-609.7397421	**-609.520676**	-608.6137032	-609.0478499	-0.0153623 **-0.0059441**
3	-609.7412543	**-609.521836**	-608.6151059	-609.0491706	-0.0169878 **-0.0062151**
4	-609.7370238	**-609.517588**	-608.6113142	-609.0458527	-0.0144062 **-0.0060876**
5	-609.7352530	**-609.516364**	-608.6087335	-609.0432045	-0.0157926 **-0.0062151**
7	-609.7362162	**-609.517088**	-608.609109	-609.0434529	-0.0172747 **-0.0063903**
R = H (**3-6R**) 1	-455.8974817	**-455.742962**	-455.0483585	-455.3672737	-0.0205575 **-0.0071075**
2	-455.8854499	**-455.730742**	-455.0352881	-455.3554901	-0.0205575 **-0.0077290**
3	-455.8854880	**-455.731089**	-455.0373616	-455.3569559	-0.0233941 **-0.0074103**
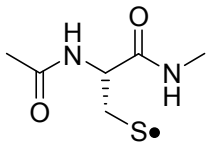 (**3-56R**)	UB3LYP		ROMP2	G3(MP2)-RAD	IEF-PCM
	E_{tot}	**H_{298}**	E_{tot}	E_{tot}	ΔG_{solv} (water) **ΔG_{solv} (heptane)**
1	-893.4003394	**-893.212432**	-891.9864284	-892.3938784	-0.0172268 **-0.0058007**
2	-893.4042928	**-893.215712**	-891.9888371	-892.3968615	-0.0169559 **-0.0062310**
3	-893.3951177	**-893.206829**	-891.9794748	-892.3872680	-0.0253064 **-0.0078405**
6	-893.4003391	**-893.212435**	-891.9864258	-892.3938777	-0.0172428 **-0.0058007**
7	-893.3992237	**-893.210847**	-891.9844058	-892.3924448	-0.0224220 **-0.0074740**
14	-893.3961382	**-893.208367**	-891.9833696	-892.3905888	-0.0228045 **-0.0063585**

Table 3.41 Energies and enthalpies for open-shell peptide models at various levels of theory in the gas phase at 298.15 K and 1 atm in Hartree.

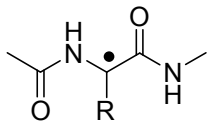	E(UB3LYP)	**H(UB3LYP)**	E(ROMP2)	E(G3(MP2)-RAD
R = CHO (**3-59R**)				
2	-569.2276250	**-569.061217**	-568.1973426	-568.5712370
4	-569.2339133	**-569.067427**	-568.2031731	-568.5764921
R = CH_3CO (**3-60R**)				
2	-608.5476982	**-608.352290**	-607.4228036	-607.8401684
3	-608.5500818	**-608.354825**	-607.4269579	-607.8440836
4	-608.5322092	**-608.337400**	-607.4127905	-607.8297855
R = H_2C=COH (**3-61Rb**)				
2	-608.5250550	**-608.330477**	-607.4088542	-607.8278750
3	-608.5236818	**-608.328792**	-607.4077166	-607.8257739
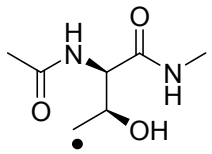 (**3-61Ra_H**)	E(UB3LYP)	**H(UB3LYP)**	E(ROMP2)	E(G3(MP2)-RAD
1	-609.7083097	**-609.491090**	-608.5909557	-609.0241559
2	-609.7153128	**-609.497839**	-608.5971186	-609.0303711
3	-609.7089514	**-609.491153**	-608.5889031	-609.0220723
4	-609.7078654	**-609.490837**	-608.5886489	-609.0216434
15	-609.7105614	**-609.492613**	-608.5911036	-609.0249362
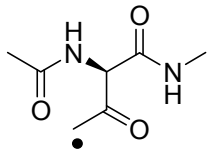 (**3-61Rb**)	E(UB3LYP)	**H(UB3LYP)**	E(ROMP2)	E(G3(MP2)-RAD
1	-608.5227376	**-608.328374**	-607.4049916	-607.8224614
2	-608.5231213	**-608.328708**	-607.4047428	-607.8224344
9	-608.5154982	**-608.321203**	-607.399195	-607.8169806

4 Calculation of Chemical Properties of Allenic Zinc Compounds

Parts of this chapter have been published in

Preparation of Tri- and Tetrasubstituted Allenes via Regioselective Lateral Metalation of Benzylic (Trimethylsilyl)alkynes Using TMPZnCl•LiCl

P. Quinio, C. François, A. Escribano Cuesta, A. K. Steib, F. Achrainer, H. Zipse, K. Karaghiosoff, P. Knochel, *Org. Lett.* **2015**, *17*, 1010 – 1013.

New In Situ Trapping Metalations of Functionalized Arenes and Heteroarenes with TMPLi in the Presence of $ZnCl_2$ and Other Metal Salts

A. Frischmuth, M. Fernandez, N. M. Barl, F. Achrainer, H. Zipse, G. Berionni, H. Mayr, K. Karaghiosoff, P. Knochel, *Angew. Chem. Int. Ed.* **2014**, *53*, 7928 – 7932.

4.1 Introduction

Since the discovery of the first organozinc compound diethyl zinc Et_2Zn by *Edward Frankland* in 1849 organometallic chemistry has witnessed an incredible and fast development.[125] Numerous syntheses and applications were only possible or in much shorter reaction steps through the processing of organometallic research. Among these, organozinc reagents possess outstanding properties concerning functional group compatibility, synthetic versatility, reactivity tuning, thermal stability, and the lack of toxicity.[126] However, the benefit of high functional group tolerance is accompanied by low reactivity compared e.g. to organolithium or *Grignard* reagents, which are characterized by a highly heteropolar carbon-metal-bond.[127] The structures of organozinc compounds in solution are comparable to the *Schlenk* equilibrium found for *Grignard* compounds and depend strongly on the solvent, temperature, concentration and the nature of the organic substituent (**Scheme 4.1**).[128]

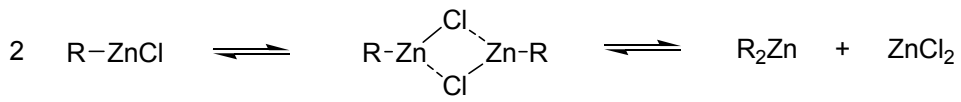

Scheme 4.1 The *Schlenk* equilibrium of organozinc compounds.

With its electron configuration $3d^{10}4s^2$ the full low-lying 3*d* shell of the Zn^{2+} ion does not generate ligand-field effects and the structural properties can therefore be supposed to be comparatively simple. Organozinc compounds possess two vacant 4*p* orbitals on the zinc atom which can accommodate two or four electrons from other organometallic derivatives to form tri- or tetrasubstituted homo- or heteroleptic ate complexes.[129] These zincates are generally more reactive than organozinc halides or diorganozinc reagents and add optionally to carbonyl groups, open epoxides without the aid of promoters or create multiple carbon-carbon bonds in a one-pot reaction.[126] The identification of structural characteristics or dynamics in solution with the help of nuclear magnetic resonance spectroscopy (NMR) is very popular, fast and reliable. Nevertheless, sometimes the assignment of signals can be difficult, time consuming and providing disputable results. Under these circumstances, NMR shift calculations using high level theory represent a helpful alternative in contrast to database search or the sometimes extensive synthesis of side products.[130] In the following chapter, in collaboration with the group of Prof. *Paul Knochel*, the formation of allenic zinc compounds has been studied spectroscopically and theoretically by NMR shift calculations and thermochemical analysis.

4.2 Allenic Organozinc Reagents – Synthesis and Reactivity

Allenes are classified as polyenes with cumulated double bonds, which exhibit higher reactivity than normal alkenes. They represent a versatile multi-reactivity functionality because they can act either as nucleophile, electrophile or as substrate for cycloadditions.[131] The central carbon atom is *sp*- and the two neighbouring carbons are sp^2-hybridized. Due to the geometrical feature of allenes they possess axial chirality, if two different substituents are connected on each of the two terminal carbon atoms.

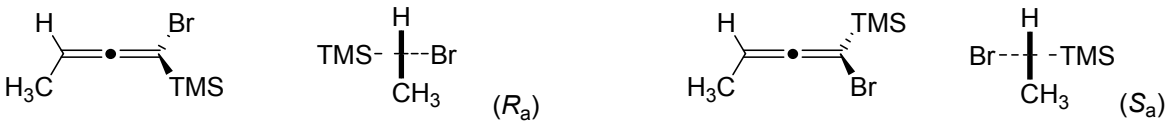

Figure 4.1 Axial chirality of allenes.

Allenes are isomers of readily-available propargylic molecules and can easily be interconverted by prototropic isomerisation. A very convenient and high-yielding synthesis of phenylallene has been published by electrocyclic ring contraction of cycloheptatriene **4-1** followed by acidic isomerisation.[132]

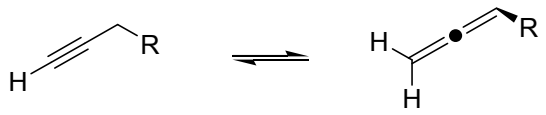

Scheme 4.2 The acetylene-allene rearrangement.

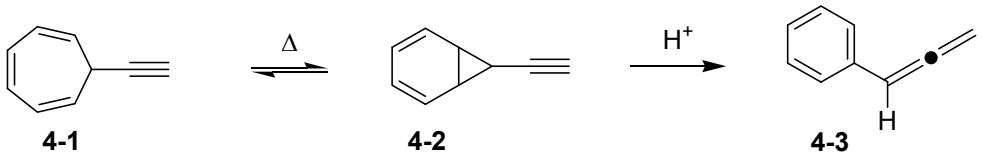

Scheme 4.3 Acid-catalyzed rearrangement of cycloheptatriene **4-1** to phenylallene (**4-3**).

Another well examined process is the ability of conjugated enyne-allenes and their benzannulated derivatives to cyclize under mild thermal conditions to form biradicals, which react further in H-abstraction reactions. The preferred outcome of cyclization is dictated by the substituent at the acetylenic position.[133]

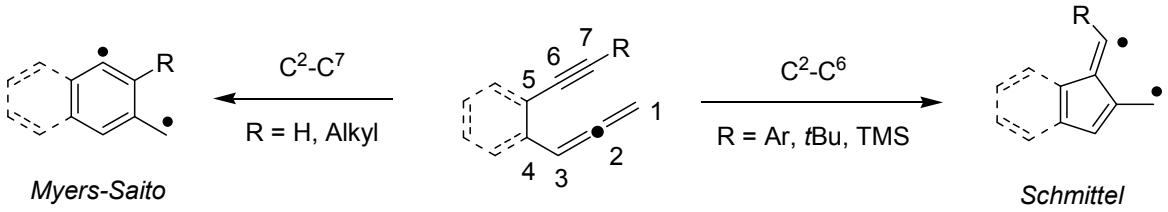

Scheme 4.4 The *Myers-Saito* vs. the *Schmittel* cyclisation.

The use of organometallic reagents for the synthesis of allenes is highly developed and covers a wide range of reactions, the most important of which are S_N2' reactions with unsaturated electrophiles to generate allenic molecules.[131] One disadvantage of this strategy is the need of already functionalized starting materials with leaving groups or electron acceptors.

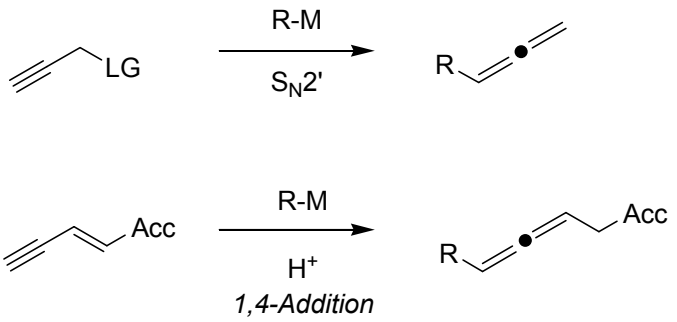

Scheme 4.5 Metal-mediated syntheses of allenes.

An alternative route is available in the already mentioned deprotonation of terminal protected acetylenes at the propargylic position, followed by isomerization and electrophilic interception. Usually the product outcome is non-selective with respect to the formation of allenic or propargylic molecules. But in general the regioselectivity is mainly provided by the nature of the starting material and the applied conditions. For example, *Ma* recently discovered a highly selective allene synthesis from 1-aryl-1-propynes by varying the metallation reagent.[134] He also investigated the influence of substituent effects on the product formation.[135]

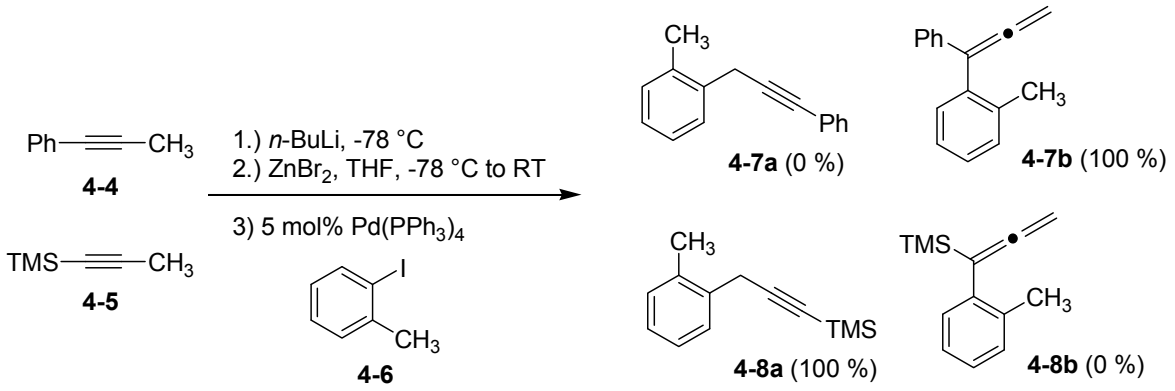

Scheme 4.6 Influence of the substituent on the propargyl-allenyl isomerization.

4.3 NMR Properties of the *Reformatsky* Reagent – Method Benchmarking

It seems, that limited literature is found for the theoretical description of NMR shifts of organozinc compounds.[126] Therefore a short preliminary benchmark study using the *Reformatsky* reagent **4-10** as model compound has been conducted to verify a reliable and even for larger systems applicable computation routine. The classic

Reformatsky reaction involves the addition of α-halocarboxylic ester to a carbonyl compound in the presence of zinc to form β-hydroxy esters.[136]

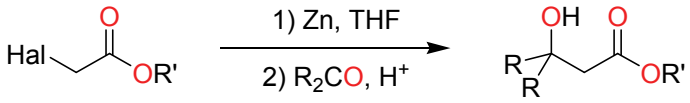

Scheme 4.7 The classical *Reformatsky* reaction.

The currently accepted mechanism proposes a preceding equilibrium between enolate and alkyl zinc intermediate, in which only the enolate is capable of attacking the electrophile.

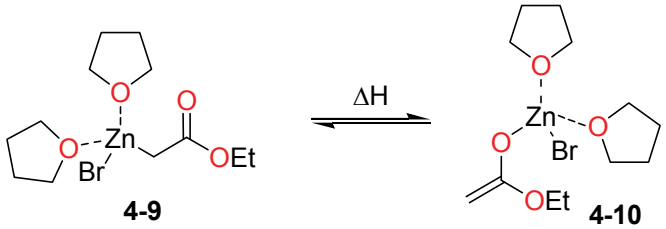

Scheme 4.8 Ester-enol equilibrium of *Reformatsky* reagent **4-9** to **4-10**.

The *Reformatsky* reagent containing a Zn-C bond is more stable by +51.8 kJ mol^{-1} (B3LYP/631SVP) than the respective compound having an enolate structure. Implicit solvation in a THF continuum lowers the endothermicity only marginally to +48.9 kJ mol^{-1} (SMD/B3LYP/6-31G(d)//B3LYP/631SVP). This is in agreement with already published results by *Dewar* and *Cossio*, who investigated the kinetics of the *Reformatsky* addition to formaldehyde and identified the zinc enolate as attacking intermediate and the enolisation as rate-determining step.[137] The structure of *Reformatsky* esters have been the objective of investigations over decades and includes NMR studies,[138] EXAFS investigations in solution[139] and X-ray single crystal determination.[140] The results indicate, that in coordinating polar solvents the *Reformatsky* compounds are best represented as dimers of structure **4-11**, which are in equilibrium with the monomer (**4-9**) and the enolate form (**4-10**), respectively.

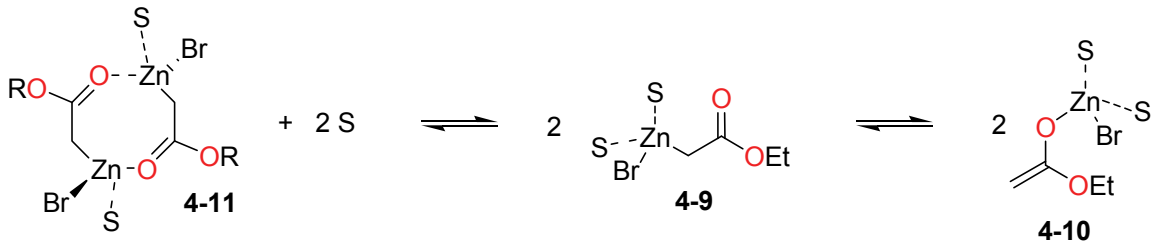

Scheme 4.9 Equilibrium of *Reformatsky* enolates in solution (S = coordinating polar solvent).

In order to identify the most reliable method for calculating chemical shifts of organozinc compounds, ^{1}H and ^{13}C NMR spectra of **4-9** in THF-d_8 have been measured which are displayed in **Figure 4.2** and **Figure 4.3**. The reagent was synthesized by insertion of activated zinc into the C-Br bond of bromo ethyl acetate in THF.[140b]

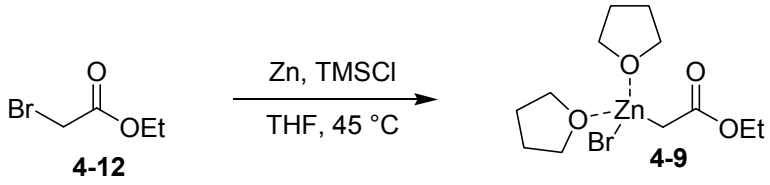

Scheme 4.10 Synthesis of the *Reformatky* reagent EtO_2CCH_2ZnBr • 2 THF (**4-9**).

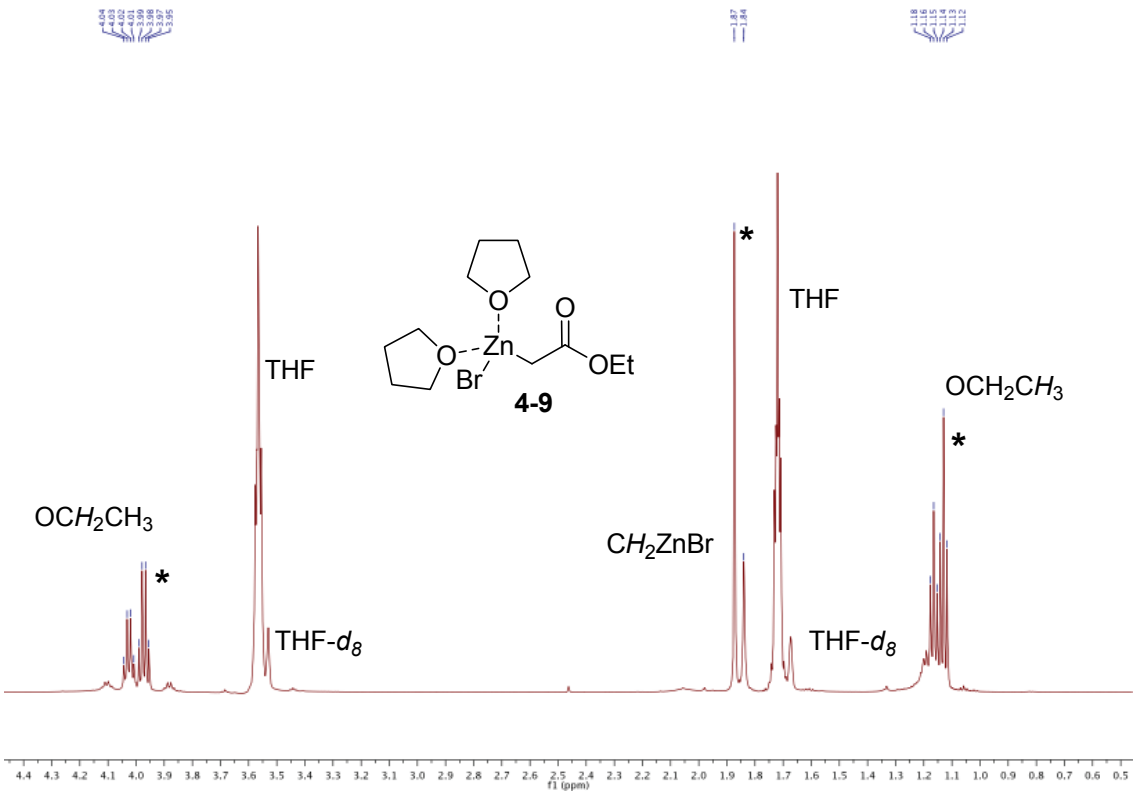

Figure 4.2 ^{1}H NMR (600 MHz, THF-d_8) at 298 K of the *Reformatsky* reagent EtO_2CCH_2ZnBr•2 THF (**3-9**). Ethyl acetate formed as a result of hydrolysis is marked by an asterisk.

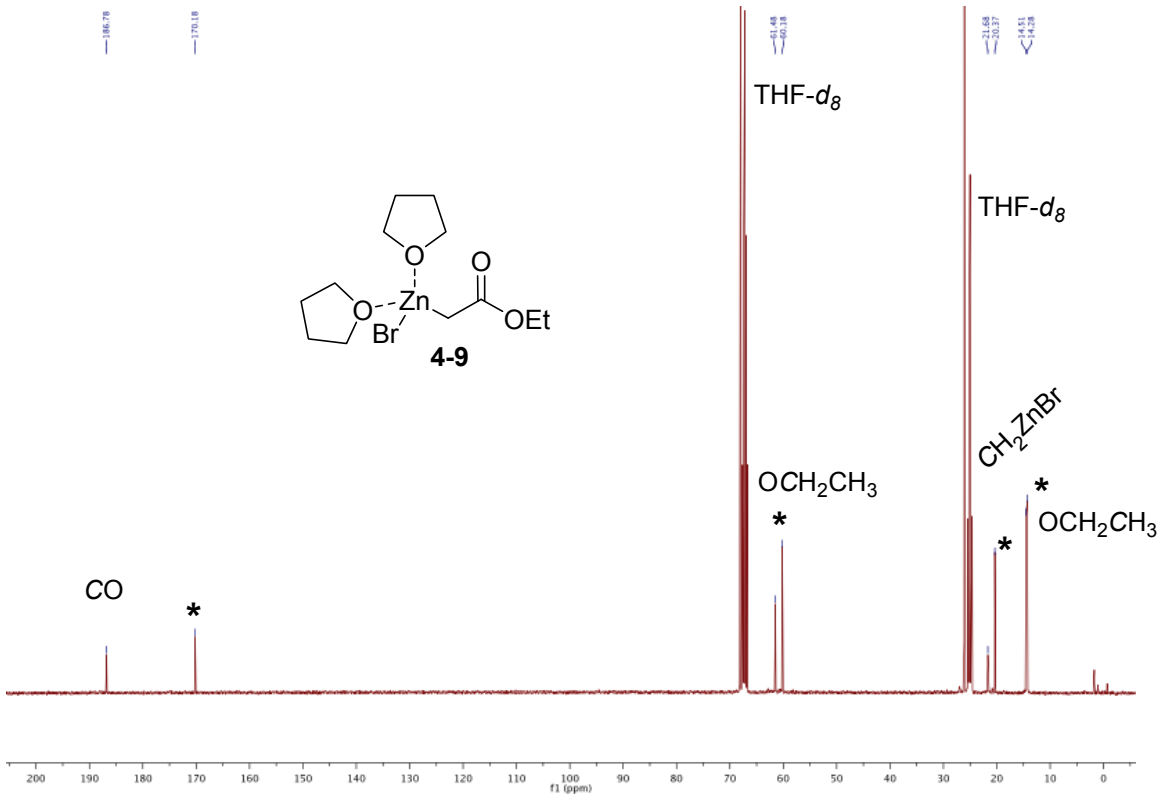

Figure 4.3 ^{13}C NMR (100 MHz, THF-d_8) at 298 K of the *Reformatsky* reagent EtO_2CCH_2ZnBr•2 THF (**4-9**). Ethyl acetate formed as result of hydrolysis is marked by an asterisk.

Due to the three different existing isomers of **4-9** in solution all structures have been evaluated theoretically. The number of basis sets for zinc and bromine as 4th row elements are usually limited to expensive basis sets, like *Ahlrichs'* def2[141] or *Dunning's* correlation consistent sets.[142] With the elemental decomposition C, H, O, Zn and Br only one Pople basis set (3-21G) is available. The B3LYP optimized structural parameters for the *Reformatsky* dimer **4-11** at three different levels are summarized together with the experimentally determined values via single crystal X-ray diffraction of (tBuO$_2$CCH$_2$ZnBr • THF)$_2$ in **Table 4.1**.[140a] The B3LYP/631SVP approach was recently used by *Thaler et al.* for the investigation of diastereoselective Negishi cross coupling reactions of cycloalkylzinc compounds[143] and includes for C, H, O, Cl the 6-31G(d,p) and for Zn the all-electron def2-SVP basis set. The overall DFT-optimized structure applying the 631SVP basis set gives good geometrical agreement compared to the X-ray structure in solid state including the twisted boat conformation, but overestimates the bond lengths in all cases. The more expensive double ξ basis set cc-pVDZ gives related results, but takes almost four times longer to fulfill its task.

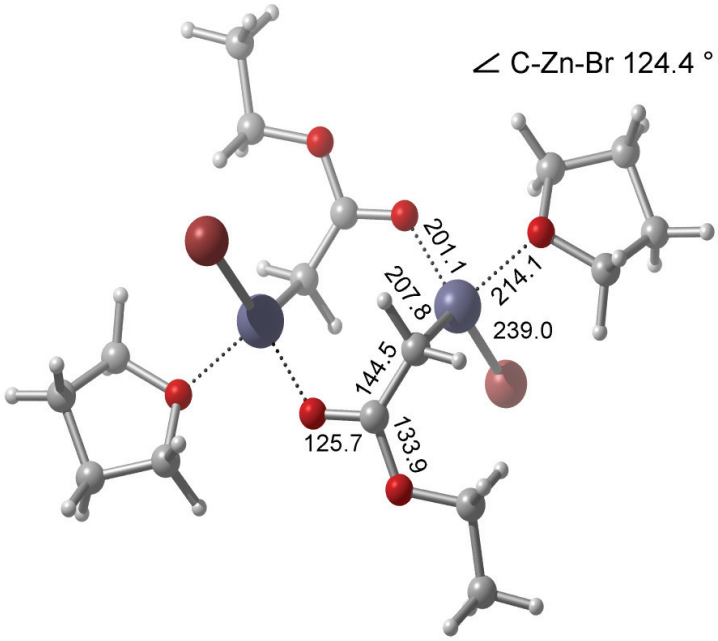

Figure 4.4 Graphical representation of the B3LYP/631SVP optimized gas phase structure of dimer **4-11**.

Table 4.1 Selected bond lengths (in pm) and angles (in °) for the DFT-optimized *Reformatsky* dimer **4-11**.

	B3LYP/3-21G[a]	B3LYP/cc-pVDZ	B3LYP/631SVP[b]	(tBuO$_2$CCH$_2$ZnBr • THF)$_2$ [X-ray]
Zn-O$_{CO}$	187.2	201.7	201.1	202.0 (1)
Zn-CH$_2$	196.7	207.9	207.8	198.0 (2)
Zn-O$_{THF}$	192.4	215.9	214.1	205.0 (1)
Zn-Br	245.5	237.8	239.0	234.6 (3)
O$_2$C-CH$_2$	141.9	144.6	144.5	141.0 (2)
Br-Zn-CH$_2$	115.1	125.9	124.4	127.6 (5)
O$_{CO}$-Zn-O$_{THF}$	102.5	89.2	90.4	93.2 (4)
O$_{THF}$-Zn-CH$_2$	113.6	105.5	109.3	106.9 (6)
O$_{CO}$-Zn-CH$_2$	110.5	109.6	109.7	111.2 (6)
Zn-O$_{CO}$-C$_{CO}$	144.6	131.1	128.5	125.0 (1)

[a]Averaged arithmethically. [b] 6-31G(d,p) for C, H, O, def2-SVP basis set for Zn and Br.

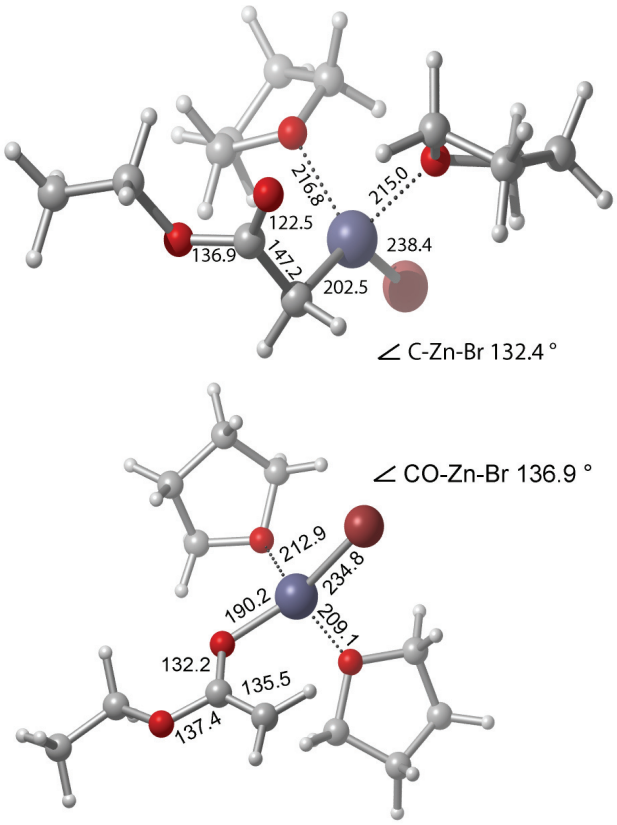

Figure 4.5 Graphical representation of the B3LYP/631SVP optimized gas phase structure of monomeric **4-9** in the ester (top) and enol form (bottom).

Usually, basis sets are developed in order to predict bonding phenomena in an accurate way, thus putting particular emphasis on the valence region. A proper description of the molecular orbital structure and thus the electron density near the nucleus is essential for the simulation of spectroscopic data like NMR shifts or EPR *g*-values. An all-purpose basis set for NMR shift calculations is the IGLO-III set[144] developed by *Kutzelnigg* and already used for the ^{13}C NMR evaluation of alkyl and aryl lithium compounds.[145] Recently, *Jensen* proposed a polarization-consistent set of basis sets with hybrid-DFT methods termed “pc-n”, which are applicable even for 4th row elements.[146] The benchmark results for the different isomers of the *Reformatsky* reagent together with the experimental NMR shifts calculated by the GIAO scheme[147] are collected in **Table 4.2** and **Table 4.3**.

Table 4.2 Method benchmarking using the GIAO method in combination with the IGLO-III[a] basis set for the calculation of chemical shifts for the *Reformatsky* reagent.

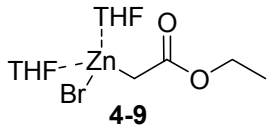

4-9

	Chemical shift δ						
	B3LYP Gas phase	mPW1K Gas phase	B3LYP SMD[b]	mPW1K SMD[b]	B3LYP UAHF[c]	mPW1K UAHF[c]	δ(exp.)
C***H***$_2$Zn	1.70	1.57	1.67	1.56	1.87	1.77	**1.84**
CH$_3$C***H***$_2$O	4.01	3.90	3.98	3.89	4.09	4.00	**3.97**
C***H***$_3$CH$_2$O	1.19	1.14	1.21	1.18	1.24	1.22	**1.16**
CH$_2$Zn	19.41	17.34	20.28	18.28	19.86	18.07	**21.67**
CO$_2$	191.94	193.07	194.51	195.62	196.00	197.13	**186.78**
CH$_3$***C***H$_2$O	65.52	62.85	67.12	64.39	66.24	63.60	**61.48**
CH$_3$CH$_2$O	16.37	15.83	16.69	16.08	16.00	15.45	**14.51**
MAD	**1.90**	**2.25**	**2.83**	**2.90**	**3.15**	**3.45**	

Table 4.3 Method benchmarking using the GIAO method in combination with the IGLO-III[a] basis set for the calculation of the dimeric (**4-10**) and the enol form (**4-11**) of the *Reformatsky* reagent.

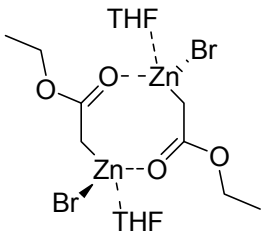

4-11

	Chemical shift δ						
	B3LYP Gas phase	mPW1K Gas phase	B3LYP SMD[b]	mPW1K SMD[b]	B3LYP UAHF[c]	mPW1K UAHF[c]	δ(exp.)
C***H***$_2$Zn	2.00	1.92	2.09	2.02	2.26	2.22	**1.84**
$CH_3C\boldsymbol{H}_2O$	4.39	4.28	4.44	4.34	4.51	4.43	**3.97**
$C\boldsymbol{H}_3CH_2O$	1.34	1.31	1.33	1.32	1.36	1.35	**1.16**
CH_2Zn	24.15	23.00	25.82	24.60	25.43	24.32	**21.67**
CO_2	201.73	203.74	203.81	205.76	204.19	206.11	**186.78**
$CH_3\boldsymbol{C}H_2O$	71.26	68.36	73.15	70.19	72.45	69.60	**61.48**
CH_3CH_2O	16.66	16.19	17.40	16.83	16.78	16.26	**14.51**
MAD	**5.35**	**5.77**	**6.10**	**6.42**	**6.12**	**6.50**	

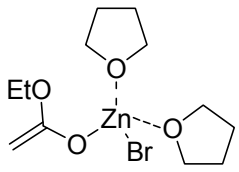

4-10

	B3LYP Gas phase	mPW1K Gas phase	B3LYP SMD[b]	mPW1K SMD[b]	B3LYP UAHF[c]	mPW1K UAHF[c]	δ(exp.)
C***H***$_2$Zn	2.80	2.81	2.65	2.69	2.70	2.75	**1.84**
$CH_3C\boldsymbol{H}_2O$	3.94	3.78	4.00	3.87	4.10	3.98	**3.97**
$C\boldsymbol{H}_3CH_2O$	1.16	1.11	1.16	1.13	1.19	1.17	**1.16**
CH_2Zn	53.56	55.95	50.40	52.84	51.53	54.27	**21.67**
CO_2	181.85	180.77	184.98	182.76	183.93	182.79	**186.78**
$CH_3\boldsymbol{C}H_2O$	64.79	61.90	66.30	63.43	65.46	62.65	**61.48**
CH_3CH_2O	17.49	16.88	18.00	17.30	17.36	16.72	**14.51**
MAD	**10.59**	**11.57**	**9.56**	**10.43**	**9.92**	**11.00**	

[a]IGLO-III for C, H, O; pc-4 for Zn and Br. [b]SMD/B3LYP/IGLO-III//B3LYP/631SVP in THF. [c]PCM/UAHF/B3LYP/IGLO-III//B3LYP/631SVP.

Two hybrid functionals have been applied, namely the well-established B3LYP[148] and the one-parameter hybrid functional mPW1K developed by *Truhlar et al.* [149] The two different functionals give almost the same results for shift calculations, wether in the gas phase or including continuum solvation in THF. The overall performance of the PCM/SMD and the PCM/UAHF model is better in combination with the mPW1K functional. The mean absolute deviation (MAD) for the gas phase calculations have the lowest value compared to the simulation in a solvent continuum. The monomeric species **4-9** gives the best agreement between theory and experiment, thus confirming its presence in THF solution.

4.4 NMR Shifts of Allenic Zinc Compounds

In order to provide structural information on the metallation of allenes using different reagents (see **Scheme 4.11**), their formation has been investigated by *Quinio* NMR spectroscopically. Therefore, aryl substituted propargyl silanes of type **4-13** have been deprotonated with two different organometallic bases (TMPZnCl•LiCl or *n*-BuLi), followed by, if required, transmetallation to zinc with the aid of $ZnCl_2$ in THF-d_8.

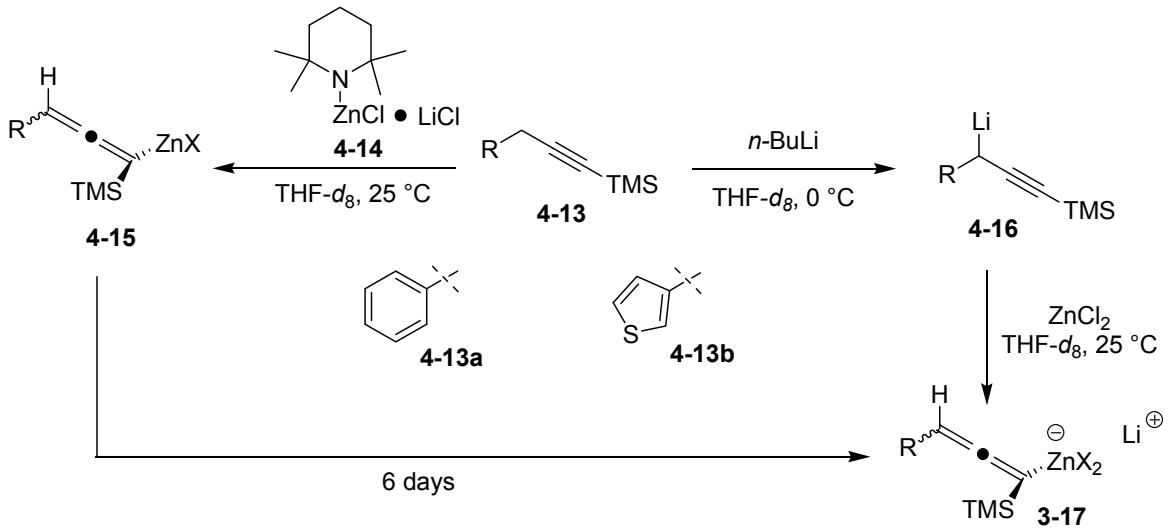

Scheme 4.11 Syntheses of allenic zinc compounds of proposed structure **4-15** and **4-17**.

NMR analysis of the reaction of **4-13** with TMPZnCl•LiCl indicated complete conversion within 5 min affording direct formation of allenylzinc species **4-15** identified by the appearance of an allenic ^{13}C signal at around 200 ppm. On the other

hand, lithiation of **4-13** with *n*-BuLi gave rise to a propargylic lithium species **4-16**, as evidenced by the appearance of a propargyl signal at 3.33 ppm in the ^{1}H NMR spectrum. No allenic carbon resonance has been observed.[150] Nevertheless, after the addition of $ZnCl_2$ an allenic species (**4-17**) was formed. This compound is the final product upon metalation, since it is also formed after six days from intermediate **4-15**. Comparison of the NMR spectra for the two distinguishable zinc species indicates only small differences in chemical shifts for the allenic carbon atoms C^2, C^3 and its attached proton H^3 irrespective of the nature of the organometallic reagent. Interestingly, the higher electron density in the proposed zincate **4-17a** has no influence on the chemical shift of C^1.

To support the hypothesis, what kind of metalation is present, the chemical shifts of allenes **4-15a** and **4-15b** together with their ate counterparts have been calculated with chlorine ligands and THF molecules to saturate their coordination sphere as benchmarked for the *Reformatsky* reagent (X/IGLO-III//B3LYP/631SVP).

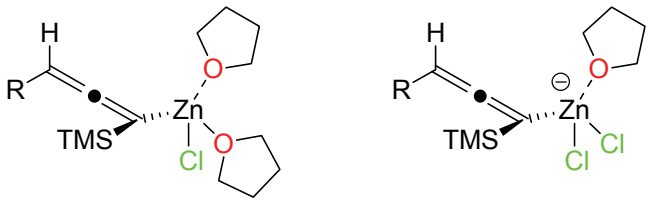

R = Ph (**4-15a**), 3-thioph (**4-15b**) R = Ph (**4-17a**), 3-thioph (**4-17b**)

Figure 4.6 Lewis structures of the theoretically considered zinc allenes.

Although allenes are quite rigid, a complete conformational search is in principle advisable for any organic molecule to evaluate the degree of error introduced by only one considered conformation. The global minimum is arguably the best choice for a single conformation. Therefore, the conformers for all examined allenes have been preselected with the MM3* force field[79] and after DFT optimization *Boltzmann*-averaged over free energies, enthalpies and free solvation energies. This *Boltzmann*-approach has been proposed by *Hoye* and *Cramer* for the calculation of ^{1}H and ^{13}C shifts of stereoisomers and rotamers of cyclohexanols.[151] The obtained results for phenyl allene **4-15a** and **4-17a** are shown in **Table 4.4**. The GIAO prediction in

combination with the two functionals B3LYP and mPW1K gives almost the same results regarding the protons.

Table 4.4 *Boltzmann*-averaged chemical shifts <δ>[a] at various levels of theory (in ppm).

	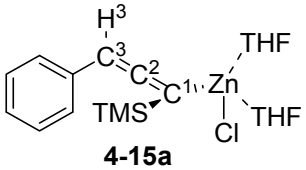 **4-15a**					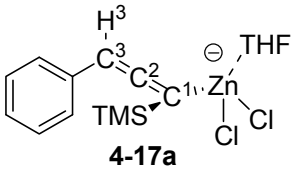 **4-17a**				
	H^3	C^3	C^2	C^1	Si	H^3	C^3	C^2	C^1	Si
δ(exp)[a]	4.99	70.18	202.83	93.97	-4.59	4.62	70.25	197.36	93.94	-6.16
Gas phase	<δ> (GIAO/B3LYP/IGLO-III//B3LYP/631SVP)									
E[b]	5.16	77.85	212.61	101.94	-7.07	4.87	75.41	206.24	104.13	-9.79
H	5.16	78.13	213.15	101.62	-7.08	4.83	75.32	204.82	104.32	-9.77
G	5.15	78.17	213.02	101.65	-7.03	4.80	75.30	203.82	104.43	-10.09
G_{sol}[c]	5.14	78.32	212.26	101.59	-7.04	4.77	74.98	202.45	104.67	-10.09
	RMSD Δδ (G_{sol}) **4.79**					**RMSD** Δδ (G_{sol}) **4.95**				
Gas phase	<δ> (GIAO/mPW1K/IGLO-III//B3LYP/631SVP)									
E[b]	5.16	76.34	213.53	100.30	-6.03	4.85	73.75	207.47	102.80	-8.75
H	5.16	76.60	214.04	99.98	-6.03	4.82	73.65	206.23	103.04	-8.70
G	5.15	76.62	213.90	100.01	-6.00	4.78	73.63	205.36	103.19	-8.93
G_{sol}[c]	5.14	76.76	214.13	99.93	-6.00	4.76	73.27	204.06	103.49	-8.95
	RMSD Δδ (G_{sol}) **4.62**					**RMSD** Δδ (G_{sol}) **4.42**				
THF	<δ> (GIAO/SMD/mPW1K/IGLO-III//B3LYP/631SVP)									
E[b]	5.38	75.86	213.10	102.06	-6.35	5.16	73.24	209.14	103.85	-8.32
H	5.37	76.03	213.47	101.83	-6.34	5.15	73.34	208.43	103.74	-8.25
G	5.37	76.12	213.42	101.77	-6.31	5.14	73.43	207.97	103.66	-8.40
G_{sol}[c]	5.36	76.24	213.58	101.75	-6.31	5.14	73.25	207.77	103.62	-8.35
	RMSD Δδ (G_{sol}) **4.65**					**RMSD** Δδ (G_{sol}) **4.99**				

[a] Using tetramethylsilane $Si(CH_3)_4$ as standard for experimental and calculated values, respectively. [b] Only global minimum structure considered. [c] SMD/B3LYP/6-31G(d)//B3LYP/631SVP (THF).

The B3LYP functional predicts chemical shifts in all cases low field-shifted compared to mPW1K and they are not depending on the overall averaged extensive property (H, G, H_{sol}, G_{sol}) for the individual nuclei. The induced error by examining only the global minimum structures is negligible (see line E in **Table 4.4**).

Table 4.5 Experimentally measured and theoretically calculated chemical shifts δ obtained in the gas phase at mPW1K/IGLO-III/B3LYP/631SVP level of theory (in ppm).[a,b]

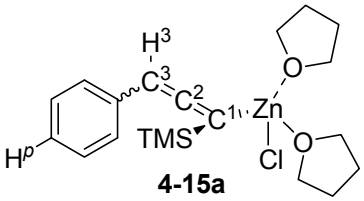

4-15a

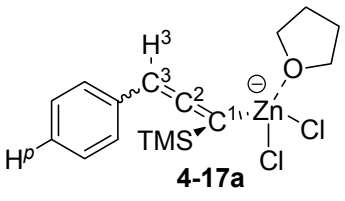

4-17a

Gas	mPW1K/ IGLO-III	δ(*exp.*)[c]	Δδ	mPW1K/ IGLO-III	δ(*exp.*)[c]	Δδ
H^3	5.14	4.99	0.15	4.76	4.62	0.14
H^p	7.21	6.78	0.43	6.72	6.65	0.07
C^3	76.76	70.2	6.58	73.27	70.3	3.02
C^2	214.13	202.8	11.30	204.06	197.4	6.70
C^1	99.93	94.0	5.96	103.49	93.9	9.55
TMS	-6.00	-4.59	-1.41	-8.95	-6.16	-2.79

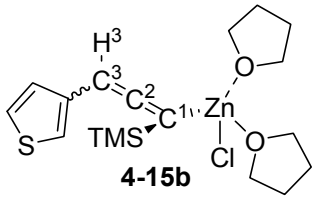

4-15b

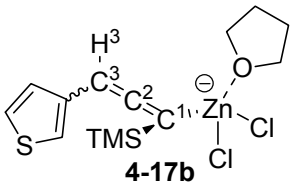

4-17b

Gas	mPW1K/ IGLO-III	δ(*exp.*)[c]	Δδ	mPW1K/ IGLO-III	δ(*exp.*)[c]	Δδ
H^3	5.16	5.11	0.05	4.80	4.71	0.09
C^3	71.78	68.7	3.08	68.45	65.5	2.95
C^2	216.87	204.5	12.37	207.43	199.0	8.43
C^1	99.14	93.6	5.54	103.49	93.9	9.59
TMS	-6.07	-5.0	-1.07	-9.81	-3.01	-3.01

[a]Using tetramethylsilane $Si(CH_3)_4$ as standard for experimental and calculated values, respectively. [b] Applying *Boltzmann*-averaged shielding tensors σ obtained from $G + \Delta G_{solv}$. [c] Measured in THF-d_8.

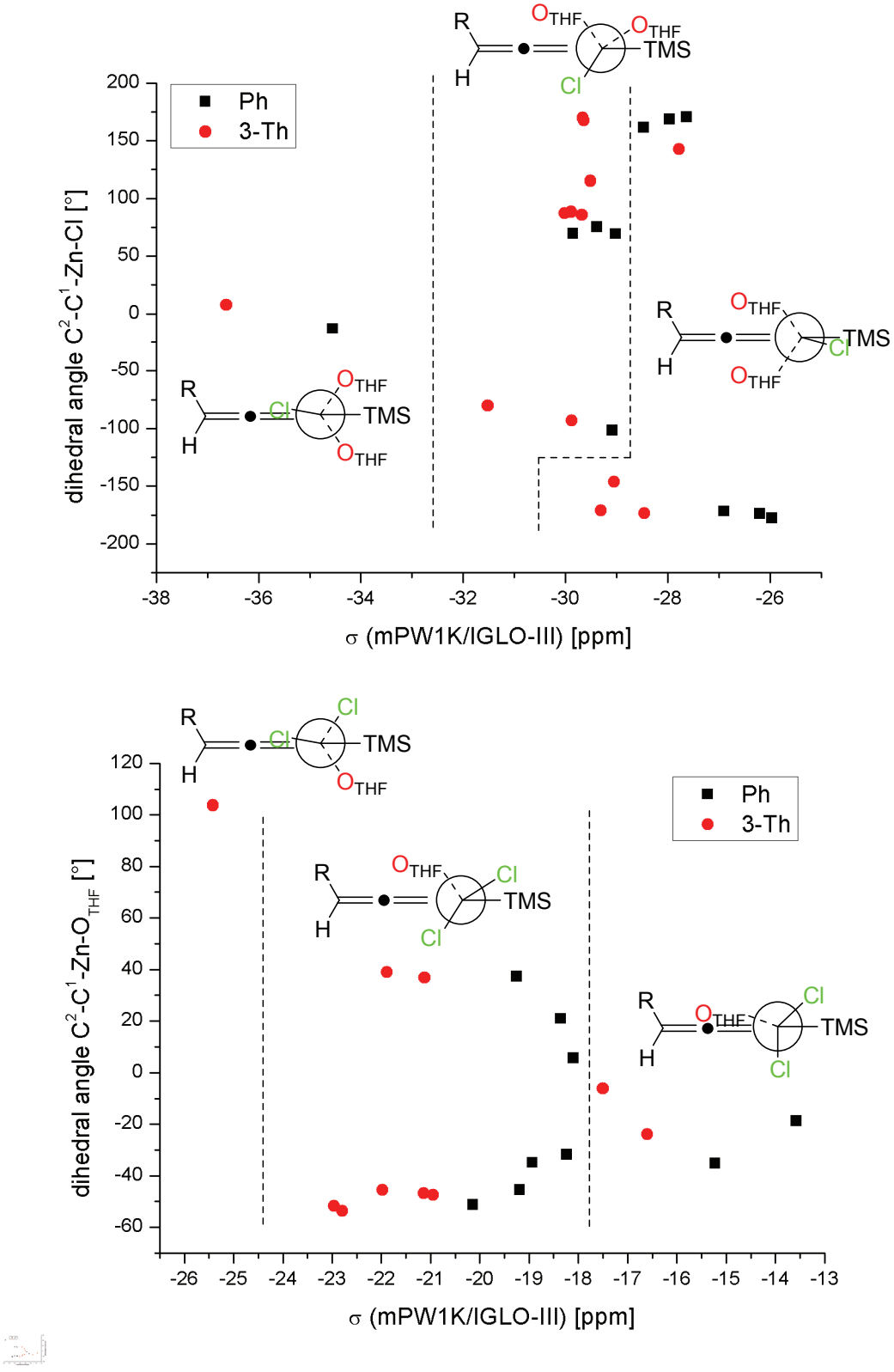

Figure 4.7 Conformational dependence of calculated shielding tensors σ of the allenic carbon atom C^2 in neutral allenic zinc reagents (top) and zincate (bottom).

The mPW1K/IGLO-III gas phase calculation performs best in all four studied cases (R = Ph, 3-thioph). The simulation for the specific allenic carbon atoms C^3 and its attached protons H^3 is in good agreement with the experimental results, regarding the effective range of the corresponding nuclei. The largest deviations are observed for the *sp*-hybridized carbon atom C^2 (see **Table 4.5**). The differences $\Delta\delta$ are smaller for the zincates than the neutral zinc allenes. In **Figure 4.7** the influence of the chloro ligand as virtual dipole to the calculated shielding tensor is plotted against the dihedral angle C^2-C^1-Zn-Cl to provide a criterion for dipole-nucleus interactions and the complete conformational space has to be examined for accurate chemical shift calculations. The most negative σ-values are found for compounds with a *syn*-chloro-C^{sp} conformation, whereupon the *anti* conformation gives values of 8 ppm shifted to higher field. The dihedral angle dependence of allene **4-15b** is not so distinctive due to the higher polarity of the thiophene group.

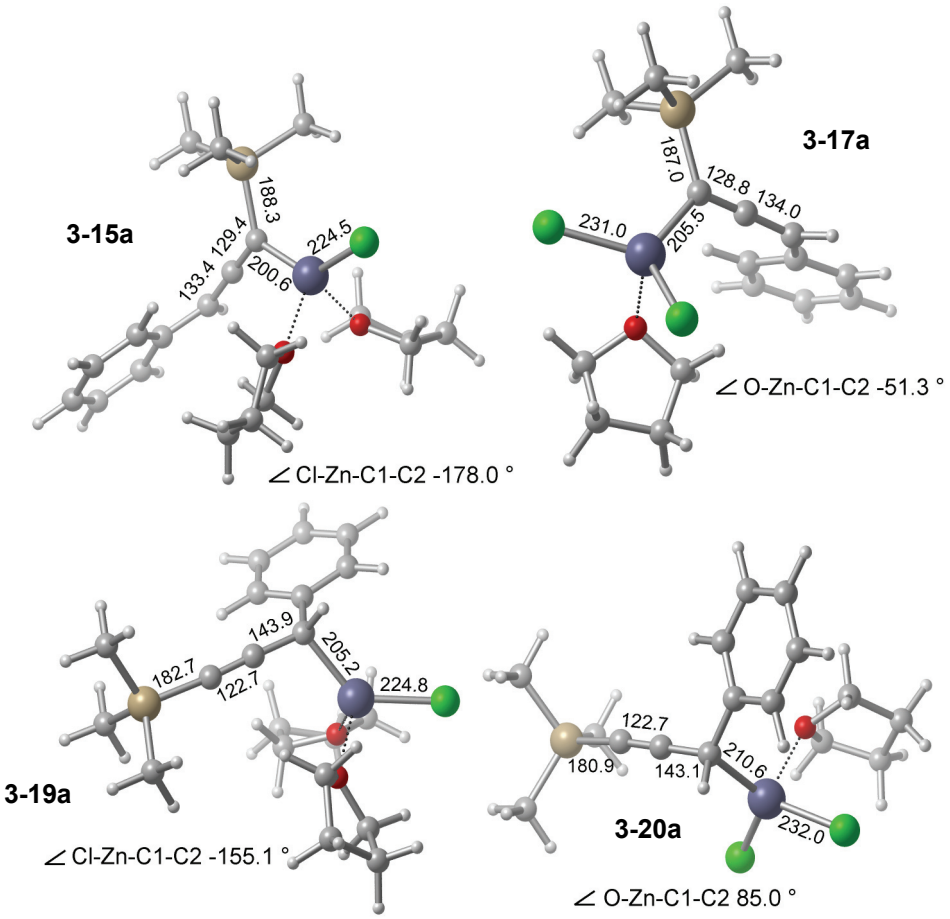

Figure 4.8 B3LYP/631SVP optimized structures of the energetically most favored conformers of allenic and propargylic zinc reagents in the gas phase.

The presence of corresponding phenyl substituted propargylic zinc compounds in solution can be excluded due to the large deviation from experimental chemical shifts (see **Table 4.6**). On the other hand, intermediate **4-16a** generated by the reaction of **4-13a** with *n*-BuLi can be verified by the NMR shift calculations. Since the structure of organolithium reagents has a major impact on the molecular properties, the optimization of **4-16a** has been conducted by attaching three THF to the lithium atom.[152]

Table 4.6 Calculated chemical shifts δ[a] for propargylic and allenic organozinc and -lithium reagents at GIAO/mPW1K/IGLO-III//B3LYP/X[b] level of theory (in ppm).[c]

δ	H^p	H^3	C^3	C^2	C^1	TMS
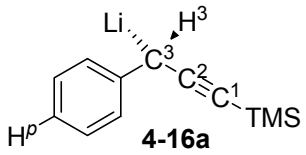 **4-16a** (exp. in THF-d_8)	**6.07**	**3.33**	**51.9**	**151.4**	**95.0**	**-18.83**
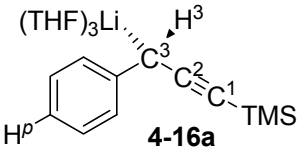 **4-16a**	6.53	3.10	42.90	140.30	97.71	-26.66
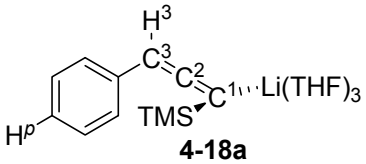 **4-18a**	6.82	4.16	64.10	184.84	108.89	-15.47
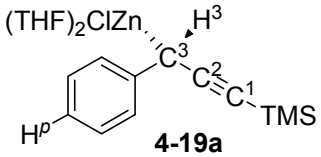 **4-19a**	7.25	3.46	23.81	127.75	91.31	-24.86
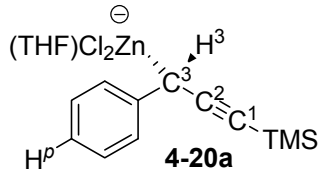 **4-20a**	6.81	3.39	29.64	132.62	87.30	-27.84

[a] Using tetramethylsilane $Si(CH_3)_4$ as standard for experimental and calculated values, respectively. [b] 6-31+G(d) for Li, 631SVP for Zn. [c] Using the global minimum of all structures.

The quantum chemical treatment of organolithium compounds has been the subject of numerous publications including explicit solvation[153] and aggregate formation.[154]

Accordingly the lithium species **4-16a** and **4-18a** have been optimized using the B3LYP functional in combination with the double ξ basis set 6-31+G(d). The characteristic shift for the *sp*-hybridized C^2 has a deviation of Δδ(**4-16a**)= +11.1 ppm at GIAO/mPW1K/IGLO-III level. For the allenic form **3-18a** a deviation of Δδ(**4-18a**) = -33.44 ppm was found. Interestingly, the chemical shift for the C^1 atom in **4-16a** reveals the overall best match in all calculations (Δδ(**4-16a**) = -2.71 ppm) and in addition confirms the presence of the propargylic lithium intermediate **4-16a** in THF.[155]

4.5 Thermochemical Analysis

^1H and ^{13}C NMR spectroscopy (see **Chapter 4.4**) shows that two allenylzinc species are generated, which most likely differ by the second substituent at zinc (monomeric or dimeric organozinc halide or LiCl-complexed ate complex). Thermochemical analysis of the organic zinc species optimized at B3LYP/631SVP level of theory in combination with solvation free energies for THF at SMD/B3LYP/6-31G(d) level reveals, that the isomerization to the phenyl-substituted allenic moiety is exothermic by -25.5 kJ mol^{-1} in its monomeric zinc form **4-15a** and -23.8 kJ mol^{-1} in its anionic ate complex **4-17a** (**Table 4.7**).

Table 4.7 Reaction enthalpies for the propargyl-allenyl isomerization (in kJ mol^{-1}).

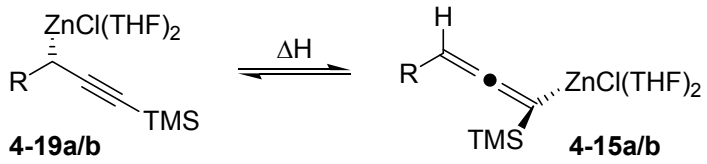

4-19a/b **4-15a/b**

R	ΔH_{298} (gas) B3LYP/631SVP[a]	ΔH_{sol} (THF) SMD/B3LYP/6-31G(d)// B3LYP/631SVP
Phenyl (**4-15a**)	-25.76	-25.50
3-Thienyl (**4-15b**)	-19.64	-18.92

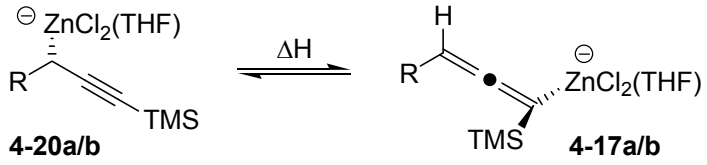

4-20a/b **4-17a/b**

R	ΔH_{298} (gas) B3LYP/631SVP[a]	ΔH_{sol} (THF) SMD/B3LYP/6-31G(d)// B3LYP/631SVP
Phenyl (**4-17a**)	-29.86	-23.75
3-Thienyl (**4-17b**)	-28.25	-21.34

[a] 6-31G(d,p) for C, H, O, Si, Cl, def2-SVP basis set for Zn.

Moving from the phenyl to the thiophene-3-yl substituted systems lowers the reaction enthalpy to -18.9 kJ mol^{-1} ($ZnCl(THF)_2$) and to -21.3 kJ mol^{-1} ($ZnCl_2$-(THF)), respectively. Furthermore, according to the NMR studies, it is evident that the propargyl isomer (**4-16a**) is the most stable organometallic species in the case of the lithium cation, whereas the allenyl structure (**4-15a**) is the dominant species in solution for zinc.[156] Single-point calculations at MP2(FC)/6-31+G(d,p) level of theory including implicit THF solvation (SMD/B3LYP/6-31G(d)) confirms a major difference in stability order for the propargyl and allenyl isomers of the respective organometallics. A reaction enthalpy of +1.4 kJ mol^{-1} for the two organolithium isomers has been calculated (see **Figure 4.9**) as opposed to -7.8 for the neutral zinc and -8.2 kJ mol^{-1} for the ate complex, respectively.

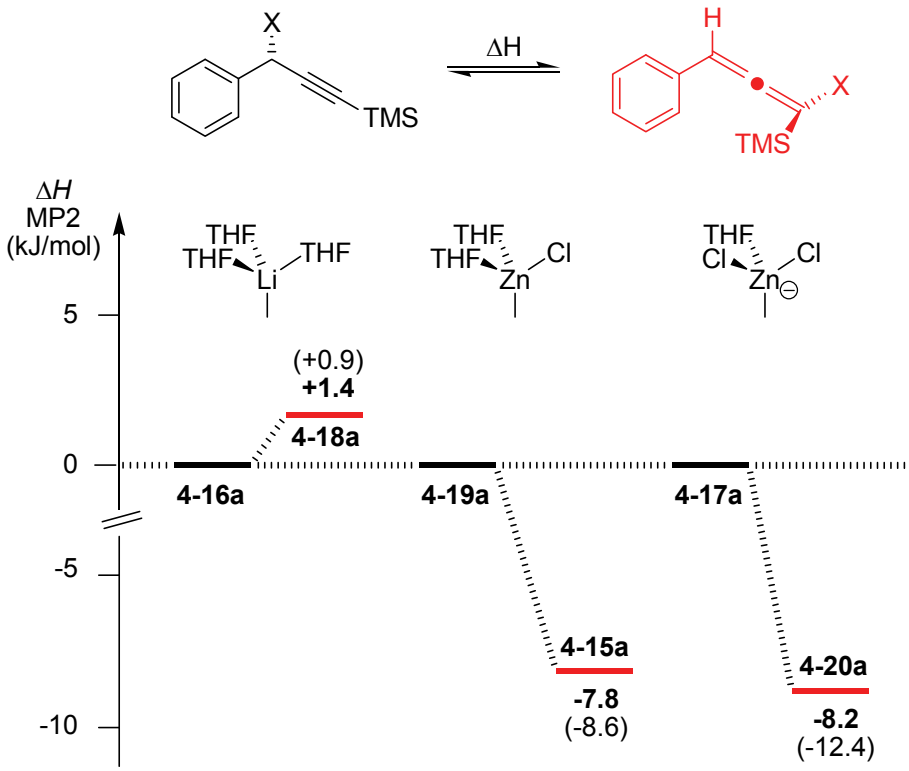

Figure 4.9 Propargyl to allenyl isomerization in THF solution (SMD/B3LYP/6-31G(d)) at MP2(FC)/6-31+G(d,p) level (gas phase values in parenthesis).

In agreement with these theoretical results only allenic products have been isolated after *Negishi* cross-coupling. This reaction sequence can even be extended to a subsequent metalation with TMPZnCl•LiCl (**4-14**) to yield, after successful trapping with various electrophiles, tetra-substituted allenes in a one-pot fashion. As example, allene **3-39** was isolated in 63 % yield after two-step metalation with 1.2 eq of TMPZnCl•LiCl (**4-14**) at room temperature within an hour, respectively. Full conversion to tri-substituted allene **4-40** using phenyl iodide as electrophile and 2 mol% $Pd(OAc)_2$/S-Phos was accomplished within 4 h, followed by the second coupling step with 3-bromothiophene within 12 h at 25 °C.

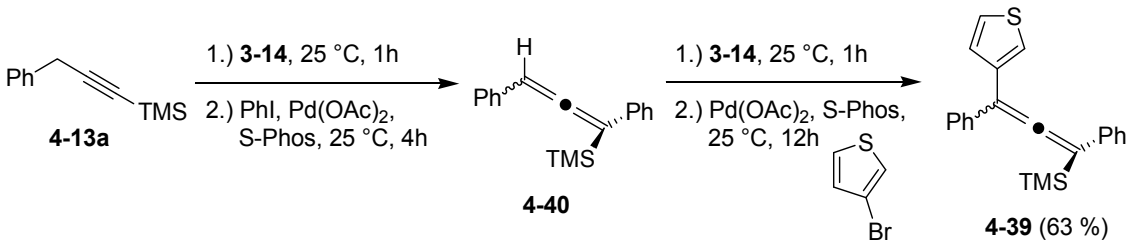

Scheme 4.12 Successive zincation of **4-13a** with TMPZnCl•LiCl (**4-14**) and subsequent Negishi-cross coupling.

4.6 Calculation of Relative pK_a Values of Weak C-H Acids in DMSO Solution

The conversion of organic molecules into organometallics by metalation with a strong base is a well-established, fast and reliable method to synthesize polyfunctionalized molecules. In numerous publications non-nucleophilic amide bases, like lithium diisopropyl amide (LDA, **4-21**), lithium bis(trimethylsilyl)amide (LiHMDS, **4-22**) or lithium tetramethylpiperidinide (LiTMP, **4-23**) have been used for this purpose. The thermodynamic driving force for this kind of reaction is a reflection of different pK_a values. Not included in this consideration are interactions of Lewis basic moieties which interact with Lewis acidic metal ions to form stable chelates (direct metalation group, DMG).

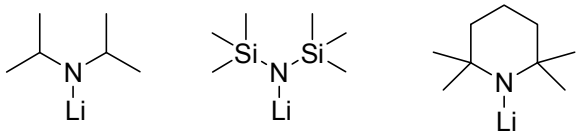

4-21 (+35.7) **4-22** (+25.8) **4-23** (+37.3)

Figure 4.10 Lewis structures of commonly used lithium amide bases (pK_a values in THF in parenthesis).[157]

Since the experimental determination of acidities or basicities of organic and inorganic compounds is rather challenging, a computational method that predicts protonation patterns in terms of pK_a values in a fast and reliable way would be of general use. The B3LYP/6-311++G(2df,2p) level of theory has been identified as a good compromise between accuracy and computational effort. Recently, *Guo* and coworkers used a similar approach to calculate pK_a values of related heteroaromatic compounds (B3LYP/6-311++G(2df,2p)//B3LYP/6-31G(d)).[158] Relative acidities in solution have been calculated using the thermochemical cycle of **Scheme 4.13** and compared with pK_a values of a test set of ten organic compounds.

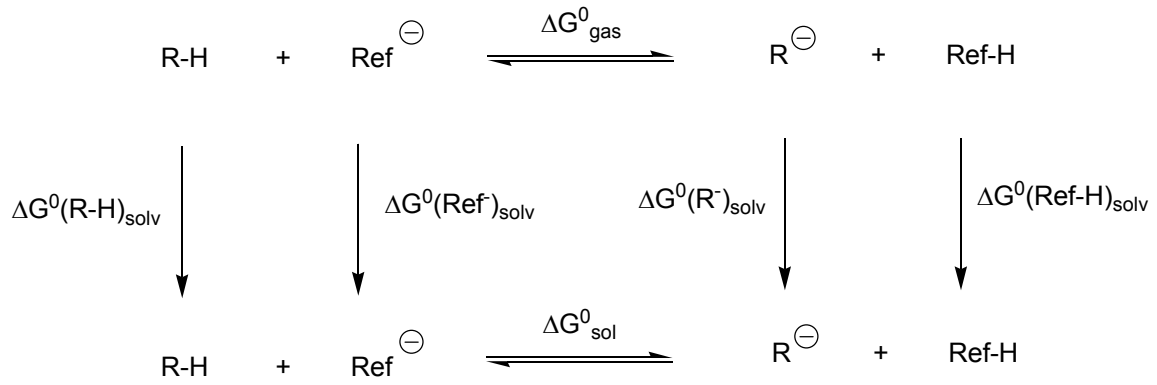

Scheme 4.13 Thermochemical cycle for the calculation of pK_a values in solution.

The definition of pK_a is

$$pK_a = -\log K_a \qquad \textbf{(eq. 4.1)}$$

and since free energies are connected to equilibrium constants K by the *Boltzmann* equation, the pK_a values can be calculated by

$$\Delta G^0 = -2.303\ R\ T \log K_a \qquad \textbf{(eq. 4.2)}$$

ΔG^0 under standard conditions (T = 298.15 K, p = 1 atm) can be calculated according to **Scheme 4.13** as

$$\Delta G^0_{sol} = \Delta G^0_{gas} - \Delta G^0(\text{R-H})_{solv} - \Delta G^0(\text{Ref}^-)_{solv} + \Delta G^0(\text{R}^-)_{solv} + \Delta G^0(\text{Ref-H})_{solv} \qquad \textbf{(eq. 4.3)}$$

Finally, relative acidities in condensed phase are obtained according to **eq. 4.4**:

$$pK_a\,(\text{R-H}) = pK_a\,(\text{Ref-H}) + \Delta G^0_{sol}/2.303\ RT \qquad \textbf{(eq. 4.4)}$$

The passage from gas phase to liquid phase has been accomplished by employing a polarizable continuum model (PCM) for DMSO (**4-24H**) as the respective solvent. The *solvent model density* by *Truhlar* and coworkers (SMD)[60] in combination with the B3LYP functional and the 6-31G(d) basis set has been identified to perform best in the calculation of pK_a values of aromatics and heteroaromatics. As expected, errors depend on the accuracy of the calculations of ΔG_{gas} and ΔG_{solv}. In these cycles ΔG_{gas} is usually calculated with high-level *ab initio* or density functional methods and ΔG_{solv} is a result of isotropic solute-solvent interactions on a molecular cavity of electrostatic origin. Thus, the major incorrect contribution can be considered in the solvent

calculation. As a starting point to find the best reference compound in the thermodynamic cycle of **Scheme 4.13** the free solvation energies of the deprotonation by different reference anions have been examined. The largest absolute value of the free reaction energies $|\Delta\Delta G_{solv}|$ has been found for DMSO (**4-24H**) and the smallest for thiophene (**4-27H**) as reference system (see **Figure 4.11**).

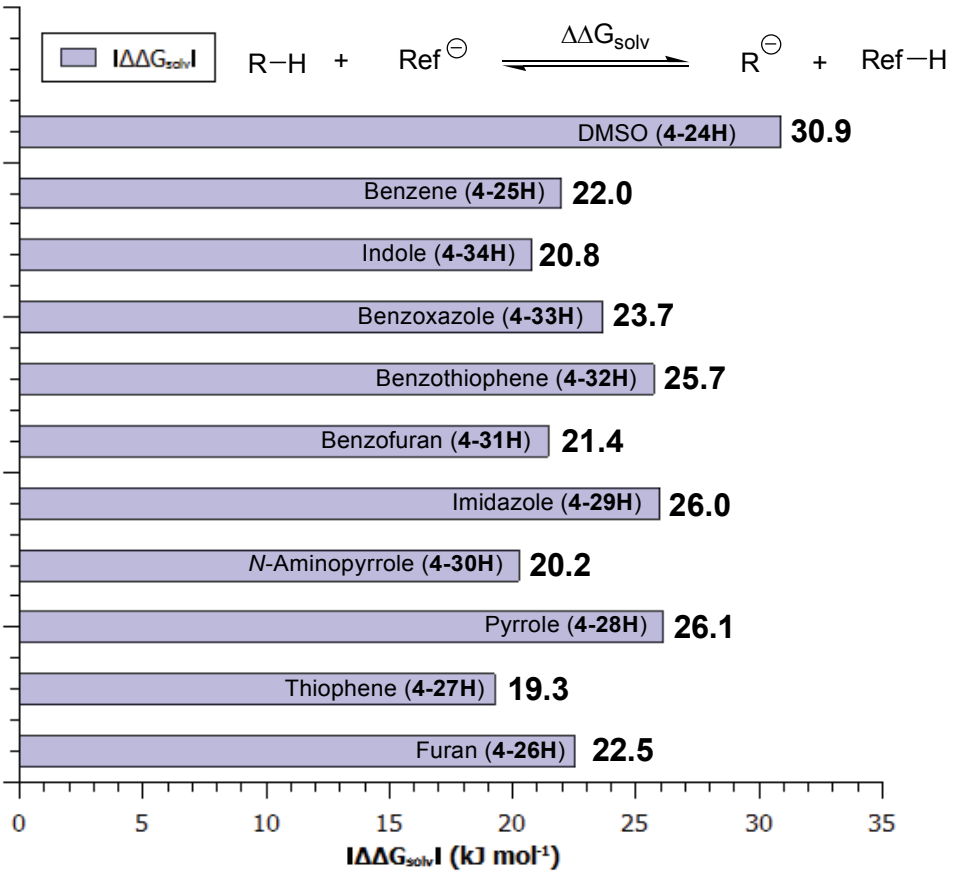

Figure 4.11 Reference-dependent differences in free solvation energies $|\Delta\Delta G_{solv}|$ in DMSO at SMD/B3LYP/ 6-31G(d)//B3LYP/6-311++G(2df,2p) level of theory.

Using **eq. 4.4** and DMSO (**4-24H**), and thiophene (**4-27H**) as the references the obtained pK_a values of the test set are summarized in **Table 4.8**.

Table 4.8 Comparison of literature values with theoretically calculated pK_a values in DMSO (SMD/B3LYP/6-31G(d)//B3LYP/6-311++G(2df,2p)).

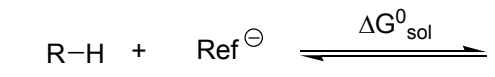

Ref-H	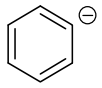 **4-25**	 **4-26**	 **4-27**	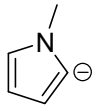 **4-28**	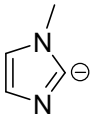 **4-29**
pK_a (exp.)	~ +43[159]	+35.0[160]	+32.5[160]	+38.7[160] (corr.)[b]	+33.1[160]
 **4-24H**[a]	+45.05	+37.40	+35.57	+39.98	+36.07
 **4-27H**	41.98	+34.34	n/a	+36.91	+33.01
Ref-H	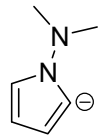 **4-30**	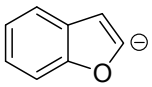 **4-31**	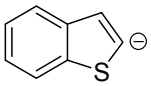 **4-32**	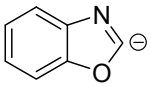 **4-33**	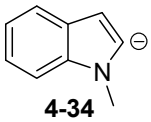 **4-34**
pK_a (exp.)	+36.4[160]	+32.7[161]	+32.9[160]	+24.4[161]	+37.3[160]
 **4-24H**[a]	+38.88	+36.12	+34.75	+29.09	+38.80
 **4-27H**	+35.82	+33.05	+31.68	+26.02	+35.73

[a] pK_a (DMSO) = -35.1[162]. [b] Using the pK_a value in THF and corrected it with *Streitwieser*'s correlation.

All considered compounds of **Table 4.8** are predicted to be less acidic if DMSO/dimsyl anion is used as the reference, indicated by larger pK_a values. As expected from the previous $\Delta\Delta G_{solv}$ survey (**Figure 4.11**), thiophene gives the overall best correlation of theory and experiment, which is shown in **Figure 4.12**. The arithmetic mean deviation of +1.47 pK_a units with respect to the reference thiophene (**4-27H**) reflects a good procedure to estimate C-H acidities in organic compounds.

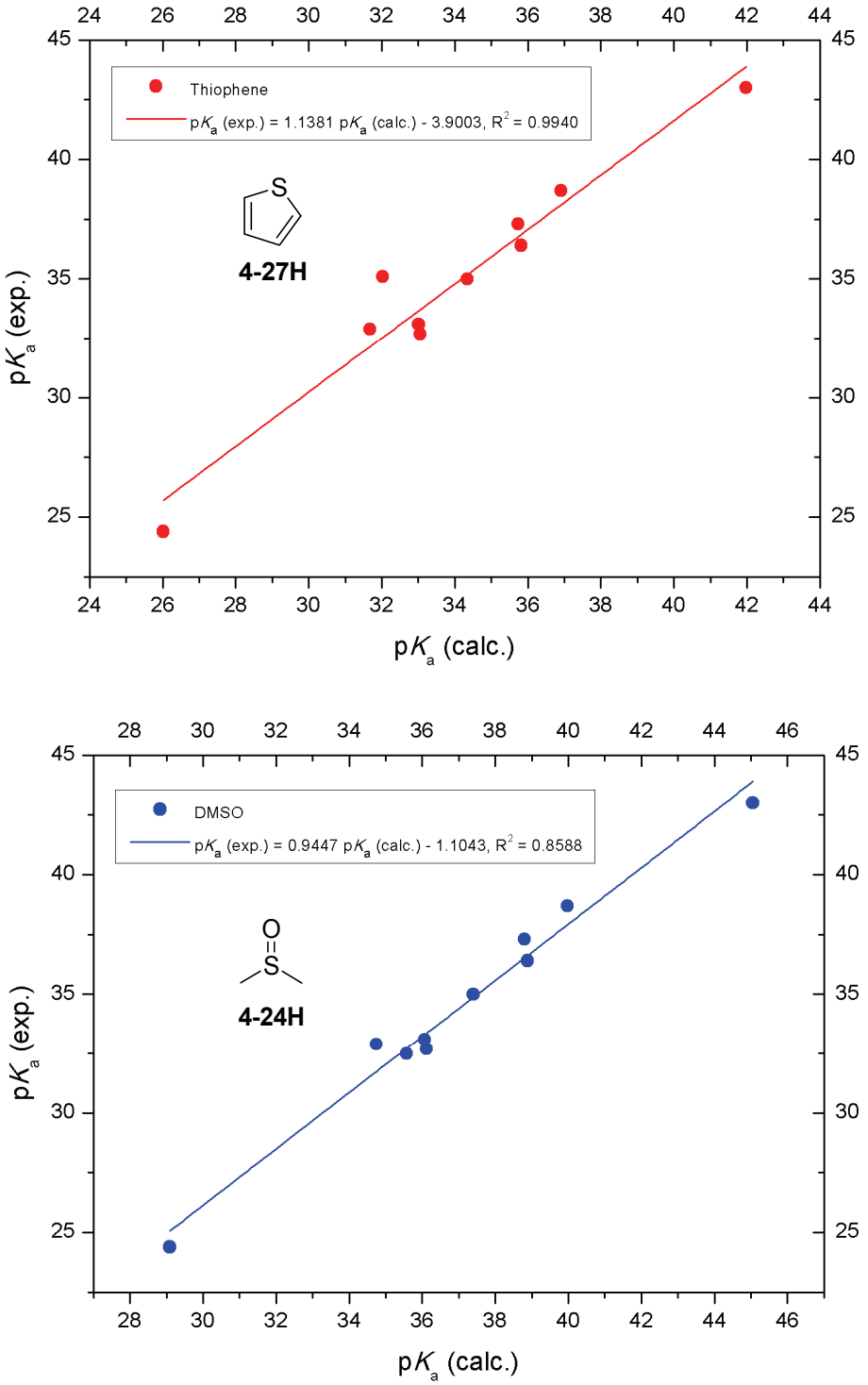

Figure 4.12 Test set correlation of calculated vs. experimental pK_a values in DMSO using either thiophene (**4-27H**, top) or DMSO (**4-24H**, bottom) as the reference.

Nevertheless, applying the $|\Delta\Delta G_{solv}|$ approach for experimentally relevant substrates like benzonitrile **4-35H** or thiophene ester **4-37H** yielded in the case of DMSO as reference the smallest differences in free solvation energies $|\Delta\Delta G_{solv}|$ (see

Theoretical Appendix Table 4.30). Related results for aqueous systems have already been described by *Liptak* and *Shields*[163] and in DMSO by *Liu* and *Guo*[164] for the absolute pK_a calculations of carboxylic acids, wherein the combination of solvent and reference system gave good results in agreement with experimental condensed phase acidities. This endorsed the use of DMSO and its dimsyl anion as reference system for the ongoing pK_a evaluation despite of the inferior correlation to thiophene (**4-27H**). Since almost all organometallic transformations are performed in THF solution, the obtained acidity values in DMSO have been corrected to "contact ion pair" values using *Streitwieser*'s linear correlation:[165]

$$\text{p}K_a\,(\text{THF}) = 1.046\ \text{p}K_a\,(\text{DMSO}) - 0.963 \qquad (\textbf{eq. 4.5})$$

This procedure has now been used to identify the most acidic positions in a variety of aromatic and heterocyclic compounds to predict the outcome of metalation reactions. The so obtained values, corrected as numbers for THF, are depicted in **Figure 4.13**.

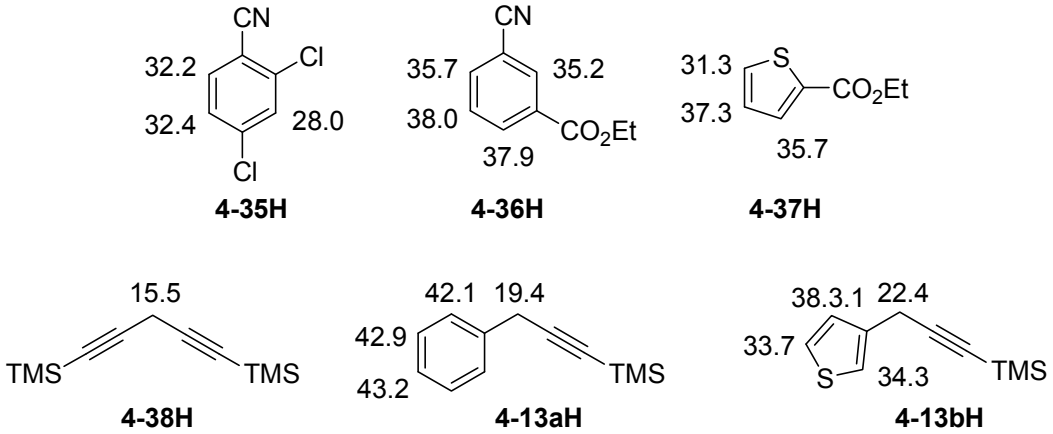

Figure 4.13 SMD/B3LYP/6-31G(d)//B3LYP/6-311++G(2df,2p) calculated pK_a values using DMSO and the dimsyl anion as reference (corrected to THF solution).

As expected, the most acidic centers are the propargylic CH positions with pK_a values of +19.4 for the phenyl (**4-13aH**) and +22.4 for the thienyl system (**4-13bH**), respectively. Interestingly, the introduction of a TMS acetylene group increases the aciditiy dramatically. For example, the pK_a value of the benzylic position in diphenylmethane is +32.3 in DMSO[166] (+32.8 corr. in THF) and is almost divided by half in the case of **4-38H**. Apparently, the π system of the alkyne is easily able to transfer electron density to the electropositive silicon center and therefore possesses

greater abilities to stabilize negative charge than a thienyl or phenyl substituent, indicated by an even lower pK_a value of +15.5 in **4-38H**. Implying the pK_a value of +37.3 of the TMP anion (**4-23**) in THF[157] the preferred metalation of the propargylic position is supported.

4.7 Conclusion

The zinc base TMPZnCl•LiCl (**4-14**) has been used to synthesize neutral allenic zinc intermediates from benzylic propynes, which can be quenched by the addition of various electrophiles. The analogous zincates have been prepared by transmetallation of the corresponding Li organyls with $ZnCl_2$ in THF. In order to support their presence in solution, the experimental NMR shifts have been matched with theoretical ^1H and ^{13}C shielding calculations.

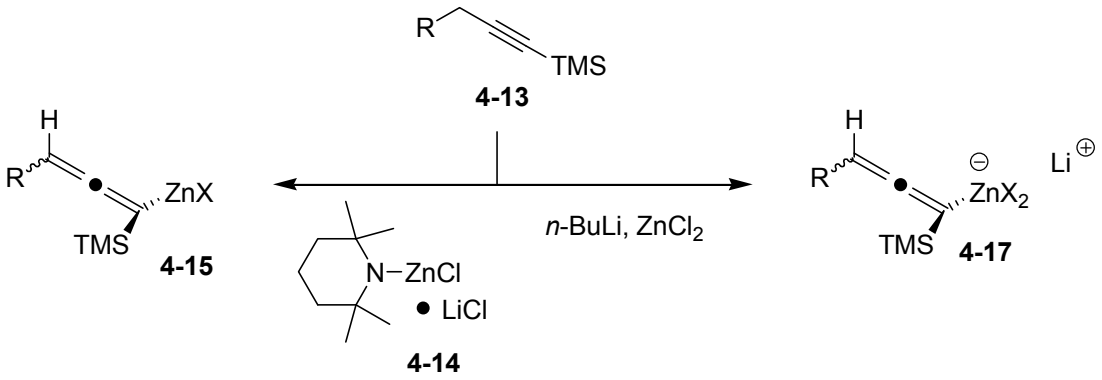

Scheme 4.14 Syntheses of allenic zinc compounds of type **4-15** and **4-17**.

Different basis sets, functionals and solvation states have been benchmarked with the well-known *Reformatsky* reagent **4-9**. B3LYP/631SVP geometries in combination with GIAO/mPW1K/IGLO-III calculations in the gas phase are sufficient enough to perform well in calculating NMR shifts of organozinc reagents in THF solution. The reaction outcome of neutral and anionic zinc allenes **4-15** and **4-17**, as well as for the corresponding organolithium isomers **4-16a** and **4-18a**, were successfully predicted by thermochemical analysis of the propargyl-allenyl isomerization.

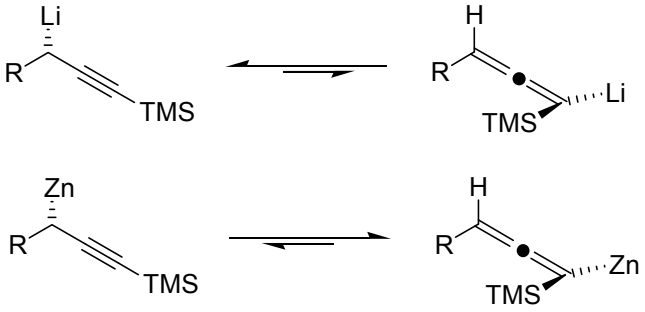

Scheme 4.15 Propargyl-allenyl isomerization of organometallics.

4.8 Experimental

All reactions were carried out under magnetic stirring in flame-dried glass flasks using standard *Schlenk* techniques and P_4O_{10}-predried N_2 as inert gas. Syringes were used to transfer reagents and solvents and were purged with N_2 prior to use. Nuclear magnetic resonance spectra were recorded on a *Varian Mercury 600* spectrometer. The chemical shifts δ were specified in ppm relative to the partially deuterated solvent THF-d_8 (^{1}H: 1.72 and 3.58, ^{13}C: 67.2 and 25.3).[167]

4.8.1 EtO_2CCH_2ZnBr•2 THF (4-9)

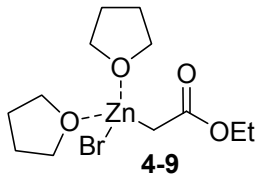

4-9

A 10 mL round bottom flask equipped with stirring bar and gas inlet was charged under nitrogen atmosphere with zinc dust (0.52 g, 7.95 mmol) and THF (2 mL) followed by TMSCl (0.05 mL, 0.043 g, 0.40 mmol). The suspension was stirred for 40 min at room temperature before a solution of bromoethyl acetate (0.44 mL, 0.66 g, 3.95 mmol) in 5 mL THF was slowly added dropwise over 10 min resulting in an exothermic reaction. After heating the suspension for one hour to 45 °C, followed by cooling to room temperature the suspension was allowed to settle. 2 ML of the supernatant yellowish solution was cannulated to a *Schlenk* flask and concentrated under reduced pressure. The resulting yellow solid was dried under high vacuum and redissolved in 1 mL THF-d_8. 0.6 ML of the deuterated THF solution were transferred to a dry nitrogen-flushed NMR tube and flame sealed.

^{1}H NMR (600 MHz, THF-d_8) δ 4.03 (q, OCH_2CH$_3$, ^3J 7.1 Hz), 3.58 – 3.54 (m, CH_2O$_{THF}$), 1.84 (s, CH_2Zn), 1.73 – 1.71 (m, C$H_{2,THF}$), 1.16 (t, OCH$_2$CH_3, ^3J 7.1 Hz) ppm.
^{13}C NMR (100 MHz, THF-d_8) δ 186.78 (*C*O), 68.01 (*C*H$_2$O$_{THF}$), 61.48 (O*C*H$_2$CH$_3$), 26.08 (*C*H$_{2,THF}$), 21.67 (*C*H$_2$Zn), 14.51 (OCH$_2$*C*H$_3$) ppm.

4.9 Theoretical Appendix

Geometry optimizations have been performed at the B3LYP/631SVP level of theory. This involves the all-electron 6-31G(d,p) basis set for the elements H, C, Si, O, S, and Cl; the all-electron def2-SVP basis set by *Ahlrichs* and coworkers[168] for Zn. For organo lithium compounds the previously used 6-31+G(d) basis set has been used for optimization,[153-154] followed by single point calculations at MP2(FC)/6-31+G(d,p) level. Thermal corrections to enthalpies at 298.15 K have been calculated at the same level using the rigid rotor/harmonic oscillator model. Initial structures have been searched extensively with the MM3* force field[79] and the systematic search routine implemented in *MACROMODEL 9.7*[80] in order to identify all possible low energy conformations which were finally *Boltzmann*-averaged. These B3LYP/631SVP optimized minima have been directly used for the gas phase NMR shift calculations. NMR shielding tensors σ have then been calculated using DFT methods (B3LYP, mPW1K) and the Gauge-Invariant Atomic Orbital (GIAO)[147, 169] method including *Kutzelnigg's* IGLO-III basis set[144] for the elements H, C, Si, O, S, Cl and *Jensen's* pc-4 basis set for Zn[146] and Li.[170] Solvent effects have been included using an IEF-PCM model with either UAHF radii or *Truhlar's* SMD model[60] and THF as solvent, respectively. The shielding tensors have been averaged arithmetically and by using the *Boltzmann*-weighting factorsand energies obtained at B3LYP/631SVP level:[151]

$$w_i = \left. \exp\left(\frac{-\Delta E}{R\,T}\right) \middle/ \sum_{i=1}^{n} \frac{-\Delta E}{R\,T} \right.$$

$$<E> = \sum_{i=1}^{n} w_i E \qquad \textbf{(eq. 4.6)}$$

Relative ^{1}H, ^{13}C, and ^{29}Si chemical shifts δ between Zn compounds **X** and tetramethylsilane ($Si(CH_3)_4$, **TMS**, $\delta(^{1}H) = 0.0$, $\delta(^{13}C) = 0.0$, $\delta(^{29}Si) = 0.0$) can then be derived from differences in shielding values σ as expressed in **eq. 4.7**.

$$\delta(\mathbf{X}) = \sigma(\mathrm{TMS}) - \sigma(\mathbf{X}) + \delta(\mathrm{TMS}) \qquad \textbf{(eq. 4.7)}$$

Calculated shielding tensors have been averaged arithmetically for magnetically equivalent nuclei. The B3LYP/6-311++G(2df,2p) level of theory was recently used to calculate C-H pK_a values of heteroaromatic compounds in solution.[158, 171] The SMD model in combination with B3LYP/6-31G(d) was again used to describe the transition from gas to liquid phase. ΔG_{solv} was determined at 298.15 K with DMSO as the respective solvent and corresponding ΔG^0_{sol} values have been calculated using **Scheme 4.13** and **eq. 4.8**.

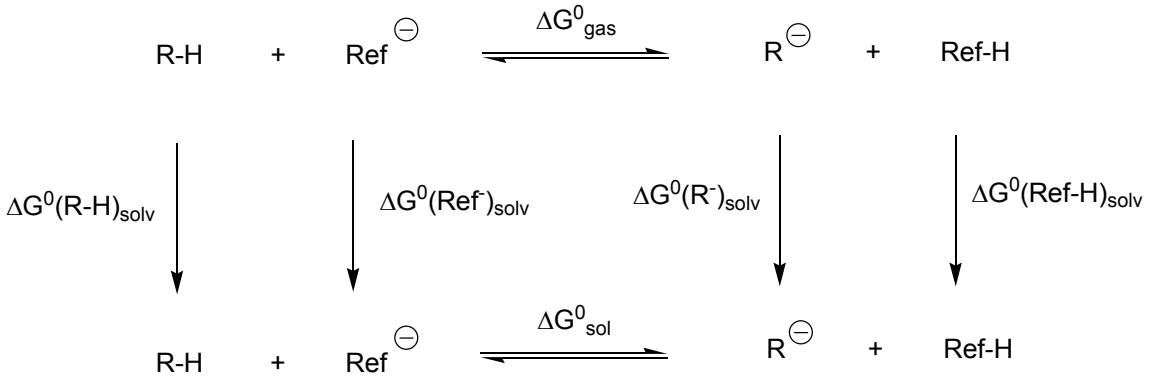

Scheme 4.16 Thermochemical cycle for the calculation of pK_a values in solution.

$$\Delta G^0_{sol} = \Delta G^0_{gas} - \Delta G^0(\text{R-H})_{solv} - \Delta G^0(\text{Ref}^-)_{solv} + \Delta G^0(\text{R}^-)_{solv} + \Delta G^0(\text{Ref-H})_{solv} \qquad \textbf{(eq. 4.8)}$$

Finally, the pK_a values have been calculated using DMSO (**4-24H**) and its dimsyl anion as reference (pK_a(DMSO) = +35.1)[162] according to **eq. 4.9**:

$$pK_a(\text{R-H}) = pK_a(\text{Ref-H}) + (\Delta G^0_{sol} / 2.303 \cdot R \cdot T) \qquad \textbf{(eq. 4.9)}$$

where R is the universal gas constant (8.3145 J K^{-1} mol^{-1}) and T the absolute temperature.

Streitwieser's linear correlation was used to transform the calculated pK_a values in DMSO to „ion pair" pK_a numbers in THF (**eq. 4.10**).[165]

$$pK_a(\text{THF}) = -0.963 + 1.046\ pK_a(\text{DMSO}) \qquad \textbf{(eq. 4.10)}$$

All calculations have been performed with *Gaussian 09* Rev. C.01.[86]

Table 4.9 Total energies, enthalpies and free solvation energies of different isomers of the *Reformatsky* reagent in Hartree (at 298.15 K and 1 atm).

	B3LYP/631SVP		SMD/B3LYP/6-31G(d) (THF)
	E_{tot}	$\mathbf{H_{298}}$	ΔG_{solv}
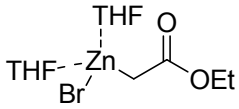 (**4-9**)	-5125.1946380	**-5124.823121**	-0.0213224
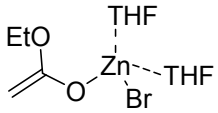 (**4-10**)	-5125.1741519	**-5124.803403**	-0.0224220
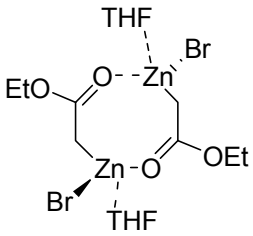 (**4-11**)	-9785.4749940	**-9784.980758**	-0.0224220

Table 4.10 Calculated shielding tensors σ in ppm.

	$Si(CH_3)_4$ (**TMS**)					
	B3LYP/IGLO-III//B3LYP/6-31G(d,p)			mPW1K/IGLO-III//B3LYP/6-31G(d,p)		
	$\sigma(^1H)$	$\sigma(^{13}C)$	$\sigma(^{29}Si)$	$\sigma(^1H)$	$\sigma(^{13}C)$	$\sigma(^{29}Si)$
Gas phase	31.72	180.08	330.11	31.63	187.33	356.95
SMD	31.66	181.37	330.00	31.58	188.61	356.93
PCM/UAHF	31.68	181.08	329.92	31.60	188.31	356.83

Table 4.11 Calculated shielding tensors σ in ppm.

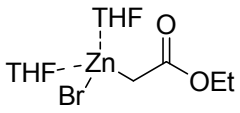

(**4-9**)

	σ	B3LYP Gas Phase	mPW1K Gas phase	B3LYP SMD (THF)	mPW1K SMD (THF)	B3LYP UAHF (THF)	mPW1K UAHF (THF)
^{1}H	C***H***$_2$Zn	29.87, 30.17	29.92, 30.20	29.87, 30.11	29.91, 30.13	29.69, 29.93	29.72, 29.94
	CH$_3$C***H***$_2$O	27.63, 27.79	27.64, 27.8	27.64, 27.71	27.65, 27.73	27.55, 27.63	27.56, 27.63
	C***H***$_3$CH$_2$O	30.39, 30.64, 3.57	30.33, 30.52, 30.61	30.42, 30.44, 30.49	30.35, 30.39, 30.45	30.40, 40.43, 30.48	30.34, 30.37, 30.44
^{13}C	***C***H$_2$Zn	160.67	169.99	161.09	170.33	161.22	170.24
	CO$_2$	-11.86	-5.74	-13.14	-7.01	-14.92	-8.82
	CH$_3$***C***H$_2$O	114.56	124.48	114.25	124.22	114.84	124.71
	CH$_3$CH$_2$O	163.71	171.50	164.68	172.53	165.08	172.86

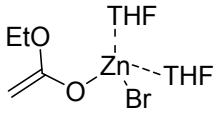

(**4-10**)

	σ	B3LYP Gas Phase	mPW1K Gas phase	B3LYP SMD	mPW1K SMD	B3LYP UAHF	mPW1K UAHF
^{1}H	C***H***$_2$CO$_2$Zn	28.73, 29.11	28.60, 29.04	28.85, 29.16	28.70, 29.08	28.86, 29.10	28.70, 29.00
	CH$_3$C***H***$_2$O	27.68, 27.88	27.76, 27.94	27.57, 27.74	27.63, 27.79	27.49, 27.66	27.54, 27.70
	C***H***$_3$CH$_2$O	30.43, 30.47, 30.79	30.37, 30.41, 30.77	30.47, 30.48, 30.56	30.40, 30.42, 30.53	30.46, 30.47, 30.55	30, 39, 30.40, 30.51
^{13}C	***C***H$_2$CO$_2$Zn	126.52	131.38	130.97	135.77	129.55	134.04
	CO$_2$	-1.77	6.56	-3.61	4.57	-2.85	5.52
	CH$_3$***C***H$_2$O	115.92	125.43	115.07	125.18	115.62	125.66
	CH$_3$CH$_2$O	162.59	170.48	163.37	171.31	163.72	171.59

Table 4.12 Calculated shielding tensors σ in ppm.

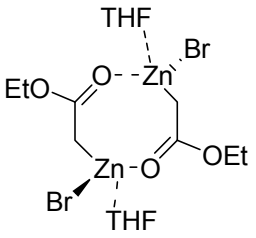

(**4-11**)

	σ	B3LYP Gas Phase	mPW1K Gas phase	B3LYP SMD	mPW1K SMD	B3LYP UAHF	mPW1K UAHF
^{1}H	C***H***$_2$Zn	29.57, 29.86	29.84, 29.58	29.51, 29.63	29.64, 29.47	29.42, 29.41	29.36, 29.40
	CH$_3$C***H***$_2$O	27.74, 26.91	27.74, 26.96	27.44, 27.00	27.43, 27.05	26.98, 27.35	27.32, 27.01
	C***H***$_3$CH$_2$O	30.14, 30.35, 30.66	30.07, 30.28, 30.62	30.24, 30.30, 30.46	30.16, 30.22, 30.40	30.22, 30.29, 30.46	30.14, 30.20, 30.40
^{13}C	***C***H$_2$Zn	155.93	164.32	155.55	164.01	155.65	163.99
	CO$_2$	-21.65	-16.42	-22.44	-17.15	-23.11	-17.80
	CH$_3$***C***H$_2$O	108.82	118.98	108.22	118.42	108.63	118.71
	CH$_3$CH$_2$O	163.42	171.14	163.97	171.78	164.30	172.05

Table 4.13 Total energies, enthalpies and free solvation energies of **4-15a** in Hartree (at 298.15 K and 1 atm).

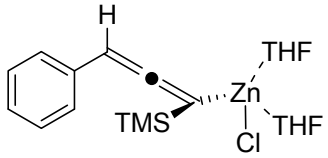

(**4-15a**)

		B3LYP/631SVP		SMD/B3LYP	MP2
	E_{tot}	**H_{298}**	G_{298}	ΔG_{solv}	E_{tot}
1	-2460.2235667	**-2459.721792**	-3459.826439	-0.0298482	-3544.9094366
5	-2460.2250223	**-2459.723067**	-3459.825295	-0.0283024	-3544.9119578
7	-2460.2217673	**-2459.719701**	-3459.820211	-0.0274259	-3544.9082162
8	-2460.2177352	**-2459.715763**	-3459.817379	-0.0326370	-3544.9028967
10	-2460.2250945	**-2459.723322**	-3459.827646	-0.0290832	-3544.9125564
11	-2460.2236684	**-2459.721644**	-3459.824388	-0.0278084	-3544.9085784
14	-2460.2217544	**-2459.719778**	-3459.822219	-0.0294020	-3544.9049148
15	-2460.2242080	**-2459.722411**	-3459.826278	-0.0293064	-3544.9100470
16	-2460.2216530	**-2459.719669**	-3459.820610	-0.0283980	-3544.9090319
17	-2460.2211686	**-2459.719098**	-3459.819452	-0.0291151	-3544.9082162
18	-2460.2251529	**-2459.723305**	-3459.826534	-0.0289876	-3544.9126771

Table 4.14 Total energies, enthalpies and free solvation energies in Hartree (at 298.15 K and 1 atm).

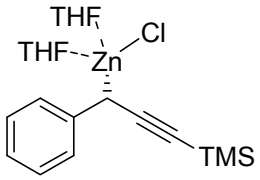

(**4-19a**)

		B3LYP/631SVP		SMD/B3LYP	MP2
	E_{tot}	**H_{298}**	G_{298}	ΔG_{solv}	E_{tot}
2	-2460.2138479	**-2459.7118720**	-3459.815277	-0.0290832	-3454.9075078
3	-2460.2117067	**-2459.7098590**	-3459.813324	-0.0318880	-3454.9010496
5	-2460.2156417	**-2459.7136830**	-3459.815631	-0.0293382	-3454.9097070
6	-2460.2138453	**-2459.7118180**	-3459.815112	-0.0294657	-3454.9078462
8	-2460.2123887	**-2459.7105170**	-3459.815268	-0.0304378	-3454.9049108
9	-2460.2138616	**-2459.7119440**	-3459.814610	-0.0295932	-3454.9078222
12	-2460.2151100	**-2459.7131030**	-3459.815577	-0.0292904	-3454.9094722

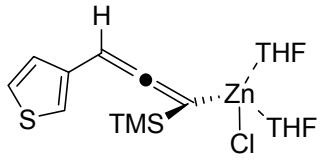

(**4-15b**)

		B3LYP/631SVP		SMD/B3LYP	MP2
	E_{tot}	**H_{298}**	G_{298}	ΔG_{solv}	E_{tot}
1	-3780.9732450	**-3780.505355**	-3780.608750	-0.0284299	-3775.3569190
2	-3780.9746331	**-3780.506602**	-3780.608455	-0.0270116	-3775.3591841
3	-3780.9713809	**-3780.503567**	-3780.606594	-0.0287167	-3775.3553078
4	-3780.9721540	**-3780.504374**	-3780.610830	-0.0278721	-3775.3555891
5	-3780.9725124	**-3780.504382**	-3780.607480	-0.0261670	-3775.3556898
6	-3780.9672297	**-3780.499160**	-3780.601472	-0.0311549	-3775.3504956
8	-3780.9708862	**-3780.502745**	-3780.602890	-0.0280315	-3775.3539561
10	-3780.9716599	**-3780.503839**	-3780.607685	-0.0280793	-3775.3568773
11	-3780.9699013	**-3780.502067**	-3780.603768	-0.0279359	-3775.3566107
15	-3780.9706366	**-3780.502795**	-3780.604568	-0.0276649	-3775.3570922
16	-3780.9734251	**-3780.505482**	-3780.608617	-0.0271709	-3775.3584101
17	-3780.9705937	**-3780.502414**	-3780.602394	-0.0259120	-3775.3563550
18	-3780.9695579	**-3780.501451**	-3780.602659	-0.0270116	-3775.3535887

Table 4.15 Total energies, enthalpies and free solvation energies in Hartree (at 298.15 K and 1 atm).

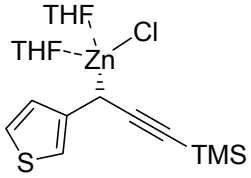

(**4-19b**)

		B3LYP/631SVP		SMD/B3LYP	MP2
	E_{tot}	**H_{298}**	G_{298}	ΔG_{solv}	E_{tot}
1	-3780.9665092	**-3780.498456**	-3780.600321	-0.0279359	-3775.3582295
2	-3780.9608671	**-3780.492884**	-3780.596218	-0.0301350	-3775.3534099
3	-3780.9620110	**-3780.493939**	-3780.597975	-0.0301988	-3775.3526579
5	-3780.9628285	**-3780.494770**	-3780.597945	-0.0286052	-3775.3542749
6	-3780.9613990	**-3780.493518**	-3780.597627	-0.0313621	-3775.3475100

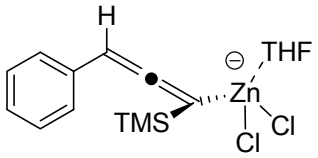

(**4-17a**)

		B3LYP/631SVP		SMD/B3LYP	MP2
	E_{tot}	**H_{298}**	G_{298}	ΔG_{solv}	E_{tot}
1	-3688.0719896	**-3687.693414**	-3687.786168	-0.0762858	-3682.8824531
2	-3688.0722292	**-3687.693606**	-3687.785142	-0.0757121	-3682.8820555
7	-3688.0735875	**-3687.694931**	-3687.785920	-0.0749949	-3682.8833878
8	-3688.0723486	**-3687.693692**	-3687.785373	-0.0760148	-3682.8813569
9	-3688.0721910	**-3687.693476**	-3687.785602	-0.0760627	-3682.8804562
14[a]	-3688.0713331	**-3687.692687**	-3687.784824	-0.0765089	-3682.8786147
15	-3688.0725306	**-3687.693788**	-3687.787050	-0.0744531	-3682.8797354
16	-3688.0726681	**-3687.694022**	-3687.785553	-0.0755049	-3682.8809793
17	-3688.0741545	**-3687.695395**	-3687.786495	-0.0730507	-3682.8834618
18	-3688.0717977	**-3687.693246**	-3687.785854	-0.0751543	-3682.8804076

[a] Using restrained coordinates to force optimization.

Table 4.16 Total energies, enthalpies and free solvation energies in Hartree (at 298.15 K and 1 atm).

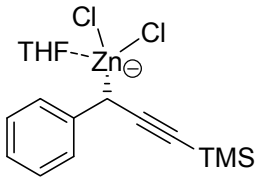

(**4-20a**)

		B3LYP/631SVP		SMD/B3LYP	MP2
	E_{tot}	**H_{298}**	G_{298}	ΔG_{solv}	E_{tot}
1	-3688.0605715	**-3687.681771**	-3687.775234	-0.0788674	-3682.8741867
2	-3688.0614695	**-3687.682867**	-3687.775953	-0.0782937	-3682.8785420
3	-3688.0607572	**-3687.681957**	-3687.775688	-0.0776722	-3682.8735734
4	-3688.0592234	**-3687.680587**	-3687.773992	-0.0795208	-3682.8742431
5	-3688.0625832	**-3687.683682**	-3687.774626	-0.0755368	-3682.8786483
6	-3688.0610365	**-3687.682392**	-3687.775398	-0.0779750	-3682.8767889
7	-3688.0623077	**-3687.683550**	-3687.776206	-0.0762061	-3682.8757391
8	-3688.0619711	**-3687.683165**	-3687.775091	-0.0765726	-3682.8775199
12	-3688.0621295	**-3687.683318**	-3687.774773	-0.0762220	-3682.8776639

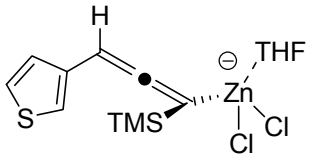

(**4-17b**)

		B3LYP/631SVP		SMD/B3LYP	MP2
	E_{tot}	**H_{298}**	G_{298}	ΔG_{solv}	E_{tot}
1	-4008.8210986	**-4008.476162**	-4008.570217	-0.0739432	-4003.3266690
2	-4008.8238141	**-4008.478849**	-4008.569453	-0.0714731	-4003.3312010
4	-4008.8198341	**-4008.475003**	-4008.568221	-0.0747559	-4003.3268852
5	-4008.8226499	**-4008.477819**	-4008.568931	-0.0736244	-4003.3290626
6	-4008.8231466	**-4008.478293**	-4008.568886	-0.0735129	-4003.3309767
8	-4008.8231735	**-4008.478356**	-4008.569517	-0.0734173	-4003.3310242
10	-4008.8216037	**-4008.476852**	-4008.567891	-0.0742141	-4003.3294869
11	-4008.8184093	**-4008.473645**	-4008.566962	-0.0762220	-4003.3242123
16	-4008.8208156	**-4008.476123**	-4008.568404	-0.0741503	-4003.3286354
17	-4008.8212911	**-4008.476358**	-4008.567482	-0.0740069	-4003.3280411

Table 4.17 Total energies, enthalpies and free solvation energies of **4-20b** in Hartree (at 298.15 K and 1 atm).

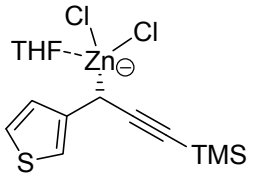

(**4-20b**)

	B3LYP/631SVP			SMD/B3LYP	MP2
	E_{tot}	**H_{298}**	G_{298}	ΔG_{solv}	E_{tot}
1	-4008.8130686	**-4008.468214**	-4008.559655	-0.0752977	-4003.3274624
2	-4008.8119697	**-4008.466978**	-4008.559097	-0.0738954	-4003.3249972
3	-4008.8099782	**-4008.465250**	-4008.560166	-0.0775447	-4003.3226299
4	-4008.8112271	**-4008.466397**	-4008.560000	-0.0770029	-4003.3219456
5	-4008.8118210	**-4008.466881**	-4008.559429	-0.0746125	-4003.3248949
6	-4008.8118150	**-4008.466847**	-4008.558957	-0.0747400	-4003.3241502

Table 4.18 Total energies, enthalpies and free solvation energies in Hartree (at 298.15 K and 1 atm).

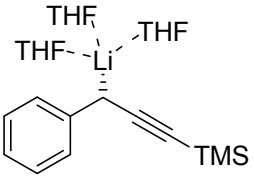

(**4-16a**)

	B3LYP/6-31+G(d)		SMD/B3LYP	MP2
	E_{tot}	**H_{298}**	ΔG_{solv}	E_{tot}
3	-1460.7994348	**-1460.176430**	-0.0284617	-1456.6433032
4	-1460.7995235	**-1460.176295**	-0.0279518	-1456.6434036
5	-1460.7992019	**-1460.176071**	-0.0277446	-1456.6416497

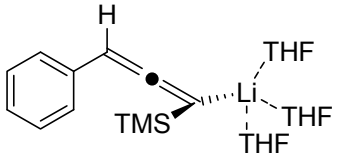

(**4-18a**)

	B3LYP/6-31+G(d)		SMD/B3LYP	MP2
	E_{tot}	**H_{298}**	ΔG_{solv}	E_{tot}
1	-1460.8026118	**-1460.179279**	-0.0281908	-1456.6434157
2	-1460.8019447	**-1460.178848**	-0.0287167	-1456.6418434
4	-1460.8013881	**-1460.178152**	-0.0296729	-1456.6396068

Table 4.19 Calculated shielding tensors σ in ppm.

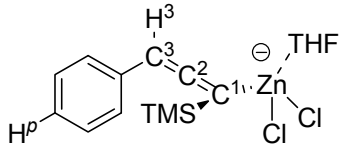

(**4-17a**)

	GIAO/B3LYP/IGLO-III//B3LYP/631SVP					
	σ(^{1}H): H^3	σ(^{1}H): H^p	σ(^{13}C): C^1	σ(^{13}C): C^2	σ(^{13}C): C^3	σ(^{29}Si)
1	27.0419	25.1793	74.7547	-19.1184	105.8530	340.6620
2	26.9711	25.1629	74.7995	-20.7684	105.6005	339.4856
7	26.8616	25.1128	75.7013	-25.0502	104.6823	339.8060
8	26.8687	25.1494	75.9990	-24.635	104.5175	340.0766
9	26.8886	25.1608	75.7486	-23.9344	104.8137	340.2231
15	26.9306	25.1203	75.6984	-23.6962	104.4586	340.8834
16	26.9143	25.1018	76.1071	-25.0986	104.5973	338.9028
17	26.8549	25.0956	75.9525	-26.1560	104.6718	339.9045
18	26.9433	25.1152	75.8582	-23.9450	104.6640	339.4440
	GIAO/mPW1K/IGLO-III//B3LYP/631SVP					
	σ(^{1}H): H^3	σ(^{1}H): H^p	σ(^{13}C): C^1	σ(^{13}C): C^2	σ(^{13}C): C^3	σ(^{29}Si)
1	26.9566	24.9308	83.0329	-13.5690	114.9418	366.3391
2	26.8862	24.9150	83.1302	-15.2213	114.6450	365.3920
7	26.7872	24.8798	84.2504	-19.1866	113.6198	365.5947
8	26.7942	24.9121	84.5450	-18.9294	113.4017	365.8010
9	26.8131	24.9168	84.2626	-18.2341	113.6943	365.9216
15	26.8616	24.8805	84.1882	-18.1010	113.3394	366.3607
16	26.8514	24.8644	84.6237	-19.2478	113.5188	364.7725
17	26.7797	24.8668	84.5278	-20.1369	113.5757	365.7010
18	26.8763	24.8746	84.3829	-18.3639	113.4851	365.1852

Table 4.20 Calculated shielding tensors σ in ppm.

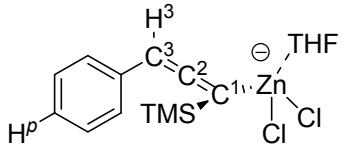

(**4-17a**)

	GIAO/SMD/mPW1K/IGLO-III//B3LYP/631SVP (THF)					
	σ(^{1}H): H^3	σ(^{1}H): H^p	σ(^{13}C): C^1	σ(^{13}C): C^2	σ(^{13}C): C^3	σ(^{29}Si)
1	26.4370	24.3157	85.0200	-19.1359	115.5896	365.4336
2	26.5069	24.3241	84.2214	-17.0715	115.7315	365.0973
7	26.4146	24.2926	84.8590	-20.0663	115.1888	365.1791
8	26.4245	24.3108	85.1433	-19.6006	115.4009	365.2749
9	26.4370	24.3157	85.0200	-19.1359	115.5896	365.4336
15	26.4404	24.3027	85.0255	-18.9153	114.8359	365.7981
16	26.4304	24.2980	85.3173	-19.9873	114.7491	364.3494
17	26.4191	24.2823	84.7598	-20.5278	115.3682	365.2488
18	26.4533	24.3021	84.9653	-18.8310	115.0803	364.6411

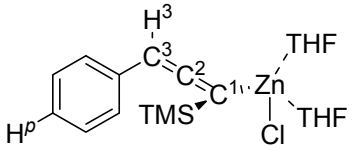

(**4-15a**)

	GIAO/B3LYP/IGLO-III//B3LYP/631SVP					
	σ(^{1}H): H^3	σ(^{1}H): H^p	σ(^{13}C): C^1	σ(^{13}C): C^2	σ(^{13}C): C^3	σ(^{29}Si)
1	26.6051	24.6617	78.8024	-34.3752	101.0584	337.1566
5	26.5353	24.6541	78.4265	-33.2387	102.1859	337.4016
7	26.4695	24.6269	80.1499	-35.5752	100.4296	337.9006
8	26.482	24.6261	81.5347	-40.8681	99.6810	339.0575
10	26.5682	24.6550	78.2969	-32.3068	102.2055	337.1369
11	26.5427	24.6473	79.7069	-34.8300	101.0329	336.6207
14	26.5988	24.6433	79.3078	-35.3809	99.9032	337.4662
15	26.5834	24.6550	78.7602	-34.0915	101.2989	337.0951
16	26.4365	24.6311	80.4088	-36.0630	100.4525	337.6731
17	26.4368	24.6549	80.0196	-35.2743	100.6147	338.0755
18	26.5550	24.6515	78.1437	-32.5336	102.2296	337.1765

Table 4.21 Calculated shielding tensors σ in ppm.

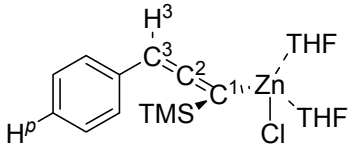

(**4-15a**)

	GIAO/mPW1k/IGLO-III//B3LYP/631SVP					
	σ(^{1}H): H^3	σ(^{1}H): H^p	σ(^{13}C): C^1	σ(^{13}C): C^2	σ(^{13}C): C^3	σ(^{29}Si)
1	26.5074	24.4255	87.8244	-27.9567	109.9269	362.9305
5	26.4450	24.4101	87.2718	-26.8995	110.8801	363.1391
7	26.3621	24.3910	89.1785	-29.3781	109.2944	363.6957
8	26.3686	24.3989	91.0664	-34.5480	108.3170	364.7236
10	26.4836	24.4165	87.1390	-25.9555	110.9815	362.9738
11	26.4419	24.4131	88.5876	-28.4687	109.8706	362.4954
14	26.4981	24.4044	88.5555	-29.0783	108.7832	363.1642
15	26.4922	24.4176	87.7072	-27.6296	110.1868	362.8467
16	26.3320	24.3946	89.4645	-29.8458	109.2608	363.5168
17	26.3377	24.4136	89.1642	-29.0169	109.4297	363.8779
18	26.4728	24.4105	87.0253	-26.1986	110.9886	362.9796
	GIAO/SMD/mPW1K/IGLO-III//B3LYP/631SVP (THF)					
	σ(^{1}H): H^3	σ(^{1}H): H^p	σ(^{13}C): C^1	σ(^{13}C): C^2	σ(^{13}C): C^3	σ(^{29}Si)
1	26.2499	24.1641	86.9022	-25.7456	111.8495	363.1832
5	26.2053	24.1524	86.4940	-24.7708	112.9123	363.4125
7	26.2131	24.1271	88.0969	-27.1584	112.0795	363.5087
8	26.2238	24.1391	87.9221	-29.0669	112.5638	364.2381
10	26.2038	24.1579	86.8260	-24.3428	112.7042	363.3046
11	26.2057	24.1495	87.6950	-26.3705	111.8810	362.6835
14	26.2573	24.1591	87.1226	-26.5071	111.1853	363.0666
15	26.2256	24.1545	87.1764	-25.8432	111.9808	363.1213
16	26.2069	24.1338	87.9999	-27.1487	112.4159	363.3187
17	26.2123	24.1479	87.6315	-26.3140	112.6266	363.6543
18	26.2003	24.1528	86.5519	-24.4931	112.7545	363.2828

Table 4.22 Calculated shielding tensors σ in ppm.

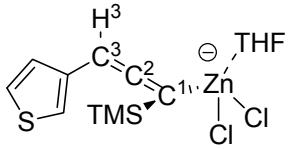

(**4-17b**)

	GIAO/B3LYP/IGLO-III//B3LYP/6-31SVP				
	σ(^{1}H): H^{3}	σ(^{13}C): C^{1}	σ(^{13}C): C^{2}	σ(^{13}C): C^{3}	σ(^{29}Si)
1	26.9272	74.1563	-23.7436	110.2325	342.8789
2	26.7073	75.8214	-29.5419	109.4911	340.3628
4	26.9654	74.7536	-22.5989	111.9348	340.9445
5	26.7741	76.1486	-28.3332	109.6256	339.8813
6	26.6905	75.5766	-29.3084	109.4231	339.8064
8	26.7146	75.5958	-28.4320	109.5018	340.3072
10	26.8273	75.8292	-27.3896	111.0311	340.2457
11	26.8578	77.2211	-31.6816	110.2289	340.7022
16	26.9196	76.9756	-27.3800	111.5279	340.7720
17	26.8453	75.9696	-27.1628	111.1166	340.1540
	GIAO/mPW1K/IGLO-III//B3LYP/631SVP				
	σ(^{1}H): H^{3}	σ(^{13}C): C^{1}	σ(^{13}C): C^{2}	σ(^{13}C): C^{3}	σ(^{29}Si)
1	26.8751	82.5198	-17.4951	118.8347	367.9506
2	26.6592	84.4790	-22.9563	117.8597	366.0002
4	26.9415	83.1604	-16.5972	120.5637	366.4606
5	26.7367	84.7275	-21.8900	118.0205	365.4962
6	26.6373	84.1876	-22.7903	117.8221	365.5078
8	26.6660	84.2119	-21.9849	117.9008	365.9243
10	26.8096	84.4472	-21.1387	119.5133	365.9045
11	26.8337	85.9408	-25.4151	118.5472	366.2148
16	26.9155	85.5272	-21.1174	119.9434	366.2903
17	26.8227	84.5030	-20.9488	119.6227	365.8415

Table 4.23 Calculated shielding tensors σ in ppm j.

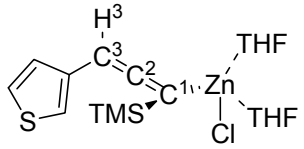

(**4-15b**)

	GIAO/B3LYP/IGLO-III//B3LYP/631SVP				
	σ(^{1}H): H^{3}	σ(^{13}C): C^{1}	σ(^{13}C): C^{2}	σ(^{13}C): C^{3}	σ(^{29}Si)
1	26.4686	78.9243	-36.6134	105.8408	337.7144
2	26.3852	78.6151	-36.2092	106.7342	337.8413
3	26.5115	79.9489	-36.1014	106.3188	338.0071
4	26.5310	79.1958	-36.4010	107.2456	337.1532
5	26.3754	78.9628	-35.9189	105.7133	337.2498
6	26.3046	81.9903	-43.4055	104.4132	338.8146
8	26.5792	79.8350	-38.3813	104.3257	339.0615
10	26.5576	79.8267	-34.3732	107.8626	337.1358
11	26.4272	80.4914	-36.2075	106.9437	338.4037
15	26.3445	80.2023	-36.5935	105.6971	338.7701
16	26.4769	78.8225	-35.1925	108.2039	337.8392
17	26.4719	80.5538	-36.5195	106.6178	337.9188
18	26.6759	79.8832	-36.5573	105.7533	338.2955
	GIAO/mPW1K/IGLO-III//B3LYP/631SVP				
	σ(^{1}H): H^{3}	σ(^{13}C): C^{1}	σ(^{13}C): C^{2}	σ(^{13}C): C^{3}	σ(^{29}Si)
1	26.3947	87.9712	-29.6598	114.3578	363.3270
2	26.3221	87.5672	-29.3111	115.0492	363.4326
3	26.4654	89.0618	-29.5071	114.9262	363.6901
4	26.4932	88.2232	-29.6423	115.7504	362.9070
5	26.3165	87.9701	-29.0488	114.1479	362.8977
6	26.2116	91.6279	-36.6278	112.7093	364.5438
8	26.4721	88.9546	-31.5219	112.9134	364.5591
10	26.5105	88.7003	-27.7834	116.3827	362.9476
11	26.3846	89.5100	-29.6792	115.4397	364.0040
15	26.2677	89.2529	-29.8928	114.1759	364.3182
16	26.4471	87.7133	-28.4586	116.5490	363.4686
17	26.4208	89.4726	-30.0156	115.1695	363.6263
18	26.6078	88.9339	-29.8801	114.4911	363.9341

Table 4.24 Calculated shielding tensors σ in ppm.

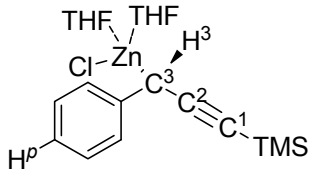

(**4-19a**)

	GIAO/B3LYP/IGLO-III//B3LYP/631SVP					
	σ(^{1}H): H^3	σ(^{1}H): H^p	σ(^{13}C): C^1	σ(^{13}C): C^2	σ(^{13}C): C^3	σ(^{29}Si)
8	28.0951	24.5848	89.5381	53.8391	151.9756	358.0297
	GIAO/mPW1K/IGLO-III//B3LYP/631SVP					
	σ(^{1}H): H^3	σ(^{1}H): H^p	σ(^{13}C): C^1	σ(^{13}C): C^2	σ(^{13}C): C^3	σ(^{29}Si)
8	28.1932	24.3778	96.0178	59.5771	163.5208	381.8059

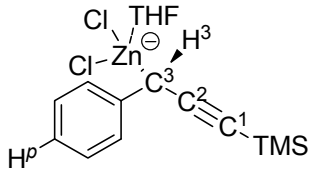

(**4-20a**)

	GIAO/B3LYP/IGLO-III//B3LYP/631SVP					
	σ(^{1}H): H^3	σ(^{1}H): H^p	σ(^{13}C): C^1	σ(^{13}C): C^2	σ(^{13}C): C^3	σ(^{29}Si)
2	28.1671	25.0274	93.5889	48.4984	146.0357	361.3098
	GIAO/mPW1K/IGLO-III//B3LYP/631SVP					
	σ(^{1}H): H^3	σ(^{1}H): H^p	σ(^{13}C): C^1	σ(^{13}C): C^2	σ(^{13}C): C^3	σ(^{29}Si)
2	28.2372	24.8228	100.0251	54.7082	157.6873	384.7873

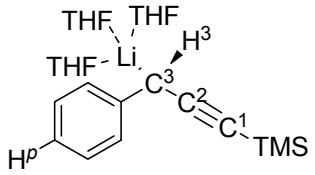

(**4-16a**)

	GIAO/B3LYP/IGLO-III//B3LYP/6-31+G(d)					
	σ(^{1}H): H^3	σ(^{1}H): H^p	σ(^{13}C): C^1	σ(^{13}C): C^2	σ(^{13}C): C^3	σ(^{29}Si)
3	28.5360	25.3371	82.7383	39.9845	134.3370	359.6495
	GIAO/mPW1K/IGLO-III//B3LYP/6-31+G(d)					
	σ(^{1}H): H^3	σ(^{1}H): H^p	σ(^{13}C): C^1	σ(^{13}C): C^2	σ(^{13}C): C^3	σ(^{29}Si)
3	28.5347	25.1027	89.6174	47.0322	144.4308	383.6148

Table 4.25 Calculated shielding tensors σ in ppm.

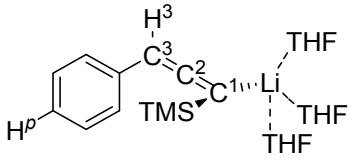

(**4-18a**)

	GIAO/B3LYP/IGLO-III//B3LYP/6-31+G(d)					
	σ(^{1}H): H^3	σ(^{1}H): H^p	σ(^{13}C): C^1	σ(^{13}C): C^2	σ(^{13}C): C^3	σ(^{29}Si)
1	27.5121	25.0578	71.0520	-3.8333	113.8368	347.1823
	GIAO/mPW1K/IGLO-III//B3LYP/6-31+G(d)					
	σ(^{1}H): H^3	σ(^{1}H): H^p	σ(^{13}C): C^1	σ(^{13}C): C^2	σ(^{13}C): C^3	σ(^{29}Si)
1	27.4701	24.8131	78.4381	2.4868	123.2315	372.4195

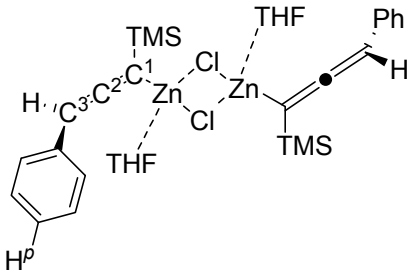

(**4-41**)

	GIAO/B3LYP/IGLO-III/B3LYP/631SVP					
	σ(^{1}H): H^3	σ(^{1}H): H^p	σ(^{13}C): C^1	σ(^{13}C): C^2	σ(^{13}C): C^3	σ(^{29}Si)
	26.5119	24.6165	78.9529	-33.0180	100.3440	338.2550
	26.5073	24.6082	79.3858	-33.8617	100.1750	337.7420
	GIAO/mPW1K/IGLO-III					
	σ(^{1}H): H^3	σ(^{1}H): H^p	σ(^{13}C): C^1	σ(^{13}C): C^2	σ(^{13}C): C^3	σ(^{29}Si)
	26.4038	24.3773	88.4831	-26.7817	109.0900	363.9970
	26.4033	24.3738	88.8302	-27.6173	109.3060	363.5270

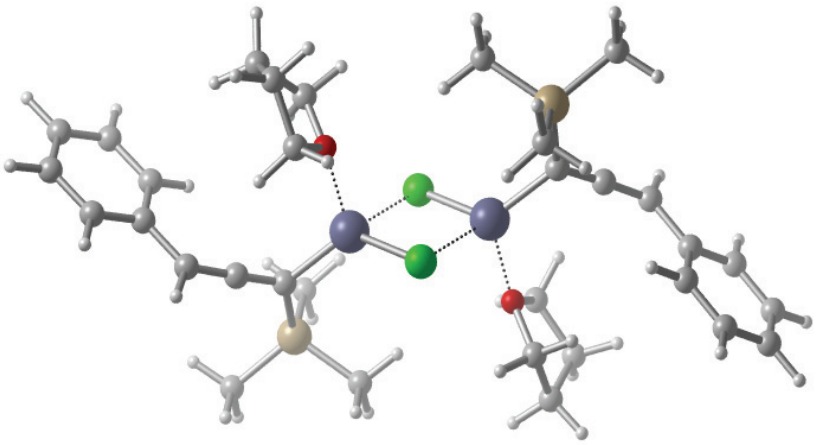

Figure 4.14 Graphical representation of the neutral zinc dimer **4-41** optimized at B3LYP/631SVP level of theory in the gas phase.

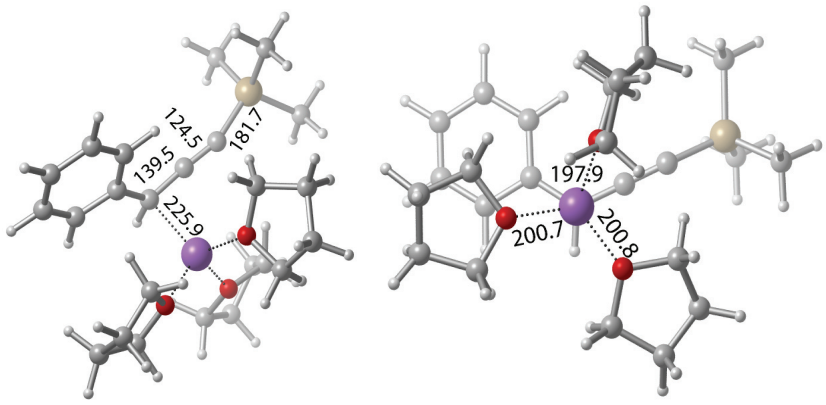

(**4-16a**)

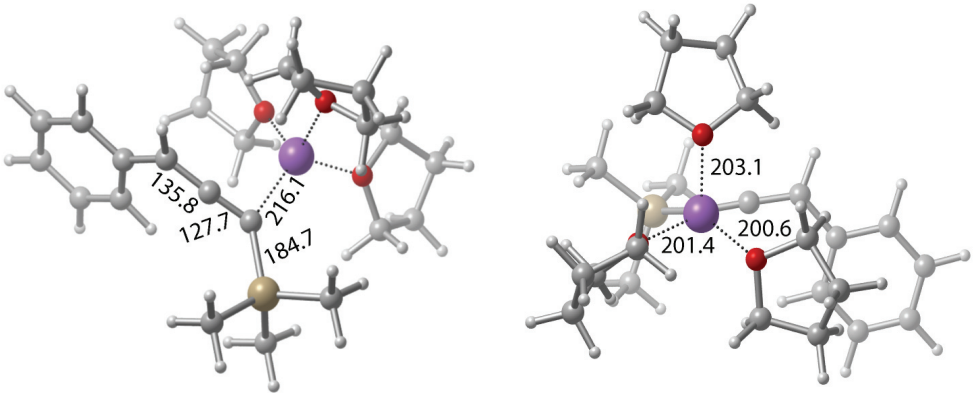

(**4-18a**)

Figure 4.15 Graphical representation of the energetically most stable Li species **4-16a** and **4-18a** optimized at B3LYP/6-31+G(d) level of theory in the gas phase.

Table 4.26 *Boltzmann*-averaged chemical shifts <δ>[a] at various levels of theory (in ppm).

	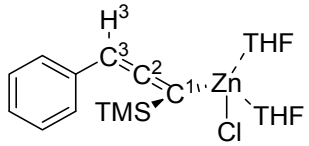 (**4-15a**)					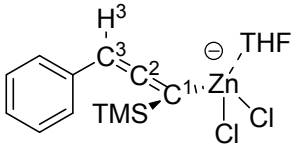 (**4-17a**)				
	H^3	C^3	C^2	C^1	Si	H^3	C^3	C^2	C^1	Si
δ(exp)[a]	4.99	70.18	202.83	93.97	-4.59	4.62	70.25	197.36	93.94	-6.16
Gas phase	<δ> (GIAO/B3LYP/IGLO-III//B3LYP/631SVP)									
H	5.16	78.13	213.15	101.62	-7.08	4.83	75.32	204.82	104.32	-9.77
H_{sol}[b]	5.15	78.22	213.22	101.62	-7.07	4.80	75.15	203.50	104.50	-9.80
G	5.15	78.17	213.02	101.65	-7.03	4.80	75.30	203.82	104.43	-10.09
G_{sol}[b]	5.14	78.32	212.26	101.59	-7.04	4.77	74.98	202.45	104.67	-10.09
Ø[c]	5.19	79.07	215.04	100.67	-7.41	4.80	75.21	203.68	104.46	-9.82
E[d]	**5.16**	**77.85**	**212.61**	**101.94**	**-7.07**	**4.87**	**75.41**	**206.24**	**104.13**	**-9.79**
Gas phase	<δ> (GIAO/mPW1K/IGLO-III//B3LYP/631SVP)									
H	5.16	76.60	214.04	99.98	-6.03	4.82	73.65	206.23	103.04	-8.70
H_{sol}[b]	5.15	76.68	214.10	99.70	-6.03	4.79	73.45	205.03	103.28	-8.72
G	5.15	76.62	213.90	100.01	-6.00	4.78	73.63	205.36	103.19	-8.93
G_{sol}[b]	5.14	76.76	214.13	99.93	-6.00	4.76	73.27	204.06	103.49	-8.95
Ø[c]	5.20	77.52	215.96	98.88	-6.35	4.78	73.53	205.22	103.23	-8.72
E[d]	**5.16**	**76.34**	**213.53**	**100.30**	**-6.03**	**4.85**	**73.75**	**207.47**	**102.80**	**-8.75**
THF	<δ> (GIAO/SMD/mPW1K/IGLO-III//B3LYP/631SVP)									
H	5.37	76.03	213.47	101.83	-6.34	5.15	73.34	208.43	103.74	-8.25
H_{sol}[b]	5.37	76.12	213.54	101.80	-6.31	5.14	73.28	207.94	103.66	-8.22
G	5.37	76.12	213.42	101.77	-6.31	5.14	73.43	207.97	103.66	-8.40
G_{sol}[b]	5.36	76.24	213.58	101.75	-6.31	5.14	73.25	207.77	103.62	-8.35
Ø[c]	5.36	76.34	214.77	101.30	-6.41	5.14	73.33	207.86	103.68	-8.23
E[d]	**5.38**	**75.86**	**213.10**	**102.06**	**-6.35**	**5.16**	**73.24**	**209.14**	**103.85**	**-8.32**

[a] Using tetramethylsilane $Si(CH_3)_4$ as standard for experimental and calculated values, respectively. [b] SMD/B3LYP/6-31G(d)//B3LYP/631SVP (THF). [c] Averaged arithmetically. [d] Only global minimum structure considered.

Table 4.27 B3LYP/6-311++G(2df,2p) optimized energies and solvation free energies ΔG_{solv} (DMSO, SMD/B3LYP/6-31G(d)) of some selected hydrocarbons and heterocycles in Hartree..

	 (**4-24H**)	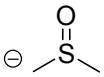 (**4-24**)	 (**4-25H**)	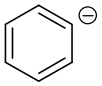 (**4-25**)	 (**4-26H**)	 (**4-26**)
E_{tot}	-553.3002559	-552.6882201	-232.3270529	-231.6744645	-230.1034710	-229.4676588
G_{298}	**-553.249510**	**-552.651429**	**-232.254150**	**-231.617052**	**-230.059831**	**-229.438939**
ΔG_{solv}	-0.0105178	-0.0918074	-0.0053226	-0.1039985	-0.0039681	-0.1030583
	 (**4-27H**)	 (**4-27**)	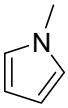 (**4-28H**)	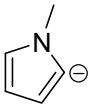 (**4-28**)	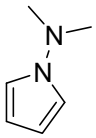 (**4-30H**)	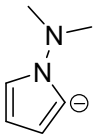 (**4-30**)
E_{tot}	-553.0919720	-552.4671930	-249.5657763	-248.9222598	-344.2213801	-343.5851177
G_{298}	**-553.052618**	**-552.441980**	**-249.484854**	**-248.856438**	**-344.099106**	**-343.477640**
ΔG_{solv}	-0.0044780	-0.0973054	-0.0083505	-0.1093689	-0.0083983	-0.1048431
	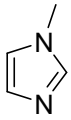 (**4-29H**)	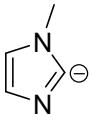 (**4-29**)	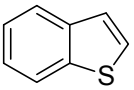 (**4-32H**)	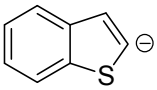 (**4-32**)	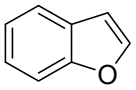 (**4-31H**)	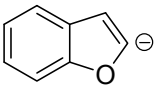 (**4-31**)
E_{tot}	-265.6193273	-264.9847240	-706.7864623	-706.1726751	-383.8002709	-383.1799253
G_{298}	**-265.549409**	**-264.929543**	**-706.703490**	**-706.104012**	**-383.713229**	**-383.107924**
ΔG_{solv}	-0.0150595	-0.1160143	-0.0076971	-0.0911541	-0.0072350	-0.0935285
	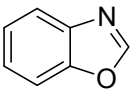 (**4-33H**)	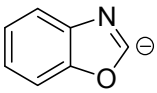 (**4-33**)	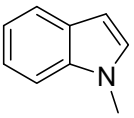 (**4-34H**)	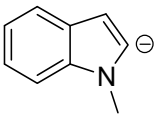 (**4-34**)		
E_{tot}	-399.8545995	-399.2505594	-403.2602311	-402.6338978		
G_{298}	**-399.778927**	**-399.190621**	**-403.135882**	**-402.523940**		
ΔG_{solv}	-0.0079999	-0.0925883	-0.0110118	-0.0981181		

Table 4.28 B3LYP/6-311++G(2df,2p) optimized energies and solvation free energies ΔG_{solv} (DMSO, SMD/B3LYP/6-31G(d)) in Hartree.

	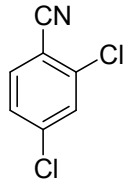 (**4-35H**)	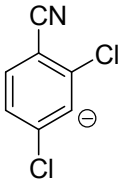 (**3-35-3H**)	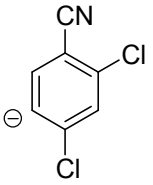 (**4-35-5H**)	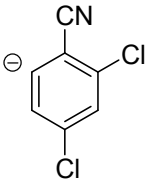 (**4-35-6H**)
E_{tot}	-1243.8459213	-1243.2576137	-1243.2483261	-1243.2478735
G_{298}	**-1243.800541**	**-1243.227241**	**-1243.217865**	**-1243.217406**
ΔG_{solv}	-0.0102787	-0.0769391	-0.0765726	-0.0774810
	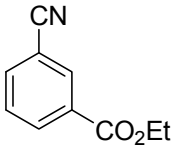 (**4-36H**)		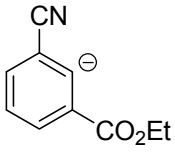 (**4-36-2H**)	
E_{tot}	-591.8888823	-591.8893222	-591.2708217	-591.2750953
G_{298}	**-591.758834**	**-591.758734**	**-591.156069**	**-591.160173**
ΔG_{solv}	-0.0132110	-0.0128763	-0.0898792	-0.0871223
	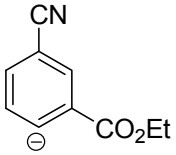 (**4-36-6H**)		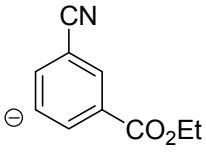 (**4-36-5H**)	
E_{tot}	-591.2719228	-591.2684706	-591.2712926	-591.2707768
G_{298}	**-591.157241**	**-591.153801**	**-591.156832**	**-591.155925**
ΔG_{solv}	-0.0841741	-0.0863255	-0.0864689	-0.0867557
	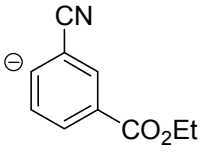 (**4-36-4H**)		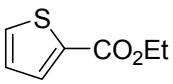 (**4-37H**)	
E_{tot}	-591.2766748	-591.2772253	-820.3845102	-820.3849336
G_{298}	**-591.161083**	**-591.161382**	**-820.283442**	**-820.283448**
ΔG_{solv}	-0.0869788	-0.0866601	-0.0095616	-0.0094501
	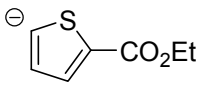 (**4-37-5H**)		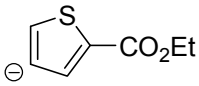 (**4-37-4H**)	
E_{tot}	-819.7771653	-891.7780388	-819.7593926	-819.7596643
G_{298}	**-819.690267**	**-819.690634**	**-819.672857**	**-819.672742**
ΔG_{solv}	-0.0885087	-0.0883493	-0.0930505	-0.0930186
	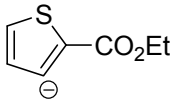 (**4-37-3H**)			
E_{tot}	-819.7622994	-819.7599345		
G_{298}	**-819.675949**	**-819.673398**		
ΔG_{solv}	-0.0922058	-0.0936720		

Table 4.29 B3LYP/6-311++G(2df,2p) optimized energies and free solvation energies ΔG_{solv} (DMSO, SMD/B3LYP/6-31G(d)) in Hartree.

	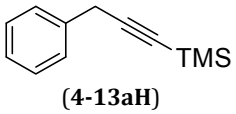 (**4-13aH**)	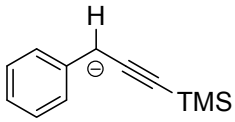 (**4-13a**)	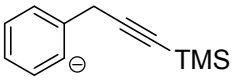 (**4-13a-2H**)	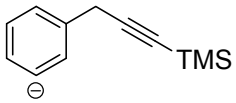 (**4-13a-3H**)
E_{tot}	-756.5923863	-756.0201032	-755.9520498	-755.9466344
G_{298}	**-756.397948**	**-755.840553**	**-755.773740**	**-755.767789**
ΔG_{solv}	-0.0064222	-0.0760627	-0.0928911	-0.0969707

	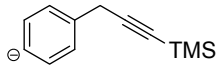 (**4-13a-4H**)	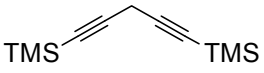 (**4-38H**)	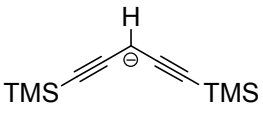 (**4-38**)
E_{tot}	-755.9455281	-1010.4046243	-1009.8411516
G_{298}	**-755.766319**	**-1010.185825**	**-1009.637799**
ΔG_{solv}	-0.0979747	-0.0025338	-0.0712978

	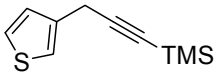 (**4-13bH**)	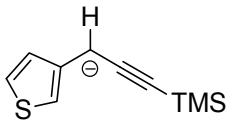 (**4-13b**)
E_{tot}	-1077.3581882	-1077.3576215	-1076.7800454	-1076.7800108
G_{298}	**-1077.198727**	**-1077.196687**	**-1076.633781**	**-1076.633874**
ΔG_{solv}	-0.0054661	-0.0059282	-0.0763495	-0.0750746

	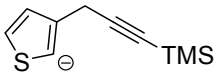 (**4-13b-2H**)	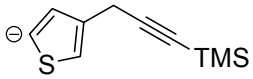 (**4-13b-5H**)
E_{tot}	-1076.7430600	-1076.7430445	-1076.7382618	-1076.7382573
G_{298}	**-1076.595754**	**-1076.596313**	**-1076.593545**	**-1076.593061**
ΔG_{solv}	-0.0874888	-0.0874888	-0.0915206	-0.0915206

	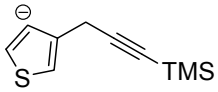 (**4-13b-4H**)
E_{tot}	-1076.7285417
G_{298}	**-1076.583510**
ΔG_{solv}	-0.0913134

Table 4.30 Reference-depending free solvation energies $\Delta\Delta G_{solv}$ in kJ mol^{-1} (PCM/SMD/B3LYP/6-31G(d)//B3LYP/6-311++G(2df,2p)).

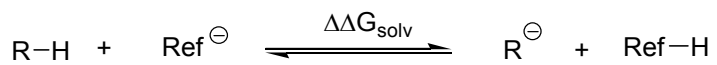

	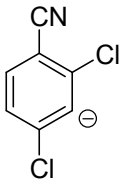 (**4-35-3H**)	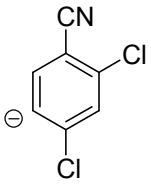 (**4-35-5H**)	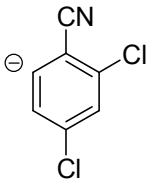 (**4-35-6H**)	
 (**4-24H**)	+38.41	+39.37	+36.99	
 (**4-27H**)	+68.70	+69.66	+67.28	
	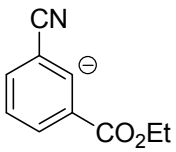 (**4-36-2H**)	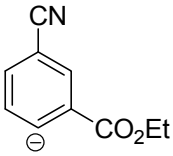 (**4-36-6H**)	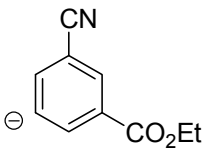 (**4-36-5H**)	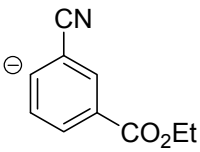 (**4-36-4H**)
 (**4-24H**)	+12.14	+21.63	+20.29	+19.73
 (**4-27H**)	+42.43	+51.92	+50.58	+50.03
	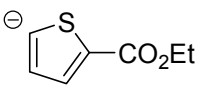 (**4-37-5H**)	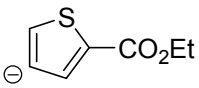 (**4-37-4H**)	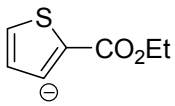 (**4-37-3H**)	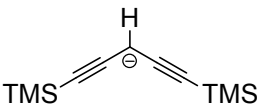 (**4-38**)
 (**4-24H**)	+6.20	-5.87	-6.87	+32.89
 (**4-27H**)	+36.50	+24.42	+23.42	+63.18

Table 4.31 Reference-depending free solvation energies $\Delta\Delta G_{solv}$ in kJ mol^{-1} (PCM/SMD/B3LYP/6-31G(d)//B3LYP/6-311++G(2df,2p)).

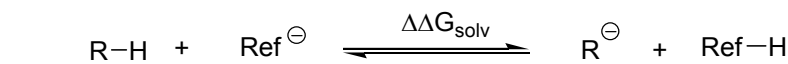

	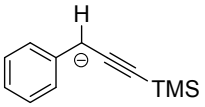 (**4-13a**)	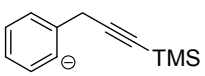 (**4-13a-2H**)	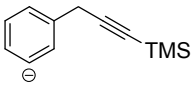 (**4-13a-3H**)	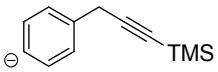 (**4-13a-4H**)
 (**4-24H**)	+30.58	-13.60	-24.31	-26.95
 (**4-27H**)	+60.88	+16.69	+5.98	+3.35
	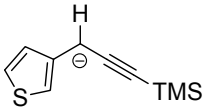 (**4-13b**)	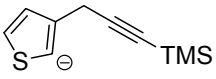 (**4-13b-2H**)	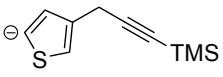 (**4-13b-5H**)	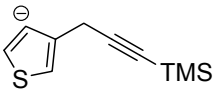 (**4-13b-3H**)
 (**4-24H**)	+28.76	-1.17	-11.76	-11.21
 (**4-27H**)	+59.06	+29.12	+18.53	+19.08

T**able 4.32** At PCM/SMD/B3LYP/6-31G(d)//B3LYP/6-311++G(2df,2p) level of theory calculated pK_a values using DMSO/dimsyl as reference system.

	pK_a(gas)	pK_a(DMSO)	pK_a(DMSO, corr.)[a]	pK_a(THF)[b]
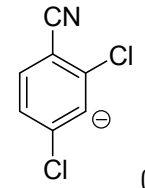 (**4-35-3H**)	+23.70	+30.43	+27.64	+27.95
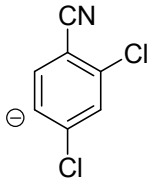 (**4-35-5H**)	+28.01	+34.91	+31.88	+32.38
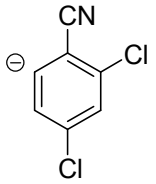 (**4-35-6H**)	+28.23	+34.71	+31.69	+32.18
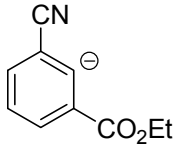 (**4-36-2H**)	+35.38	+37.73	+34.54	+35.17
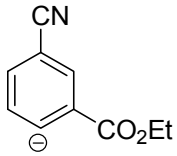 (**4-36-6H**)	+36.72	+40.51	+37.17	+37.91
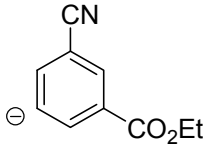 (**4-36-5H**)	+37.00	+40.55	+37.20	+37.95
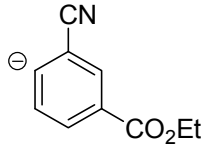 (**4-36-4H**)	+34.84	+38.30	+35.08	+35.73

[a] Using the test set correlation fit: pK_a(exp.) = 0.9447 pK_a(calc.) – 1.1043.

[b] Corrected with *Streitwieser*'s linear correlation pK_a (THF) = 1.046 pK_a (DMSO) – 0.963.

Table 4.33 At PCM/SMD/B3LYP/6-31G(d)//B3LYP/6-311++G(2df,2p) level of theory calculated pK_a values using DMSO/dimsyl as reference system.

	pK_a(gas)	pK_a(DMSO)	pK_a(DMSO, corr.)[a]	pK_a(THF)[b]
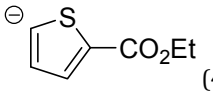 (**4-37-5H**)	+32.75	+33.84	+30.86	+31.32
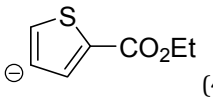 (**4-37-4H**)	+40.87	+39.85	+36.54	+37.26
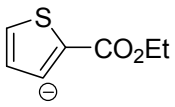 (**4-37-3H**)	+39.49	+38.29	+35.07	+35.72
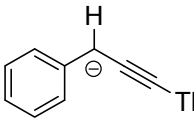 (**4-13a**)	+16.39	+21.75	+19.44	+19.37
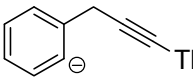 (**4-13a-2H**)	+47.12	+44.73	+41.15	+42.08
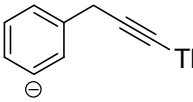 (**4-13a-3H**)	+49.85	+45.59	+41.96	+42.93
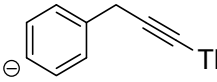 (**4-13a-4H**)	+50.53	+45,81	+42.17	+43.15
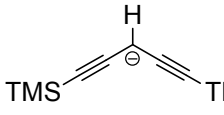 (**4-38**)	+12.08	+17.84	+15.75	+15.51
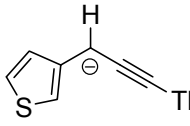 (**4-13b**)	+19.73	+24.77	+22.30	+22.36
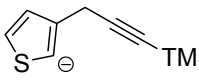 (**4-13b-2H**)	+37.06	+36.86	+33.72	+34.31
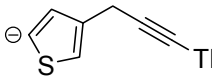 (**4-13b-5H**)	+38.35	+36.29	+33.18	+33.74
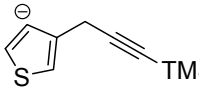 (**4-13b-4H**)	+42.87	+40.90	+37.53	+38.30

[a] Using the test set correlation fit: pK_a(exp.) = 0.9447 pK_a(calc.) – 1.1043.

[b] Corrected with *Streitwieser*'s linear correlation pK_a (THF) = 1.046 pK_a (DMSO) – 0.963.

5 The Chemical Fate of Paroxetine Metabolites

Parts of this chapter have been published in

The chemical fate of paroxetine metabolites. Dehydration of radicals derived from 4-(4-fluorophenyl)-3-(hydroxymethyl)piperidine

D. Šakić, F. Achrainer, V. Vrček, H. Zipse, *Org. Biomol. Chem.* **2013**, *11*, 4232 – 4239.

5.1 Introduction

The supply of drinking water is one of the biggest challenges of humanity in the next decades or even centuries. According to the *World Health Organisation* (WHO) since 1990 over two billion people have gained access to drinking water and improved sanitation. But more than 700 million of earth's population still lack free entrance to improved sources of drinkable water.[172] It is known, that the degree of industrialization is correlating with the analyzable amount of micro pollutants or organic metabolites in municipal wastewater.[173] A well-known established procedure to remove organic compounds is, aside from ozonization or UV irradiation, the chlorination with agents like Cl_2/ClO^-, NH_2Cl or ClO_2, which therefore plays an important role in environmental and biological chemistry.[174] The development of cheap disinfectants, which produce nontoxic, biodegradable byproducts or can be handled safely, is still an ongoing scientific challenge. The main byproducts of organic compounds upon chlorination are chloroform $CHCl_3$, haloacetic acids, haloketones, cyanogen chloride and chloramines.[175] Due to the potential carcinogenicity of those compounds a regular monitoring of their concentrations is highly regulated in the municipal water system.[176]

The risk assessment of only a small number of organic compounds is known and documented. The amino moiety present in amines, amides or sulfonamides is an example for compounds with a well-known behavior against chlorination.[177]

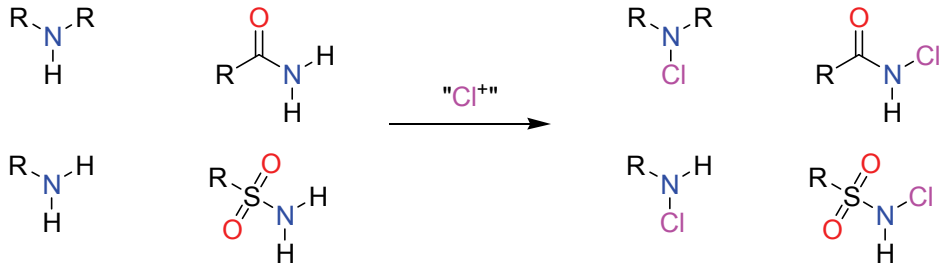

Scheme 5.1 Electrophilic chlorination of nitrogen containing compounds.

N-Chlorosuccinimide (**5-1**) and chloramine T (**5-2**) are widely used reagents in synthesis.[178] Even the oxidizing potential of *N*-chlorosaccharin (**5-3**) as a source for electrophilic chlorine cations has been studied.[179] Saccharin is an example of a food additive, which is accumulated in wastewater undigested by our body.[180]

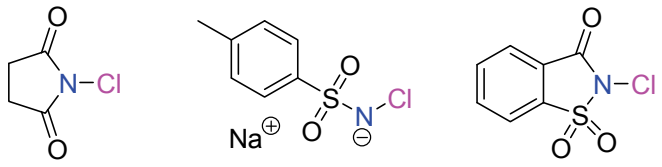

Figure 5.1 Commonly used *N*-chloramines.

Halogenated carboxylic amides readily undergo a Hofmann-type rearrangement to generate mutagenic isocyanates or the respective primary amines upon hydrolysis.[181]

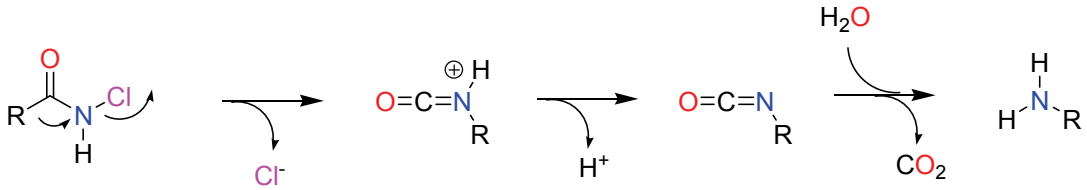

Scheme 5.2 Mechanism of the *Hofmann* rearrangement.

5.2 The Chemistry of *N*-centered Radicals

The chemistry of *N*-chloro amines is dominated by ionic reactions involving electrophilic chlorine and radical reactions involving *N*-centered radicals. The term "nitrogen centered radical" refers to a species where the initial unpaired electron is localized on the nitrogen atom. *N*-Centered radicals can be divided into four classes:

Neutral aminyl radicals $R_2N^{\bullet}$ (**5-4**), protonated aminyl radicals $R_2NH^{\bullet+}$ (**5-5**), aminyl radical metal complexes $R_2N^{\bullet}$-$M^{+}Cl$ (**5-6**)[182] and triarylaminium radicals $Ar_3N^{\bullet+}$.[183]

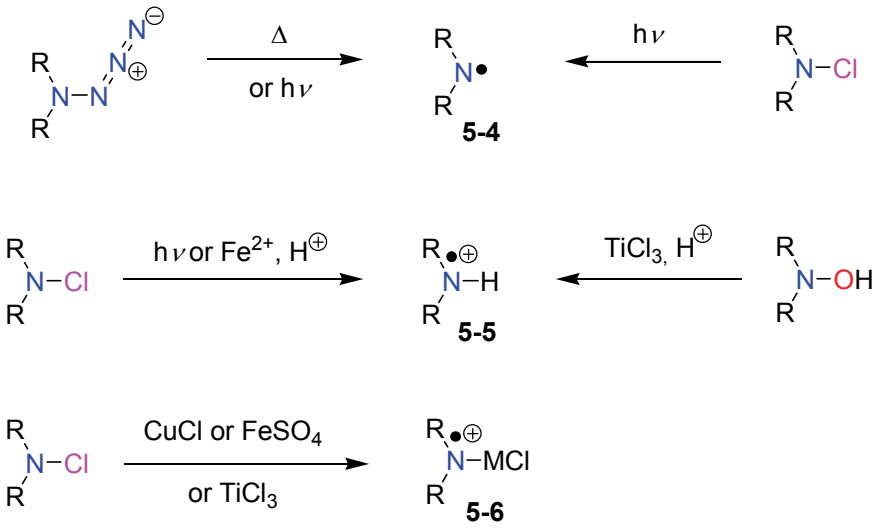

Scheme 5.3 Generation of *N*-centered radicals.

These species can easily be generated by photolysis or single electron transfer (SET) reactions. Free aminyl radicals of type **5-4** are unique in that a lone pair and an unpaired electron are localized at the same atom. Therefore they are capable of existing in either a π or σ electronic state. By EPR spectroscopy the π state has been identified for many alkylaminyl radicals as ground state.[182a]

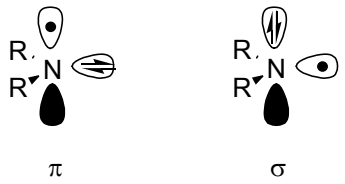

Figure 5.2 Electronic states of neutral aminyl radicals of type **5-4**.

Neutral dialkylaminyl radicals $R_2N^{\bullet}$ (**5-4**) prefer dimerization to hydrazines and then disproportionate to amines and imines. In the presence of olefins or arenes they strongly tend to abstract hydrogen atoms forming stabilized allyl or benzyl radicals rather than to add to the C-C double bond. Homolytic decomposition of *N*-chloramines in acidic media leads to the formation of aminium radicals $R_2NH^{\bullet+}$ (**5-5**) which behave very differently than their neutral counterparts. The positive charge reduces the propensity to dimerize or disproportionate and increases the tendency to abstract

exposed or activated hydrogen atoms (*Hofmann-Löffler-Freytag* reaction)[184] or the addition to sp^2-hybridized hydrocarbons.[182b] Fragmentation reactions of the aminium radicals to imines and stabilized C-centered radicals are also common.[185]

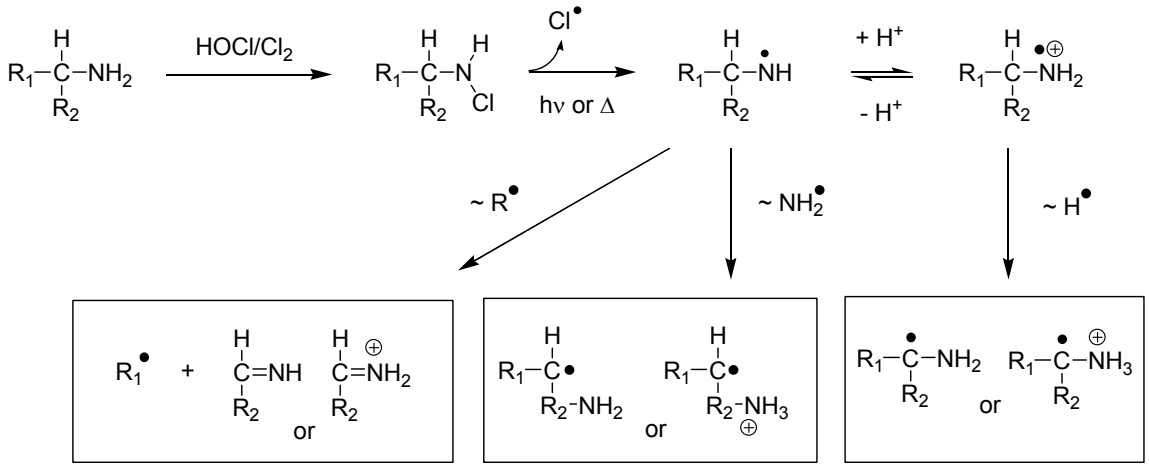

Scheme 5.4 Generally accepted reaction pathways of aminyl radicals.

Single electron reduction of *N*-chloramines in pH-neutral solution by metal salts, like Fe^{2+}, Cu^{+} or Ti^{3+} chlorides, leads to complexed radicals with the lowest reactivity in the row of aminyl radicals, only capable of addition reactions. Triarylaminium radicals are mainly used as one electron oxidants with tuneable redox potentials through the substitution pattern of the phenyl rings.[186] Their main application is found in the initiation of radical cation Diels-Alder reactions of electroneutral dienes and dienophiles.[187]

5.3 Paroxetine – a Selective Serotonine Reuptake Inhibitor

Paroxetine (Paxil©, **5-7**) is an often prescribed antidepressant of the class of selective serotonine (5-hydroxytryptamine, **5-8**) reuptake inhibitors (SSRI).[188] It is used to treat major depression, obsessive-compulsive disorder, social anxiety, and panic and stress attacks. Paroxetine represents one of the most specific selective SSRIs.

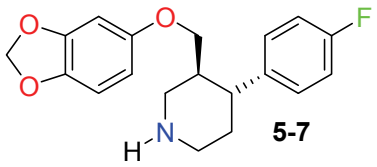

Figure 5.3 Paroxetine© (**5-7**).

Messages are passed through cerebral nerve cells via a small gap by releasing neurotransmitters, e.g serotonine (**5-8**), from the presynaptic cell into it. In the so called synapse the neurotransmitters are then recognized by receptors on the surface of the postsynaptic cell, which upon stimulation relays the signal. About 90 % of the neurotransmitter are again released from the receptors and are then taken up by monoamine transporters to the presynaptic cell. Serotonine reuptake inhibitors as the name implies inhibit the reuptake into the presynaptic cell, which results in a longer presence in the synapse increasing the signal relay between neurons followed by a serotonine receptor down-regulation in the central nervous system.

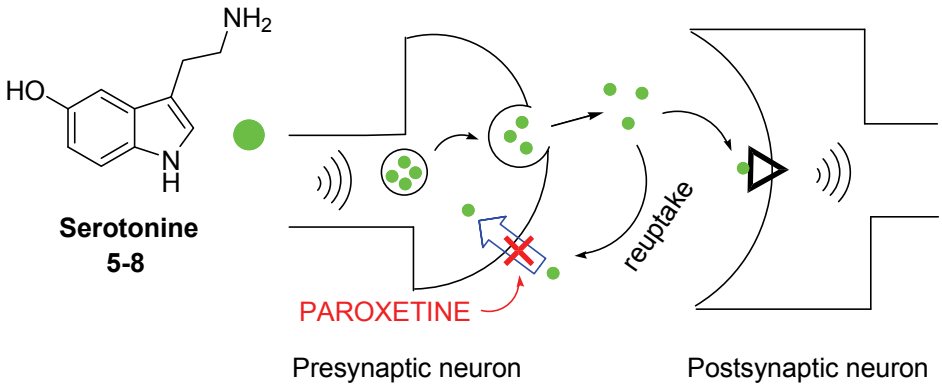

Figure 5.4 Schematic overview for the mechanism of serotonine reuptake.

In many examples the lead motif for serotonine reuptake inhibitors possesses a piperidine moiety. Related pharmaceuticals are Femoxetine© (**5-9**),[189] Litoxetine© (**5-10**)[190] and Ifoxetine© (**5-11**),[191] where the latter two never reached market.

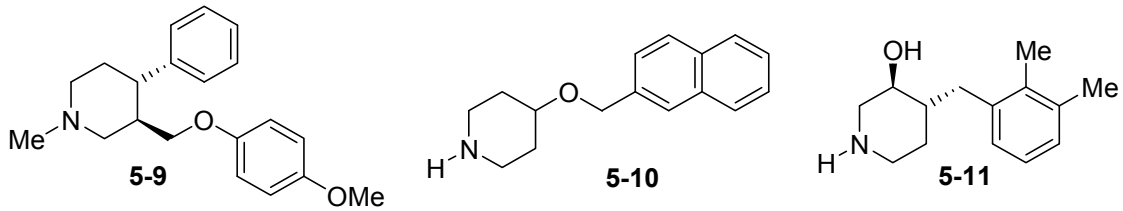

Figure 5.5 Femoxetine© (**5-9**), Litoxetine© (**5-10**) and Ifoxetine© (**5-11**).

Starting in 1977 with the patent of *Christensen* and *Squires* using a selective diastereomer recrystallization strategy,[192] in the past years numerous enantioselective syntheses of paroxetine have been established. These include, for example, enzymatic resolution of intermediates,[193] chiral auxiliary-assisted synthesis,[194] desymmetrization of prochiral diesters[195] or the catalytic selective formation of the β-stereocenter of a 2-piperidone derivative.[196]

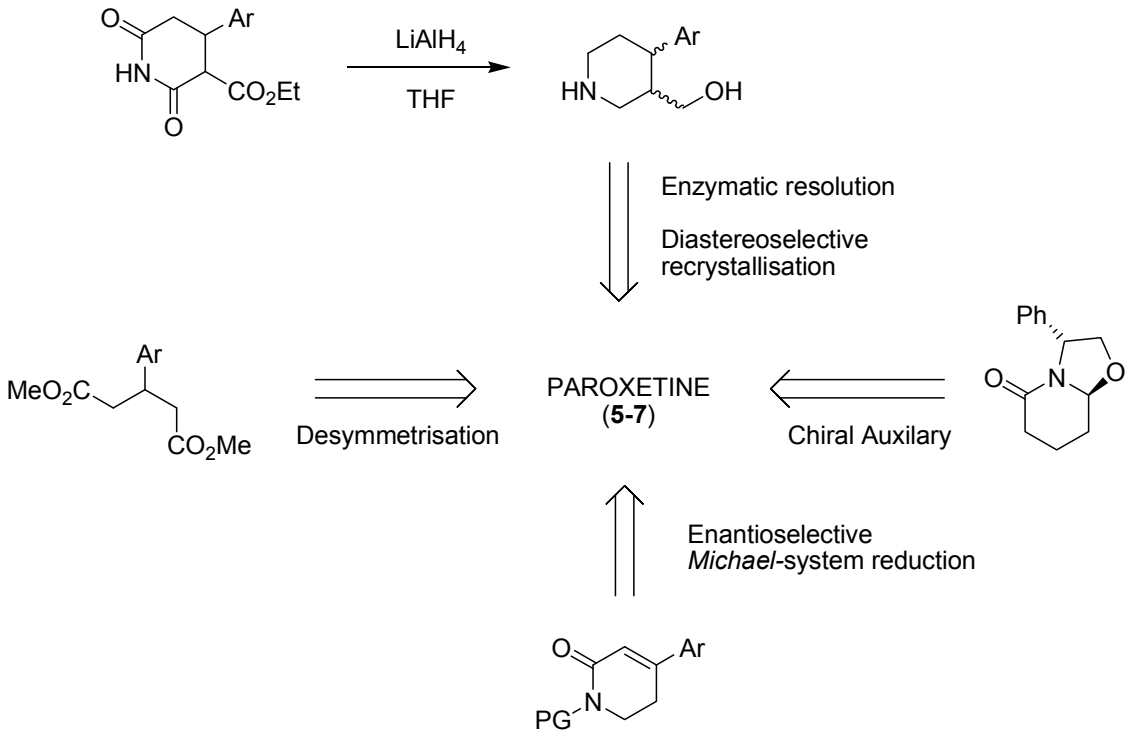

Scheme 5.5 Schematic overview of different paroxetine syntheses.

5.4 Photolysis of Paroxetine

Recent studies have shown, that paroxetine and its metabolites can accumulate in wastewaters,[197] but also in the tissue of fish.[198] With respect to environmental risk assessment only paroxetine (**5-7**) itself and its major human metabolite **5-12** have been studied in more detail until today.[199] Paroxetine appears to be hydrolytically stable, but *Kwon* and *Armbrust* have shown, that the compound exposed to simulated sunlight easily undergoes hydrolysis to **5-12** and furthermore dehydrates to an unknown photoproduct.[200] No mechanistic pathway has been provided and the only structural information for the dehydrated product is the mass spectrum signal *m/z*

192 $[M + H]^+$, which they proposed to be **5-13**. *Vrček* and coworkers recently investigated a number of possible base-catalyzed rearrangements of the *N*-chlorinated piperidine derivate **5-12Cl** in aqueous media. In addition to hydrolyzed product **5-13** alternative products have been suggested for the chemical fate of paroxetine (**5-7**). Nevertheless, these investigations included only closed-shell intermediates, no open-shell compounds which can occur upon photolysis, have been studied.[201]

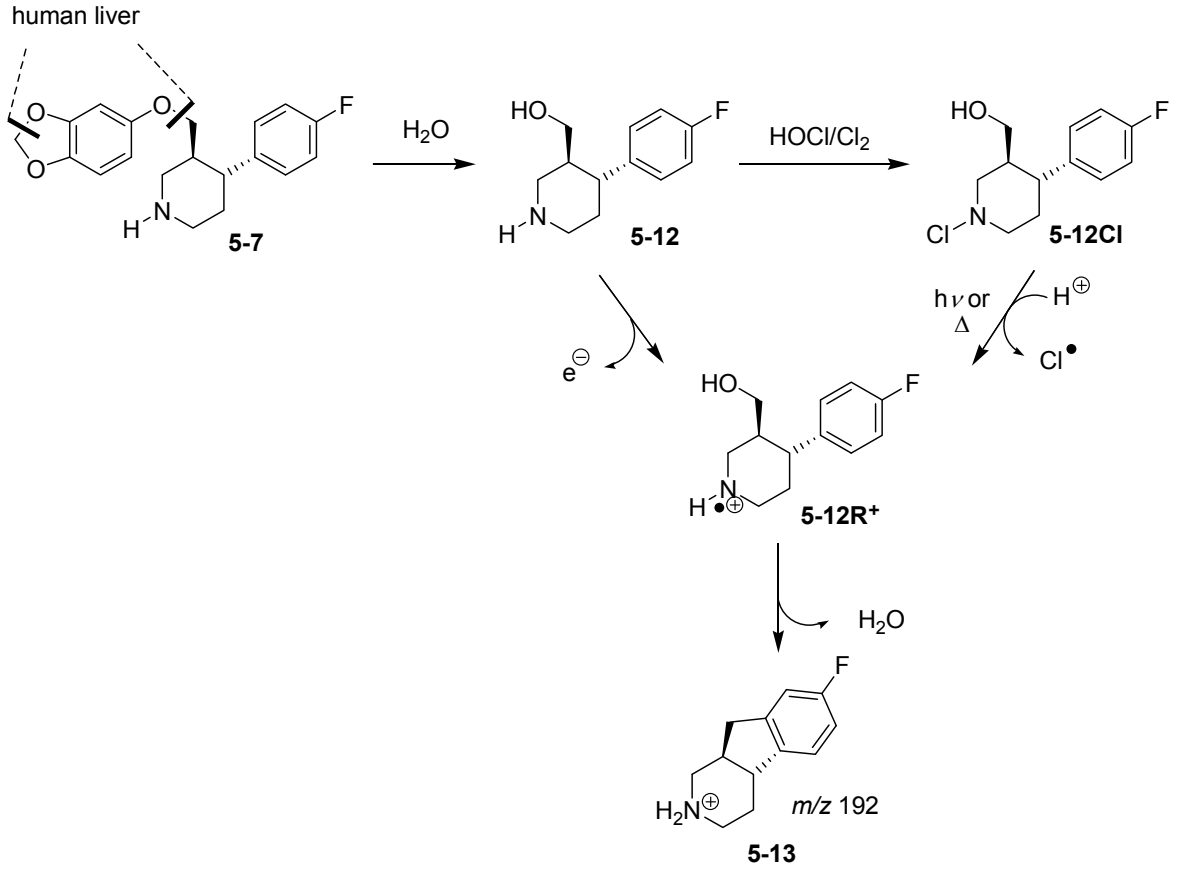

Scheme 5.6 Degradation of paroxetine (**5-7**) and proposed formation of key intermediate **5-12R**$^+$ in the environment.

5.5 Computation of Chemical Properties of *N*-centered Piperidinyl Radicals

The formation of the *N*-centered piperidyl radical (**5-12R**$^+$) is the initial key step for the following reaction pathway[202] and therefore has been specifically examined. The BDE (bond dissociation energy) can easily be calculated by combining the isodesmic

reaction enthalpy $\Delta_{rxn}H$, which is nothing else than a reflection of the radical stability and the experimentally measured bond strength of the reference (Ref-H).

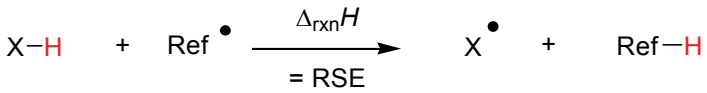

BDE (X-H) = RSE + BDE (Ref-H)

Scheme 5.7 General definition of radical stability and calculation of bond dissociation energies.

The theoretical results for different piperidine derivatives are summarized in **Table 5.1** and **Table 5.2**

Table 5.1 Theoretically calculated reaction enthalpies and N-X BDEs of differently substituted piperidines.

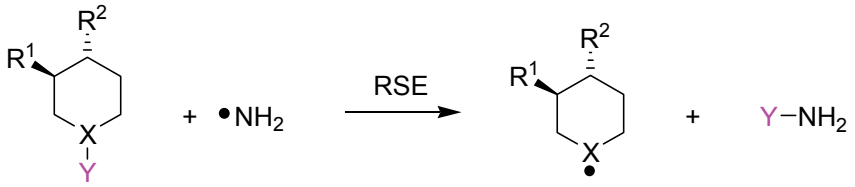

	X	Y	R^1	R^2	RSE UB3LYP[a]	RSE ROMP2[b]	RSE G3(MP2)-RAD	BDE (X-Y)[d] G3(MP2)-RAD
5-14Cl	N	Cl	H	H	-22.94	+10.71	-1.24	+251.86
5-14Cl$^+$	NH^+	Cl	H	H	-72.17	-22.05	-38.33	+214.77
5-14	N	H	H	H	-52.21	-43.62	-46.68	+403.40
5-14H	NH^+	H	H	H	-37.86	-35.29	-28.01	+422.07
5-12Cl	N	Cl	CH_2OH	Ar[c]	-27.13	+6.79	-5.22	+247.88
5-12	N	H	CH_2OH	Ar[c]	-53.70	-45.20	-48.49	+401.59
5-12H	NH^+	H	CH_2OH	Ar[c]	-39.40	-14.33	-22.52	+427.56

[a] B3LYP/6-31G(d). [b] ROMP2(FC)/6-311+G(3df,2p)//UB3LYP/6-31G(d). [c] *p*-F-C_6H_5. [d] BDE(NH_2Cl) = +253.1 kJ mol^{-1}; BDE(NH_3) = +450.08 kJ mol^{-1}.[115]

Upon protonation the stabilization of *N*-centered piperidine radical **5-12R$^+$** is decreased by approximately 25 kJ mol^{-1} at G3(MP2)-RAD level in the gas phase.[203] Also, the impact of the attached residues is enhanced due to the introduction of the positive charge on the nitrogen center (see **Figure 5.6**). The formation of *N*-centered radical **5-12R** by photolytic cleavage of the N-Cl compared to the N-H bond is favored by ΔBDE = +153.7 kJ mol^{-1}.

Table 5.2 Theoretically obtained reaction enthalpies and C-H-BDEs of differently charged piperdines.

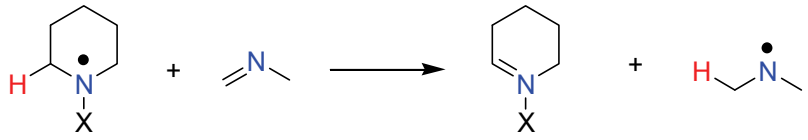

X	$\Delta_{rxn}H$ UB3LYP[a]	$\Delta_{rxn}H$ ROMP2[b]	$\Delta_{rxn}H$ G3(MP2)-RAD	BDE (Z-H)[c] G3(MP2)-RAD
H (**5-14R**$^+$)	-29.62	-31.50	-28.59	+75.21
/ (**5-14R**)	-14.21	-10.59	-8.68	+95.12

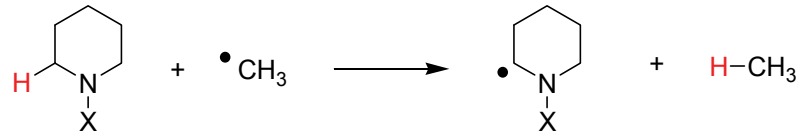

X	$\Delta_{rxn}H$ UB3LYP[a]	$\Delta_{rxn}H$ ROMP2[b]	$\Delta_{rxn}H$ G3(MP2)-RAD	BDE (Z-H)[c] G3(MP2)-RAD
H (**5-14**)	-63.74	-47.87	-48.79	+390.51
H_2 (**5-14H**)	-14.43	+1.35	+1.17	+440.47

[a] B3LYP/6-31G(d). [b] ROMP2(FC)/6-311+G(3df,2p)//UB3LYP/6-31G(d). [c] BDE(CH_4) = +439.3 kJ mol^{-1}; BDE ($(H_3C)_2N^\bullet$) = ($\Delta_fH(CH_2{=}NCH_3)$ + $\Delta_fH(H^\bullet)$) - $\Delta_fH((H_3C)_2N^\bullet)$ = +103.8 kJ mol^{-1}.[115]

The N-Cl bond of protonated *N*-chloropiperidine (**5-14ClH**) is weakened by 37.1 kJ mol^{-1} compared to that in neutral *N*-chloropiperidine. On the other hand the homolytic N-H cleavage of piperidinium ion **5-14H** is raised to a value of +422.1 kJ mol^{-1} in the gas phase. The experimental determined BDE of **5-14H** in DMSO was estimated to be +431.4 kJ mol^{-1}. Applying a continuum model (SMD/UB3LYP/ 6-31G(d))[60] to the isodesmic reaction the theoretical BDE values is matching the experiment well (BDE_{sol}(**5-14H**) = +425.88 kJ mol^{-1}). The results for piperidinium ion **5-14ClH** and the chloro derivative **5-14Cl** can easily be explained by the increase of polarization of the N-halogen bond upon charge induction. The weakest bond is not the N-Cl but the C-H bond in the neighboring α-position of protonated piperidinyl radical **5-14R**$^+$ (BDE = +75.21 kJ mol^{-1}), which is displayed graphically in **Figure 5.6**.

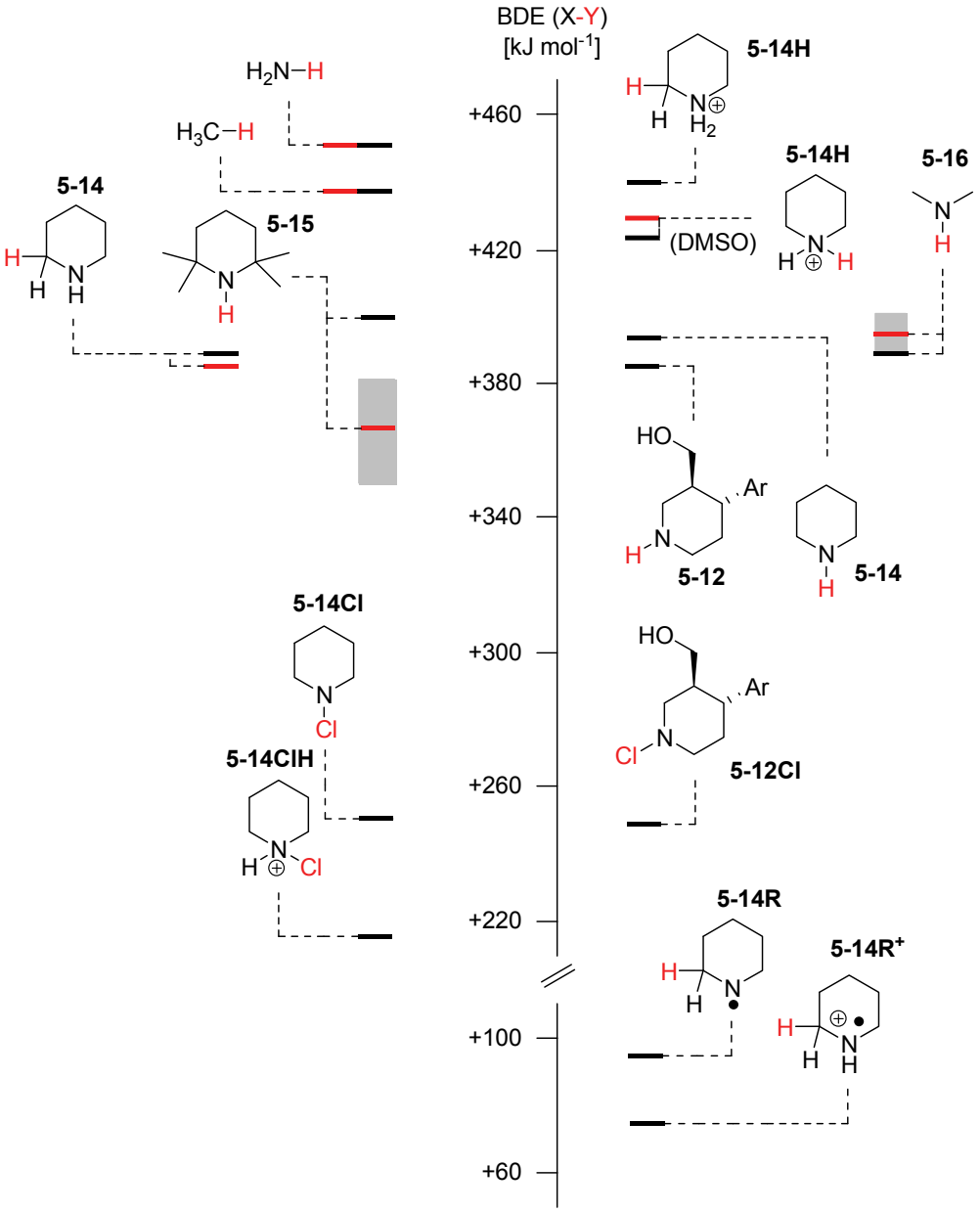

Figure 5.6 Experimental[115] (red bars) vs calculated (black bars, G3(MP2)-RAD) bond dissociation energies in the gas phase (Ar = *p*-F-C_6H_5).

The α-CH bond in neutral piperidinyl radical **5-14R** is about 20 kJ mol^{-1} stronger. This low bond energy is not only the result of inductive effects induced by the positive charged nitrogen center, but can mainly be explained by the bond situation in the newly formed product. Upon CH bond homoysis of **5-14R** or **5-14R⁺** a π bond is formed together with the hydrogen atom. For closed-shell molecules like neutral (**5-14**) or protonated piperidine (**5-14H**) such gain in energy is not possible (**Figure 5.7**).

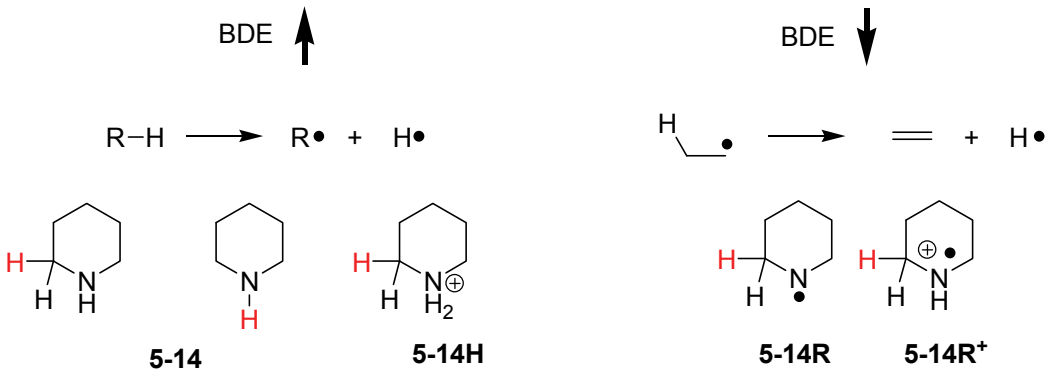

Figure 5.7 Homolytic cleavage with high (left) and low BDE (right) due to the formation of double bonds.

Secondly, in the case of saturated *N*-heterocycles the unpaired electron in the nitrogen π orbital interacts with the σ*(C-H). For the closed-shell piperidinium ion **5-14H** this overlap is reduced, resulting in the highest BDE of +440 kJ mol^{-1} (see **Figure 5.8**). Therefore a mechanism involving the cleavage of α-CH bonds in paroxetine metabolite **5-12R$^+$** is very likely to proceed and indeed such intermediates have been identified computationally by *Vrçek*.[204]

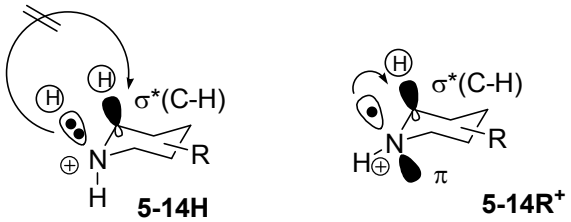

Figure 5.8 Secondary orbital interactions responsible for the low α-CH bond dissociation energy of aminyl radicals.

The pK_a values for protonated amines and aminyl radicals have been calculated according to the equations in **Chapter 4.6** using H_2O/H_3O^+ as reference (pK_a = -15.7) and the so obtained results for piperidinium ion **5-14H** and its radical **5-14R** are in good agreement with literature known numbers (see **Table 5.3**). The acidity of the respective open-shell intermediate **5-12R$^+$** is quite similar to its parent aminyl radical **5-14R,** which in general is the result of the larger amount of *s* character in the lone pair orbital (sp^2) compared to the closed-shell amine with its sp^3 configuration. The pK_a value of +3.8 suggests that both species, the neutral and the protonated radical, can coexist in neutral media.

Table 5.3 *Boltzmann*-averaged free energies of proton transfer at various levels of theory (in kJ mol^{-1}, at 298.15 K and 1 atm, Ar = *p*-F-C_6H_5). Aqueous solvation free energies ΔG_{solv} for individual components are obtained from SMD/(U)HF/6-31G(d)//(U)B3LYP/6-31G(d).

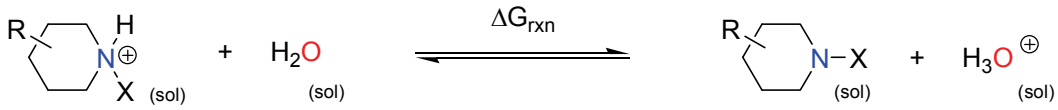

		(U)B3LYP[a]	(U)CCSD(T)[b]	(RO)MP2[c]	G3(MP2)-RAD	**Exp.**
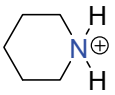	ΔG_{gas}	+260.07	+263.45	+262.20	+265.19	
	ΔG_{sol}	+142.08	+145.46	+144.21	+147.20	
5-14H	pK_a	**+9.19**	**+9.78**	**+9.56**	**+10.08**	**+11.2**[205]
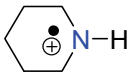	ΔG_{gas}	+245.67	+234.50	+241.17	+246.46	
	ΔG_{sol}	+111.15	+99.98	+106.65	+111.94	
5-14R$^+$	pK_a	**+3.77**	**+1.81**	**+2.98**	**+3.91**	**+5.8**[206]
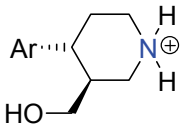	ΔG_{gas}	+280.90	+279.79	+275.36	+278.03	
	ΔG_{sol}	+152.36	+151.25	+146.82	+149.49	
5-12H	pK_a	**+10.99**	**10.79**	**+10.02**	**+10.49**	
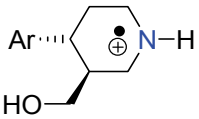	ΔG_{gas}	+267.60	+248.52	+245.34	+252.96	
	ΔG_{sol}	+125.79	+106.71	+103.53	+111.15	
5-12R$^+$	pK_a	**+6.33**	**+2.99**	**+2.43**	**+3.77**	

[a] UB3LYP/6-31G(d). [b] (U)CCSD(T)/6-31G(d). [c] (RO)MP2(FC)/6-311+G(3df,2p).

5.6 Hydrogen Atom Transfer

5.6.1 Intramolecular Pathways

As already mentioned in **Chapter 5.2**, aminium radicals $R_2NH^{\bullet+}$ easily abstract exposed hydrogen atoms either intra- or intermolecularly to form more stable open-shell intermediates and ammonium ions. Hydrogen atom transfer (HAT) is per definition the concerted movement of a proton and an electron in a single kinetic step from one group to another. In piperidinyl radical **5-12R$^+$** of paroxetine metabolite **5-12** four exposed positions are feasible and have been examined theoretically. *Kwon* and *Armbrust* have estimated the unimolecular rate constant for photodegradation of paroxetine metabolite **5-12** to be 0.0529 h^{-1} (calculated as the rate of disappearance

of paroxetine **5-7**) which corresponds to a barrier of ca. 100 kJ mol^{-1} at pH 7 and 25 °C.[200] All theoretically calculated barriers should therefore not exceed this value.

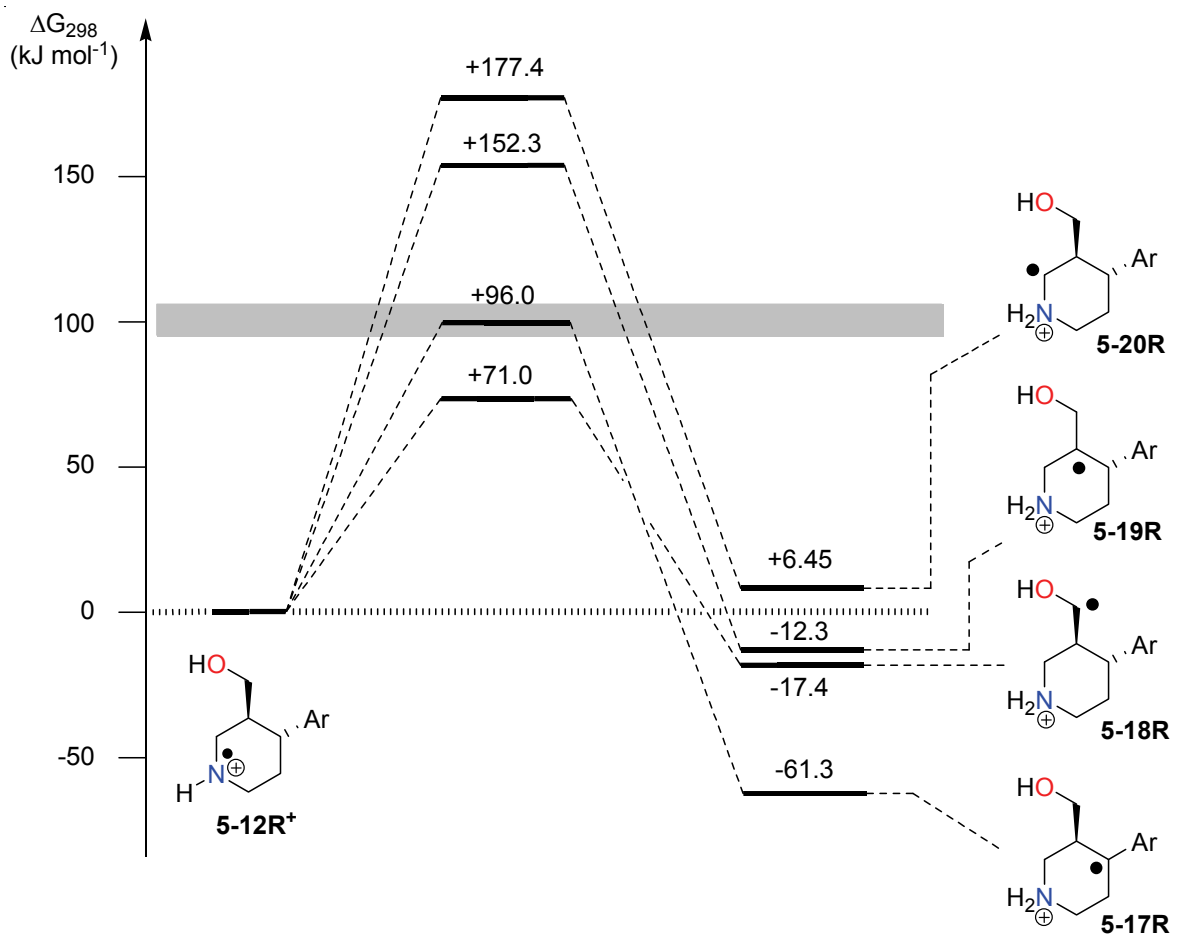

Figure 5.9 Schematic energy profile of hydrogen atom transfer in the gas phase at G3(MP2)-RAD level of theory at 298.15 K and 1 atm (Ar = *p*-F-C_6H_5).

Besides the well-established G3(MP2)-RAD approach,[81] *Radom* recently benchmarked various methods to obtain accurate barriers for water-mediated proton transfer and identified the dispersion-corrected double hybrid functional B2PLYP-D as a reasonable compromise of accuracy and computing time.[207] The results are summarized together with the G3(MP2)-RAD results in **Table 5.4**. Solvation effects have been included using a conductor-like polarizable continuum model (C-PCM) with United Atom Hartree-Fock (UAHF) radii and B3LYP/6-31G(d) single point calculation.[82] The differences in reaction barriers for both methods are almost identical, but reaction free energies ΔG_{298} (G3(MP2)-RAD) are more negative, especially in the case for the generation of open-shell intermediate **5-17R**.

Considering gas phase calculations only the barriers for the formation of intermediates **5-17R** and **5-18R** are lower than the experimental threshold of +100 kJ mol^{-1} (see **Table 5.4**).

Table 5.4 *Boltzmann*-averaged free energy differences for H-atom transfer of *N*-centered paroxetine metabolite **5-12R$^+$** in the gas phase or in solution[a] (in kJ mol^{-1}, at 298.15 K and 1 atm, Ar = *p*-F-C_6H_5).

	UB3LYP[b]		ROMP2[c]		UB2PLYP[d]		G3(MP2)-RAD	
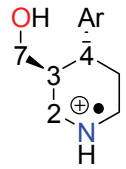 **5-12R$^+$**	<ΔG‡> **<ΔG$_{sol}$‡>**	<ΔG> **<ΔG$_{sol}$>**	<ΔG‡> **<ΔG$_{sol}$‡>**	<ΔG> **<ΔG$_{sol}$>**	<ΔG‡> **<ΔG$_{sol}$‡>**	<ΔG> **<ΔG$_{sol}$>**	<ΔG‡> **<ΔG$_{sol}$‡>**	<ΔG> **<ΔG$_{sol}$>**
N →C2	+201.2	+32.2	+154.6	-9.00	+181.9	+13.8	+177.4	+6.55
	+195.8	**+29.4**	**+150.0**	**-12.8**	**+173.4**	**+8.25**	**+172.0**	**+1.41**
N →C3	+167.6	+8.08	+126.7	-26.7	+153.8	-5.83	+152.3	-12.2
	+190.7	**+2.93**	**+150.7**	**-29.0**	**+174.9**	**-11.5**	**+175.5**	**-16.5**
N →C4	+98.9	-46.9	+67.7	-70.9	+93.3	-48.8	+96.0	-61.2
	+130.1	**-41.5**	**+99.7**	**-64.7**	**+122.4**	**-45.6**	**+127.3**	**-73.9**
N →C7	+78.9	+7.71	+40.2	-33.7	+67.1	-12.2	+71.0	-17.2
	+88.6	**-11.1**	**+50.7**	**-50.1**	**+74.7**	**-30.4**	**+80.8**	**-35.2**

[a] C-PCM/UAHF/UB3LYP/6-31G(d)//UB3LYP/6-31G(d). [b] UB3LYP/6-31G(d). [c] ROMP2(FC)/6-311++G(3df,2p)//UB3LYP/6-31G(d) [d] UB2PLYP-D/aug-cc-pVDZ//UB3LYP/6-31G(d).

The identified transition states are displayed in **Figure 5.10**. All methods predict the lowest barrier for transfer of the hydrogen atom in α-position of the hydroxyl group to the nitrogen center. The chair-like 5-membered transition state is favored by ca. 11 kJ mol^{-1} over the alternative boat-shaped transition state with the large phenyl group in equatorial position.

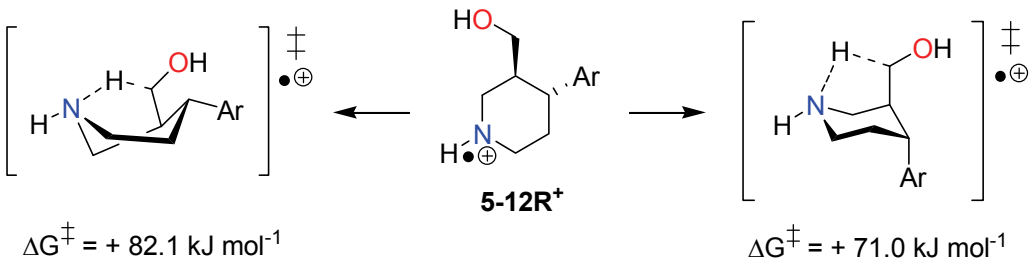

Scheme 5.8 Boat- vs. chair-like transition states for the N→C7-hydrogen atom transfer at G3(MP2)-RAD level of theory in the gas phase (Ar = *p*-F-C_6H_5).

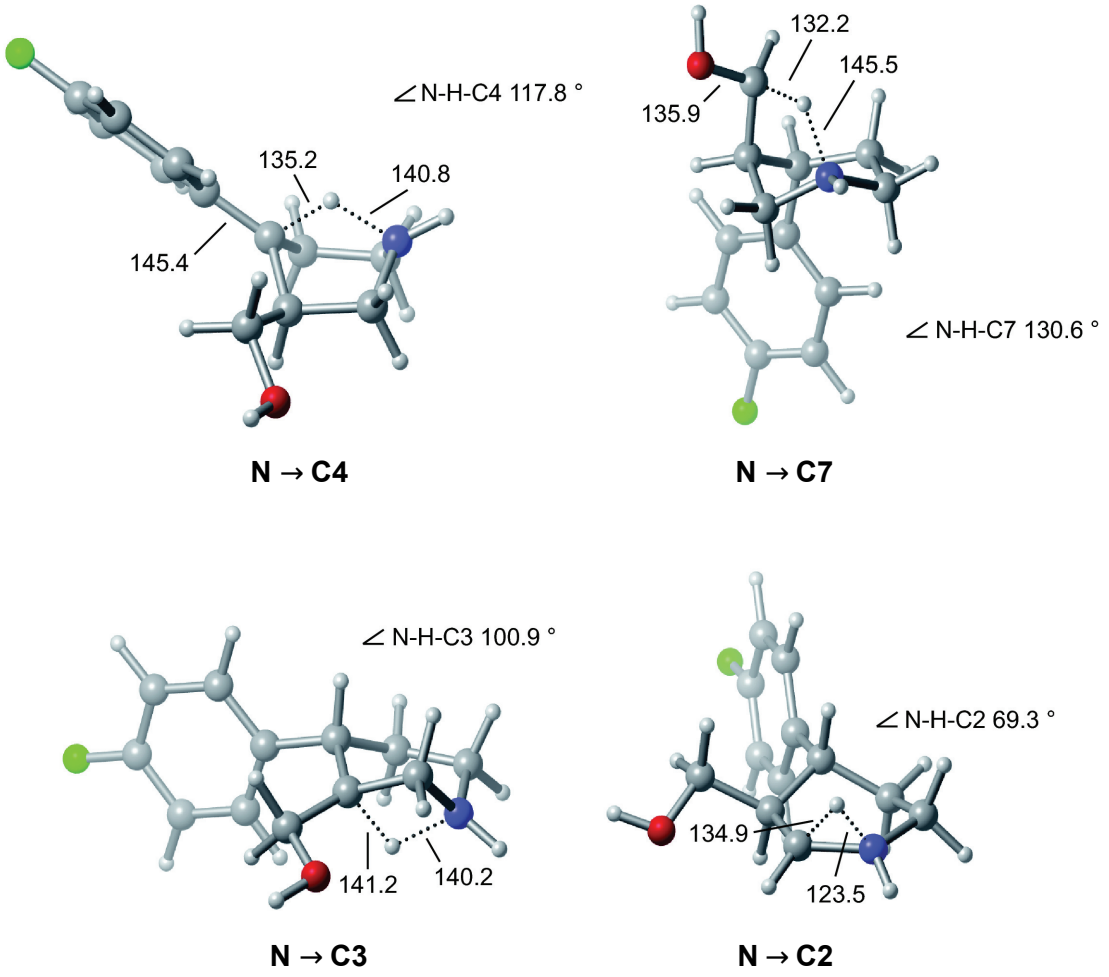

Figure 5.10 Graphical representation of the UB3LYP/6-31G(d) optimized transition states of the hydrogen atom transfer reactions for **5-12R⁺**. Distances are given in pm.

5.6.2 Water-assisted Pathways

For the correct description of open-shell systems in water the inclusion of specific solvent effects in either implicit or explicit form is mandatory. According to *Pliego*'s approach,[208] *Vrček* identified the most stable structures by varying the number of explicit water molecules (n = 0-3) and compared the resulting Gibbs energies of solvation.[204] He found that one water molecule added to **5-12R⁺** gives the most negative ΔG_{solv} and substantially lowers all examined barriers. The most suitable coordination site for H_2O was assigned upon *Mulliken* charge analysis for the most positively charged hydrogen atom and nearest proximity to the reaction centers.

Three different transfer modes have been examined theoretically and are depicted graphically in **Scheme 5.9**. In the spectator mode (TS_1) the water molecule has no influence on the transfer of the respective hydrogen atom to the electrophilic nitrogen center. However, in the shuttle (TS_2) or carrier mode (TS_3) the H_2O molecule facilitates the transfer in a cooperative way comparable to the well known histidine proton shuttle in proteins. The calculated Gibbs energies are collected in **Table 5.5** and shown graphically in **Figure 5.10**.

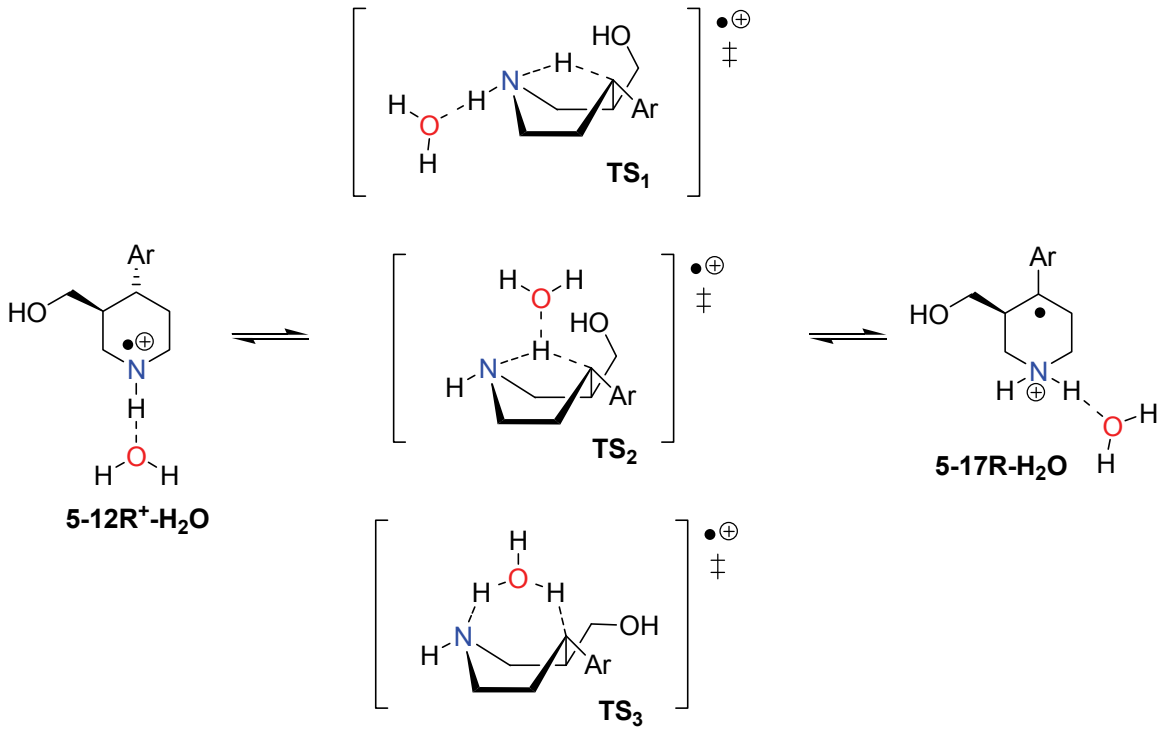

Scheme 5.9 Theoretically examined water-assisted transfer modes: spectator (TS_1), carrier (TS_2) and shuttle mode (TS_3).

Table 5.5 *Boltzmann*-averaged barriers and free reaction energies for water-assisted H-atom transfer of *N*-centered paroxetine metabolite **5-12R**$^{+}$ in the gas phase or in solution[a] (in kJ mol^{-1}, at 298.15 K and 1 atm, Ar = *p*-F-C_6H_5).

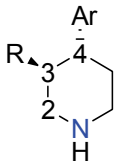

	UB3LYP[b]		ROMP2[c]		UB2PLYP[d]		G3(MP2)-RAD	
TS$_1$	<ΔG‡> **<ΔG$_{sol}^{‡}$>**	<ΔG> **<ΔG$_{sol}$>**	<ΔG‡> **<ΔG$_{sol}^{‡}$>**	<ΔG> **<ΔG$_{sol}$>**	<ΔG‡> **<ΔG$_{sol}^{‡}$>**	<ΔG> **<ΔG$_{sol}$>**	<ΔG‡> **<ΔG$_{sol}^{‡}$>**	<ΔG> **<ΔG$_{sol}$>**
N$^{+\bullet}$ → C2	+200.7 **+193.2**	+44.8 **+24.5**	+161.5 **+153.9**	+10.5 **-10.1**	+184.0 **+176.4**	+28.7 **+8.08**	+182.8 **+175.0**	+23.2 **+2.38**
N$^{+\bullet}$ → C3	+175.1 **+190.1**	+9.69 **+0.94**	+138.6 **+153.4**	-17.9 **-23.7**	+162.6 **+177.4**	-2.26 **-9.19**	+162.8 **+177.5**	-6.54 **-12.8**
N$^{+\bullet}$ → C4	+113.0 **+131.4**	-44.6 **-43.9**	+85.1 **+103.3**	-62.0 **-61.6**	+107.6 **+125.8**	-45.4 **-45.0**	+111.0 **+129.1**	-55.5 **-55.1**
TS$_2$	<ΔG‡> **<ΔG$_{sol}^{‡}$>**		<ΔG‡> **<ΔG$_{sol}^{‡}$>**		<ΔG‡> **<ΔG$_{sol}^{‡}$>**		<ΔG‡> **<ΔG$_{sol}^{‡}$>**	
N$^{+\bullet}$ → C2	+193.8 **+193.9**		+152.8 **+152.7**		+173.5 **+173.4**		+172.2 **+172.1**	
N$^{+\bullet}$ → C3	+172.2 **+172.3**		+147.2 **+147.2**		+164.0 **+164.0**		+163.7 **+163.5**	
N$^{+\bullet}$ → C4	+196.1 **+132.0**		+161.8 **+97.6**		+182.0 **+117.9**		+176.7 **+112.4**	
TS$_3$	<ΔG‡> **<ΔG$_{sol}^{‡}$>**		<ΔG‡> **<ΔG$_{sol}^{‡}$>**		<ΔG‡> **<ΔG$_{sol}^{‡}$>**		<ΔG‡> **<ΔG$_{sol}^{‡}$>**	
N$^{+\bullet}$ → C2	+205.0 **+121.2**		+176.5 **+92.6**		+192.7 **+108.7**		+195.6 **+111.5**	
N$^{+\bullet}$ → C3	+189.0 **+204.6**		+207.0 **+222.5**		+195.7 **+211.2**		+220.4 **+235.8**	
N$^{+\bullet}$ → C4	+136.5 **+147.0**		+123.5 **+133.9**		+132.6 **+142.9**		+156.6 **+166.8**	

[a] C-PCM/UAHF/UB3LYP/6-31G(d)//UB3LYP/6-31G(d). [b] UB3LYP/6-31G(d). [c] ROMP2(FC)/6-311+G(3df,2p)//UB3LYP/6-31G(d) [d] UB2PLYP-D/aug-cc-pVDZ//UB3LYP/6-31G(d).

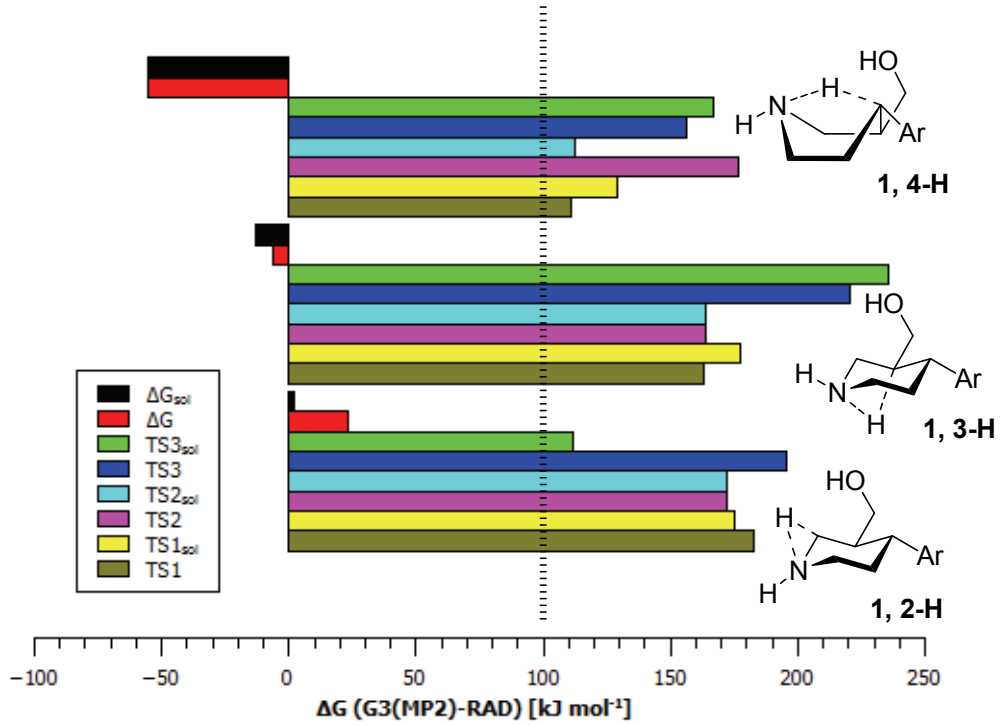

Figure 5.11 Graphical representation of the obtained barriers and reaction free energies at G3(MP2)-RAD level in gas phase and solution.

Again, the most exergonic pathway is that for the formation of C4-centered benzylic radical **5-17R** at G3(MP2)-RAD level (ΔG_{298} = -55.5 kJ mol^{-1}, ΔG_{sol} = -55.1 kJ mol^{-1}). Feasible barriers in solution with one explicit water molecule have been identified for the hydrogen transfer to yield either C2-centered radical **5-20R-H_2O** (carrier mode TS_3, $\Delta G^{\ddagger}_{sol}$ = +111.5 kJ mol^{-1}) or C4 radical **5-17R-H_2O** (shuttle mode TS_2, $\Delta G^{\ddagger}_{sol}$ = +112.4 kJ mol^{-1}). Nevertheless, the formation of C2 radical **5-20R-H_2O** can be neglected due to its endergonic free reaction energies (ΔG_{298} = +23.2 kJ mol^{-1}, ΔG_{sol} = +2.38 kJ mol^{-1}). The optimized transition states for the three modes to form radical **5-17R-H_2O** are shown in **Figure 5.12**.

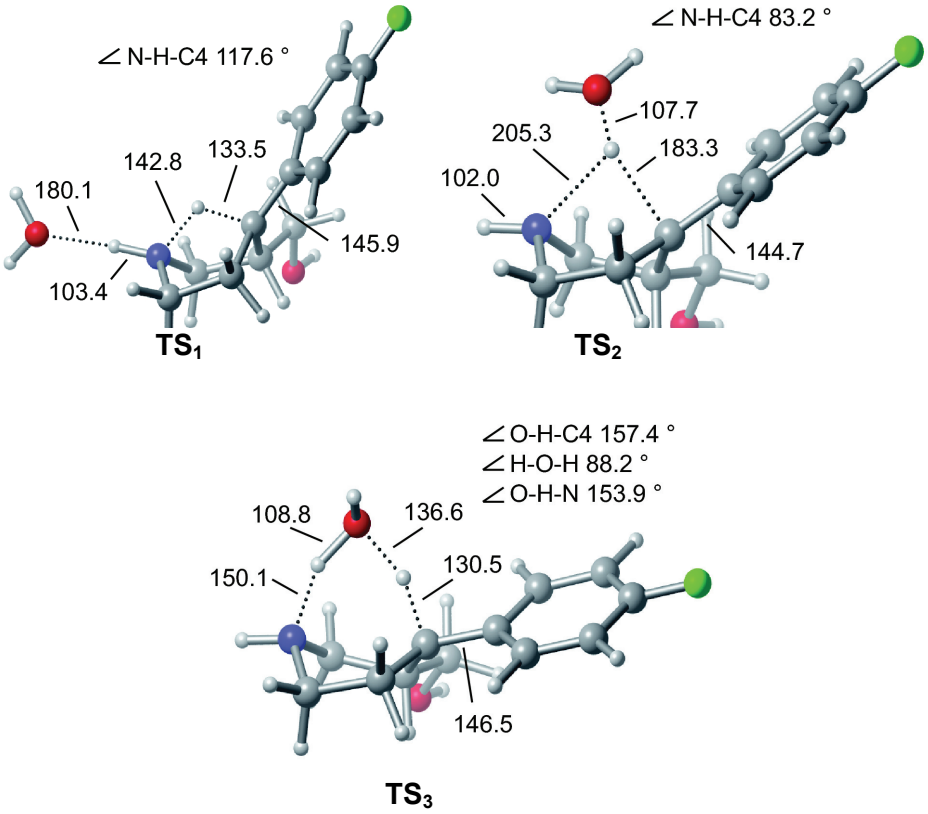

Figure 5.12 Graphical representation for the UB3LYP/6-31G(d) optimized transition states TS_1 (spectator mode), TS_2 (shuttle mode) and TS_3 (carrier mode) for the hydrogen atom transfer from position C4. Distances are given in pm.

5.7 Radical-induced Dehydration Pathways

As already shown in **Chapter 5.5** the C_α-H BDE with the very low value of +75.2 kJ mol^{-1} at G3(MP2)-RAD level of theory is a preferential point of attack for chemical transformations of paroxetine metabolite **5-12** upon excitation. As an alternative unimolecular pathway *N*-centered radical cation **5-12R$^+$** ican involve C_α-H cleavage, in which the hydrogen atom at C2 position will be transferred to the C7-hydroxy group to form the appropriate water leaving group. The resulting iminium radical **5-22R$^+$** can now either attack the phenyl ring nucleophilly to generate *Kwan*'s proposed tricycle **5-26R$^+$** ($\Delta G^{\ddagger}_{sol}$ = +72.9 kJ mol^{-1}) or forms allyl-stabilized radical cation **5-24R$^+$** via 1,2-H-shift ($\Delta G^{\ddagger}_{sol}$ = +76.9 kJ mol^{-1}). Radical **5-24R$^+$** represents the most exergonic product of all considered reaction pathways in solution (ΔG_{sol} = -102.3

kJ mol^{-1}) at G3(MP2)-RAD level in combination with explicit and implicit water solvation (**Figure 5.13**).

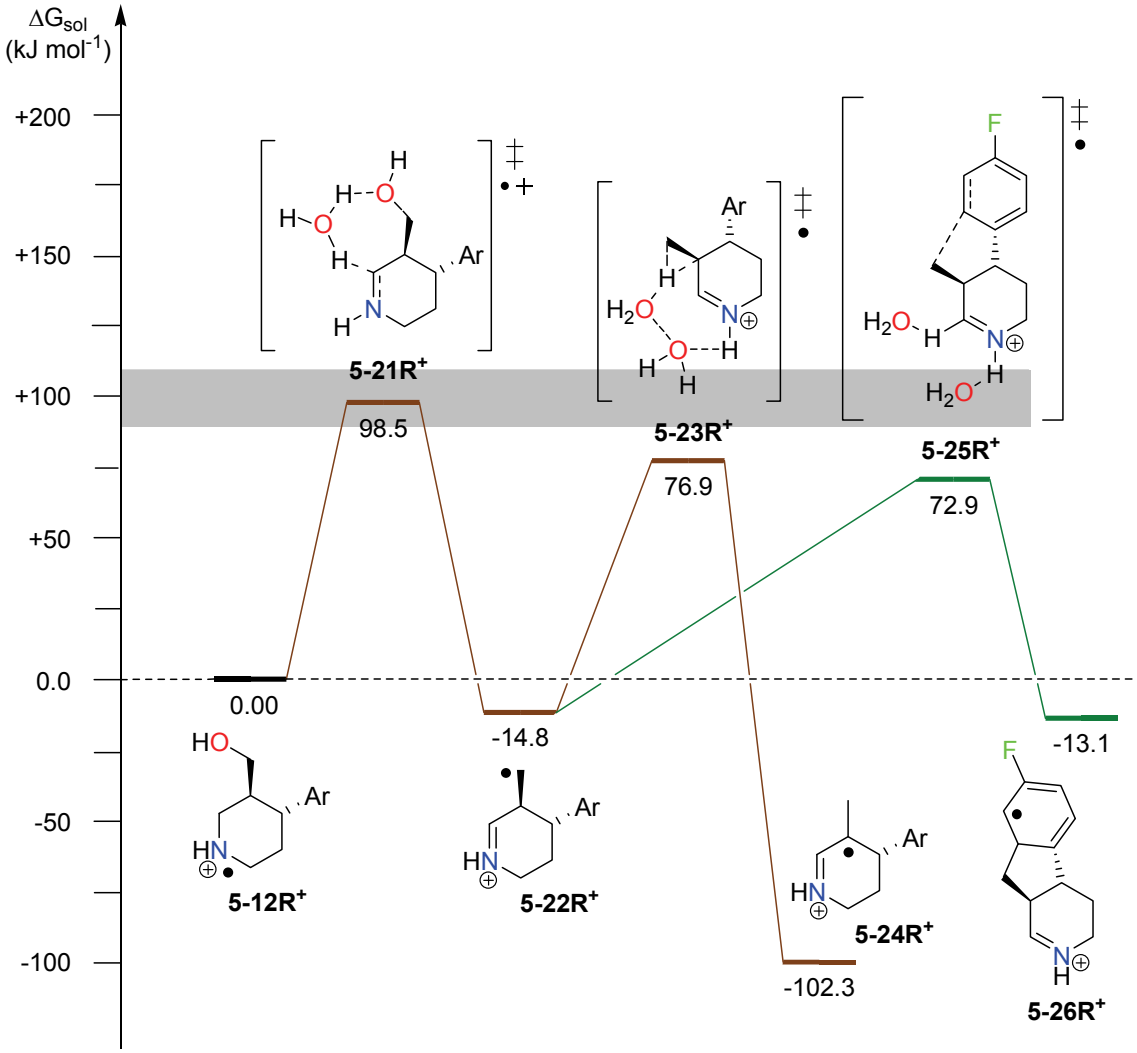

Figure 5.13 Schematic free energy profile in solution $\Delta G_{298} + \Delta G_{solv}$ (C-PCM/UAKS/UB3LYP/6-31G(d)) for dehydration of **5-12R**$^+$ (imine formation in brown, cyclodehydration formation in green) at G3(MP2)-RAD level of theory. Explicit water molecules have been omitted for clarity.[204]

The *Vrçek* group, who was responsible for the identification of these structures, studied additional pathways including the formation of bycyclic pyridines **5-30R** and **5-32R** or allyl radical **5-28R** starting from C4-centered radical **5-17R**.[204] Unfortunatelly, these reactions are unfeasible, because either the barrier is too high or endergonic products are formed (**Figure 5.14**).

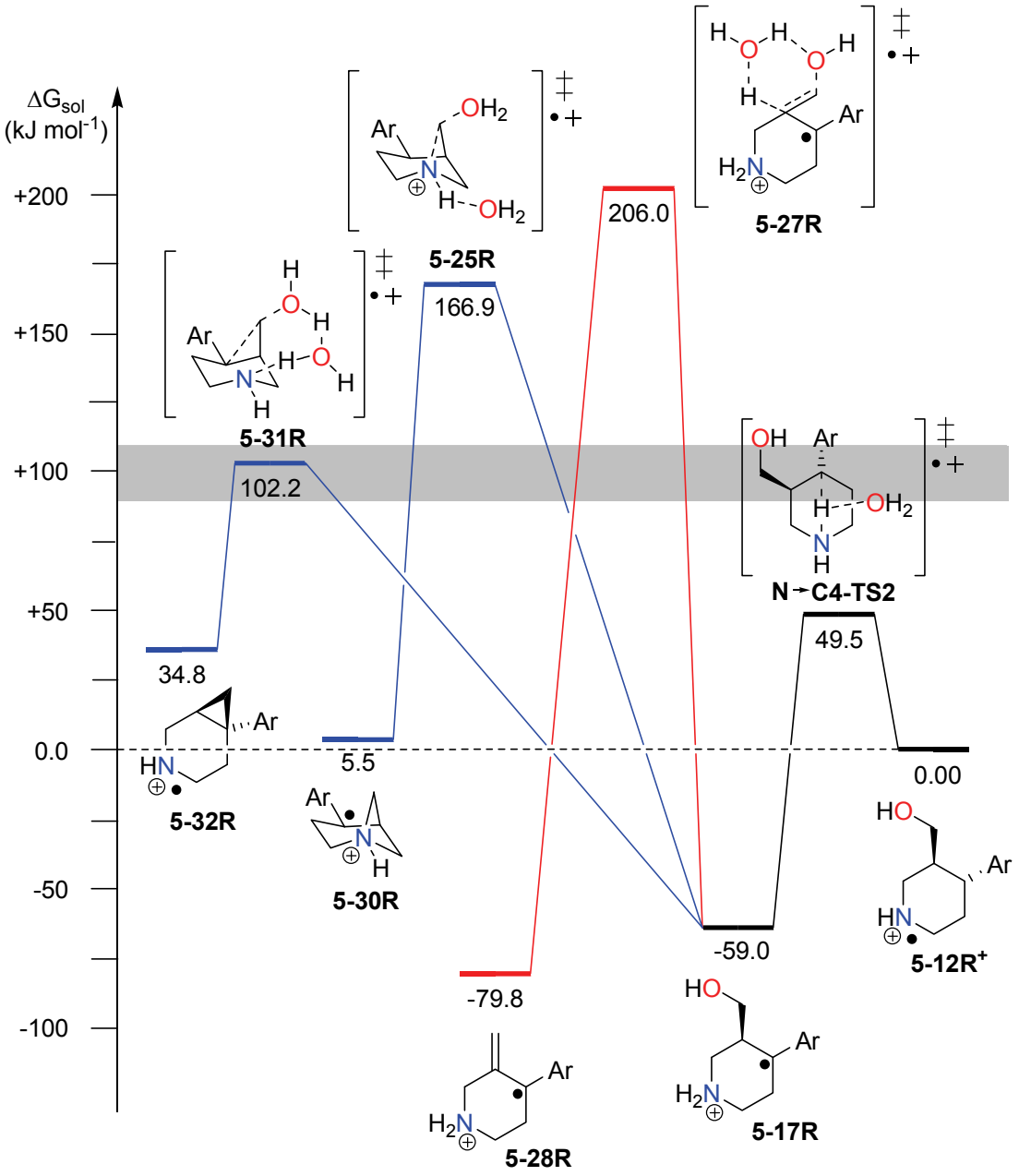

Figure 5.14 Schematic free energy profile in solution ΔG_{298} + ΔGsolv (C-PCM/UAKS/UB3LYP/6-31G(d)) for dehydration of **5-12R⁺** (alkene formation in red, three-membered ring formation in blue) at G3(MP2)-RAD level of theory. Explicit water molecules have been omitted for clarity.[204]

From a kinetic point of view the formation of imines **5-22R**, **5-24R** and the tricycle **5-26R** is favoured compared to alkene **5-28R** or bicyclic intermediates **5-30R** and **5-32R**. But the opposite is observed from the thermochemical standpoint.

In 2004 *Potáček* and coworkers examined the *N*-methyl derivative of paroxetine metabolite **5-12** for possible ionic elimination reactions and indeed were able to isolate under microwave irradiation in the presence of alumina or KF-alumina

mixtures of the two isomeric piperidyl alkenes **5-28a** and **5-28b**.[209] The existence of **5-28a**/**5-28b** has also been confirmed by applying electrospray ionization mass-spectrometry (ESI-MS).

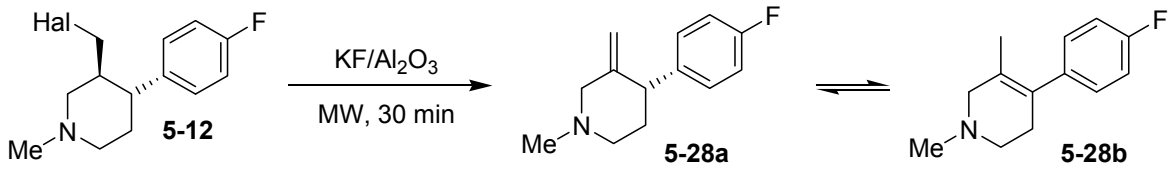

Scheme 5.10 Ionic elimination to **5-28a** according to *Potáček et al.*[209]

In order to complete this project considering not only kinetic but also thermodynamic stability, radical stabilization energies of all products are explored.

5.7.1 RSE of Hydrolysis Intermediates

Based on the computational results presented herein, a central position in the reaction cascade is occupied by the initial hydrogen atom transfer, which serves as the starting point for all outlined pathways. The stabilization energies for these intermediates at different levels of theory have been summarized in **Table 5.6**.

The benzylic radical **5-17R** is the most stable open-shell species with an RSE of -71.8 kJ mol^{-1} at G3(MP2)-RAD level among the four considered key intermediates for the dehydration process. Radical **5-19R** is a typical example of a stabilized tertiary radical and features an RSE of -21.1 kJ mol^{-1}, which is slightly decreased compared to the archetypical *tert*-butyl radical **5-34R** (RSE = -28.5 kJ mol^{-1}).[93] This is mainly the results of the presence of stereoelectronic interactions. The α-hydroxy substituted radical **5-18R**, for which the lowest barrier of its formation was found, is stabilized by -30.4 kJ mol^{-1}. The worst stabilization is found for open-shell species **5-20R** with the unpaired spin located in direct proximity to the positively charged ammonium group (RSE = -4.0 kJ mol^{-1} at G3(MP2)-RAD level of theory). In conclusion, oxygen-centered radical **5-33R**, which could be formed via a 6-membered transition state, cannot be considered as a likely intermediate due to its high O-H dissociation energy of +461.6 kJ mol^{-1} as compared to the less stabilized radical **5-20R** (BDE = +435.3 kJ mol^{-1}).

Table 5.6 Theoretical *Boltzmann*-averaged radical stabilization energies of *C*-centered radicals (in kJ mol^{-1}, Ar = *p*-F-C_6H_5).

R•	UB3LYP[a]	ROMP2[b]	G3(MP2)-RAD	BDE[c]
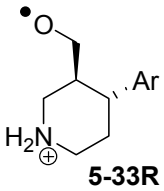 **5-33R**	-42.29	-27.84	-35.53	+461.6
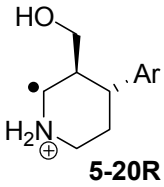 **5-20R**	-19.76	-2.09	-4.04	+435.3
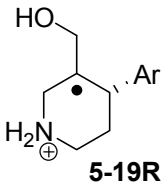 **5-19R**	-41.96	-18.16	-21.13	+418.2
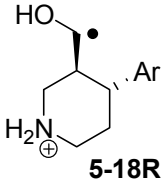 **5-18R**	-46.72	-29.28	-30.38	+408.9
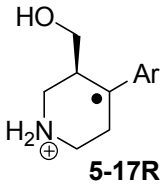 **5-17R**	-98.63	-64.03	-71.76	+367.5

[a] UB3LYP/6-31G(d). [b] ROMP2(FC)/6-311+G(3df,2p)//UB3LYP/6-31G(d). [c] BDE (R-H) = RSE (R•) + BDE (Ref), BDE(CH_4) = +439.3, BDE (H_2O) = +497.1 kJ mol^{-1}.[115]

The role of benzyl radical **5-17R** as key intermediate of *Vrçek*'s reaction pathways is confirmed here, since it displays the overall most stable open-shell species compared to all *C*-centered and aminyl radicals (see **Figure 5.15**).

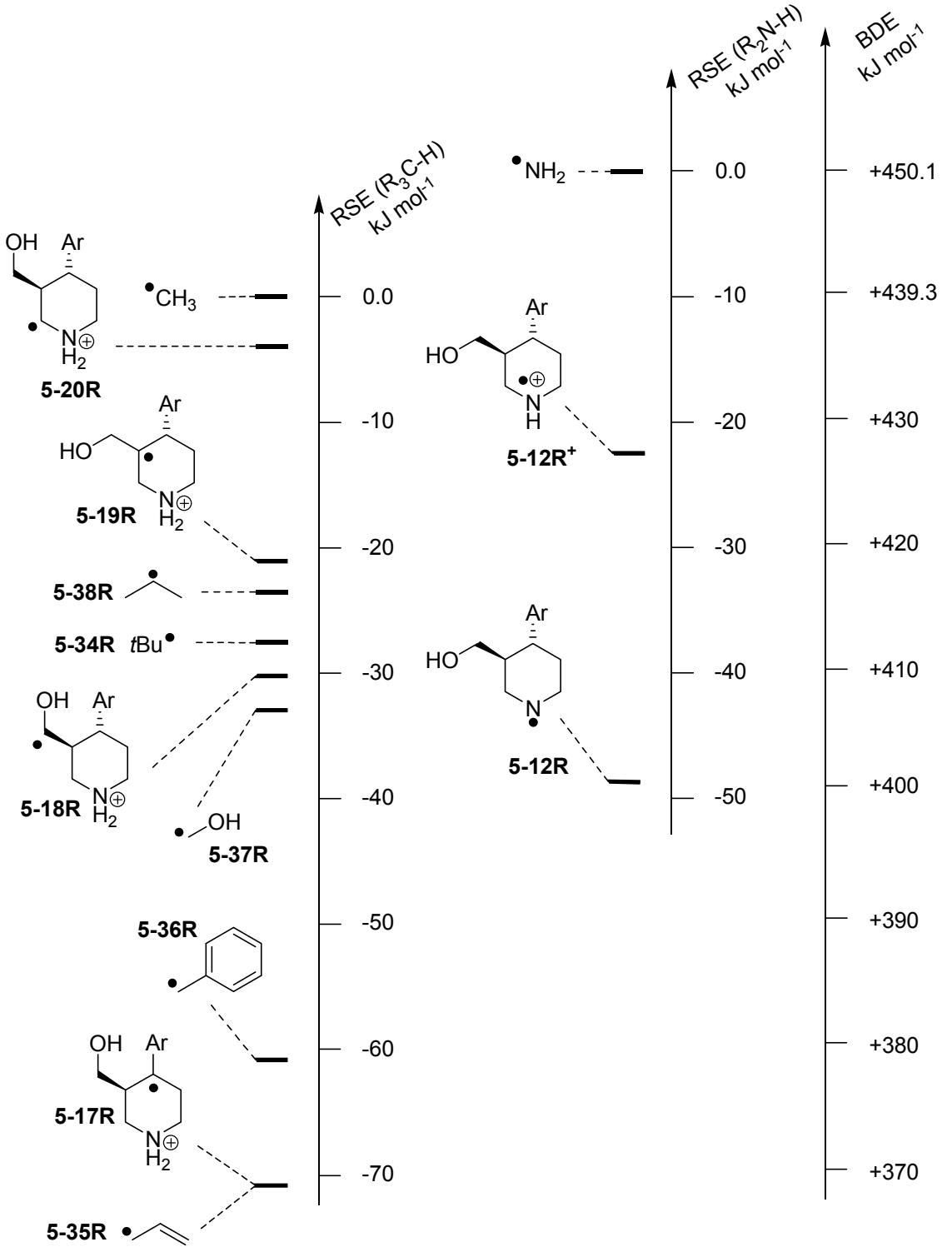

Figure 5.15 RSE and BDE values of a variety of *C*- and *N*-centered radicals in the gas phase (G3(MP2)-RAD, in kJ mol^{-1}).[93]

5.7.2 RSE of Dehydration Products

What all reaction products of this survey have in common are, that they mainly belong to the class of trisubstituted benzyl radicals. The effect of the electron-withdrawing fluoro substituent in *para* position of the phenyl ring is small and lowers the RSE by about 2 kJ mol^{-1} compared to the dimethyl benzyl radical **5-40R**. This incidence is known for *para* substituted benzyl radicals and is indicated by smaller spin densities at the benzylic position (**5-40R**: 0.751, **5-17R**: 0.734, **5-30R**: 0.713). Interestingly, allylic radical **5-39R** shows the same stability compared to *Kwon*'s postulated tricycle **5-13R**[200] (see **Figure 5.16**).

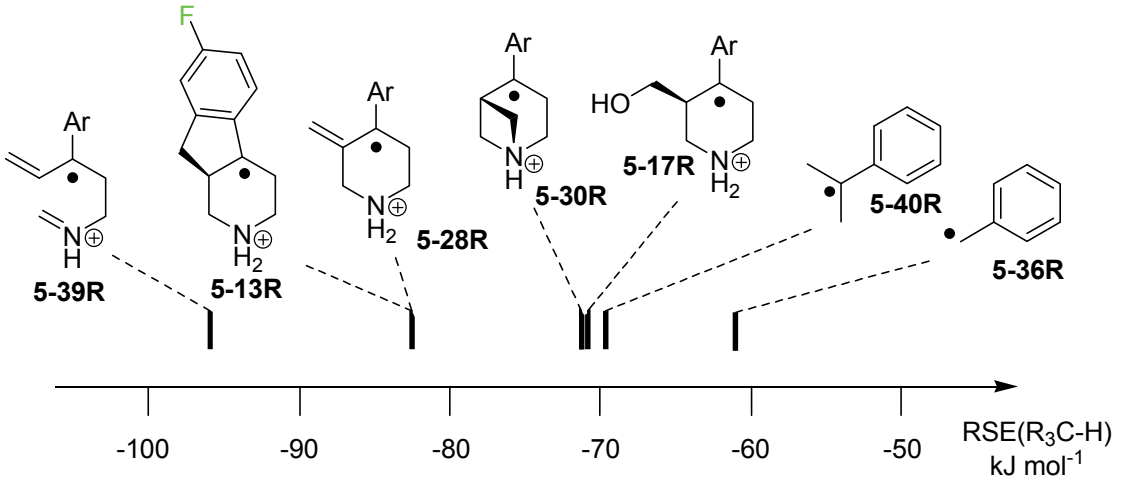

Figure 5.16 *Boltzmann*-averaged RSE of benzylic radicals at G3(MP2)-RAD level in the gas phase (in kJ mol^{-1}).

The stabilization energies for all, in principle, feasible *C*-centered radicals considered by *Vrçek* are depicted in **Table 5.7**.

Table 5.7 Theoretical *Boltzmann*-averaged radical stabilization energies of *C*-centered radicals (in kJ mol^{-1}, Ar = *p*-F-C_6H_5).

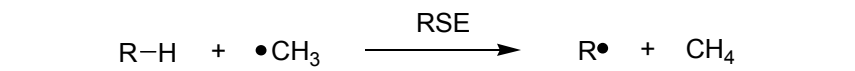

R•	UB3LYP[a]	ROMP2[b]	G3(MP2)-RAD	BDE[c]
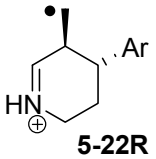 **5-22R**	-15.20	+0.95	-0.87	+438.4
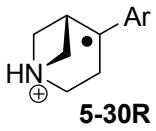 **5-30R**	-96.35	-63.27	-70.79	+368.5
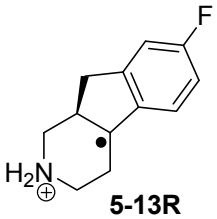 **5-13R**	-109.29	-76.64	-82.35	+356.9
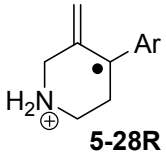 **5-28R**	-111.65	-79.56	-82.54	+356.8
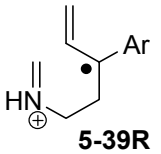 **5-39R**	-134.62	-94.26	-95.74	+343.6
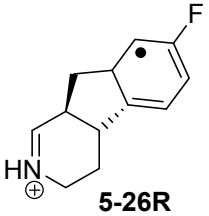 **5-26R**	-117.47	-101.61	-97.03	+342.3
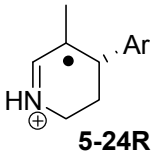 **5-24R**	-132.87	-101.99	-100.14	+339.2

[a] UB3LYP/6-31G(d). [b] ROMP2(FC)/6-311+G(3df,2p)//UB3LYP/6-31G(d). [c] BDE (R-H) = RSE (R•) + BDE (CH_4), BDE(CH_4) = +439.3 kJ mol^{-1}.[115]

It is known in the literature, that protonated aminyl radicals undergo fragmentation if highly stabilized radicals are formed.[185] Under these circumstances, allyl radical

5-39R is generated as dehydration product, which is characterized by the largest radical stabilization of all benzyl radicals. Unfortunately, all attempts to find a reaction pathway to its formation, particularly the proton transfer from the ammonium to the hydroxyl group, was not found by DFT theory (UB3LYP/6-31G(d)). Nevertheless, optimization of intermediate **5-17R** led to the instantaneous elimination of water and **5-39R**.

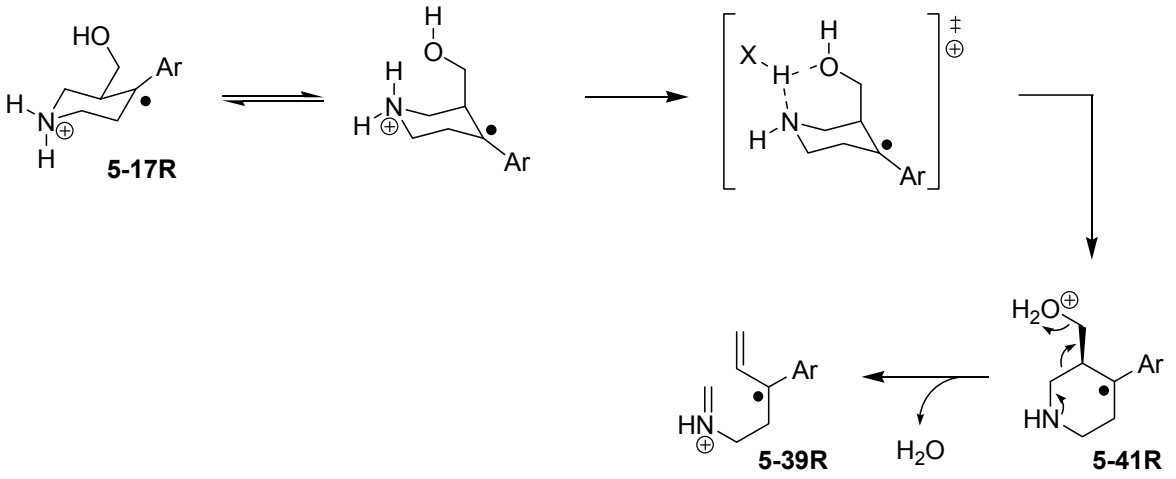

Scheme 5.11 Proposed mechanism of the formation of allyl benzyl radical **5-39R**.

The piperidinium radical **5-22R** located on the pathway for the cyclization to **5-26R** represents a very reactive primary radical as indicated by an almost thermoneutral stabilization of -0.9 kJ mol^{-1} in the gas phase. The probability to handle this reactivity by the subsequent [1,2-H] migration to form heteroallylic **5-24R** or cyclization to **5-26R** is verified by its low RSE and barriers. Similar results are found for the biologically important adenosyl radical (**5-42R**), which either undergoes cyclization to open-shell 8,5'-anhydroadenosine (**5-43R**) or hydrogen transfer to 5'-desoxyadenosine (**5-44**).[210]

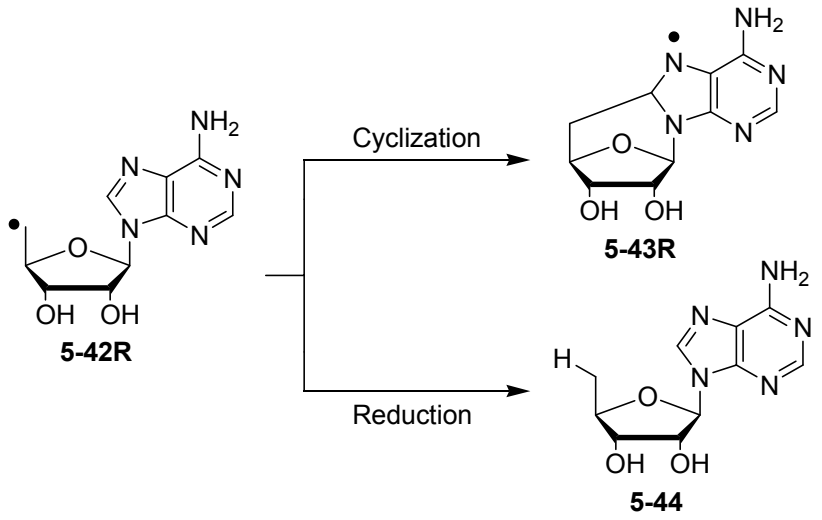

Scheme 5.12 Possible reactions of 5'-adenosyl radical **5-42R**.

Heteroallyl radical **5-24R** is the most stable among all reaction products either on enthalpic or on kinetic scale with an RSE value of -100.1 kJ mol^{-1}. The protonation state has almost no influence on the radical stabilization energy as indicated in **Figure 5.17** with the more simple iminyl radicals **5-46R** and **5-46R$^+$**. Similarly, the spin densities as indicators for delocalization are not changed.

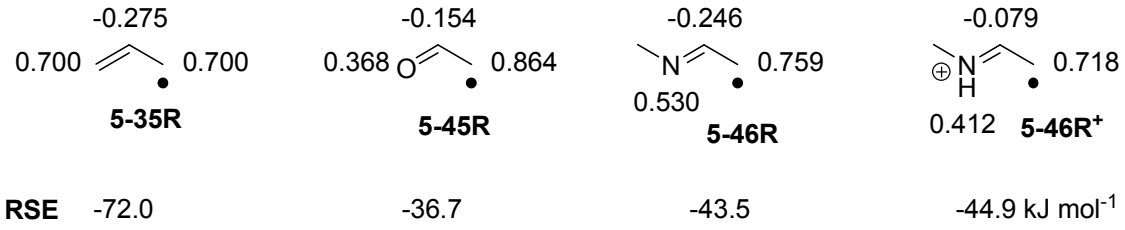

Figure 5.17 Mulliken spin densities and RSEs at G3(MP2)-RAD level (in kJ mol^{-1}).[93]

The influence of the substitution pattern of delocalized aminyl radical **5-46R** and **5-46R$^+$** has been examined carefully by simple addition of methyl groups. The comparison with the isolelectronic all-carbon derivatives are depicted in **Figure 5.18**.

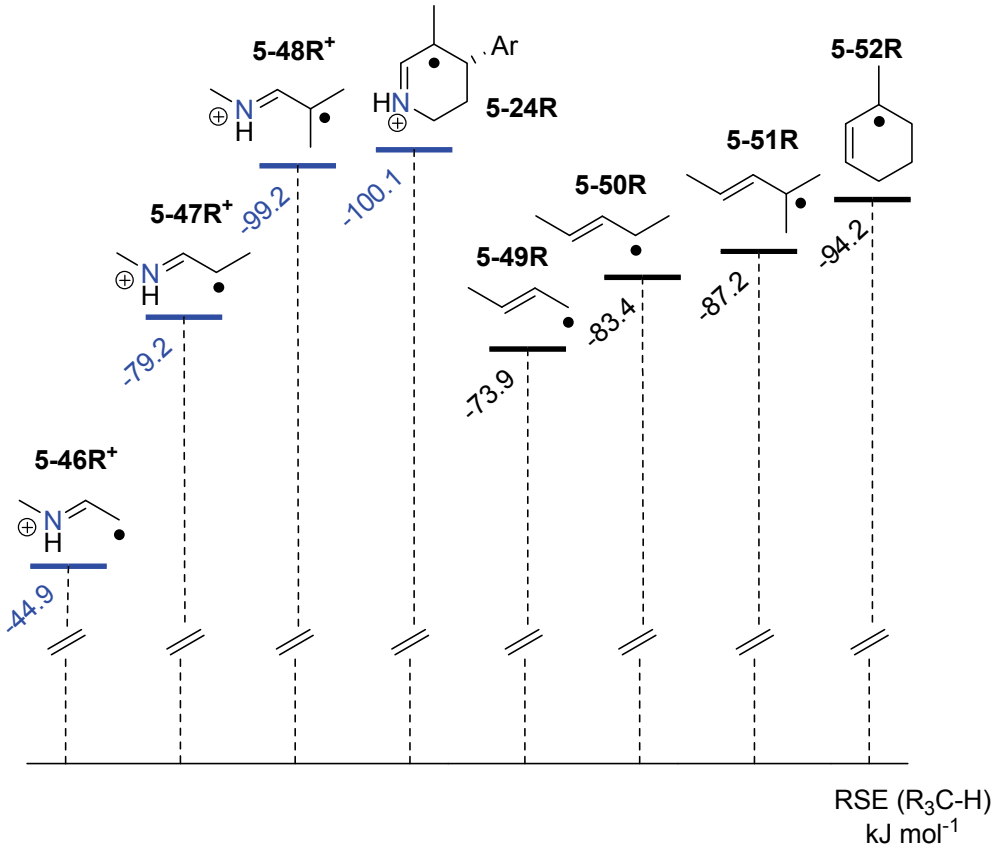

Figure 5.18 Saturation behavior of multiply substituted *C*-centered radicals at G3(MP2)-RAD level.[93]

One notices immediately, that the stabilities of the four respective systems are not equally spaced. The enthalpy differences are significantly larger for the more electrophilic nitrogen containing radicals than the allylic counterparts. This behavior of saturation can be observed by repeated addition of the same residue both with simple alkyl and more strongly interacting substituents[211]. The influence of the ring conformation is negligible upon replacement of a CH with an NH^+ group.

5.8 Conclusion

The accumulation of pharmaceutically active compounds in waste or drinking water is of growing importance for the world's population. Therefore, quantum chemical calculations have been used to evaluate the chemical properties and possible reaction channels of open-shell piperidine **5-12R⁺,** which is considered to be the key intermediate in the environmental (photo)degradation of paroxetine (**5-7**). This

included, for example, bond dissociation energies, hydrogen atom transfer reactions and radical-induced dehydrations.

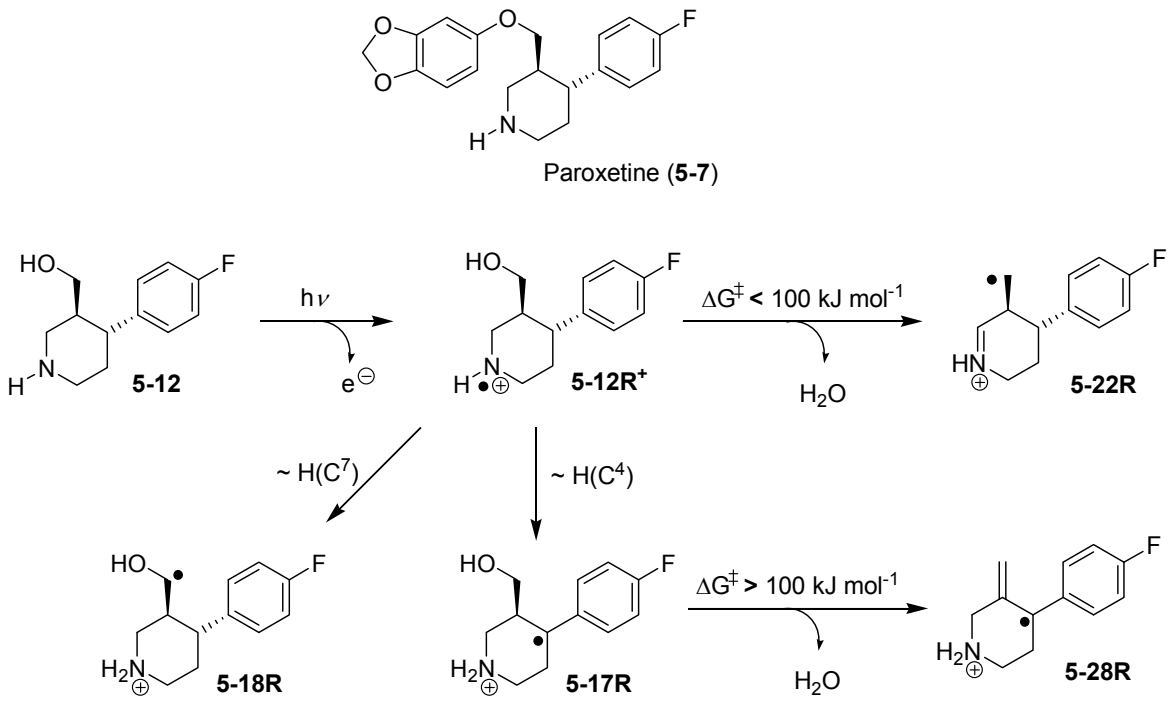

Scheme 5.13 Exemplary reaction pathways of the hydrolysis product **5-12** of paroxetine (**5-7**) upon photolysis.

Considering the hydrogen atom transfer, the [1,4]-H shift to yield **5-17R** is the most favorable pathway if a cluster continuum model with water as solvent and reagent is included. In the gas phase without explicit solvation the formation of α-hydroxy radical **5-18R** is preferred.

The unpaired spin at the nitrogen atom has a significant impact on the bond strength of the α-CH bond, which is decreased dramatically and opens a dehydration pathway never considered before with iminium radical **5-22R** as intermediate.

Table 5.8 Theoretical obtained bond dissociation energies (G3(MP2)-RAD level) in the gas phase for varies piperidines

	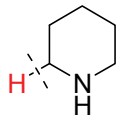 **5-14**	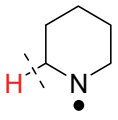 **5-14R**	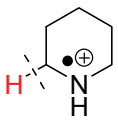 **5-14R$^+$**	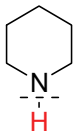 **5-14**	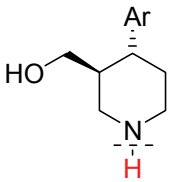 **5-12**	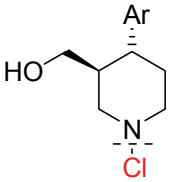 **5-12Cl**
BDE (kJ mol^{-1})	+390.5	+95.1	+75.2	+403.4	+401.7	+247.2

In addition, the stability of different dehydrated product radicals has been evaluated to support the existence of proposed reaction products even on a thermochemical scale.

For structures **5-28R** and **5-30R** the experimentally observed reaction barrier of around +100 kJ mol^{-1} is exceeded, but nevertheless it has to be noted that the formation of **5-28** has already been proven and most likely proceeds without the intermediacy of free radicals. *Kwon*'s tricyclic piperidine **5-13** and the newly proposed enamine **5-24** are up to now the most relevant intermediates to be formed in the (photo)degradation either from the kinetic or the thermochemical point of view.

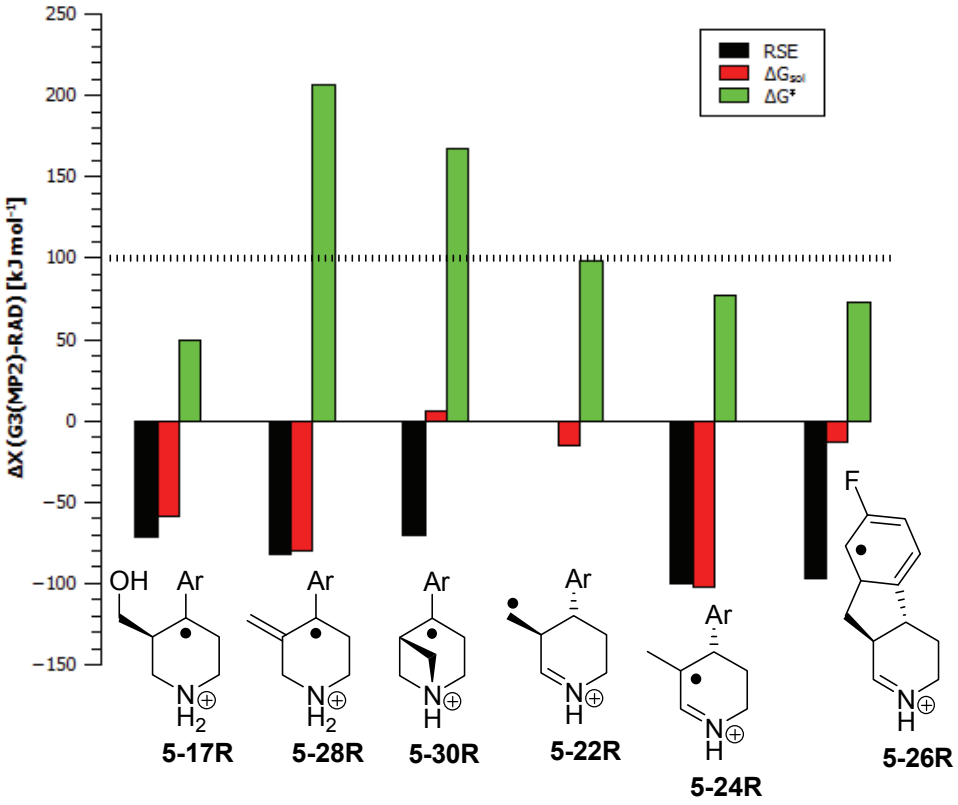

Figure 5.19 Comparison of barriers, reaction free energies and radical stabilities.

5.9 Theoretical Appendix

Geometry optimizations of all systems have been performed at the (U)B3LYP/ 6-31G(d) level of theory. Thermochemical corrections to 298.15 K have been calculated at the same level of theory using the rigid rotor/harmonic oscillator model. A scaling factor of 0.9806 has been used for this latter part. Single point energies have then been calculated at different levels of theory, including the (RO)MP2(FC)/ 6-311+G(3df,2p) and (U)B2PLYP-D/aug-cc-pVDZ level. Combination of these total energies with thermochemical corrections obtained at B3LYP level yield the enthalpies termed as "MP2" or “B2PLYP” in the text:

$$H(HL) = E_{tot}(HL) + H(B3LYP, 0.9806) - E_{tot}(B3LYP) \qquad \textbf{(eq. 5.1)}$$

Improved relative energies are obtained using the G3(MP2)-RAD scheme proposed by *Radom et al.*[81] These are based on the same geometries and thermal corrections as the MP2 level:

$$E_{tot}(G3(MP2)\text{-}RAD) = E_{tot}((U)CCSD(T)/6\text{-}31G(d)//UB3LYP/6\text{-}31G(d) + \\ + DE(G3MP2large) + DE(HLC) \qquad \textbf{(eq. 5.2)}$$

$$DE(G3MP2large) = (RO)MP2(FC)/G3MP2large - (RO)MP2(FC)/6\text{-}31G(d) \qquad \textbf{(eq. 5.3)}$$

$$DE(HLC) = -A\, n(\beta) - B\,(n(\alpha) - n(\beta)) \qquad \textbf{(eq.5.4)}$$

with A = 9.413×10^{-3} au, B = 3.969×10^{-3} au and n(α) and n(β) represent the valence electrons, respectively. Finally, enthalpies are averaged by the *Boltzmann* method:

$$w_i = \exp\left(\frac{-\Delta H_{298}}{R\,T}\right) \Big/ \sum_{i=1}^{n} \frac{-\Delta H_{298}}{R\,T}$$

$$\langle H_{298} \rangle = \sum_{i=1}^{n} w_i H_i \qquad \textbf{(eq. 5.5)}$$

Additional consideration of solvation was included by calculating free energies using the polarizable continuum solvation model in its C-PCM[119] or SMD[60] variant and adding them to the gas phase enthalpies. (U)CCSD(T) calculations have been

performed with *MOLPRO*,[84] the geometry optimizations, frequencies and C-PCM calculations with *Gaussian03* Rev. D.01.[85] The SMD model is implemented in *Gaussian09* Rev. C.01.[86]

Table 5.9 Energies and enthalpies of studied compounds (closed- and open-shell) at various levels of theory in the gas phase in Hartree (298.15 K, 1 atm).

	E_{tot}(B3LYP)	**H_{298}(B3LYP)**	E_{tot}(MP2)	E_{tot}(G3(MP2)-RAD)
CH_4	-40.5183890	**-40.470240**	-40.4055437	-40.4651605
$\bullet CH_3$	-39.8382922	**-39.804975**	-39.7316815	-39.7851922
NH_3	-56.5479476	**-56.510271**	-56.4504323	-56.5036014
$\bullet NH_2$	-55.8726187	**-55.850247**	-55.7686657	-55.8192957
NH_2Cl	-516.1034330	**-516.073561**	-515.5082404	-515.6084632
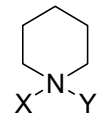	E_{tot}(B3LYP)	**H_{298}(B3LYP)**	E_{tot}(MP2)	E_{tot}(G3(MP2)-RAD)
X = H (**5-14**)	-251.9043988	**-251.740953**	-251.3373000	-251.5876572
X = • (**5-14R**)	-251.2503261	**-251.100813**	-250.6735196	-250.9225046
X, Y = H (**5-14H**)	-252.2859532	**-252.107338**	-251.7102525	-251.9636606
X = H, Y = • (**5-14R$^+$**)	-251.6243289	**-251.461735**	-251.0364096	-251.2893059
X = Cl (**5-14Cl**)	-711.4700162	**-711.315399**	-710.4148056	-710.7088087
X = H, Y = Cl (**5-14ClH**)	-711.8264093	**-711.657573**	-710.7663371	-711.0626184
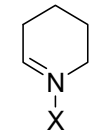	E_{tot}(B3LYP)	**H_{298}(B3LYP)**	E_{tot}(MP2)	E_{tot}(G3(MP2)-RAD)
X = / (**5-53**)	-250.6879270	**-250.548845**	-250.1275807	-250.3643284
X = H (**5-53H**)	-251.0687400	**-250.915636**	-250.4993520	-250.7396565
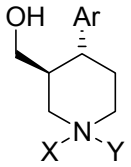	E_{tot}(B3LYP)	**H_{298}(B3LYP)**	E_{tot}(MP2)	E_{tot}(G3(MP2)-RAD)
X = H (**5-12**) 1	-696.7047170	**-696.429590**	-695.3578394	-695.8880547
2	-696.7052976	**-696.429916**	-695.3589258	-695.8890284
3	-696.7053907	**-696.430212**	-695.3593569	-695.8894093
4	-696.7058900	**-696.430492**	-695.3603363	-695.8902106
5	-696.69181855	**-696.416383**	-695.3453579	-695.8762566
6	-696.6982159	**-696.422306**	-695.3502836	-695.8810932
7	-696.6965504	**-696.421012**	-695.3502359	-695.8810534
8	-696.6980953	**-696.422529**	-695.3524956	-695.8831429
9	-696.7059898	**-696.429713**	-695.3571829	-695.8873961

Table 5.10 Energies and enthalpies of studied compounds (closed- and open-shell) at various levels of theory in the gas phase in Hartree (298.15 K, 1 atm).

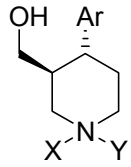	E_{tot}(B3LYP)	**H_{298}(B3LYP)**	E_{tot}(MP2)	E_{tot}(G3(MP2)-RAD)
X, Y = H (**5-12H**) 1	-697.0973763	**-696.806475**	-695.7400695	-696.2729667
3	-697.0796011	**-696.789152**	-695.7244486	-696.2578215
4	-697.0904568	**-696.800185**	-695.7339445	-696.2671066
X = Cl (**5-12Cl**) 1	-1156.2701199	**-1156.003759**	-1154.4363418	-1155.0098548
2	-1156.2640590	**-1155.997352**	-1154.4310511	-1155.0050468
3	-1156.26877040	**-1156.001610**	-1154.4334001	-1155.0069384
X = • (**5-12R**) 1	-696.0521673	**-695.790747**	-694.6966258	-695.2252238
2	-696.0416065	**-695.780204**	-694.6850463	-695.2144278
3	-696.0510773	**-695.789096**	-694.6922163	-695.2213836
X = •, Y = H (**5-12R$^+$**) 1	-696.4344588	**-696.160120**	-695.0609196	-695.5939959
2	-696.4364562	**-696.161715**	-695.0631977	-695.5966076
3	-696.4300297	**-696.155932**	-695.0518066	-695.5860462
4	-696.4312302	**-696.157060**	-695.0594352	-695.5925036
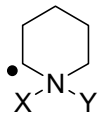	E_{tot}(B3LYP)	**H_{298}(B3LYP)**	E_{tot}(MP2)	E_{tot}(G3(MP2)-RAD)
X = H (**5-54R**)	-251.2501181	**-251.099965**	-250.6832114	-250.9278106
X, Y = H (**5-54R$^+$**)	-251.6113195	**-251.447570**	-251.0358414	-251.2836958
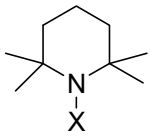	E_{tot}(B3LYP)	**H_{298}(B3LYP)**	E_{tot}(MP2)	E_{tot}(G3(MP2)-RAD)
X = H (**5-15**)	-409.1596691	**-408.881243**	-408.2301409	-408.6488242
X = • (**5-15R**)	-408.5056768	**-408.240617**	-407.5652418	-407.9828487
	E_{tot}(B3LYP)	**H_{298}(B3LYP)**	E_{tot}(MP2)	E_{tot}(G3(MP2)-RAD)
X = H (**5-16**)	-135.1628504	**-135.066310**	-134.8608089	-134.9999147
X = • (**5-16R**)	-134.5094855	**-134.427626**	-134.1990378	-134.3362540
 (**5-55**)	-133.9423365	**-133.870244**	-133.6497130	-133.7754365

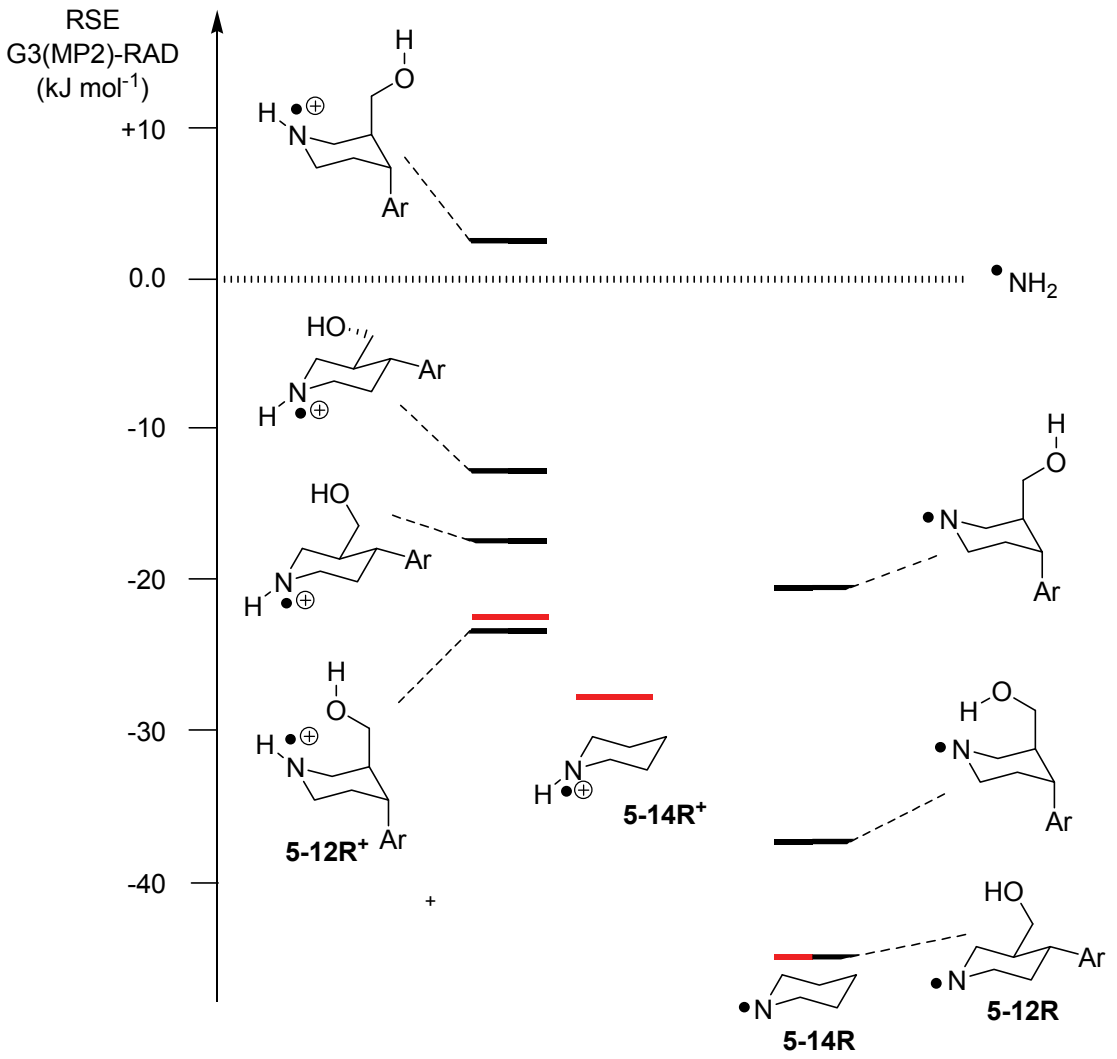

Figure 5.20 Conformational dependence of the radical stability of **5-12** and **5-14** in their neutral and protonated forms (Ar = *p*-F-C_6H_5). Red bars represent *Boltzmann*-averaged values.

Table 5.11 Total and Gibbs free energies at various levels of theory for the calculation of pK_a values in aqueous media in Hartree (SMD/HF = SMD/HF/6-31G(d)//B3LYP/6-31G(d)).

	E_{tot}(B3LYP) **G_{298}(B3LYP)**	E_{tot}(CCSD(T))	E_{tot}(MP2)	E_{tot}(G3(MP2)-RAD)	ΔG_{solv} (SMD/HF)
H_2O	-76.4089533 **-76.405863**	-76.2078377	-76.3181017	-76.3633998	–0.0149002
H_3O^+	-76.6890842 **-76.673565**	-76.4874515	-76.5888203	-76.6360307	–0.1534321
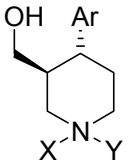	E_{tot}(B3LYP) **G_{298}(B3LYP)**	E_{tot}(CCSD(T))	E_{tot}(MP2)	E_{tot}(G3(MP2)-RAD)	ΔG_{solv} (SMD/HF)
X = H (**5-12**) 1	-696.7047170 **-696.485403**	-694.6929141	-695.3578394	-695.8880547	-0.0202388
2	-696.7052976 **-696.485561**	-694.6942974	-695.3589258	-695.8890284	-0.0196013
3	-696.7053907 **-696.485834**	-694.6937394	-695.3593569	-695.8894093	-0.0183583
4	-696.7058900 **-696.485973**	-694.6950801	-695.3603363	-695.8902106	-0.0173384
5	-696.69181855 **-696.471530**	-694.6804747	-695.3453579	-695.8762566	-0.0197925
6	-696.6982159 **-696.476783**	-694.6872663	-695.3502836	-695.8810932	-0.0182468
7	-696.6965504 **-696.476032**	-694.6852116	-695.3502359	-695.8810534	-0.0213383
8	-696.6980953 **-696.477606**	-694.6871978	-695.3524956	-695.8831429	-0.0171631
9	-696.7059898 **-696.483142**	-694.6952591	-695.3571829	-695.8873961	-0.0142309
X, Y = H (**5-12H**) 1	-697.0973763 **-696.860408**	-695.0869582	-695.7400695	-696.2729667	-0.0946281
3	-697.0796011 **-696.844746**	-695.0684628	-695.7244486	-696.2578215	-0.1102614
4	-697.0904568 **-696.856005**	-695.0793122	-695.7339445	-696.2671066	-0.1064845

Table 5.12 Total and Gibbs ree energies at various levels of theory for the calculation of pK_a values in aqueous media in Hartree (SMD/HF = SMD/(U)HF/6-31G(d)//(U)B3LYP/6-31G(d)).

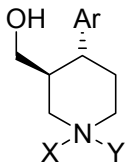	E_{tot}(B3LYP) **G_{298}(B3LYP)**	E_{tot}(CCSD(T))	E_{tot}(MP2)	E_{tot}(G3(MP2)-RAD)	ΔG_{solv} (SMD/HF)
X = • (**5-12R**) 1	-696.0521673 **-695.847245**	-694.0519473	-694.6966258	-695.2252238	-0.0236172
2	-696.0416065 **-695.836191**	-694.0411763	-694.6850463	-695.2144278	-0.0244618
3	-696.0510773 **-695.843391**	-694.0504012	-694.6922163	-695.2213836	-0.0152348
X = H, Y = • (**5-12R$^+$**) 1	-696.4344588 **-696.216665**	-694.4248535	-695.0609196	-695.5939959	-0.1049228
2	-696.4364562 **-696.217042**	-694.4285135	-695.0631977	-695.5966076	-0.0961102
3	-696.4300297 **-696.212552**	-694.4151135	-695.0518066	-695.5860462	-0.1088749
4	-696.4312302 **-696.213835**	-694.4228363	-695.0594352	-695.5925036	-0.1053690
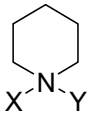	E_{tot}(B3LYP) **G_{298}(B3LYP)**	E_{tot}(CCSD(T))	E_{tot}(MP2)	E_{tot}(G3(MP2)-RAD)	ΔG_{solv} (SMD/HF)
X = H (**5-14**)	-251.9043988 **-251.776169**	-251.0941830	-251.3373000	-251.5876572	-0.0060397
X, Y = H (**5-14H**)	-252.2859532 **-252.142928**	-251.4765055	-251.7102525	-251.9636606	-0.0996320
X = • (**5-14R**)	-251.2503263 **-251.136930**	-250.4510442	-250.6735352	-250.9225045	-0.0124142
X = •, Y = H (**5-14R$^+$**)	-251.6243289 **-251.498203**	-250.8202743	-251.0364096	-251.2893059	-0.0997117

Table 5.13 Total and Gibbs free energies at various levels of theory in Hartree (298.15 K, 1 atm, CPCM/UB3LYP = C-PCM/UAHF/UB3LYP/6-31G(d)//UB3LYP/6-31G(d)).

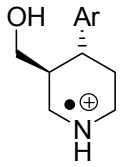	E_{tot}(UB3LYP) **G_{298}(UB3LYP)**	E_{tot}(ROMP2)	E_{tot} (UB2LPYP)	E_{tot} (G3(MP2)-RAD)	G_{solv} (CPCM/UB3LYP)
(**5-12R$^+$**) 1	-696.4344588 **-696.216665**	-695.0609196	-695.861664	-695.5939959	-0.0977675
2	-696.4364562 **-696.217042**	-695.0631977	-695.8648262	-695.5966076	-0.0905166
3	-696.4300297 **-696.212552**	-695.0518066	-695.8553786	-695.5860462	-0.0934807
4	-696.4312302 **-696.213835**	-695.0594352	-695.8597707	-695.5925036	-0.0992336
N→C2‡	-696.3529656 **-696.1401680**	-694.9973444	-695.7885658	-695.5220389	-0.0994249
N→C3‡	-696.3665174 **-696.152968**	-695.008717	-695.8000126	-695.5323474	-0.0885406
N→C4‡	-696.3946218 **-696.179113**	-695.0331669	-695.8250143	-695.5557395	-0.0854808
N→C7‡ (chair)	-696.4035768 **-696.186743**	-695.0449624	-695.8363187	-695.5665728	-0.0936720
N→C7‡ (boat)	-696.4003917 **-696.184401**	-695.2761532	-695.8311545	-695.5615451	-0.0940066
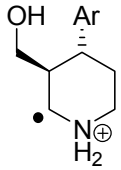	E_{tot}(UB3LYP) **G_{298}(UB3LYP)**	E_{tot}(ROMP2)	E_{tot} (UB2LPYP)	E_{tot} (G3(MP2)-RAD)	G_{solv} (CPCM/UB3LYP)
(**5-20R**) 1	-696.4156447 **-696.197155**	-695.0585586	-695.8511515	-695.5862724	-0.1059905
2	-696.4247646 **-696.204571**	-695.0670447	-695.8600108	-695.5945270	-0.0961899
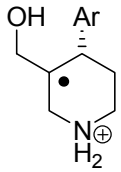	E_{tot}(UB3LYP) **G_{298}(UB3LYP)**	E_{tot}(ROMP2)	E_{tot} (UB2LPYP)	E_{tot} (G3(MP2)-RAD)	G_{solv} (CPCM/UB3LYP)
(**5-19R**) 1	-696.4342693 **-696.213753**	-695.074138	-695.8678203	-695.6020398	-0.0960783
2	-696.4283820 **-696.209893**	-695.067528	-695.8613575	-695.5958137	-0.1032495

Table 5.14 Total and Gibbs free energies at various levels of theory in Hartree (298.15 K, 1 atm, CPCM/UB3LYP = C-PCM/UAHF/UB3LYP/6-31G(d)//UB3LYP/6-31G(d)).

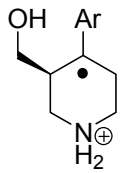	E_{tot}(UB3LYP) **G_{298}(UB3LYP)**	E_{tot}(ROMP2)	E_{tot} (UB2LPYP)	E_{tot} (G3(MP2)-RAD)	G_{solv} (CPCM/UB3LYP)
(**5-17R**) 1	-696.4562821 **-696.234665**	-695.0920655	-695.8852521	-695.6217839	-0.0952974
2	-696.4308613 **-696.210506**	-695.0668778	-695.861375	-695.6141778	-0.1085084
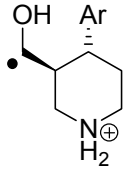	E_{tot}(UB3LYP) **G_{298}(UB3LYP)**	E_{tot}(ROMP2)	E_{tot} (UB2LPYP)	E_{tot} (G3(MP2)-RAD)	G_{solv} (CPCM/UB3LYP)
(**5-18R**) 1	-696.4311173 **-696.211875**	-695.0729357	-695.8659587	-695.6003529	-0.1065005
2	-696.4362715 **-696.214079**	-695.0786122	-695.8719957	-695.6057780	-0.0965564

Table 5.15 Total and Gibbs free energies at various levels of theory in Hartree (298.15 K, 1 atm, CPCM/UB3LYP = C-PCM/UAHF/UB3LYP/6-31G(d)//UB3LYP/6-31G(d)).

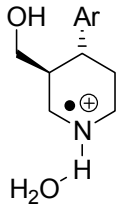	E_{tot}(UB3LYP) **G_{298}(UB3LYP)**	E_{tot}(ROMP2)	E_{tot}(UB2LPYP)	E_{tot}(G3(MP2)-RAD)	G_{solv} (CPCM/UB3LYP)
(**5-12R$^+$-H$_2$O**)	-772.8719350	-771.4064873	-772.2675860	-771.9833326	-0.0861502
1	**-772.637845**				
2	-772.8709712 **-772.630781**	-771.4037671	-772.2671892	-771.980868	-0.0843813

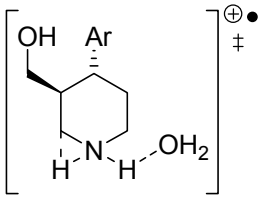

TS_1	E_{tot}(UB3LYP) **G_{298}(UB3LYP)**	E_{tot}(ROMP2)	E_{tot}(UB2LPYP)	E_{tot}(G3(MP2)-RAD)	G_{solv} (CPCM/UB3LYP)
N→C2‡	-772.7921261 **-772.561400**	-771.3416131	-772.1941070	-771.9103794	-0.0890346
N→C3‡	-772.8020679 **-772.571137**	-771.3505172	-772.2024973	-771.9181955	-0.0804929
N→C4‡	-772.8266104 **-772.594778**	-771.3717919	-772.2243403	-771.9388298	-0.0792021

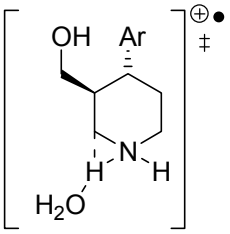

TS_2	E_{tot}(UB3LYP) **G_{298}(UB3LYP)**	E_{tot}(ROMP2)	E_{tot}(UB2LPYP)	E_{tot}(G3(MP2)-RAD)	G_{solv} (CPCM/UB3LYP)
N→C2‡	-772.7978756 **-772.564034**	-771.3480438	-772.201239	-771.9175147	-0.0861502
N→C3‡	-772.8102189 **-772.572230**	-771.3542959	-772.2089998	-771.924913	-0.0861502
N→C4‡	-772.8010445 **-772.563160**	-771.3486481	-772.2020261	-771.9198588	-0.1105801

Table 5.16 Total and Gibbs free energies at various levels of theory in Hartree (298.15 K, 1 atm, CPCM/UB3LYP = C-PCM/UAHF/UB3LYP/6-31G(d)//UB3LYP/6-31G(d)).

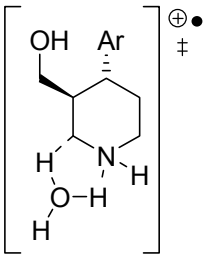

TS₃	E_{tot}(UB3LYP) **G_{298}(UB3LYP)**	E_{tot}(ROMP2)	E_{tot}(UB2LPYP)	E_{tot}(G3(MP2)-RAD)	G_{solv} (CPCM/UB3LYP)
N→C2‡	-772.7948956 **-772.559756**	-771.3402911	-772.1952354	-771.9098993	-0.1181178
N→C3‡	-772.8020962 **-772.565853**	-771.3298024	-772.1951882	-771.9015625	-0.0802379
N→C4‡	-772.8231060 **-772.585846**	-771.3625955	-772.2202325	-771.9268777	-0.0821980
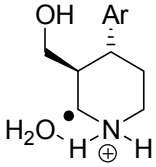	E_{tot}(UB3LYP) **G_{298}(UB3LYP)**	E_{tot}(ROMP2)	E_{tot}(UB2LPYP)	E_{tot}(G3(MP2)-RAD)	G_{solv} (CPCM/UB3LYP)
(**5-20R-H_2O**) 1	-772.8556732 **-772.620967**	-771.4033039	-772.2574901	-771.9754045	-0.0938154
2	-772.8557696 **-772.618741**	-771.4037982	-772.2580406	-771.9759132	-0.0922058
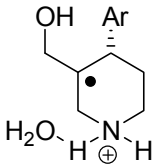	E_{tot}(UB3LYP) **G_{298}(UB3LYP)**	E_{tot}(ROMP2)	E_{tot}(UB2LPYP)	E_{tot}(G3(MP2)-RAD)	G_{solv} (CPCM/UB3LYP)
(**5-19R-H_2O**) 1	-772.8709036 **-772.634136**	-771.4161773	-772.2714117	-771.9887242	-0.0865326
2	-772.8665353 **-772.631041**	-771.4109351	-772.2662921	-771.9835952	-0.0925086
3	-772.8761873 **-772.634214**	-771.4190663	-772.2754790	-771.9908176	-0.0896083

Table 5.17 Total and Gibbs free energies at various levels of theory in Hartree (298.15 K, 1 atm, CPCM/UB3LYP = C-PCM/UAHF/UB3LYP/6-31G(d)//UB3LYP/6-31G(d)).

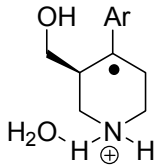	E_{tot}(UB3LYP) **G_{298}(UB3LYP)**	E_{tot}(ROMP2)	E_{tot}(UB2LPYP)	E_{tot}(G3(MP2)-RAD)	G_{solv} (CPCM/UB3LYP)
(**5-17R-H_2O**) 1	-772.8926329 **-772.654803**	-771.4338376	-772.2886123	-772.0082323	-0.0859271
2	-772.8697636 **-772.633118**	-771.4108941	-772.2667916	-771.9851624	-0.0974169
3	-772.8697039 **-772.630890**	-771.4109150	-772.2669858	-771.9851492	-0.0954568

Table 5.18 Energies and enthalpies for closed- and open-shell compounds at various levels of theory in the gas phase in Hartree (298.15 K, 1 atm).

	E_{tot}(B3LYP)	**H_{298}(B3LYP)**	E_{tot}(MP2)	E_{tot}(G3(MP2)-RAD)
CH_4	-40.5183890	**-40.470240**	-40.4055437	-40.4651605
$\bullet CH_3$	-39.8382922	**-39.804975**	-39.7316815	-39.7851922
H_2O	-76.4089533	**-76.384416**	-76.3181017	-76.3633998
•OH	-75.7234547	**-75.712016**	-75.6176489	-75.6628743
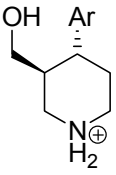 (**5-12H**)	E_{tot}(B3LYP)	**H_{298}(B3LYP)**	E_{tot}(MP2)	E_{tot}(G3(MP2)-RAD)
1	-697.0973763	**-696.806475**	-695.7400695	-696.2729667
3	-697.0796011	**-696.789152**	-695.7244486	-696.2578215
4	-697.0904568	**-696.800185**	-695.7339445	-696.2671066
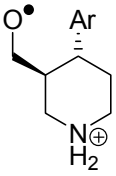 (**5-33R**)	E_{tot}(UB3LYP)	**H_{298}(UB3LYP)**	E_{tot}(ROMP2)	E_{tot}(G3(MP2)-RAD)
1	-696.4264601	**-696.150172**	-695.0487338	-695.5844400
2	-696.4162231	**-696.139959**	-695.0396277	-695.5742936
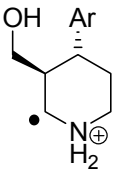 (**5-20R**)	E_{tot}(UB3LYP)	**H_{298}(UB3LYP)**	E_{tot}(ROMP2)	E_{tot}(G3(MP2)-RAD)
1	-696.4156447	**-696.140255**	-695.0585586	-695.5862724
2	-696.4247646	**-696.148674**	-695.0670447	-695.5945270
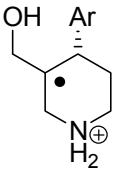 (**5-19R**)	E_{tot}(UB3LYP)	**H_{298}(UB3LYP)**	E_{tot}(ROMP2)	E_{tot}(G3(MP2)-RAD)
1	-696.4342693	**-696.157174**	-695.074138	-695.6020398
2	-696.4283820	**-696.152041**	-695.067528	-695.5958137
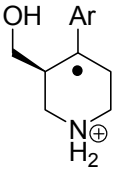 (**5-17R**)	E_{tot}(UB3LYP)	**H_{298}(UB3LYP)**	E_{tot}(ROMP2)	E_{tot}(G3(MP2)-RAD)
1	-696.4562821	**-696.178740**	-695.0920655	-695.6217839
2	-696.4308613	**-696.153677**	-695.0668778	-695.6141778

Table 5.19 Energies and enthalpies for closed- and open-shell compounds at various levels of theory in the gas phase in Hartree (298.15 K, 1 atm).

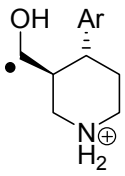 (**5-18R**)	E_{tot}(B3LYP)	**H_{298}(B3LYP)**	E_{tot}(MP2)	E_{tot}(G3(MP2)-RAD)
1	-696.4311173	**-696.154748**	-695.0729357	-695.6003529
2	-696.4362715	**-696.158990**	-695.0786122	-695.6057780
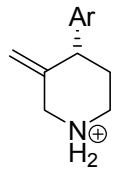 (**5-28**)	-620.6476626	**-620.387070**	-619.390153	-619.8807985
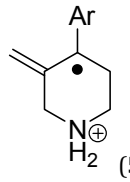 (**5-28R**)	-620.0119822	**-619.764330**	-618.7484839	-619.2341610
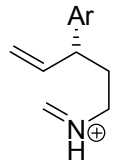 (**5-39**)	E_{tot}(B3LYP)	**H_{298}(B3LYP)**	E_{tot}(MP2)	E_{tot}(G3(MP2)-RAD)
9	-620.6172567	**-620.360248**	-619.3556370	-619.8496166
6	-620.6163369	**-620.359351**	-619.3553544	-619.8493633
3	-620.6146982	**-620.357753**	-619.3484535	-619.8431816
8	-620.6144354	**-620.357447**	-619.3518305	-619.8462650
7	-620.6141452	**-620.356940**	-619.3493499	-619.8437562
17	-620.6139230	**-620.356849**	-619.3484900	-619.8430658
1	-620.6139336	**-620.356791**	-619.3484656	-619.8430437

Table 5.20 Energies and enthalpies for closed- and open-shell compounds at various levels of theory in the gas phase in Hartree (298.15 K, 1 atm).

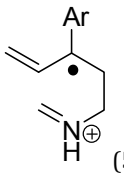 (**5-39R**)	E_{tot}(B3LYP)	**H_{298}(B3LYP)**	E_{tot}(MP2)	E_{tot}(G3(MP2)-RAD)
3	-619.9903176	**-619.746164**	-618.7197996	-619.2082755
9	-619.9882919	**-619.744311**	-618.7192621	-619.2076865
10	-619.9886573	**-619.744288**	-618.7169172	-619.2057050
18	-619.9850393	**-619.740921**	-618.7094029	-619.1992911
5	-619.9850445	**-619.740920**	-618.7092833	-619.1991655
4	-619.9852604	**-619.741175**	-618.7091540	-619.1990094
6	-619.9857357	**-619.741936**	-618.7188697	-619.2059670
2	-619.9849875	**-619.740825**	-618.7095568	-619.1995824
 (**5-30**)	-620.6329420	**-620.371872**	-619.3772914	-619.8651080
 (**5-30R**)	-619.9909782	**-619.743305**	-618.7289607	-619.2135363
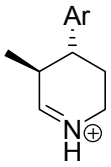 (**5-22**)	-620.6679645	**-620.408967**	-619.4039932	-619.8950718
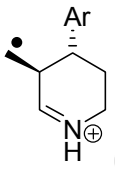 (**5-22R**)	-619.9943128	**-619.749493**	-618.7304221	-619.2160875
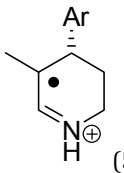 (**5-24R**)	-620.0400565	**-619.794308**	-618.7705607	-619.2548263

Table 5.21 Energies and enthalpies for closed- and open-shell compounds at various levels of theory in the gas phase in Hartree (298.15 K, 1 atm).

	E_{tot}(B3LYP)	**H_{298}(B3LYP)**	E_{tot}(MP2)	E_{tot}(G3(MP2)-RAD)
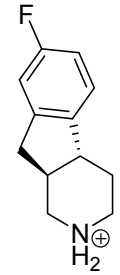 (**5-13**)	-620.6740891	**-620.412081**	-619.4200626	-619.9066648
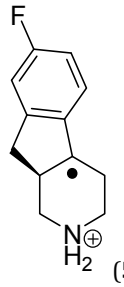 (**5-13R**)	-620.0370841	**-619.788444**	-618.7768548	-619.2595265
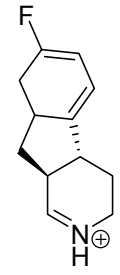 (**5-26**)	-620.6257278	**-620.366155**	-619.3633574	-619.8596808
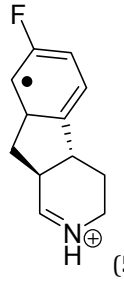 (**5-26R**)	-619.9911960	**-619.745631**	-618.7290217	-619.2174915

Table 5.22 Energies and enthalpies for closed- and open-shell compounds at various levels of theory in the gas phase in Hartree (298.15 K, 1 atm).

	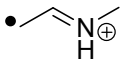 (**5-46R$^+$**)	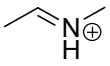 (**5-46$^+$**)	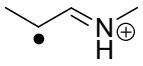 (**5-47R$^+$**)	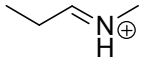 (**5-47$^+$**)
	E_{tot} **H_{298}**	E_{tot} **H_{298}**	E_{tot} **H_{298}**	E_{tot} **H_{298}**
B3LYP	-172.9850104 **-172.882792**	-173.6389523 **-173.523493**	-212.3172722 **-212.185736**	-212.9553790 **-212.810184**
G3(MP2)-RAD	-172.7516328 **-172.6494144**	-173.4129251 **-173.2974658**	-212.0280626 **-211.8965264**	-212.6766973 **-212.5315023**
	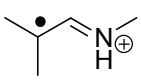 (**5-48R$^+$**)	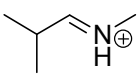 (**5-48$^+$**)	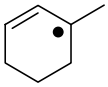 (**5-52R**)	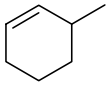 (**5-52**)
	E_{tot} **H_{298}**	E_{tot} **H_{298}**	E_{tot} **H_{298}**	E_{tot} **H_{298}**
B3LYP	-251.6434184 **-251.482641**	-252.2724055 **-252.098081**	-273.3286682 **-273.162659**	-273.9630016 **-273.783331**
G3(MP2)-RAD	-251.3021794 **-251.1414020**	-251.9430866 **-251.7687621**	-272.9565059 **-272.7904967**	-273.5994374 **-273.4197668**

6 Abbreviations

(d)A	(Desoxy)adenosine (adenine)
(d)C	(Desoxy)cytidine (cytosine)
(d)G	(Desoxy)guanosine (guanine)
(d)T	(Desoxy)thymidine (thymine)
(U)HF	(Unrestricted) *Hartree-Fock*
3-thioph	3-thienyl
Ac	Acetyl
AID	Activation-induced deaminase
AP	Abasic site
Ar	Aryl
ATR	Attenuated total reflectance
aug-cc-pVXZ	*Dunning*'s correlation consistent basis set (X = D(double), X = T (triple)), augmented (aug) with diffuse functions
B2PLYP-D	Double-hybrid density functional by *Grimme* including dispersion corrections
B3LYP	Hybrid density functional including *Becke*'s three-parameter exchange functional and *Lee-Yang-Parr*'s correlation functional
B98	Becke's 1998 hybrid density functional
BDE	Bond dissociation energy
BER	Base excision repair
BGVA	*Benson* increment values for the estimation of $\Delta_f H$
Bn	Benzyl
Boc	*tert*-Butoxycarbonyl
Bu	Butyl
Bz	Benzoyl
C(ys)	Cysteine
ca^{5}dC	5-Carboxyl desoxycytosine
calc.	Calculated
CBS	Complete basis set
CBz	Benzyloxycarbamate
CCSD(T)	Coupled-cluster with single, double and perturbative triple excitations
C_p	Heat capazity at constant pressure
C-PCM	Conductor-like PCM
CpG	Cytosine-phosphatidyl-guanine
D	Dihydrouridine (dihydrouracil)
δ	Chemical shift
DCE	1,2-dichlorethane
DCM	Dichloromethane
DDQ	2,3-Dichloro-5,6dicyano-1,4-benzoquinone
$\Delta_f H^0$	Heat of formation under standard conditions
DFT	Density functional theory
ΔG_{298}	Gibbs free energy at 298 K
ΔG_{solv}	Free solvation energy
$\Delta_{hyd} H$	Heat of hydrogenation
DIBAL	Di-*iso*butylaluminium hydride
DMAP	4-Dimethylaminopyridine
DMF	*N*,*N*-Dimethylformamide
DMSO	Dimethyl sulfoxide
$\Delta_{rxn} H$	Heat of reaction
$\Delta_{sub} H$	Heat of sublimation
$\Delta_{trh} H$	Heat of transfer hydrogenation
$\Delta_{vap} H$	Heat of vaporization
E	Glutamate
EI	Electron impact ionisation
ENDOR	Electron nuclear double resonance
EPR	Electron paramagnetic resonance
eq.	equation

ESI	Electron spray ionisation	M	Molar
Et	Ethyl	m^3U	3-Methyl uridine
EtOAc	Ethyl acetate	m^5dC	5-Methyl desoxycytosine
eV	Electron volt	MCA	Methyl cation affinity
EXAFS	Extended X-ray absorption fine structure	Me	Methyl
exp.	Experimental	min	Minute
f^5dC	5-Formyl desoxycytosine	MM3	Molecular mechanics developed by *Allinger*
FGE	Formyl-generating enzyme	MP*n*(FC)	N^{th} order *Møller-Plesset* perturbation theory with frozen core approximation
G3(MP2)-RAD	Adaption of G3(MP2) theory on open-shell species	MP*n*(Full)	N^{th} order *Møller-Plesset* perturbation theory with inner core electrons included
G3B3	Gaussian 3-theory with geometries and zero-point vibrational energies calculatedat B3LYP/6-31G(d) level	mPW1K	Modified *Perdew-Wang* one parameter hybride density functional for kinetics
G3large	Extension of the 6-311G(d,p) basi set with more flexible polarization functions (2df) and polarization of the core electrons (3d2f on Na-Ar)	*m*RNA	Messenger RNA
G3MP2large	G3large basis set excluding core polarization functions	MW	Micro wave
GIAO	Gauge including (invariant) atomic orbitals	ν	frequency
h	Hour	N	Asparagine
hm^5dC	5-Hydroxymethyl desoxycytosine	ν	Wave number
HMBC	Heteronuclear multiple-bond correlation	n/a	Not available
HOMO	Highest occupied molecular orbital	NADP	Nicotineamide adenine dinucleotide phosphate
HRMS	High resolution mass spectrometry	NMR	Nuclear magnetic resonance
HSQC	Heteronuclear single quantum correlation	PCC	Pyridinium chlorochromate
IEF-PCM	Integral equation formalism variant of PCM	PCM	Polarizable continuum model
IGLO	Individual gauge for localized orbitals	PE	Petrol ether
IR	Infrared	Ph	Phenyl
k	Rate constant	p	Partial pressure
K	Equilibrium constant	pK_a	Negative lg of acid dissociation constant (K_a)
LDA	Lithium di*iso*propylamide	py	Pyridine
LiHMDS	Lithium hexamethyldisilazide	PP	Diphosphate
m	Mass	Q	Glutamine
M	Molar mass	QCISD(T)	Quadratic configuration interaction with single, double and perturbative triple excitations

R	Universal gas constant (8.3145 J mol^{-1} K^{-1})	TS	Transition state
R	Organic rest	UAHF	United atom Hartree-Fock
refl.	reflux	UAKS	United atom Kohn-Sham
RMSE	Root mean square deviation	Um	2'-Methoxy uridine
RNR	Ribonucleotide Reductase	UV	Ultraviolet
RO	Restricted open-shell	*V*	Volume
RP-18	Reverse phase silica chain length 18	w	Boltzmann factor
*r*RNA	Ribosomal RNA	W*n*	Weizmann *n*-theory
RSE	Radical stabilization energy	X-YZ+G(ndf,mpd)	Valence-double-ζ basis set by *Pople et al.* Supplemented by polarization (df,pd) and diffuse (+ or ++) functions, *e.g.* 6-31+G(2d,p)
RT	Room temperature	X-YZW+G(ndf,mpd)	Valence-triple-ζ basis set by *Pople et al.* Supplemented by polarization (df,pd) and diffuse (+ or ++) functions, *e.g.* 6-311++G(3df,2p)
σ	Shielding tensor	Y	Tyrosine
S(er)	Serine	Ψ	Pseudouridine
SMD	Solvent model density		
sol	In solution		
SOMO	Semi-occupied molecular orbitals		
SSRI	Selective serotonine reuptake inhibitor		
T	Temperature		
T(hr)	Threonine		
TBAI	Tetrabutylammonium iodide		
T_c	Coalescence temperature		
TDG	Thymine DNA glycolase		
TET	Ten-eleven translocation		
TFA	Trifluoracetic acid		
THF	Tetrahydrofuran		
TLC	Thin layer chromatography		
TMP	2,2,6,6-Tetramethylpiperidine		
TMS	Trimethylsilyl		
*t*RNA	Transfer RNA		

7 Literature

[1] J. M. Berg, J. L. Tymoczko, L. Stryer, *Biochemistry*, 5th ed., W. H. Freeman and Company, New York, **2002**.
[2] J. D. Watson, F. H. C. Crick, *Nature* **1953**, *171*, 737.
[3] T. R. Cech, *Gene* **1993**, *135*, 33.
[4] J. J. Dalluge, T. Hashizume, A. E. Sopchik, J. A. McCloskey, D. R. Davis, *Nucleic Acids Research* **1996**, *24*, 1073.
[5] H. Shi, P. B. Moore, *RNA* **2000**, *6*, 1091.
[6] R. Da Roza, E. C. Friedberg, B. K. Duncan, H. R. Warner, *Biochemistry* **1977**, *16*, 4934.
[7] L. B. Maia, J. J. G. Moura, *Chemical Reviews* **2014**, *114*, 5273.
[8] V. Labet, C. Morell, T. Douki, J. Cadet, L. A. Eriksson, A. Grand, *The Journal of Physical Chemistry A* **2010**, *114*, 1826.
[9] G. B. Kistiakowsky, J. R. Ruhoff, H. A. Smith, W. E. Vaughan, *Journal of the American Chemical Society* **1936**, *58*, 146.
[10] A. Fattahi, L. Lis, S. R. Kass, *Journal of the American Chemical Society* **2005**, *127*, 13065.
[11] K. B. Wiberg, *Angewandte Chemie International Edition in English* **1986**, *25*, 312.
[12] L. A. Curtiss, K. Raghavachari, P. C. Redfern, V. Rassolov, J. A. Pople, *The Journal of Chemical Physics* **1998**, *109*, 7764.
[13] a) J. A. Montgomery, M. J. Frisch, J. W. Ochterski, G. A. Petersson, *The Journal of Chemical Physics* **1999**, *110*, 2822; b) J. A. Montgomery, M. J. Frisch, J. W. Ochterski, G. A. Petersson, *The Journal of Chemical Physics* **2000**, *112*, 6532.
[14] a) J. M. L. Martin, G. de Oliveira, *The Journal of Chemical Physics* **1999**, *111*, 1843; b) S. Parthiban, J. M. L. Martin, *The Journal of Chemical Physics* **2001**, *114*, 6014.
[15] *CRC Handbook of Chemistry and Physics*, 88 ed., CRC Press, Boca Raton, USA, **2008**.
[16] G. B. Kistiakowsky, A. G. Nickle, *Discussions of the Faraday Society* **1951**, *10*, 175.
[17] G. B. Kistiakowsky, J. R. Ruhoff, H. A. Smith, W. E. Vaughan, *Journal of the American Chemical Society* **1936**, *58*, 137.
[18] W. R. Roth, H.-W. Lennartz, *Chemische Berichte* **1980**, *113*, 1806.
[19] D. W. Rogers, E. Crooks, K. Dejroongruang, *The Journal of Chemical Thermodynamics* **1987**, *19*, 1209.
[20] R. K. Hill, G. H. Morton, D. W. Rogers, L. S. Choi, *The Journal of Organic Chemistry* **1980**, *45*, 5163.
[21] D. W. Rogers, Y. Zhao, M. Traetteberg, M. Hulce, J. Liebman, *The Journal of Chemical Thermodynamics* **1998**, *30*, 1393.
[22] H. A. Skinner, A. Snelson, *Transactions of the Faraday Society* **1959**, *55*, 404.
[23] K. B. Wiberg, L. S. Crocker, K. M. Morgan, *Journal of the American Chemical Society* **1991**, *113*, 3447.
[24] M. A. Dolliver, T. L. Gresham, G. B. Kistiakowsky, E. A. Smith, W. E. Vaughan, *Journal of the American Chemical Society* **1938**, *60*, 440.

[25] H. Shimizu, I. Nagasaki, K. Matsumura, N. Sayo, T. Saito, *Accounts of Chemical Research* **2007**, *40*, 1385.
[26] N. J. A. Martin, B. List, *Journal of the American Chemical Society* **2006**, *128*, 13368.
[27] C. Zhu, T. Akiyama, *Advanced Synthesis & Catalysis* **2010**, *352*, 1846.
[28] C. Saluzzo, M. Lemaire, *Advanced Synthesis & Catalysis* **2002**, *344*, 915.
[29] a) R. Kawahara, K.-i. Fujita, R. Yamaguchi, *Angewandte Chemie International Edition* **2012**, *51*, 12790; b) R. Kawahara, K.-i. Fujita, R. Yamaguchi, *Journal of the American Chemical Society* **2012**, *134*, 3643.
[30] a) D. Kulikov, S. P. Verevkin, A. Heintz, *Fluid Phase Equilibria* **2001**, *192*, 187; b) D. H. Zaitsau, S. P. Verevkin, Y. U. Paulechka, G. J. Kabo, V. M. Sevruk, *Journal of Chemical & Engineering Data* **2003**, *48*, 1393.
[31] H.-D. Beckhaus, G. Kratt, K. Lay, J. Geiselmann, C. Rüchardt, B. Kitschke, H. J. Lindner, *Chemische Berichte* **1980**, *113*, 3441.
[32] G. E. Hilbert, T. B. Johnson, *Journal of the American Chemical Society* **1930**, *52*, 4489.
[33] U. Niedballa, H. Vorbrüggen, *Angewandte Chemie International Edition in English* **1970**, *9*, 461.
[34] W. Micklitz, B. Lippert, H. Schöllhorn, U. Thewalt, *Journal of Heterocyclic Chemistry* **1989**, *26*, 1499.
[35] A. C. Spivey, T. Fekner, S. E. Spey, H. Adams, *The Journal of Organic Chemistry* **1999**, *64*, 9430.
[36] S. Jaime-Figueroa, A. Zamilpa, A. Guzmán, D. J. Morgans, *Synthetic Communications* **2001**, *31*, 3739.
[37] D. J. Brown, L. Strekowski, *Australian Journal of Chemistry* **1981**, *34*, 1157.
[38] H. Wang, K. Wen, L. Wang, Y. Xiang, X. Xu, Y. Shen, Z. Sun, *Molecules* **2012**, *17*, 4533.
[39] a) Y. Wei, G. N. Sastry, H. Zipse, *Journal of the American Chemical Society* **2008**, *130*, 3473; b) Y. Wei, T. Singer, H. Mayr, G. N. Sastry, H. Zipse, *Journal of Computational Chemistry* **2008**, *29*, 291.
[40] S. Thumser, in *Die Hydrierung von C5-modifizierten Cytosinen zur Erforschung des Demethylierungsprozesses, Bachelor-Arbeit*, Ludwig-Maximilians-Universität, München, **2013**.
[41] C. K. Lee, J. Y. Shim, *Bulletin of the Korean Chemical Society* **1991**, *12*, 343.
[42] R. S. Hosmane, N. J. Leonard, *Synthesis* **1981**, *1981*, 118.
[43] K. Ciszweski, L. Celewicz, K. Golankiewicz, *Synthesis* **1995**, *1995*, 777.
[44] a) V. Sbkaric, B. Gaspert, M. Hohnjec, G. Lacan, *Journal of the Chemical Society, Perkin Transactions 1* **1974**, 267; b) E. B. Brown, T. B. Johnson, *Journal of the American Chemical Society* **1924**, *46*, 702; c) W. E. Cohn, D. G. Doherty, *Journal of the American Chemical Society* **1956**, *78*, 2863.
[45] a) D. M. Brown, M. J. E. Hewlins, *Journal of the Chemical Society C: Organic* **1968**, 2050; b) C. C. Cheng, L. R. Lewis, *Journal of Heterocyclic Chemistry* **1964**, *1*, 260.
[46] V. Skaric, B. Gaspert, I. Jerkunica, D. Skaric, *Croatica Chemica Acta* **1965**, *37*, 199.
[47] Y. K. Kang, H. S. Park, *Journal of Molecular Structure: THEOCHEM* **2004**, *676*, 171.

[48] T. Drakenberg, K.-I. Dahlqvist, S. Forsen, *Acta Chemica Scandinavica* **1970**, *24*, 694.
[49] T. Bally, P. Diehl, E. Haselbach, A. S. Tracey, *Helvetica Chimica Acta* **1975**, *58*, 2398.
[50] S. R. Wilson, I. D. Watson, G. N. Malcolm, *The Journal of Chemical Thermodynamics* **1979**, *11*, 911.
[51] M. A. V. Ribeiro da Silva, L. M. P. F. Amaral, P. Szterner, *The Journal of Chemical Thermodynamics* **2011**, *43*, 1924.
[52] S. Murata, M. Sakiyama, S. Seki, *Thermochimica Acta* **1985**, *88*, 121.
[53] T. L. P. Galvão, I. M. Rocha, M. D. M. C. Ribeiro da Silva, M. A. V. Ribeiro da Silva, *The Journal of Physical Chemistry A* **2013**, *117*, 5826.
[54] G. Buechi, M. A. Francisco, J. M. Liesch, P. F. Schuda, *Journal of the American Chemical Society* **1981**, *103*, 3497.
[55] a) A. Skladanowski, P. Bozko, M. Sabisz, *Chemical Reviews* **2009**, *109*, 2951; b) P. Koepf-Maier, H. Koepf, *Chemical Reviews* **1987**, *87*, 1137.
[56] a) J.-L. Fischel, P. Formento, J. Ciccolini, M.-C. Etienne-Grimaldi, G. Milano, *Anti-Cancer Drugs* **2004**, *15*, 969; b) A. B. P. van Kuilenburg, R. Meinsma, A. H. van Gennip, *Nucleosides, Nucleotides and Nucleic Acids* **2004**, *23*, 1371.
[57] R. A. L. Peerboom, S. Ingemann, N. M. M. Nibbering, J. F. Liebman, *Journal of the Chemical Society, Perkin Transactions 2* **1990**, 1825.
[58] a) C. A. M. Seidel, A. Schulz, M. H. M. Sauer, *The Journal of Physical Chemistry* **1996**, *100*, 5541; b) K. Aflatooni, G. A. Gallup, P. D. Burrow, *The Journal of Physical Chemistry A* **1998**, *102*, 6205.
[59] a) E. A. Green, R. D. Rosenstein, R. Shiono, D. J. Abraham, B. L. Trus, R. E. Marsh, *Acta Crystallographica Section B* **1975**, *31*, 102; b) N. Leulliot, M. Ghomi, G. Scalmani, G. Berthier, *The Journal of Physical Chemistry A* **1999**, *103*, 8716.
[60] A. V. Marenich, C. J. Cramer, D. G. Truhlar, *The Journal of Physical Chemistry B* **2009**, *113*, 6378.
[61] E. Bártová, J. Krejčí, A. Harničarová, G. Galiová, S. Kozubek, *Journal of Histochemistry & Cytochemistry* **2008**, *56*, 711.
[62] T. Carell, C. Brandmayr, A. Hienzsch, M. Müller, D. Pearson, V. Reiter, I. Thoma, P. Thumbs, M. Wagner, *Angewandte Chemie International Edition* **2012**, *51*, 7110.
[63] R. Straussman, D. Nejman, D. Roberts, I. Steinfeld, B. Blum, N. Benvenisty, I. Simon, Z. Yakhini, H. Cedar, *Nat Struct Mol Biol* **2009**, *16*, 564.
[64] M. M. Suzuki, A. Bird, *Nat Rev Genet* **2008**, *9*, 465.
[65] M. Tahiliani, K. P. Koh, Y. Shen, W. A. Pastor, H. Bandukwala, Y. Brudno, S. Agarwal, L. M. Iyer, D. R. Liu, L. Aravind, A. Rao, *Science* **2009**, *324*, 930.
[66] T. Pfaffeneder, B. Hackner, M. Truß, M. Münzel, M. Müller, C. A. Deiml, C. Hagemeier, T. Carell, *Angewandte Chemie International Edition* **2011**, *50*, 7008.
[67] a) S. Ito, L. Shen, Q. Dai, S. C. Wu, L. B. Collins, J. A. Swenberg, C. He, Y. Zhang, *Science* **2011**, *333*, 1300; b) Y.-F. He, B.-Z. Li, Z. Li, P. Liu, Y. Wang, Q. Tang, J. Ding, Y. Jia, Z. Chen, L. Li, Y. Sun, X. Li, Q. Dai, C.-X. Song, K. Zhang, C. He, G.-L. Xu, *Science* **2011**, *333*, 1303.
[68] S. Schiesser, B. Hackner, T. Pfaffeneder, M. Müller, C. Hagemeier, M. Truss, T. Carell, *Angewandte Chemie International Edition* **2012**, *51*, 6516.

[69] a) C. Popp, W. Dean, S. Feng, S. J. Cokus, S. Andrews, M. Pellegrini, S. E. Jacobsen, W. Reik, *Nature* **2010**, *463*, 1101; b) P. Hajkova, S. J. Jeffries, C. Lee, N. Miller, S. P. Jackson, M. A. Surani, *Science* **2010**, *329*, 78.

[70] S. Schiesser, T. Pfaffeneder, K. Sadeghian, B. Hackner, B. Steigenberger, A. S. Schröder, J. Steinbacher, G. Kashiwazaki, G. Höfner, K. T. Wanner, C. Ochsenfeld, T. Carell, *Journal of the American Chemical Society* **2013**, *135*, 14593.

[71] W. L. F. Armarego, C. Li Lin Chai, *Purification of Laboratory Chemicals*, 6th ed., Elsevier Inc., Oxford, **2009**.

[72] W. C. Still, M. Kahn, A. Mitra, *The Journal of Organic Chemistry* **1978**, *43*, 2923.

[73] H. E. Gottlieb, V. Kotlyar, A. Nudelman, *The Journal of Organic Chemistry* **1997**, *62*, 7512.

[74] F. Achrainer, V. N. Emel'yanenko, W. Tantawy, S. P. Verevkin, H. Zipse, *The Journal of Physical Chemistry B* **2014**, *118*, 10426.

[75] D. G. Hartzfeld, S. D. Rose, *Journal of the American Chemical Society* **1993**, *115*, 850.

[76] Y. J. Ham, D.-H. Lee, H. G. Choi, J.-M. Hah, T. Sim, *Tetrahedron Letters* **2010**, *51*, 4609.

[77] Integrated Spectral Database System of Organic Compounds (SDBS), National Institute of Advanced Industrial Science and Technology, Japan, **2015**.

[78] A. Robin, K. Julienne, J.-C. Meslin, D. Deniaud, *European Journal of Organic Chemistry* **2006**, *2006*, 634.

[79] N. L. Allinger, Y. H. Yuh, J. H. Lii, *Journal of the American Chemical Society* **1989**, *111*, 8551.

[80] a) F. Mohamadi, N. G. J. Richards, W. C. Guida, R. Liskamp, M. Lipton, C. Caufield, G. Chang, T. Hendrickson, W. C. Still, *Journal of Computational Chemistry* **1990**, *11*, 440; b) Schrödinger, *MACROMODEL 9.7*, **2009**.

[81] D. J. Henry, M. B. Sullivan, L. Radom, *The Journal of Chemical Physics* **2003**, *118*, 4849.

[82] J. Tomasi, B. Mennucci, R. Cammi, *Chemical Reviews* **2005**, *105*, 2999.

[83] V. Barone, M. Cossi, J. Tomasi, *The Journal of Chemical Physics* **1997**, *107*, 3210.

[84] H.-J. Werner, P. J. Knowles, G. Knizia, F. R. Manby, M. Schütz, MOLPRO 2010.1, a package of *ab-initio* programs.

[85] M. J. Frisch, G. W. Trucks, H. B. Schlegel, G. E. Scuseria, M. A. Robb, J. R. Cheeseman, J. Montgomery, T. J. A.; Vreven, K. N. Kudin, J. C. Burant, J. M. Millam, S. S. Iyengar, J. Tomasi, V. Barone, B. Mennucci, M. Cossi, G. Scalmani, N. Rega, G. A. Petersson, H. Nakatsuji, M. Hada, M. Ehara, K. Toyota, R. Fukuda, J. Hasegawa, M. Ishida, T. Nakajima, Y. Honda, O. Kitao, H. Nakai, M. Klene, X. Li, J. E. Knox, H. P. Hratchian, J. B. Cross, V. Bakken, C. Adamo, J. Jaramillo, R. Gomperts, R. E. Stratmann, O. Yazyev, A. J. Austin, R. Cammi, C. Pomelli, J. W. Ochterski, P. Y. Ayala, K. Morokuma, G. A. Voth, P. Salvador, J. J. Dannenberg, V. G. Zakrzewski, S. Dapprich, A. D. Daniels, M. C. Strain, O. Farkas, D. K. Malick, A. D. Rabuck, K. Raghavachari, J. B. Foresman, J. V. Ortiz, Q. Cui, A. G. Baboul, S. Clifford, J. Cioslowski, B. B. Stefanov, G. Liu, A. Liashenko, P. Piskorz, I. Komaromi, R. L. Martin, D. J. Fox, T. Keith, M. A. Al-Laham, C. Y. Peng, A. Nanayakkara, M. Challacombe, P. M. W. Gill, B. Johnson, W. Chen, M. W. Wong, C. Gonzalez, J. A. Pople, *Gaussian 03* Rev. D.01, Gaussian, Inc., Wallingford CT, USA, **2004**.

[86] M. J. Frisch, G. W. Trucks, H. B. Schlegel, G. E. Scuseria, M. A. Robb, J. R. Cheeseman, G. Scalmani, V. Barone, B. Mennucci, G. A. Petersson, H. Nakatsuji, M. Caricato, X. Li, H. P. Hratchian, A. F. Izmaylov, J. Bloino, G. Zheng, J. L. Sonnenberg, M. Hada, M. Ehara, K. Toyota, R. Fukuda, J. Hasegawa, M. Ishida, T. Nakajima, Y. Honda, O. Kitao, H. Nakai, T. Vreven, J. A. Montgomery Jr., J. E. Peralta, F. Ogliaro, M. J. Bearpark, J. Heyd, E. N. Brothers, K. N. Kudin, V. N. Staroverov, R. Kobayashi, J. Normand, K. Raghavachari, A. P. Rendell, J. C. Burant, S. S. Iyengar, J. Tomasi, M. Cossi, N. Rega, N. J. Millam, M. Klene, J. E. Knox, J. B. Cross, V. Bakken, C. Adamo, J. Jaramillo, R. Gomperts, R. E. Stratmann, O. Yazyev, A. J. Austin, R. Cammi, C. Pomelli, J. W. Ochterski, R. L. Martin, K. Morokuma, V. G. Zakrzewski, G. A. Voth, P. Salvador, J. J. Dannenberg, S. Dapprich, A. D. Daniels, Ö. Farkas, J. B. Foresman, J. V. Ortiz, J. Cioslowski, D. J. Fox, *Gaussian 09* Rev. C.01, Gaussian, Inc., Wallingford, CT, USA, **2009**.
[87] R. A. W. Johnstone, A. H. Wilby, I. D. Entwistle, *Chemical Reviews* **1985**, *85*, 129.
[88] R. Noyori, S. Hashiguchi, *Accounts of Chemical Research* **1997**, *30*, 97.
[89] a) J. W. Yang, M. T. Hechavarria Fonseca, B. List, *Angewandte Chemie International Edition* **2004**, *43*, 6660; b) S. G. Ouellet, J. B. Tuttle, D. W. C. MacMillan, *Journal of the American Chemical Society* **2005**, *127*, 32.
[90] a) H. G. Viehe, Z. Janousek, R. Merenyi, L. Stella, *Accounts of Chemical Research* **1985**, *18*, 148; b) R. Sustmann, H.-G. Korth, in *Advances in Physical Organic Chemistry, Vol. Volume 26* (Ed.: D. Bethell), Academic Press, **1991**, pp. 131.
[91] G. P. F. Wood, D. Moran, R. Jacob, L. Radom, *The Journal of Physical Chemistry A* **2005**, *109*, 6318.
[92] a) A. E. Wagner, P. Huebbe, T. Konishi, M. M. Rahman, M. Nakahara, S. Matsugo, G. Rimbach, *Journal of Agricultural and Food Chemistry* **2008**, *56*, 11694; b) E. Niki, *American Journal of Clinical Nutrition* **1991**, *54*, 11195.
[93] J. Hioe, H. Zipse, in *Encyclopedia of Radicals in Chemistry, Biology and Materials*, John Wiley & Sons, Ltd, **2012**.
[94] H. Zipse, E. Artin, S. Wnuk, G. J. S. Lohman, D. Martino, R. G. Griffin, S. Kacprzak, M. Kaupp, B. Hoffman, M. Bennati, J. Stubbe, N. Lees, *Journal of the American Chemical Society* **2008**, *131*, 200.
[95] a) P. Nordlund, P. Reichard, *Annual Review of Biochemistry* **2006**, *75*, 681; b) P. Reichard, A. Baldesten, L. Rutberg, *Journal of Biological Chemistry* **1961**, *236*, 1150.
[96] U. Uhlin, H. Eklund, *Nature* **1994**, *370*, 533.
[97] a) W. Tong, D. Burdi, P. Riggs-Gelasco, S. Chen, D. Edmondson, B. H. Huynh, J. Stubbe, S. Han, A. Arvai, J. Tainer, *Biochemistry* **1998**, *37*, 5840; b) P. Nordlund, H. Eklund, *Journal of Molecular Biology* **1993**, *232*, 123.
[98] J. Stubbe, D. G. Nocera, C. S. Yee, M. C. Y. Chang, *Chemical Reviews* **2003**, *103*, 2167.
[99] A. N. I. Lin, G. W. Ashley, J. Stubbe, *Biochemistry* **1987**, *26*, 6905.
[100] R. Lenz, B. Giese, *Journal of the American Chemical Society* **1997**, *119*, 2784.
[101] A. Kasrayan, A. L. Persson, M. Sahlin, B.-M. Sjöberg, *Journal of Biological Chemistry* **2002**, *277*, 5749.
[102] F. Z. Avval, A. Holmgren, *Journal of Biological Chemistry* **2009**, *284*, 8233.
[103] M. W. Ruszczycky, S.-h. Choi, S. O. Mansoorabadi, H.-w. Liu, *Journal of the American Chemical Society* **2011**, *133*, 7292.

[104] A. G. Baboul, L. A. Curtiss, P. C. Redfern, K. Raghavachari, *Journal of Chemical Physics* **1999**, *110*, 7650.
[105] J. D. Cox, G. Pilcher, *Thermochemistry of organic and organometallic compounds*, Academic Press, **1970**.
[106] M. L. Coote, *The Journal of Physical Chemistry A* **2004**, *108*, 3865.
[107] J. L. Holmes, F. P. Lossing, P. M. Mayer, *Journal of the American Chemical Society* **1991**, *113*, 9723.
[108] G. P. F. Wood, L. Radom, G. A. Petersson, E. C. Barnes, M. J. Frisch, J. A. Montgomery, *The Journal of Chemical Physics* **2006**, *125*.
[109] M. Cord, B. Husson, J. C. Lizardo Huerta, O. Herbinet, P.-A. Glaude, R. Fournet, B. Sirjean, F. Battin-Leclerc, M. Ruiz-Lopez, Z. Wang, M. Xie, Z. Cheng, F. Qi, *The Journal of Physical Chemistry A* **2012**, *116*, 12214.
[110] a) M. Bennati, M. Lendzian, M. Schmittel, H. Zipse, *Biological Chemistry* **2005**, *386*, 1007; b) H. Zipse, *Organic and Biomolecular Chemistry* **2003**, *1*, 692; c) M. Mohr, H. Zipse, *Chemistry - A European Journal* **1999**, *5*, 3046.
[111] J. Tomasi, B. Mennucci, E. Cancès, *Journal of Molecular Structure: THEOCHEM* **1999**, *464*, 211.
[112] a) D. Rabuka, J. S. Rush, G. W. deHart, P. Wu, C. R. Bertozzi, *Nat. Protocols* **2012**, *7*, 1052; b) P. Bojarová, S. J. Williams, *Current Opinion in Chemical Biology* **2008**, *12*, 573.
[113] J. Hioe, G. Savasci, H. Brand, H. Zipse, *Chemistry – A European Journal* **2011**, *17*, 3781.
[114] J. Hioe, H. Zipse, *Faraday Discussions* **2010**, *145*, 301.
[115] Y.-R. Luo, *Comprehensive Handbook of Chemical Bond Energies*, CRC Press, Boca Raton, USA, **2007**.
[116] a) G. Gryn'ova, M. L. Coote, *Journal of the American Chemical Society* **2013**, *135*, 15392; b) G. Gryn'ova, D. L. Marshall, S. J. Blanksby, M. L. Coote, *Nat Chem* **2013**, *5*, 474.
[117] O. Schiemann, E. Feresin, T. Carl, B. Giese, *ChemPhysChem* **2004**, *5*, 270.
[118] I. Dąbkowska, J. Rak, M. Gutowski, *Eur. Phys. J. D* **2005**, *35*, 429.
[119] M. Cossi, N. Rega, G. Scalmani, V. Barone, *Journal of Computational Chemistry* **2003**, *24*, 669.
[120] A. Bhattacharya, S. Shivalkar, *Journal of Chemical & Engineering Data* **2006**, *51*, 1169.
[121] J. Berkowitz, G. B. Ellison, D. Gutman, *The Journal of Physical Chemistry* **1994**, *98*, 2744.
[122] N. Cohen, *Journal of Physical and Chemical Reference Data* **1996**, *25*, 1411.
[123] W. Tsang, *Heats of Formation of Organic Free Radicals.*, Blackie Academic and Professional, New York, **1996**.
[124] J. L. Holmes, F. P. Lossing, A. Maccoll, *Journal of the American Chemical Society* **1988**, *110*, 7339.
[125] a) E. von Frankland, *Justus Liebigs Annalen der Chemie* **1849**, *71*, 171; b) D. Seyferth, *Organometallics* **2001**, *20*, 2940.
[126] Z. Rappoport, I. Marek, *The Chemistry of Organozinc Compounds: R-Zn*, Wiley-VCH, **2006**.
[127] T. Klatt, J. T. Markiewicz, C. Sämann, P. Knochel, *The Journal of Organic Chemistry* **2014**, *79*, 4253.

[128] C. Elschenbroich, *Organometallics, Vol. 3rd*, Wiley-VCH, **2006**.
[129] A. F. Holleman, E. Wiberg, N. Wiberg, *Lehrbuch der Anorganischen Chemie*, 102 ed., de Gruyter, Berlin, **2007**.
[130] H.-U. Siehl, in *Advances in Physical Organic Chemistry, Vol. Volume 42* (Ed.: J. P. Richard), Academic Press, **2007**, pp. 125.
[131] N. Krause, A. S. K. Hashmi, *Modern Allene Chemistry*, Wiley-VCH, Weinheim, **2004**.
[132] T. Kitagawa, J. Kamada, S. Minegishi, K. i. Takeuchi, *Organic Letters* **2000**, *2*, 3011.
[133] a) B. Engels, C. Lennartz, M. Hanrath, M. Schmittel, M. Strittmatter, *Angewandte Chemie International Edition* **1998**, *37*, 1960; b) S. Sakai, M. Nishitani, *The Journal of Physical Chemistry A* **2010**, *114*, 11807.
[134] S. Ma, Q. He, X. Zhang, *The Journal of Organic Chemistry* **2005**, *70*, 3336.
[135] S. Ma, A. Zhang, *The Journal of Organic Chemistry* **2002**, *67*, 2287.
[136] a) S. Reformatsky, *Berichte der deutschen chemischen Gesellschaft* **1887**, *20*, 1210; b) A. Fürstner, *Synthesis* **1989**, *1989*, 571.
[137] a) M. J. S. Dewar, K. M. Merz, *Journal of the American Chemical Society* **1987**, *109*, 6553; b) J. Maiz, A. Arrieta, X. Lopez, J. M. Ugalde, F. P. Cossío, B. Lecea, *Tetrahedron Letters* **1993**, *34*, 6111.
[138] a) F. Orsini, F. Pelizzoni, G. Ricca, *Tetrahedron Letters* **1982**, *23*, 3945; b) F. Orsini, F. Pelizzoni, G. Ricca, *Tetrahedron* **1984**, *40*, 2781; c) D. Pini, G. Uccello-Barretta, A. Mastantuono, P. Salvadori, *Tetrahedron* **1997**, *53*, 6065.
[139] W. Hörner, H. Bertagnolli, *Journal of Organometallic Chemistry* **2002**, *649*, 128.
[140] a) J. Dekker, P. H. M. Budzelaar, J. Boersma, G. J. M. Van der Kerk, A. J. Spek, *Organometallics* **1984**, *3*, 1403; b) S. Miki, K. Nakamoto, J.-i. Kawakami, S. Handa, S. Nuwa, *Synthesis* **2008**, *2008*, 409.
[141] a) F. Weigend, R. Ahlrichs, *Physical Chemistry Chemical Physics* **2005**, *7*, 3297; b) F. Weigend, *Physical Chemistry Chemical Physics* **2006**, *8*, 1057.
[142] a) T. H. Dunning Jr., *Journal Of Chemical Physics* **1989**, *90*, 1007; b) R. A. Kendall, T. H. Dunning Jr., R. J. Harrison, *Journal of Chemical Physics* **1992**, *96*, 6796; c) D. E. Woon, T. H. Dunning, *The Journal of Chemical Physics* **1993**, *98*, 1358.
[143] T. Thaler, B. Haag, A. Gavryushin, K. Schober, E. Hartmann, R. M. Gschwind, H. Zipse, P. Mayer, P. Knochel, *Nat Chem* **2010**, *2*, 125.
[144] W. Kutzelnigg, U. Fleischer, M. Schindler, *NMR Basics and Principles*, Springer, Berlin/Heidelberg, **1991**.
[145] M. Buehl, N. J. R. Van Eikema Hommes, P. v. R. Schleyer, U. Fleischer, W. Kutzelnigg, *Journal of the American Chemical Society* **1991**, *113*, 2459.
[146] F. Jensen, *The Journal of Chemical Physics* **2013**, *138*, 014107.
[147] J. R. Cheeseman, G. W. Trucks, T. A. Keith, M. J. Frisch, *The Journal of Chemical Physics* **1996**, *104*, 5497.
[148] a) A. D. Becke, *Physical Review A* **1988**, *38*, 3098; b) C. Lee, W. Yang, R. G. Parr, *Physical Review B* **1988**, *37*, 785.
[149] B. J. Lynch, P. L. Fast, M. Harris, D. G. Truhlar, *The Journal of Physical Chemistry A* **2000**, *104*, 4811.
[150] H. J. Reich, J. E. Holladay, *Journal of the American Chemical Society* **1995**, *117*, 8470.

[151] K. W. Wiitala, Z. F. Al-Rashid, V. Dvornikovs, T. R. Hoye, C. J. Cramer, *Journal of Physical Organic Chemistry* **2007**, *20*, 345.
[152] H. J. Reich, *Chemical Reviews* **2013**, *113*, 7130.
[153] S. Seel, G. Dagousset, T. Thaler, A. Frischmuth, K. Karaghiosoff, H. Zipse, P. Knochel, *Chemistry – A European Journal* **2013**, *19*, 4614.
[154] a) O. Kwon, F. Sevin, M. L. McKee, *The Journal of Physical Chemistry A* **2000**, *105*, 913; b) T. Brinck, *Organometallics* **2001**, *20*, 5134.
[155] P. I. Dem'yanov, I. M. Styrkov, D. P. Krut'ko, M. V. Vener, V. S. Petrosyan, *Journal of Organometallic Chemistry* **1992**, *438*, 265.
[156] M. Gaudemar, *Bulletin de la societé chimique de france* **1962**, 974.
[157] R. R. Fraser, T. S. Mansour, S. Savard, *The Journal of Organic Chemistry* **1985**, *50*, 3232.
[158] K. Shen, Y. Fu, J.-N. Li, L. Liu, Q.-X. Guo, *Tetrahedron* **2007**, *63*, 1568.
[159] A. Streitwieser, P. J. Scannon, H. M. Niemeyer, *Journal of the American Chemical Society* **1972**, *94*, 7936.
[160] R. R. Fraser, T. S. Mansour, S. Savard, *Canadian Journal of Chemistry* **1985**, *63*, 3505.
[161] F. G. Bordwell, *Accounts of Chemical Research* **1988**, *21*, 456.
[162] W. S. Matthews, J. E. Bares, J. E. Bartmess, F. G. Bordwell, F. J. Cornforth, G. E. Drucker, Z. Margolin, R. J. McCallum, G. J. McCollum, N. R. Vanier, *Journal of the American Chemical Society* **1975**, *97*, 7006.
[163] M. D. Liptak, G. C. Shields, *International Journal of Quantum Chemistry* **2001**, *85*, 727.
[164] Y. Fu, L. Liu, R.-Q. Li, R. Liu, Q.-X. Guo, *Journal of the American Chemical Society* **2003**, *126*, 814.
[165] A. Streitwieser, D. Z. Wang, M. Stratakis, A. Facchetti, R. Gareyev, A. Abbotto, J. A. Krom, K. V. Kilway, *Canadian Journal of Chemistry* **1998**, *76*, 765.
[166] F. G. Bordwell, W. S. Matthews, N. R. Vanier, *Journal of the American Chemical Society* **1975**, *97*, 442.
[167] G. R. Fulmer, A. J. M. Miller, N. H. Sherden, H. E. Gottlieb, A. Nudelman, B. M. Stoltz, J. E. Bercaw, K. I. Goldberg, *Organometallics* **2010**, *29*, 2176.
[168] F. Weigend, R. Ahlrichs, *Physical Chemistry Chemical Physics* **2005**, *7*, 3297.
[169] a) R. Ditchfield, *Molecular Physics* **1974**, *27*, 789; b) K. Wolinski, J. F. Hinton, P. Pulay, *Journal of the American Chemical Society* **1990**, *112*, 8251.
[170] F. Jensen, *The Journal of Physical Chemistry A* **2007**, *111*, 11198.
[171] A. Frischmuth, M. Fernández, N. M. Barl, F. Achrainer, H. Zipse, G. Berionni, H. Mayr, K. Karaghiosoff, P. Knochel, *Angewandte Chemie International Edition* **2014**, *53*, 7928.
[172] *Progress on Drinking Water and Sanitation 2014 Update*, WHO Press, Geneva, Switerland, **2014**.
[173] S. Suthar, J. Sharma, M. Chabukdhara, A. Nema, *Environmental Monitoring and Assessment* **2010**, *165*, 103.
[174] D. Li, J. Qu, *Journal of Environmental Sciences* **2009**, *21*, 713.
[175] a) S. W. Krasner, H. S. Weinberg, S. D. Richardson, S. J. Pastor, R. Chinn, M. J. Sclimenti, G. D. Onstad, A. D. Thruston, *Environmental Science & Technology* **2006**, *40*, 7175; b) E. M. Fiss, K. L. Rule, P. J. Vikesland, *Environmental Science &*

Technology **2007**, *41*, 2387; c) S. H. Joo, W. A. Mitch, *Environmental Science & Technology* **2007**, *41*, 1288.
[176] D. Liviac, E. D. Wagner, W. A. Mitch, M. J. Altonji, M. J. Plewa, *Environmental Science & Technology* **2010**, *44*, 3527.
[177] a) X. L. Armesto, M. Canle L, M. V. Garcia, J. A. Santaballa, *Chemical Society Reviews* **1998**, *27*, 453; b) J. M. Antelo, F. Arce, M. Parajó, *International Journal of Chemical Kinetics* **1995**, *27*, 637; c) L. Abia, X. L. Armesto, M. L. Canle, M. V. García, J. A. Santaballa, *Tetrahedron* **1998**, *54*, 521; d) M. Bedner, W. A. MacCrehan, *Chemosphere* **2006**, *65*, 2130.
[178] a) M. M. Campbell, G. Johnson, *Chemical Reviews* **1978**, *78*, 65; b) R. Filler, *Chemical Reviews* **1963**, *63*, 21.
[179] H.-S. Dawn, I. H. Pitman, T. Higuchi, S. Young, *Journal of Pharmaceutical Sciences* **1970**, *59*, 955.
[180] a) I. J. Buerge, M. Keller, H.-R. Buser, M. D. Müller, T. Poiger, *Environmental Science & Technology* **2010**, *45*, 615; b) R. Banerjee, P. M. Bhatt, N. V. Ravindra, G. R. Desiraju, *Crystal Growth & Design* **2005**, *5*, 2299.
[181] C. L. Arcus, J. Kenyon, *Journal of the Chemical Society (Resumed)* **1939**, 916.
[182] a) L. Stella, *Angewandte Chemie International Edition in English* **1983**, *22*, 337; b) R. S. Neale, *Synthesis* **1971**, *1971*, 1; c) J. Hu, J. Wang, T. H. Nguyen, N. Zheng, *Beilstein Journal of Organic Chemistry* **2013**, *9*, 1977.
[183] R. I. Walter, *Journal of the American Chemical Society* **1955**, *77*, 5999.
[184] M. E. Wolff, *Chemical Reviews* **1963**, *63*, 55.
[185] J. H. Horner, F. N. Martinez, O. M. Musa, M. Newcomb, H. E. Shahin, *Journal of the American Chemical Society* **1995**, *117*, 11124.
[186] R. I. Walter, *Journal of the American Chemical Society* **1966**, *88*, 1923.
[187] a) D. J. Bellville, D. W. Wirth, N. L. Bauld, *Journal of the American Chemical Society* **1981**, *103*, 718; b) D. J. Bellville, N. L. Bauld, *Journal of the American Chemical Society* **1982**, *104*, 2665.
[188] a) S. H. Preskorn, R. Ross, C. Y. Stanga, in *Antidepressants: Past, Present and Future, Vol. 157* (Eds.: S. Preskorn, J. Feighner, C. Stanga, R. Ross), Springer Berlin Heidelberg, **2004**, pp. 241; b) K. Dechant, S. Clissold, *Drugs* **1991**, *41*, 225.
[189] J. B. Lassen, E. Petersen, B. Kjellberg, S. O. Olsson, *European Journal of Pharmacology* **1975**, *32*, 108.
[190] I. Angel, H. Schoemaker, M. Prouteau, M. Garreau, S. Z. Langer, *European Journal of Pharmacology* **1993**, *232*, 139.
[191] P. C. Waldmeier, L. Maître, P. A. Baumann, K. Hauser, S. Bischoff, H. Bittiger, R. Paioni, *European Journal of Pharmacology* **1986**, *130*, 1.
[192] J. A. Christensen, R. F. Squires, *Vol. US4007196*, USA, **1977**.
[193] G. de Gonzalo, R. Brieva, V. M. Sánchez, M. Bayod, V. Gotor, *The Journal of Organic Chemistry* **2001**, *66*, 8947.
[194] M. Amat, J. Bosch, J. Hidalgo, M. Cantó, M. Pérez, N. Llor, E. Molins, C. Miravitlles, M. Orozco, J. Luque, *The Journal of Organic Chemistry* **2000**, *65*, 3074.
[195] M. S. Yu, I. Lantos, Z.-Q. Peng, J. Yu, T. Cacchio, *Tetrahedron Letters* **2000**, *41*, 5647.
[196] G. Hughes, M. Kimura, S. L. Buchwald, *Journal of the American Chemical Society* **2003**, *125*, 11253.

[197] a) T. Vasskog, T. Anderssen, S. Pedersen-Bjergaard, R. Kallenborn, E. Jensen, *Journal of Chromatography A* **2008**, *1185*, 194; b) M. Segura, J. Ortuño, M. Farré, R. Pacifici, S. Pichini, J. Joglar, J. Segura, R. d. l. Torre, *Rapid Communications in Mass Spectrometry* **2003**, *17*, 1455.
[198] S. Chu, C. D. Metcalfe, *Journal of Chromatography A* **2007**, *1163*, 112.
[199] V. L. Cunningham, D. J. C. Constable, R. E. Hannah, *Environmental Science & Technology* **2004**, *38*, 3351.
[200] J.-W. Kwon, K. L. Armbrust, *Environmental Toxicology and Chemistry* **2004**, *23*, 1394.
[201] D. Sakic, H. Zipse, V. Vrcek, *Organic & Biomolecular Chemistry* **2011**, *9*, 4336.
[202] V. Vrček, H. Zipse, *The Journal of Organic Chemistry* **2009**, *74*, 2947.
[203] R. J. O'Reilly, A. Karton, L. Radom, *The Journal of Physical Chemistry A* **2011**, *115*, 5496.
[204] D. Sakic, F. Achrainer, V. Vrcek, H. Zipse, *Organic & Biomolecular Chemistry* **2013**, *11*, 4232.
[205] H. K. Hall, *Journal of the American Chemical Society* **1957**, *79*, 5441.
[206] M. Jonsson, D. D. M. Wayner, J. Lusztyk, *The Journal of Physical Chemistry* **1996**, *100*, 17539.
[207] A. Karton, R. J. O'Reilly, L. Radom, *The Journal of Physical Chemistry A* **2012**, *116*, 4211.
[208] J. R. Pliego Jr, *Chemical Physics* **2004**, *306*, 273.
[209] H. Navrátilová, Z. Kříž, M. Potáček, *Synthetic Communications* **2004**, *34*, 2101.
[210] a) B. P. Hay, R. G. Finke, *Journal of the American Chemical Society* **1986**, *108*, 4820; b) K. M. Doll, B. R. Bender, R. G. Finke, *Journal of the American Chemical Society* **2003**, *125*, 10877.
[211] F. G. Bordwell, T. Y. Lynch, *Journal of the American Chemical Society* **1989**, *111*, 7558.

8 Curriculum Vitae

Personal data

Name	Florian Achrainer
Place of Birth	Munich, Germany
Nationality	German
Marital status	unmarried

Education and Studies

11/2008 – 9/2014	Ph.D. Thesis under the supervision of *Prof. Dr. Hendrik Zipse*, Ludwig-Maximilians-Universität Munich Focus: organic synthesis, microwave synthesis, computational chemistry, kinetics
10/2005 – 9/2008	Master of Science (M.Sc), department of chemistry, Ludwig-Maximilians-Universität Munich
10/2001 – 7/2005	Bachelor of Science (B.Sc), department of chemistry, Ludwig-Maximilians-Universität Munich
9/2000 – 8/2001	Civil service at the Alten- und Service Zentrum Untergiesing, Munich
9/1991 – 5/2000	Abitur, Pater-Rupert-Mayer-Gymnasium Pullach